

Department of Civil, Environmental and Geomatic Engineering, University
College London, Gower Street, London, WC1E 6BT

Feasibility assessment and informed survey design of cavity
detection by forward geophysical modelling

Engineering Doctorate

Paul James

September 2014

Supervisors: Dr. Pedro Ferreira, Prof. Peter Sammonds and
Tim Hartlib

A dissertation submitted in partial fulfilment of the
requirements for the degree of Engineering Doctorate,
University College London.

Declaration of originality

This is to certify that the work is entirely my own and not of any other person, unless explicitly acknowledged (including citation of published and unpublished sources). The work has not previously been submitted in any form to the University College London or to any other institution for assessment for any other purpose.

Signed _____

Date _____

Abstract

Feasibility analysis of near-surface cavity detection is presented using modelling of the gravity, gravity gradient, magnetic, magnetic gradient, and ground penetrating radar techniques. The geophysical signal is modelled over typical cavity shapes in three-dimensional subsurface environments with varying geologies and survey parameters. The cavity detection probability is calculated for each technique in the outlined environments and these values are used to aid technique choice, assess the feasibility of cavity detection, assess the limits of detection for each technique, and optimise survey design before entering the field.

The “halo” effect is quantified by simulating the halo around cavities and calculating the change to the gravity and magnetic anomalies by geophysical modelling. The magnitude of the effect is shown to be more complicated than existing literature implies, depending heavily on the fracture percentage in the halo area and the halo spread.

Tests in a range of conditions show that technique choice is conditional to site characteristics and site parameters, and highlight the need for modelling in the desk study stage of site investigation and survey design. Detection probability results show that standard survey direction practice in magnetometry is not always optimal, and demonstrate the importance of site specific noise level consideration. Comparisons with case study measurements demonstrate that modelling and subsequent detection probability calculation chose appropriate techniques and survey parameters, but also highlighted the limitations of the method.

Acknowledgements

I would like to thank my supervisors, Dr. Pedro Ferreira, Prof. Peter Sammonds and Tim Hartlib, for all their help and guidance throughout the project. I thank Ramboll, UCL and the EPSRC for this opportunity and the funding they have provided. I would like to thank my colleagues in Urban Sustainability and Resilience for the interesting discussions, candour and support. Finally, I would like to thank Anne Cole for her encouragement throughout.

Contents

Abstract	3
Acknowledgements	4
Contents.....	5
List of Figures	12
1 Introduction.....	26
1.1 Aim and Objectives	28
1.2 Thesis Organisation	28
1.3 Applications	29
2 Literature Review.....	30
2.1 Cavity hazards.....	30
2.1.1 Cavity collapse.....	31
2.1.2 Contamination.....	32
2.1.3 Mine flooding.....	33
2.2 Land use and engineering	33
2.3 Social and biological interest.....	34
2.4 Cavity location	34
2.5 Cavity formation and typical shapes.....	36
2.5.1 Man-made cavities	36
2.5.2 Natural.....	40
2.6 Current cavity detection techniques in engineering.....	45
2.6.1 Intrusive	45
2.6.2 Desk study	46
2.7 Geophysics for cavity detection.....	47

2.7.1	Reputation in engineering	47
2.7.2	Benefits of a geophysical survey	48
2.7.3	Considerations	50
2.8	Geophysical techniques.....	52
2.8.1	Ground Penetrating Radar	52
2.8.2	Gravity.....	59
2.8.3	Magnetometry	62
2.8.4	Gradient.....	66
2.8.5	Resistivity	67
2.8.6	EM	68
2.8.7	Seismic techniques	69
2.9	Choice of technique	73
2.10	Cavity detection database	74
2.11	Generalised protocol for U.K. cavity detection.....	76
2.12	Current use of modelling in near surface geophysics	78
2.12.1	Finite element method.....	80
2.12.2	Software available.....	80
2.12.3	Software requirements	82
2.13	Chapter Summary	83
3	Methodological framework	85
3.1	Modelling approach.....	86
3.2	Modelling method overview.....	87
4	Cavity modelling.....	88
4.1	Modelling techniques	88
4.1.1	3D.....	89
4.1.2	Potential methods	89
4.1.3	Ground penetrating radar.....	91
4.1.4	Resistivity	92

4.1.5	Electromagnetic induction.....	92
4.2	MATLAB implementation.....	93
4.2.1	Graphical user interface.....	93
4.2.2	Data structure	93
4.2.3	Usability	94
4.3	Variable parameters.....	95
4.3.1	Predetermined variables.....	96
4.3.2	User variables.....	96
4.4	Noise level	99
4.4.1	Literature noise measurements.....	100
4.4.2	Field measurements of magnetic noise	102
4.5	Probabilistic approach to detection in noise	104
4.5.1	Single survey line probability	107
4.5.2	Total survey probability.....	109
4.5.3	Monte Carlo method	110
4.6	Running the program.....	110
4.6.1	Begin modelling.....	110
4.7	Output	111
4.7.1	Visualisation	111
4.7.2	Survey cost and time	113
4.7.3	Collapse height	115
4.8	Chapter summary	117
5	Modelling Results and Data Analysis Implementation	119
5.1	Cavity variation	120
5.1.1	Cavity depth	121
5.1.2	Cavity shape.....	121
5.1.3	Shaft size.....	124
5.1.4	Rounded gallery	126

5.1.5	Fill material	127
5.1.6	Lining material	128
5.1.7	Lining thickness	129
5.2	Site conditions.....	130
5.2.1	Geology	130
5.2.2	Noise level.....	133
5.2.3	Profile and station spacing.....	135
5.2.4	Survey direction.....	137
5.2.5	Survey size	139
5.2.6	Data deletion percentage.....	140
5.2.7	Parameter variation	143
5.2.8	Small variations in antenna height	145
5.3	Limit of detection	145
5.4	Chapter Summary	148
6	The Halo effect	150
6.1	Introduction.....	150
6.2	Halo variables.....	151
6.2.1	Halo spread	151
6.2.2	Fracture patterns.....	151
6.2.3	Fracture aperture	154
6.2.4	Layer thickness.....	157
6.2.5	Joint spacing and bed thickness ratio.....	160
6.2.6	Orientation.....	160
6.2.7	Fracture fill.....	161
6.2.8	Within the halo system.....	161
6.2.9	Excavation cracks	163
6.3	Effect on geophysical techniques.....	165
6.4	Halo generation methodology.....	165

6.5	Geophysical modelling.....	166
6.6	Chapter summary	167
7	Halo Results.....	168
7.1.1	Fracture configuration.....	169
7.1.2	Fracture percentage.....	171
7.1.3	Cavity depth	173
7.1.4	Halo spread.....	176
7.1.5	Fracture aperture	179
7.1.6	Fracture angle.....	182
7.1.7	Fracture patterns.....	184
	The impact of varying the indent size was tested by modelling a.....	185
7.1.8	Micro-fractures.....	188
7.2	Comparison with rules of thumb	191
7.3	Comparison with previous work.....	194
7.4	Discussion	196
7.5	Chapter summary	196
8	Cavity Case Studies and Modelling Comparison	198
8.1	Equipment list.....	198
8.2	Middlesex Hospital, London	199
8.2.1	Pavement vault modelling	199
8.2.2	Field measurements.....	200
8.3	Oslo sewerage tunnel	202
8.3.1	Tunnel modelling.....	202
8.3.2	Field measurements.....	204
8.3.3	Interpretation.....	207
8.4	West Wycombe Caves	208
8.4.1	Cave design.....	209
8.4.2	Land surveying	210

8.4.3	Cave geophysical modelling	212
8.4.4	Field measurements.....	214
8.5	Coatbridge, Scotland	217
8.5.1	Geology	218
8.5.2	Shaft modelling.....	219
8.5.3	Geophysical survey	220
8.5.4	Survey locations	220
8.5.5	Field techniques.....	221
8.5.6	Results and interpretation	224
8.5.7	Discussion	229
8.6	Chapter summary	230
9	Summary and Conclusions	232
9.1	Review of objectives and findings	233
9.1.1	Objective 1	233
9.1.2	Objective 2	234
9.1.3	Objective 3	235
9.1.4	Objective 4	236
9.1.5	Objective 5	237
9.2	Discussion	237
9.2.1	Practical merits of approach	237
9.2.2	Critique of methodology.....	238
9.2.3	Comparison with other modelling techniques	240
9.2.4	Modelling approach weaknesses	241
9.2.5	Lessons learnt from the case studies	243
9.3	Continuation and Future Work.....	245
9.3.1	Alternative approach to halo modelling	245
9.3.2	Site specific parameter measurement	246
9.3.3	Further techniques.....	246

9.3.4	Multiple techniques and joint inversion.....	247
9.3.5	Alternative modelling approaches	247
9.3.6	Comparison with other targets.....	247
9.3.7	Application to other near surface targets.....	248
9.3.8	Processing analysis.....	248
9.3.9	On site noise measurements	248
9.3.10	Field work and literature comparison	248
9.4	Final Conclusion.....	248
10	References	250
11	Appendices	271

List of Figures

FIGURE 2.1. HAZARDS ASSOCIATED WITH CAVITIES. FROM LEFT: PREVIOUSLY UNKNOWN BLACKHEATH MEDIEVAL CHALK MINE COLLAPSE (BRITISH GEOLOGICAL SOCIETY, 2010); RESCUE FROM BREACH OF PREVIOUSLY UNKNOWN MINE IN XIANGNING, CHINA (BRANIGAN, 2010); CONTAMINATION OF WATER FLOWING THROUGH MINE, (UNITED STATES GEOLOGICAL SURVEY, 2006).	32
FIGURE 2.2. POTENTIAL CAVITY LOCATIONS IN GREAT BRITAIN. LEFT: ACTIVE AND CEASED MINE WORKS COMPILED BY THE DIRECTORY OF MINES AND QUARRIES (BRITISH GEOLOGICAL SURVEY, 2010B). RIGHT: POTENTIAL FOR DISSOLUTION TO BE A HAZARD (BRITISH GEOLOGICAL SOCIETY, 2011).	35
FIGURE 2.3. SHAFT DIAMETER (LEFT) AND DEPTH (RIGHT) INCREASES THROUGH TIME (OVE ARUP AND PARTNERS, 1976).	37
FIGURE 2.4. DISTRIBUTION OF SOLUBLE (KARSTIC) ROCKS IN GREAT BRITAIN (BRITISH GEOLOGICAL SURVEY, 2010A).....	41
FIGURE 2.5. WORLD MAP OF CARBONATE ROCK OUTCROPS (SCHOOL OF ENVIRONMENT, UNIVERSITY OF AUCKLAND, 2010 BASED ON DATA FROM FORD & WILLIAMS, 2007).....	41
FIGURE 2.6. DEVELOPMENT OF CAVITIES IN CHALK OVER GEOLOGICAL TIME (EDMONDS, 2008). A BURIED SOLUTION SINKHOLE IS CREATED AND INCREASED BY WATER FLOW (THIS CAN BE NATURAL OR MANMADE E.G. A BROKEN PIPE OR QUARRY DEWATERING CHANGING THE WATER TABLE). A VOID WILL FORM IN THE OVERBURDEN AND WILL MIGRATE UPWARDS WITH EROSION LEAVING INFILL BENEATH. MIGRATION WILL CEASE IF THERE IS A COMPETENT STRATA ABOVE OR EROSION STOPS. A SINKHOLE FORMS IF THE VOID REACHES THE SURFACE OR THE OVERBURDEN COLLAPSES.	43
FIGURE 2.7. DEVELOPMENT OF SUBSIDENCE IN SAND ABOVE ERODED BEDROCK (TOP) AND DROPOUT IN CLAY (BOTTOM) (CULSHAW AND WALTHAM 1987).	43
FIGURE 2.8. THE POSSIBILITY OF MISSING CAVITIES WITH DISCRETE BOREHOLE SAMPLING. DEPENDING ON BOREHOLE GRID DENSITY AND CAVITY SIZE, WHOLE CAVITIES MAY BE MISSED BETWEEN BOREHOLES BOREHOLE GRID PATTERNS MAY EVEN MATCH MINE PILLAR PATTERNS, MEANING ALL AREAS OF MINING ACTIVITY GO UNDETECTED. ALSO MANY MORE BOREHOLES THAN NEEDED ARE DRILLED ADDING UNNECESSARY EXPENSE (KENDORSKI, 2004).	46
FIGURE 2.9. GENERAL BENEFITS OF USING GEOPHYSICS IN SITE INVESTIGATION.	49
FIGURE 2.10. GROUND PENETRATING RADAR EQUIPMENT AND PRINCIPLE (XU <i>ET AL.</i> , 2009).	53
FIGURE 2.11. GPR SURVEY OF A TEST PIT USING 300, 500 AND 900 MHZ ANTENNAS (TOP, MIDDLE AND BOTTOM RESPECTIVELY). HERE WE CAN SEE THE DEEPER PENETRATION OF THE LOWER	

FREQUENCIES AND THE INCREASED RESOLUTION OF THE HIGHER FREQUENCY. ALSO NOTE HOW THE FEATURES ABOVE THE VOID MAY OBSCURE THE VOIDS SIGNAL. D IS A BURIED AIR VOID, E ARE PIPES AND P IS THE PIT LIMIT (GRANDJEAN <i>ET AL.</i> , 2000).	55
FIGURE 2.12. DIFFRACTION HYPERBOLA OVER A CAVITIES WITHIN LIMESTONE (TERRADAT UK LTD., 2005).	57
FIGURE 2.13. GPR SURVEY OVER A COLLAPSED DOLINE. THE GREY AREA WAS CHARACTERISED BY PENETRATION VARIANCE AND THE INSET SHOWS THE ONLAP REFLECTION FEATURES AT THE BORDER OF THE COLLAPSE (MOCHALES <i>ET AL.</i> , 2007A).	58
FIGURE 2.14. A) OSCILLATIONS WITHIN AN AIR FILLED SINKHOLE AT DEPTH 1.1 M IMAGED IN ORTHOGONAL DIRECTIONS (KOFMAN <i>ET AL.</i> , 2006). B) MULTIPLE REFLECTION ANOMALIES HIGHLIGHTING HIGH CONDUCTIVITY MATERIAL (MOCHALES <i>ET AL.</i> , 2007A).	59
FIGURE 2.15. MODEL OF A VOID AND ITS ASSOCIATED MAGNETIC ANOMALY (RYBAKOV <i>ET AL.</i> , 2005).	65
FIGURE 2.16. MAGNETIC AND GRAVITY ANOMALIES OVER A SINKHOLE AT HEVER SOUTH SITE, NEAR THE DEAD SEA (RYBAKOV <i>ET AL.</i> , 2005) AND AN ANOMALY DETECTED OVER A DOLINE IN NORTHERN SPAIN (MOCHALES <i>ET AL.</i> , 2007B).	65
FIGURE 2.17. MAGNETIC CONTOUR PLOT OF A BRICK LINED SHAFT AND A WOOD LINE SHAFT NEAR LEEDS (BACKGROUND VALUE OF 48,000 NT) (RAYBOULD & PRICE, 1966).	67
FIGURE 2.18. WAVEFIELD TRANSFORMATION OF ONE MULTICHANNEL RECORD TO A DISPERSION IMAGE SHOWING THE ENERGY ACCUMULATION OF SEISMIC WAVES (PARK SEISMIC, 2010B).	71
FIGURE 2.19. SHEAR-WAVE VELOCITY MODEL FOR HISTORICAL MINES IN MINNESOTA. VELOCITY VALUES ARE IN FEET/SECOND (BILLINGTON, 2006).	73
FIGURE 2.20. CAVITIES SUCCESSFULLY DETECTED USING GROUND PENETRATING RADAR IN DIFFERENT GEOLOGIES COMPILED FROM ACADEMIC LITERATURE (APPENDIX C). BALLOON SIZE REPRESENTS THE LARGEST CAVITY DIMENSION (SCALE IS EQUAL TO THE DEPTH AXIS). ONLY CAVITIES WITH ALL OF THE FOLLOWING INFORMATION WERE USED: CAVITY SIZE, DEPTH AND SURROUNDING GEOLOGY.	75
FIGURE 2.21. DEPTH OF CAVITIES DETECTED AND THE ANTENNA FREQUENCY USED. DATA IS FROM RECENT LITERATURE ON CAVITY DETECTION (APPENDIX C).	76
FIGURE 2.22. PROPOSED GEOPHYSICAL ROUTINE FOR CAVITY DETECTION IN THE U.K. N.B. THIS ROUTINE MUST BE ADAPTED FOR EACH SITE AND DOES NOT REPLACE A DESK STUDY AND EXPERIENCED GEOPHYSICIST. AFTER PUEYO-ANCHUELA <i>ET AL.</i> (2010).	79
FIGURE 3.1. PROPOSED INTEGRATION OF GEOPHYSICS AND MODELLING INTO SITE INVESTIGATION.	86
FIGURE 4.1. GRAPHICAL USER INTERFACE OF THE CAVITY MODELLING PROGRAM. THIS OPENING PAGE OFFERS THE USER ALL THE OPTIONS AVAILABLE TO START THE PROGRAM. VARIABLES ARE CHANGED EITHER BY TYPING IN THE TEXT BOXES OR USING THE DROP DOWN MENUS AND SLIDERS. THE IMAGE OF THE SUBSURFACE IS REDRAWN WHEN THE 'SHOW' BUTTON IS PRESSED. MIGRATION IS AUTOMATICALLY REDRAWN WITH CHANGES.	94

FIGURE 4.2. STRUCTURE OF THE CAVITY MODELLING SOFTWARE. EACH BOX REPRESENTS AN M-FUNCTION WITH ITS GIVEN NAME NOTED. ARROWS REPRESENT INTERACTION BETWEEN FUNCTION. DIAMONDS ARE CLICKABLE BUTTONS ON THE GUI.....	95
FIGURE 4.3. TYPICAL CAVITY SHAPES USED IN MODELLING. A) SHAFT, B) BELL PIT, C) LINED SHAFT, D) CAPPED SHAFT, E) HORIZONTAL GALLERY (DOTTED LINES - MORE ROUNDED GALLERY), F) MIGRATING VOID.....	98
FIGURE 4.4. ELECTROMAGNETIC NOISE SPECTRUM HIGHLIGHTING POTENTIAL NOISE SOURCES ACROSS ALL RANGES OF FREQUENCY UTILISED BY GEOPHYSICAL METHODS. (EVERETT & MEJU, 2005) AFTER (PALACKY & WEST, 1991).....	100
FIGURE 4.5. GENERAL LOCATION OF NOISE MEASUREMENTS (GOOGLE, 2011). MORE DETAILED MAPS IN APPENDIX C. SITES WERE: A) REGENTS PARK. LOCATIONS IN THE CENTRE OF A FIELD (RP1), AND BESIDE A ROADSIDE AND FENCE (RP2). B) MIDDLESEX HOSPITAL SITE. LOCATIONS NEAR THE CHURCH (M1 AND 2), BY A RUBBLE MOUND (M3), BY THE PERIMETER FENCE (M4) AND 1.5 M FROM FENCE (M5). C) UCL QUAD. LOCATIONS ON THE GRASS (Q1), ON A PAVED FOOTPATH (Q2), BY THE LARGE PORTICO BUILDING (Q3), BY A SMALL BUILDING (Q4), INSIDE THE DOORWAY (Q5), ON THE STAIRS (Q6), INSIDE A SECOND STORY ROOM (Q7). D) WEST WYCOMBE CAVES (35 MILES EAST OF LONDON). LOCATIONS IN THE CENTRE OF THE FIELD (W1), WITH TREE COVERAGE (W2), BY THE EQUIPMENT (W3), AND BY THE MAUSOLEUM (W4).	102
FIGURE 4.6. NOISE LEVEL DEPENDENT ON SITE TYPE. THE WIDE RANGE HIGHLIGHTS THE IMPORTANCE OF SITE SPECIFIC MEASUREMENTS OF NOISE.	104
FIGURE 4.7. A) TOTAL MAGNETIC FIELD FROM A 1-M CUBE AIR CAVITY AT 3-M DEPTH IN LIMESTONE. GREEN LINES DENOTE THE SURVEY LINES WHERE THE ANOMALY IS LARGER THAN THE INSTRUMENTAL NOISE VALUE OF A TYPICAL MAGNETOMETER (GEOMETRICS G858). B) THE DISTANCE FROM THE CAVITY CENTRE THAT THE CAVITY ANOMALY IS GREATER THAN TYPICAL MAGNETOMETER SENSITIVITY (TOP CURVE) AND INSTRUMENTAL NOISE (BOTTOM CURVE) AT INCREASING DEPTHS. C) THE SAME CAVITY BUT IN SANDSTONE. D) THE APPLICATION OF NOISE SHOWN TO HIGHLIGHT THE OBSCURING OF CAVITY SIGNAL.	105
FIGURE 4.8. MODELLED RESULTS SHOWING THE DETECTION PROBABILITY OF A 1-M CUBE AIR CAVITY AT 3 M DEPTH IN LIMESTONE USING MAGNETOMETRY. COLOUR SCALE SHOWS THE PROBABILITY OF DETECTION AT EACH SURVEY LINE AT (A) 0.01 nT, (B) 0.1 nT AND (C) 1.4 nT.....	108
FIGURE 4.9. A) MODELLED RESULTS SHOWING THE PROBABILITY OF DETECTION OF A 1-M SIDED CUBE AIR CAVITY AT 3-M DEPTH IN LIMESTONE USING MAGNETOMETRY. THE GREY SCALE SHOWS THE PROBABILITY OF DETECTION IN TYPICAL MAGNETIC NOISE (TABLE 2). B) THE DETECTION PROBABILITY OF THE SAME CAVITY DECREASING WITH DEPTH IN A RANGE OF GEOLOGIES. THE PROBABILITIES SHOWN REPRESENT THAT OF A SURVEY LINE DIRECTLY ABOVE THE CAVITY.....	108
FIGURE 4.10. EXAMPLE OUTPUT OF THE CAVITY MODELLING PROGRAM. THE CAVITY MODELLED IS A 1-M CUBE WATER CAVITY AT 2-M DEPTH IN SANDSTONE. NB THE EM RESULTS ARE BASED ON THE MODELLING OF A 1-M DIAMETER SPHERE AS THE ALGORITHM DOES NOT CURRENTLY ALLOW CUBES. APPARENT RESISTIVITY IS CURRENTLY ONLY AVAILABLE IN 2D (DISTANCE ALONG SURVEY LINE ON HORIZONTAL AXIS AND DEPTH ON THE VERTICAL AXIS). OVERALL DETECTION	

PROBABILITY IS SHOWN ABOVE EACH TECHNIQUE AND PROFILE LINE DETECTION PROBABILITY IS INDICATED BY THE COLOUR SCALE TO THE RIGHT OF THE FIRST ROW OF RESULTS (WITH THE EXCEPTION OF RESISTIVITY).....	112
FIGURE 4.11. THE CAVITY IS A 1-M SIDED CUBE WATER CAVITY AT 2 M DEPTH IN SANDSTONE MODELLED WITH A) MAGNETIC, B) MAGNETIC GRADIENT, C) GRAVITY, D) GRAVITY GRADIENT, E) GPR. OVERALL DETECTION PROBABILITY IS SHOWN ABOVE EACH TECHNIQUE AND THE COLOUR BAR INDICATES PROFILE LINE DETECTION PROBABILITY. DP = OVERALL DETECTION PROBABILITY.	113
FIGURE 4.12. AN EXAMPLE OF THE OUTPUT OF THE FIELD.M COMMAND. THE RED DOTS REPRESENT SURVEY POINT FOR THE GRAVITY SURVEYS, AND THE BLACK LINES ARE THE PROFILE LINES. ESTIMATED SURVEY TIME AND RENTAL COSTS ARE LISTED BELOW.....	115
FIGURE 4.13 MAXIMUM HEIGHT COLLAPSE DEPENDANT ON GEOMETRY. FROM BELL (2004) BASED ON PIGGOTT & EYNON (1978)	116
FIGURE 4.14. MODELLED POTENTIAL MIGRATION HEIGHT OF A 1-M CUBE, 3 M DEEP IN LIMESTONE. THE THREE MIGRATION TYPES ARE SHOWN, A) RECTANGULAR, B) WEDGE, AND C) CONICAL. OF THE THREE, ONLY THE CONICAL MIGRATION TYPE REPRESENTS A POSSIBILITY OF CROWNING (MIGRATING TO THE SURFACE). THE CONICAL SHAPE IS THE EXTREME OF MIGRATION AND SO CIRCULAR CAVITIES ARE MORE OF A THREAT.....	117
FIGURE 5.1. TOTAL MAGNETIC FIELD OVER A CUBOID AIR CAVITY. BASE CONDITIONS ARE A 1 M AIR FILLED CUBE AT 3 M DEPTH IN LIMESTONE, MEASURED DIRECTLY ABOVE THE CAVITY. SIGNAL AMPLITUDE DECREASES WITH A) DISTANCE FROM TARGET (0.5 M INCREMENTS FROM 0 M), B) DEPTH TO TARGET (0.2 M INCREMENTS FROM 0.1 M DEPTH), C) DECREASING CAVITY SIZE (0.4 M INCREMENTS DOWN TO 0.1 M CUBE), D) DECREASING MAGNETIC SUSCEPTIBILITY OF CAVITY MATERIAL, E) DECREASING MAGNETIC SUSCEPTIBILITY OF HOST MATERIAL. IT CAN BE SEEN THAT SMALL CHANGES IN EACH PARAMETER AFFECT THE SIGNAL IN A LOGICAL MANNER BUT THE COMBINATION OF THESE FACTORS CAN MAKE ACCURATE PREDICTION OF GEOPHYSICAL SIGNAL COMPLICATED.	120
FIGURE 5.2. A) DETECTION PROBABILITY OF A 1-M CUBE AIR CAVITY IN LIMESTONE AT TYPICAL NOISE LEVELS OVER A RANGE OF DEPTHS ACROSS A 15 M GRID. B) ANOMALY SIZE OVER THE SAME CAVITY EXPRESSED AS A PERCENTAGE OF THE ANOMALY SIZE AT 1-M CAVITY DEPTH (ORIGINAL RESULTS OF ANOMALY SIZES IN APPENDIX A).....	122
FIGURE 5.3. (PREVIOUS PAGE) MODELLED SIGNAL OVER TYPICAL CAVITY SHAPES IN LIMESTONE. A 1 M SQUARE, 1 M DEEP, 6 M TALL A) AIR SHAFT, B) WATER SHAFT, C) AIR SHAFT WITH 0.5 M STEEL CAP, D) AIR SHAFT WITH STEEL LINING AND CAP (0.5 M), AND E) AIR SHAFT WITH 4 M SQUARE, 2 M TALL BELL PIT BENEATH. THE COLOUR BAR INDICATES DETECTION PROBABILITY (%). TOTAL DETECTION PROBABILITY IS OVER 99% FOR ALL MAGNETIC MODELS AND, FROM TOP, 79%, 71%, 72%, 84% AND 94%, FOR GRAVITY.....	124
FIGURE 5.4. SHAFT DIAMETER (LEFT) AND DEPTH (RIGHT) INCREASES THROUGH TIME (OVE ARUP AND PARTNERS, 1976).	124

FIGURE 5.5. 2-M DEEP AIR SHAFT, WITH HEIGHT OF 20 M IN CLAY, AT BROWNFIELD NOISE LEVELS (AS WOULD BE TYPICAL ON A SITE WITH A MINE SHAFT).A) DETECTION PROBABILITY AND B) ANOMALY SIZE OF SIGNAL ABOVE THE 2-8 M DIAMETER SHAFT. GRAVITY GRADIENT IS AT 100% FOR ALL SHAFT SIZES WHILE GPR ANOMALY IS VERY SMALL (6.61×10^{10} MICROV).....	125
FIGURE 5.6. DOTTED LINE SHOWS ORIGINAL GALLERY CROSS-SECTION, SOLID FILL SHOWS ROUNDED GALLERY CROSS-SECTION; A THIRD OF THE HEIGHT AND THE WIDTH ARE REMOVED.....	126
FIGURE 5.7. MODELLING ABOVE A 1-M SQUARE, 15 M LONG GALLERY IN LIMESTONE AT TYPICAL NOISE LEVELS. A) DETECTION PROBABILITY OF A ROUNDED AND NON-ROUNDED GALLERY WITH INCREASING DEPTH. B) EFFECT ON ANOMALY SIZE DUE TO ROUNDING OF GALLERY.	127
FIGURE 5.8. DETECTION PROBABILITY OF 1-M SIDED CUBE (WITH VARIOUS FILL MATERIAL), 3 M DEEP IN LIMESTONE ACROSS A 15 M SQUARE SITE. DENSITY (LEFT TO RIGHT): 1.5 G/CM ³ (ERKAN & JEKELI, 2011), 1 G/CM ³ (MILSOM & ERIKSEN, 2011), 0.0012 G/CM ³ (INTERNATIONAL STANDARD ATMOSPHERE), 1.4 G/CM ³ , 1.8 G/CM ³ (AVERAGE FROM PUEYO-ANCHUELA <i>ET AL.</i> , 2010). MAGNETIC SUSCEPTIBILITY: 1×10^{-7} (MILSOM, 2003), -9.051×10^{-9} (ARRIGHINI, 1968), 0 (MILSOM, 2003), 0.05, 0.005 (AVERAGE FROM PUEYO-ANCHUELA <i>ET AL.</i> , 2010) SI UNITS.	128
FIGURE 5.9. MODELLED DETECTION PROBABILITY OVER A 1 M DEEP, 10 M TALL, AIR SHAFT IN LIMESTONE, AT BROWNFIELD NOISE LEVELS. LINING AND CAP ARE BOTH 0.2 M THICK.	129
FIGURE 5.10. A) (PREVIOUS PAGE) MODELLING RESULTS FOR THE MAGNETIC (LEFT COLUMN) AND GRAVITY (RIGHT COLUMN) TECHNIQUES OVER A 1 M DEEP, 10-M HEIGHT, AIR SHAFT IN LIMESTONE, AT BROWNFIELD NOISE LEVELS WITH CONCRETE LINING. GREY BOX REPRESENTS THE LINING THICKNESS IN THAT ROW'S MODELS. COLOUR BAR REPRESENTS THE DETECTION PROBABILITY, DP = OVERALL SURVEY DETECTION PROBABILITY. B) THE OVERALL DETECTION PROBABILITY FOR ALL LINING THICKNESSES.	132
FIGURE 5.11. DETECTION PROBABILITY OF THE RANGE OF TECHNIQUES FOR A 1-M CUBE AIR CAVITY, 3 M DEEP IN TYPICAL NOISE CONDITIONS IN A RANGE OF GEOLOGIES. SEE TABLE 4.1 FOR GEOPHYSICAL PARAMETERS. GRAVITY GRADIENT HAS ABOVE 99% DETECTION PROBABILITY IN ALL GEOLOGIES.....	132
FIGURE 5.12. MODELLED MAGNETOMETER SIGNAL OF A 1 M SQUARE AND 6 M TALL AIR SHAFT IN LIMESTONE AT 1 M DEPTH IN DIFFERENT NOISE CONDITIONS: A) GREENFIELD, B) URBAN AND BUILDINGS, C) BROWNFIELD AND D) INDOOR. THE COLOUR BAR INDICATES PROFILE DETECTION PROBABILITY. DP = OVERALL DETECTION PROBABILITY.....	134
FIGURE 5.13. PROGRAM OUTPUT OF THE MODELLING FOR A 1 M AIR CUBE IN LIMESTONE AT 3 M DEPTH. FROM LEFT, THE TECHNIQUES MODELLED ARE: MAGNETIC, GRAVITY GRADIENT, GRAVITY. FROM THE TOP, THE NOISE LEVELS ARE: BROWNFIELD, TYPICAL, INSTRUMENTAL. THESE VARIABLES CAN BE FOUND IN SECTIONS 4.3.2.4 AND THE SET_PARAMETERS CODE (APPENDIX AV). DP = OVERALL DETECTION PROBABILITY.....	134
FIGURE 5.14. THEORETICAL RESPONSE TO A 1-M CUBE CAVITY AT 3 M DEPTH IN LIMESTONE OVER A 15 M SQUARE GRID BY: A) MAGNETOMETRY, B) GRAVITY, C) GRAVITY GRADIENT AND D) GPR TECHNIQUES. COLOUR SCALE REPRESENTS THE DETECTION PROBABILITY FOR EACH SURVEY LINE. DP = OVERALL DETECTION PROBABILITY.....	136

FIGURE 5.15. PLAN VIEW OF A MODELLED MAGNETIC FIELD CONTOURS OVER A 1 M SIDED AIR CUBE AT 3 M DEPTH IN LIMESTONE. ALTHOUGH DETECTION AT THE LEVEL OF SIGNAL INDICATED BY THE CONTOURS (DOWN TO 0.0005 nT) IS UNACHIEVABLE IN THE FIELD, THE CONTOURS SHOW THE EXPANSE OF EACH LEVEL OF SIGNAL ACROSS THE SITE. THE SHAPE WILL BE SIMILAR FOR HIGHER MAGNITUDE ANOMALIES DEPENDENT ON THE DEPTH, SIZE AND MAKEUP OF THE CAVITY AND CAN BE SCALED UP APPROPRIATELY. SIGNAL LEVELS HIGHLIGHTED IN FIGURE 5.15 ARE LABELLED.	138
FIGURE 5.16. DIFFERENCE BETWEEN THE DETECTION PROBABILITY OF A MAGNETIC SURVEY RUNNING EAST-WEST AND A SURVEY RUNNING NORTH-SOUTH OVER THE CAVITY SHOWN IN FIGURE 5.15. A POSITIVE RESULT INDICATES THE EAST-WEST SURVEY HAS A HIGHER DETECTION PROBABILITY. THE SHAPE AND AMPLITUDE OF THIS GRAPH WILL CHANGE DEPENDANT ON CAVITY TYPE AND SUBSURFACE ENVIRONMENT.	139
FIGURE 5.17. 1-M AIR CUBE, 3 M DEEP IN LIMESTONE, AT TYPICAL NOISE LEVELS MODELLED AT VARIOUS SURVEY SIZES. X AXIS REPRESENTS THE LENGTH OF SIDE OF A SQUARE SURVEY. GPR AND GRAVITY GRADIENT DETECTION PROBABILITY IS ABOVE 99% FOR ALL SURVEY SIZES.	140
FIGURE 5.18. A) DETECTION PROBABILITY DECREASING WITH INCREASED DATA DELETION FOR POTENTIAL TECHNIQUES OVER A 1 M SIDED AIR CUBE AT 3 M DEPTH IN LIMESTONE IN TYPICAL NOISE WITH 2 M PROFILE SPACING. B) VARIANCE OF DETECTION PROBABILITY OVER 100 SIMULATIONS OVER THE SAME CAVITY.	141
FIGURE 5.19. A) (PREVIOUS PAGE) PROGRAM OUTPUT SHOWING HISTOGRAMS OF DETECTION PROBABILITY OVER 100 MONTE CARLO SIMULATIONS FOR THE GRAVITY METHOD OVER A 1-M AIR CUBOID AT 3 M DEPTH IN LIMESTONE AT TYPICAL NOISE LEVELS (AXIS SHOWS FREQUENCY). THE LEFT COLUMN SHOWS 0% DATA DELETION, THE RIGHT 50% DATA DELETION. THE TOP ROW IS AT 1 M PROFILE SPACING, THE MIDDLE 2 M SPACING, AND THE BOTTOM 3 M SPACING. THE BOTTOM PLOT SHOWS THE DATA DELETION TREND AS SPACING IS INCREASED.....	143
FIGURE 5.20. A) HISTOGRAMS OF DETECTION PROBABILITY OVER 100 MONTE CARLO SIMULATIONS FOR THE GPR METHOD OVER A 1-M AIR CUBOID AT 3 M DEPTH IN LIMESTONE AT BROWNFIELD NOISE LEVELS. TOP LEFT AT 0% DATA DELETION, RIGHT 50%. Y-AXIS IS FREQUENCY. B) SHOWS DECREASE IN DETECTION PROBABILITY AS DATA DELETION INCREASES.	144
FIGURE 5.21. SINGLE MAGNETIC SURVEY LINE OVER 1-M AIR CUBE AT 3 M DEPTH IN LIMESTONE, SHOWN WITH VARIATION IN HEIGHT TO REPRESENT SMALL CHANGES WHICH MAY OCCUR IN THE FIELD.	146
FIGURE 5.22: CHANGE IN MINIMUM DETECTABLE CAVITY SIZE WITH DEPTH USING THE MAGNETIC METHOD. BASE CONDITIONS WERE A CUBE VOID (WITH SIDE LENGTH REPRESENTED BY THE X-AXIS ON THE PLOTS) IN LIMESTONE AT INSTRUMENTAL NOISE, 1 M LINE SPACING AND 0% DATA DELETION, DETECTED TO 95% RELIABILITY. ALTERED PARAMETERS WERE: A) GEOLOGY, B) PROFILE LINE SPACING, C) NOISE LEVEL AND D) PROCESSING DATA DELETION PERCENTAGE. CAVITY SIZE WAS INCREASED AT 0.2 M INCREMENTS CAUSING SOME LINEAR GROUPING OF DATA; A LINEAR BEST LINE WAS ADDED ACROSS THE DATA TO FIND THE OVERALL TREND. SUSCEPTIBILITY VALUES AS IN TABLE 4.1	147

FIGURE 5.23. A) THE SMALLEST CUBE DETECTABLE (TO 95% RELIABILITY) IN LIMESTONE AT DEPTHS FROM 0-15 M USING: GPR (GREEN), GRAVITY GRADIENT (BLACK), GRAVITY (RED) AND MAGNETICS (BLUE).	148
FIGURE 6.1. AVERAGE FREQUENCY OF FRACTURES MEASURED IN FOUR BOREHOLES IN CHALK (THIN SOLID LINE) AND CENTRAL BOREHOLE (THICK SOLID LINES) SHOWS THE VARIATION IN NUMBER OF FRACTURES WITH DEPTH (HARTMANN <i>ET AL.</i> , 2007).	157
FIGURE 6.2. RELATIONSHIP BETWEEN LAYER THICKNESS AND JOINT SPACING (NARR & SUPPE, 1991).	160
FIGURE 6.3 SCHEMATIC SHOWING THE SYSTEMATIC CROSS JOINTS (ENGELDER, 2012). JOINTS RUN IN TWO SETS PERPENDICULAR TO ONE ANOTHER. THE MODELLING USES THIS FORM OF FRACTURE SYSTEM.	162
FIGURE 6.4. ORTHOGONAL JOINTS BETWEEN BEDS (HIGHLIGHTED WITH BLUE AND GREEN) SHOWN IN NW ENGLAND CHALK (HARTMANN <i>ET AL.</i> , 2007).	162
FIGURE 6.5. WANG <i>ET AL.</i> , (2012) NUMERICAL SIMULATION OF A CIRCULAR VOID A LATERAL CONFINING PRESSURE OF 7.5 MPa. STAGES A TO F SHOW THE DEVELOPMENT OF THE FRACTURES AROUND THE CAVITY.	163
FIGURE 6.6. MICROCRACK GROWTH AROUND A TUNNEL THOUGH TIME (GOLSHANI <i>ET AL.</i> , 2007). GROWTH INCREASES RAPIDLY BEFORE FAILURE. CRACKS DEVELOP MOSTLY IN THE SIDE WALLS AS VERTICAL STRESS IS LARGER THAN THE HORIZONTAL STRESS.	164
FIGURE 6.7. STRESS CONCENTRATION AROUND A CAVITY (WONG, LIN, TANG, & CHAU, 2002). STRESS CONCENTRATION DECREASES WITH DISTANCE FROM THE CAVITY. THE CIRCULAR CAVITY IS SHOWN; 'R' IS THE DISTANCE FROM THE CAVITY.	164
FIGURE 6.8. A) SCHEMATIC OF THE HALO SYSTEM USED IN THE MODELLING. BLUE REPRESENTS THE HALO AREA, WHITE THE CAVITY AND A FEW EXAMPLE FRACTURES. B ,C) TWO VIEWS OF AN EXAMPLE FRACTURE SYSTEM AROUND A 1 M CUBE CAVITY AT 3 M DEPTH. HALO SPREAD IS TWO TIMES THE CAVITY DIMENSION (2 M), TOTAL FRACTURE PERCENTAGE IS 1% OF HALO AREA, APERTURE IS 10 MM AND FRACTURES ARE ANGLED 3° OFF HORIZONTAL AND PERPENDICULAR TO THE SURFACE.....	166
FIGURE 7.1. MODELLING RESULTS WITH: A) NO HALO, B) HALO AS IN FIGURE 6.8. MAGNETIC DETECTION PROBABILITY: 46.2% (A), 62.3% (B). GRAVITY DETECTION PROBABILITY: 92.9% (A), 98.8% (B). FRACTURE CONFIGURATION.....	169
FIGURE 7.2. THREE EXAMPLE FRACTURE CONFIGURATIONS WITH 0.5% OF THE HALO AREA FILLED WITH FRACTIONS. HALO SPREAD IS 1 M AND APERTURE IS 0.1 M. SYSTEM A: LARGE FRACTURES, B - A MIXTURE OF SMALL AND LARGE FRACTURES, C - MANY SMALL FRACTURES. MODELLING RESULTS ARE SHOWN IN TABLE 7.1.	170
FIGURE 7.3. TWO EXAMPLE FRACTURE CONFIGURATIONS FOR 25% OF THE HALO AREA FILLED WITH FRACTIONS. FROM LEFT (MORE ANGLED FRACTURES) TO RIGHT (CLOSE TO HORIZONTAL AND VERTICAL FRACTURES): MAGNETIC DETECTION PROBABILITY 100%, 100%; MAGNETIC ANOMALY 2.44 nT, 1.75 nT; GRAVITY DETECTION PROBABILITY 89.2%, 87.1%; GRAVITY ANOMALY 0.0269 MG, 0.0200 MG.	170

FIGURE 7.4. MODELLED RESULTS OVER A 1 M CUBE AIR CAVITY AT 2 M DEPTH IN LIMESTONE WITH UP TO 0.1 M APERTURE FRACTURES. A, B) (PREVIOUS PAGE) AVERAGE SIZE OF ANOMALY AS FRACTURE PERCENTAGE IS INCREASED. C) INCREASE IN DETECTION PROBABILITY WITH FRACTURE PERCENTAGE. CROSSES DISPLAY THE AVERAGE PEAK-TO-PEAK ANOMALY OVER 20 FRACTURE SYSTEMS GENERATIONS AND ERROR BARS SHOW THE MAXIMUM AND MINIMUM ANOMALIES RECORDED.....	173
FIGURE 7.5. MODELLED RESULTS OF FRACTURE SYSTEMS AROUND A 1-M AIR CUBE CAVITY BETWEEN 2 M AND 10 M DEPTH. THE FRACTURE PERCENTAGE WAS 1% OF THE HALO AREA, AND THE SPREAD OF FRACTURES WAS 1 M. CROSSES SHOW THE AVERAGE OF 5 ITERATIONS (WITH VARYING FRACTURE CONFIGURATIONS) AND THE BARS INDICATE THE MINIMUM AND MAXIMUM RESULTS FOR THE ITERATIONS. BLUE CROSSES INDICATE THE RESULTS FOR THE SAME CAVITY WITHOUT THE HALO SYSTEM. A) (PREVIOUS PAGE) ANOMALY SIZE FOR GRAVITY MODELLING, B) (PREVIOUS PAGE) ANOMALY SIZE FOR GRAVITY MODELLING, C) DETECTION PROBABILITY FOR GRAVITY TECHNIQUE, D) DETECTION PROBABILITY FOR MAGNETIC TECHNIQUE.	175
FIGURE 7.6. MODELLED RESULTS OF FRACTURE SYSTEMS AROUND A 1-M AIR CUBE CAVITY BETWEEN 2 M AND 10 M DEPTH. THE FRACTURE PERCENTAGE WAS VARIED FROM 0-16% (LEGEND) OF THE HALO AREA, AND THE SPREAD OF FRACTURES WAS 2 M. LEFT – MAGNETIC RESULTS, RIGHT, GRAVITY RESULTS. THE MODELLED ANOMALY DECREASES IN SIZE WITH DEPTH OF CAVITY AS DOES THE IMPACT OF VARIATION IN FRACTURE PERCENTAGE.....	176
FIGURE 7.7. SCHEMATIC SHOWING THE HALO ZONE AND THE HALO SPREAD DISTANCE. CAVITIES ARE RANDOMLY GENERATED AROUND THE CAVITY UNTIL THE CHOSEN FRACTURE PERCENTAGE IS REACHED (EXAMPLES BELOW USE 1% FRACTURE PERCENTAGE).....	177
FIGURE 7.8. CHANGE IN A) (PREVIOUS PAGE) MAGNETIC ANOMALY, B) GRAVITY ANOMALY, C) DETECTION PROBABILITY WITH HALO SPREAD. FRACTURE SYSTEMS ARE AROUND A 1-M AIR CUBE CAVITY WITH FRACTURE PERCENTAGE ALWAYS 1%. CROSSES DISPLAY THE AVERAGE PEAK-TO-PEAK ANOMALY OVER 5 FRACTURE SYSTEMS GENERATIONS AND ERROR BARS SHOW THE MAXIMUM AND MINIMUM RESULTS.....	178
FIGURE 7.9. EFFECT OF CHANGING FRACTURE APERTURE ON A) GRAVITY ANOMALY, B) MAGNETIC ANOMALY. FRACTURE SYSTEMS ARE AROUND A 1-M AIR CUBE CAVITY IN LIMESTONE WITH FRACTURE PERCENTAGE 1% AND HALO SPREAD 1 M.....	180
FIGURE 7.10. INCREASE IN DETECTION PROBABILITY WITH INCREASE IN FRACTURE PERCENTAGE ACROSS A RANGE OF FRACTURE APERTURES (SEE LEGEND) FOR THE A) MAGNETIC TECHNIQUE AND B) GRAVITY TECHNIQUE. THE CHANGE IN FRACTURE APERTURE HAS LITTLE INFLUENCE ON DETECTION PROBABILITY. FRACTURE SYSTEMS ARE AROUND A 1-M AIR CUBE CAVITY IN LIMESTONE WITH FRACTURE PERCENTAGE 1% AND HALO SPREAD 1 M IN TYPICAL NOISE CONDITIONS. NOTE NON-ZERO AXIS START.	181
FIGURE 7.11. VARYING FRACTURE ANGLE AROUND A 1-M AIR CUBE CAVITY IN LIMESTONE WITH FRACTURE PERCENTAGE 1% AND HALO SPREAD 1 M IN TYPICAL NOISE CONDITIONS. A) MAGNETIC ANOMALY, B) GRAVITY ANOMALY (PREVIOUS PAGE), C) DETECTION PROBABILITY (RED CROSSES ARE THE MAGNETIC DETECTION PROBABILITY, BLUE GRAVITY). NOTE NON-ZERO AXIS	

START. CROSSES MARK THE AVERAGE FOR 5 FRACTURE CONFIGURATIONS; BARS MARK THE MAXIMUM AND MINIMUM RESULTS.	183
FIGURE 7.12. VARYING FRACTURE ANGLE AND FRACTURE PERCENTAGE AROUND A 1-M AIR CUBE CAVITY IN LIMESTONE WITH HALO SPREAD 1 M IN TYPICAL NOISE CONDITIONS. ANGLE OF BARS REPRESENTS THE FRACTURE ANGLE; AXIS SHOWS DETECTION PROBABILITY AND LEGEND SHOW FRACTURE PERCENTAGE.	184
FIGURE 7.13. A LATER STAGE OF A NUMERICAL SIMULATION OF CRACK EVOLUTION AROUND A CIRCULAR VOID. SMALL CRACKS ARE SEEN TO DEVELOP AND COALESCE INTO LARGER CRACKS (WANG <i>ET AL.</i> , 2012). B) MICROCRACK CONFIGURATION JUST BEFORE FAILURE SHOWING MORE CRACKS IN THE SIDE WALLS AS VERTICAL STRESS IS LARGER THAN HORIZONTAL STRESS (GOLSHANI <i>ET AL.</i> , 2007). IT SHOULD BE NOTED THAT THESE PATTERNS DEPEND UPON THE ROCK STRENGTH AND CONFINING PRESSURES.	185
FIGURE 7.14. A) SCHEMATIC SHOWING THE CREATION OF STRESS RELATED FRACTURE PATTERNS. INDENTS ARE CALCULATED AS FOLLOWS: $Z = \text{HALO SPREAD} \times \text{INDENT}$, $X = \text{CAVITY SIZE} \times \text{INDENT}$, WHERE INDENT IS USER CHOSEN. B) EXAMPLE MODELLED FRACTURES AROUND A CAVITY (GREY). UNLIKE PREVIOUS MODELS, THESE FRACTURES DON'T NECESSARILY HAVE TO BE JOINED TO THE MAIN CAVITY; THE FRACTURES JUST MUST WITHIN THE STRESS DISTRIBUTION ZONE.	185
FIGURE 7.15. MODELLED AIR TUNNEL: 1-M SQUARE, 5 M LONG, LIMESTONE SURROUNDING MATERIAL.	186
FIGURE 7.16. EXAMPLE MODELLING OUTPUTS SHOWING THE AIR TUNNEL WITH A) (PREVIOUS PAGE) 30% OF HALO SPREAD INDENTATION (0.3 M) AND B) 70% HALO INDENTATION (0.7 M). OTHER INDENTATION PERCENTAGE FIGURES ARE IN APPENDIX F. GREEN SQUARE REPRESENTS THE CAVITY, BLACK LINES ARE THE FRACTURES. COLOUR BAR SHOWS THE DETECTION PROBABILITY.	187
FIGURE 7.17. THE EFFECT OF HALO INDENTATION ON THE GRAVITY ANOMALY SIZE. RESULTS SHOWN ARE MODELLED ABOVE THE AIR TUNNEL IN FIGURE 7.15. CROSSES ARE THE AVERAGE OF ALL 20 FRACTURE CONFIGURATIONS MODELLED AT EACH INDENT PERCENTAGE; BARS ARE THE MINIMUM AND MAXIMUM ANOMALIES FOR ALL CONFIGURATIONS.	187
FIGURE 7.18. MICRO-FRACTURE HALO SYSTEM AROUND A 1-M SQUARE, 5 M LONG AIR TUNNEL IN LIMESTONE AT TYPICAL NOISE LEVEL. FRACTURES ARE RANDOM DIMENSIONS UP TO 1 CM AND THE FRACTURE PERCENTAGE IS 1%. HALO INDENTATION IS 0.7 M.	188
FIGURE 7.19. MICRO-FRACTURE HALO SYSTEM AROUND A 1-M SQUARE, 5 M LONG AIR TUNNEL IN LIMESTONE AT TYPICAL NOISE LEVEL. FRACTURES RANGE FROM 1 M TO 1 CM, DECREASING WITH DISTANCE FROM THE CAVITY. THE FRACTURE PERCENTAGE IS 0.1%, FRACTURE WIDTH 1 CM AND HALO INDENTATION IS 0.7 M. THIS LOW FRACTURE PERCENTAGE IS SHOWN HERE TO HIGHLIGHT THE CHANGE IN FRACTURE LENGTH WITH DISTANCE FROM THE CAVITY. BOTTOM IMAGES SHOW THE MODELLED RESULTS FOR THE GRAVITY (LEFT) AND MAGNETIC (RIGHT) TECHNIQUES. COLOUR BAR REPRESENTS DETECTION PROBABILITY.	189

FIGURE 7.20. THE SAME CAVITY AND FRACTURE CONDITIONS AS FIGURE 7.19 BUT WITH 1% FRACTURE PERCENTAGE SO COMPARISONS CAN BE MADE WITH PREVIOUS RESULTS.....	190
FIGURE 7.21. MODELLED RESULTS COMPARED WITH RULE OF THUMB ESTIMATES. MODELLED SYSTEM IS A 1-M CUBE AIR CAVITY AT 2 M DEPTH IN LIMESTONE WITH UP TO 0.1 M APERTURE FRACTURES. A) MAGNETIC AND B) GRAVITY AVERAGE SIZE OF ANOMALY AS FRACTURE PERCENTAGE IS INCREASED. CROSSES DISPLAY THE AVERAGE PEAK-TO-PEAK ANOMALY OVER 20 FRACTURE SYSTEMS GENERATIONS AND ERROR BARS SHOW THE MAXIMUM AND MINIMUM ANOMALIES RECORDED. THE BLUE DOTTED LINE INDICATES THE ANOMALY SIZE ACCORDING TO THE RULE OF THUMB (INCREASE TO THE SIZE OF A GEOPHYSICAL ANOMALY BY A FACTOR OF TWO OVER THE CAVITY WITH NO HALO).....	192
FIGURE 7.22. COMPARISON OF ANOMALY SIZE AT DEPTH WITH RULES OF THUMB. MODELLED RESULTS OF FRACTURE SYSTEMS AROUND A 1-M AIR CUBE CAVITY BETWEEN 2 M AND 10 M DEPTH. THE FRACTURE PERCENTAGE WAS VARIED FROM 0-16% (LEGEND) OF THE HALO AREA, AND THE SPREAD OF FRACTURES WAS 2 M. A) MAGNETIC RESULTS, B) GRAVITY RESULTS. THE BLUE DOTTED LINE HIGHLIGHTS THE ANOMALY SIZE OF THE CAVITY WITH NO HALO AT 2 M DEPTH. THE SECTION INDICATED BY THE ARROWED LINE IS THE DEPTH THE RULE OF THUMB SUGGESTS THE CAVITY WITH A HALO WILL BE DETECTABLE (1.5-2 TIMES DEEPER THAN THE CAVITY ALONE).	193
FIGURE 7.23. INTERPRETIVE MODELLING OF AN AIR FILLED CAVITY IN COMPARISON WITH THE OBSERVED RESULTS (PÁNISOVÁ & PAŠTEKA, 2009).....	194
FIGURE 7.24. MODELLED RESULTS OF THE CAVITY IN PÁNISOVÁ & PAŠTEKA (2009). DIMENSIONS USED ARE FROM THE PAPER (1.3 M DEPTH, 5.5 M BY 3 M ACROSS, 1.8 M TALL IN SOIL). THE RIGHT IMAGE SHOWS A PROFILE VIEW FOR COMPARISON WITH FIGURE 7.23.....	195
FIGURE 7.25. A) THE ORIGINAL CAVITY DIMENSIONS REDUCED BY 5%. A HALO WITH 2% OF THE HALO SPREAD (1 M) FILLED WITH FRACTURES. THE PERCENTAGE OF FRACTURES REQUIRED WAS FOUND BY MODELLING THE HALO WHILE INCREASING THE FRACTURE PERCENTAGE UNTIL THE GRAVITY ANOMALY REACHED THAT OF THE ORIGINAL SIZED CAVITY. B) THE MODELLED GRAVITY RESULT FOR THE CAVITY AND HALO CONFIGURATION. THE AMPLITUDE AND SHAPE CLOSELY MATCH THAT OF THE ORIGINAL CAVITY ANOMALY (FIGURE 7.24).....	195
FIGURE 8.1. SATELLITE IMAGE OF THE MIDDLESEX HOSPITAL SITE. RED LINE INDICATES LOCATION OF SURVEY (GOOGLE 2011).	199
FIGURE 8.2. GEOPHYSICAL SIGNAL MODELLED OVER PAVEMENT VAULTS WITH THE SAME DIMENSIONS AS AN EXPOSED VAULT AT MIDDLESEX HOSPITAL SITE. DP= OVERALL DETECTION PROBABILITY. A) MAGNETIC, B) GRAVITY, C) GRAVITY GRADIENT AND D) GPR. COLOUR BAR REPRESENTS THE DETECTION PROBABILITY ON EACH SURVEY LINE.	200
FIGURE 8.3. LEFT: PROCESSED SECTION ABOVE TWO PAVEMENT VAULTS (SURVEY LOCATION SHOWN IN FIGURE 8.1) SHOWING THE STRONG REFLECTION FROM THE VAULTS (RED DOTTED LINE). RIGHT: GPR TRACES DIRECTLY ABOVE THE VAULTS. POSITIONS OF TRACES ARE INDICATED BY THE ARROWS ON THE SECTION (TOP TRACE IS LEFT ARROW AND BOTTOM IS RIGHT).....	201

FIGURE 8.4. MAGNITUDE OF SIGNAL ABOVE BOTH PAVEMENT VAULTS COMPARED WITH THE MODELLED RESULTS AND WITH THE MODELLED RESULTS WHEN USING THE GEOPHYSICAL PARAMETERS OF PORTLAND CEMENT. A MUCH CLOSER MATCH IS MADE WHEN USING THE PORTLAND CEMENT PARAMETERS.	202
FIGURE 8.5. ESTIMATED TARGET TUNNEL LOCATION ABOVE THE EXISTING TUNNEL, AND CLOSE TO THE PROPOSED TUNNEL. THE GREEN LINE IS THE LEFT BOREHOLE AND THE RED LINE IS THE RIGHT BOREHOLE IN THE ROOF OF THE EXISTING TUNNEL. NORTH IS INTO THE PAGE. SCALE ON THE LEFT IS IN METERS.	203
FIGURE 8.6. MODELLED RESULTS OF THE ESTIMATED TARGET TUNNEL LOCATION AND DIMENSIONS (13 M FROM THE EXISTING TUNNEL, 4 M WIDE, 5 M HIGH AIR TUNNEL IN GRANITE IN BROWNFIELD NOISE). LEFT: GPR RESULTS, RIGHT: GRAVITY RESULTS. GPR HAS AN OVERALL DETECTION PROBABILITY OF 99% WHILE GRAVITY HAS 68%.	204
FIGURE 8.7. PROCESSED RADAR SECTIONS FROM A) LEFT BOREHOLE AND B) RIGHT BOREHOLE. Y-AXIS SHOWS DISTANCE ALONG THE PROFILE. RED CROSSES INDICATE SUSPECTED REFLECTIONS FROM POINT SOURCES, YELLOW FROM FRACTURES CROSSING THE BOREHOLE, PURPLE FRACTURES WITHIN THE ROCK.	205
FIGURE 8.8. STRONG AMPLITUDES REFLECTORS FROM THE BOREHOLE RADARS OVERLAID ON THE TUNNELS PROFILE. BLUE REFLECTORS ARE FROM THE LEFT BOREHOLE AND RED REFLECTORS ARE FROM THE RIGHT BOREHOLE. THE ANTICIPATED TUNNEL LOCATION IS DRAWN IN BROWN.	206
FIGURE 8.9. MODELLED ROOF OF TUNNEL WITH AIR FRACTURE AND AIR FILLED TARGET TUNNEL IN GRANITE. THE BOREHOLE IS ALONG THE LEFT AXIS. Y-AXIS SHOWS DISTANCE ALONG THE BOREHOLE.	207
FIGURE 8.10. A) MODELLING RESULTS FROM MATGPR R2 (TZANIS, 2006) FOR THE TUNNEL AND FRACTURE SHOWN IN FIGURE 8.9. B) RECORDED GPR RESULTS FOR THE LEFT BOREHOLE RE-SCALED TO MATCH THE MODELLED RESULTS. BLUE BOXES HIGHLIGHT THE SIGNAL FROM THE FRACTURE; RED CURVES HIGHLIGHT THE RESULTS FROM THE TUNNEL. Y-AXIS SHOWS DISTANCE ALONG THE BOREHOLE.	208
FIGURE 8.11. CURRENTLY ACCEPTED WEST WYCOMBE CAVE LAYOUT (NOT TO SCALE).(HELL FIRE CAVES, 2012).	209
FIGURE 8.12. SATELLITE IMAGE OF THE WEST WYCOMBE CAVES SITE (GOOGLE, 2011). LEFT INSET IS INSIDE THE TUNNELS, RIGHT INSET SHOWS THE TUNNEL ENTRANCE.	210
FIGURE 8.13. LOCATION OF THE CAVES BENEATH THE SURFACE (GOOGLE, 2011). WHITE LINE INDICATES THE CAVE ROUTE AND THE RED DOTS ARE THE TOTAL STATION SURVEY LOCATIONS.	211
FIGURE 8.14. ELEVATION OF THE CAVE AND THE SURFACE ABOVE THE CAVE. TOP: LOOKING NORTH, BOTTOM: LOOKING EAST.	212
FIGURE 8.15. MODELLED RESULTS ABOVE THE DESCENDING CAVE (2-M HEIGHT, 1-M WIDTH AIR GALLERY, DESCENDING 13.0 M TO 21.5 M OVER THIS 25 M STRETCH IN CHALK) FOR FOUR GEOPHYSICAL TECHNIQUES: A) MAGNETIC, B) GRAVITY, C) GRAVITY GRADIENT, D) GPR. COLOUR	

SCALE INDICATES SURVEY LINE DETECTION PROBABILITY (%). DP= OVERALL DETECTION PROBABILITY.	213
FIGURE 8.16. TOTAL MAGNETIC FIELD MEASURED OVER THE CAVE. THE INSET SHOWS THE COLOUR SCALE IN NT. THE MEASUREMENTS ARE POSITIONED ON A SATELLITE AND TOPOGRAPHIC IMAGE OF THE AREA WITH THE WHITE LINE REPRESENTING THE SURFACE PROJECTION OF THE CAVE (GOOGLE, 2011).....	215
FIGURE 8.17. MAGNETIC FIELD WITH DIURNAL CHANGE AND LINEAR UPHILL TREND REMOVED. THE LARGE MAGNETIC HIGH ABOVE THE “STEWARDS GATE” IS STILL VISIBLE THE RED SECTION TO THE EAST OF THE SURVEY. THE INSET SHOWS THE COLOUR SCALE IN NT. THE MEASUREMENTS ARE POSITIONED ON A SATELLITE IMAGE OF THE AREA WITH THE WHITE LINE REPRESENTING THE SURFACE PROJECTION OF THE CAVE (GOOGLE 2011).	215
FIGURE 8.18. MOST EASTERLY MAGNETIC SURVEY LINE MEASUREMENTS. THE LARGE ANOMALY AT 30 M IS PROPOSED TO BE METAL INSIDE THE CAVE. THE DECREASE IN MAGNETIC FIELD OVER THE CAVE IS OBSCURED BY THE SCALE USED TO SHOW THE LARGER ANOMALY.	217
FIGURE 8.19. COLLAPSED BOREHOLE AT SITE FOLLOWING AN INVESTIGATION BOREHOLE (PHOTO COURTESY OF RAMBOLL, 2010).	217
FIGURE 8.20. GEOLOGICAL MAP OF SURVEY AREA. THE BROWN UNIT IS A SUPERFICIAL DEPOSIT OF PEAT OF QUATERNARY AGE. THE BLUE UNIT IS A SUPERFICIAL DEPOSIT OF TILL (DEVENSIAN) OF QUATERNARY AGE. THE LIGHT PINK UNIT IS A SUPERFICIAL DEPOSIT OF GLACIOLACUSTRINE DEPOSITS (UNDIFFERENTIATED) (CLAY, SILT AND SAND) OF QUATERNARY AGE. DOTTED BLACK LINES ARE INFERRED COAL SEAMS, AND DASHED, DOTTED LINES ARE INFERRED NORMAL FAULTS (N.E.R.C., 2010). A BROADER GEOLOGICAL MAP CAN BE SEEN IN FIGURE 11.8	218
FIGURE 8.21. MODELLED RESULTS OVER A 2-M SQUARE AND 10-M TALL AIR SHAFT AT 3 M DEPTH IN PEAT. LEFT TO RIGHT: MAGNETIC, GRAVITY AND GPR TECHNIQUES. TOP ROW SHOWS UNCAPPED AND LINED, BOTTOM SHOWS A STEEL LINED AND CAPPED SHAFT. COLOUR BAR SIGNALS THE DETECTION PROBABILITY ON SURVEY LINES.	219
FIGURE 8.22. MAP SHOWING SITE LOCATION (INSET) AND SATELLITE IMAGE (GOOGLE MAPS, 2010) SHOWING THE LOCATION OF SURVEY AREAS. BLUE – MAGNETIC SURVEY, RED – GPR, YELLOW – SEISMIC (USED IN ANOTHER PROJECT).	221
FIGURE 8.23. SATELLITE IMAGE (GOOGLE MAPS, 2010) WITH MAGNETIC RESULTS (DIURNALLY CORRECTED, IN NT). RED LINE – GOALPOSTS, RED DOTTED RECTANGLE – PATH, BLACK DOTTED RECTANGLES – LINEAR ANOMALIES, GREY DOTTED RECTANGLES – DIPOLE ANOMALIES INDICATIVE OF VOIDS.	225
FIGURE 8.24. SATELLITE IMAGE (GOOGLE MAPS, 2010) WITH MAGNETIC RESULTS (DIURNALLY CORRECTED IN NT). RED RECTANGLE – ANOMALY FROM METAL FENCE, WHITE RECTANGLE – LINEAR NEGATIVE ANOMALY, BLACK LINES – GPR SURVEY LINES (STRONG BLACK LINE - SURVEY SHOWN IN FIGURE 8.25, RED CIRCLES – GPR EVIDENCE OF VOIDS. NOTE THE HERRINGBONING ON THE ANOMALY CAUSED BY THE OFFSET OF BI-DIRECTIONAL FIELD PROCEDURE.	226
FIGURE 8.25. GPR SECTION OF LINE SHOWN IN FIGURE 8.24. BLACK LINES INDICATE THE REVERBERATION. BLACK ARROWS POINT OUT SIGNIFICANT STRATA. THE DOUBLE ENDED BLACK	

ARROW INDICATES THE ESTIMATE OF VOID WIDTH. THE BROWN ARROW INDICATES THE REFLECTION FROM THE HOUSE. THE FIRST, STRONG ARRIVAL IS THE DIRECT AIR WAVE.	227
FIGURE 8.26. SATELLITE IMAGE (GOOGLE MAPS, 2010) WITH MAGNETIC RESULTS (DIURNALLY CORRECTED IN nT). STRONG BLACK LINE - SURVEY SHOWN IN FIGURE 8.27. SEE FIGURE 8.24 FOR FURTHER LABELS.	228
FIGURE 8.27. GPR SECTION OF PROFILE SHOWN IN FIGURE 8.26. BLACK LINES INDICATE THE REVERBERATION. BLACK ARROWS POINT OUT SIGNIFICANT STRATA. THE DOUBLE ENDED BLACK ARROW INDICATES THE ESTIMATE OF VOID WIDTH. THE FIRST, STRONG ARRIVAL IS THE DIRECT AIR WAVE.	229
FIGURE 11.1. REGENTS PARK NOISE MEASUREMENTS.	334
FIGURE 11.2. MIDDLESEX NOISE MEASUREMENTS.	334
FIGURE 11.3. UCL QUAD NOISE MEASUREMENTS.	335
FIGURE 11.4. UCL QUAD NOISE MEASUREMENTS.	336
FIGURE 11.5. WEST WYCOMBE NOISE MEASUREMENTS.	337
FIGURE 11.6. DEPTH TO CAVE FROM SURFACE AT SURVEY POINTS. DIGITAL ELEVATION MODELS: GE – GOOGLE EARTH, ASTER - ADVANCED SPACEBORNE THERMAL EMISSION AND REFLECTION RADIOMETER, STRM - SHUTTLE RADAR TOPOGRAPHY MISSION.	349
FIGURE 11.7 GEOLOGICAL AND OS MAPS. TOP: BASEMENT GEOLOGY. MIDDLE: SUPERFICIAL GEOLOGY. BOTTOM: OS MAP.	350
FIGURE 11.8 - GEOLOGICAL MAP OF SURVEY AREA. THE BROWN UNIT IS A SUPERFICIAL DEPOSIT OF PEAT OF QUATERNARY AGE. THE BLUE UNIT IS A SUPERFICIAL DEPOSIT OF TILL (DEVENSIAN) OF QUATERNARY AGE. THE PINK UNIT IS A SUPERFICIAL DEPOSIT OF GLACIOLACUSTRINE DEPOSITS (UNDIFFERENTIATED) (CLAY, SILT AND SAND) OF QUATERNARY AGE. DOTTED BLACK LINES ARE INFERRED COAL SEAMS, AND DASHED, DOTTED LINES ARE INFERRED NORMAL FAULTS (N.E.R.C., 2010).	351
FIGURE 11.9 - MADE GROUND THICKNESS (M)	352
FIGURE 11.10 - DEPTH TO BEDROCK (M)	352
FIGURE 11.11 - DEPTH TO GLACIOMARINE (M)	353
FIGURE 11.12 - APPROXIMATE LOCATIONS OF BOREHOLES, COAL OUTCROPS AND COAL SHAFTS (URS).	356
FIGURE 11.13 – 1859 O.S. MAP. RED BOX INDICATES LOCATION OF COAL PIT.	357
FIGURE 11.14 – 1860 O.S. MAP. RED BOX INDICATES LOCATION OF COAL PIT.	357
FIGURE 11.15 – 1864 O.S. MAP. RED BOX INDICATES LOCATION OF COAL PIT.	358
FIGURE 11.16 – 1898 O.S. MAP. RED BOXES INDICATE SHAFTS. GREEN BOX INDICATES OLD RAILWAY – NOW A PATH.	358
FIGURE 11.17 - 1898 O.S. MAP. ZOOM OF SHAFT AREA.	359
FIGURE 11.18 - 1898 O.S. MAP. ZOOM OF NORTHERN SHAFT AREA.	359
FIGURE 11.19 – 1899 O.S. MAP. RED BOX INDICATE SHAFT AND MINE (HERE NOT LABELLED AS SUCH).	360

FIGURE 11.20 – 1912 O.S. MAP. RED BOXES INDICATE AREAS OF SHAFTS – NO LONGER MARKED ON THESE MAPS INDICATING INACTIVITY. RAILWAY NOW NOTED AS DISMANTLED.....	360
FIGURE 11.21 - 1912 O.S. MAP. ZOOM OF TANK.....	361
FIGURE 11.22 – 1914 O.S. MAP. MINING ACTIVITY NO LONGER NOTED.....	361
FIGURE 11.23 – 1935 O.S. MAP. NO MENTION OF MINING ACTIVITY. RAILWAY LINE NOW PATH.	362
FIGURE 11.24 – 1936 O.S. MAP. NO MENTION OF MINING ACTIVITY.	362
FIGURE 11.25 – 1955 O.S. MAP. NEW CUTTING ACTIVITY.....	363
FIGURE 11.26 - 1955 O.S. MAP. ZOOM OF CUTTING.....	363
FIGURE 11.27 – 1958 O.S. MAP.	364
FIGURE 11.28 – 1967 O.S. MAP.	364
FIGURE 11.29- 1982 O.S. MAP. LANDFILL AREA NOW PLAYING FIELDS.....	365
FIGURE 11.30 - 1993 O.S. MAP.....	365

Chapter 1

1 Introduction

Subsurface cavities are a major engineering concern. Cavities can place restrictions on the location of development, and are a potential hazard during and after construction. The time-scale of the associated hazards varies greatly. Settlement and subsidence can happen slowly over time; changing the topography and density of the subsurface, further complicating the engineering process. Of greater immediate threat is the migration of a void to the surface, resulting in a rapid dropout and potential damage to people and property. The location of these cavities should therefore be a high priority before any construction begins. Unfortunately, natural cavities often have no surface expression, historic mines have long since been filled or covered and mining maps are frequently inaccurate. This leaves a wealth of unmapped or unknown hazards throughout the U.K. With the government drive to redevelop brownfield sites (including old mining areas) the detection of these cavities is of growing importance.

Improved understanding of ground behaviour and advances in geotechnical engineering has increased the possibility of development on sites previously thought to be too complex or dangerous. Key to this understanding is the accurate description of the very

heterogeneous subsurface. The development of karstic or under-mined land is hazardous and can be prohibitively expensive, so opportunities to save money are eagerly sought. Every attempt should be made to detect and image subsurface cavities early in site development to aid foundation design and reduce the risk of danger.

Detection is usually limited to a borehole grid and geophysics is rarely successfully used. This is due to indiscriminate technique choice and inadequate understanding of the limitations of certain methods. Engineers require reliable techniques and it is therefore imperative to outline the spectrum of where and when techniques work or do not. This will result in the correct choice and use of geophysical techniques. Currently cavity detection technique choice is largely heuristic which is only feasible for experienced practitioners. The increased popularity and ease of use of geophysics means less experienced users are designing surveys and may choose inappropriate techniques. Here we show that forward modelling of these techniques in various situations can aid this decision, improve survey design, increase survey success and consequently improve the reputation of geophysics in the engineering industry.

In near surface geophysics, including cavity detection, field work is very rarely preceded by forward modelling of the site environment. This leads to incorrect choice of technique and failure to detect a target, both in the academic literature, and within industry.

It is imperative that a geophysical survey is designed relevant to the specific site and target and with the ability and judgement to rule out some, and possibly all, techniques and highlights the uses and limitations of geophysics.

Here, we investigate the geophysical signature of various cavity targets by introducing modelling software which computes the theoretical signal of a range of techniques. The likelihood of their detection is assessed in typical subsurface and noise conditions. This allows comparison and prediction of the suitability of a range of techniques in any site specific conditions. Modelling provides a more quantified approach than rules of thumb, removes guesswork in technique choice and highlights the uses, and limitations of geophysics.

The resulting software will allow more discriminate choice of technique and easier understanding of the limitations and uses of geophysics. The modelling and calculation of detection probability will aid survey design. Different survey parameters can be modelled to find the optimum survey design for a given environment. This is a much more effective and efficient way to design a survey than relying on default profile and survey position spacing.

1.1 Aim and Objectives

The overall aim of this research is to develop geophysical modelling software that will: 1) assess the feasibility of using geophysics to detect cavities in the near surface, and 2) inform any subsequent geophysical survey design. To achieve these aims the following objectives must be met:

1. Understand cavity processes and the likely subsurface conditions related to cavities. Review current approaches to cavity detection, including geophysical approaches, assessing their benefits and limitations.
2. Develop modelling software that can simulate geophysical signal over cavities
3. Build in functions to allow the calculation of cavity detection probability for comparison between techniques, and to inform survey design
4. Expand the investigation of cavities to include the area surrounding the cavities, the halo, and assess the impact on geophysical signal and detection probability
5. Evaluate the modelling technique by using the approach on real world cavity detection scenarios.

1.2 Thesis Organisation

Chapter 2 contains the Literature Review and so fulfils objective 1. This first part of this Chapter will cover our current understanding of cavities and why their detection is of such importance. This detail will give an overview of the problem but will also inform the modelling design. The second section will review current cavity detection techniques (including geophysical methods) and the limitations associated and how geophysical modelling could fit into the current process

Chapter 3, the methodological framework, introduces the modelling approach informed by the literature review. This Chapter will highlight the need for this modelling software as well as an overview of the methodology of fulfilling the objectives.

Chapter 4 starts with a review of the relevant geophysical modelling approaches (and so satisfies some of objective 1) and continues to detail the modelling approach. The software is introduced and the functionality explored (objective 2). The core part of this Chapter is the analysis and process of calculating the probability of detection of a signal in noise and hence the meeting of objective 3.

In Chapter 5, the cavity modelling software is explored and tested by varying the range of input parameters and assessing their effect on the geophysical signal and detection probability. This Chapter will practically demonstrate how the software can aid technique choice and inform survey design through numerous simulations (objective 3)

The next two Chapters (6 and 7) are concerned with the halo effect (the collection of fractures surrounding a cavity). Chapter 6 explores the halo through a literature review providing key parameters required in the modelling of the halo. This Chapter also introduces the halo modelling approach (objective 4). Chapter 7 models the halo and analyses the effect on the detection probability results.

Chapter 8 fulfils the final objective by using the modelling approach to choose the geophysical technique and survey parameters on four field sites. Data collected on the sites is also presented and used to review the effectiveness of the software.

The final Chapter summarises key findings and contributions of the Thesis. It includes discussion on the limitations of the modelling approach presented and the potential future progression of this research.

1.3 Applications

As an Engineering Doctorate project, this work must have practical application within the relevant industry. Here, the most obvious application is in the engineering industry. Engineers will use the software to assess whether geophysics is suitable for cavity detection on a particular site. The software can calculate the limits of detection in a given environment showing the user the depth of penetration of the techniques and the size of cavities that can be detected.

Near surface geophysicists will be able to use the software to assess the theoretical feasibility of techniques. They will be able to compare techniques to find the most suitable and calculate the most efficient survey parameters. As the program is extended by users and within this project it will gain a wider breadth of use. The modelled results can also be used to compare with field measurements to assist interpretation.

The program can be used in education to provide students experience of the shapes and sizes of anomalies associated with cavities. The lack of field experience is a limitation to education in geophysics due to time and money constraints. Though modelling does not replace field experience, it can provide some understanding of what results may look like and the techniques and survey parameters needed to achieve such results. The students can change parameters and environments easily and immediately see the change in geophysical signal.

Modelling offers the opportunity to test geophysical techniques in a range of environments without the expense of entering the field. This means survey parameters, cavity type, and environment can all be altered with ease at no expense and without the difficulties in finding an appropriate site. By modelling these variables concurrently the feasibility of detection can be calculated in conditions relevant to any given environment.

Chapter 2

2 Literature Review

Cavity detection remains an important but challenging aspect of near surface geophysics. Although cavity delineation has long been studied in the geophysics academic and industrial communities it is becoming a more pressing issue with the increased use land above brownfield sites and karstic environments to accommodate a growing population. In this chapter a review of the hazards associated with this type of development, along with other applications of cavity detection, are outlined. A detailed study of the cavity types associated with these hazards follows as well as a detailed review of current cavity detection techniques and the geophysical techniques relevant to cavity detection.

2.1 Cavity hazards

The primary rationale for detecting cavities is to alleviate the concern of hazards. Cavities must be mapped before any construction begins as they affect subsurface stresses and hence foundation design. The location of voids is expensive, difficult, and time consuming but the threat they present is of far greater concern. If the engineering industry

is to adopt a standard geophysical survey for cavity detection, the important reasons for their detection must be emphasised. There are three major categories of potential hazards.

2.1.1 Cavity collapse

Inherent to areas of subsurface cavities is the risk of ground collapse. In karstic environments, and in mining regions, once stable systems can erode through a variety of mechanisms to weaken roofs or walls causing collapse over years or a matter of hours. The dangers were dramatically shown with the recent collapse of a huge sinkhole in Guatemala City (Walker, 2010), swallowing an entire intersection.

The potential hazard of full or differential collapse or settlement into cavities is dependent on the proximity of buildings, services, infrastructure or people. In the UK, historic mines are often located in areas that are now very urban, significantly increasing the risk. Subsidence above rock salt mines in Northwich was so common that houses were built on jacks allowing re-leveling after subsidence (Branston & Styles, 2003). In Pennsylvania, where some 1,000,000 houses are positioned above mines (Pennsylvania Department of Environmental Protection, 2010), residents routinely take out “Mine Subsidence Insurance”. However, only 56,000 of these properties are covered for catastrophic damage (Hopey, 2008) indicating ignorance of the significant associated risks. The Ohio Mine Subsidence Insurance Underwriting Association has estimated \$1,189,000 of mining subsidence damage between 1987 and 2006.(Clarke *et al.*, 2006).

Even if in a shaft is in equilibrium subsidence may be induced by groundwater movement, vibration, ground movement, increase of surface loading. The risk is especially high when mining continues in the area and heavy vehicles are used on the site – Styles *et al.* (2006) noted several collapses in the area of Kalgoorlie Consolidated Gold Mines, Australia. Mining shafts permit water flow which affects the stability of mine galleries (Rodriguez Castillo & Reyes Gutierrez, 1992) increasing collapse potential. Collapse is especially prevalent in the growing economies that rely heavily on money from mining. In developing countries, mines that have been abandoned because they are no longer economically viable or are too dangerous, are often re-mined by local people. This illegal mining is done outside of safety regulations increasing the danger of collapse or mine breach. In Ghana 15 miners were killed in an illegal collapsed gold mine in 2009 (B.B.C., 2009b).

The risk of road collapse is also of serious concern. Numerous recent examples in the U.K. have thankfully yielded no personal injuries but have caused significant infrastructure damage (the collapse of a medieval chalk mine on the A2 road, Blackheath, London in 2002 (Figure 2.1 and Styles *et al.*, 2006), and a main road in Manchester due to a burst pipe (B.B.C., 2009a)). The East Coast rail line in Scotland had to be rerouted after mine collapse

costing £56 million between 1988 and 2001 (Clarke *et al.*, 2006). In Ohio in 1995 a 3.5 m sinkhole opening over an abandoned coal mine on a busy interstate causing the closure of the road for 3.5 months (Hammack, 2004).

Similarly, there are high risk environments over karstic subsurface, leading to building collapses across the U.K. (T. Waltham, Bell, & Culshaw, 2004) and worldwide (e.g., the City of Beni-Mellal, Morocco (Filahi *et al.*, 2008)). A sinkhole opening on a highway in Maryland in 1993 killed a driver whose car entered the sinkhole (Hammack, 2004). All of these hazards can present themselves on construction sites and so pre-emptive cavity detection is preferable.



Figure 2.1. Hazards associated with cavities. From left: Previously unknown Blackheath medieval chalk mine collapse (British Geological Society, 2010); Rescue from breach of previously unknown mine in Xiangning, China (Branigan, 2010); Contamination of water flowing through mine, (United States Geological Survey, 2006).

2.1.2 Contamination

Cavities, especially in karstic environments, create conduits for the rapid flow of fluids. This can serve to accelerate the flow of contaminants from the surface ; especially hazardous in proximity to sources of radioactive material (geophysics was used to map voids near the Y-12 nuclear plant in Oak Ridge, USA (Doll *et al.*, 1998)). Flow through cavities also avoids natural filtration through the subsurface. Cavities within waste lagoons can allow leaking of hazardous waste (Wadhwa, Ghosh, Chaudhari, Chandrashekar, & Sinharay, 2008). The unpredictable formation of cavities means the path of flow is similarly unpredictable, favouring geophysics to interpretation between boreholes.

Groundwater flow through mines will be contaminated by any residual materials, and consequently pollute water supplies and threaten human and wildlife health. Extensive mining in Wales has contributed to 108 km of waterways failing to meet water quality objectives (Johnston, 2004). The mapping of unknown mines in water catchment areas will help prevent this level of contamination.

2.1.3 Mine flooding

A major hazard in mining is the breach of the mine-face into an unknown, abandoned mine. Should this mine be filled with water the inrush of water can be catastrophic. China's massive scale mining industry has suffered major flooding disasters in recent years: twice in 2005, in 2006, 2007 (Yanrong, 2009) and 2010 when 38 miners confirmed dead after an old shaft was breached in Wangjialing coal mine, Shanxi Province, China, (Global Times, 2010). In total, 122 flooding incidences have been recorded in China in the past 30 years (Yang, 2007). Two recent, large US events have highlighted the dangers: Quecreek (2002), where a flooded mine was breached and approximately 250 million gallons of mine waste water and slurry was released trapping 9 miners for 77 hours; and Inez (2000) where breached slurry flooded rivers and streams - disrupting local water supply and causing environmental damage (Gochioco, 2003). There were approximately 100 breaches in the U.S. alone between 1995 and 2002 (Gardner & Wu, 2005) and with 500,000 abandoned mines in the U.S. (MSHA, 2001) and 30,000 unmapped in the U.K. (Littlejohn, 1979) the problem is still very present. Accurate mapping of historic mines could help prevent further breach accidents.

2.2 Land use and engineering

With population rising and land a finite resource, the redevelopment of brownfield sites in the UK is a growing necessity. Brownfield is defined as previously developed land that is now vacant, derelict, or with known potential for redevelopment. Government statistics collected in 2008 show 63,750 ha (approximately 0.49%) of England is classified as brownfield (Homes and Community Agency, 2010). The government predicts that 3.8 million houses will be needed by 2021 (King *et al.*, 2000) and plans to continue building at least 60% of houses on brownfield sites (in 2008 79% of new housing was built on brownfield, an increase from 56% in 1997 (Barclay, 2010)).

The development of such land requires continuous investigation of the subsurface integrity and stability, and the risk assessment of subsidence or collapse. Karstic and mining environments can hence restrict development as they present an on-site safety concern, and lateral variation of subsurface bearing strengths complicates foundation design. Cavities remain a concern well into the lifespan of a development as void migration, or subsurface collapse, may damage structures and services. Also, clay filled cavities may jam boring machines used in site investigation and construction. The mapping of these features is therefore of great significance to design and construction.

Potentially, near surface cavities of sufficient size could feasibly be used to bury Intermediate Level radioactive waste (ILW) (including chemical sludge, resins and material from decommissioned reactors). Short lived ILW contains radioactivity that may require

shielding by concrete or bitumen. Cavity volume and shape, found using geophysical techniques, could be used to inform the amount and location of shielding required.

Cavities must be considered when mining in carbonate environments. Increased water flow into tunnels and alteration of the permeability and flow through tunnel face can be hazardous and slow tunnelling. Currently probes check the conditions ahead of the face and water can be drained. Geophysics can work in tandem to check the face conditions. Cavities beneath a tunnel may cause non-uniform settling, these need to be detected.

Cavities in purpose built waterways, such as canals, can lead to expensive loss of water and threaten the integrity of structure (Wadhwa *et al.*, 2008). Water can also flow into quarries through solution cavities causing pumping costs of \$5000 per month (Hammack, 2004), mapping cavities can help blocking these leaks.

2.3 Social and biological interest

Besides hazards and in construction, subsurface cavities are of social interest to various parties. Tunnels are used in illegal smuggling activities and cavities in military storage and underground facilities. Buried contraband or victims will often be housed in an object detectable as a cavity. Forensic geophysics is a relatively modern application used to detect bodies (notably in the Fred West case in the 1990s (Fenning & Donnelly, 2004) and more recently the Pentagon's plans to detect Iran's nuclear facilities (Hambling, 2010)). Archeologically, burial sites (Edwards, Okita, & Goodman, 2000) and historic mines (Bates & Duff, 2006) offer an insight in past rituals and a record of human development.

Cavities created by animals are of interest to zoologists. The mapping of burrows of subterranean animals can provide interesting information and by using geophysics the structure of the burrow will not have to be disturbed (e.g. Tortoise burrows in Kinlaw *et al.*, 2007). Habitats can also cause structural problems, as is the case with termite nests in levees in China and the U.S. (X. Yang, Henderson, Mao, & Evans, 2009), creating leaks, weaknesses and possible collapses.

2.4 Cavity location

Cavities are widely spread across the U.K. (Figure 2.2). They can be generally classified into two categories: manmade and natural. The majority of manmade mines are coal mines due to its availability and use as a fuel. Coal mining has left an estimated 1,000 million m³ of voids in the U.K. alone (Norton, 1996). However, lead, copper, iron, tin, and slate mines were once prevalent. It is estimated, for example, that there are between 50,000 and 100,000 lead mines in the U.K. (Healy & Head, 1984). Natural mines in the UK usually form by

dissolution of carbonate rock such as limestone, dolomite and chalk but can also form in weaker material such as salt or, more rarely, in resistive materials.

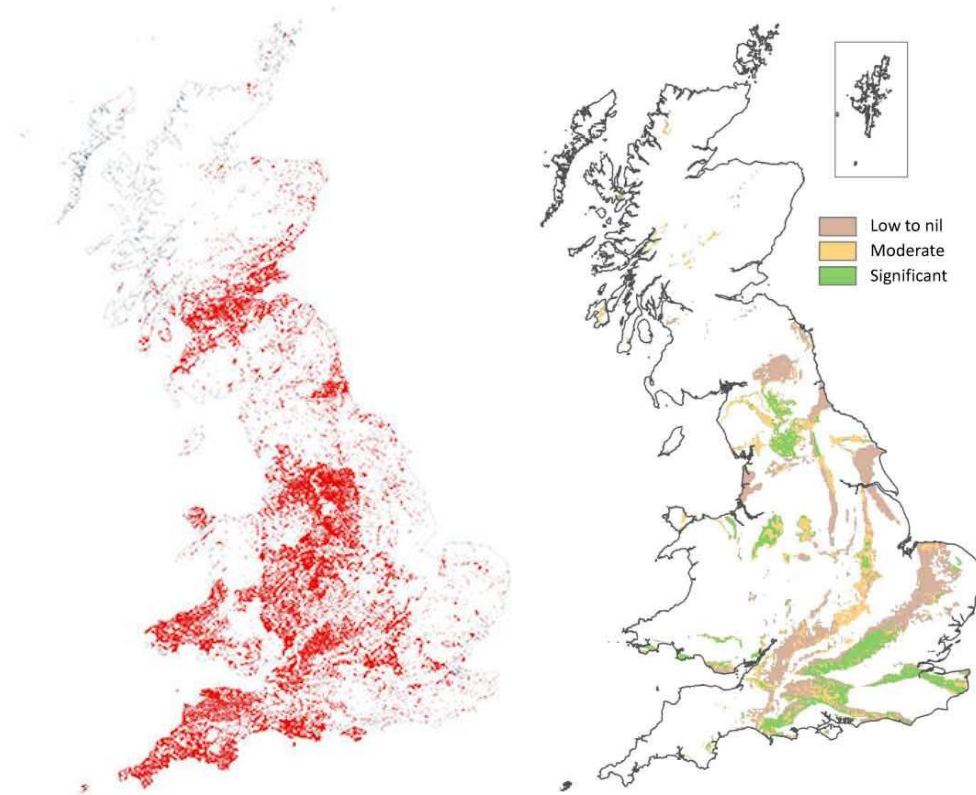


Figure 2.2. Potential cavity locations in Great Britain. Left: Active and ceased mine works compiled by the Directory of Mines and Quarries (British Geological Survey, 2010b). Right: Potential for dissolution to be a hazard (British Geological Society, 2011).

Though the general spread of likely cavity locations is known (Figure 2.2), cavities are not all accurately mapped. Since 1872, the Coal Mines Regulation Act has required that all areas of mining activity be mapped. Despite this, the extensive mining of coalfields before the Regulation Act means that an estimated 30,000 of 100,000 mine workings in the U.K. remain unmapped (Littlejohn, 1979). Of mines that are mapped, the accuracy of old mining maps is questionable. Projections changes through time mean the mine locations become less reliable and the same shaft can be mistakenly mapped more than once. Over 12,000 natural cavities exist in chalk (and 3,500 chalk mines) in the U.K. but most natural cavities remain unrecorded (Edmonds 2008). Across the globe the practice of illegal, unlicensed mining and hence unmapped is still prevalent; it is estimated that 65,000 unlicensed mines in China were shut down between 2005 and 2008 (Ali, 2008). Therefore, there are a large number of unmapped and potentially hazardous mines. Before any development of potentially hazardous sites can begin such cavities must be detected and delineated.

2.5 Cavity formation and typical shapes

One of the major difficulties in using geophysical techniques to detect voids is the variety in shape, size, make-up and depth; the factors which also control the possibility of hazard occurring. To understand which technique, or group of techniques, to employ, we must first understand their creation. It is of utmost importance to understand the target before planning the approach to utilise. To find typical cavity parameters, a comprehensive review of typical cavity shapes and their formation is presented. The parameters of typical cavity shapes are researched to inform our models and form the basis of our initial tests to determine optimum survey parameters and technique choice.

Generally speaking a cavity is a hole in the subsurface with contrasting properties to the surrounding strata but there is a wide variety of structures in both mining and natural cavities. The depth of interest of most geotechnical investigations is less than 15 m (Roth *et al.*, 2002). More specifically, depth of proof required is also dependent upon area and building type, from 1.5 m for a light bridge caissons in North Carolina to 5 m required for pile tips cavernous karst in Florida, (Waltham & Fookes, 2003). As we aim to cover to the depth that may affect the design, cavities within this region were researched.

2.5.1 Man-made cavities

Manmade cavities are intrinsically related to brownfield sites and their remediation is vital to the development of these areas. Mined materials in the U.K. include coal (long used as a cheap and efficient energy source in Britain), metal ores, minerals, evaporates (salt), aggregates and precious metals. Initially only surface outcrops were mined but as resources became scarcer and demand greater, miners were forced to dig into the subsurface. Old mine workings are expected in areas near a mineral outcrop if superficial deposits are suitably shallow.

Until the 18th century mines were rarely deeper than 60 m (Healy & Head, 1984; Figure 2.3) and shallow, abandoned mine workings have been found in New Jersey just 2-3 m below surface (Ghatge, 1993) and beneath heavily urbanised areas of Mexico City where mining has left cavities 5-8 m deep, and main chambers 2-30 m deep (Chavez Segura *et al.*, 2011).

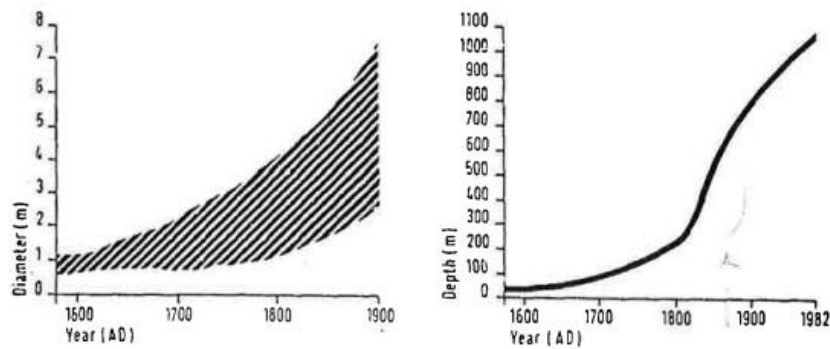


Figure 2.3. Shaft diameter (left) and depth (right) increases through time (Ove Arup and Partners, 1976).

2.5.1.1 Bell pit

Bell pits were first used the 13th century (Healy & Head, 1984) and are predominantly found in areas of thin superficial deposit where the dip of the seam is low (Healy & Head, 1984). Mining continued radially from the shaft until the artificial or natural support was not sufficient, ventilation was too poor, or ground water inflow exceeded bailing (Healy & Head, 1984). Once ceased, a new shaft was sunk a sufficient distance from the old shaft (sometimes as close as 5 m apart (Healy & Head, 1984)). Bell pits may follow the outcrop of a seam, noticeable by cones of mine waste or depressions near outcrops, with depth increasing further from the outcrop. The spoil from the new pit was used to fill the previous pit. They are not always backfilled solidly, so will collapse or have a low bearing capacity – either way of interest to site investigation. The shaft diameter is usually around 1 m and pit diameter was 8-20 m (Littlejohn, 1979). Depth is seam dependent but rarely over 12 m (Clarke *et al.*, 2006).

2.5.1.2 Shafts

To enable further extraction from the seam, miners dug deep shafts with diameters increasing from 2 m in 1600 up to 8 m in modern times (Culshaw & Waltham, 1987). In the 18th Century water pumps allowed deeper mines to be dug (Figure 2.3). Circular shaped shafts were popular in England while other regions (especially Scotland) preferred square and rectangular shapes (Healy & Head, 1984). From 1852 more than 2 shafts were required by legislation either close together or at the ends of the mine to avoid accident; before this only a single shaft was used (Healy & Head, 1984). From 1872 shafts were required to be at least 3 m apart, increased to 13.6 m in 1887 but by the end of 19th Century fewer shafts were dug as underground transport improved.

2.5.1.3 Deeper mining techniques

Pillar and stall mining first evolved in the 15th and 16th century, using a high density of shafts instead of digging long roadways. Pillar stall mines can be accessed through a shaft or adit with pillars left for support. They are still used today in limestone, ironstone and gypsum mining. Pillars may be robbed (the removal of material from the pillars at the end of mining when structural integrity is perceived to be of less import) on the way out of the mine. Pillars may settle into the mine floor, or weather and collapse, causing unpredictable subsidence localised to a few pillar collapses. Often the stalls would fail as upward stoping (sometimes 100s of m) of the roof caused collapse (Piggott & Eynon, 1978). Precise pillar location and condition was usually unmapped and maps would not account for any robbing.

Drift mining is used when the seam dip is shallow and the outcrop is near to the surface. It is used now instead of shafts, digging at approximately 15° until the seam is reached.

Since 18th century since then longwall mining has been the predominant method. Coal is mined from longwall with roadway away at right angles. Roadways are supported by timber, stone, steel supports. The process involved the deliberate collapse of the mining face after the extraction. The material above would subside and the cavities may be filled upon completion. This left a surface with uneven strain and a large potential sinkhole hazard. Subsidence may occur up to 2 years after mining (Healy & Head, 1984).

2.5.1.4 Fill and lining

Since the 17th century mines have been lined. The material used depends on the ground material, materials available and when the shaft was dug. Wood was the first to be used, followed by bricks and stone, metal from the 18th Century and concrete was used from 1890s (Culshaw & Waltham, 1987) – each a very different geophysical target. In competent rock lining may not be required. Three types of lining exist: open – horizontal timber or steel frames to stop large rock falls down shaft; closed – boards or wall to stop all falls; and sealed – to prevent water inflow (concrete, steel etc.). If the lining collapses, or is purposefully removed, the surrounding strata may fall into the shaft creating a crown larger in diameter than the shaft. If in equilibrium, a shaft may subside from groundwater movement, vibration, ground movement, or increased surface loading.

Capping material, when used, is also dependent on local resources and materials available but can include brick, slate, steel rimmed or wood (Roe, 2008). Before 1945 caps were often poor standard (Pringle *et al.*, 2008). Plugs (a tree, pit tubs or scaffold) were sometimes placed close to the surface, with fill on top. The plug would eventually degrade, leading to collapse.

Empty shafts are rare (Healy & Head, 1984) but shafts were not always backfilled solidly, so may collapse or have a low bearing capacity – either of interest to a site investigation. It is unlikely for a deep shaft to have been completely filled, more likely just the top of the shaft is filled (Culshaw & Waltham, 1987). Also fill can often migrate to the roadways, creating air cavities in the shaft. Compression of fill in the field is impractical so fill is only consolidated under its own weight which is limited by lining friction and arching (Healy & Head, 1984). Composition varies but generally involves mineral waste or superficial material collapsed into the shaft (including deteriorated lining) and may contain building debris (rope, ash, iron, tubs, and equipment); all potentially hazardous, especially if the material is easily eroded. Before 1945 the fill material used was unregulated (Pringle *et al.*, 2008).

The fill material is of great importance to the choice of technique: an unfilled shaft will be a good gravity target, but metal debris or burnt shale fill will be an excellent magnetic target (providing the made ground across the site does not contain similar levels of metal). Shaft fill can migrate to the roadways, leading to cavities throughout the shaft. Shafts permit water flow which can affect the stability of mine galleries (e.g. Rodriguez Castillo & Reyes Gutierrez (1992)) and also create an excellent electromagnetic target. Cavities filled with rubble (either from collapse or by fill from local rock) will produce a gradual loss of energy or signal from remote techniques; not the strong return that we would expect from a perfect void. If the fill is sufficiently similar in geophysical parameters to the surrounding strata mine cavities may even behave as a continuous rock and go undetected. Voids, migrated above the rubble by stoping, far above the mine itself, may be easily detected but give a false impression of the size of the mine. Initially, mines seem a good geophysical target, with strongly contrasting properties and distinct boundaries, but collapse and filling will cloud this definition. We must therefore consider how the mines may have changed since mine maps were drawn in order to assess the likelihood of detection.

As the cap, lining, and fill are of importance when choosing which geophysical technique will have the highest likelihood of detecting the shaft present, the clarification of the mining type and materials in the area is of great importance to the modelling and consequent survey success (Table 2.1).

Table 2.1. Location and details of mining of the most commonly mined materials.

Material	Location and mining details
Iron	Open cast in Northamptonshire, Lincolnshire, and Cleveland Hills. Also pillar and stall. Mostly well documented.
Lead, Zinc, Tin	North Pennine, North Wales, The Peaks and Lakes. Tin copper in Cornwall. Mining is localised so subsidence unlikely. Shallow copper has caused subsidence in Cornwall.
Gypsum, anhydrite	Cumbria, Staffordshire, Leicestershire, Derbyshire, Teeside. Deep, pillar stall mining.
Limestone	Usually at outcrops but may subside if mined and then weathered (Figure 2.6).
Chalk or flint	Underlies many urban areas especially in the Home Counties. Bell pits up to 30 m deep with chambers running off (2-8 m wide, 2-12 m high, up to 20 m long). Migration can create crown holes (Figure 2.6). Could be caused by the changing of draining regime by development. Most are unrecorded but 12,000 natural cavities on chalk, 3500 chalk mines are mapped (Edmonds, 2008). Mines are associated with urban areas e.g. Norwich. May not form under clay where percolation is prevented.
Sandstone	Scotland, Manchester, West Yorkshire. Roofs can spall leading to possible crown holes.
Salt brining	Cheshire, Yorkshire, Lancashire, Shropshire. Bands up to 30 m in two levels, pumping caused erratic subsidence. Subsidence may occur 30-60 m from pump.
Coal	Present across much of the UK. If good quality coal is present it can be assumed the area has been mined, but maybe unsystematically.

2.5.1.5 Non mining cavities

Outside of mining, other manmade cavities are found often in industrialised areas including: service, road and canal tunnels, sewers, pipes (water, utilities), basements of demolished buildings (especially from 19th century when cities rapidly expanded (Culshaw & Waltham, 1987)), graves and burial mounds, wells, vaults, concrete bubbles, and ungrouted masonry cells. Some of these cavities will be well mapped but may be in unknown states of decay and collapse depending on age and construction quality.

2.5.2 Natural

Natural cavities exist natively in many types of rock by dissolution of widespread soluble bedrock. Cavities in limestone are most common because karstic environments are so prevalent; 20% of the Earth's near surface has solution susceptible rock (D. Butler, 2008).

Figure 2.4 shows the distribution of karstic environments in Great Britain and Figure 2.5 the distribution across the world.

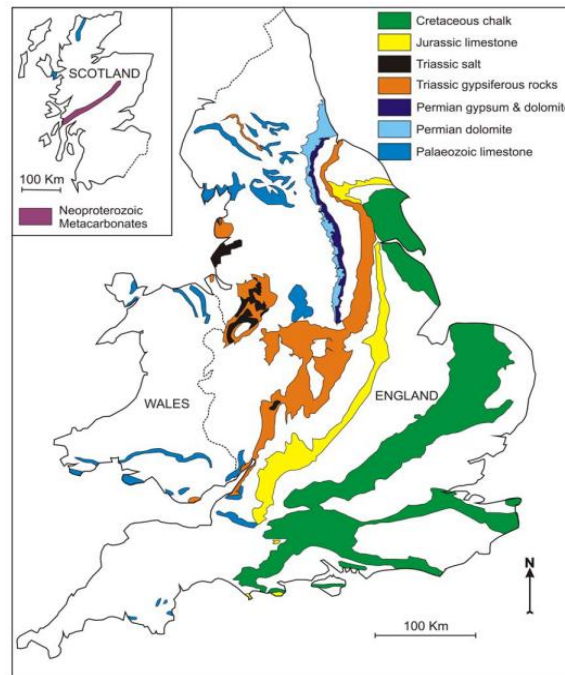


Figure 2.4. Distribution of soluble (karstic) rocks in Great Britain (British Geological Survey, 2010a)

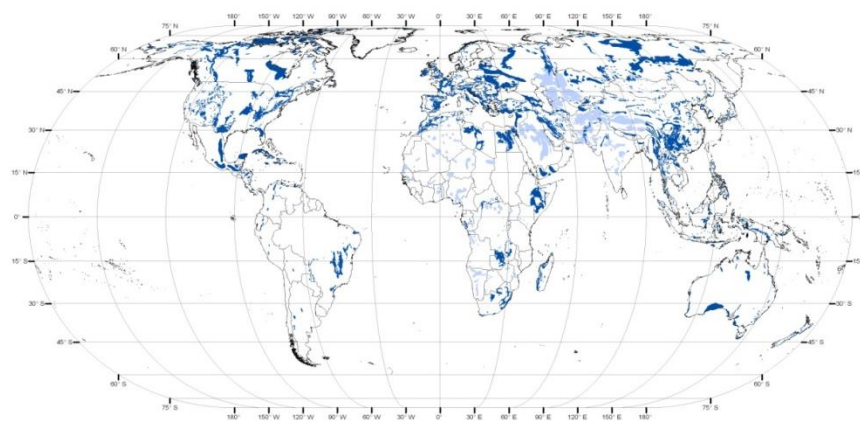


Figure 2.5. World map of carbonate rock outcrops (School of Environment, University Of Auckland, 2010 based on data from Ford & Williams, 2007)

Rock strength dictates the size of the cavity leading to a wide variety in structure. Weaker rocks (less than 30-100 MPa) do not have the strength to support large distance spans and collapse easily so cavities are smaller: weak chalk (rarely more than 10 m deep and 20 m diameter (Culshaw & Waltham, 1987)), gypsum or porous limestone. Cavities develop

best in strong, competent and fractured rocks (Waltham & Fookes, 2003): large karstic environments in dolomite, marble and more compact limestone (Culshaw and Waltham, 1987). Salt is rapidly dissolved so cavities act differently to those in limestone and gypsum. Sinkholes indicate a cavity or karstic feature at greater depth and can range from 0.5 to 500 meters in depth and radius, however, in Britain cavities are usually less than 10 m in diameter (Culshaw and Waltham 1987). Cavities will be water filled if below the water table (Pueyo-Anchuela *et al*, 2010) or air or sediment filled if above (Waltham & Fookes, 2003).

The formation, shape and size of such cavities are dependent on a number of factors: location, local drainage, topography, and fractures. Underground drainage and rainfall will cause the dissolution of soluble rocks to create cavities, caves or sinkholes meaning cavities are common at springs and along geological flow-paths. Dissolution rate of calcium carbonate depends upon the presence of biogenic carbon dioxide, especially prevalent in tropical and deep soil where decomposition of organic matter is fast, and the speed of water recharge (Waltham & Fookes, 2003). Therefore wet, tropical conditions are most likely to create large caves; in southwest China the karst area is 430,000 km², and the population living above is over 100,000,000 (Zhang *et al*, 2001) apud (Xu *et al*, 2009). Dissolution is a slow process, just a few mm per 100 years for walls and ceilings (Waltham & Fookes, 2003), but possibly faster in fissures with rapid water flow. Dissolution in gypsum is faster, potentially 1 m over 100 years.

Providing the rock is not very weak or loading very great, a solid roof of 10 m depth should be safe (Culshaw & Waltham, 1987). However, threat to engineering if width is greater than the roof cover (not including soil and fractured cover) (Waltham & Fookes, 2003). Natural cavities can be connected along the same flow path. Caves are abandoned if water finds preferred flow path or they are filled with sediment, stalagmites or collapse material (leaving large breccia).

2.5.2.1 Migrating cavity

Although solution cavities form slowly and their collapse is considered a rare occurrence (Fehdi *et al*, 2010), a more common hazard is the formation of cavities in soil cover over eroded bedrock (Figure 2.6). Subsidence cavities are formed as cover material enters the rock following dissolution at exposed outcrops, the rock head, or within fractures of the rock by downward percolation of water. The speed of enlargement is dependent on flow rate and water aggressiveness (degree of chemical under-saturation). If the cover material is cohesive enough a bridge may form creating a cavity, while weaker rocks will gradually subside into the cavity (slow subsidence- Figure 2.7). If the migration (through stoping) reaches the surface the collapse is termed a dropout failure (Waltham & Fookes, 2003). In a subsidence

pipe, 8.6% will be the void space migrating to the surface over geological time, beneath which lie loose, deep columns of infilling deposits (Edmonds, 2008). If a dropout failure does occur, the sinkhole can be infilled with available nearby material, altering the geophysical target (Mochales *et al.*, 2007). Near the surface the corrosive soil water causes rapid dissolution. Formation usually occurs where cover is less than 20 m and the water table is in decline (Culshaw & Waltham, 1987) and often there is no surface expression prior to collapse. When sinkholes do occur they may indicate further cavities at depth (Batayneh *et al.*, 2002).

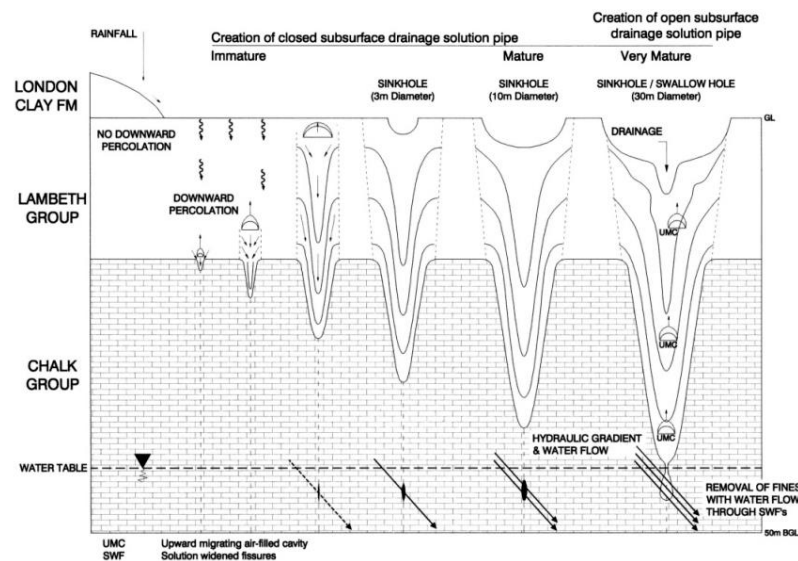


Figure 2.6. Development of cavities in chalk over geological time (Edmonds, 2008). A buried solution sinkhole is created and increased by water flow (this can be natural or manmade e.g. a broken pipe or quarry dewatering changing the water table). A void will form in the overburden and will migrate upwards with erosion leaving infill beneath. Migration will cease if there is a competent strata above or erosion stops. A sinkhole forms if the void reaches the surface or the overburden collapses.

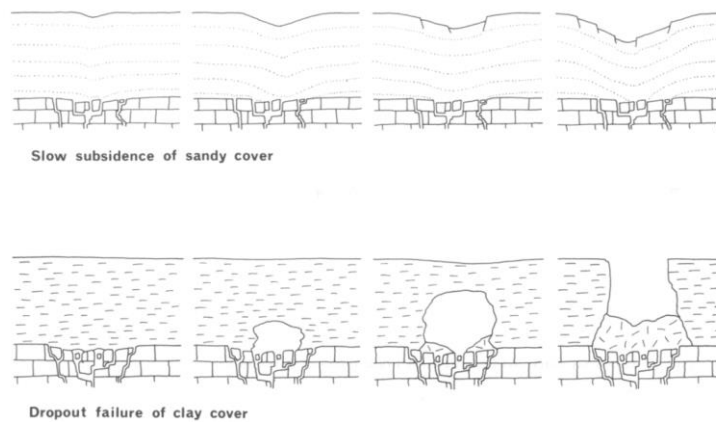


Figure 2.7. Development of subsidence in sand above eroded bedrock (top) and dropout in clay (bottom) (Culshaw and Waltham 1987).

Dissolution on the bed rock is extremely irregular and locally varied so migrating cavities of this sort are difficult to predict and can give rise to a range of engineering hazards. The soil above a karstic environment may be the insoluble element of the bedrock and hence will be loosely packed (an engineering hazard). Collapse of these cavities (cover collapse sinkholes) is a major and unpredictable engineering concern and can be onset by engineering activity (also loading, vibration, drainage leaks, heavy rainfall, and mine, quarry or groundwater dewatering as the water table passes the rockhead draining sediment down into voids). Most problems occur when soil 2 m to 10 m thick lies over fissured bed rock (providing the soil has enough cohesion to arch over the void). Natural cavity boundaries are much less defined than those in mining (at the base of the manmade cavity strength increases rapidly beneath, but this is not so with dissolution) and so the location of these migrating cavities is difficult.

2.5.2.2 Non-karstic cavities

Cavities can rarely form in insoluble rock known as 'pseudokarsts'. The solution of evaporates and subsequent collapse is a common problem (especially in Spain - Pueyo-Anchuela *et al.*, 2010), as are rapid washout voids in sand and gravel by a sudden flood of water. The weakening of exposed roof layers in layered rocks, e.g. shale, weakens support and will encourage ceiling collapse. Other, less common, natural cavities can form as: lava tubes (the hardened, cooled skin remains as the lava flows away); sandstone and quartzite hydrothermal solution cavities; cavities in landslip fissures (usually very small); soil pipes (ephemeral); and melted ice wedges.

2.5.2.3 Geophysics

Ideally a migrating cavity will be detected whilst still in the formation stages before a dropout occurs and geophysics offers many techniques applicable to this task. All land over carbonates has potential of cavity collapse. As noted by McMechan *et al.* (1998), the origin of cavities is well known but their internal structure and their distribution (some follow drainage flow, some joints and bedding) are still relatively unexplored. Natural cavities are a complex and unpredictable mess of collapses, weakened rock, drainage paths, and in some cases various human filling and mining. And it is variation of their internal structure and properties that make natural cavities so difficult to map and such a difficult geophysical target. The subsurface structure is difficult to estimate from the surface expression and without geophysical techniques. This especially true is karstic environments which present a different problem to air and water filled voids; local geology is of great importance and the void properties may not be as distinct from the host material.

2.6 Current cavity detection techniques in engineering

Encouragement of integration of geophysical techniques into current site investigation techniques is the overarching aim of this work, most likely with geophysics assessing the ground before using boreholes to verify. If there are any techniques already in use that can be utilised to aid a geophysics investigation, time and money can be saved. However, a geophysical investigation will provide a wealth of information that may mean some of these more expensive current techniques will not be required.

2.6.1 Intrusive

The current standard technique for detecting cavities in the site investigation process is a borehole grid, with the hope of void encounter. If a water flush (used to cool the drill bit and help return rock chips) is used the return rate may also be indicative of voids. Cameras can be inserted into the hole when void encountered. Boreholes cost \$25 per foot (increasing with depth and in mining (Kendorski, 2004)), not including the expensive cost of an onsite geologist and drilling contractor (Wadhwa *et al.*, 2008) and only sample a 4-6 inch diameter cylinder of the subsurface.

Cores or trials pits can highlight bed separation which may be indicative of stoping above a ceased mine. Digging such pits may be difficult or restricted on slopes, where the overburden is too large, on ground that cannot be disturbed, or in built up areas. Backfilling may change conditions that must be considered for foundations. A trial shaft can be used for deep examination of open workings or of overlying rocks where void migration is suspected (Healy & Head, 1984). Other common technique include: dynamic probing (testing subsurface resistance to a cone driven into the material).

These techniques are intrusive, non-continuous, slow, expensive, require specialist safety precautions, and, when large numbers of boreholes are used, can decrease the integrity of the subsurface. They can also increase the potential of immediate hazard (cavity collapse, hitting a tank or pipe, mine water breach) and create new flow paths for hazardous materials. These techniques are affected by the site geology; it is also possible that the drill may not be able to penetrate through a material, which not only limits depth of investigation but can cause expensive and hazardous damage to the equipment. The discrete nature of these techniques means 3D imaging of cavities (useful in remediation) is impossible (excluding prohibitively expensive laser techniques that rely on a borehole “hitting” an air void (Liu *et al.*, 2008)) and extrapolations between boreholes are only as accurate as the density of the coverage.

A borehole grid is likely to miss cavities smaller than the borehole spacing (Figure 2.8) and so hole spacing should be irregular to avoid matching pillar patterns (Healy & Head, 1984). Spacing will be smaller if faulting or mining have complicated the subsurface.

However, the closer the borehole spacing the larger the threat to structural integrity and risk of hitting and underground utility (Mellett, 1995). A density of probes of 2500/ha is required to have a 90% chance of finding one cavity of 2.5 m diameter (Waltham & Fookes, 2003) which may prohibitively expensive. In Belgium 31 boreholes missed two caves only revealed during excavation; unfortunately often the time when true ground conditions are found (Waltham & Fookes, 2003). These techniques are generally adequate, and in some places enforced, and the industry is understandable adverse to risk, meaning new techniques are treated with caution.

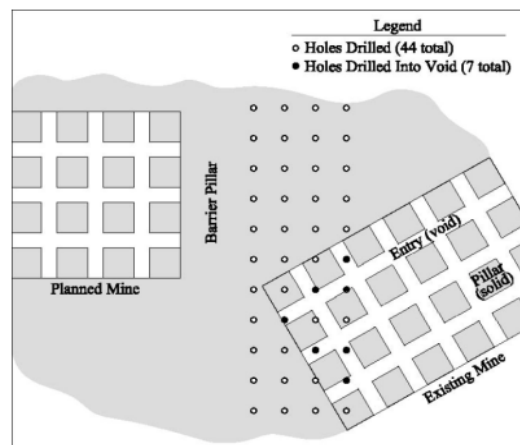


Figure 2.8. The possibility of missing cavities with discrete borehole sampling. Depending on borehole grid density and cavity size, whole cavities may be missed between boreholes Borehole grid patterns may even match mine pillar patterns, meaning all areas of mining activity go undetected. Also many more boreholes than needed are drilled adding unnecessary expense (Kendorski, 2004).

2.6.2 Desk study

Visual site inspections and desk studies are non-invasive and useful but not conclusive. This can include: aerial photographs (subsidence and change in soil or vegetation can be indicative of mining), local interviews, historical maps (railways, canals, chimneys or engine houses maybe associated with old mining work), mine maps, geological maps (Culshaw & Waltham (1987) suggest that any marked coal seam or mineral vein should be assumed to have been mined), aeronautical and geophysical maps, topographic study (analyse the area for crown holes, spoil heaps, shafts, outcrop workings, buildings cracked), chemical tests (methane often associated with abandoned mining and groundwater may contain evidence of mining) and field walkovers (potentially hazardous in cavity areas). The accuracy of this information is dependent on the quality, availability, or existence of relevant maps, and knowledge of how the landscape may have changed through time. Much of this information is nullified if the area has been built over. All of this information must be treated with optimistic caution.

2.7 Geophysics for cavity detection

Detection and characterization of subsurface cavities, tunnels and abandoned mines remains one of the most difficult classes of problems addressed by near-surface geophysics. (Butler, 2008)

As we have seen, the formation of underground cavities is complex and varied; the same can be said of their detection. The importance of such work was confirmed in 2003 when the U.S. congress authorised the MSHA (Mine Safety and Health Administration) to focus on using remote sensing technologies to find abandoned mines (Gochioco, 2003).

A new robust investigation standard in the detection of cavities is needed and geophysical techniques offer an attractive alternative. A range of geophysical techniques have been successfully utilised in cavity detection in various geologies across the globe: microgravity (Rybakov *et al.*, 2001; Styles *et al.*, 2006; Tuckwell *et al.*, 2008), resistivity (Rodriguez Castillo and Reyes Gutierrez, 1992; Elawadi *et al.*, 2001; Roth *et al.*, 2002), a variety of seismic techniques (refraction - Ballard *et al.*, 1982; reflection - Miller and Steeples, 1991; surface wave diffraction - Xia *et al.*, 2007), and recently multidisciplinary techniques (Filahi *et al.*, 2008; Cardarelli *et al.*, 2009; Pueyo-Anchuela *et al.*, 2010). However, techniques that are viable on one site may not be applicable to another. The complexity and variation of cavities and their surroundings mean there is no standard technique, or collection of techniques, to detect and map cavity location. Especially limited in the literature is testing on sites that are commonly used by engineering companies. There is a lack of published information comparing responses of different geophysical techniques to cavities on such sites. No consensus on which technique is suitable in a given situation is available, or if geophysics will be suitable at all.

If we can establish a robust methodology for cavity detection in the U.K., we can integrate geophysics in the current site investigation techniques and enable the development of brownfield sites.

2.7.1 Reputation in engineering

Using geophysics for cavity detection is still relatively new and unconstrained and has an uncertain reputation in some areas of the engineering industry. Users are unsure of the techniques, and the industry is inclined to rely on tried and tested techniques than utilise new, unfamiliar technologies. The industry can often be legally tied to certain borehole techniques in the U.K. (Styles, 2003), in the U.S.A. (the Mine Safety and Health Administration and several states require probe drilling (Kendorski, 2004), and the regulations of the Al-Ain Municipality (U.A.E.) require detailed geophysical investigations

for new construction projects because of the high cavity risk in the limestone (Bloushi, 2011).

Compounding this, geophysics for cavity detection has an uncertain reputation in some areas of the engineering industry. Users often recall bad experiences with geophysical surveys: the target remained undetected despite assurances of detection; more questions were created than answers; or results were obscured by noise (EAGE Conference and Exhibition workshop discussion, 2012). Reasons for these experiences include: unfamiliarity with the techniques and subsequent unreasonable expectations; use of geophysics as a last resort when the subsurface is so complex that other techniques have failed (“emergency geophysics” (Meglich, 2013); overselling of certain techniques to win tenders (Loulizi, Barker, Brown, Flintsch, & Riad, 2001); indiscriminate choice of particular techniques (EAGE Conference and Exhibition workshop discussion, 2012); or use of geophysics by personnel without the required knowledge (Loulizi *et al.*, (2001) mentions the use of GPR by civil engineers without understanding of the system capabilities or the electromagnetic properties of the subsurface). Communication between geophysicists and engineers is of paramount importance. Honesty in the limitations of techniques is required but also the championing of good practice and successes. A stronger understanding of how a technique will perform in a given situation will lead to correct utilisation.

Techniques that are viable on one site may not be applicable on another, and there is no consensus on which technique is suitable in a given situation, or if geophysics will be suitable at all. Comparison of the effectiveness of different geophysical techniques on sites that are commonly used by engineering companies is limited in the literature.

2.7.2 Benefits of a geophysical survey

The general benefits of using geophysics in a site investigation are highlighted in Figure 2.9. Geophysics is non-destructive and so the subsurface can be investigated on protected sites or on hazardous sites without exposure to hazardous materials. As the site remains unchanged, geophysical measurements can be repeated recording temporal results or continuously monitoring a hazardous subsurface. This non-destructive quality is especially important in areas with cavities as any alteration may increase the potential for collapse. In some cases, such as nuclear waste depository construction, further subsurface openings are not allowed. In such a case boreholes would be ruled out and geophysics must be used. Geophysics also offers continuous coverage of the subsurface while boreholes are discrete and represent a very small percentage of the subsurface. Geophysical survey time is generally low and so is cost and time efficient and on-site analysis of the techniques allows real time response to target detection or problems.

With cavity detection additional benefits include the ability to monitor any change in cavity structure or migration rate without intrusion, monitoring how successful the remediation techniques applied were, and the techniques are much quicker, have better coverage than borehole techniques and are in three dimensions aiding calculations of filling costs. Especially in karst environments, there is wide variety in subsurface properties over a short distance (Doolittle & Collins, 1998) and extrapolations between too few boreholes will not meet the required accuracy.

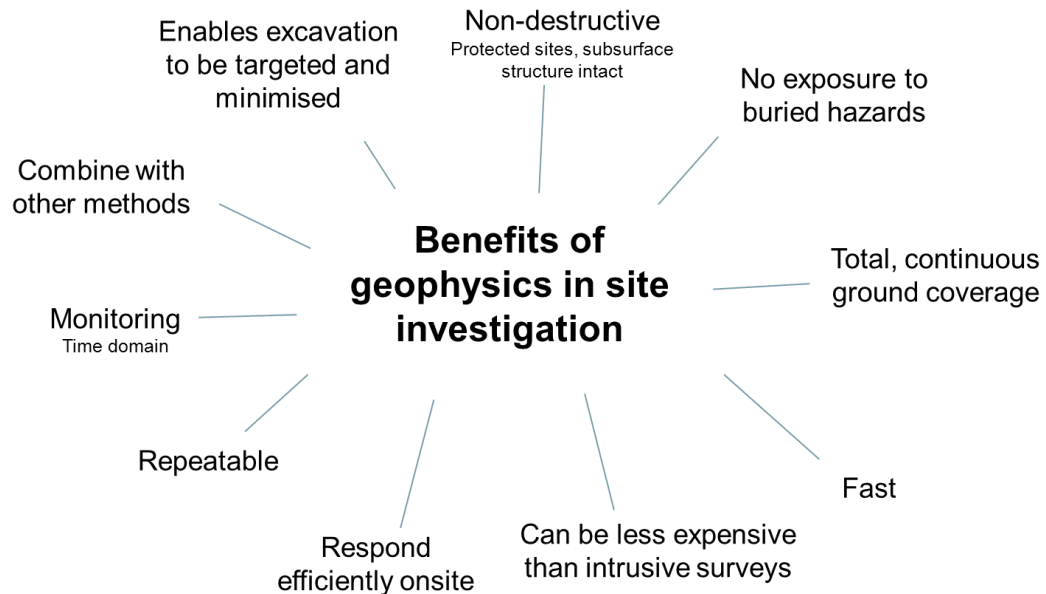


Figure 2.9. General benefits of using geophysics in site investigation.

The variation in cavity size, location, makeup and surroundings make it difficult to decide which of many techniques should be employed and ultimately, any results from geophysical techniques need verification from intrusive methods. Here, we propose that geophysical methods for cavity detection and analysis be integrated into the standard borehole regime currently utilised by engineering companies. Over large sites it is infeasible to, or at least prohibitively expensive, to cover the area with enough boreholes to detect voids. It is therefore sensible to cover the area with geophysical techniques and use boreholes for verification in positions that will give us the most information; termed “smart holes” by Benson & La Fountain (1984). Consequently, fewer expensive boreholes are required. Of course this will require more faith in the techniques and proof of their success in varying subsurface structures. This study aims to find techniques, or range of techniques, appropriate for various geologies and cavity geometries, taking into account the constraints of time, budget and site specific inhibitions. Most previous studies focus on rural locations

and few on brownfield sites in the U.K. If the civil engineering industry is to adopt geophysics as part of its standard site investigation, more robust and U.K. specific techniques (or collection of techniques) are required.

2.7.3 Considerations

As will be shown in Section 2.8, each geophysical method has its own particular limitations and so no method can be used routinely in all circumstance. There are a number of general considerations should be made before applying geophysics to a problem.

2.7.3.1 Cavity considerations

Detection of cavities using geophysics is reliant on a number of key factors: penetration, resolution, signal-to-noise ratio, and contrast in physical properties (McCann *et al.*, 1987). In cavity detection, often both deep penetration and high resolution are required, and so a trade-off is required. The relationship between the depth of a target and how large that target needs to be for detection is unpredictable and so “rules of thumb” are often employed; McCann *et al.* (1987) suggest cavities with depth less than twice its diameter can be detected in favourable conditions.

With the exception of gravity we are not looking for ‘nothing’; we hope to detect the contrast in properties between the cavity and the surrounding strata. Cavities will disturb their immediate surroundings with fractures, redistributed stress or small collapses, creating a “halo” effect in the strata up to two or more diameters from the cavity (Daniels, 1988). This enlarged target improves the chances of a geophysical anomaly being detected but reduces the accuracy of estimated dimensions.

The cavity will also affect subsurface drainage and changes in water content can indicate a cavity beneath (Chamon & Dobereiner, 1988). A number of geophysical techniques cannot reach the large depths of some mines, thus limiting the choice of technique for direct detection. However, shallower indicators: the shaft, the mine yard, and mine fill, are easier to detect.

Geophysical methods detect contrasts in subsurface properties. In its purest sense, a void is the perfect target; the contrasts between air and any type of rock will be large enough for detection providing the target is large enough. However, there are a numbers of other factors complicating the process. A subsurface cavity is rarely empty and has at least some material within, collapsed or otherwise (with the exception of a void; strictly defined to be air filled only – see Daniels (1988) for precise clarification of related mining terms for cavities). Of course, below the water table the cavity will be filled with water, but geological material can also be present or remnants of previous activity (e.g. mining equipment). The cavity and its material are referred to as the “cavity system” (Butler, 2008).

2.7.3.2 Site considerations

Any prior knowledge of the cavity system (shape, size and depth, surrounding and internal geology, natural or manmade) will greatly assist the survey design and the chance of detection. It is important to note that these factors affect different techniques in different ways. So in one environment, for example clay, the high electromagnetic wave attenuation may render GPR useless at depth, and we may consider using a non EM technique (see section 2.9). It is therefore vital that a desk study take place. This knowledge will inform the choice of equipment and survey design, perhaps the most important decisions involved.

Signal to noise ratio at particular sites can be limiting, especially in an urban setting. The subtle anomalies from cavities need to rise above, and be distinctive from, this noise. Surface and subsurface objects prominent in urban areas (buildings, tress, pipes, service etc.) and background noise (magnetic and electrical, e.g. magnetic storms and power lines) will be identified by the geophysical survey and may obscure the true target. Natural noise is also a problem; wind, magnetic storms, ground currents and natural seismic activity. Again, this will depend upon the technique utilised and a good knowledge of potential sources noise at the site will inform the choice of technique prior to the surveys undertaking. Constantly changing ground conditions will also vary results obscuring subtler signals.

Field conditions can also inhibit techniques; space and access are required and some techniques require ground contact. Some techniques can be very slow in the field (microgravity) or in processing (seismic). Surface condition variation such as changing from tarmac to soil, anthropological activity, or the variation of the thickness of any made ground will result in changes to the geophysical signal that must be removed or may obscure the target or be falsely interpreted as a target (Tuckwell *et al.*, 2008) Cavity detection in particular requires very sensitive equipment which can be expensive. Field technicians need to be well trained in order to adapt in the field. The communication of results to non-geophysicists can be challenging, and a skill that is often overlooked.

A common trade-off of using geophysics is that signal resolution is lost with depth, and penetration is inhibited by higher resolution. Another inhibiting problem is, because results are taken remotely, intrusive verification is required. Finally, because results from a single technique can be ambiguous and non-unique, multiple complementary techniques may be required.

Geophysics involves assumptions and uncertainties that simplify the true subsurface. As the science progresses, the signatures associated with subsurface variations are better understood, but the complexity of the near surface is still difficult to interpret. This complexity is also difficult to model, so we usually interpret a simplified version of the subsurface.

2.8 Geophysical techniques

Although each case study has an individual context meaning it is difficult to discern whether the technique will work elsewhere, by assessing and comparing existing technologies, good practice can be evaluated to improve the reliability of geophysical techniques for cavity detection. Here, techniques used to currently detect cavities are reviewed.

2.8.1 Ground Penetrating Radar

Ground penetrating radar (GPR) surveys have been used since at least 1929, though the crude technique has been available since 1904 (the year of Christian Hulsmeyer's patent (Daniels *et al.*, 1988)). In the Earth Sciences, GPR was initially used for ice soundings in the 1950s (Olhoeft, 1996). The introduction of commercial systems and the use in the Apollo Space programme in the 1970s (Daniels *et al.*, 1988; Monaghan *et al.*, 2003) led to wider application of the technique in rock and soil. GPR has since progressed greatly and is used in a myriad of applications including: geological, archaeological, criminological, environmental, engineering, construction and hydrology, and is showcased in a wider range of applications at the frequent GPR specialised Symposiums on the Application of Geophysics to Environmental and Engineering Problems.

In the geological application of GPR, a transmitter antenna radiates pulses of high frequency electromagnetic energy (between 10 MHz and 1 GHz) that are reflected in the subsurface and recorded by a receiver (Figure 2.10). When the radar pulse reaches an electrical discontinuity (a change in dielectric constant) the signal is reflected, refracted, or scattered. The dielectric constant (or permittivity) is related to a materials reaction to a steady state electric field and ranges from 1 (air – its low value allowing cavities to be easily identified on a profile) to 88 (sea water), with most soils and geological materials below 15 (clay, however, can reach up to 40) (Conyers, 2004). Dielectric constant is a function of porosity, mineralogy, water saturation and frequency (Monaghan *et al.*, 2003).

The amount of reflected energy is dependent upon the size of the target, surface of the target, water content, and the amplitude reflection coefficient, which is controlled by the dielectric constant (Equation 2.1). The bigger the contrast in dielectric properties, the stronger the reflection will be. The received energy is digitised and either displayed in-field or stored as a chart of horizontal distance versus time. If we know the velocity of the pulse in the material (Equation 2.2), the two-way time (Δt) can give us a simple measurement of distance (or depth) (Equation 2.3). The amplitude can give us information about the difference in electrical properties.

$$R = \frac{1 - \sqrt{\epsilon_2/\epsilon_1}}{1 + \sqrt{\epsilon_2/\epsilon_1}} \quad \text{Equation 2.1}$$

where ϵ_1 and ϵ_2 are the dielectric constants of the two materials.

$$v = c/\epsilon_r\mu_r \quad \text{Equation 2.2}$$

where $\epsilon_r = \epsilon/\epsilon_0$ (the ratio of dielectric permittivity of the medium to free space), $\mu_r = \mu/\mu_0$ (the relative magnetic permeability of a medium, which is so close to unity in most rocks it's effect is negligible. In iron-bearing materials it may be important), and $c = 3 \times 10^8$ m/s (velocity of EM waves in free space) (Batayneh *et al.*, 2002).

$$D = v \cdot \frac{\Delta t}{2} \quad \text{Equation 2.3}$$

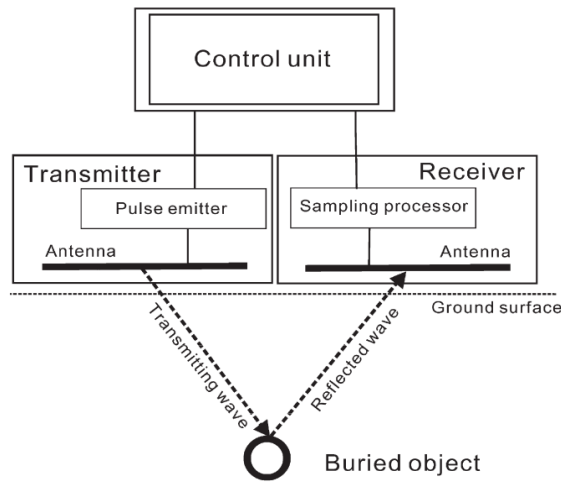


Figure 2.10. Ground penetrating radar equipment and principle (Xu *et al.*, 2009).

The recent popularity of GPR lies in its repeatability, rapid use, relative ease, non-intrusive nature, high resolution and versatility. If using shielded antennas, the technique has an advantage over other geophysical techniques as it can be used in urban settings (Mellett, 1995). As GPR is a reflective technique, depths to targets can be found more accurately than other techniques if subsurface parameters are known (Mellett, 1995). Also, in the case of spherical targets, the lateral location is accurately found from the top of the reflection hyperbola (Mellett, 1995). Because of these attributes, GPR is frequently, and successfully, used in cavity detection in various geologies (typically electrically resistive) (Appendix A), though penetration is often prohibitive (Doolittle & Collins, 1998; Butler, 2008). The large contrast between the electromagnetic properties of an empty or water filled cavity and the host rock creates strong reflectors at the boundary, often resulting in distinct hyperbola on a profile (section 2.8.1.3.1). The reflective nature of the technique allows us to easily determine cavity depths (if the dielectric constant is known or calculated) and

accurately map the location (using hyperbola peaks or other geophysical signatures). Typically, detected voids in the literature are either shallow or large or both (Appendix A), and the specific nature of each site means the techniques reliability in other conditions is uncertain. In response to this a number of studies have been completed in test sites (Grandjean *et al.*, 2000; Kofman *et al.*, 2006; Xu *et al.*, 2009) showing the GPR response in near perfect situations. This is of great use but neglects problems encountered in the field.

2.8.1.1 Considerations and limitations

A number of factors affect GPR signal; velocity and density contrasts, propagation velocity, layer thickness and homogeneity (of mineralogy, porosity, grain size and water content), electrical properties (dielectric contrast, magnetic permeability, conductivity), site conditions and background noise. In addition to spherical divergence, attenuation (α in dB/M) will also decrease the amplitude of a GPR pulse propagating through a material by dispersion or absorption. Attenuation is dominated by conductivity in most materials. Attenuation occurs when resistivity is low (conductive environments) and dielectric constant high (exceptions occur in exceptionally heterogeneous or homogeneous materials (Daniels, 1988)) and the two properties are mostly independent. High conductivity soils can become radar opaque (Doolittle & Collins, 1998) and so ideal conditions for GPR penetration are low clay content and low water content where there is little attenuation of energy (Finck, 2003), i.e., dry, resistive environments with sandy soil. Unfortunately, clay is common across Britain, inhibiting GPR use. However, only mineralogical clays (e.g. montmorillonite) restrict GPR (Olhoeft, 1996). High frequency GPR (above 400 MHz (Olhoeft, 1996)) may be unaffected by mineralogical clay but the high frequency will limit penetration depth. Highly conductive soils will also rapidly attenuate signal and hence the most successful uses of GPR are in electrically resistive environments such as karstic (Beres *et al.*, 2001) and testing is often completed in sand to negate attenuation as much as possible (Kofman *et al.*, 2006).

The water table can limit penetration of GPR as the present ions increase bulk conductivity and water absorbs electromagnetic energy over about 1000 MHz (Geomatrix, 2010a). However, if the water is not highly conductive (salt water is more conductive) and the water content of the soil is below 40%, GPR may be of use (Wadhwa *et al.* (2008); Olhoeft (1996)). It should be remembered that electrical conductivity is affected by water content, soil type, salinity and dielectric constant, not merely by the presence of water (Chung *et al.*, 2013). Seasonal and meteorological variance has little effect on detection of voids below 50 cm as rain only varies moisture in the very near surface soils (Xu *et al.*, 2009)

especially when using longer wavelengths. There may be a slight increase in velocities in moist materials which can be advantageous.

We can increase the frequency of the transmitted pulse to increase the resolution of the signal but this will decrease the depth of penetration because energy is attenuated (and the opposite is true) or dissipated through heat. Figure 2.11 shows this effect in a test pit and Figure 2.21 shows the depth of cavities found by recent workers with different frequency antennas. However, too low a frequency and EM field will not propagate as waves but diffuse (as in inductive EM). In some countries certain frequencies are restricted; in the U.S. these include most of the frequencies below 100 MHz, though specific frequencies are still available (Sternberg, 2004). We can also increase the transmitter power to increase depth though we need a great deal of power to increase penetration by any meaningful distance (Geomatrix, 2010a).

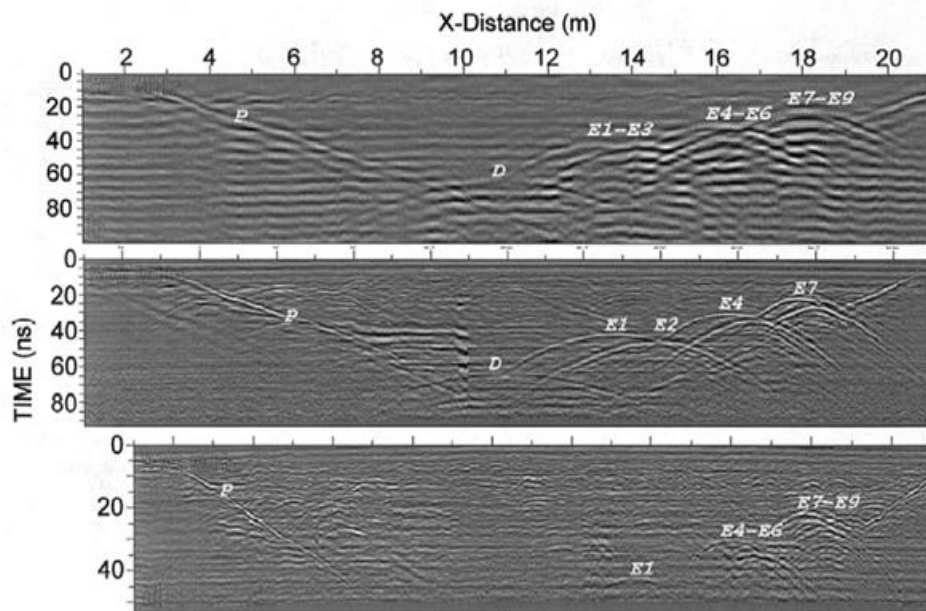


Figure 2.11. GPR survey of a test pit using 300, 500 and 900 MHz antennas (top, middle and bottom respectively). Here we can see the deeper penetration of the lower frequencies and the increased resolution of the higher frequency. Also note how the features above the void may obscure the voids signal. D is a buried air void, E are pipes and P is the pit limit (Grandjean *et al.*, 2000).

If possible, we should avoid noise from phones, radios, strong sources of electricity, and reflections from buildings, metal and even trees that commonly are detected with low frequency antennas. If not, extensive notes should be taken in order to recognise features on profiles. Rebars can often disrupt GPR signal but high frequency antenna may be able to detect targets in between rebars (Olhoeft, 1996). GPR samples in 3D and hence off-line reflections will be seen on a 2D profile (Beres *et al.*, 2001), obscuring features and complicating depth estimates. Depth estimates to cavities are only as accurate as the velocity

values obtained for the subsurface. Therefore inaccuracies in this value or lateral and vertical variation in velocity will disrupt depth estimates. Finding the height of a cavity is also troublesome. The strong reflection from the top of a cavity will mask or interfere with the reflection from the base. Kinlaw *et al.* (2007) found estimates of tunnel height by GPR were exaggerated by 1.43. The typically diffraction hyperbola of a cavity must be treated with caution as it could be another feature with strongly contrasting electrical properties. Xu *et al.* (2009) found, after excavation, that 11% of suspected cavities were incorrectly interpreted.

2.8.1.2 Typical depths of penetration

Anderson & Ismail (2003) note that the depth of penetration of GPR is usually less than 10 m, however, depth of penetration GPR varies greatly from site to site but there are a number of estimates for a variety of materials (Table 2.2). These numbers are highly variable depending on frequency and local material makeup and that depths will also decrease as porosity, concentration of electrolyte, and cation exchange capacity of clay increase (Doolittle & Collins, 1998). It must be noted this is not a maximum penetration, just the depth of the cavity. Maximum depths of penetration, and other measured parameters (velocity, attenuation, dielectric constant, etc.) measured in various geologies in the recent literature are compiled in Appendix B.

Table 2.2. Maximum penetration estimates compiled from a range of authors.

Geology	Depth (m)	Reference
Dry salt	1000+	Daniels., 1988
Ice	1000+	Daniels, 1988
Hard frozen ice	5000	Western Mining Resource Center, 2007
Igneous	up to 30	Daniels, 1988
Metamorphic	up to 30	Daniels, 1988
Limestone (low clay)	up to 30	Daniels, 1988
Karst	30-40	Xu <i>et al.</i> 2009
Dry sand	30	Western Mining Resource Center, 2007
Sandy soils	5-30	Doolittle, 1998
Loamy soils	1-5	Doolittle, 1998
Limestone	~3	Daniels, 1988
Volcanics	~3	Daniels, 1988
High clay content	<1	Daniels, 1988
Bentonite	<1	Western Mining Resource Center 2007
Clayey soils	<0.5	Doolittle, 1998

The Radar Range Equation can help predict the instrumental losses accurately. This will be discussed in further detail later.

2.8.1.3 Geophysical signature

The strength of reflection from a cavity will depend upon its size, depth and the contrast of properties. However, there are 3 main signatures related to cavities discussed here. Smaller cavities will be notable by a diffraction hyperbola, and larger cavities may have a more chaotic signal (Casas *et al.*, 1996).

2.8.1.3.1 Diffraction hyperbola

This is the most common method of detection of cavities using GPR (Appendix A). The contrast in electrical properties (permittivity) between the cavity and the surrounding rock reflects the transmitted EM energy back to the receiver. We see a hyperbolic shape because reflections from an offset surface position takes longer to arrive than from directly above the subsurface object (Figure 2.11; Figure 2.12). The apex of the hyperbola is therefore directly above the object. As can be seen in Figure 2.11, pipes give a similar hyperbolic response and therefore care must be taken in interpretation to avoid confusion with other subsurface objects with contrasting permittivity. This can be done by employing further geophysical investigation or a more detailed survey.

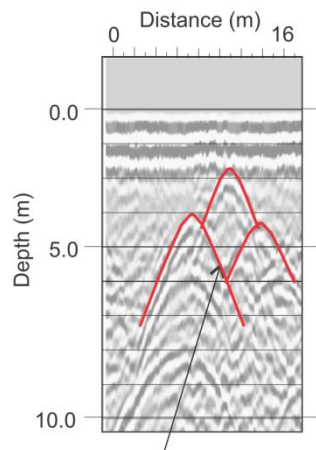


Figure 2.12. Diffraction hyperbola over a cavities within limestone (TerraDat UK Ltd., 2005).

2.8.1.3.2 Lateral variation (penetration variance, onlap geometry and pull-up)

A region of collapse may be indicative of deeper cavities or may be the migration of a cavity to the surface. Either way, the area will be of interest as further subsidence may occur and the integrity of the material has been weakened. A collapsed area will have a number of features on a GPR survey. The area may be characterised by a change in the wave features (propagation, depth of penetration, amplitude, density of reflectors) because the collapse properties will be different to the surrounding strata (Pueyo-Anchuela *et al.*, 2010). At the

edge of the zone of collapse we may see in-dipping onlap geometry where the collapsed sides do not align with the adjacent strata (Figure 2.13). The exact makeup of the subsurface is uncertain with these indicators; is the collapse total or partial, or do the irregular signals indicate an irregularly shaped cavity (Mochales *et al.*, 2007a)?

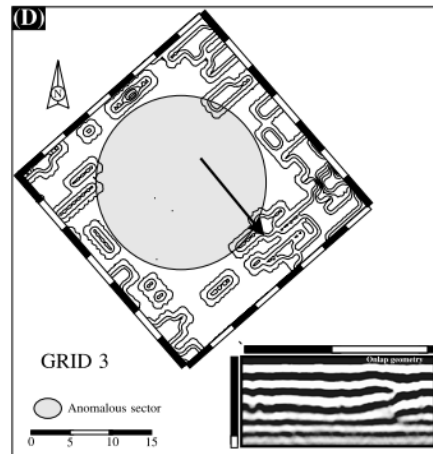


Figure 2.13. GPR survey over a collapsed doline. The grey area was characterised by penetration variance and the inset shows the onlap reflection features at the border of the collapse (Mochales *et al.*, 2007a).

The maximum penetration of the GPR signal across the site can be mapped and used as an indication of anomalous areas and cavities. This type of evidence needs verification as conductive materials also allow deeper penetration. Individual traces can also be analysed for the strong reflections indicative of strong contrasts found in cavities (complex trace analysis (Taner *et al.*, 1979; Beres *et al.*, 2001)). This method also helps delineate cavities as profiles directly above a cavity will have the strongest reflections with reflections gradually weakening with distance.

The presence of a cavity creates lateral velocity variation. We expect signals from beneath the cavity to arrive earlier than those adjacent to the cavity as EM waves travel faster in air. This will be noticeable on a GPR section as a “pull-up” of horizons (Leckebusch, 2007).

2.8.1.3.3 Reverberation and resonance

Of the energy that is not reflected on the boundary of a cavity, some may reflect within the cavity numerous times (reverberate). The receiver antenna will detect the EM energy that ‘escapes’ from the cavity reverberation at each upper reflection point. The GPR trace will therefore show a pattern of a number of similarly shaped, high amplitude, low frequency reflections (multiples) above the point of the cavity (Mellett, 1995; (Kofman *et al.*, 2006) - Figure 2.14) allowing lateral mapping of cavities. As the wave has travelled further (by

reflecting within the cavity) the reflections will *appear* on the profile to be arriving from deeper in the subsurface, though they are just arriving later; this obscures the vertical dimension of the cavity. These reverberations can also occur in a zone of subsidence (Ulugergerli & Akca, 2006) or in a cavity filled with highly conductive material (Mochales *et al.*, 2007a). It must be noted that a highly conductive near surface objects, e.g., metal manholes or concrete, may cause a similar reverberation effect (David, 2008) and hence care must be taken in the field to note any such objects.

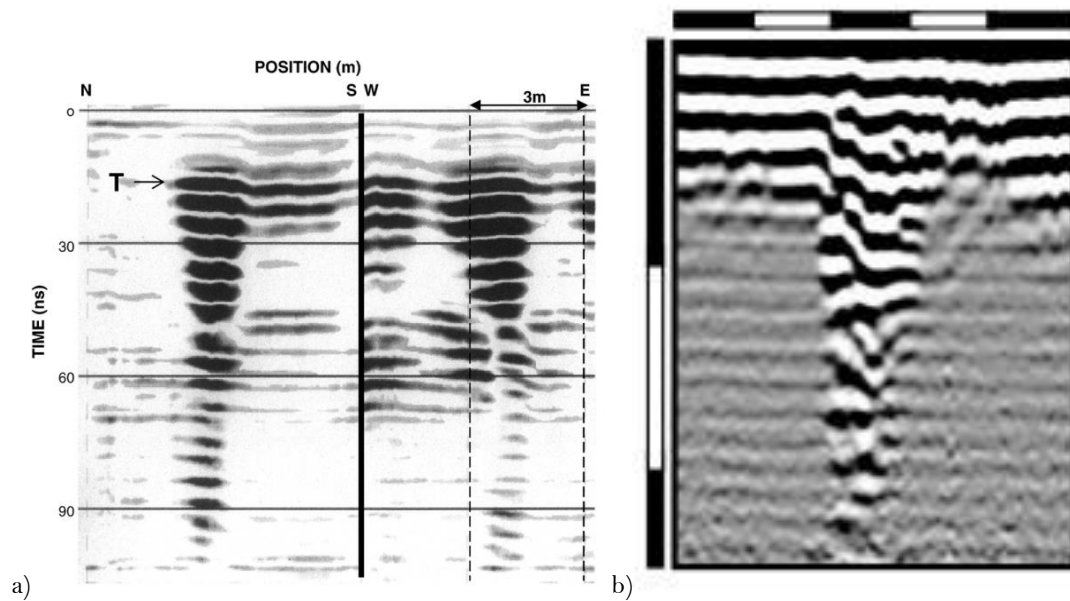


Figure 2.14. a) Oscillations within an air filled sinkhole at depth 1.1 m imaged in orthogonal directions (Kofman *et al.*, 2006). b) multiple reflection anomalies highlighting high conductivity material (Mochales *et al.*, 2007a).

2.8.2 Gravity

Very small changes in the Earth's gravity field are detected over varying densities in the subsurface. Measuring these changes requires very sensitive instrumentation. In the case of void detection we can detect a decrease in the gravity (negative gravity anomaly), corresponding to the void's "missing" mass. When searching for voids it is, therefore, in theory the most apt technique as it is directly measuring the presence of the cavity. Because voids generally produce small gravity variations, mostly due to their small size, normal gravity techniques may not detect these subtleties and so microgravity must be used. Microgravity allows detection of anomalies on the microGal scale (1/1,000,000 Gal) and therefore can build a very detailed image of gravity variation. Air filled voids generally offer a high density contrast to the surrounding material (depending on the density of the material – see **Table 4.1** for typical density values), but water less so resulting in an anomaly 60% that of air and rubble less still with an anomaly of 40% that of air (suggesting

that infilled shafts or collapsed cavities may be difficult to detect with this technique) (Styles *et al.*, 2005). Though these density contrasts are large, targets are typically quite small. The anomaly amplitude may also tell us something about the size or depth of the anomaly (small anomalies are not usually associated with mining (Branston & Styles, 2003) but results must be treated with caution as with gravity interpretations are non-unique. The same gravity anomaly can be produced from a wide range of subsurface cavities with varying depth, size and host rock density (Branston & Styles, 2003). Other techniques or modelling using well constrained subsurface parameters may be required to verify which combination of parameters is correct.

Disturbed or fractured rock surrounding the cavity will decrease the density contrast, but increase the size of the effective target, especially in the case of natural cavities. The so called 'halo' effect can reach 2 meters around the void allowing smaller voids to be detected than theoretically possible (Butler, 2008). The halo effect is discussed in much further detail in Chapter 6. The same is true in karst environments where dissolution, sinkholes and joint systems increase the potential target size.

2.8.2.1 Considerations and limitations

Gravity surveys are slow and labour intensive and are hence expensive when considered in terms of area covered compared with other faster techniques, especially magnetic, limiting their commercial appeal (Tuckwell *et al.*, 2008). It is therefore more useful on a small detailed scale, on large scale features across a large area where fewer measurements are required (Linford, 1998) and especially good on flat terrain where few corrections are required. The acquisition of data has to be strict and uniform (readings are often subjective and can be affected by small vibrations from roads, machinery, tree roots moved in the wind and even distant earthquakes (Milsom, 2003) and require repeat readings), as do the corrections which can complicate the analysis - (Doll *et al.*, 1998) suggest that elevation accuracy needs to be 0.3-3 cm for void detection). We must also ensure that the spacing of the measurements is dense enough to detect our target; (Waltham & Fookes, 2003) suggest for example that a 2 m grid is sufficient for a 1 m cavity. There are also possible errors in interpretation by assuming the water table is constant across a potentially cavernous site, the cavity may take in more water than the surrounding material (Branston & Styles, 2003). It can be especially useful in conductive soils when GPR may not be applicable, on sites with limited access as little extra room outside the target is required (Beres *et al.*, 2001) and industrial and developed sites as it is unaffected by electricity or acoustic noise. Only voids with a large enough density contrast and size will be detected and even then detection depends upon the resolution of the chosen gravity meter.

Modern instruments may measure down to $0.01 \mu\text{m/s}^2$ sensitivity, although repeatable meter reading error including unclamping, re-levelling and moving the meter may lower the error to $\pm 0.05 \mu\text{m/s}^2$ and new electronic instruments down to $\pm 0.02\text{--}0.03 \mu\text{m/s}^2$ (United States Army Corps of Engineers, 1995). However, these estimates can be optimistic and many factors can decrease the accuracy of measurement: wind, traffic, and ground hardness may all contribute to increasing the reading error to ± 0.08 to $0.1 \mu\text{m/s}^2$ (United States Army Corps of Engineers, 1995). Other estimations of the resolution of microgravity techniques include: in the microGal range (Linford, 1998); $4 \mu\text{Gal}$ (Patterson *et al.*, 1995); $1 \mu\text{Gal}$ for the Scintrex CG5 gravity meter (Tuckwell *et al.*, 2008); $1 \mu\text{Gal}$ for the Scintrex CG-3M gravity meter (Styles, McGrath, *et al.*, 2005); 0.001 mGal precision and 0.003 mGal repeatability for the Burris Gravity meter (Mochales, *et al.*, 2007); detection of anomalies of $19 \mu\text{Gal}$ with a repeatability of a few microGal (Styles *et al.*, 2006).

As gravity measures density change, the cause of the negative anomaly which is interpreted as a void could be a number of things; a variation in water levels, a thickening or changing lithology of superficial deposits (McCann *et al.*, 1987). To verify a void we may need to use additional Geophysical techniques. The interpretation of the negative gravity anomaly is also subjective; an anomaly is affected by shape, depth and density contrast and different variations of these may produce similar anomalies. We must also be cautious of the halo effect around a cavity, which, though helping us detect smaller voids, could be confused in interpretation; (Chamon & Dobereiner, 1988) found an anomaly to be twice as big as the void present alone would have created.

2.8.2.2 Cavity detection examples

There are numerous examples in the literature of successful uses of microgravity to detect subsurface cavities. Many of these have been collected in a database to compare which equipment was successful in which geology (Appendix D). (Styles *et al.*, 2005) offer a good history of success in void detection in various conditions, with depths ranging up to 50 m and cavity diameters of $2\text{--}5 \text{ m}$. In fact (Chamon & Dobereiner, 1988) concluded that microgravity was the only method that should be used to find caverns. As well as detection the gravity can be used to monitor migrating cavities and collapsing mines through time (Branston & Styles, 2003). It should also be noted that cavity detection is not always direct and may rely on the cavity casing. For example, the lining or collapsed lining of a tomb or shaft, or the infill of a cavity may create a positive anomaly.

Estimations of the maximum depth of cavity detection and the minimum size of anomaly required to detect a cavity are varied. Patterson *et al.* (1995) suggest that in voids of 4 m diameter can be detected to 12 m depth. Styles *et al.*, (2006) found that microgravity was

suitable for both open and infilled voids on a mining pit floor up to 30 m. (Doll *et al.*, 1998) suggest that typical cave and void anomalies are between 10-100 mGal. McCann *et al.*, (1987) show a spherical air cavity with a 0.042 mGal anomaly when at 2 m depth will reduce to just 0.01 mGal when the depth is 10 m. Further examples of successful detection include: 0.5-3.5 m diameter shallow coal mining voids at 12-14 m depth in Bristol (Styles *et al.*, 2005); 2-5 m diameter caverns in sandstone, at depths of 40-50 m detected through the halo effect (and were hence estimated to be twice as large as actual features). (Chamon & Dobereiner, 1988); cavities with 20 m or greater width creating 0.05 mGal anomaly (Styles *et al.*, 2005); 2-3 m deep abandoned mine workings in New Jersey (Ghatge (1993) apud Styles *et al.* (2005); further examples still, with typical anomaly shapes are shown in Appendix D.

2.8.3 Magnetometry

Magnetic methods have been used since the Middle Ages to detect variations in geology (Milsom, 2003) and since then ever increasing equipment sensitivity has allowed smaller features to be detected. Magnetometry is used to find rock types, toxic materials, pipes, archaeological items, and cavities. The magnetic field of subsurface objects cause slight variations in the Earth's total magnetic field (which itself varies with latitude). These variations are caused by permanently magnetised objects (remnant) or variations in magnetic susceptibility. A material in a magnetic field will acquire a magnetisation (induced) – susceptibility is a measure of the materials ability to do this (Equation 2.4). Susceptibility is controlled by the density, moisture content and composition of a material (Dearman *et al.*, 1977). Therefore, it is changes in these properties that will result in the distortion of flux lines (and anomalous readings) at the surface, providing the susceptibility contrast is large enough. Air has a magnetic susceptibility of -1×10^{-6} (Mochales *et al.*, 2007b), and anthropological filling varies from 1×10^{-1} to 1×10^{-3} (Pueyo-Anchuela *et al.*, 2010), in comparison with agricultural soil, 300×10^{-6} (Mochales *et al.*, 2007b), and common rocks ranging from 10×10^{-6} (limestone) to 0.15 (dolerite) (Milsom, 2003). It is possible that cavities will be undetected in certain geologies (e.g. gypsum, salt) as the susceptibility contrast is not great enough. Numerous features can be detected in this subtle manner, cavities being one of these but also pipes, bricks and changes in soil type.

$$M = kH \quad \text{Equation 2.4}$$

where M is the induced magnetization, k is the susceptibility, and H is the magnetic field intensity

The amplitude of the anomaly will also depend upon the size, shape and depth of the object, and the lateral distance from it. For example a screwdriver would create a 5-10 nT anomaly at 1.5 m, and a 0.5-1 nT anomaly at 3 m, where a 1 tonne car would create a 40 nT anomaly at 9 m and 1 nT at 30 m (Geomatrix, 2010b). A useful rule of thumb estimates that

the magnetic field falls off by $1/8$ as the distance is doubled, and linearly with mass (Geomatrix, 2010b). Similarly, increasing the depth of an object will result in a smaller anomaly. Deeper objects are also characterized by wider anomaly widths. It is problematic that magnetic anomalies are non-unique; a shallow small object may create a similar anomaly to a deeper, larger object.

The magnitude of the total magnetic field is measured with a magnetometer. A gradiometer uses two sensors to measure the difference in magnetic field. Workers detecting evidence of cavities or mining utilise both types (gradiometer - Mochales *et al.*, 2007b; total field - Rybakov *et al.*, 2005; Dearman *et al.*, 1977). Though using the total field technique requires the use of a base station to measure diurnal variations in magnetic field, it is more sensitive to small variations (Geomatrix, 2010b) and therefore the small variations of a cavity are more likely to rise above noise level.

It is theoretically possible to detect anomalies below 1 nT, though practically, with noise limitations, 5 nT was suggested as feasible by McCann *et al.* (1987) and, with the sensitivity of modern instrumentation, values below this are not unlikely. In mine detection it is the ferromagnetic material that will be most easily identified. Often shafts will be lined with brick, or were infilled with highly magnetic material associated with the mining process or with clay (McCann *et al.*, 1987). The high susceptibility of these objects (anthropological fill susceptibility ranges from 10^{-1} – 10^{-3} SI units, and ferromagnetic material much higher (Pueyo-Anchuela *et al.*, 2010)), even when present in small quantities, will contrast strongly with the surrounding material, creating anomalies 40–850 nT (Pueyo-Anchuela *et al.*, 2010). In the case of detecting graves, it has been shown that fluid from recent graves have an increase in iron levels that will aid detection (Juerges *et al.*, 2010). Air cavities or filled cavities will create much smaller anomalies, dependent upon the dimensions, depth and the susceptibility contrast, but are feasibly distinct from the background magnetic field.

2.8.3.1 Considerations and limitations

Magnetic surveys can cover a large area in a short amount of time and are thus a cost effective way of exploring a site. It is relatively unaffected by high electrical ground conductivity in comparison to GPR and EM, so is useful in clay, saline or contaminated ground. However, if the top soil contains crushed igneous rock, a material with high magnetic susceptibility, magnetic noise may be too high to detect cavities (Linford, 1998)

Caution must be used in locating the source of anomalies. Anomalies are mostly dipolar and the peaks will be offset from the centre of the object, meaning uncertainty in lateral positioning. The “herringbone effect” confuses this position further, caused by the offset of the GPR from the sensor. As already mentioned, object depth is uncertain as magnetic

anomalies are non-unique. We can use certain “rules of thumb” to estimate this depth which are accurate to approximately 30% (Milsom, 2003). A better approach is to use another technique to corroborate the depth and model the subsurface based on this.

The process is complicated by the changing magnetic field of the Earth, both daily and during magnetic storms. The former can be accounted for by continually monitoring the magnetic field at a base station and the latter usually requires the delay of field work. A major limitation of magnetic surveys is the presence of magnetic noise, especially prevalent in urban areas. Buildings, power lines, cables, cars, railway lines, and any ferrous debris in the near surface, will all obscure the signal and may mean a survey is of little use. Brownfield sites can have any number of objects creating unwanted noise on the survey, so we must note any such objects meticulously. It can also be difficult to pick out the magnetic anomaly from natural changes in bedrock height and subsurface deposits (Bates & Duff, 2006).

2.8.3.2 Geophysical signature

The detection of cavities using magnetometry is mostly dependant on the cavity creating a large enough susceptibility contrast to rise above the background field. This is made more likely by the inclusion of ferromagnetic materials within mines, but workers have detected large enough negative anomalies associated with a natural cavity.

Natural cavities

The detection of a pure cavity, i.e., one filled with only water or air, is difficult with a magnetic survey as anomalies rarely rise over noise levels. However, if the cavity is filled by anthropological material (section 2.8.3.3) or a material with contrasting susceptibility, a significant anomaly may be detected. Clay filled sink holes are such an example; they are common in chalk (clay has a higher susceptibility than chalk) and McDowell (1975) noted a magnetic high of almost 20 nT and two other anomalies of 10 nT in Hampshire, U.K.

We can expect a regular dipolar anomaly to be associated with a cavity. However, as we are looking for a non-magnetic target, in the northern hemisphere, a strong low will be in the south and a weaker positive peak in the north. Figure 2.15 shows this effect over a cylindrical void (5 m length, 10 m depth) producing 5 nT negative anomaly – this may, however, be obscured by normal noise levels. The modelled void was moved to a depth of 20 m creating a 0.3 nT anomaly. This suggests a limitation of detection of approximately two times the void diameter.

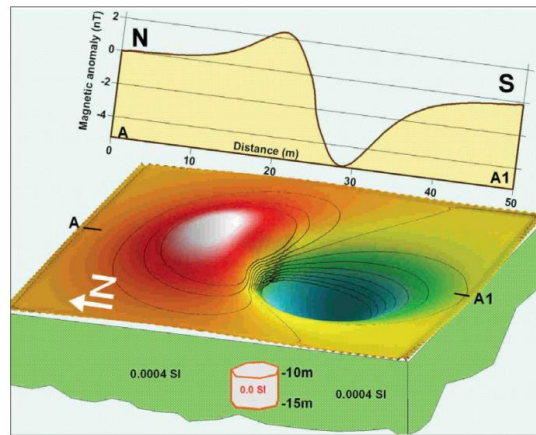


Figure 2.15. Model of a void and its associated magnetic anomaly (Rybakov *et al.*, 2005).

In practice, Rybakov *et al.* (2005) measured an approximately 12 nT anomaly (Figure 2.16) over a 7 m wide and 8.5 m deep sinkhole (Rybakov, 2001), and an approximately 6 nT anomaly over a 1.5 m wide and 7 m deep sinkhole. Manzanilla *et al.* (1994) measured a dipolar anomaly with the low to the south as expected, over a tunnel modelled to be at 3 m depth. Mochales *et al.* (2007b) detected a large (24 m deep) alluvial filled doline with a 650 nT anomaly (Figure 2.16). The anomaly was this large because the doline was at the surface, very large, and the filling had a strong susceptibility contrast with the surrounding material. Saribudak (2001) also found a large magnetic anomaly (~ 400 nT) over a shallow, soil filled cave in Texas, using conductivity and resistivity for verification. Pueyo-Anchuela *et al.* (2010) recorded a 200 nT anomaly over a collapse filled with urban debris (hence the large value) and a 50 nT anomaly at a similar, older collapse. Chamon & Dobereiner (1988) unsuccessfully used magnetometry in attempting to detect caverns in sandstone; anomalies were not significant enough to be detected. Linford (1998) found a negative magnetic anomaly and associated it with either a buried plastic water pipe, a low susceptibility material or a remnant magnetic field in the opposite direction to the current Earth field.

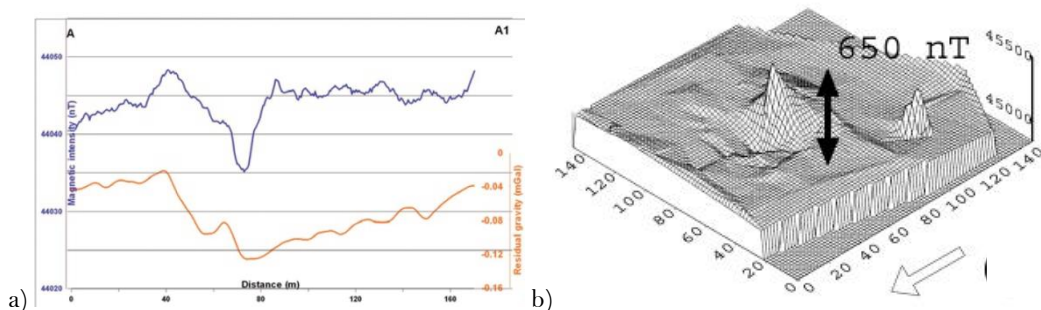


Figure 2.16. Magnetic and gravity anomalies over a sinkhole at Hever South site, near the Dead Sea (Rybakov *et al.*, 2005) and an anomaly detected over a doline in Northern Spain (Mochales *et al.*, 2007b).

2.8.3.3 Industrial works

As we have seen, some success has been achieved in the detection of natural cavities with magnetometry. The technique is, however, more suited to finding ferromagnetic material and is hence an efficient technique for detecting mining activity. An old mine may contain a number of materials that can offer strong susceptibility contrasts to the surroundings materials: rail tracks, wall linings, tools, scrap iron, burnt rocks, ash, bricks. The material used to fill a mine may also be of a contrasting susceptibility or contain fragments of ferromagnetic material - burnt shale has susceptibility of 5,000 – 11,300 nT and colliery ashes has 11,300 – 25,100 nT (Maxwell, 1975). However, should the surrounding strata have similar susceptibilities, detection will not be possible. Also, many of these materials can be found elsewhere, with no relevance to mining activity, and were used as fill near mining activity (Dearman *et al.*, 1977). The age and location of the mine will affect the likelihood of detection, as this will dictate whether wood or brick was used as a lining and the nature of the fill (Maxwell, 1976).

Again, anomalies will be dipolar, though if we are detecting ferromagnetic material we can expect a large positive anomaly to the south. Bates & Duff (2006) detected a large positive anomaly over an abandoned sewage works and over a cellar of an old house in Fife. Dearman *et al.* (1977) successfully detected mineshafts in Newcastle by identifying positive anomalies to the north of the associated shaft. Similar results were found by Raybould & Price (1966) over shafts near Leeds (Figure 2.17).

Further examples of successful employment of the magnetic technique to detect cavities and typical geophysical signatures are shown in Appendix D.

2.8.4 Gradient

In magnetometry, gradient measurements are very common. Magnetometers generally come with two sensors for this application (e.g. the Geometrics G-858 Caesium magnetometer). Vertical gradient is more suited to cavity detection than horizontal gradient as it allows the detection of very subtle changes in magnetic field along a profile. The top sensor is positioned at a fixed distance above the bottom sensor.

Gravity gradient techniques are less common mainly because of time constraints (and hence cost). Gravity is a time consuming process and finding the vertical gradient at any point will nearly double that time (magnetic gradient surveys can be completed at the same speed as total field surveys). In near surface applications of gravity gradient, a two tier tower is used to keep a constant height distance between the upper and lower measurement positions. The technique has been sporadically used in cavity detection literature over the last 30 years; Fajkiewicz *et al.* (1982) detected mine workings and karstic forms; Pánisová &

Pašteka (2009) detected church crypts; Butler (1984) detected tunnels and cavities in Florida. The gravity gradient technique produces more sensitive subsurface information than the gravity technique alone and is hence a more effective technique in detecting subtle cavity anomalies.

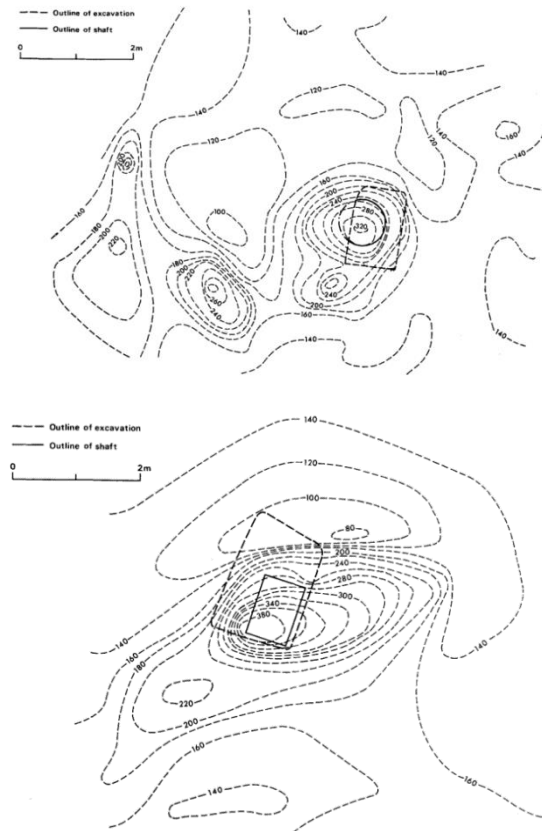


Figure 2.17. Magnetic contour plot of a brick lined shaft and a wood line shaft near Leeds (background value of 48,000 nT) (Raybould & Price, 1966).

2.8.5 Resistivity

Resistivity is recommended for detection of bell pits and shafts (Healy & Head, 1984), in areas of highway collapse (minimally affected by traffic) and The National Energy Technology Laboratory use resistivity to detect near surface voids associated with mines (Hammack, 2004). Fehdi *et al.* (2010) also suggest that resistivity is most used in karstic environments, especially in clay rich soils. The technique can also be of use when searching for graves as any *grave fluid* will be observed as a low resistivity anomaly (Juerges *et al.*, 2010).

Rules of thumb about the depth of use of resistivity vary in the literature: suitable when width or diameter of the target is less than the depth (Healy & Head, 1984); possible detection with standard geoelectrical techniques when depth/radius=5 (Rodriguez Castillo & Reyes Gutierrez, 1992); when depth/target width>2 (from modelling by Johnson (2003)).

2.8.5.1 Considerations

Different results may be recorded at different times of the year because resistivity is easily affected by moisture (however, anomalous subsurface areas may still be detectable). Small size cavities may be hard to distinguish from other environmentally caused variations of the same size. Also, low resistivity could be due to ground saturation from canopy shading of ground (Scott & Hunter, 2004) and might be confuse or obscure deeper results. It is difficult to estimate the vertical extent of voids from resistivity results and resolution decreases quickly with depth, we must increase electrode spacing to increase penetration (Johnson, 2003). It should be noted that there may be a decrease in resistivity with depth below about 10 m. This is not a true measure of the subsurface but a 3D effect, as the electrode spacings get larger the current is more likely to find a less resistive path (through fractures or joints (Roth *et al.*, 2002)).

In practical terms, the length of the profile must be correct for the depth of target which might not be possible on all sites; e.g. to image to a depth of 50 m a pole-dipole line would need to be 400 m (Johnson, 2003). Also the electrode spacing must be adequate, (Buck, 2003) failed to detect a grave target by using a spacing larger than the target (Scott & Hunter, 2004). Also, survey lines must be offset close to the target; (Roth *et al.*, 2002) found that offsets greater than 4 m did not detect voids. Inversion and smoothing add further problems to interpreting voids due to the spread of the signal in 3D (Roth *et al.*, 2002).

2.8.6 EM

Electromagnetic waves travel from the transmitter through air and into the medium. If the medium is conductive, the magnetic component of wave induces eddy currents in the conductor, these then generate a secondary electromagnetic field which can be detected by a receiver. The receiver also detects the primary field that has travelled through the air, and so an overall response is measured. The addition of the secondary wave means a change in the phase and amplitude of the signal with respect to the primary signal – this change reveals details about the subsurface.

Electromagnetic methods are mainly used for horizontally stratified layers. But there has been some use in cavity detection; slingram sources, TimeDomain Electromagnetic and very low frequency have all been used successfully in karst detection often detecting the associated water paths and fractures (Chalikakis *et al.*, 2011); The Time Domain Electromagnetic Method was used to detect variation in conductivity to map changes to the salt layer related to sinkhole collapse (Frumkin *et al.*, 2011); time domain electromagnetic method to map covered deep karst in Greece (Chalikakis *et al.*, 2011); in an industrial setting detecting remains old mine buildings (Bates & Duff, 2006).

In an isotropic resistive medium electromagnetic waves would travel indefinitely. We can calculate an estimate for the depth of penetration by finding the skin depth which is the depth at which signal amplitude has decreased to $1/e$ or 37%.

2.8.6.1 Considerations

Electromagnetic techniques are usually light weight, quick and do not require ground contact. Ground conductivity methods cannot be used in buildings because of ambient noise from mains power lines (Reynolds, 1997).

2.8.7 Seismic techniques

Seismic techniques have been used successfully in cavity detection because the techniques are sensitive to changes in density and in bulk and shear stiffness. However, most techniques are not applicable to the very near surface as the air and ground wave obscure the signal. Seismic techniques are not as limited in penetration as GPR (we can increase the source energy to penetrate deeper) and have the potential for high resolution results (seismic tomography for example). In seismic surveys, identification of voids will depend on, as with other geophysical techniques, the geology and geometry of the void and the surroundings, and the nature of the wave. Voids can offer significantly large density contrasts to the surrounding material and can slow seismic waves, create a drop in frequency of the amplitude spectrum (only shallow voids - (Grandjean & Leparoux, 2004)), act as a diffracting body, mask deeper reflections, or produce attenuation patterns (Grandjean & Leparoux, 2004).

2.8.7.1 Seismic reflection

Seismic reflection surveys use common midpoint stacked sections to identify the amplitude, frequency, and phase anomalies indicative of voids. Miller & Steeples (1991) detected water filled cavities (0.6 m height, 7 m depth) by their variation in frequency in comparison to the surrounding coal seam. Other successful use of reflection includes: Walters *et al.* (2009) identifying tunnels using an automated processing algorithm; high resolution reflection using land streamers (Inazaki *et al.*, 2005) capable of detecting cavities of less than 2 m diameter, at 5-10 m depth. In the U.K., reflection has been used in 2D and 3D reflection seismic to identify the cavities in gypsum responsible for subsidence (Sargent & Goulty, 2009). Higher resolution imaging of smaller voids can be achieved with the use of cross borehole seismic tomography (Louis *et al.*, 2005). Tomography has also been used in mapping old mining areas by identifying the high stress areas of pillars and low stress of collapsed ceilings (Gritto, 2003). Though reflection is well suited to the detection of cavities, seismic techniques can be slow, expensive, and the deployment of geophones can be

impossible in hard ground situations (Tuckwell *et al.*, 2008). Cavities may also be too small in comparison to seismic wavelengths or the variation of mechanical properties in the near subsurface may be too complicated to isolate cavities. The wavelength of incident seismic wave must be smaller than the diameter of the cavity, otherwise very little energy will be reflected (McCann *et al.*, 1987). In the shallow subsurface large amplitude surface waves can easily obscure any features (McCann *et al.*, 1987).

2.8.7.2 Multi-channel analysis of surface waves

Some relatively recent work has been focused on the use of surface wave diffraction in cavity detection (successful feasibility studies of the technique recorded by Luke & Chase (1997) and Xia *et al.* (2007)), especially multi-channel analysis of surface waves (MASW). Park *et al.* (1999) introduced the technique to utilise the dispersion characteristics of Rayleigh waves. Rayleigh waves carry 67% of a seismic waves energy (Woods, 1968) and therefore the much smaller sources (e.g., sledgehammer) can be used. Shots are recorded on multiple channels, and multiple shots are recorded to increase the signal to noise ratio (noise is problematic in urban areas). The shot record is converted by a wavefield transformation to a dispersion image (frequency vs. phase velocity) showing the accumulation of energy from the wavetrains (Figure 2.18). Dispersion curves are extracted from the image based on the energy trends depicted, allowing the effective removal of body waves (Xia *et al.*, 2007). The inversion of these curves supplies the depth variations of shear-wave velocities (V_s) at the centre point of each record. Shear-wave velocities values can be used as an indicator of stiffness, to calculate Young's modulus, or interpolated to create 2D or 3D maps.

The depth and resolution of MASW is dependent on the subsurface complexity and the survey parameters. Depths of up to 50 m can be achieved if a large source (20 lb) and a receiver spread of 150 m are used (Park Seismic, 2010a). Resolution will be improved by a small receiver spacing and a small move of the entire setup after each gather. When compared to borehole data the error associated with shear-wave velocities found using MASW is approximately 15% (Xia *et al.*, 2000).

Using MASW in cavity detection has had mixed success. We can expect to find an area of low velocity using the technique, indicative of a cavity or a collapsed cavity. A survey for voids under paving slabs found that the thick paving trapped much of the signal, leading to the incorrect interpretation of only one void (Trainum, 2006). Historic mines of depth 30-45 m were detected as a distinct region of low velocity and correlated well with the locations on historical mine maps and with drilling (Figure 2.19). Nasser-Moghaddam *et al.* (2007) showed a concentration of energy in the frequency domain, as well as amplitude increase on

the seismic traces, in the vicinity of 50 m depth voids. It was found that the width of the energy was a good estimate for void width.

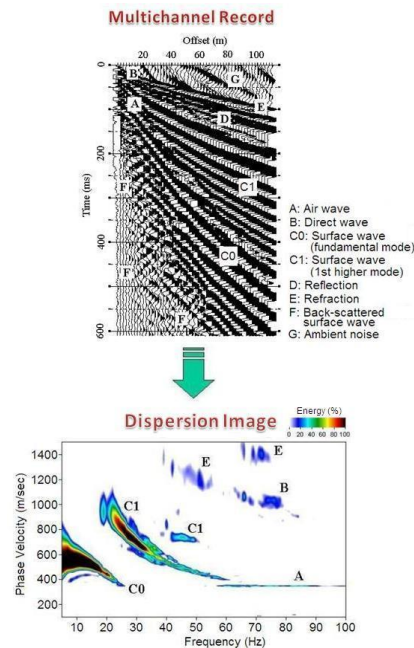


Figure 2.18. Wavefield transformation of one multichannel record to a dispersion image showing the energy accumulation of seismic waves (Park Seismic, 2010b).

2.8.7.3 Other techniques

Cross hole tomography can find caves but requires deep boreholes so is not often suitable for near surface (Waltham & Fookes, 2003).

Seismic refraction is usually used for depth to bedrock analysis but can be used to detect large object using low frequency.

Near surface geophysics problems have never had the financial investment afforded to the oil, gas and mining industries. Most techniques used in near surface geophysics are borrowed and adapted from their original exploration purposes. This is particularly true in seismic methods. The primary technique used in exploration, industry is constantly improving and inventing new niches in the seismic method. Many of these techniques are applicable to near surface geophysics and some to cavity detection, though very little testing has been completed. A number of cutting edge techniques may be applicable in the pursuit of a technique for deeper near surface cavity detection (greater than 20 m).

Shallow S wave seismic reflection: Shear waves are generally limited to borehole and refraction use. For small targets, such as some cavities, S-waves offer a higher resolution than P-wave, and have been suggested to resolve targets less than 1.3 m (Sloan & Harris, 2010). S-waves also offer better results in areas of unconsolidated, saturated shallow sediments (where P-wave velocity is much faster).

ConsoliTest: An adaptation of the MASW pioneered by (Park *et al.*, 1999), the ConsoliTest (Westerhoff *et al.*, 2004) uses surface waves to determine the shear wave velocity profile of the subsurface. The ConsoliTest has been specifically developed for use in unconsolidated sediments and for areas with complex alternating strata where the MASW technique inversion process struggles. MASW has been successful in detection of cavities (Billington, 2006) though not tested in a variety of environments. Problems could include resolution limitations with smaller cavities, the complexity of the inversion, and access to the software.

Seismic attribute analysis: The establishment of mathematical relationships between traces of a section and application to specific attributes. Similarity and variances attributes may be used to detect low amplitude patches indicative of cavities, or reflection strength attributes may indicate the large reflection contrast between the cavity and the surrounding strata. However, the technique is complex (neural networks required), slow (1-2 days processing for each attribute, 3D data is better) and expensive software is required.

2.8.7.4 Considerations

General limitations of seismic surveys include the site not being able to accommodate the length of survey required, number of geophones available and using the correct source. (Nasseri-Moghaddam *et al.*, 2007) suggest a maximum depth of 30 m for void detection as the longer wavelengths required for these depths are hard to generate with high signal to noise ratios. In terms of very shallow targets seismic surveys can't see less than 3 m because there is too much noise from the ground roll (Rick Miller, 2013). If a cavity depth is greater than its diameter, the resolution of refraction results may be too low and may not be detectable at all if the halo system is less than 6 m (McCann *et al.*, 1987). If the subsurface is dry, high attenuation of energy means that voids less than 20 m in width will not be detected (Bell, 2004). If the bedrock is shallow and irregular surface, seismic reflection methods do not provide reliable data (Roth *et al.*, 2002).

As the surface wave technique is a relatively new technique, interaction of Rayleigh waves in voids are still not fully understood in all settings. In scaled lab tests Grandjean & Leparoux (2004) found Rayleigh waves performed poorly in cavity detection below 0.2 m which scales up to a real world depth of 2 m. Seismic surface waves only offer resolution of a few metres in lateral and vertical directions (Laake & Strobbia, 2012).

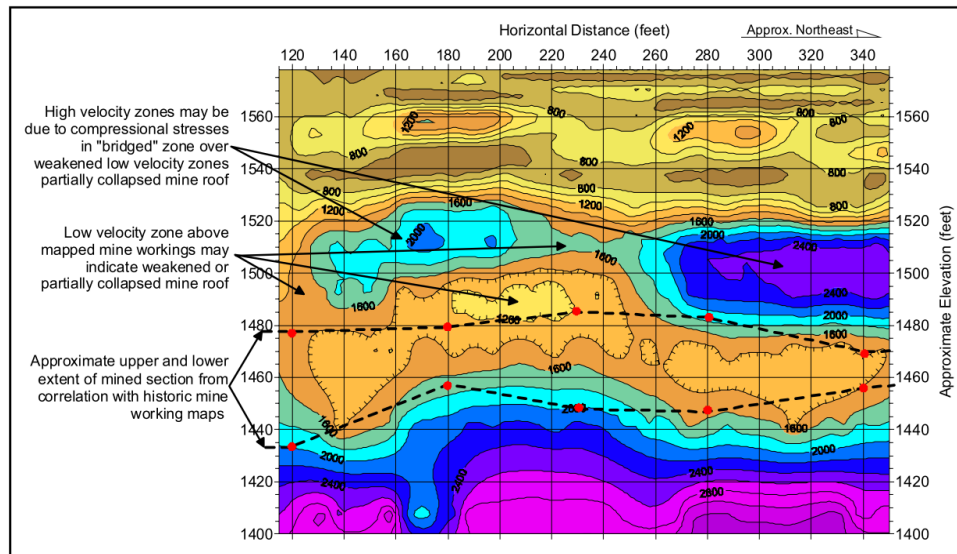


Figure 2.19. Shear-wave velocity model for historical mines in Minnesota. Velocity values are in feet/second (Billington, 2006)

2.9 Choice of technique

Technique choice is a key issue in cavity detection and is the major point of this research. Geophysics has been proven successful in cavity detection (Section 2.8) but only if the correct technique is chosen relevant to the site. Factors affecting the possible detection of voids are so numerous it is impossible to choose a single, or combination, of geophysical techniques that will work universally - there is no *silver bullet*. Each case must be looked at individually, to evaluate a fair compromise of resolution, penetration and accepted ambiguity, as well as the more practical factors of time and budget constraints. For geophysics to be trusted within the engineering industry a robust method for choosing and utilising geophysical techniques must be found.

Of utmost importance to technique choice is a site investigation study. The physical properties of the subsurface area of study and likely properties of the cavity must be found. McCann *et al.* (1987) suggest finding estimates of the physical properties to at least an order of magnitude to give an idea of the expected contrasts. These details may be found by desk study or from boreholes drilled in the initial site investigation. The resolution required must be found which will include the common compromise of depth against resolution. The amount of information required is of great importance - do we want to just map the location of the cavities or do we need to know details about the depth and geometry of the cavity? It will be useful to give a likelihood of detecting cavities in the given situation. If cavities are expected beyond the depth of penetration of a given technique, or are smaller than the technique resolution, other options must be considered (e.g., cross borehole techniques).

The popularity of geophysical technique for cavity detection has changed through time and is dependent on region (Butler, 2008). Appendix C collects various authors preferred techniques for cavity detection, often regardless of situation, with fairly varied conclusions though the most popular techniques seem to be: GPR, resistivity and microgravity. Of course, we must consider the site situation and some workers have compared techniques in a number of environments and made suggestions based on their results. Using resistivity, magnetic, gravity and EM in cavity detection in sandstone, Chamon & Dobereiner (1988) found microgravity to be the only successful technique. Butler (2008) considers microgravity, EM, GPR and resistivity the best techniques in karstic environments. A hypothetical example of an air cavity in limestone in McCann *et al.* (1987) stated there would be little resistivity contrast with resistivity methods, P-wave may be attenuated, S-waves may have too long wavelengths, gravity would work only if the limestone was homogenous, GPR could penetrate greater than 5 m, and a magnetic survey may only work if mining material was present. In the same situation but with rain and 1-2 m of alluvium soil this would be very different: the moisture in the limestone would aid resistivity detection, drainage above the cavity could be detected by low frequency EM, P-wave refraction may show velocity perturbations, but the soil may obscure gravity results and attenuate the GPR. These simple hypothetical examples show the variation of success is very dependent upon the geology, and also how a small change in the situation (here rainfall) can completely change the choice of technique.

Here, it is suggested that a more discerning method of technique choice should be encouraged, taking into account the geology, potential cavity size and the noise level. Initially we approach this by comparing more results in the literature, and then by the application of numerical modelling to the problem. Practically, we must also consider the size of the site, the time and budget available, and limit our techniques based on these factors. Brownfield sites offer further constraints on the use of techniques; services, buildings, access, complex, disturbed subsurface and surface covering, all make geophysical application difficult.

2.10 Cavity detection database

To assess the current uses of geophysics in cavity detection and the comparison of techniques used in different environments, the relevant literature was studied in depth and a database was created showing the uses of geophysical techniques and their potential for success in various environments (GPR example in Appendix A). This highlighted the particular strengths and weaknesses of the techniques. Technique survey parameters used in various geologies were compiled to add detail to site specific survey design (GPR example in

Appendix B). Attempts to access data from geophysical companies around the globe, and in particular in the U.K., for comparison and championing of good practice was mostly unsuccessful due to client privacy issues.

Figure 2.20-Figure 2.21 show the depths and sizes of cavities detected using GPR and the frequencies used. It is seen that the technique is used mostly to detect cavities within the first 5 m of the subsurface. Only much larger cavities are detected deeper or those within karstic environment. This confirms the attenuation of GPR within most environments (especially clay rich). Most cavities are detected in karstic environments, again due to the low attenuation. As can be seen much deeper cavities were detected with the lower frequency antenna. Over 100 MHz no cavities below 5 m were detected. However below 100 MHz cavities up to 20 m depth were detected. This is because attenuation of GPR signal is greater at these higher frequencies.

Although the database showed that some techniques were suited or unsuited to particular environments (GPR and resistivity in karstic environments; gravity used to detect air cavities), the database emphasised that cavity detection technique choice is very site dependent.

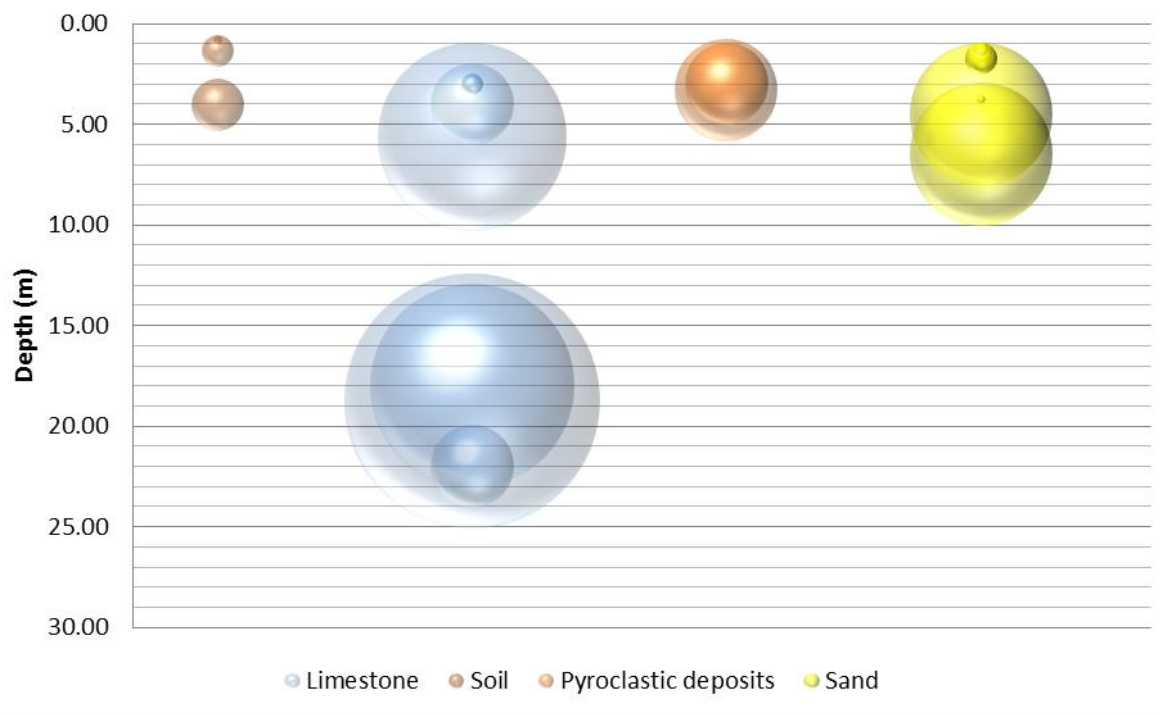


Figure 2.20. Cavities successfully detected using ground penetrating radar in different geologies compiled from academic literature (Appendix C). Balloon size represents the largest cavity dimension (scale is equal to the depth axis). Only cavities with all of the following information were used: cavity size, depth and surrounding geology.

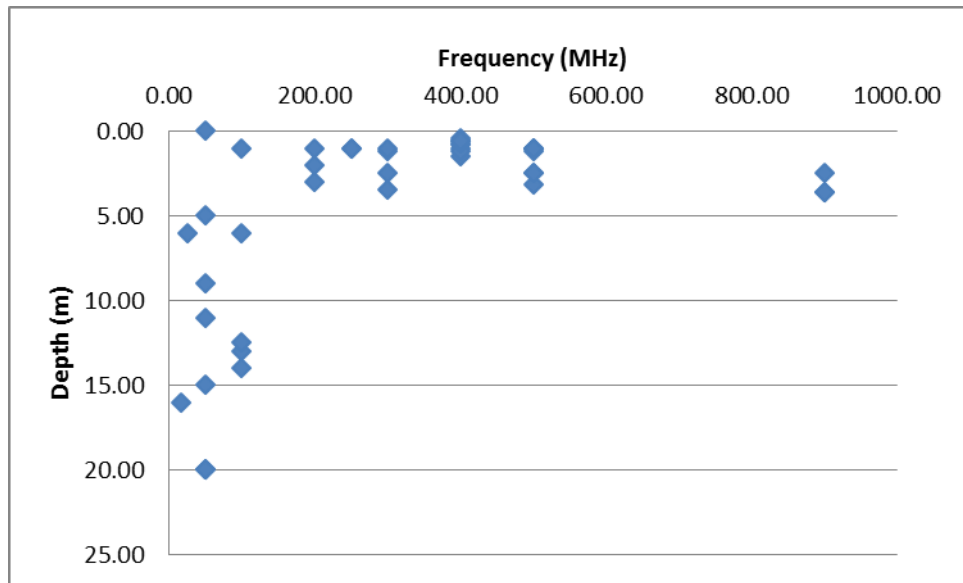


Figure 2.21. Depth of cavities detected and the antenna frequency used. Data is from recent literature on cavity detection (Appendix C).

2.11 Generalised protocol for U.K. cavity detection

Though a *silver bullet* technique is sought in the detection of cavities, in some circumstances the best use of geophysics is to utilise complementary techniques. These techniques can be applied simultaneously (as with the recent popularisation of carts/chariots carrying numerous pieces of equipment) or in succession, gradually increasing the resolution. The latter offers greater variety and option of adaptation in the field depending on site specific requirements.

Having reviewed the literature, and through analysis of the successes and problems encountered during my own field work (including magnetic noise, GPR attenuation (see Chapter 8)), a general protocol for geophysical detection of cavities (particularly in the U.K.) was realised (Figure 2.22) based on a previous protocol by Pueyo-Anchuela *et al.* (2010). This process involves the informed choice of successive, complimentary techniques that work to gradually increase the resolution of the subsurface and cavity structure.

An initial, detailed desk study can aid targeting areas of potential cavities, saving time, and later help to confirm any results interpreted. The two major considerations are the noise levels of the site, and the budget and time available to the project. An urban setting (geophysically noisy) limits the use of a number of techniques for various reasons (magnetometry - magnetic noise; seismic and resistivity - impenetrable surfaces; GPR - surface reflections). Budget and time clearly limit the amount of techniques utilized and the survey parameters chosen.

Techniques should be chosen to detect different properties of the cavity and thus their use together will strengthen the case for cavity presence or reveal further details (geometry, depth, surrounding material, cavity makeup). As sites are commonly large, the first technique may be rapid, covering the whole site and detecting areas of ambiguity and possible cavities. Both electromagnetic and magnetometry suit this purpose as they can be applied at walking speed. The choice between the two will depend on the site: noise level (ferromagnetic material), conductivity and the specific target.

The second technique should focus on any anomalous areas found with the first technique using a suitable higher resolution technique. This technique will provide us with more detail about a subsurface parameter (seismic – density, elastic moduli; GPR - dielectric constant, conductivity; electrical resistivity - resistivity). Again choice will be dependent on site conditions, but GPR (still with the choice of frequency), seismic, or resistivity may be suitable. Any further techniques should focus on assessing the size, makeup and geometry of the cavity. Higher frequency GPR, or microgravity can provide direct information about the cavity. By combining these complementary techniques we can delineate the cavities across the site.

- 1) *Broadly cover the area to identify any anomalous areas of interest.* This technique must be fast to cover large areas quickly. In areas of suspected mining magnetometry is a good first choice because old mining materials will create a distinct, and strong, anomaly. In urban areas shielded GPR may be the only option. These techniques may not detect the cavities directly but rather indications of possible voiding such as the ferrous material associated with mining or the change in water flow above regions of cavities.
- 2) *Analysis of structure of subsurface at anomalous areas.* This stage of the process aims to reveals the location and depth of regions of the subsurface with properties different from the surrounding material, and those properties that are indicative of voids. The properties of contrast found using these techniques (dielectric constant, wave velocity, resistivity) will be different to those found in stage one (susceptibility, conductivity) and will therefore corroborate any findings and will not be influenced by the same noise limitations. Each technique has its limitations and the choice must be made on both the site conditions and the results from stage 1.

A very useful exercise here is to take a conductivity reading of the site in general (an EM survey will have already achieved this). If the conductivity is below 0.01 S/m, a GPR survey may be of use, above this value it is unlikely any useful results will be obtained and another technique should be used (Kathage, 2010). Other techniques available include seismic (MASW, reflection) and electric (resistivity).

- 3) *Cavity dimension measurements.* Precise knowledge of their dimensions and volume aids construction design and remediation.

By this stage the location, depth and size of possible cavities should be known. Precise knowledge of their dimensions and volume aids construction design and remediation. In order to achieve this 3D image microgravimetry can be used. The technique is slow but instrumentation is very accurate, and survey size should not be too large as we have already delineated cavity positions. Accurate data processing becomes arduous in urban areas where we must correct for every surface object of significant mass. We can use models, utilising the information from the previous stages (gravity anomalies are non-unique), to accurately map locations, depths and volumes of cavities (Styles *et al.*, 2005; Tuckwell *et al.*, 2008). Other techniques available at this stage, though only offering indirect measurements of the cavity system, include higher frequency GPR if the target is fairly shallow (Kinlaw *et al.*, 2007), or cross borehole seismic tomography (Louis *et al.*, 2005). All of these techniques would require very accurate measurements and high resolution survey parameters to achieve cavity geometries.

The proposed routine was still very general and led to the conclusion that continuation of the project should involve discriminate cavity detection technique choice on a site by site basis depending upon site conditions and cavity type.

2.12 Current use of modelling in near surface geophysics

In seeking the best techniques for cavity detection, relying on past field use is highly inefficient. As has been seen, subsurface and surface characteristics vary greatly from site to site, and so techniques which can be applied to one site may not be applicable on another. This approach also limits itself to site conditions which have already been encountered. Cavity detection on brownfield sites is limited in the literature and so best technique choice is still uncertain. Physical testing offers an alternative but it is often impossible or at least prohibitively expensive to utilise for every site condition. Modelling offers the opportunity to vary site, subsurface and cavity conditions to endless scenarios for little cost.

Modelling is used in two ways in geophysics. Forward modelling is the technique of calculating a mathematical, theoretical response to a given constrained model. The parameters, shape and size of the model are known previously. Inversion is the process of matching geophysical measurements to a geological model using an iterative process. Forward modelling is therefore a vital part of the inversion process. Most of the work done in geophysical modelling is used during inversion, with little use of modelling prior to field work in near surface geophysics.

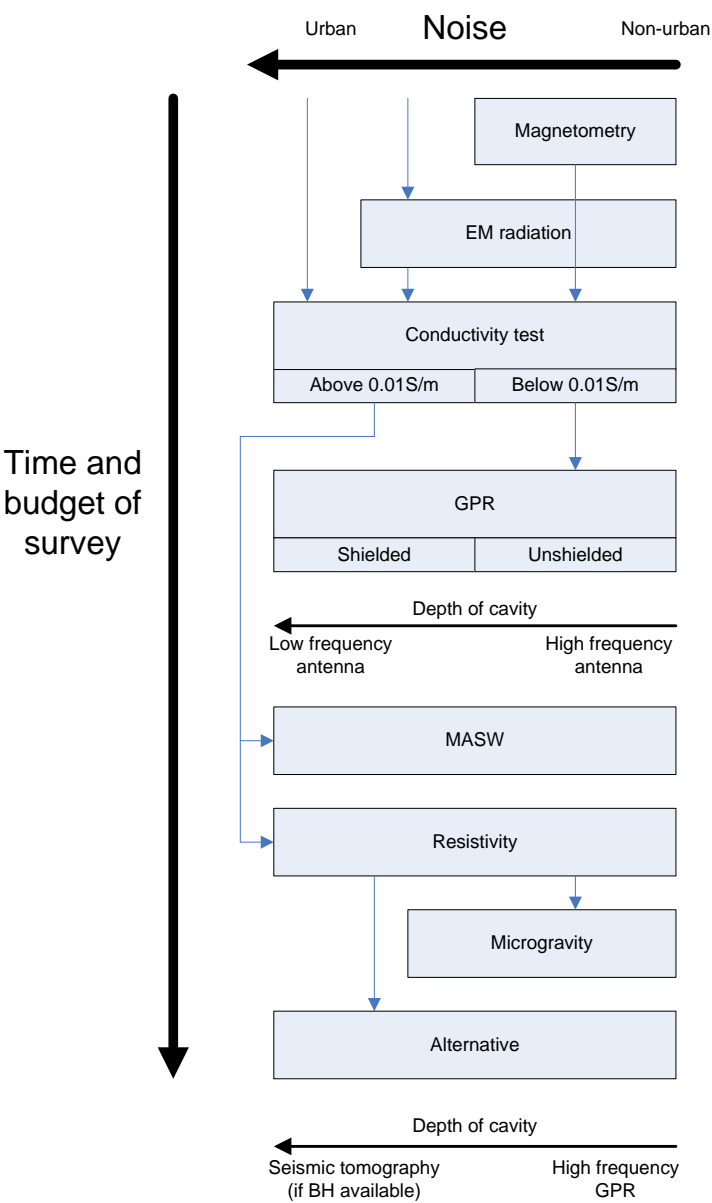


Figure 2.22. Proposed geophysical routine for cavity detection in the U.K. N.B. this routine must be adapted for each site and does not replace a desk study and experienced geophysicist. After Pueyo-Anchuela *et al.* (2010).

In potential modelling techniques the theoretical field that results from a subsurface object is calculated. Progress has been made from the calculation of analytical solutions of simple prism shapes (see, for example, Parasnis (1996)) to more complicated shapes by dividing arbitrary shapes into prisms. This was completed in two important publications by Manik Talwani: the gravity method (Talwani & Ewing, 1960) and magnetic method (Talwani, 1965). Later, the field resultant from a uniformly magnetized polyhedron was computed through calculation of the volume integral of dipoles over the surfaces (Barnett,

1976) and then line integrals (Singh & Guptasarma, 2001). This allows the calculation of the potential magnetic field of any given polyhedron shape at any point on the surface.

Though a recently adopted technique, there have been a range of methods of modelling ground penetrating radar. Ray tracing modelling calculates the ray path of an electromagnetic wave as it propagates from the transmitter through the subsurface to the receiver following Fermat's principles (e.g. Cai & McMechan (1995)). Finite difference time domain methods are well suited to GPR modelling as a range of frequencies can be incorporated, but the technique is computationally slow (e.g. Roberts (1997); Uduwawala & Norgren (2004)). Finally the radar range equation offers a simple analysis of signal amplitude losses in a given environment (Daniels *et al.*, 1988); this is discussed further in Section 4.1.3.

2.12.1 Finite element method

With advanced computer power, Finite element method simulation has become a more popular as a way of modelling complex subsurfaces. Although analytical solutions, like those discussed above are adequate and efficient for simple bodies, for more complex heterogeneity the finite element method can approximate the solution and can be more efficient. Finite element modelling works by breaking down complex bodies of varying geophysical parameters into smaller blocks, each with an individual geophysical parameter. Each of these simple blocks is modelled and combined to approximate the solution to the whole system.

This approach has been used frequently in geophysical modelling, particularly in geophysical flow studies, but also in other work more closely related to near surface geophysics. Sasaki (1994) used the finite element method for 3D resistivity inversion. Mallick and Sharma (1999) used the method to model a regional gravity anomaly, as do Cai and Wang (2005). Zerwer *et al.* (2003) used the method to model Raleigh waves in near surface discontinuities. There appears to be little in the literature using the method to model cavities specifically.

The finite element method could be applied to cavity modelling at different of levels of complexity. The cavity itself could be modelled in any shape, allowing the typical cavities shapes discussed to be modelled and indeed more complicated shapes. It could also allow variation in geophysical parameters within the shape. The approach could also be used to represent variation with the geological background.

2.12.2 Software available

There are numerous software programs available to model a range of geophysical techniques. Here we look at the key techniques that are used to detect cavities and summarise the commonly used software and the approach of previous modellers.

2.12.2.1 Magnetic and gravity

Magnetic and gravity are often seen in the same software. Potent is a package by Geophysical Software Solutions (www.geoss.com.au) that models magnetic and gravity in 3D. Various 3D subsurface shapes can be modelled in combination, and so typical cavity shapes are possible. The method used is similar to that described above, based on the field component normal the prism. Unfortunately, the software is not free and it is not possible to adapt to include other techniques.

Pblock and Pdyke are freeware versions of these software but only offer modelling in 2D and only rectangular prisms. As such typical cavity shapes cannot be modelled and we cannot get a sense of the anomaly across the site (essential for detection probability calculations). The modelling method is based on anomalies for a semi-infinite slab.

GeoModel is freeware software created by Gordon Cooper at University of Witwatersrand. It offers simultaneous gravity and magnetic forward modelling. Unfortunately, the modelling is only available in 2.5D and so is not possible to model typical cavity shapes of finite size and it is also not possible to model the anomaly size on survey lines across the site.

Another similar piece of software is GravMag from the University of Colorado (cires1.colorado.edu/people/jones.craig/GSSH/002-GravMag). Again the software only allows modelling of simple shapes in 2.5D.

Mag2Data (Stocco *et al.*, 2009) is a MATLAB based program for 2D magnetic modelling and inversion. It allows modelling of 2D shapes made up a collection of prisms. The modelling algorithm is based on the analytical solution to a 2.5D model (as in Telford *et al.* (1990)). It is therefore possible to build the typical cavity shapes and, because the code is in MATLAB, it is possible to adapt the code to suit the needs of this project. Unfortunately, again, it only allows 2D modelling.

Mag3D and Grav3D are produced by University of British Columbia (https://gif.eos.ubc.ca/software/main_programs) and offer FORTRAN based 3D modelling of both techniques. The algorithm works in a finite element way, by dividing the subsurface into 3D cells and assuming constant geophysical parameters in each. Although it may be free to universities, for commercial use, a licence is required. Since the main target of this project is engineering companies, the barrier of a licence may limit the user base.

2.12.2.2 Electromagnetic

Geophysical Software Solutions also produce electromagnetic software called EM-Q which models transient electromagnetic anomalies. Unfortunately, it is currently only

possible to model only a sphere or a dipping sphere and so typical cavity shapes cannot be modelled.

2.12.2.3 Resistivity

RES3D and RES2D (Loke, 2011) are well used software for forward modelling of resistivity using finite difference and finite element methods. Although this is freeware, it is a self-contained and therefore not adaptable to allow inclusion of other techniques or to include the calculation of detection probability.

FW2_5D (Pidlisecky and Knight, 2008) is 2.5D resistivity model based on Dey and Morrison's (1979) technique which calculates the potential about a point source in a half space. The code is written in MATLAB and it is therefore possible that the work could be incorporated into this project. However, as it only models 2.5D we cannot model the anomaly across the site.

2.12.2.4 GPR

Reflexw is a popular near surface GPR software by Sandmeier (www.sandmeier-geo.de/reflexw.html). It is commonly used for processing and interpretation but does not have a finite difference simulation element as well. This is a very useful way to model simple shapes in the subsurface, but requires a licence and is not adaptable.

gprMax (www.gprmax.com) uses the Finite Difference Time Domain method to simulate GPR. This method provides flexibility and accuracy in the response of GPR to various subsurface anomalies. The software is open source but not easily adaptable to meet the needs of this project.

2.12.3 Software requirements

The key requirements for this software are to model the most commonly used geophysical techniques over typical cavity shapes and to calculate the detection probability for each of those techniques. To be able to do this, the modelling techniques need to all be 3D. This rules out quite a lot of the available software and modelling approaches.

It is also important that the software output provides simple, clear comparison between techniques over the same cavity. This means all techniques will ideally be modelled within the same environment. Most of the current available software models only individual techniques (or two in the case of the potential methods). It is therefore better to incorporate individual techniques into the same programming language. This way all the techniques can be modelled at the same time with shared inputs and additional techniques can be added to the software if required at a later stage.

Ease of use is of paramount importance. It is hoped this software will be used by people of a range of geophysical experience and ability. A key user group is geotechnical engineers. These users will be very familiar with some of the parameters associated with geophysical techniques but not with the techniques, survey design or with geophysical results themselves. Therefore the software needs to be usable with little prior knowledge of the techniques and should therefore have a simple user interface.

The modelling approach for each technique should also be as simple as possible while still fulfilling the requirements of the project. If this is achieved it will be much easier for users to understand and adapt the code if particular circumstances require. This adaptation could be changing the parameters that are not shown on the user interface or adding extra functionality. Modelling simplicity will also ensure that the software runs quickly. Modelling techniques such as the Finite element method are appropriate but since there are simpler analytical modelling techniques that meet the project requirements, these are preferred. If the requirements of the software alters in the future, these more complicated methods should be considered.

These factors were considered when choosing the modelling approach for each technique and the layout and functionality of the software. The final approach used is described in detail in Chapter 4.

2.13 Chapter Summary

This chapter has outlined the current understanding of cavities and the potential hazard they present. This information is vital in making sure that the modelling process captures the typical cavity conditions that may be found on a site. As modelling of these cavities is the key aim, focus has been placed on the practical aspects of the cavities, such as size and makeup.

A key aspect of this Chapter is the discussion around current cavity detection techniques and their limitations. It is clear that the current approach, though useful in some situations where the subsurface conditions are well known, is outdated and certainly not optimal for most sites. This Thesis proposes that geophysics be used before or alongside such techniques in the aim of producing a much clearer picture of the subsurface in a more efficient way. However, in order to convince geotechnical engineers that geophysics is a viable option, proof of concept and improved utilisation of geophysics must be sought. It is hoped that the modelling approach here will improve technique choice and consequently improve the success rate of cavity detection surveys. The software aspect will also allow the engineers themselves to understand the key drivers in survey success.

A sizable part of this Chapter is devoted to understanding the current state-of-the-art geophysical approaches to cavity detection. By reviewing the most popular techniques and their ability to detect cavities of all types, we can make an informed decision as to which techniques to model in the software.

The current use of forward modelling for survey parameter optimisation is very limited in the literature, especially on brownfield sites that are typical in the engineering industry. Here, it is suggested that forward modelling before embarking on a survey is of great importance, especially so when hoping to detect cavities which have such small associated signals. It is noted that there is no comparison package available currently that helps in the technique choice for any near surface survey and certainly none that aids cavity detection.

Chapter 3

3 Methodological framework

The literature review highlighted the importance of detecting cavities on site, not just in terms of the hazards they represent but in the limitations they place on construction. Cavities remain an ever important consideration in risk reduction and foundation design. Current techniques were shown to be slow, intrusive and give an incomplete picture of the subsurface. As discussed, the benefits of incorporating geophysics into site investigations are manifold. However, geophysics still has an uncertain reputation in the industry because of experiences with failed surveys.

An informed survey should involve smooth integration of geophysics (Figure 3.1). Here, we propose that geophysical modelling is an important element of successful integration. The modelling presented will inform correct technique choice and aid successful application of geophysics. Modelling after the desk study and initial soil sampling can inform the parameters associated with the site and increase modelling accuracy. After modelling the geophysical techniques, users will have a better understanding of the applicability of geophysics to a particular site. A site specific survey can then be designed and carried out,

followed by informed intrusive investigations and interpretation using both geophysical and geotechnical data.

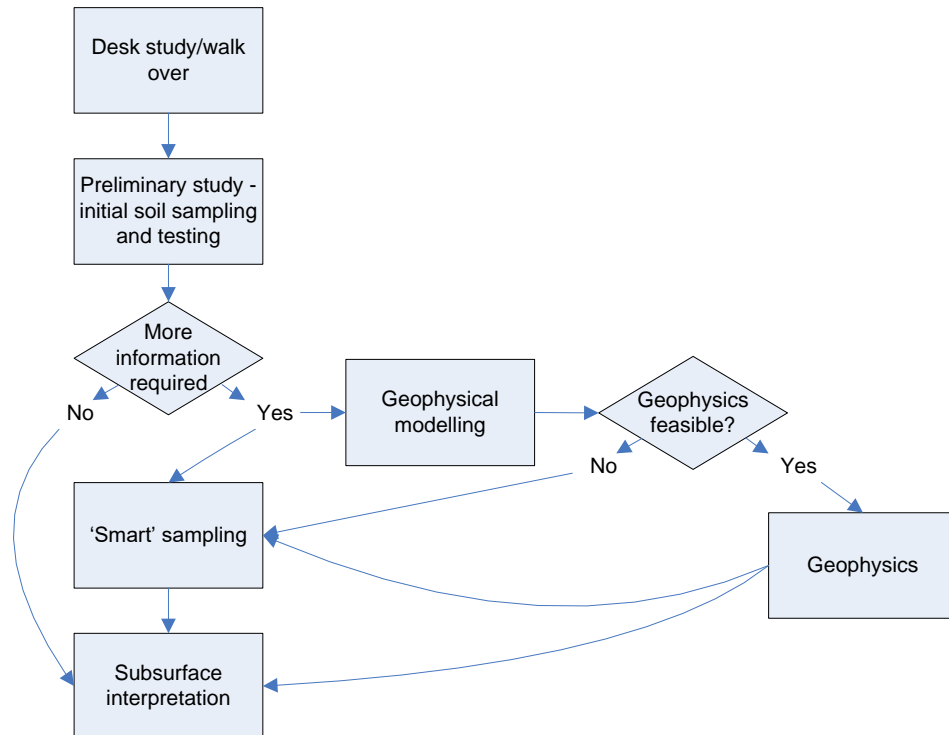


Figure 3.1. Proposed integration of geophysics and modelling into site investigation.

3.1 Modelling approach

Correct choice of relevant geophysical technique or techniques is vital in the success of a cavity detection survey. Particular geophysical techniques are more applicable to certain environments and cavity dimensions and depths than others. Currently technique choice is largely informed by experience and knowledge. However, the increased popularity and ease of use of geophysics means more less experienced users are designing surveys and may choose inappropriate techniques.

'Rules of thumb' can be of use and are usually grounded in theory but too often are not used in conjunction with or presented alongside any intended constraints. Additionally, these rules vary vastly from source to source. In gravimetry, it is suggested that cavities can be detected when depth to diameter ratio is 8–10:1 (Butler, 2008), 2:1 (McCann *et al.*, 1987), 1:1 (U.S. Army Corps of Engineers, 1995) or when depth is less than 1.5 times the width or diameter (Healy & Head, 1984). 'Rules of thumb' provide a tempting but inherently simplistic approach to a feasibility assessment where modelling and subsequent assessment provides a more accurate alternative, with the advantage of applying site specific

parameters. Modelling minimises dependence on rules of thumb and informs correct, efficient and effective use of geophysical techniques.

A more robust approach to technique choice is sought. Here, near surface geophysical modelling is proposed as a useful tool for assessing the feasibility of a range of techniques to detect subtle signals such as those associated with cavities. By comparing the theoretical geophysical response to typical noise values associated with the instrument or with typical site conditions the probability of detection can be assessed. This step is rarely applied in survey planning and, as such, surveys are completed, both in industry and in academic studies, with no hope of target detection.

To this author's knowledge no comparative software exists to aid technique choice. Also, previous single technique modelling software limits the shapes of bodies and hence typical cavity shapes are not represented.

3.2 Modelling method overview

A number of factors affect the likelihood of cavity detection, broadly these are: depth of target, distance from target, size of target, surrounding geology, cavity makeup, technique utilised, survey parameters and noise level and approach used, and, most importantly, signal to noise ratio (SNR). This complexity means prediction of the geophysical response to a particular cavity is difficult but with modelling the theoretical response of different techniques in endless subsurface scenarios can be assessed.

The cavity modelling software presented here requires user input (through a graphical user interface) of known variables acquired from a desk study, a site investigation or estimated from similar sites in the literature. Parameters of interest include:

- Local geology
- Cavity: Size, depth, shape, makeup, lining and cap
- Noise level (manmade/natural)
- Constraints: Time, budget and techniques available, data deletion percentage

Using these parameters, the subsurface is modelled with the relevant geophysical parameters for each technique (taken from measured values of materials in the literature). The response from a range of geophysical techniques is then simulated. The detection probability for a range of techniques is then calculated. These results are used to inform the choice of technique and improve survey design through finding optimal survey parameters to use in that particular example.

Chapter 4

4 Cavity modelling

4.1 Modelling techniques

Five geophysical techniques are compared: gravimetry, gravity gradient, magnetometry, magnetic gradient and ground penetrating radar (GPR). Gravimetric methods were chosen for analysis as they are ranked the most commonly used and preferred method of cavity detection in Europe and third most popular in the U.S. (Butler, 2008). Similarly, electromagnetic methods (including GPR) are the most preferred in the US and second in Europe (Butler, 2008), despite the limitations of penetration in conductive media. Numerous other sources highlight the applicability of these two techniques to cavity detection and offer examples of their successful application (e.g. Reynolds, 1997; Sharma, 1997; Anderson & Ismail, 2003). Magnetometry is less commonly associated with cavity detection as the susceptibility contrast between most geologies and an air or water filled cavity is very small. However, it is possible to detect such a cavity if the noise level is low enough (Manzanilla *et al.*, 1994; Rybakov *et al.*, 2005; Chamon & Dobereiner, 1988). Also, magnetometry is often used to detect filled natural cavities (Saribudak, 2001; Mochales *et al.*, 2007) and especially cavities associated with mining where the discarded ferromagnetic material is often used to

fill shafts, or caps and lining are installed (Pueyo-Anchuela *et al.*, 2010; Raybould & Price, 1966). Magnetometry is therefore worth considering when attempting to detect cavities, and is hence compared with the other techniques.

A subsurface model of the relevant geophysical parameters for each technique is created and the response from a range of geophysical techniques is modelled. Numerous modelling techniques have been incorporated into MATLAB and tested. Techniques ranged from analytical techniques of very simple shapes, to 2, 2.5 and 3 dimensional numerical modelling. The most important aim was to represent the typical cavity shapes found in underground cavities (section 4.3.2.1) and to model in three dimensions to allow calculation of detection probability over a range of survey parameters were of highest importance in choosing an appropriate modelling algorithm.

However, it was also important to use modelling techniques that all work within the MATLAB environment (so comparisons can be made) and that are computationally efficient.

4.1.1 3D

Cavities were modelled in three dimensions to allow variation of the survey parameters (profile and survey point spacing). From these values the most efficient survey parameters to detect a given cavity can be later calculated. This is new work as previous cavity modelling focused on sphere or cube shapes and most often in just 2 or 2.5 dimensions.

4.1.2 Potential methods

Gravity and magnetic fields are naturally occurring and so their measurement is passive. Techniques which measure these fields are known as potential methods. Magnetic and gravity fields can be understood by similar representations: gravity force from a point mass, and magnetic force from a magnetic monopole. The magnitude of the anomaly over a body is dependent on the density or magnetic susceptibility contrast of the body to the surrounding material. However, a magnetic anomaly is also dependent upon the orientation of the magnetic field and the object and is hence a more challenging prospect.

Although analytical solutions to gravity and magnetic anomalies of spherical and cylindrical shapes are well established (Parasnis, 1996), more complex shapes are required to represent the most common cavity types (Figure 4.3). Addition of spheres and cylinders can go some way to representing complicated polygons (gravity method (Talwani and Ewing, 1960); magnetic method (Talwani, 1965)), but in the very near surface the resultant disparity in anomaly size and shape will be of importance to the detection probability. A more suitable method is modelling the potential field of a polyhedron made up of any number of polygons, allowing flexible creation of all the typical 3D cavity shapes.

4.1.2.1 Magnetometry

Initially, the theoretical magnetic anomaly of a sphere was considered, following Parasnis (1996) (Appendix Ai). The clear limitation being the mismatch between a sphere and the typical cavity shapes researched (Figure 4.3). A further iteration was considered in 2.5 dimensions (meaning infinitely uniform in one direction). Won & Bevis (1987) created code in Fortran to compute anomalies in magnetic field over a 2D polygon (with infinite strike) based on theory by Talwani *et al.* (1959). The polygon can be of any shape with straight sides. This code was translated into the MATLAB environment (code in Appendix Aii) and tested against analytical methods for accuracy (Won & Bevis, 1987; Becerra, 2004). The limitation to two dimensions inhibited the use of survey parameters. The requirement of 3D modelling and flexible cavity shapes limits the algorithm choice but Guptasarma and Singh's (1999) modelling of a polyhedron made up of any number of polygons was suitable. More recently the theory was updated to three dimensional modelling of a polyhedron made up of any number of polygons (Guptasarma & Singh, 1999). This theory is based upon proving the equality of the magnetic field of a polyhedron and the field of the surface distribution of magnetic pole density equal to the normal component of magnetisation intensity. In practical terms this polyhedron field is calculated by translating each polygon face surface integral into a line integral of the face edge. This method allows the use of any shape cavity, providing the cavity can be created by flat face polygons, and so was very applicable to this work. The algorithm was incorporated into MATLAB code and tested for accuracy against analytical solutions (Parasnis, 1996; Singh & Guptasarma, 2001).

4.1.2.2 Gravity

Gravity modelling is simpler than magnetic modelling as the anomaly is only dependant on the density contrast and geometry of cavity. Following Equation 4.1 (Lillie, 1998) MATLAB code was created to model the gravimeter response to a subsurface sphere (Appendix Aiii)

$$\Delta g_z = \frac{4\pi R^3 G(\Delta\rho)}{3} \frac{z}{(x^2 + z^2)^{3/2}} \quad \text{Equation 4.1}$$

Δg_z = vertical component of gravitational attraction (as in that measured by a gravimeter), R=radius of sphere, G=gravitational constant, $\Delta\rho$ =change in density, z=depth to sphere, x=distance to sphere.

Though possible to use in three dimensions, more complicated shapes were required. The (Guptasarma & Singh, 1999) magnetic theory utilised can be adapted to gravity use. In a similar approach to the magnetic method, we consider the field due to the distribution of surface mass density to be equivalent to the field of the uniform density polyhedron. The

surface mass density is calculated on each face by the product of the body volume density and the scalar product of the unit vector normal to the face and the direction vector of the face to the current observation point (proof for the equality in Singh & Guptasarma (2001)). This technique allows concurrent calculation with the magnetic calculation, making the process computationally efficient. The algorithm was incorporated into MATLAB code and tested for accuracy against analytical solutions and other gravity modelling software (Cooper, 2010; Geophysical Software Solutions & TGT Consulting, 2009; Singh & Guptasarma, 2001).

4.1.2.3 Gradient

As mentioned vertical gradient methods are suited to cavity detection and are common in magnetometry. In most modern magnetometers the top sensor can be positioned at a fixed distance above the bottom sensor; this MATLAB program uses 1 m separation, though this can be altered. The gradient is calculated by finding the difference between the magnetic field measured at both sensors and dividing by the sensor separation. This requires the modelling algorithm to run twice (at each height), slowing down the operation, (users can choose to remove this calculation if speed is of importance).

Gravity gradient techniques are less common as the technique is very slow. When used a tower system is set up measuring the gravity field at both levels. This program uses 1 m separation for the tower though this can be simply altered. The gradient is calculated in the same way as the magnetic gradient calculation.

4.1.3 Ground penetrating radar

The voltage recorded at the GPR receiver, and its amplitude compared to the site noise level, must be calculated to test the methods applicability to cavity detection. Methods for modelling GPR include: ray tracing (e.g. Cai and McMechan, 1995); finite difference time domain methods which can incorporate a range of frequencies but are slow in computation (e.g. Roberts, 1997; Uduwawala and Norgren, 2004); and the radar range equation, utilised here, that offers a simple analysis of signal amplitude losses in a given environment (Daniels *et al.*, 1988). A subsurface variation of the radar range equation (Daniels, 2004) determines the voltage received by calculating the loss of energy through attenuation as an electromagnetic wave propagates through the subsurface.

The model is frequency and attenuation dependant; the governing parameters in GPR propagation.

$$v(r, \eta) = \frac{V_0 A \sigma \kappa}{c r'^2 \tau} \tau_g \rho_t 10^{-3} e^{(-2kr)} \quad \text{Equation 4.2}$$

Where, V_0 =peak radiated voltage (V), τ =pulse duration (seconds), c =speed of light (m/s), A =antenna effective aperture (m^2), σ =target cross section (m^2), κ =number of averages, τ_g =transmission coefficient into subsurface, ρ_t =target reflection coefficient, k =propagation coefficient, r =range (m), r' =equivalent range taking antenna beam pattern into account.

The radar parameters used in the calculation were based on values for the Sensors and Software pulseEKKO PE-100A 100 MHz GPR, and from standard parameter values for materials (Milsom, 2003; Sensors Software Inc., 2003). This theory was converted into MATLAB code (Appendix Aiv) and incorporates the calculations of the parameters required in Equation 4.2.

It should be noted that this technique is primarily aimed at use beyond 2 m depth (Daniels, 2004) and is not a full waveform model. Further iterations of this MATLAB software may utilise a full waveform model but comparison with case studies in this work show the radar range technique is applicable (Chapter 8.2.2).

4.1.4 Resistivity

The resistivity modelling algorithm used currently is based on theory in Dey & Morrison (1979) which allows the modelling of any 2D shape. This algorithm has been incorporated into the MATLAB environment by Pidlisecky & Knight (2008) with improvements in speed and in restricting boundary effects on the original algorithm. Unfortunately, in the current state the resistivity modelling is only in two dimensions and so later calculations of survey parameters and detection probability cannot be completed. Future work on this project will incorporate a 3D resistivity model.

4.1.5 Electromagnetic induction

Electromagnetic induction modelling follows the theory of Wait (1951). The solution is currently only applicable to a sphere target and is therefore not comparable to the other modelling techniques and so is removed from later comparisons. Future work on this project will incorporate more target shapes (Figure 4.3). The vertical component of the induced field that can be calculated at each survey point is:

$$H_z(r) = 4 \frac{m(\omega)}{r^6} \quad \text{Equation 4.3}$$

Where r is the square distance of the sphere centre to the survey point, $m(\omega)$ is the induced dipole moment, and ω is the frequency.

4.2 MATLAB implementation

MATLAB was chosen to host the cavity detection program for a number of reasons: MathWorks software is available across platforms (Windows, Macintosh and Linux); MATLAB has extensive visualisation options (including 3D) allowing effective communication of results; there are numerous relevant statistical and numerical functions available; graphical user interface (GUI) options are available; and importantly MATLAB is frequently used within the geophysical and engineering disciplines (e.g. Witten (2004); Johnson (2008)). The MATLAB interrelated function and file system means that the program is also extendable. Further techniques can be coded, or converted from other languages, and incorporated into the program for comparison by capable users with a few minor changes. This flexibility is required to keep the software suited to user needs as new techniques emerge and progress. More complex modelling algorithms can be incorporated if required. The code is well commented and parameters clearly labelled allowing simple alteration to suit requirements.

However, MATLAB code is generally slower than other languages (e.g. C and FORTRAN) but the aforementioned benefits of usability and readability are seen to outweigh this. MATLAB is not open source which may limit use; however, there are a few techniques to export programs for universal use (section 4.2.3).

4.2.1 Graphical user interface

A MATLAB GUI was developed for the program allowing the widest range of users and ensuring convenient and intuitive use (Figure 4.1). Parameters can be entered into the GUI using text boxes, sliders and drop-down boxes. These values are then used in the modelling calculations. The interface options are limited to essential variables and kept non-technical meaning in depth understanding of the geophysical techniques is not essential, increasing ease of use within various areas of engineering. A basic understanding of near surface techniques may aid interpretation.

4.2.2 Data structure

The program primarily uses 33 m-files (text files of MATLAB commands and functions) as well as a number of built in MATLAB functions (Figure 4.2). Parameter values are stored in cell arrays, matrices, and as single variables. Using matrices is advantageous because numerous values of the same parameter can be stored together, representing the same value in different materials or the extreme values of a parameter when variance exists (i.e. maximum and minimum). Cell arrays enable storage of the same variable matrices for each

technique or material. This becomes useful in comparison of variables and also improves efficiency of data transfer between m-files by limiting the number of variables.

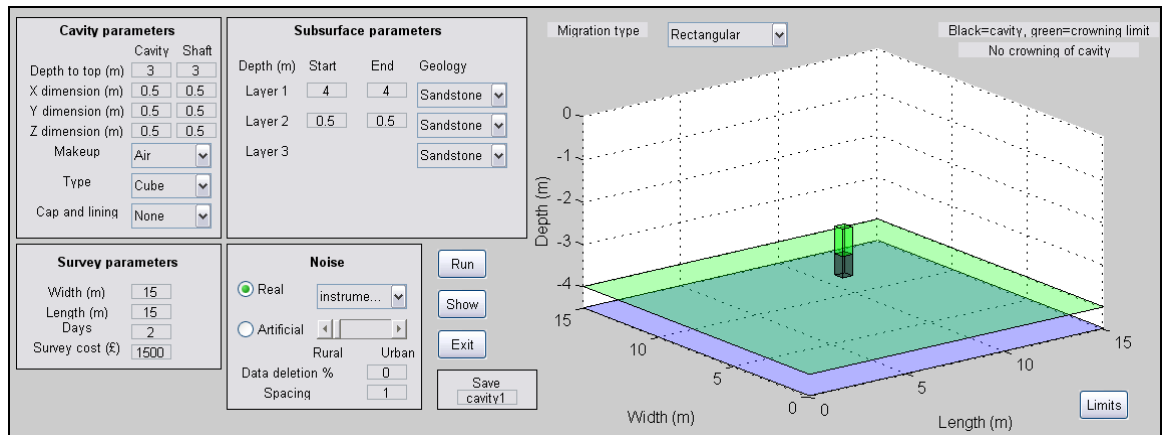


Figure 4.1. Graphical user interface of the cavity modelling program. This opening page offers the user all the options available to start the program. Variables are changed either by typing in the text boxes or using the drop down menus and sliders. The image of the subsurface is redrawn when the 'Show' button is pressed. Migration is automatically redrawn with changes.

4.2.3 Usability

4.2.3.1 Open source code

MATLAB is not free software and so the distribution of this program is limited. Although most potential users will have access to MATLAB (within the engineering, geophysics and academic communities) availability for as many users as possible is of great importance. To this end, an executable (.exe) was trialled for the GPR modelling (the fastest of the modelling techniques) which worked successfully (MATLAB code before conversion in Appendix Axvi). This can be used on any windows machine using the MATLAB Compiler.

The ability for users to adapt the code to suit specific needs is also of importance. To aid this, the code has been written in a function based manner, allowing the extension of the applications by simply incorporating new functions.

4.2.3.2 Other distribution approaches

The ideal solution would be distribution online on a web based version of the program. A Java based web application would achieve this but the program is too large and complex to support this and so traditional distribution is more applicable.

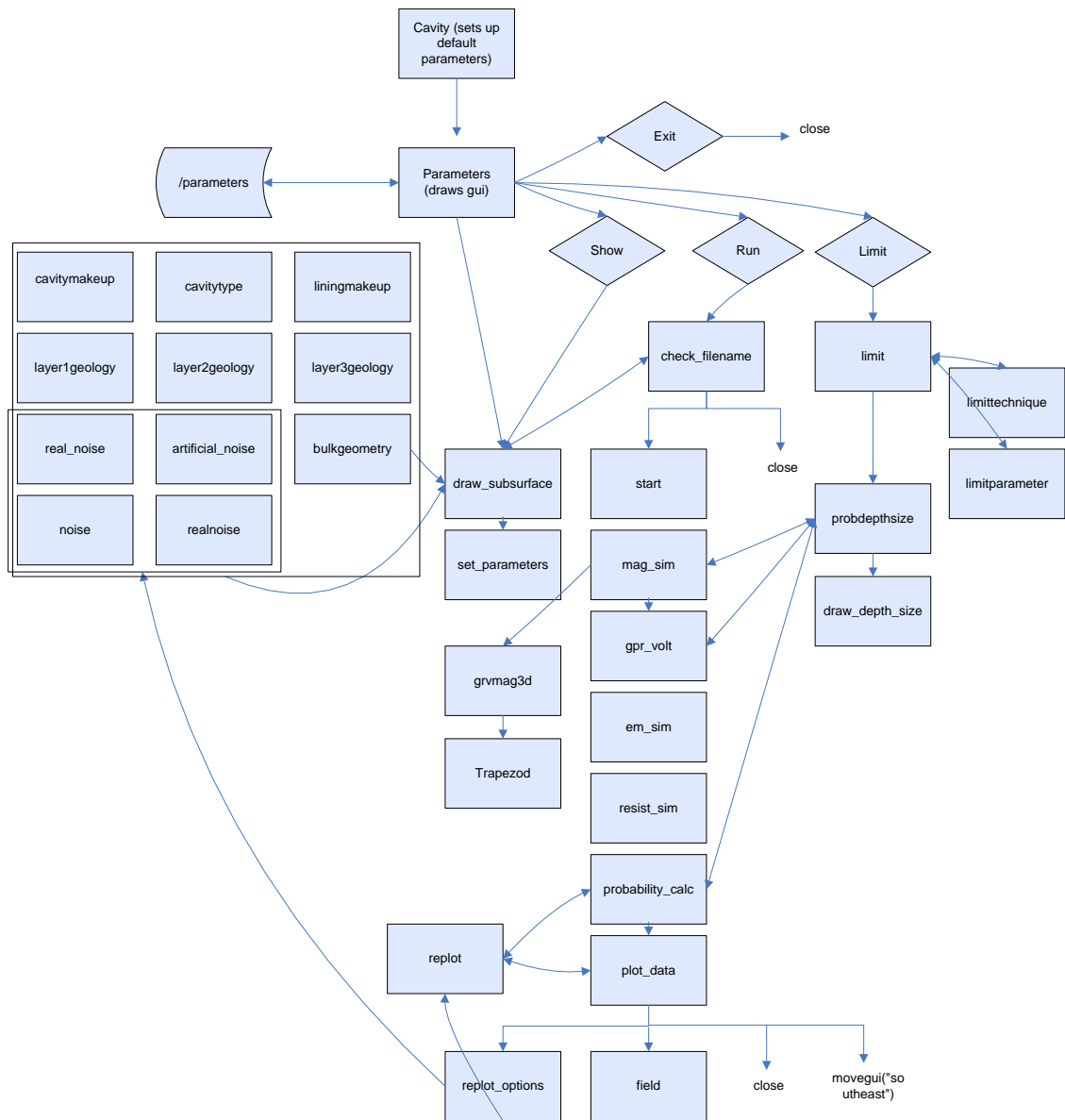


Figure 4.2. Structure of the cavity modelling software. Each box represents an m-function with its given name noted. Arrows represent interaction between function. Diamonds are clickable buttons on the GUI.

4.3 Variable parameters

In order to incorporate all techniques into the same program the various input variables were converted to the same format and name. Modelling variables are split into two types: user defined values and predetermined inputs (all variables are listed in Appendix Avii).

4.3.1 Predetermined variables

Material parameters: We define ‘geology.mat’ to store material parameters. This matrix contains the average, maximum and minimum material parameters required for each geophysical modelling technique (conductivity, dielectric constant, EM velocity, density, magnetic susceptibility, and magnetic permeability) for each geological material and cavity material modelled (values are referenced in the file ‘set_parameters.m’ (Appendix Av) and average values in **Table 4.1**).

Noise: We define ‘noise.mat’ to store noise values. Various noise scenarios are available, each with a range of values based upon literature or site measurement (see section 4.3.2.4 for further detail).

Equipment specific parameters: Values such as GPR frequency and antenna characteristics and magnetic sensor separation are pre-defined individually but removed from the matrices in order to allow easy access for alteration if using different equipment. These are defined in ‘set_parameters.m’ (Appendix Av).

Location specific parameters: Values such as magnetic field intensity are predefined for use in the U.K., but are easily accessible for alteration in ‘set_parameters.m’ (Appendix Av).

4.3.2 User variables

The probability of detection of cavity is dependent on a number of key factors. Firstly, the magnitude and shape of the anomaly. This is dependent upon the shape, makeup and depth of the target and also of the surrounding material. Secondly, the level of noise on the site. Finally the technique utilised, its sensitivity of detection and the survey parameters chosen. All these factors can be altered by the user to aid technique choice in a given scenario.

Program users are presented with a number of input options within the GUI environment. The important variables for a specific survey can be entered. Default settings are presented in the options boxes and will remain so if the user makes no alterations. Some are essential in the modelling calculation while some are used solely for additional survey design calculations. The following variable options can be seen on the GUI (Figure 4.1).

Table 4.1. Geophysical parameter values used in modelling. GPR is not modelled in soil or clay in this paper.

Material	Density (g/cm ³)	Magnetic susceptibility (k)	EM velocity (m/ns)	Conductivity (mS/m)	Dielectric constant
Limestone	2.65 ²	0.000505 ²	0.12 ²	0.0001 ³	6 ²
Soil	1.92 ¹	0.001 ³	-	-	-
Sandstone	2.35 ¹	0.00002 ²	0.15 ⁴	0.01 ³	5 ³
Clay	2.21 ¹	0.000255 ²	-	-	-
Concrete	2.3 ⁸	0.0017 ⁵	0.1 ⁶	0.001 ⁶	7 ⁷
Granite	2.6 ²	0.025 ²	0.13 ²	0.00001 ⁹	5 ²
Peat	0.15 ¹²	0.00014 ¹³	0.037 ¹⁰	0.006 ¹¹	60 ¹⁰
Air	0	0 ²	0.3 ²	0 ²	1 ²
Water	1 ¹	0 ²	0.033 ²	0.05 ²	80 ²

¹ Seigel (1995). ² Value or average of the range values listed in Milsom and Eriksen (2011). ³ Erkan and Jekeli (2011). ⁴ Martinez *et al.* (1996). ⁵ McEnroe (1998). ⁶ Reynolds (1997). ⁷ Carino (2010). ⁸ Kosmatka (2010). ⁹ Ulriksen (1982). ¹⁰ Theimer *et al.* (1994). ¹¹ Slater & Glaser (2001). ¹² Silc & Stanek (1977). ¹³ Petrovský & Ivers (2011)

4.3.2.1 Cavity shapes

Six typical cavity shapes (Figure 4.3) are modelled to give a more accurate representation of widespread manmade and natural subsurface environments than the more commonly modelled cuboid and spherical shapes. Based on research of cavity shapes in the U.K. and abroad (Section 2.5), the following typical cavity types were chosen for use in the modelling

- Shaft: Rectangular cuboid of any dimensions. Shaft diameter increased through time up to 4 m wide and 250 m deep (Ove Arup and Partners, 1976). Circular shaped shafts were used in England, other regions (especially Scotland) used rectangular (Healy and Head, 1984).
- Bell pit: Rectangular cuboid with a larger cuboid at the base. Bell pit shaft diameter was usually around 1 m and pit diameter was 8-20 m (Littlejohn, 1979). Depth was seam dependent but rarely over 12 m (Clarke *et al.*, 2006).
- Lined shaft: Rectangular cuboid with lining surrounding the four vertical sides. Thickness and material (wood, concrete or steel) chosen by the user.
- Capped shaft: Rectangular cuboid with a cap on top. Thickness and material (wood, concrete or steel) chosen by the user.

- Horizontal gallery: Rectangular cuboid representing natural cave systems or mines. Gallery can dip in either direction and the corners can be cut to closer represent a rounded gallery.
- Migrating void: cuboid of any dimension. Representing natural cavities or, as collapse of karstic cavities in rock is considered a rare occurrence (Fehdi, *et al.*, 2010), a migrating void which forms in eroded bedrock cover. Also, migrating mine shaft voids formed as fill migrates to the roadways.

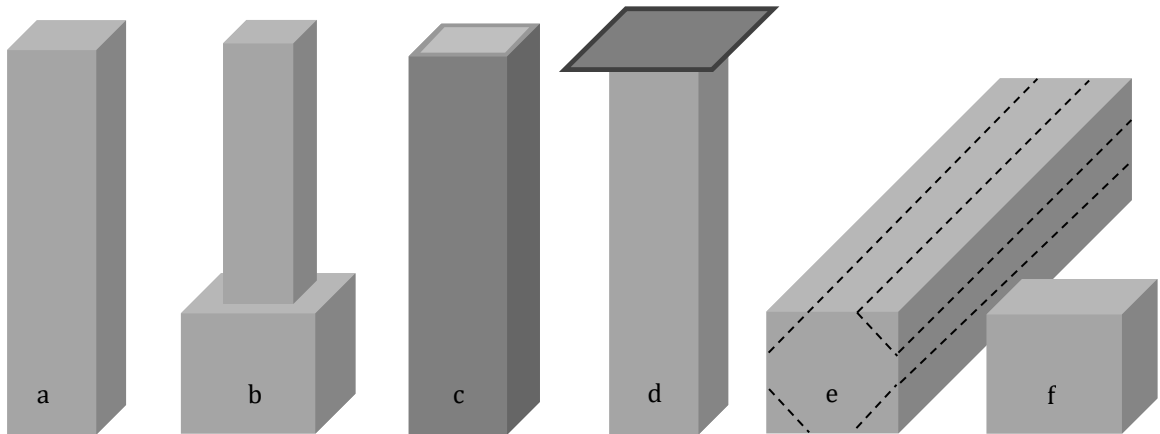


Figure 4.3. Typical cavity shapes used in modelling. a) shaft, b) bell pit, c) lined shaft, d) Capped shaft, e) Horizontal gallery (dotted lines - more rounded gallery), f) migrating void.

The depth, dimensions and fill of all cavity types can be altered by the user. The ability to model such shapes was an important factor in choosing the modelling techniques. The focus on modelling these typical cavity shapes is a unique topic to this author's knowledge; previously only sphere or cube cavities were modelled.

4.3.2.2 Cavity fill and subsurface material

The range of fill materials is only limited by knowledge of the relevant parameters used in the modelling. The most well documented and common fills have been chosen for inclusion: air, water, and soil backfilled shafts.

Shafts and bell pits are modelled with a range of cap and lining materials. As discussed (Section 2.5.1.4), the capping material is variable and each material represents a very different geophysical target.

Table 4.1 shows the range of host materials modelled, concentrating on those typical in the U.K. (limestone, soil, sandstone, cement and clay) and the corresponding geophysical parameters. This variety of subsurface scenarios means prediction of the geophysical response to a particular cavity is difficult. Further fill values and geological parameters can

easily be added to the matrix 'geology.mat'. Modelling allows the assessment of the theoretical response of different techniques in endless subsurface scenarios.

4.3.2.3 Survey size and spacing

Survey size is often an important limitation on survey design and hence feasibility of geophysical survey success. The width and length of the site are alterable parameters of the model. Also of great importance is the spacing between survey points and between profiles. This value is user variable, or the program can calculate the optimum spacing for each technique based on user specified site conditions (Section 5.2.3).

4.3.2.4 Data deletion

During processing often a number of data points are deleted, usually noisy anomalies (e.g. spikes in magnetic data, incorrectly coupled resistivity spikes). The program allows the user to choose a percentage of points to be deleted from the dataset. This will be chosen based on the users own experience. The function 'randperm.m' will delete random data points (uniformly distributed pseudorandom numbers) until the data deletion percentage is reached. The program can assess the impact data deletion has on detection feasibility (Section 5.2.6).

4.4 Noise level

The process of cavity detection is further complicated by the presence of noise at a site. Noise is a major limiting factor to survey success. Noise level varies between sites but subtle cavity signals can easily be obscured in all techniques. Noise is typically defined as 'unwanted signal' from a range of sources, with influence varying between techniques. Common incoherent noise sources include: instrumental, ambient (utilities, buildings, traffic, wind, magnetic storms, electromagnetic sources (Figure 4.4)), human interaction (including variation in sensor height for portable techniques), scattering noise from soil (Xu, 2013) and site clutter.

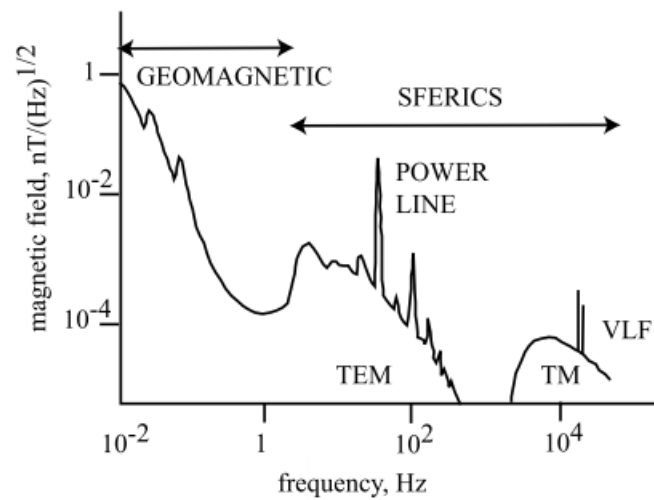


Figure 4.4. Electromagnetic noise spectrum highlighting potential noise sources across all ranges of frequency utilised by geophysical methods. (Everett & Meju, 2005) after (Palacky & West, 1991).

It is commonly the case that noise is of short wavelength and high amplitude obscuring the more subtle and smaller amplitude target signals. These characteristics can be utilised to remove noise by applying filters in the frequency or space domain, though these are both limited in their ability to distinguish between noise and features (being based solely on wavelength or width) and can distort the shape of genuine signal pulses, remove anomalies, or even create artificial anomalies (Parasnis, 1996; Salem, *et al.*, 2010). It is not certain that data can be processed to remove all traces of noise and leave the genuine signal intact. In fact, (Salem *et al.*, 2010) suggest that filters “rarely yield cleaner data”. With subtle anomalies, such as those associated with cavities, it imperative that signal is not lost in processing. This often means the original noisy data must be used for interpretation. If it can be established that the signal from the chosen target will be greater than the expected noise on the site, and distinctive in characteristic (Butler, 2008) a positive detection of the cavity can be expected. To establish whether this will be possible on a site, the level of site noise must be found or estimated.

4.4.1 Literature noise measurements

Noise can be estimated as a percentage of the data anomaly size (Ma, Li, & Huang, 2013) but this does not take into account noise variation between sites. Site specific noise levels can be estimated in a number of ways. The most accurate is to measure on the site itself. This can be impractical if the site is currently in use or inaccessible, though in construction the site is often accessible for a period during the initial site investigation. If site access is improbable the site noise must be estimated based upon noise measurements at similar sites

or estimated from relevant literature. A number of near surface noise measurements were found in the relevant literature and classified on a range from instrumental to brownfield (Table 4.2).

Table 4.2. Noise levels from the academic literature sorted by technique.

Location	Technique	Noise level
Greenfield	Magnetic	0.01 nT (Geometrics, 2006)
Typical	Magnetic	0.01 nT (Michael Rybakov <i>et al.</i> , 2005)
Typical	Magnetic	0.1 nT (Erkan & Jekeli, 2011)
Brownfield	Magnetic	1.4 nT (Munsch, Boulanger, Ulrich, & Bouiflane, 2007)
Quiet	Magnetic	1 nT (McCann <i>et al.</i> , 1987)
Noisy	Magnetic	5 nT (McCann <i>et al.</i> , 1987)
Instrumental (Scintrex CG-5)	Gravity	0.005 mGal (Scintrex, 2011)
Typical	Gravity	0.1 mGal (Laswell, Engel, Cassidy, Courtier, & Henton, 2008) and (Seigel, 1995)
Instrumental (LaCoste)	Gravity	0.01 mGal (J. Milsom, 2003)
Instrumental (Scintrex CG-5)	Gravity	0.003 mGal (J. Milsom, 2003)
Instrumental	Gravity	0.001 mGal (United States Army Corps of Engineers, 1995)
Typical	Gravity	0.005 mGal (United States Army Corps of Engineers, 1995)
Typical (electronic gravimeter)	Gravity	0.002-0.003 mGal (United States Army Corps of Engineers, 1995)
General pessimistic noise level	Gravity	0.008 - 0.01 mGal (United States Army Corps of Engineers, 1995)
Optimistic noise level in bad conditions	Gravity	0.022 mGal (United States Army Corps of Engineers, 1995)
Instrumental	Gravity	0.01 mGal (McCann, Jackson, & Culshaw, 1987)
Typical	Gravity	0.03 mGal (McCann <i>et al.</i> , 1987)
Typical	GPR	10 μ V (Erkan & Jekeli, 2011)
Typical	Gravity gradient	3 E (Erkan & Jekeli, 2011)

4.4.2 Field measurements of magnetic noise

To broaden the range of categories and number of examples within each category, magnetic noise measurements were taken across a range of sites in the U.K. Sites were chosen to reflect typical sites and to cover the spectrum of potential noise. Site locations and descriptions are shown in Figure 4.5. Measurements were taken with a Geometrics Caesium G-858 magnetometer in gradiometer mode in order to negate the effect of diurnal changes. Measurements were taken with a typical setup for gradiometry measurements in order to record typical measurements (Geometrics, 2006). The general trend of the magnetic field was noted and the standard deviation from this trend was calculated giving the noise level at the locations (Table 4.3).

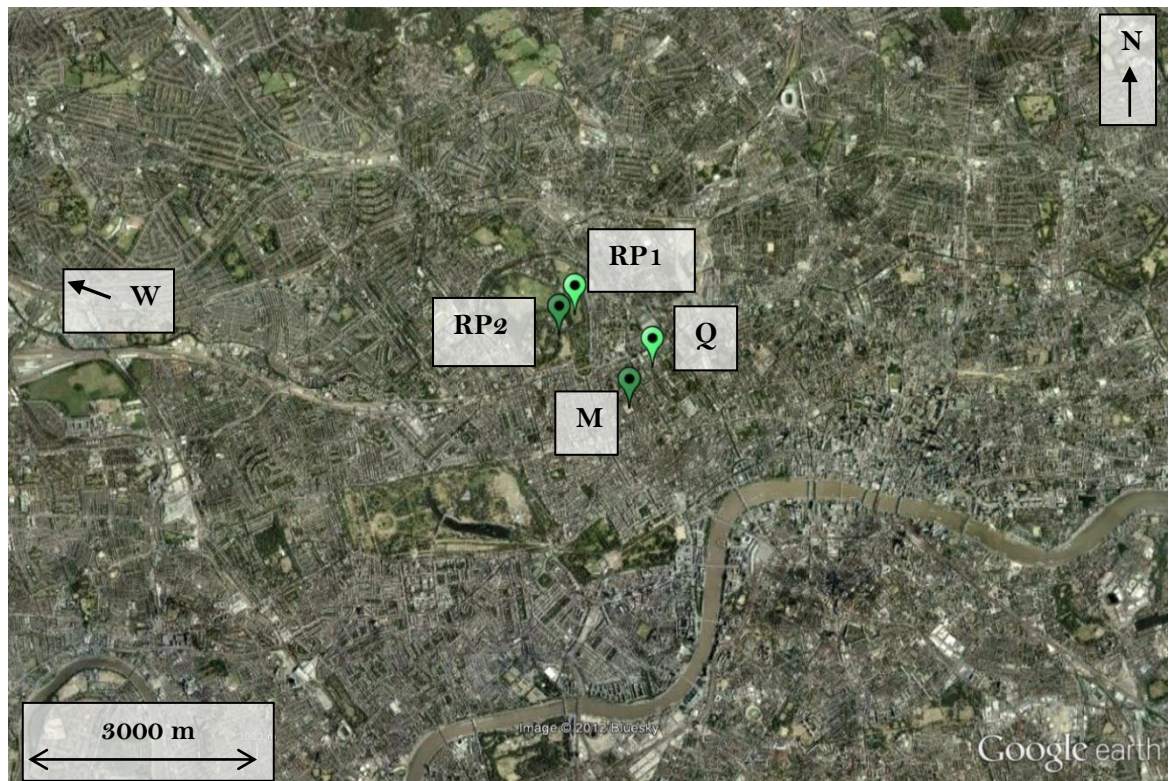


Figure 4.5. General location of noise measurements (Google, 2011). More detailed maps in Appendix C. Sites were: a) Regents Park. Locations in the centre of a field (RP1), and beside a roadside and fence (RP2). b) Middlesex Hospital site. Locations near the church (M1 and 2), by a rubble mound (M3), by the perimeter fence (M4) and 1.5 m from fence (M5). c) UCL Quad. Locations on the grass (Q1), on a paved footpath (Q2), by the large Portico building (Q3), by a small building (Q4), inside the doorway (Q5), on the stairs (Q6), inside a second story room (Q7). d) West Wycombe caves (35 miles east of London). Locations in the centre of the field (W1), with tree coverage (W2), by the equipment (W3), and by the mausoleum (W4).

Table 4.3. Recorded noise measurements at a range of sites. See Figure 4.5 for locations.

Location	Noise level (nT) (standard deviation (3 d.p.))
West Wycombe 1 (centre of hill)	0.005
West Wycombe 2 (beside trees)	0.006
Regents Park 2 (by road - 4 m from fence)	0.497
West Wycombe 3 (beside equipment)	0.694
Regents Park 2 (by road - 3 m from fence)	1.043
Regents Park 1 (field)	1.195
West Wycombe 4 (beside mausoleum)	1.210
UCL Quad 1 (on asphalt - 1 m from building)	1.464
UCL Quad 2 (paving slabs)	1.591
UCL Quad 3 (grass)	1.616
UCL Quad 1 (on asphalt - 2 m from building)	1.617
UCL Quad 1 (on asphalt - 4 m from building)	2.186
Regents Park 2 (by road - 2 m from fence)	2.637
UCL Quad 1 (on asphalt - 3 m from building)	2.712
UCL Quad 1 (on asphalt - by building)	2.796
UCL Quad 4 (observatory on grass - 1 m away)	3.889
UCL Quad 4 (observatory on grass - 0 m away)	4.139
Middlesex 1 (church)	6.883
Middlesex 3 (west)	7.259
Middlesex 4 (1.5 m away from fence)	12.931
Middlesex 2 (rock mound)	14.281
Regents Park 2 (by road - 1 m from fence)	14.405
Middlesex 5 (fence)	16.301
UCL Quad 6 (inside doorway)	24.533
UCL Quad 5 (indoor)	30.223
UCL Quad 7 (stairs)	32.837
Regents Park 2 (by road - 0 m from fence)	136.566

The noise level varies from 0.005 nT in a greenfield area (in the centre of a park, beside forested areas) to 136 nT beside a road (in central London). This range of noise would have a large influence on the detection probabilities of cavities in different environments. This is a huge scale of noise and obvious that cavities detectable on the greenfield site would be completely obscured by proximity to a road or on a number of the other noisier site locations. The sites were grouped into four categories: greenfield, urban and buildings, brownfield and indoor (Figure 4.6). Average noise levels of these groups are, respectively: 0.55 nT, 13.65 nT, 18.39 nT, and 21.21 nT. This range in site noise level will have a large influence on the cavity detection probability in different environments. This method of noise approximation is of much greater use than the single “typical” value of noise for all sites, or not considering noise level at all, as is often the case in other modelling and allows a much

more relevant estimation of the feasibility of using geophysics in cavity detection on a particular site.

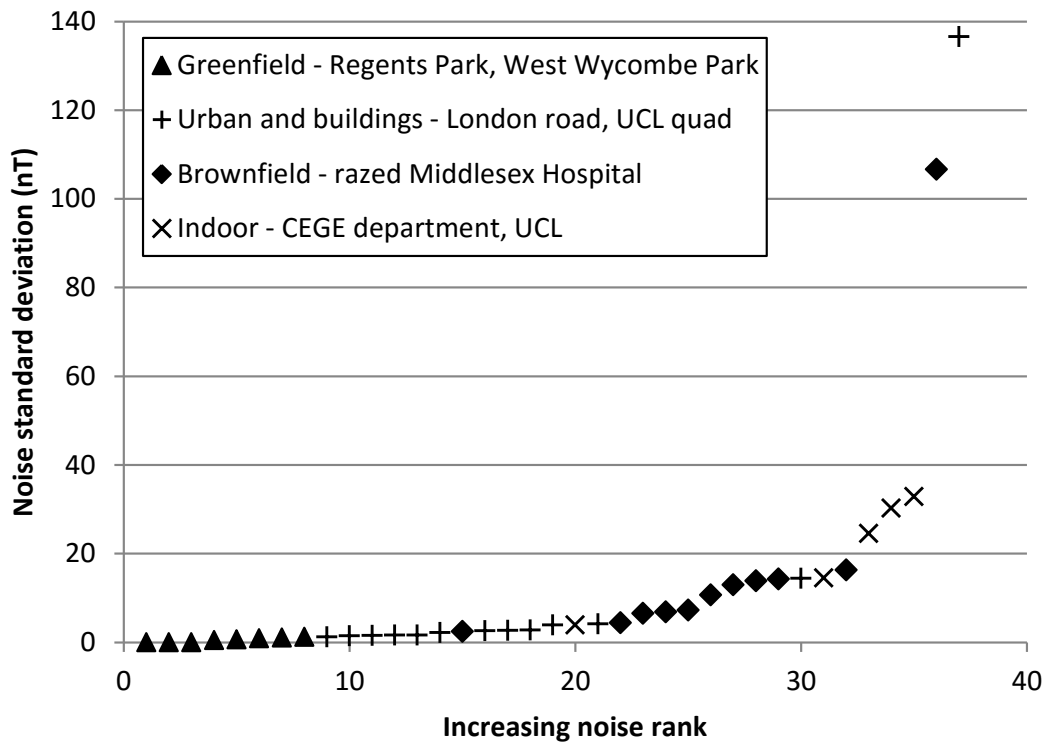


Figure 4.6. Noise level dependent on site type. The wide range highlights the importance of site specific measurements of noise.

The sites were chosen to cover a range of noise conditions but there are clearly more nuanced site conditions to be considered. Further measurements will improve the range, but on site measurements would vastly improve the usefulness of any subsequent modelling for a particular site. Further noise measurements of all techniques should be taken.

As measurements were taken from a stationary position, only time dependant sources of noise are monitored, i.e. instrumental noise and cultural noise at the survey position. This method therefore falsely assumes that cultural noise is equal along the survey line and neglects geological variation along the survey line. These limitations explain the low values of noise found in some locations (especially greenfield sites) compared to other workers estimates (Table 4.2). This is further explored in the Chapter 9.

4.5 Probabilistic approach to detection in noise

The cavity detection probability is calculated to assess and compare the suitability of each technique in any given subsurface, noise level and survey condition. The basis of this

calculation is the comparison between the level of meaningful signal as a result of the cavity, and the estimated or measured level of unwanted noise at the site represented by random noise of that amplitude. In rudimentary terms, if the signal is bigger than the noise then the signal should be detectable.

The program calculates the amplitude response of any given cavity at every survey point across the site using the algorithms for each technique (Section 4.1). Noise is estimated as in Section 4.4.

As an example, Figure 4.7a shows the total magnetic field calculated above a 3-m deep, 1-m sided air cavity in limestone positioned in the centre of a 30 m square grid. The maximum amplitude signal is small (just under 0.025 nT) but some survey lines (shown in green) have large enough amplitude to rise over the typical instrumental sensitivity of magnetometers (0.01 nT (Geometrics, 2006)).

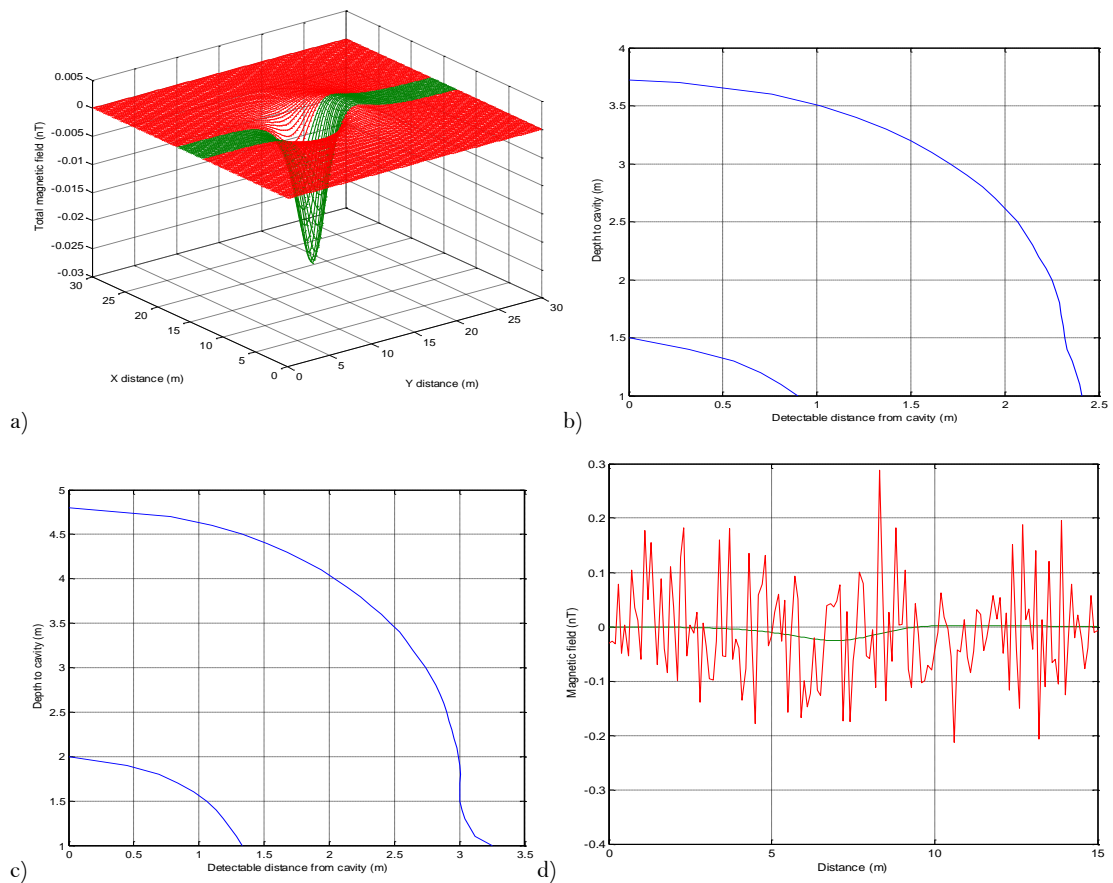


Figure 4.7. a) Total magnetic field from a 1-m cube air cavity at 3-m depth in limestone. Green lines denote the survey lines where the anomaly is larger than the instrumental noise value of a typical magnetometer (Geometrics G858). b) The distance from the cavity centre that the cavity anomaly is greater than typical magnetometer sensitivity (top curve) and instrumental noise (bottom curve) at increasing depths. c) The same cavity but in sandstone. d) The application of noise shown to highlight the obscuring of cavity signal.

The distance from the cavity centre that the cavity anomaly is greater than a certain level of noise, i.e. it is theoretically detectable, can help us understand where a cavity will be detectable. Figure 4.7b shows how this distance decreases with increasing cavity depth. This process displays the basic feasibility of theoretical detection of cavities in any environment.

It is important to progress beyond this direct comparison of signal and noise size to more precise estimation of detection probability. The first stage is to calculate a common geophysical parameter, the signal to noise ratio (SNR). SNR is a ratio of the power of the two values. This can be converted into amplitude of signal thus:

$$SNR = \frac{P_{signal}}{P_{noise}} = \left(\frac{A_{signal}}{A_{noise}} \right)^2 \text{ or } SNR = \frac{\mu}{\sigma}$$

Equation 4.4. P=power, A=amplitude, μ = signal mean, σ =standard deviation of noise.

A progression of this ratio is the calculation of the probability of isolation of the signal anomaly from the unwanted noise present in a dataset. The signal amplitude resulting from the cavity at each survey point across the site is calculated using the chosen algorithm for each technique. The probability of isolation of the signal anomaly from unwanted noise present in a dataset is calculated following Kotelnikov's criterion (Fajklewicz *et al.* (1982) apud Nikitin and Tarchov (1973)):

$$Detection\ probability = \frac{1}{\sqrt{2\pi}} \int_0^{\frac{\sqrt{\alpha}}{2}} \frac{-t^2}{e^2} dt$$

Equation 4.5. α is the amplitude characteristic of the anomaly and t is the iterated variable.

The modelling simulates the anomaly shape and amplitude and so the amplitude characteristic can be calculated thus:

$$\alpha = \frac{\sum_{i=1}^m A^2(x_i)}{\hat{\sigma}^2} = \frac{\bar{A}^2 \cdot m}{\hat{\sigma}^2}$$

Equation 4.6. $A(x_i)$ is the anomaly at point x_i along a profile, in this case caused by the presence of a cavity, m is the number of measurements and $\hat{\sigma}$ is the dispersion of the measurements or the noise level on the site. It can be seen that α in Equation 4.6 is equivalent with SNR.

Equation 4.5 is also referred to in statistics as the 'error function', and so the probability of detection of an anomaly of known form and intensity (here termed γ) in noise is simplified to:

$$\gamma = \text{erf}\left(\sqrt{\rho/2}\right)$$

Equation 4.7. ρ =the ratio of the anomaly square to the noise dispersion, erf =the error function This calculation has been previously utilised with respect to geophysical fields in Khesin *et al* (1996). and Erkan and Jekeli (2011)

This allows the calculation of a percentage probability of cavity detection with any given variables related to specific survey parameters. It allows direct comparison between techniques and across a range of noise levels associated with different sites.

4.5.1 Single survey line probability

Continuing with the example of a 1-m cube air cavity at 3-m depth in limestone (Figure 4.7), the detection probability using magnetometry is calculated in a range of noise situations (Figure 4.8). As the noise level increases the detection probability on single survey lines decreases and the distance away from the cavity that it is detectable decreases rapidly. In the lowest noise level (0.01 nT - caesium magnetometer sensitivity (Geometrics, 2006)) the cavity has over 20% chance of detection up to 3 m from the cavity centre but decreases rapidly beyond this. In the increased noise environment the detection probability is less than 10% directly above the cavity.

Figure 4.8 (a) shows the modelled result of a magnetic survey over a 1 m sided cube air cavity at 3 m depth in limestone with typical noise levels (0.1 nT (Geoscan Research, 2012)). The cavity detection probability is over 20% on each survey line up to 3 m from the cavity centre but decreases rapidly beyond this. The same cavity is modelled in a range of geologies and depths in typical noise level (Figure 4.8b). Cavity detection probability on the central survey line decreases as cavity depth increases in a similar manner for all geological materials but the probability varies greatly between materials because of the variation in host susceptibility.

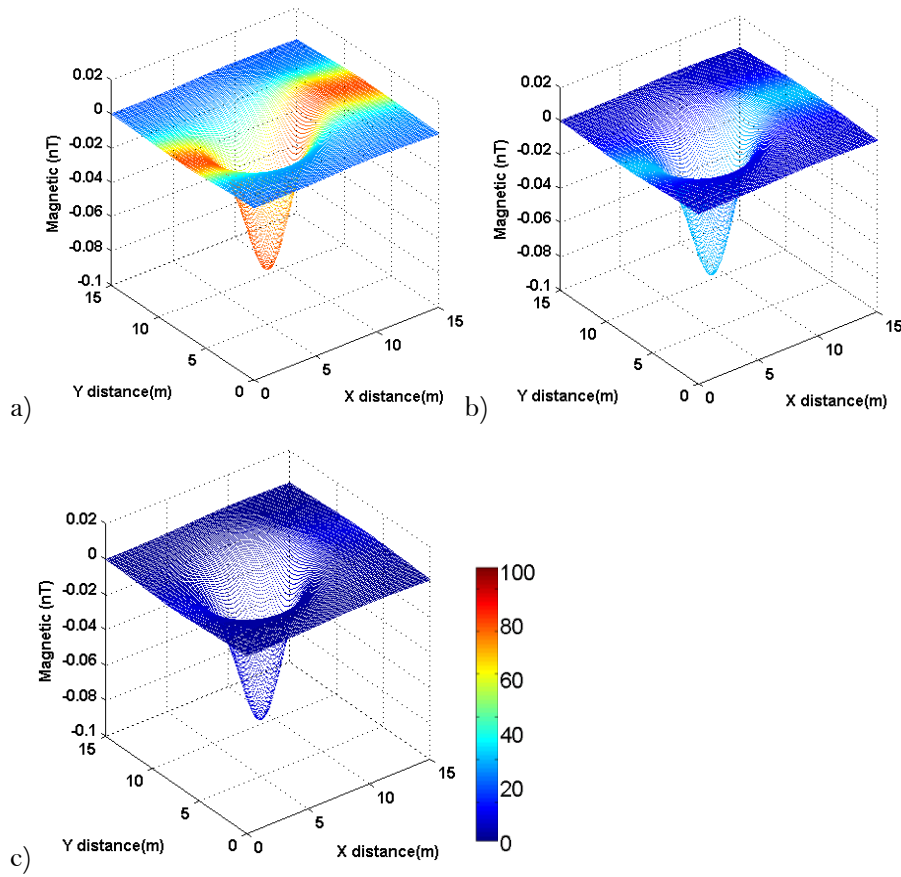


Figure 4.8. Modelled results showing the detection probability of a 1-m cube air cavity at 3 m depth in limestone using magnetometry. Colour scale shows the probability of detection at each survey line at (a) 0.01 nT, (b) 0.1 nT and (c) 1.4 nT.

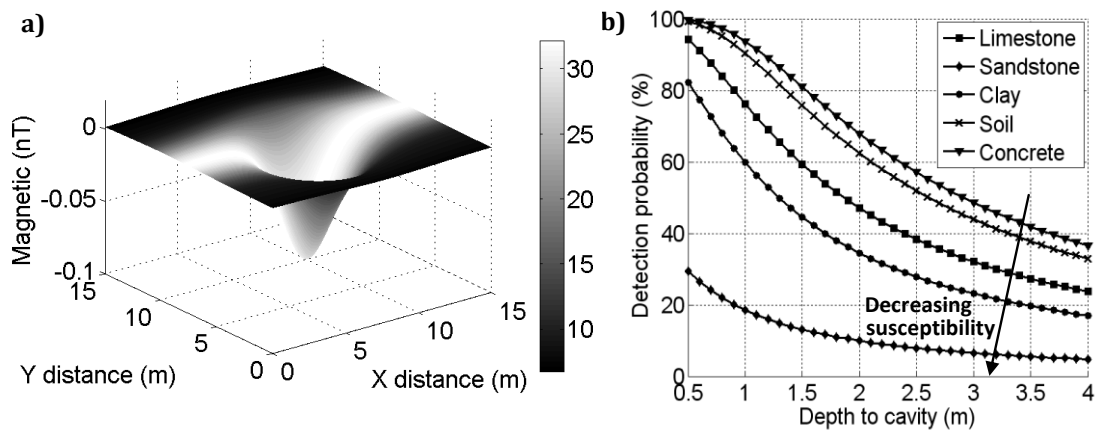


Figure 4.9. a) Modelled results showing the probability of detection of a 1-m sided cube air cavity at 3-m depth in limestone using magnetometry. The grey scale shows the probability of detection in typical magnetic noise (Table 2). b) The detection probability of the same cavity decreasing with depth in a range of geologies. The probabilities shown represent that of a survey line directly above the cavity.

Cavity detection probability on the central survey line decreases as cavity depth increases in a similar manner for all geological materials (Figure 4.9b) but the probability varies greatly between materials because of the variation in host susceptibility. Cavity detection probability is fairly low below 3 m depth when using just a single survey line in all materials has less than 50% chance of detection.

4.5.2 Total survey probability

Of course, geophysical surveys generally record measurements across a number of profiles, not just a single profile. In order to calculate a more realistic detection probability, all survey profiles are considered together. This allows analysis of change to detection probability when altering survey size, profile spacing or survey point spacing for any given cavity and site specific environment. We can subsequently calculate the optimum survey parameters for detection. Including the minimum spacing required for detection.

The probability of cavity detection is assessed on each survey line at a given spacing using Kotelnikov's criterion (Equation 4.7). As GPR records a signal that has the possibility of detecting a cavity at each survey position, the detection probability is calculated at every survey point. Since each survey line can be considered a statistically independent event the total probability of detection is calculated by multiplication of individual probabilities. The standard definition of the probability of two independent events occurring is:

$$P(A \cap B) = P(A) * P(B)$$

Equation 4.8. Probability of events A and B occurring.

The probability of not detecting a cavity on a profile is the complement of detection (or 1 minus the probability of detection). Following Equation 4.8 the probability of *not* detecting a cavity on all of the survey lines is the product of the individual probabilities of non-detection on all the survey lines:

$$P(\text{no detection}) = (1 - P(\text{detection}_{\text{line}_1})) * (1 - P(\text{detection}_{\text{line}_2})) * \dots * (1 - P(\text{detection}_{\text{line}_n}))$$

Equation 4.9. Probability of *not* detecting the cavity on all survey lines.

Therefore, the probability of detection of the cavity on at least one line is the complement of not detecting the cavity on all the survey lines:

$$P(\text{detection on any of the survey lines}) = 1 - P(\text{no detection})$$

Equation 4.10. Probability of cavity detection across the survey site.

4.5.3 Monte Carlo method

It is unreasonable to assume that the central survey line will be directly above the cavity (the best case scenario), and so the effect of altering the starting position is investigated. The Monte Carlo method of stochastic sampling is applied to calculate an unbiased value of the overall probability. Survey profile start positions are varied randomly between the best case (aforementioned) and the worst, in which the cavity lies directly between two consecutive survey lines. As gravity measurements are taken discretely along profiles (where GPR and magnetic techniques take measurements almost continuously), both the profile and station start positions are varied. The average detection probability is calculated over 100 surveys (this variable is alterable) with random start positions. This value can be calculated for any profile or station spacing. The MATLAB code created to calculate the profile probabilities, run the Monte Carlo method and calculate the final probability is shown in Appendix Axi.

4.6 Running the program

‘Cavity.m’ is the m-file that invokes the program (Appendix Avi). It sets default conditions before invoking ‘parameters.m’ that creates the GUI framework and ‘draw_subsurface.m’ that visualises the subsurface, cavity and migration potential geometry (Appendix Aviii). From the GUI the user may change various options outlined in section 4.3.2 before choosing between the buttons ‘Run’ (commence modelling), ‘Show’ (redraw subsurface), ‘Exit’ (close the program) and ‘Limits’ (calculates the limits of cavity detection) (Figure 4.1).

4.6.1 Begin modelling

Pressing the ‘Run’ button on the GUI, first checks the filename for existence and offers an overwrite option (‘check_filename.m’ –Appendix Aix). The modelling process then begins with the ‘start.m’ file that contains a list of commands to be completed successively (Appendix Ax). The modelling algorithms are run and the results stored in the cell array ‘Data’. This array is then accessed by the algorithms for calculating the probability of detection (‘probability_calc.m’) and plotting of results (‘plot_data.m’ –Appendix Axii). All the user defined parameters (excluding ‘days’ and ‘cost’ of survey which are used later to calculate time in field (Section 4.7.2)) will be taken into account in the calculation of the ‘Data’ cell array. If the other m-files are required or the code is needed in a more convenient way, please contact the author.

4.7 Output

‘Data’ contains the amplitude of response for each technique at all survey points across the survey space. All matrices have the same size and shape allowing comparison analysis and amplitude units are the same as technique noise values allowing detection probability calculation. Amplitudes are also calculated at points in between the survey points so a Monte Carlo statistical analysis can be completed (Section 4.5.3). ‘Data’ is saved as ‘Data.mat’ containing all amplitudes after modelling is completed. This allows further statistical analysis of the results of certain site conditions without repeated modelling. The final detection probabilities are saved in the matrix ‘prob_total’.

4.7.1 Visualisation

To improve usability, various inbuilt MATLAB functions are used to visualise the results. The modelled signal from each technique is visualised as a 3D surface with the z-axis indicating the amplitude of the signal, and the x and y axis representing the survey length and width. In the same image the probability of cavity detection on each survey line is indicated by the colour of the line (ranging from blue (0%) to red (100%) or black to white in the case of grayscale images). The aim of this style of visualisation is to efficiently portray all of the important information with simple clarity.

Figure 4.10 shows an example of the modelling output of all techniques over a 1-m sided cube water cavity at 2-m depth in sandstone at instrumental noise levels. The overall probability for each technique is highlighted above each visualisation. Detection probability on individual profile lines decreases rapidly with distance from the cavity. Figure 4.11 shows the same subsurface conditions at typical noise levels for the major techniques studied in this work.

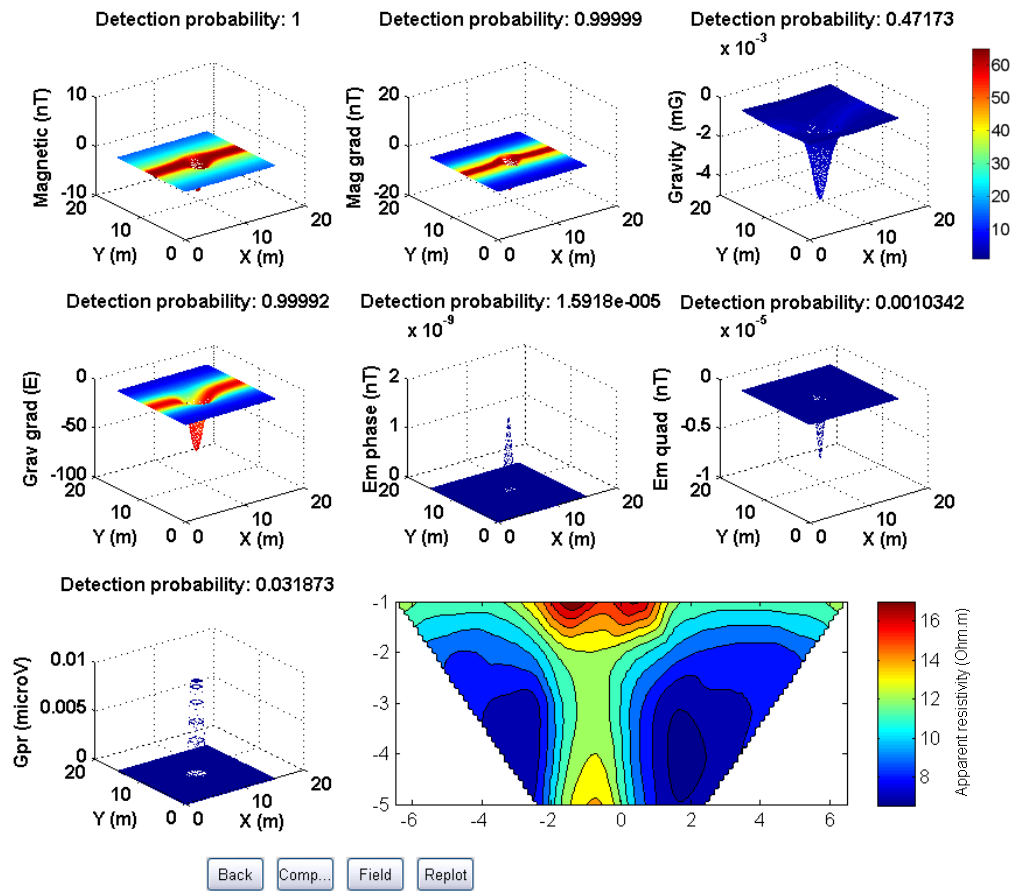


Figure 4.10. Example output of the cavity modelling program. The cavity modelled is a 1-m cube water cavity at 2-m depth in sandstone. NB the EM results are based on the modelling of a 1-m diameter sphere as the algorithm does not currently allow cubes. Apparent resistivity is currently only available in 2D (distance along survey line on horizontal axis and depth on the vertical axis). Overall detection probability is shown above each technique and profile line detection probability is indicated by the colour scale to the right of the first row of results (with the exception of resistivity).

Overall detection probability on the 15-m grid is low at these typical noise levels for the magnetic, magnetic gradient and gravity methods. The small contrast in density between water and sandstone decreases the gravity anomaly and low susceptibility of sandstone decreases the magnetic anomaly size.

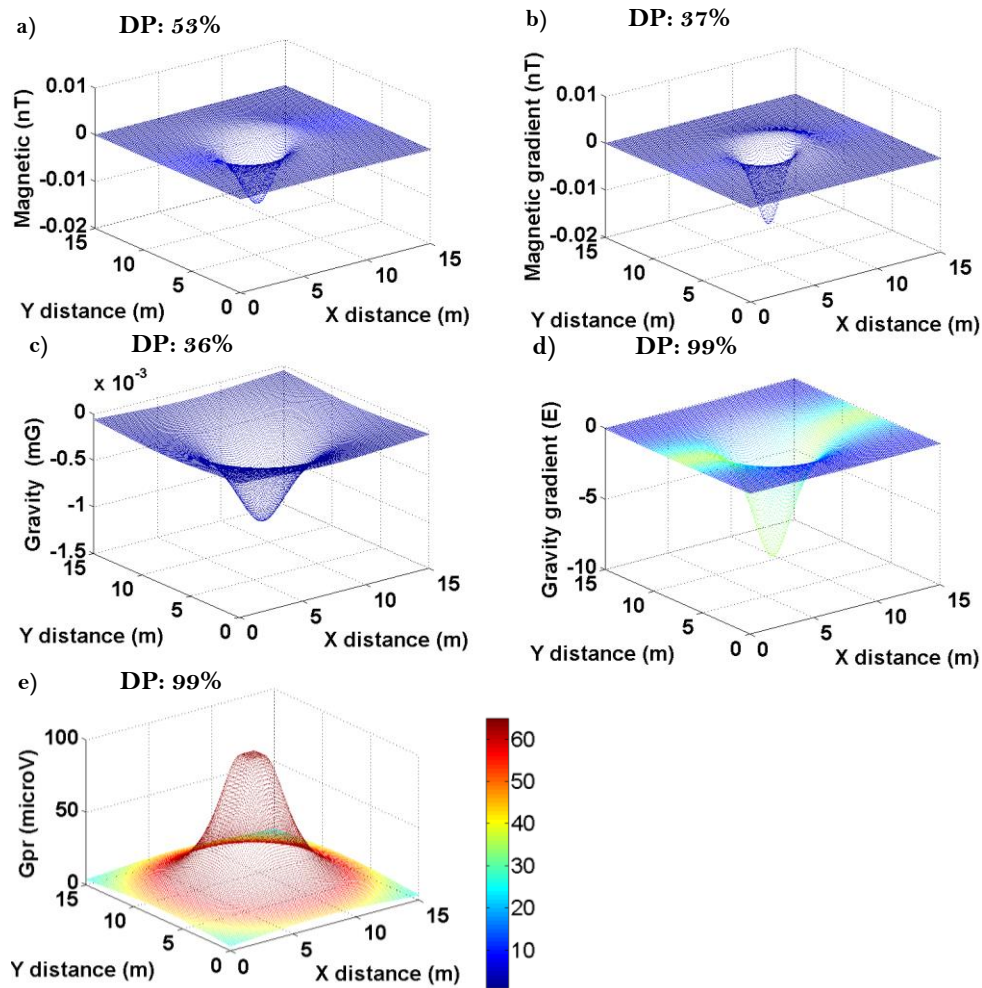


Figure 4.11. The cavity is a 1-m sided cube water cavity at 2 m depth in sandstone modelled with a) magnetic, b) magnetic gradient, c) gravity, d) gravity gradient, e) GPR. Overall detection probability is shown above each technique and the colour bar indicates profile line detection probability. DP = overall detection probability.

4.7.2 Survey cost and time

Based on the survey size and the spacing chosen by the user, the estimated time required in the field and cost of the survey are calculated. The number of profiles (for magnetic and GPR) or survey points (gravity) is calculated and divided by the average time and multiplied by the average cost for each technique. The field times and costs for each technique were found from a number of sources in the literature and from equipment manufacturers (Table 4.4). There was a wide range in estimates and field examples of the time and costs of each technique depending on when and where the survey was completed. An average of all these results was used in the calculations.

These values and the MATLAB code created are shown in 'field.m' (Appendix Axiii). The plan view of the survey, with survey points, profile lines, estimated cost and time

indicated is also visualised and presented to the user by ‘field.m’ (Figure 4.12). It should be noted that these costs and time estimates do not include post processing or planning.

Table 4.4. Geophysical survey costs and times.

Technique	Cost	Time
Boreholes	\$12,333/borehole ¹ \$90/m ¹ \$25/ft ¹⁸ \$10/ft ¹⁹	1 borehole /day ¹⁷
GPR	\$14.3/m ² \$21.42/m ³ €450/week ⁷	253 m/hour ¹² 63 m/hour ¹⁶
Resistivity	\$50/m ⁴	10 acres/day ¹⁰ 3,000 ft/day ¹⁰ 100 measurements/hour ¹⁵
Microgravity	€800/week ⁶	80 points/day ⁸ 100 points/day ¹¹ 140 points/day ¹⁴
Magnetic	€450/week ⁷	1 Ha/day ⁹ 1 Ha/hour ¹³

(Trainum, 2006): ¹Based on \$90,000–\$95,000 for 7–8 borings. ²Based on \$10,000 for two sides of a 300–400 m road. ³Based on \$15,000 for two sides of a 300–400 m road at 3 frequencies. ⁴Based on \$15,000 for 300 m road. ⁵Based on \$16,000 for 300–400 m road.

(Chalikakis *et al.*, 2011): ⁶Based on €601–1000/week for 2 people. ⁷Based on €301–600/week for 2 people.

⁸Based on 2000 m² per day on a 5 m grid (Rybakov *et al.*, 2001) and 80 stations per day (Rybakov *et al.*, 2005)

⁹(Matthews & Clayton, 2000).

¹⁰(Hutchinson & Barta, 2004)

¹¹(Reynolds International, 2009) based on a Scintrex AutoGrav.

¹²(Jol & Smith, 1995) based on 460 m and 550 m 1-m spacing profiles completed in 2 hours each

¹³(Geometrics, 2006) – G-858 MagMapper

¹⁴(Styles *et al.*, 2006)

¹⁵(Doll *et al.*, 1998)

¹⁶(Kruse *et al.*, 2006) based on a 9 m by 4.2 m at 0.2-m spacing over 3 hours.

¹⁷(McDowell, 1975) – slow rate because of large flints.

¹⁸(Kendorski, 2004) – increasing with depth.

¹⁹(Stolarczyk *et al.*, 2003) based on an estimate of \$300,000 for 100 boreholes to average depth of 300 ft.

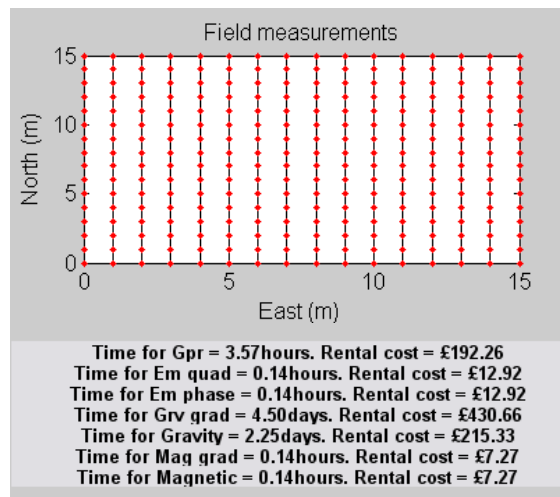


Figure 4.12. An example of the output of the field.m command. The red dots represent survey point for the gravity surveys, and the black lines are the profile lines. Estimated survey time and rental costs are listed below.

4.7.3 Collapse height

Cavity migration towards the surface is a consequence of an unstable cavity roof collapsing into the cavity itself. The deterioration of mining pillars or roofs are common causes, as is collapse of natural cavities. The roof will continue to fail causing upward stoping of the void. Stopping will continue until bulking of the collapsed material (now less dense) fills the void supporting the above material (Kendorski, 2004), a strong stratum forms a bridge over the void, or the surface is reached. This can occur anytime from a few months to years after the original cavity formation (Bell, 2004); the process will be accelerated with weaker overlying rock. Migration distance depends on a number of factors, most importantly the geology above the cavity (and how it breaks apart to bulk the void) and the dimensions of the cavity.

To assess whether the cavity parameters entered by the user indicate a risk of migration to the surface and subsequent collapse, a migration distance analysis is calculated within the GUI. The distance of migration is disputed, with a number of published rules. Healy & Head (1984) state that cavities are unlikely to migrate more than 5-10 times the seam thickness and usually less than 50 m depth. (Piggott & Eynon, 1978) give a maximum depth of possible collapse as 70 m. But (Clarke *et al.*, 2006) state that mine workings up to 300 m can still be a threat for up to 300 years. Waltham & Fookes (2003) suggest there is a threat to engineering if the cavity width is greater than the roof cover (excluding soil and fractured cover). Taylor (2000) advises that collapse is not a risk if there is 18.3 m of cover. (Littlejohn, 1979) highlight an example of 10:1 migration from a 3 m seam. Whilst (Bell, 1980) suggest the ratio is 6:1.

Here, the Piggott & Eynon (1978) theory is used, giving three possible collapse geometries for any given cavity (Figure 4.13). The migration distance is based upon the geometry of the cavity and the bulking factor of the geology above the cavity. The bulking factor for each geological material is stored in the 'geology.mat' matrix. The theory was converted into MATLAB code and incorporated into 'draw_subsurface.m' (Appendix A). The results are shown visually on the GUI (Figure 4.14).

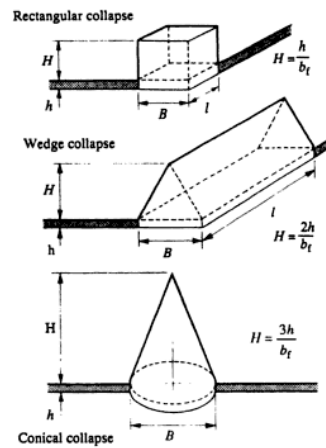


Figure 4.13 Maximum height collapse dependant on geometry. From Bell (2004) based on Piggott & Eynon (1978)

It should be noted that a competent rock above the cavity will stop the migration. It is suggested that a competent strata with thickness 1.75 times the span of the cavity will be sufficient to stop migration (Piggott & Eynon, 1978). Caves are more stable than artificial mining as the stronger arches prevent collapse. It is noted that the Piggott & Eynon (1978) theory is a general rule that does not consider the condition of the void or any changes in overlying geology and is used here only as a guideline to the hazard.

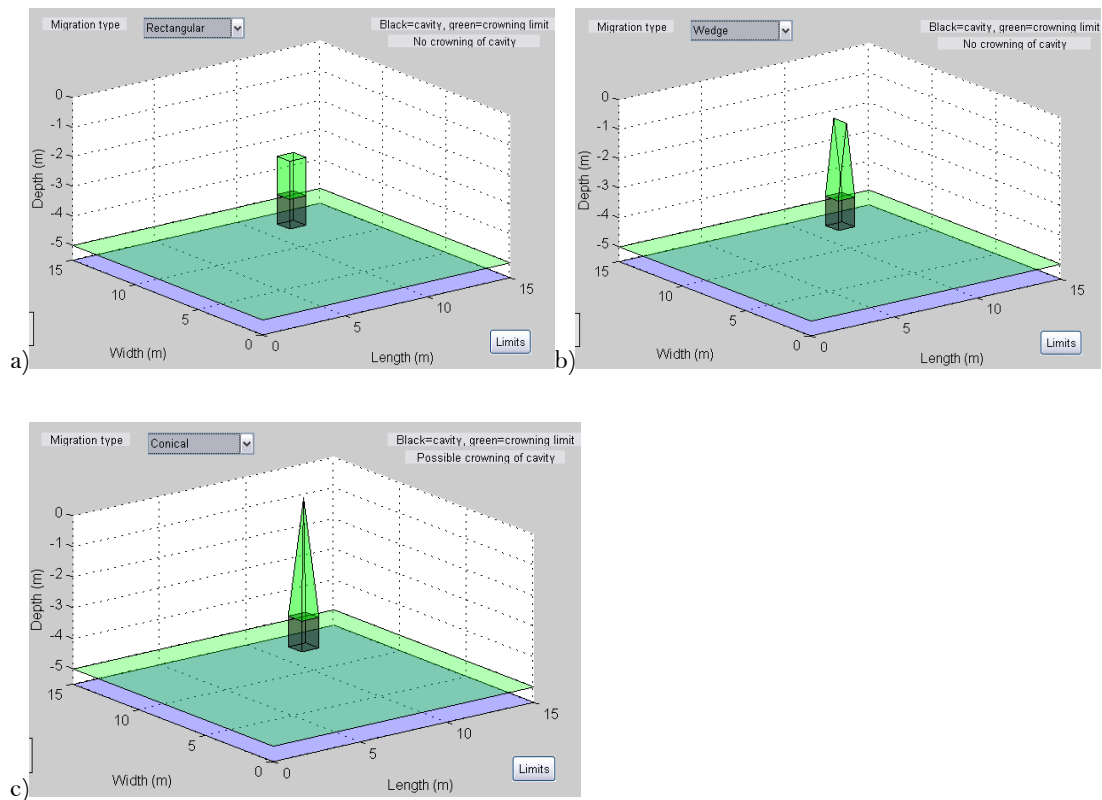


Figure 4.14. Modelled potential migration height of a 1-m cube, 3 m deep in limestone. The three migration types are shown, a) rectangular, b) wedge, and c) conical. Of the three, only the conical migration type represents a possibility of crowning (migrating to the surface). The conical shape is the extreme of migration and so circular cavities are more of a threat.

4.8 Chapter summary

This Chapter introduces the modelling process at the centre of this Thesis. Firstly, current modelling techniques at use are outlined and the limitations they have with regard to this work. Then follows detail on the geophysical modelling approach chosen for each technique.

An important element of this work is the creation of a user-friendly graphical user interface that a wide range of geophysicists and potentially geotechnical engineers can utilise to aid feasibility analysis of geophysics for cavity detection. MATLAB was chosen to be the most versatile and widely used host for the software. This Chapter highlights the numerous input options for the software and so acts as a guide for any potential users. There is some detail in the makeup of the software in the hope that future user will expand upon the functionality with more complex subsurface structures and with more techniques; the modular programming allows this flexibility.

Noise level on a site is of paramount importance to the likelihood of a successful geophysical survey. Despite this, there is little discussion, quantified or otherwise, of noise level in relation to survey planning. Here, it is at the centre of the modelling approach. In order to further understand typical noise levels a further literature review as well as in the field measurements at typical sites were completed. The noise level is the major comparator with the signal level in deciding the detection probability of a subsurface object.

The analysis and process of calculating the probability of detection of a signal in noise is laid out. This is a crucial element to the software and to this work as a whole. This process allows us to assess numerous geophysical techniques and the likelihood of survey success. It also allows us to assess the effect on detection probability that various parameter changes will have (both within the cavity system and on the site). This is explored in the next Chapters.

The addition of survey cost and time and the potential for collapse height were added to the software functionality after discussion with geotechnical engineers on additional features that would be of use. With these elements, as well as the central features (geophysical technique choice and parameter optimisation) the software represents a very useful tool for the field geophysicist as well as the geotechnical engineer looking to use geophysics on a project.

Chapter 5

5 Modelling Results and Data Analysis Implementation

The cavity modelling software can calculate the theoretical geophysical signal from a variety of cavity configurations in a range of environments. The probability of cavity detection in a given noise environment is calculated and used to analyse the feasibility of using geophysics and to compare geophysical techniques. Here, some typical simulated situations and case studies are explored to demonstrate the applications of the program and test its accuracy.

The amplitude, wavelength and shape of a cavity anomaly depend on numerous parameters. Variation of each parameter affects the signal intuitively but the complexity of the combination of parameters, especially in three dimensions, emphasises the need for mathematical modelling of geophysical methods rather than relying on rules of thumb or speculation based on previous field work.

To gauge an idea of how the signal changes with each parameter, a cuboid air cavity has been modelled for the total magnetic field technique on a single survey line, and parameters

changed individually (Figure 5.1). The parameters tested are: distance from cavity, depth to cavity, size of cavity, geology surrounding cavity, and cavity fill material. The other geophysical techniques can be modelled to show similar trends under parameter variation.

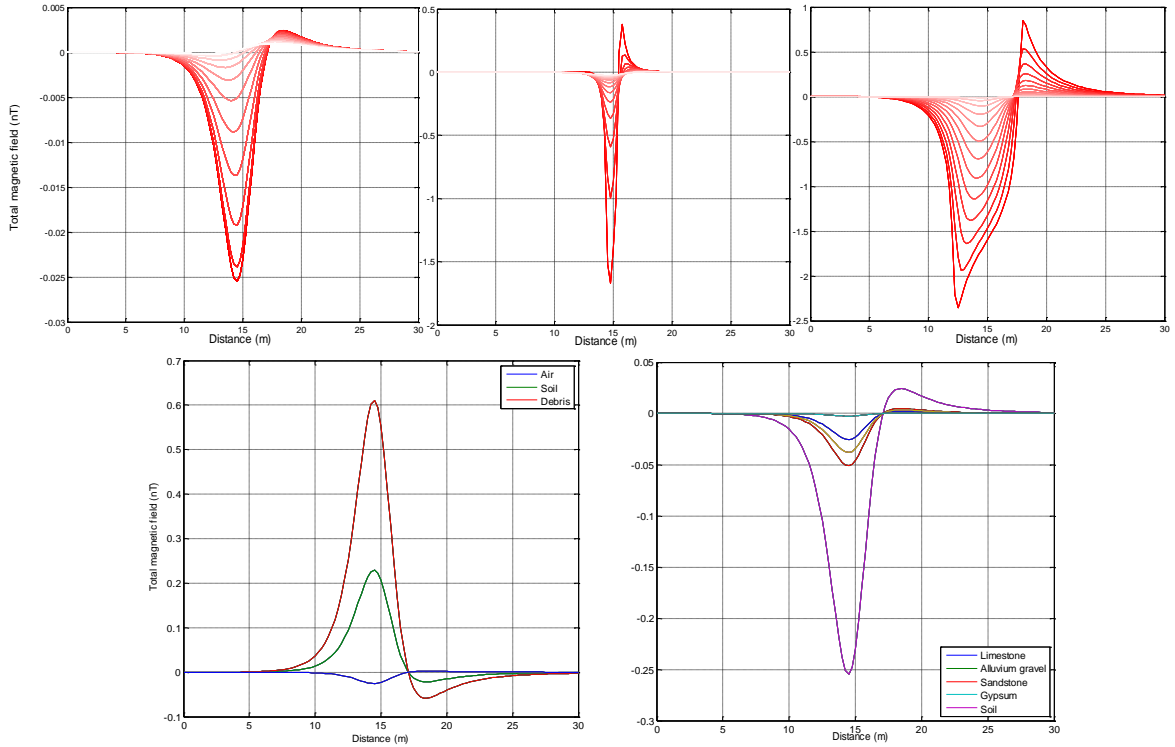


Figure 5.1. Total magnetic field over a cuboid air cavity. Base conditions are a 1 m air filled cube at 3 m depth in limestone, measured directly above the cavity. Signal amplitude decreases with a) distance from target (0.5 m increments from 0 m), b) depth to target (0.2 m increments from 0.1 m depth), c) decreasing cavity size (0.4 m increments down to 0.1 m cube), d) decreasing magnetic susceptibility of cavity material, e) decreasing magnetic susceptibility of host material. It can be seen that small changes in each parameter affect the signal in a logical manner but the combination of these factors can make accurate prediction of geophysical signal complicated.

5.1 Cavity variation

To get an accurate picture of the detection probability on a field site, modelling must be completed across the site footprint. The subsequent calculation of detection probability adds further complexity but provides vital information to the survey planners. As the problem becomes more complex, guesswork and rules of thumb lose their meaning and mathematical modelling becomes an essential part of the geophysical survey planning stage. The presented incorporation of modelling into survey planning will vastly increase the chance of survey success by providing information on technique choice and survey parameter.

In this section, numerous important subsurface parameters are altered and the subsequent effect on the detection probability presented for the range of geophysical techniques.

5.1.1 Cavity depth

From a geotechnical point of view, good knowledge of cavity depth of one of the most important factors when considering site hazards and the structural integrity of the subsurface. For geophysical survey planning, it is important to understand how deep each technique will be able to detect cavities to in given site conditions.

Figure 5.2a shows the effect of cavity depth on each of the technique's detection probability. It can be seen that in the very near surface (up to 2 m) magnetic, magnetic gradient and gravity gradient all have a very high detection probability in these conditions (see caption for site conditions). However, the magnetic gradient detection probability rapidly decreases with depth, while gravity gradient remains above 90% down to 10 m depth. Figure 5.2b shows the effect on anomaly size as depth increases. At 2 m depth all anomaly amplitudes are below 40% of anomaly amplitude at 1 m depth. This highlights how quickly signal will be obscured by noise with increasing depth.

These results show the large variation in the loss of signal with depth between techniques. These results are specific to this example, but the major advantage of modelling is that this depth trend can easily be produced for any number of environments.

5.1.2 Cavity shape

This modelling incorporates typical cavity shapes into near surface geophysics forward modelling, an important step towards accurate prediction of the feasibility of geophysics on a given site. To analyse the impact on detection probability, a range of cavity shapes, linings and fills are modelled (Figure 5.3) (for an example of a dipping gallery model, see the West Wycombe Cave case study). The magnetic and gravity methods are modelled over the different cavity shapes at 1 m depth in limestone at typical noise levels.

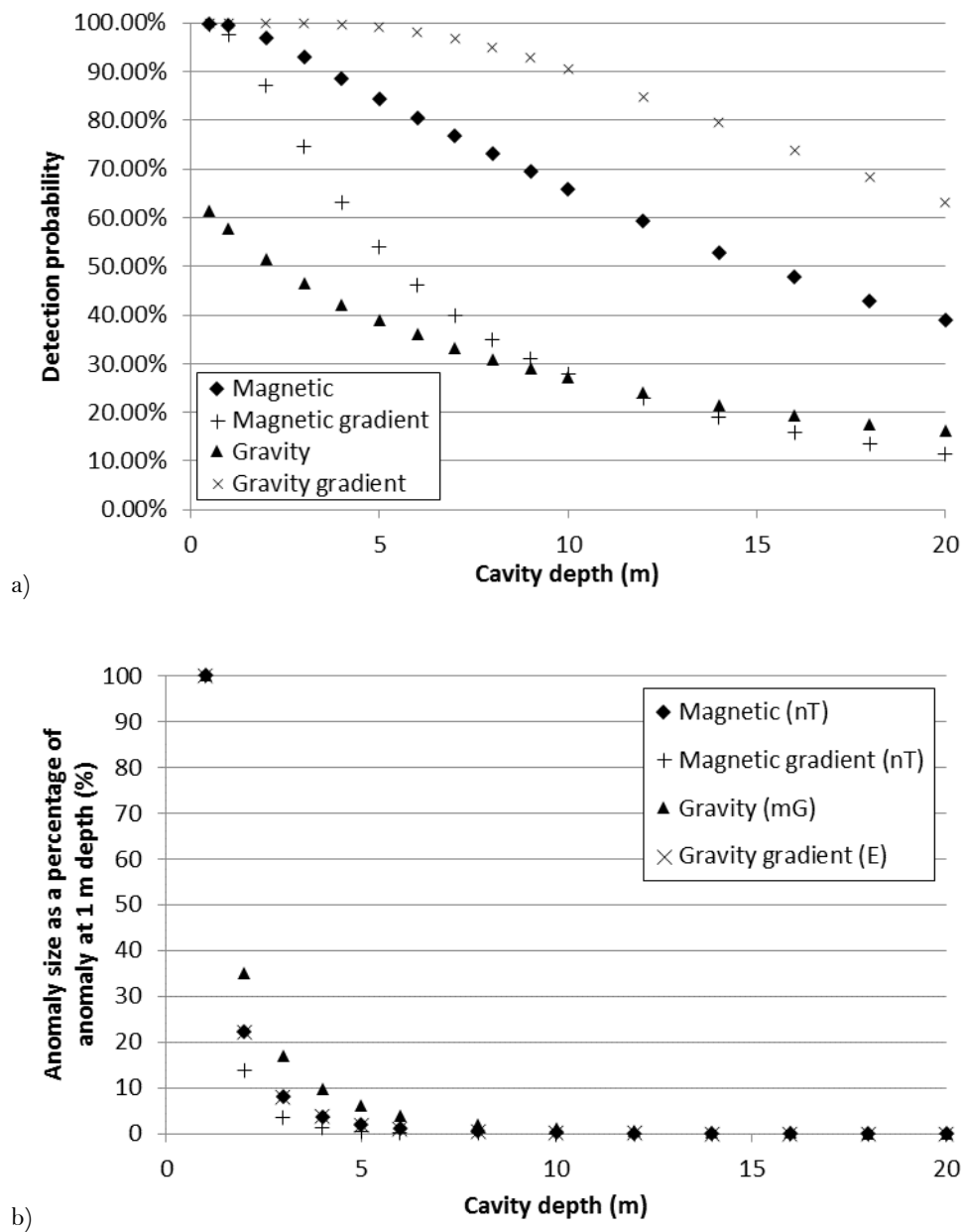


Figure 5.2. a) Detection probability of a 1-m cube air cavity in limestone at typical noise levels over a range of depths across a 15 m grid. b) Anomaly size over the same cavity expressed as a percentage of the anomaly size at 1-m cavity depth (original results of anomaly sizes in Appendix A).

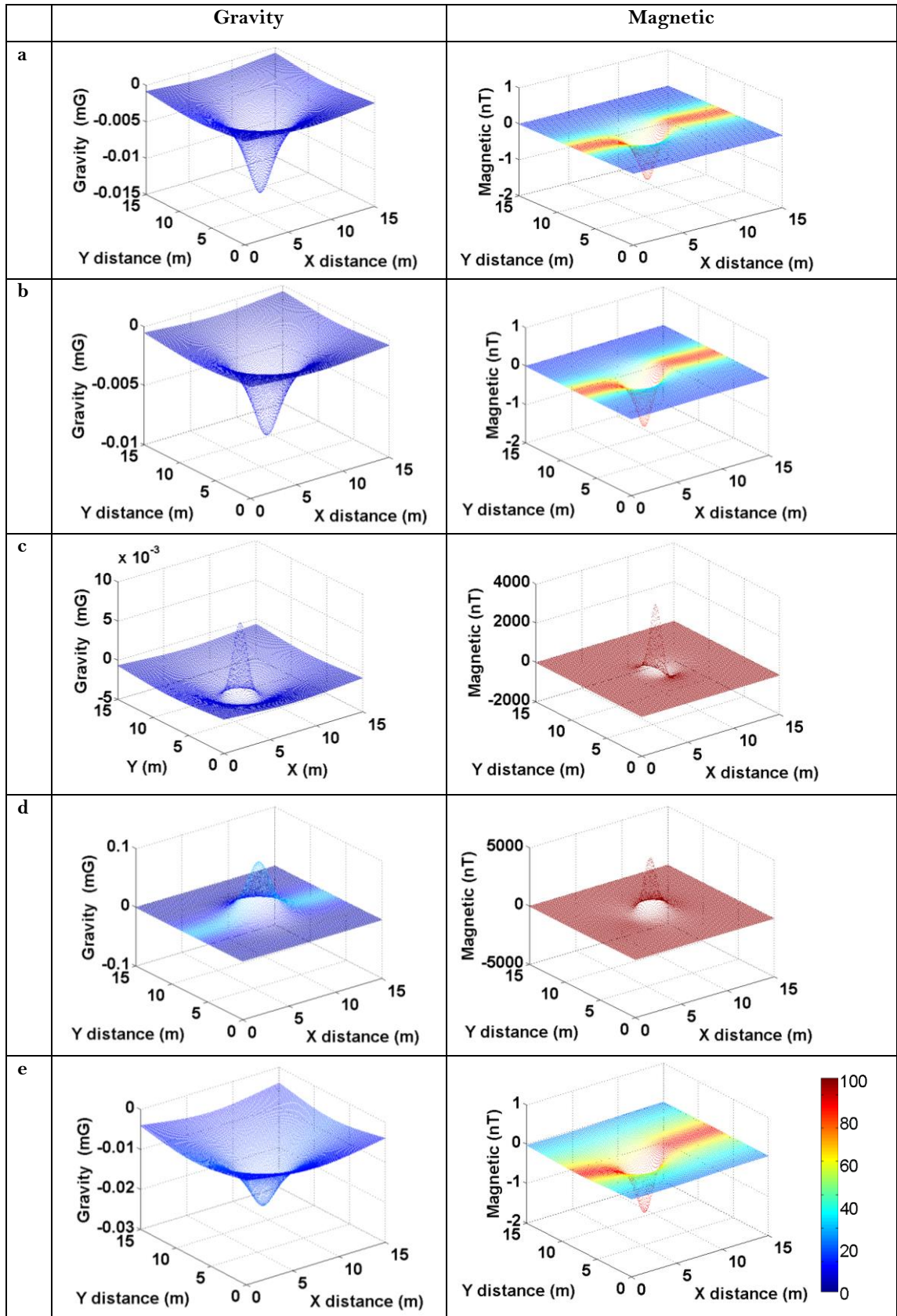


Figure 5.3. (Previous page) Modelled signal over typical cavity shapes in limestone. A 1 m square, 1 m deep, 6 m tall a) air shaft, b) water shaft, c) air shaft with 0.5 m steel cap, d) air shaft with steel lining and cap (0.5 m), and e) air shaft with 4 m square, 2 m tall bell pit beneath. The colour bar indicates detection probability (%). Total detection probability is over 99% for all magnetic models and, from top, 79%, 71%, 72%, 84% and 94%, for gravity.

Using the magnetic method, an air filled shaft and a water shaft are equally detectable. Using the gravity method, the high density contrast of an air shaft translates to an 8 percentage point higher detection probability than for a water shaft. The addition of steel lining and shaft cap increases detectability using the magnetic method across the whole site. With the gravity method over a capped shaft, the small amount of steel in the cap complicates the signal from the air shaft, resulting in lower maximum and minimum signal amplitudes and subsequently decreasing the detection probability. When the shaft is both lined and capped, the additional dense material in the subsurface results in solely a strong positive anomaly and a 5 percentage point detection probability increase using the gravity method. A bell pit beneath the shaft increases the detection probability for both magnetic and gravity techniques, though has a larger effect on the gravity method.

These examples show the significant effect that cavity shape and makeup have on detection probability. Endless other subsurface conditions can be modelled, and detection probabilities calculated for all techniques, giving an accurate assessment of the feasibility of incorporating geophysics into a project.

5.1.3 Shaft size

As noted previously, shaft diameter generally ranges from 2-8 m diameter (Figure 2.3) depending of age, local material and depth (Culshaw & Waltham, 1987). To assess the impact of these variations on geophysical anomaly size and detection probability, the range of techniques were modelled over a shaft with varying diameter (Figure 5.5).

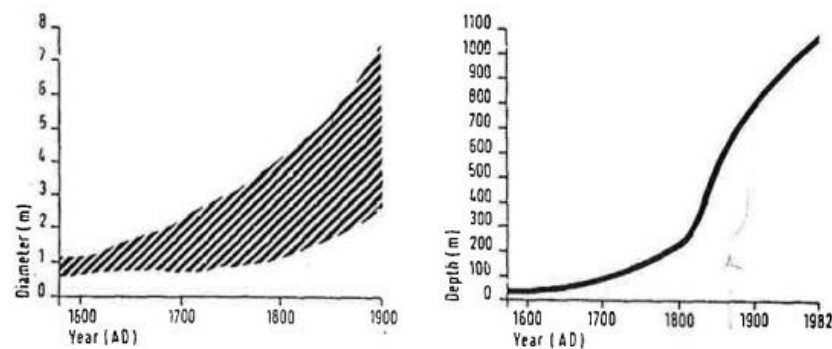


Figure 5.4. Shaft diameter (left) and depth (right) increases through time (Ove Arup and Partners, 1976).

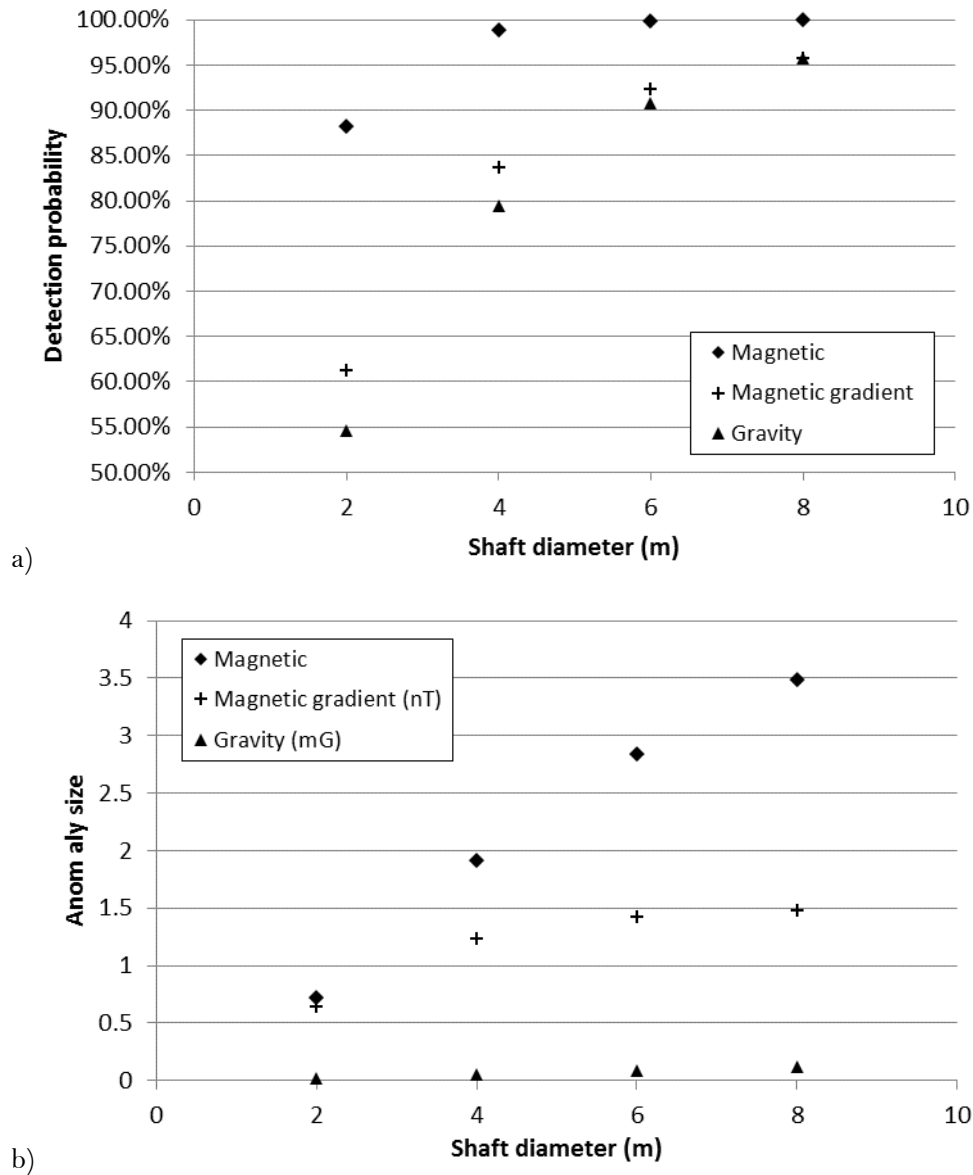


Figure 5.5. 2-m deep air shaft, with height of 20 m in clay, at brownfield noise levels (as would be typical on a site with a mine shaft).a) detection probability and b) anomaly size of signal above the 2-8 m diameter shaft. Gravity gradient is at 100% for all shaft sizes while GPR anomaly is very small (6.61×10^{10} microV).

The detection probability for the GPR and gravity gradient techniques is very high across the site and so the effect of the increased shaft diameter is negligible. However, for the other techniques where the detection probability for a 2-m shaft is low, a noticeable increase is seen with increasing shaft diameter. For the gravity technique a shaft of 2-m diameter is only 55% detectable, but an 8-m diameter shaft is above 95% detectable, a dramatically improved potential geophysical target. The magnetic gradient technique shows a similarly large increase in detection probability with increased shaft size.

These results highlight the importance of prior knowledge of the type of shafts which are likely to be present on a site. Shaft diameter, as well as height, is shown to greatly affect the geophysical anomaly and consequently the detection probability. If the target shaft diameter is unknown before the geophysical survey, this modelling software can assess the minimum size shaft which can be detected by each technique.

5.1.4 Rounded gallery

Modelling subsurface cavities as cuboids is not always the most consistent with real subsurface environments. In the case of subsurface galleries in soluble rock, the top of the cavity is often rounded as material collapses from the roof. Also, migrating voids will often be rounded at the top, again through roof collapse. To assess the impact a rounded roof section, modelling was completed for a cuboid gallery with the top corners removed (Figure 5.6).



Figure 5.6. Dotted line shows original gallery cross-section, solid fill shows rounded gallery cross-section; a third of the height and the width are removed.

Figure 5.7a shows that the decrease in detection probability for the gravity technique is minimal when the rounded gallery is modelled. This difference is more pronounced with a deeper cavity because at depth, with smaller anomaly sizes, small changes have a large effect on the detection probability. Figure 5.7b shows the percentage decrease in anomaly size caused by the rounding of the gallery for the magnetic, gravity and gravity gradient techniques. The anomaly size decrease is largest for the magnetic technique at shallow depths but the effect becomes similar at greater depths as signal amplitude becomes smaller.

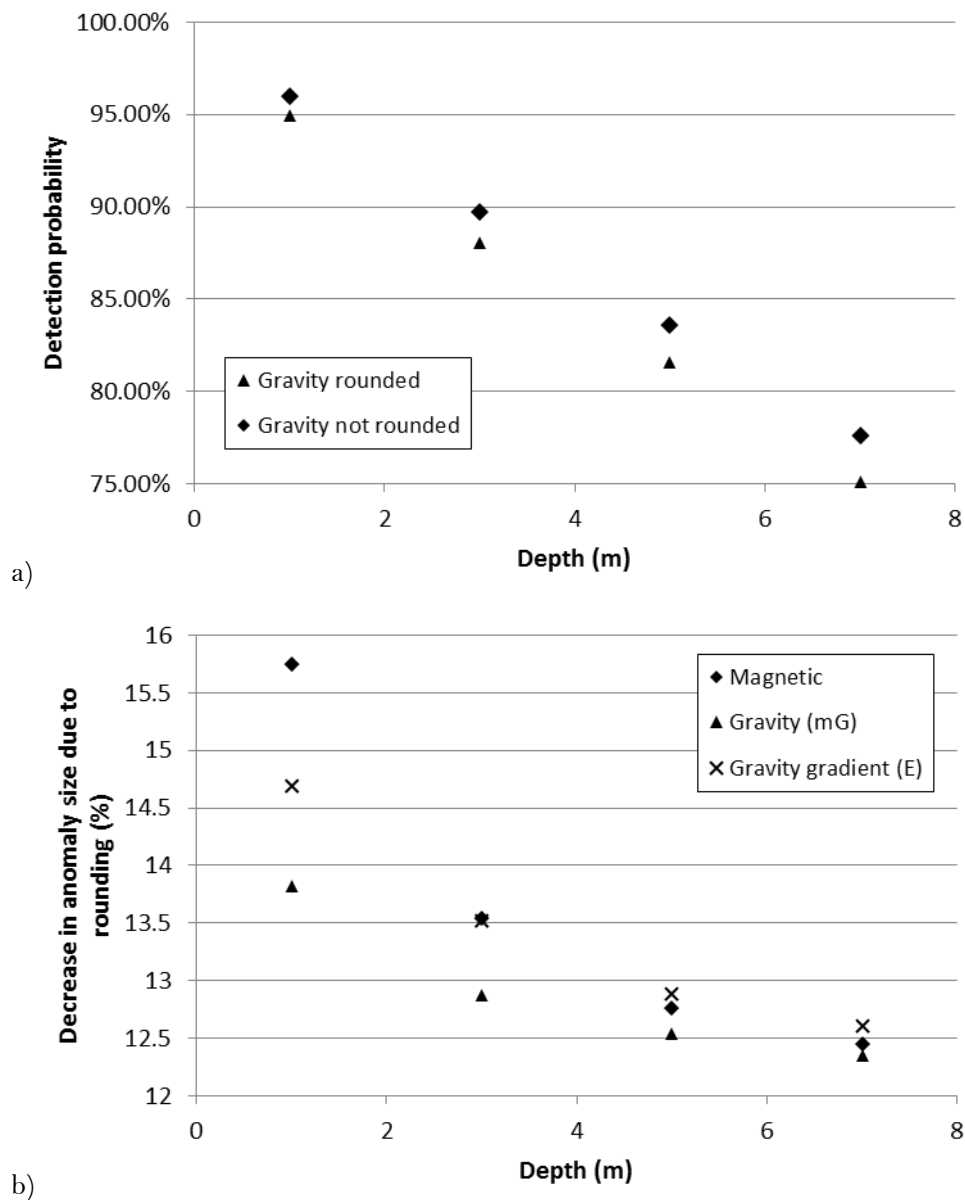


Figure 5.7. Modelling above a 1-m square, 15 m long gallery in limestone at typical noise levels. a) Detection probability of a rounded and non-rounded gallery with increasing depth. b) Effect on anomaly size due to rounding of gallery.

5.1.5 Fill material

Unless specifically designed to be so, as in mines, cavities are rarely pure air cavities. If the cavity is below the water table it will be water filled, a natural cavity will likely be rubble filled. After mine shafts are abandoned they are usually filled with local materials (natural or anthropogenic) in order to reduce the potential hazard. The bigger the cavity or shaft, the less likely it is to be completely filled (Culshaw & Waltham, 1987), and will be partially filled at the bottom of the cavity with air or water in the top section (especially as void space will migrate to the top of the cavity over time (Edmonds, 2008)).

Kendorski (2004) posit that a rubble filled cavity will cause a gradual loss of energy or signal from remote techniques, not the strong return that we would expect from a perfect void. Rybakov *et al.* (2005) observed a magnetic anomaly smaller than predicted and concluded that collapse had filled the cavity. Here, cavities with different fill materials are modelled to investigate the effect on the overall detection probability for the magnetic and gravity techniques (Figure 5.8).

For the gravity technique the air cavity gives the largest density contrast and so the highest detection probability. The remaining fill materials decrease in detection probability with their increasing density (and hence contrast from the limestone density). In this case material filled cavities do provide a smaller geophysical anomaly than the air filled cavity.

For the magnetic technique, the air cavity has the lowest detection probability, with the anthropogenic fill providing the highest detection probability (due to the increased magnetic susceptibility incorporating metal materials). These results are at odds with Kendorski (2004) and Rybakov *et al.* (2005) who suggested a filled cavity would result in a smaller geophysical signal. However, here fully filled cavities are considered, more research needs to be completed in the detection probability of partially filled cavities.

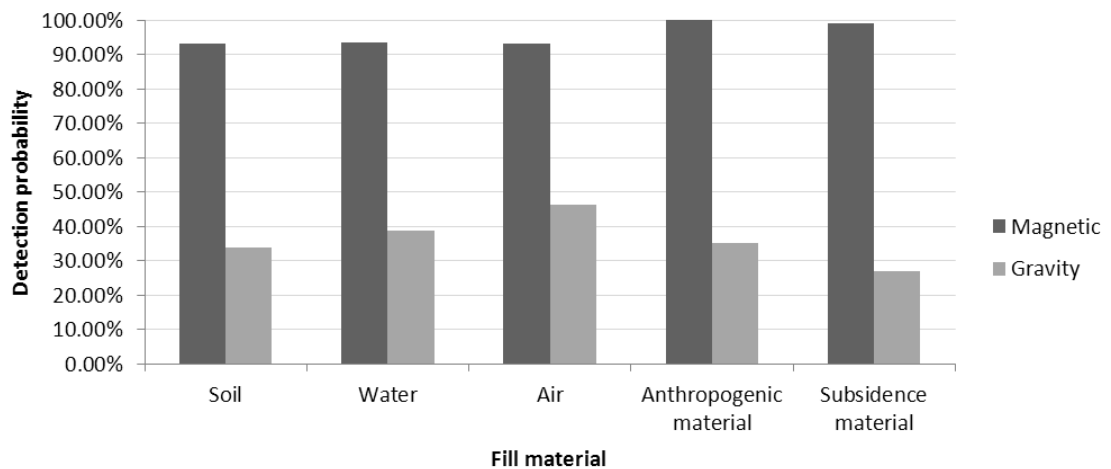


Figure 5.8. Detection probability of 1-m sided cube (with various fill material), 3 m deep in limestone across a 15 m square site. Density (left to right): 1.5 g/cm³ (Erkan & Jekeli, 2011), 1 g/cm³ (Milsom & Eriksen, 2011), 0.0012 g/cm³ (International Standard Atmosphere), 1.4 g/cm³, 1.8 g/cm³ (average from Pueyo-Anchuela *et al.*, 2010). Magnetic susceptibility: 1×10⁻⁷ (Milsom, 2003), -9.051×10⁻⁹ (Arrighini, 1968), 0 (Milsom, 2003), 0.05, 0.005 (average from Pueyo-Anchuela *et al.*, 2010) SI units.

5.1.6 Lining material

As discussed in the Literature Review, shaft lining and cap material, if utilised, depend on the date of the mine and on local materials. Here, the effect of a range of lining materials on the geophysical anomaly and the detection probability of the shaft is tested (Figure 5.9).

Wood and brick, as used before the 18th century, and metal (steel) and concrete are tested (Culshaw & Waltham, 1987) – the associated geophysical parameters are stored in `set_parameters.m` (Appendix Av).

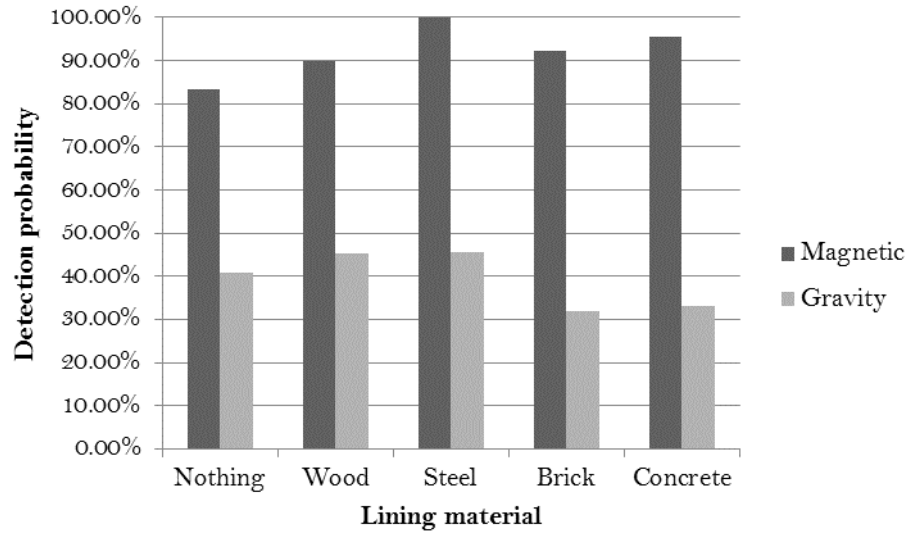


Figure 5.9. Modelled detection probability over a 1 m deep, 10 m tall, air shaft in limestone, at brownfield noise levels. Lining and cap are both 0.2 m thick.

For the magnetic method the addition of lining always increases the detection probability. The largest impact is with steel lining which has a much higher magnetic susceptibility. Brick and concrete have similar magnetic susceptibilities (0.0013 ((Hus, Ech-Chakrouni, & Jordanova, 2002) and 0.0017 (McEnroe, 1998) respectively) and so have similar detection probabilities. Although wood has susceptibility negligibly close to air (Rákoš *et al.*, 1984), the extra volume around the cavity of low susceptibility caused by the wood lining increases the detection probability.

With the gravity method, the high density steel creates a large anomaly and increases the detection probability. The addition of low density wood serves to increase the size of the low density cavity by the lining width and thus increases the detection probability. For the concrete and brick lining (average of 2.3 g/cm³ (Kosmatka, 2010) and average of 2.25 g/cm³ (Automation Creations, 2014) respectively), the addition of a dense material around the low density cavity works means the two anomalies work against one another to produce a lower amplitude anomaly, and hence a lower detection probability.

5.1.7 Lining thickness

Varying lining thickness in the modelling software produces some interesting and unintuitive results (Figure 5.10). The magnetic detection probability intuitively increases as the lining thickness increases as the concrete lining has a high susceptibility compared to

the cavity and the limestone surrounding material (Figure 5.10b). However, for the gravity method the high density lining serves to decrease the amplitude of the anomaly and lower detection probability. With thin lining (0.1 m) a large negative anomaly is seen which as a detection probability of 35%. As the lining thickness is increased the positive lining signal becomes more prominent in the overall anomaly. This serves to decrease the amplitude of the negative anomaly at the centre of the site, lowering the detection probability. With the lining thickness at 0.5 m a positive signal is seen at the centre of the site (caused by the lining) amongst the larger negative signal caused by the cavity. The maximum to minimum amplitude is still lower than other lining thicknesses and the detection probability is still lower.

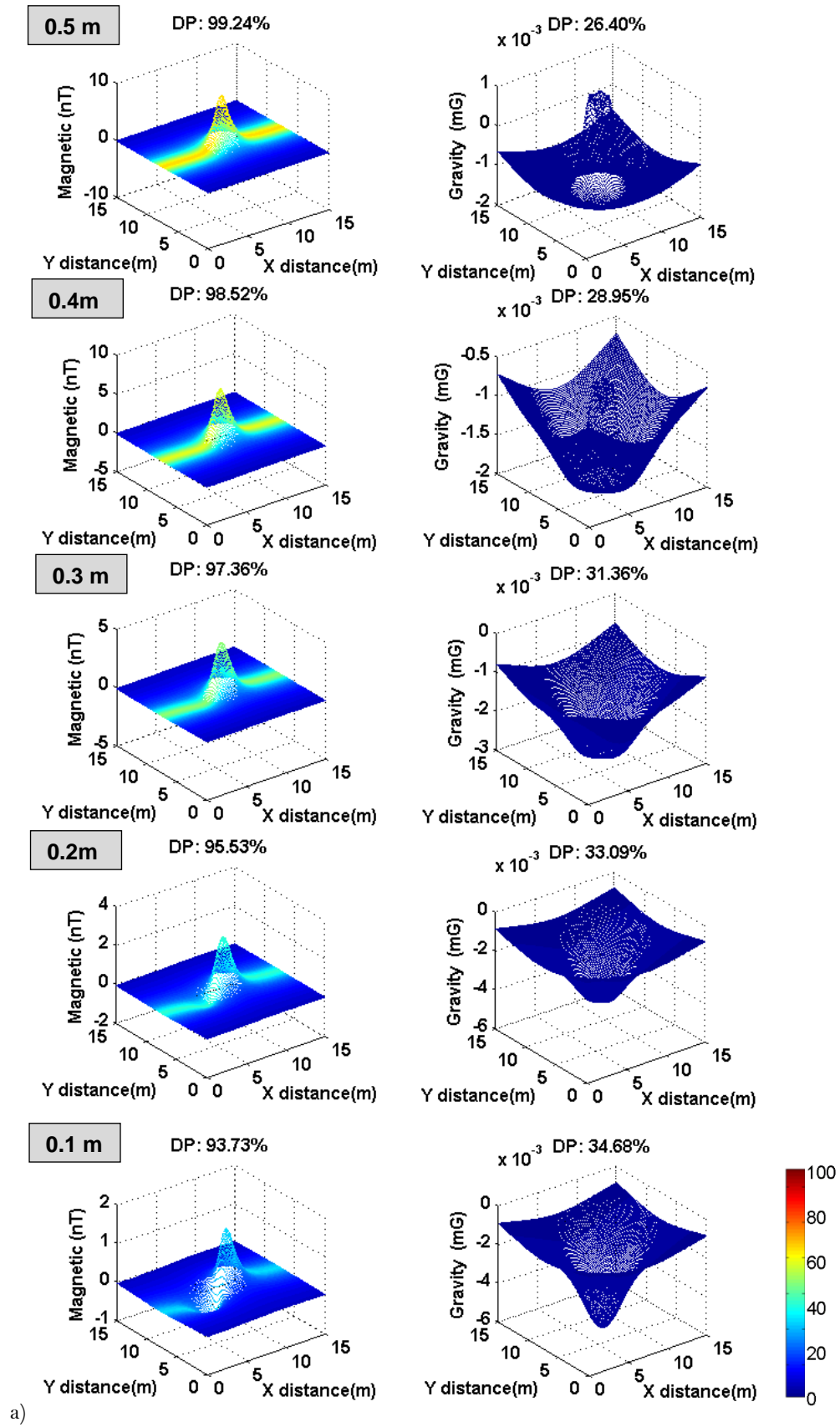
These diverging magnetic and gravity results show that non-intuitive results can be found in cavity detection and highlight the need for modelling of the techniques before the field. Modelling in this case would also help to clarify any unintuitive results that may be recorded in the field.

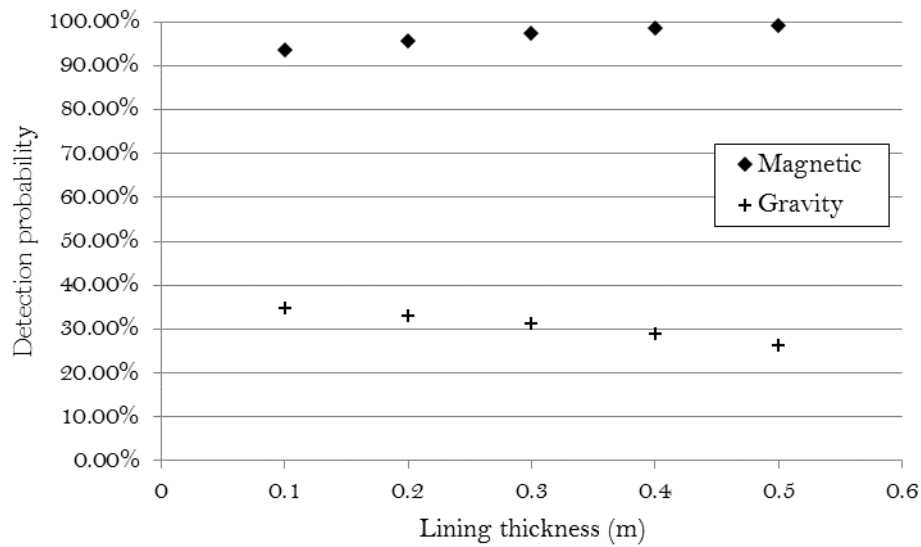
5.2 Site conditions

As well as cavity variations, the site conditions also have a large impact on the calculated detection probability and the consequent feasibility and technique choice. In this section, the effect of changing a range of site conditions on detection probability for each technique is investigated. When these factors are considered alongside the cavity parameters discussed in previous section, a detailed picture of the site conditions is built and the accuracy of detection probability calculations is improved. It is important for geophysicists and geotechnical engineers to consider all of these parameters when scoping or designing a geophysical survey.

5.2.1 Geology

The geology of the site is one of the most important factors in determining whether a geophysical technique will be feasible for cavity detection. The geology of the site should be easy to determine from geological maps or from on-site sampling. With this information, the geophysical parameters can be determined from reference material or the parameters can again be measured on site. The impact on cavity detection probability is assessed in various geologies (Figure 5.11).





b)

Figure 5.10. a) (Previous page) Modelling results for the magnetic (left column) and gravity (right column) techniques over a 1 m deep, 10-m height, air shaft in limestone, at brownfield noise levels with concrete lining. Grey box represents the lining thickness in that row's models. Colour bar represents the detection probability, DP = overall survey detection probability. b) The overall detection probability for all lining thicknesses.

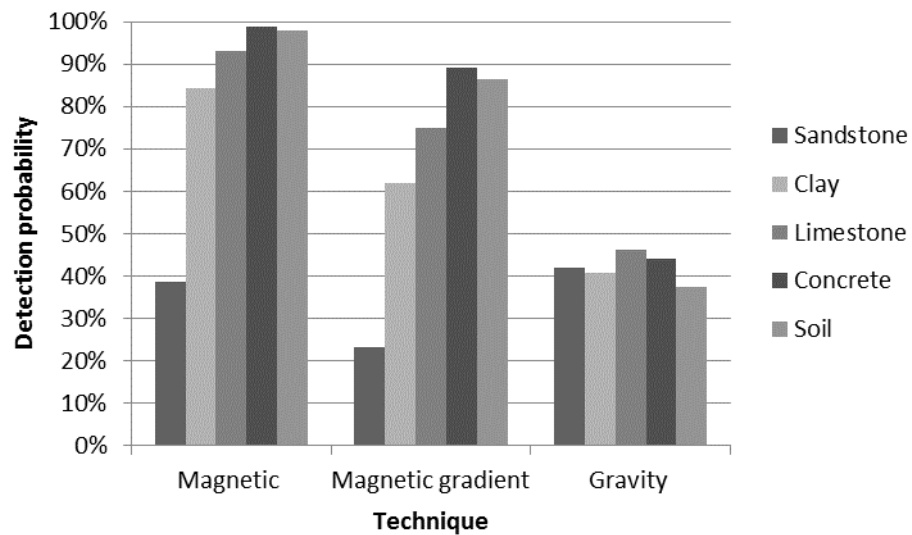


Figure 5.11. Detection probability of the range of techniques for a 1-m cube air cavity, 3 m deep in typical noise conditions in a range of geologies. See Table 4.1 for geophysical parameters. Gravity gradient has above 99% detection probability in all geologies.

The magnetic and the magnetic gradient technique follow the same trends of detection probability for the chosen geologies. A cavity in concrete has the highest detection probability because it has the highest magnetic susceptibility and so the contrast with the

zero magnetic susceptibility is the highest. A cavity in sandstone has the lowest detection probability of all the geologies tested. Although the magnetic gradient technique has a larger anomaly than the magnetic method, the detection probability is lower because a higher noise level was used (0.2 nT).

The gravity method shows little variation in detection probability between the geologies. This is due to the similarity in densities of the geologies, varying just 0.73 g/cm³ between limestone, the most dense (and hence largest density contrast and subsequent highest detection probability), and soil, the least dense.

It should be noted that estimation of geophysical parameters from geological maps can be fairly inaccurate and parameters can be wrong by orders of magnitude. This is discussed further in Section 5.2.7 (Parameter variation).

5.2.2 Noise level

In broad terms, as noise increases, the probability of detecting a cavity at a site decreases. As shown (Section 4.3.2.4) noise values can vary greatly between sites. It is important to have a good understanding of the potential noise level on a site before assessing geophysical technique applicability and feasibility.

Figure 5.12 shows the modelled magnetometry detection probabilities of an air shaft (1 m square, 6 m deep) at 1 m depth in the four noise levels previously measured in the field 4.3.2.4. At the greenfield noise level, detection probability of the shaft is above the standard 95% confidence interval. At all other noise levels the probability of cavity detection is very low and hence the magnetic method is inapplicable. Using typical noise levels, the gravity technique similarly decreased to below 50% in the brownfield noise environment.

Figure 5.13 shows the modelled detection probability results of the previous example cavity (1 m air cuboid at 3 m depth in limestone) but at three noise levels taken from the relevant literature (instrument sensitivity, instrumental noise, and typical quiet site noise). Magnetometry, gravity and gravity gradient are modelled. There is a high detection probability at the “instrument sensitivity” noise level for all techniques. The probability decreases with increased noise level but each technique is affected differently. The gravity technique shows the quickest decline in detection probability; from 95% at instrumental noise levels, to 46% and 18% at typical and brownfield noise levels. The magnetic results show inapplicability in brownfield noise conditions, a consequence of large magnetic noise level due to metal scraps present. Gravity gradient remains a viable option across all noise levels.

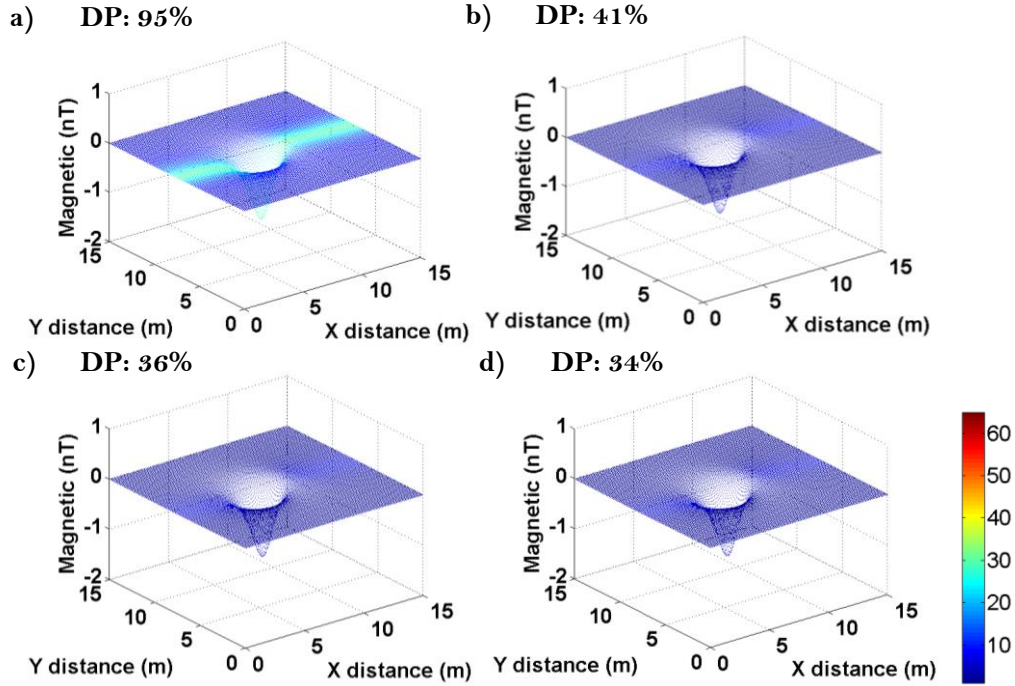


Figure 5.12. Modelled magnetometer signal of a 1 m square and 6 m tall air shaft in limestone at 1 m depth in different noise conditions: a) greenfield, b) urban and buildings, c) brownfield and d) indoor. The colour bar indicates profile detection probability. DP = overall detection probability.

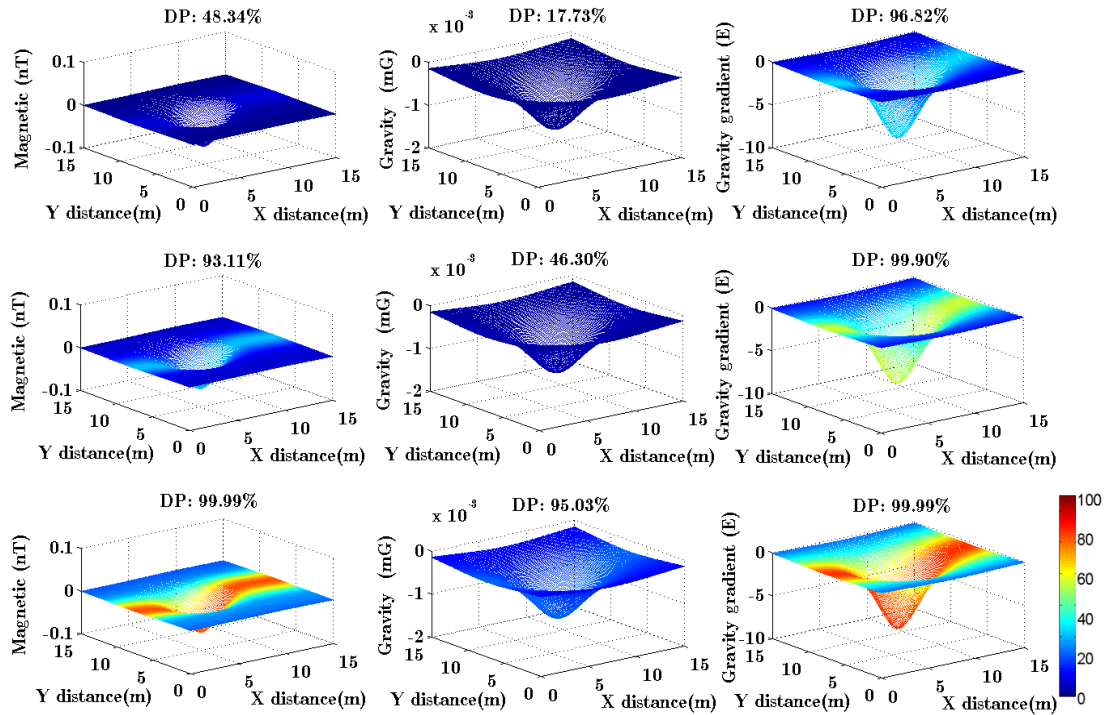


Figure 5.13. Program output of the modelling for a 1 m air cube in limestone at 3 m depth. From left, the techniques modelled are: magnetic, gravity gradient, gravity. From the top, the noise levels are: brownfield, typical, instrumental. These variables can be found in sections 4.3.2.4 and the set_parameters code (Appendix Av). DP = overall detection probability.

These tests highlight the importance of site specific noise level consideration in near surface modelling and the effect the choice has on detection probability. Despite this, consideration of site noise level in modelling and survey design are presently very uncommon and so this software is an important iteration of near surface modelling evolution. Estimating noise as a percentage of the modelled anomaly does not represent changing site conditions (Ma, Li, & Huang, 2013) and using literature noise values can be useful. However, neither are substitutes for noise measurements from a similar site or, in a perfect scenario, from the site itself as presented here.

5.2.3 Profile and station spacing

Profile and station spacing judgment is of great importance in survey design. An optimum design will detect the target with the least amount of stations possible, saving time and money. The presented modelling software can calculate the minimum spacing required to detect a cavity to a certain confidence interval (set here at 95%).

Waltham & Fookes (2003) suggest that in karst environment using microgravity a 2 m spaced grid can identify caves of 1 m across. Styles *et al.* (2005) suggest that station spacing should be chosen based on the depth and size of the cavity. However, as we have seen, the geology, fill, noise level and cavity shape are also of great importance to cavity anomaly size and consequently, as we will see here, on the optimum station spacing.

Figure 5.14 shows the modelled signal of the magnetic, gravity, gravity gradient and GPR techniques for the previously used example of a 3 m deep, 1-m cube air cavity in limestone across a 15 m survey grid. The maximum responses are small for all techniques (amplitudes of 0.08 nT, 0.0013 mGal, 8.3 E, 26 μ V) but at typical noise levels (see section 4.3.2.4 and Table 5.1) the detection probability (shown by the colour of profile lines) is over 50% for the gradient gravity and GPR method on the central profiles.

An increased number of survey points or profiles across the site will increase the detection probability of the anomaly. To assess the optimum survey design, the detection probability is calculated with a range of profile spacings (Table 5.1). The detection probability falls quickly as spacing is increased but the decrease is variable between techniques. A spacing increase to 2 m decreases the total detection probability by: 24 (GPR), 19 (gravity), 20 (magnetic) and 1 (gravity gradient) percentage points. Increasing spacing to 3 m decreases detection probability a further: 14 (magnetic), 9 (gravity) and 8 (gravity gradient) and 34 (GPR) percentage points.

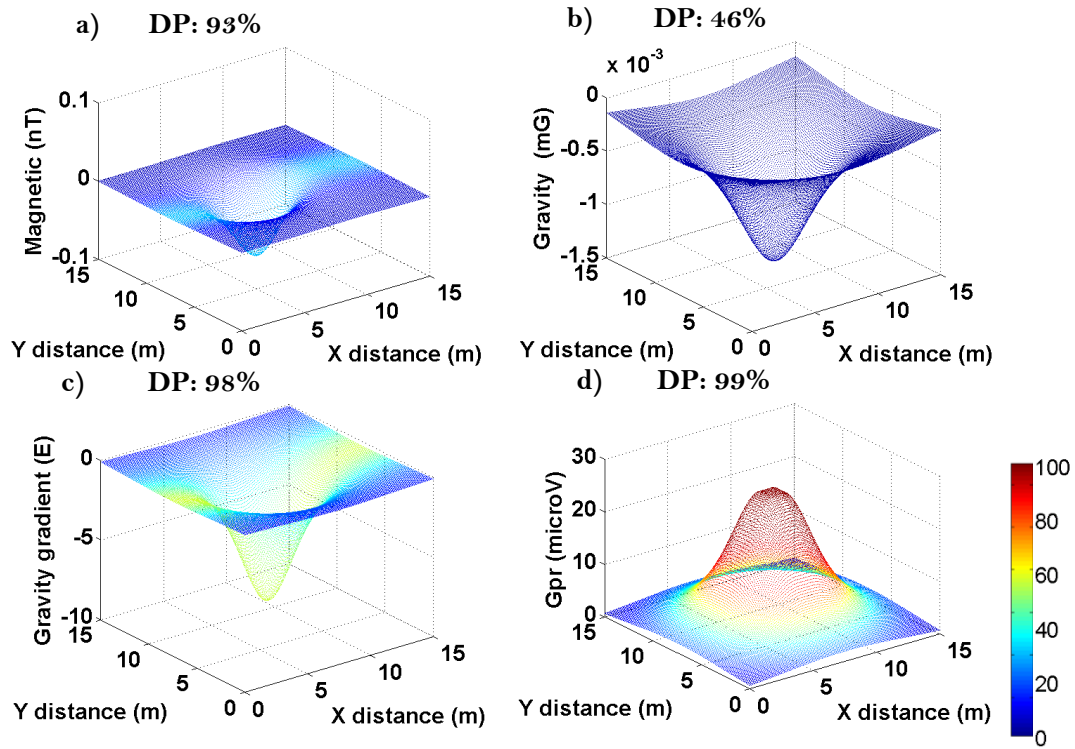


Figure 5.14. Theoretical response to a 1-m cube cavity at 3 m depth in limestone over a 15 m square grid by: a) magnetometry, b) gravity, c) gravity gradient and d) GPR techniques. Colour scale represents the detection probability for each survey line. DP = overall detection probability.

With 2 m spacing, the gravity gradient method has over 95% chance of cavity detection and is hence suitable for use in this situation. However, gravity gradient is a slow, and hence expensive, technique in the field and so GPR or magnetometry may be more cost effective solutions at this noise level. This is, of course, just one example and minor changes in any parameter will alter all of the technique's detection probabilities. Spacing intervals are forced to 1 m increments here as these are the easiest to set up in the field, though more accurate spacings can be calculated for use with, for example, a robotic survey setup.

Table 5.1. Effect of increased spacing. Detection probability (%) of a range of techniques with increasing survey spacing. Darker shade represents a higher detection probability.

Technique	Noise	Spacing		
		1 m	2 m	3 m
Magnetic	0.1 nT (Geoscan Research, 2012)	93	73	59
Gravity	0.1 mGal (Laswell <i>et al.</i> , 2008)	46	27	18
Gravity gradient	3 E (Erkan and Jekeli, 2011)	98	97	91
GPR	10 μ V (Erkan and Jekeli, 2011)	99	75	41

5.2.4 Survey direction

At any latitude the peak to peak amplitude of a magnetic anomaly is largest when measured in the north-south direction (Breiner, 1999). This often justifies the orientation of a magnetic survey in the north-south direction (Scollar, *et al.*, 2009; David, 2008). However, here it is shown that a survey in this direction is not always optimal.

Figure 5.15 shows the contoured modelled total magnetic field over a 1-m air cube at 3 m depth in limestone. In a given level of noise, only signal above certain amplitude will be detectable and so the contour shapes indicate the region that a signal of that level is detectable. For example, the 0.001 nT contour spreads across most of the survey site; if this is the lowest signal detectable at a given noise level (too subtle in reality) then a profile running through this contour will detect the target. Contour extents in the east-west and north-south direction are measured (Table 5.2) and the direction most likely to detect the target is inferred by the survey direction with the largest span.

For smaller signal levels (up to 0.001 nT) the anomaly is wider (E-W) than long (N-S) and so a survey in the north-south would be more successful. However, above this level the anomaly is longer (N-S) than wide (E-W) and so an east-west survey is more appropriate. This is clarified by calculating the detection probability using the cavity detection modelling algorithms at different noise levels. Figure 5.16 shows the detection probability of a survey running east-west minus a survey running north-south. An east-west survey is always more likely to detect the example cavity than a north-south survey above 0.1 nT noise. The peak difference occurs at 0.8 nT noise when an east-west survey is 2.3 percentage points more likely to detect the cavity than a north-south survey. The difference then decreases as the length and width of the anomaly become more similar at higher signal levels (Figure 5.15). These are very interesting results as they are in contradiction to standard practice.

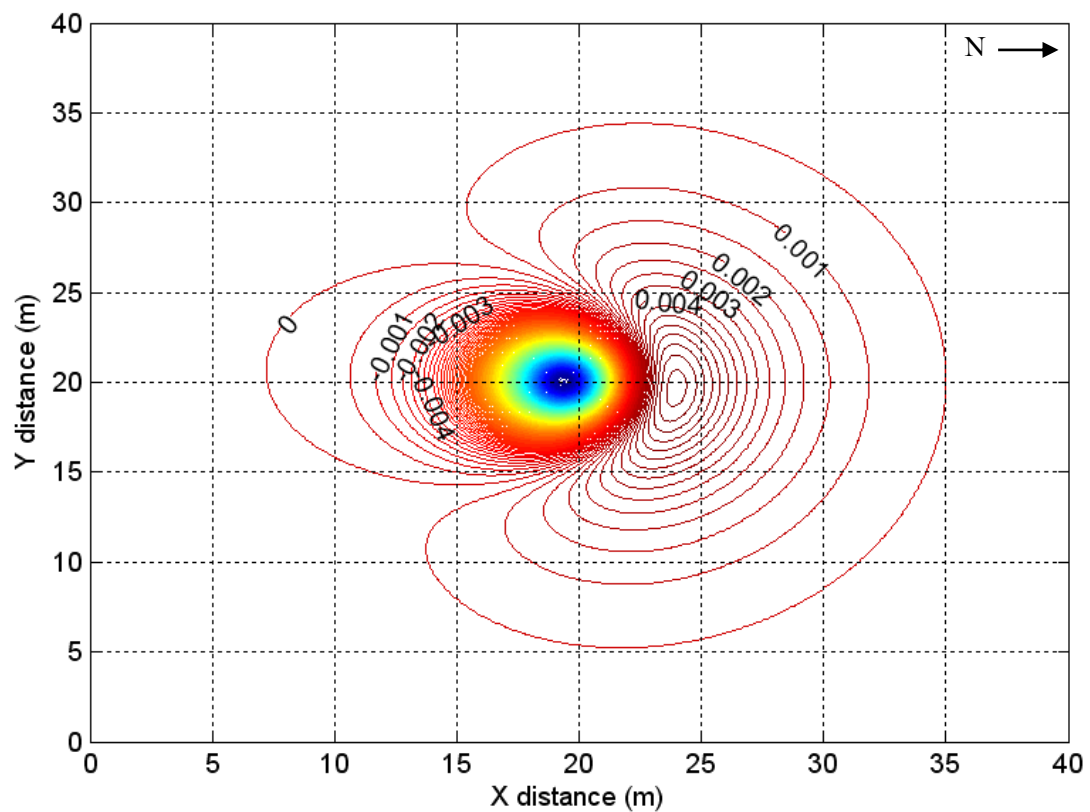


Figure 5.15. Plan view of a modelled magnetic field contours over a 1 m sided air cube at 3 m depth in limestone. Although detection at the level of signal indicated by the contours (down to 0.0005 nT) is unachievable in the field, the contours show the expanse of each level of signal across the site. The shape will be similar for higher magnitude anomalies dependent on the depth, size and makeup of the cavity and can be scaled up appropriately. Signal levels highlighted in Figure 5.15 are labelled.

Table 5.2. Comparison of magnetic anomaly size (Figure 5.15) width and length at different signal levels to assess the optimum survey direction.

Signal level (nT)	Anomaly size (m)		Difference (m)
	Width	Length	
0.0005	28.0	24.3	-3.7
0.001	22.1	20.1	-2.0
0.002	15.9	16.5	6
0.003	12.6	14.4	1.8
0.004	10.1	13.0	2.9

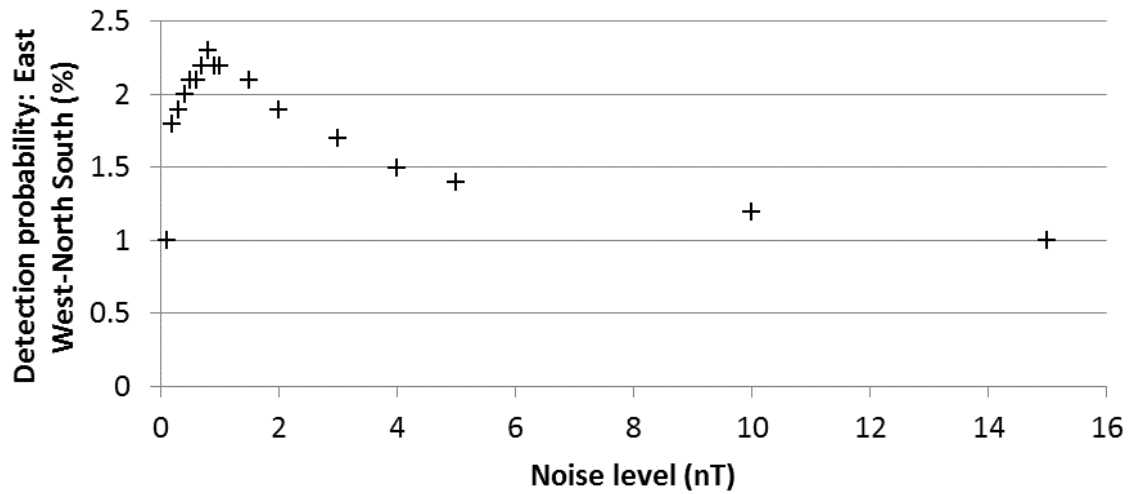


Figure 5.16. Difference between the detection probability of a magnetic survey running east-west and a survey running north-south over the cavity shown in Figure 5.15. A positive result indicates the east-west survey has a higher detection probability. The shape and amplitude of this graph will change dependant on cavity type and subsurface environment.

5.2.5 Survey size

The size of a geophysical survey can be important factor in the feasibility of using a particular technique to detect cavities. Deeper cavities have large wavelength cavity signals and so a survey requires more space to detect the whole anomaly. There can be site restrictions which can limit survey size: fences, hazardous regions, geophysically noisy areas where signal will be obscured. It is therefore important to consider survey size in the survey planning stage.

Figure 5.17 shows the effect on detection probability of increasing the survey area. For all techniques the detection probability increases with larger survey size, as more of the anomaly is recorded. The magnetic techniques reach a point where increasing the survey size has little effect on increasing the detection probability (the gravity technique still shows detection probability increase up to 20 m survey size). This analysis would be very useful in determining the maximum and minimum limits of survey size required. There is little point in spending extra money and time increasing survey size if the detection probability is not increased and the survey must be big enough to detect the cavity to a suitable degree of significance.

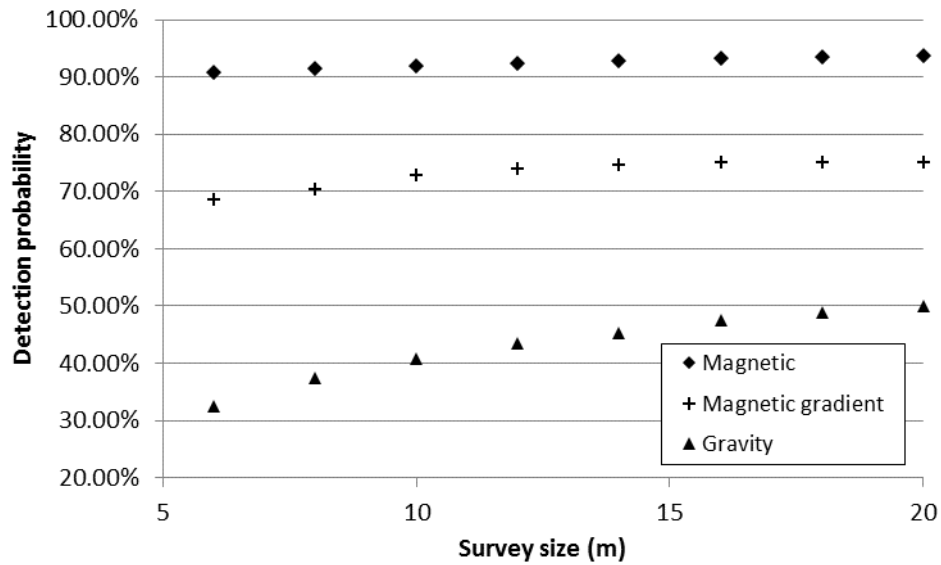


Figure 5.17. 1-m air cube, 3 m deep in limestone, at typical noise levels modelled at various survey sizes. X axis represents the length of side of a square survey. GPR and gravity gradient detection probability is above 99% for all survey sizes.

5.2.6 Data deletion percentage

Often, during data processing, a number of noisy data points need to be deleted, most often noisy anomalies (*e.g.* spikes in magnetic data, incorrectly coupled resistivity spikes). Here, the impact of random data deletion on detection probability is considered.

The potential techniques were modelled over a 1-m cube air cavity at 3 m depth in limestone with 2-m spacing at typical noise levels (Table 5.1). The data deletion had a more pronounced effect on detection probability for the gravity techniques which record fewer points along the survey line than the magnetic techniques which, even after data deletion still had a large number of survey points close enough to the target to record a high amplitude signal. As data deletion percentage was raised to 75% detection probability fell by up to: 9.5 (gravity), 14 (gravity gradient), 2.5 (magnetic) and 3.4 (magnetic gradient) percentage points (Figure 5.18a) – a significant of the survey feasibility.

As the deletion process was random, the variance of detection probability over 100 simulations was tested (Figure 5.19 and Figure 5.18b). It was found that the variance increased with both increased data deletion and increased spacing. Over the 100 simulations with 75% data deletion, the gravity detection probabilities spread over a range of 12.4% (1 m spacing) and 7.9% (2 m spacing).

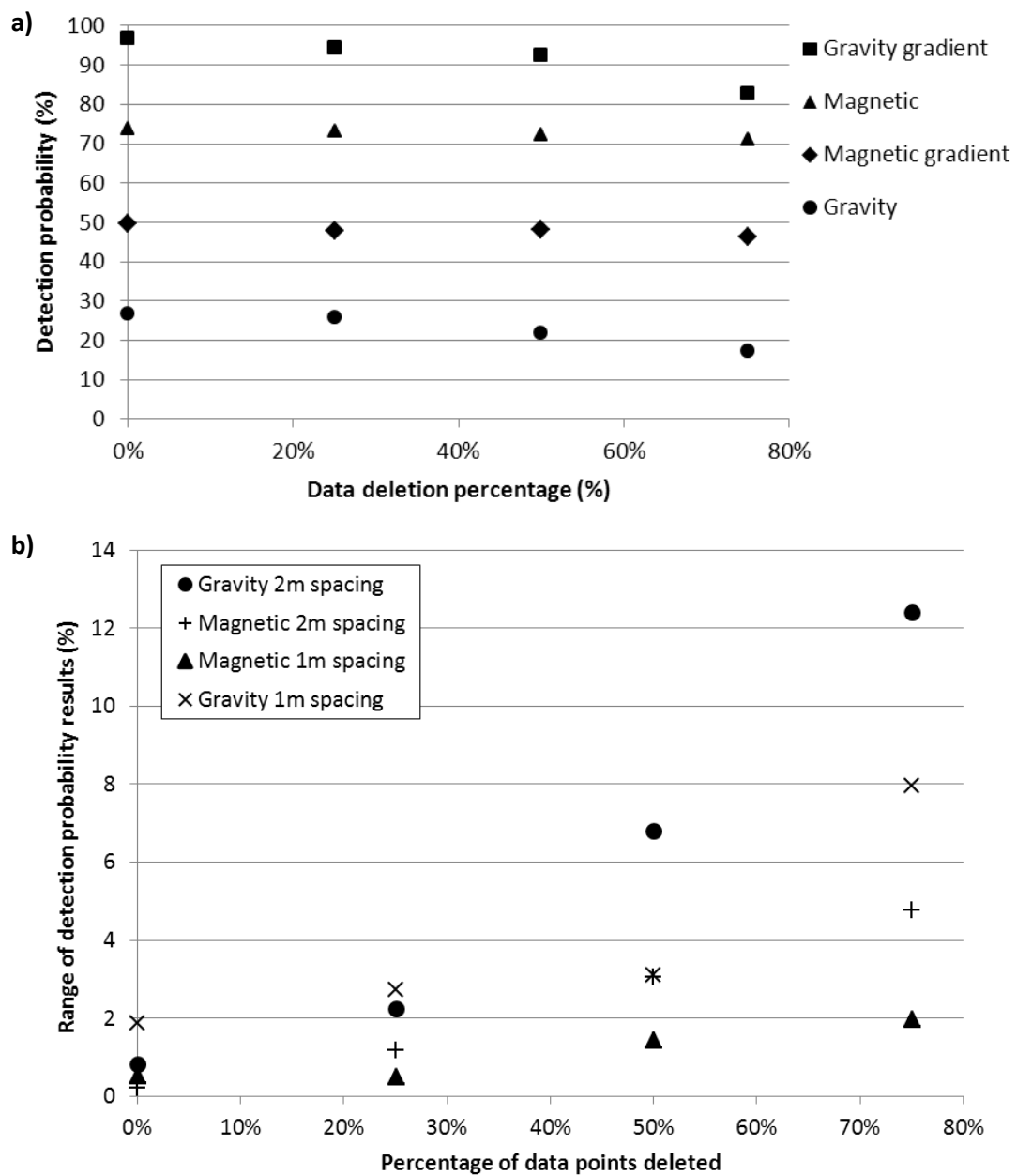
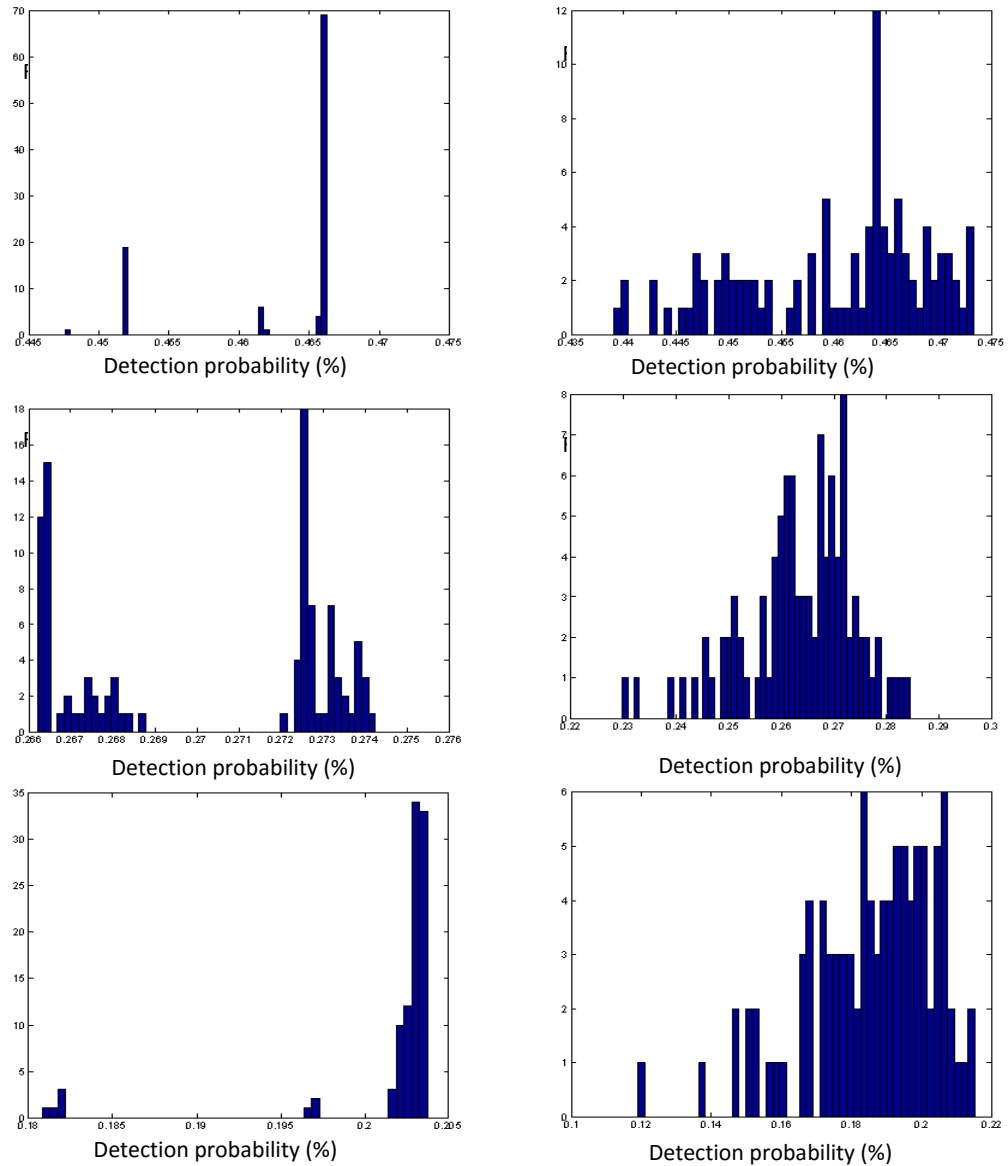


Figure 5.18. a) Detection probability decreasing with increased data deletion for potential techniques over a 1 m sided air cube at 3 m depth in limestone in typical noise with 2 m profile spacing. b) Variance of detection probability over 100 simulations over the same cavity.

Figure 5.19a shows more detail, through histograms of the detection probability for all simulated surveys with the gravity method. The results of 0% and 50% data deletion are compared. The 50% data deletion simulations show a wider range of detection probabilities. The variation also increases with increased survey point spacing. When 50% of data is deleted, the probability range increases by 1.5 percentage points at 1 m spacing, 4.7

percentage points at 2 m spacing, and 7.2 percentage points 3 m spacing (the trend is shown Figure 5.19b).

Though the average change over all simulations is not large, these results indicate that when a high level of data deletion is expected, the detection probability is not only lower but less reliable.



a)

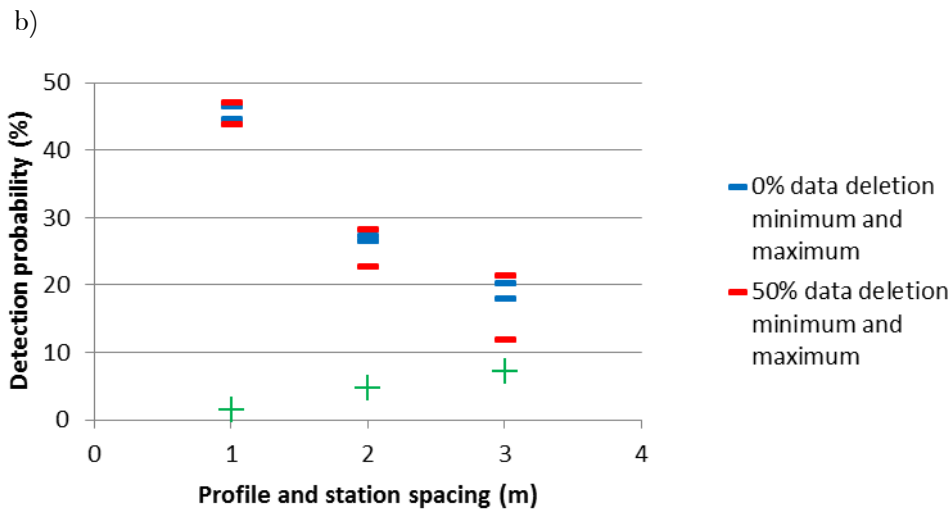


Figure 5.19. a) (previous page) Program output showing histograms of detection probability over 100 Monte Carlo simulations for the gravity method over a 1-m air cuboid at 3 m depth in limestone at typical noise levels (axis shows frequency). The left column shows 0% data deletion, the right 50% data deletion. The top row is at 1 m profile spacing, the middle 2 m spacing, and the bottom 3 m spacing. The bottom plot shows the data deletion trend as spacing is increased

At a higher noise level the data deletion process affects GPR detection probability more than the other techniques. Figure 5.20a shows histograms of the detection probability using GPR to detect the same cavity but in brownfield noise levels. With 0% data deletion the detection probability average is 79.9%, where at 50% data deletion the average is 55.1%, a decrease in probability of 24.8 percentage points. The detection probability decreases faster as the data deletion percentage increases (Figure 5.20b).

5.2.7 Parameter variation

Material parameters are not well defined and so parameters used in the modelling may be inaccurate. Parameters can vary with depth and moisture and magnetic susceptibility especially can vary by orders of magnitude (Breiner, 1999) or several orders if anthropological material is involved (Mochales *et al.*, 2007).

On site measurements may improve this but these kinds of intrusive measurements can be problematic. Often, geophysics is chosen because of its non-intrusive nature, in hazardous or culturally significant sites. Running the modelling program with the extreme material parameter values may give the user a range of possible results.

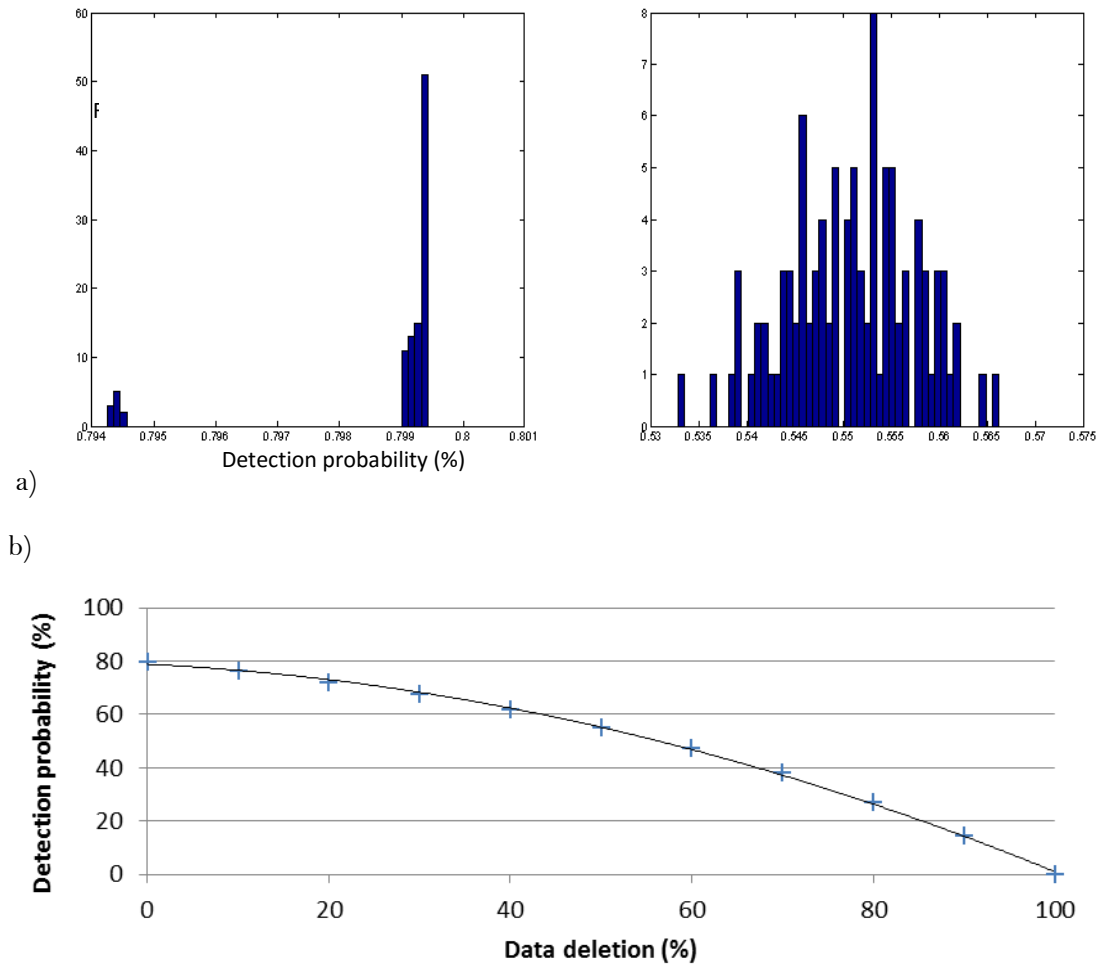


Figure 5.20. a) Histograms of detection probability over 100 Monte Carlo simulations for the GPR method over a 1-m air cuboid at 3 m depth in limestone at brownfield noise levels. Top left at 0% data deletion, right 50%. Y-axis is frequency. b) shows decrease in detection probability as data deletion increases.

Currently the program uses the average parameter value from a number of sources found for each geological material. However, the range in the literature can have a major effect on the detection probability. For example, Milsom (2003) lists limestone susceptibility ranging from 10 to 1000 ($\text{SI} \times 10^6$). This translates to a range of modelled signal amplitudes and hence a variation of detection probability (**Table 5.3**). In the case of the example 1-m air cube cavity at 3 m depth in limestone this range causes a probability detection range for the magnetic method between 29% and 98% at typical noise levels, and a 9% and 61% difference at brownfield noise levels; a range of 69 and 52 percentage points respectively.

Table 5.3. Range of probability detection values due to the disparity in parameter value. A 1-m cube air cavity at 3 m depth in limestone was modelled.

Susceptibility value	Detection probability (%) at		Magnetic signal (nT)	
	Typical noise level	Brownfield noise level	Minimum	Maximum
Maximum	98.00	61.17	-0.16	0.015
Minimum	29.22	8.70	-0.0016	1.50x10 ⁻⁴
Range	68.78	52.47		

The magnetic method has the largest variation in parameter values and so has the largest range of detection probability, but the problem still affects the other techniques.

5.2.8 Small variations in antenna height

In the field not all surveys can be completed smoothly. Undulations on the ground and shaking of the antenna can cause small disturbances in the magnetometer antenna position. These small changes in sensor height are simulated by changing the sensor position in the modelling by 2 cm (suggested in Pasion, 2007) to test the effect on detection probability.

A modelled survey was run for the magnetic method over a 1-m air cube at 3 m depth in limestone at typical noise, varying the antenna height by 2 cm above and below the typical 1 m height. There was a very small change in the anomaly size that was larger directly above the cavity (Figure 5.21). This small change translated into a minor change in the detection probability: typical antenna height: 93.11%, raised 2 cm 93.02%, lowered 2 cm 93.17%. The change in this example is negligible. However, if the ground is expected to be very rough it may be worth modelling a few scenarios with bigger changes in antenna height to estimate the impact. The approach could also be used to optimise the height of the antenna specific to the site and cavity rather than relying standard equipment suggestions.

5.3 Limit of detection

If potential cavity details are limited, the limitations of using geophysical techniques can be assessed by calculating the minimum cavity size detectable at a range of depths in any given geology. To enter this option the user pushes the 'Limits' button on the GUI, inducing the 'limit.m' function (Appendix Axiv). The user is presented with a pop-up menu with the option to alter a parameter (noise level, geology type, spacing or delete percentage) and choose the technique on which to run the limit analysis. There is also an option to set the desired detection probability confidence interval required (the default is a better than 95% probability of detection).

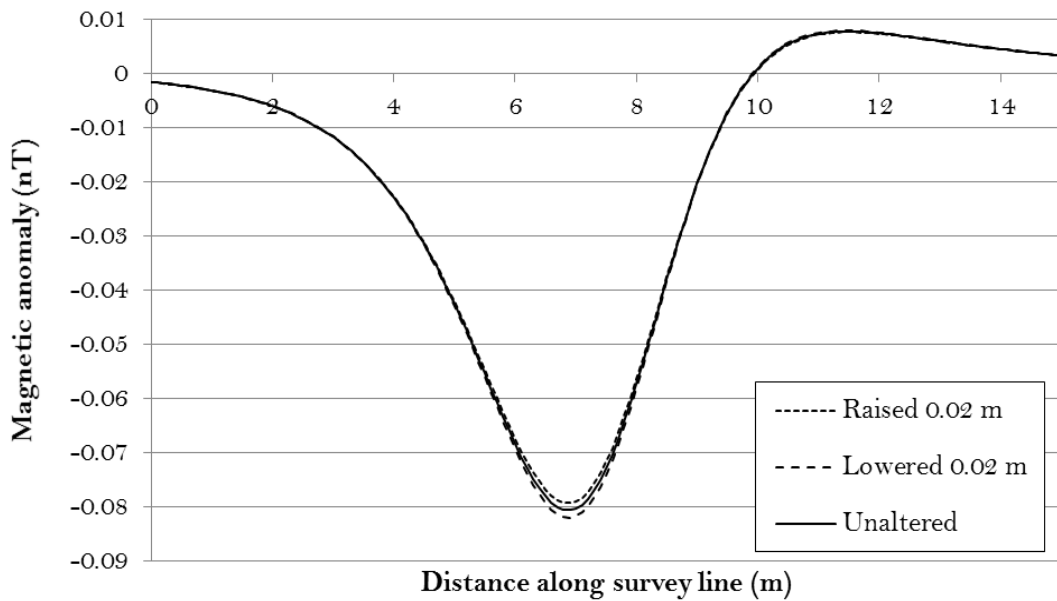


Figure 5.21. Single magnetic survey line over 1-m air cube at 3 m depth in limestone, shown with variation in height to represent small changes which may occur in the field.

The user then invokes ‘probdepthsize.m’ (Appendix A0) by clicking the ‘Run limits’ button. At each depth the cavity dimensions are increased until the cavity detection probability for each technique reaches the chosen confidence interval, thus the minimum sized detectable cavity at the current depth is found. At this point the process begins again at a deeper cavity position. This allows an assessment of the smallest cavity detectable at a given depth to any degree of probability required. This informs site specific feasibility assessment of geophysical techniques. The optimum spacing to achieve the required detection probability can be calculated in this process as in section 5.2.3. In combination, the user builds up a good idea of the survey type and technique required to detect a cavity in their chosen environment.

To highlight this technique, the minimum detectable cavity cube size is calculated for a range of parameters using the magnetic technique (Figure 5.22). By altering each variable independently the effect on the cavity detection probability is highlighted. The variation in Figure 5.22a is dominated by the difference in magnetic susceptibility of the host materials (Table 4.1). The low susceptibility of sandstone means a cavity has to be much larger at depth to be detectable than in other materials.

Site noise level has the largest influence on the minimum detectable cavity size; a 1 m cube cavity at 5 m depth would have to be 2.4 times bigger to be detected in a typical noise level than at instrumental noise level, and 8.6 times larger to be detected in brownfield noise conditions Figure 5.22c.

The cavity size required for detection increases with depth significantly more rapidly in some subsurface conditions than others. For example, because the increase in noise level up to brownfield level is much greater than the increase to the lower noise levels, the detection probability decreases much faster. Conversely, the effect of changing some parameters is negligible (e.g. increasing spacing above 4 m, and data deletion over 10% have little effect on detection probability - Figure 5.22b and d).

The effect of changing each parameter is intuitive but modelling allows accurate determination of these trends for a chosen techniques in given site conditions. By modelling a combination of all these variables, the most suitable technique and survey parameters required to detect any given cavity to a prescribed confidence interval can be established.

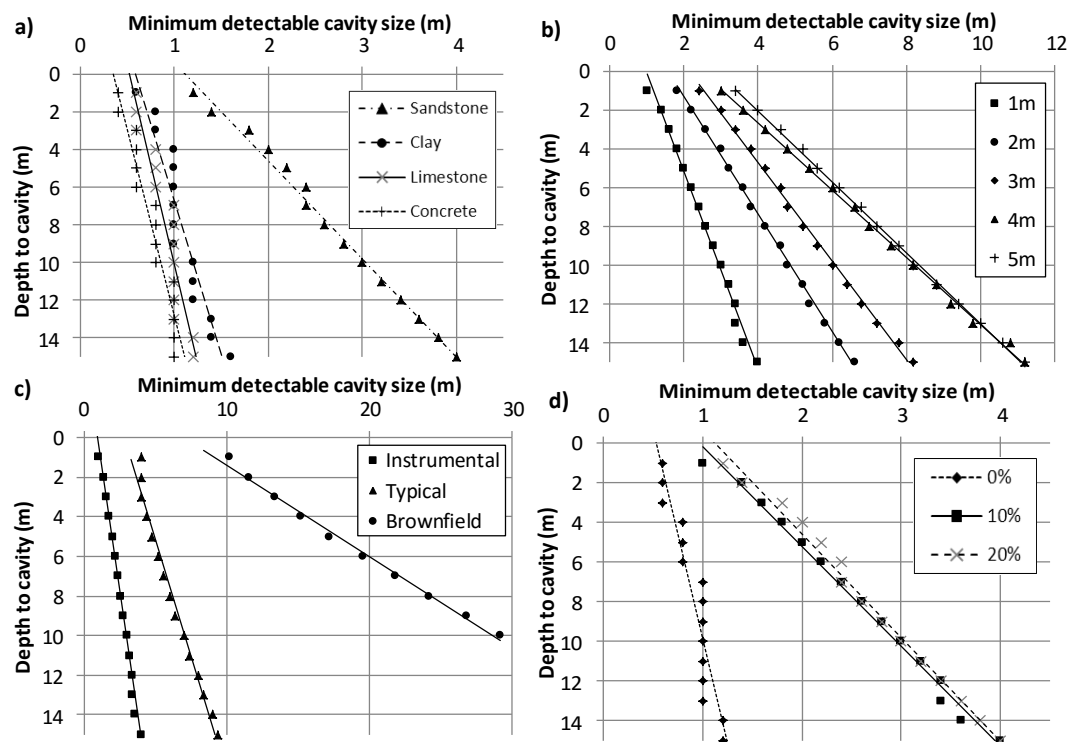


Figure 5.22: Change in minimum detectable cavity size with depth using the magnetic method. Base conditions were a cube void (with side length represented by the x-axis on the plots) in limestone at instrumental noise, 1 m line spacing and 0% data deletion, detected to 95% reliability. Altered parameters were: a) geology, b) profile line spacing, c) noise level and d) processing data deletion percentage. Cavity size was increased at 0.2 m increments causing some linear grouping of data; a linear best line was added across the data to find the overall trend. Susceptibility values as in Table 4.1.

Figure 5.23 shows the smallest cube detectable (to 95% reliability) in limestone from 0 m to 15 m depth using: GPR, gravity gradient, gravity and magnetics (this is the depth of

interest of geotechnical investigations (Roth *et al.*, 2002)). As shown, GPR and gravity gradient can detect much smaller cavities at depth than the magnetic and gravity techniques. This type of visualisation shows clearly and efficiently the feasibility of using each technique in these conditions.

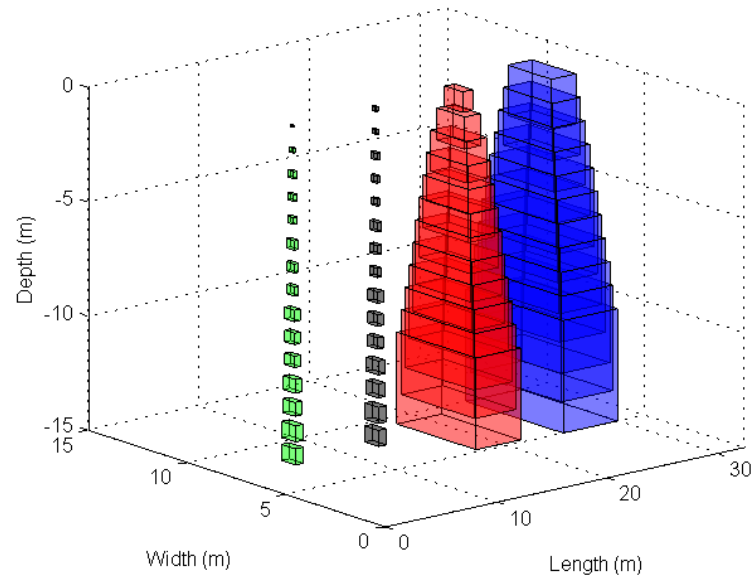


Figure 5.23. a) The smallest cube detectable (to 95% reliability) in limestone at depths from 0-15 m using: GPR (green), gravity gradient (black), gravity (red) and magnetics (blue).

5.4 Chapter Summary

This Chapter shows the results of the modelling technique and feasibility analysis developed in the previous Chapters. The impact on changing a wide variety of parameters in the subsurface environment is assessed. The results are set out in such a way that the reader can see the impact of each individual parameter on the geophysical anomaly size and the overall detection probability.

Although many of the changes to detection probability caused by parameter change are intuitive, the magnitude of the effect is not always easy to estimate. For example, it is clear that detection probability will decrease as cavity depth increases, what is not clear is the rate at which the probability decreases and how this varies between techniques. The modelling approach outlined here allows us to see this in unlimited scenarios.

However, there are also a number of results realised that do not follow intuition or that have not been considered before in the literature. A north-south direction of magnetic surveys is often stated to be best for detection of objects in the subsurface. Here it is shown, through modelling, that this direction is not always optimal. The optimal survey direction is

dependent upon anomaly size and the noise level on a site. Different typical cavity shapes have not been previously considered in forward modelling of geophysical techniques. Here, it is shown that the shape of the expected cavity makes a large difference to the likelihood of detection. Also, the level of noise on a site is not a factor in most modelling, especially not before a survey has begun. Here, it is shown that this is one of the most important factors in whether a cavity will be detectable.

In terms of visualisation of results, an important aspect of working with engineers on projects, a simple limit of detection image developed here highlights the differences between the geophysical technique, and the potential size of cavity which can be detected to each depth. This, along with the user-friendly graphical user interface, means that the software and the results can be easily understood by a wide cross section of those interested in using geophysics on projects.

Chapter 6

6 The Halo effect

6.1 Introduction

In near surface modelling and so far in this work, a subsurface cavity is commonly represented as a polyhedron in homogenous rock but this is a simplified version of the subsurface. Cavities are typically surrounded by a system of secondary fractures, created by various processes during and after the creation of the cavity including: subsidence, ground water flow, enlargement of faults and joints, stress redistribution, chemical alterations and secondary permeability or induced by tunnelling processes in manmade cavities (Benson and Yuhr, 1992; Butler, 2008; Daniels, 1988). This fracture system is commonly termed the “halo” of the cavity, while the halo, cavity and fill are collectively termed the cavity system (Butler, 2008). The fill could be empty (air), water, material deposited by water flow (e.g. mud (Doll, Nyquist, Carpenter, Kaufmann, & Carr, 1998)), or collapse from the surrounding material.

This fracture system is referenced in engineering literature, especially in relation to tunnel creation, but study is limited in geophysical literature. In this work, the effect of the halo on the magnetic and gravity techniques is assessed.

6.2 Halo variables

In order to create a model of the halo system, the creation and makeup of the halo must be understood. The most important parameters of the system when considering modelling are the halo spread, and the fracture orientation, aperture and spacing.

6.2.1 Halo spread





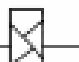

The spread of the halo around man-made tunnels and mines can be up to two or more cavity diameters from the cavity depending on cavity size, rock strength and excavation technique (Daniels, 1988; Pánisová & Pašteka, 2009) and a similar distance in natural cavities (Chamon & Dobereiner, 1988). The size of the halo is considered to be dependent upon the rock type, the size of the cavity, and the excavation technique (Daniels, 1988).

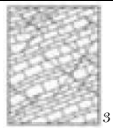
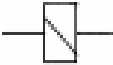
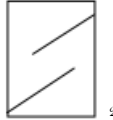
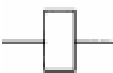
After cavity formation, fractures and the damaged zone will continue to grow around the cavity (Ewy & Cook, 1990b). There are two main processes that increase the halo spread. Firstly, stress redistribution and rock strain leads to cracking and fracturing (especially tunnelling) (Clarke, Welford, & Hughes, 2006). Secondly, weathering by solution and induced ground water flow enlarge faults, joints and fractures (especially karstic) (Styles *et al.*, 2005). Therefore, fracture spreading occurs more prevalently along rock weaknesses and so the structural patterns of rock are of great importance.

6.2.2 Fracture patterns

Fractures generally occur around a cavity as follows: spalling under compressive stress, primary under tensile stress, secondary or remote under a combination, side wall slabbing or compressive failure (Carter *et al.*, 1991; Wang *et al.*, 2012). The geometry and frequency of rock fractures depends greatly on the rock type and the particular stresses in the subsurface and many authors have classified rock masses (Table 6.1). There are a wide range of fracture categories (see Balk & Cloos (1948) and Pluijm & Marshak (2004) for a summary) and in this work the most common is concentrated on - rock structures classified between stratified, moderately jointed and blocky rock types (Terzaghi, 1946). This means that there is a system of Systematic joints (parallel joints with roughly planar geometry) and another joint set of systematic joints perpendicular. Joint sets of this type have regular spacing and this spacing is discussed in Section 6.2.5. It should be noted however, prediction of the fracture system is difficult as samples only show a few inches and variation can be great within a rock type.

Table 6.1. Literature rock classifications

Terzaghi, 1946		Wickham <i>et al</i> , 1972		Bieniawski, 1976	Hoek & Brown, 1997		Hoek & Brown, 1997 ¹ , P. Marinos & Hoek, 2000 ² , PV Marinos, 2010 ³	Hoek <i>et al</i> , 1998	Marinos & Hoek, 2001 ¹ , P. Marinos & Hoek, 2000 ²	
Classification	Definition	Classification	Definition	Definition	Classification	Definition	Classification	Definition	Examples	Examples
Crushed but chemically intact	microscopic particles of micaceous or clay minerals	Very closely jointed	< 5.08cm	< 6cm	Heavily jointed rock mass		Heavily broken rock. Also blocky/disturbed incorporating faults and folds ¹		<i>sericite metasandstone, greywacke, metasiltstone, marly</i>	
Blocky and seamy	<i>chemically intact or almost intact rock fragments</i>	Closely jointed	< 15.24cm	6-20cm	Many joints		Very blocky – 4 or more discontinuity sets ¹		<i>limestone schist</i>	<i>arkosic metasandstone,</i>
Moderately jointed	<i>joints and hair cracks</i>	Moderately jointed	< 30.48cm	20-60cm	Two joint set		Blocky – 3 orthogonal discontinuity sets ¹ Undisturbed limestone bedding		<i>limestone and fresh diabase-peridotite,</i>	

					structure ³				
Stratified	<i>individual strata with little or no resistance against separation along the boundaries between the strata</i>	Moderate to blocky	< 60.96cm		One joint set		Intact/massive – intact rock mass with a few widely spaced discontinuities ²		Flysch ¹
		Blocky to massive	< 1.21m	0.6-2m					<i>Siltstones and claystones²</i>
Intact	<i>no joints nor hair cracks</i>	Massive	> 1.21m	> 2m	Intact rock				

6.2.3 Fracture aperture

Fracture aperture (the width of a fracture) varies between geology and location (Table 6.2). Aperture increases with time and is usually in the range of micrometres to millimetres through modellers have used apertures of centimetres (Liu & Yu, 2013). Narr & Suppe (1991) note that mechanical boundary layers range from 0.1 to 15 cm with a 3 cm median. These boundaries may then be weathered to form fractures.

Apertures of outcrops can be easily measured but in situ rock measurements without stress release require more complicated methods (e.g. pressure tests in Snow (1970)). On top of this, aperture is also affected by the boring process (Keller, 1998) so samples may be misleading.

Table 6.2. Fracture aperture in various rock types.

Rock	Specifics	Romanov, <i>et al</i> 2002	Hartmann <i>et al</i> , 2007	Pastoules & Cripps, 1990	Atkinson, <i>et al</i> , 2000	Snow, 1970 Surface apertures	Keller, 1998 Core sample	Laubach <i>et al</i> , 1998	Waltham, Bell, & Culshaw, (2004) after White (1988)
Limestone	Aquifer	10 ⁻⁵ cm to 0.03 cm				0.03cm			Initially 10-25 µm increasing 5- 10mm in the first 3000-5000 yrs dependant on local conditions and climate
Chalk	Modelled		363 and 384 µm						
	Yorkshire			100-600 µm					
	Eastern England				450-460 µm				
Granite	Pike Peak					Averaged at 0.932 mm			
	General					0.011 0.017cm	- Average= 0.825mm, 0.639mm. Small aperture regions 0.553 and		

		0.459in
Granite	0.015	-
gneiss	0.024cm	
Greenstone	0.015-0.035cm	
Sandstone	0.012-0.026cm	Average=0.204mm, $\sigma=0.282\text{mm}$ Small aperture region: 0.134mm
Coal		Surface=<0.1 mm. Else: 3 to 40 μm filled fractures <0.5 cm

6.2.4 Layer thickness

Layer thickness (or distance between fractures) varies between, and within rock types (Table 6.3). Marinos *et al.* (2005) states that claystones, siltstones and weak sandstones developed in stable conditions have few discontinuities and match the blocky rock type (Table 6.1). Generally layer thickness increases with depth (Snow, 1970) ranging from centimetres to metres thick, though this relationship can be quite varied (Figure 6.1).

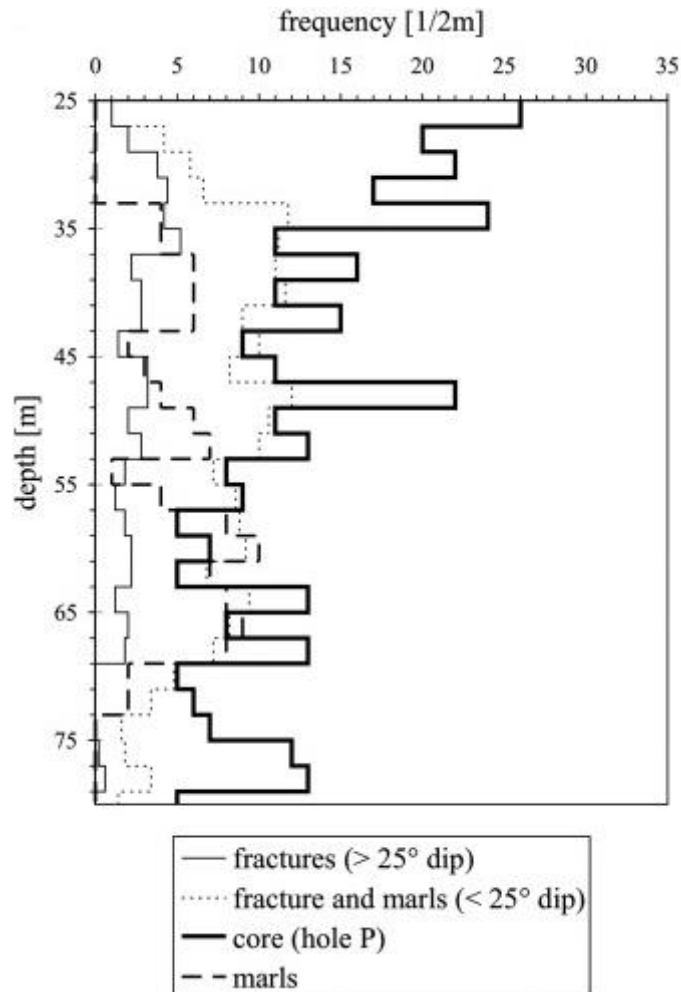


Figure 6.1. Average frequency of fractures measured in four boreholes in chalk (thin solid line) and central borehole (thick solid lines) shows the variation in number of fractures with depth (Hartmann *et al.*, 2007).

Table 6.3. Literature values of layer thickness for various rock types.

Rock type and description		Layer thickness								
		Marinos & Hoek, 2000	(Pastoules & Cripps, 1990)	Hartmann <i>et al</i> , 2007	(Wu & Pollard, 1995)	Snow, 1970	(Ji & Saruwatari, 1998)	Laubach <i>et al</i> , 1998	(Narr & Suppe, 1991)	(Atkinson, Ward, & O'Hannelly, 2000)
Siltstones and clayshales		Few mms								
Sandstone	Weak				Mostly <1m					
	General				but up to 2m		Mostly <20m, but up to 140m			
Limestone		Few to 10-20cm			10-90cm ¹ , <50cm ² , up to 12m ⁴					
Chalk	Yorkshire	0.15 to 1 m								
	Eastern England				0.18-0.85m					
	General				Few cms to 2 m					
	Modelled values				5cm-1m					
	Intensely fractured upper chalk block				5-10cm					
	Below the upper chalk 25m depth				0.2-1m					
					8cm increasing to					

	increasing to 75m depth	40cm	
Granite	1.5-16.7m increasing to 47m	0.54m increasing to 2.84m	
Flysch		Mostly 5- 100cm	
Chert			Mostly 20-50cm
Dolostone			Mostly <60cm
Greywacke		Mostly under 4m ³	
Porcelanite and siliceous shale		5-55cm	<90cm
Coal			Mostly <40cm
<i>'after Huang and Angelier 1989, 'after Price 1966, 'after Ladeira and Price 1981, 'after McQuillan 1973</i>			

6.2.5 Joint spacing and bed thickness ratio

Joint spacing is dependent on material properties but within beds is mostly consistent and increases proportionally with bed thickness (Figure 6.2) in both extensional and compressional stress situations (Huang & Angelier, 1989; Twiss & Moores, 2006) although this is questioned (Rives *et al.*, 1992). Wu & Pollard (1995) note that joint density is not affected by lithology or location in hard beds (in their case the Monterey Formation) Under stress, fractures are likely to appear in the middle of existing cracks with the largest spacing (Rives *et al.*, 1992) indicating that joint spacing will tend towards uniformity.

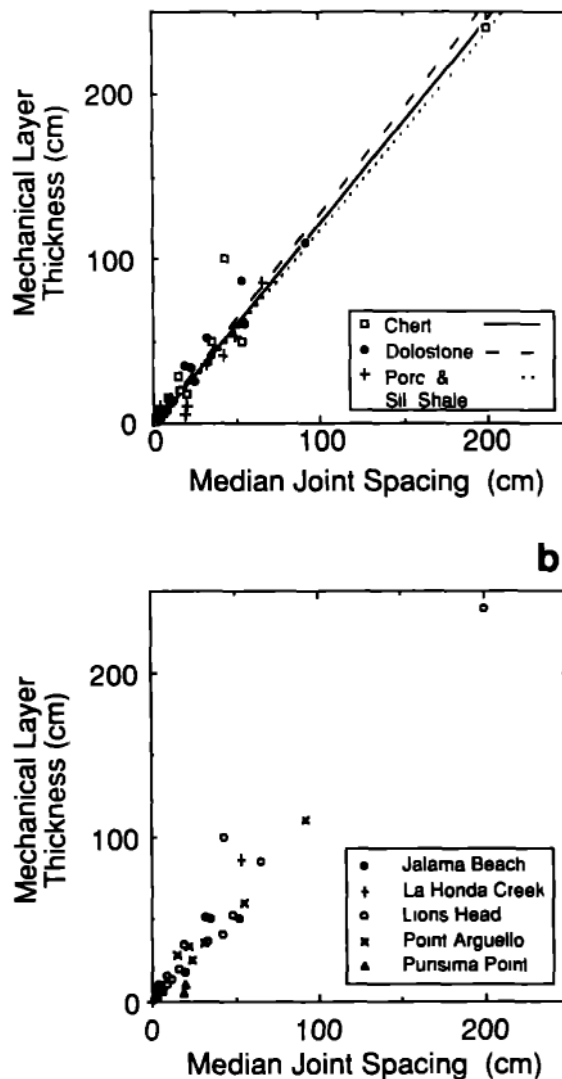


Figure 6.2. Relationship between layer thickness and joint spacing (Narr & Suppe, 1991).

6.2.6 Orientation

Most joint systems comprise systematic joints (parallel joints with roughly planar geometry and regular joint spacing) with another joint set of systematic joints perpendicular (Twiss & Moores, 2006). Orientation is related to rock stresses and this often means

systematic joints are horizontal or sub-horizontal. In sedimentary rocks bedding planes are also generally sub parallel with perpendicular sets of joints (Narr & Suppe, 1991). Rock joints are parallel to bedding (Twiss & Moores, 2006) and commonly follow the systematic and cross joint orientation shown in Figure 6.3. Figure 6.4 shows this situation in NW England chalk with orthogonal joints between beds. In igneous rocks such as granite, fractures generally originate as extensional fractures with sub-horizontal sheeting joints, longitudinal parallel to flow lines and cross joints perpendicular (Engelder, 2012). Coal fractures are termed cleats, occurring in two sets perpendicular to each other and to bedding (Laubach *et al.*, 1998).

Wickham & Tiedemann (1974) categorise joint dip into: flat (0-20°), dipping (20-50°) and vertical (50-90°). Golshani *et al.* (2007) orientate microcracks in their models at four angles: vertical, horizontal, 45° and 135° (note these are two orthogonal sets). Fractures are planar and have the same strike across large regions (Laubach *et al.*, 1998).

As the most common case is systematic joints that are horizontal or sub-horizontal, many of the examples presented here will use that orientation. However, the program allows variation in the orientation angle (Section 7.1.6).

6.2.7 Fracture fill

Fractures can be filled with air, water (if beneath the water table) or rock material. Mechanical boundary layers can be filled with softer material such as mudstone.

6.2.8 Within the halo system

The formation of the cavity or creation of a tunnel changes the stress in the surrounding rock. Stress is released around the cavity and the rock will deform elastically. If stresses are high enough inelastic deformation will result in fracturing (Ewy & Cook, 1990a). Fractures and the damaged zone will continue to grow around the cavity (Ewy & Cook, 1990a).

This fracturing occurs initially in areas where the compressive stress is greatest. Ewy & Cook, (1990a) note that many field studies show this occurs around tunnels and galleries on the two opposite sides of the hole, termed sidewall failure. Wang *et al.*, (2012) ran numerous modelled tests on a circular opening under various stress conditions. Figure 6.5 shows the fracture development around a circular void under lateral pressure. Peripheral cracks appear first, followed by growth of the damage area and joining of some of the smaller fractures into larger cracks. Cracks start to develop in groups around the void and eventually a failure occurs on the bottom right corner. It was found that a void in a more homogenous material produced much less microcracking under the same pressure. Increasing the confining pressure restricts tensile crack related failure and microcracks are concentrated around the sides of a circular cavity.

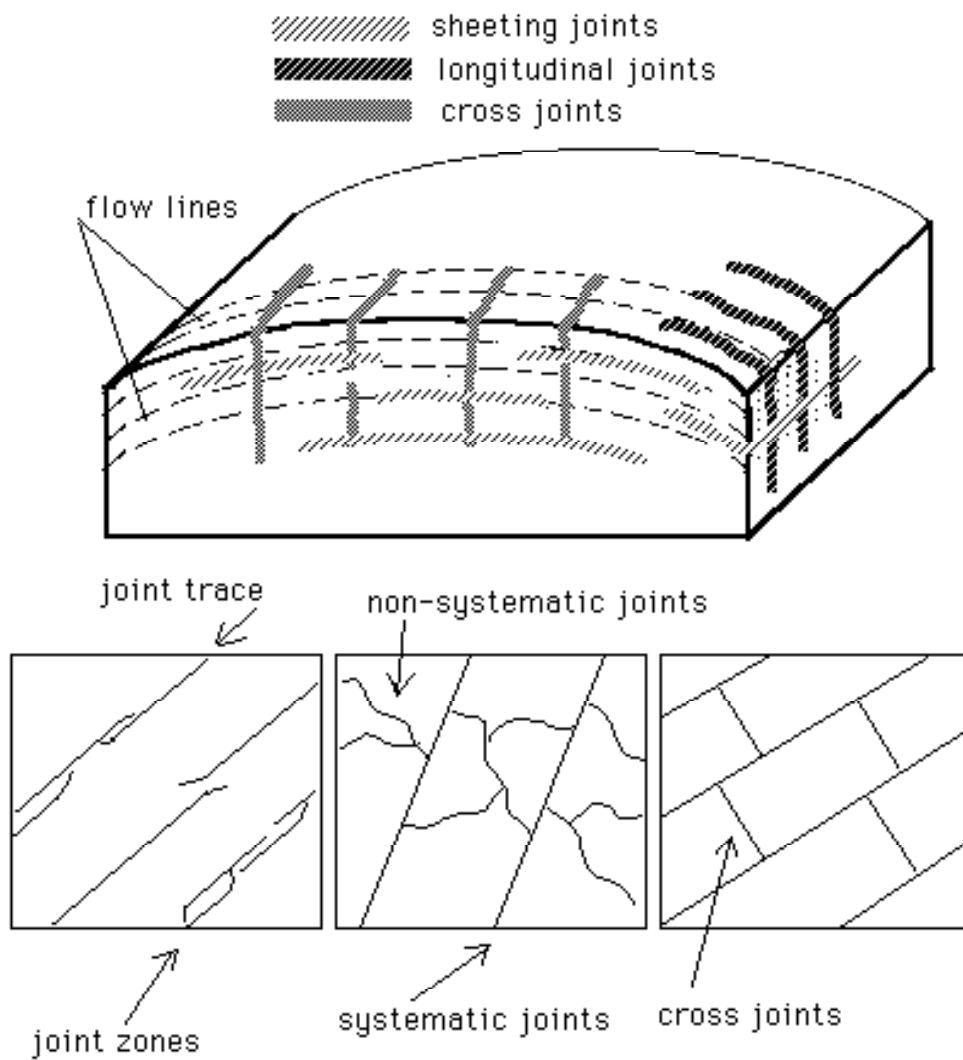


Figure 6.3 Schematic showing the systematic cross joints (Engelder, 2012). Joints run in two sets perpendicular to one another. The modelling uses this form of fracture system.



Figure 6.4. Orthogonal joints between beds (highlighted with blue and green) shown in NW England chalk (Hartmann *et al.*, 2007).

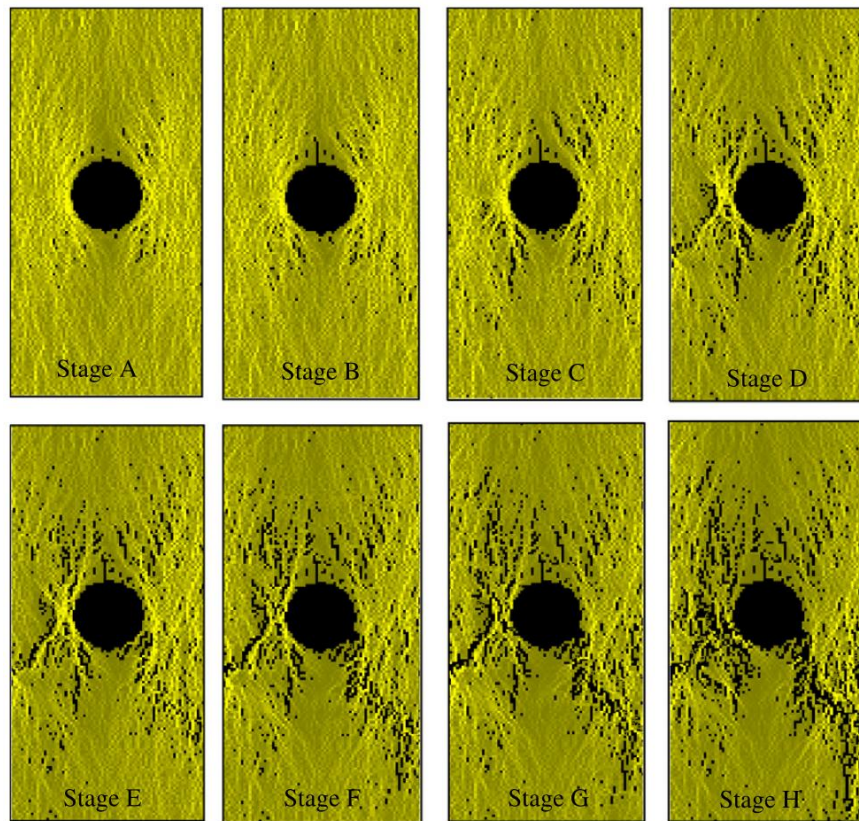


Figure 6.5. Wang *et al.*, (2012) numerical simulation of a circular void a lateral confining pressure of 7.5 MPa. Stages A to F show the development of the fractures around the cavity.

6.2.9 Excavation cracks

Rock excavation alters stress distribution and mechanical strength around the created cavity. This leads to a network of cracks and possibly a plastic zone around the cavity (Golshani *et al.*, 2007). Damage growth is concentrated around the tunnel and spreads further from the cavity at the side walls (Figure 6.6 and summarised in (Golshani *et al.*, 2007)). This agrees with the known decrease in stress with distance from the cavity (Figure 6.7) and the association between damage zones and compressive stress (Golshani *et al.*, 2007).

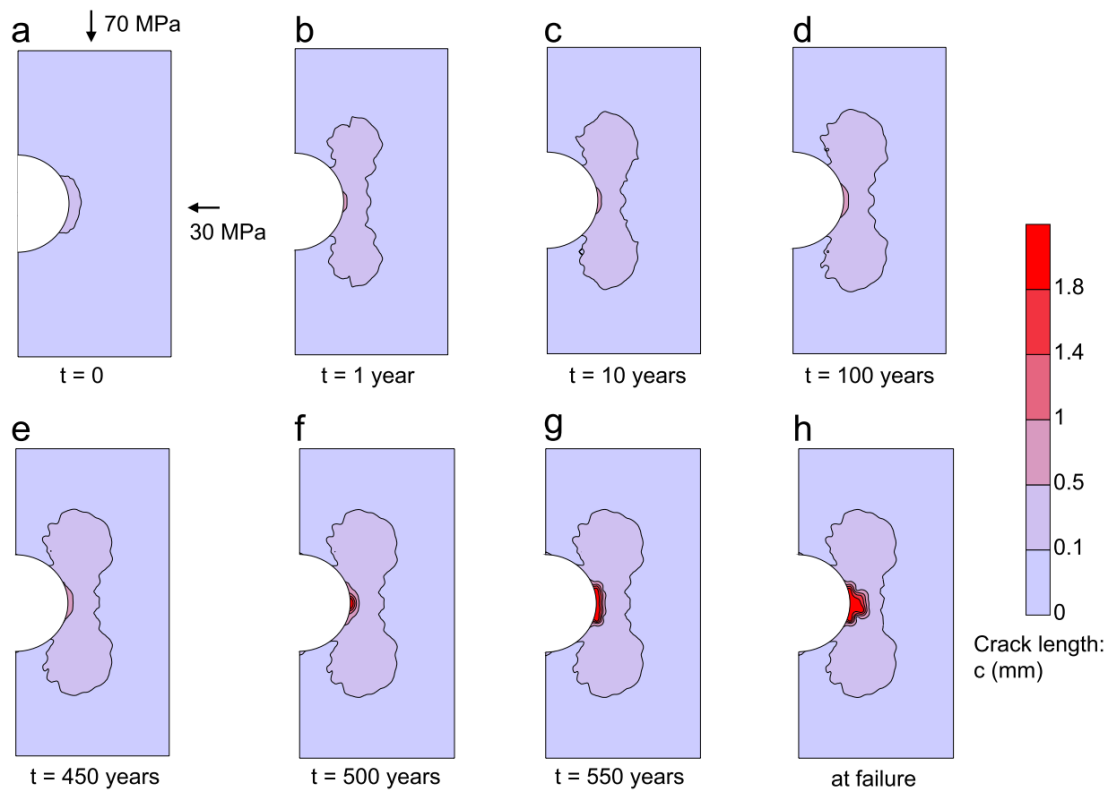


Fig. 12. (a)–(h) Time-dependent development of damage zone around the opening.

Figure 6.6. Microcrack growth around a tunnel through time (Golshani *et al.*, 2007). Growth increases rapidly before failure. Cracks develop mostly in the side walls as vertical stress is larger than the horizontal stress.

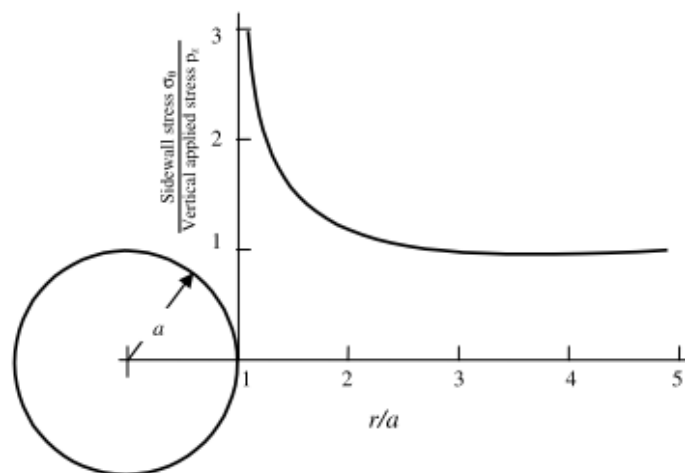


Figure 6.7. Stress concentration around a cavity (Wong, Lin, Tang, & Chau, 2002). Stress concentration decreases with distance from the cavity. The circular cavity is shown; 'r' is the distance from the cavity.

6.3 Effect on geophysical techniques

Halo presence increases the size of the detectable area and hence improves the likelihood of detection using geophysical techniques in most situations. The “effective size” of the cavity for geophysical detection becomes the cavity plus the space within the surrounding fractures. This allows smaller cavities than expected to be indirectly sensed by geophysical techniques (see examples in Styles *et al.* (2005)).

Evaluation of the significance of the halo effect on geophysical techniques is limited to qualitative descriptions and rules of thumb. The presence of a halo is estimated to increase the size of a geophysical anomaly often larger than a factor of two (Butler, 2008). Benson & Yuhr (1993) suggest a cavity halo allows detection 1.5-2 times the depth than the theoretical cavity alone. Chamon & Dobereiner (1988) state that gravity anomalies specifically are generally a factor of two larger than for the cavity alone.

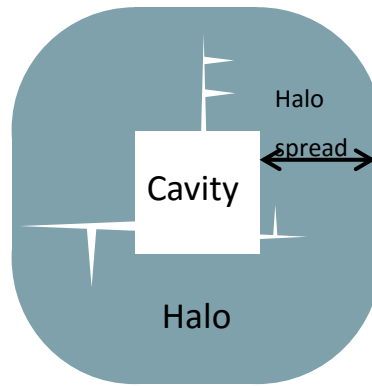
The potentially large impact on cavity detection probability should mean the halo is considered in all cavity modelling: predictive and interpretation. In this work, halos are modelled with various fracture configurations and the effect on geophysical signal and detection probability assessed.

6.4 Halo generation methodology

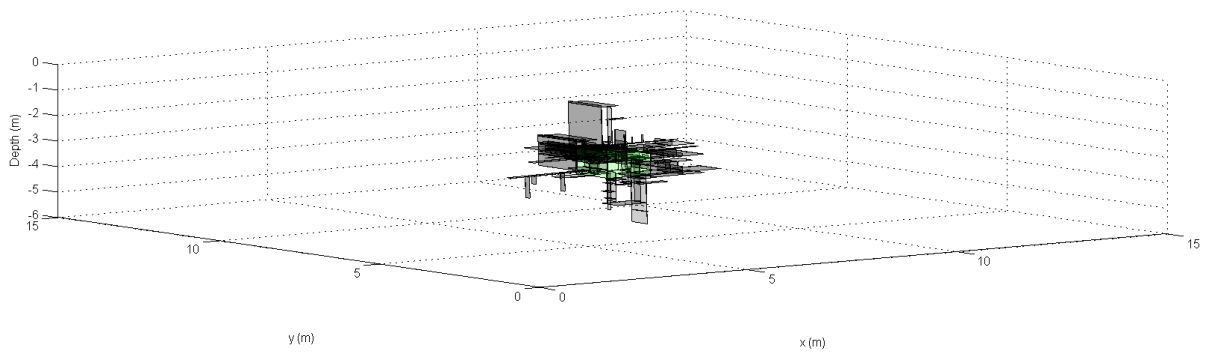
To quantitatively evaluate the effect, the halo system is synthesized and the gravity and magnetic responses are modelled from the surface. The fracture system is created randomly but with some important restrictions. There are two types of fracture; those that originate from the cavity itself and those that originate on other fractures. The fracture base is randomly assigned to any cavity side or existing fracture side. Many aspects of the fractures surrounding the cavity are variable. Fractures are directed in two planes at 90 degrees to each other simulating the natural planar fracture patterns found in most rocks (Reches, 1998; Waltham *et al.*, 2004). The angle of this system relative to the surface can be altered. The length and spread of the fractures is randomised up to the maximum halo spread which can be up to the two times the cavity size as indicated by previous literature. The fracture aperture is variable but values found in the literature will be used. Fractures are tapered to a point at their end. Fractures are randomly added to the cavity system until the fractures reach a chosen percentage of the surrounding halo area. Finally, the cavity can also be altered as in the previous Chapter (e.g. depth, size, shape, geology).

Figure 6.8 shows an example generated fracture system. As fractures are randomly generated, each test is completed a number of times (generally twenty) and the results compared, analysed and averaged (code in Appendix Axvii).

a)



b)



c)

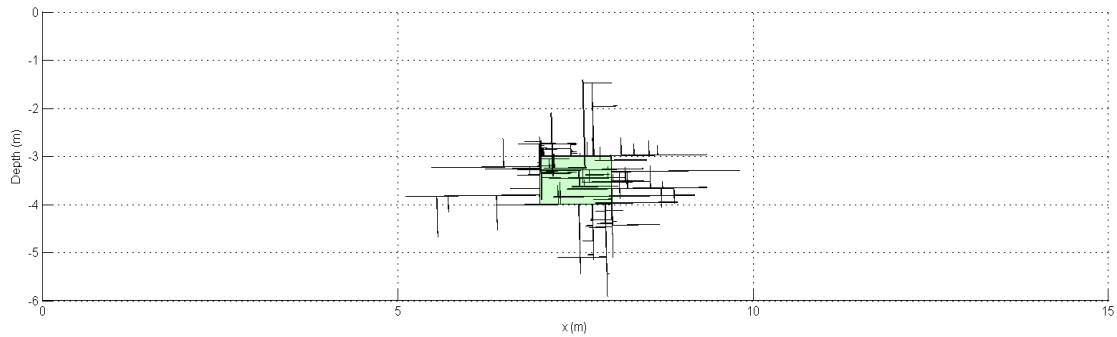


Figure 6.8. a) Schematic of the halo system used in the modelling. Blue represents the halo area, white the cavity and a few example fractures. b ,c) Two views of an example fracture system around a 1 m cube cavity at 3 m depth. Halo spread is two times the cavity dimension (2 m), total fracture percentage is 1% of halo area, aperture is 10 mm and fractures are angled 3° off horizontal and perpendicular to the surface.

6.5 Geophysical modelling

The generated fracture system is numerically modelled using two geophysical techniques: gravimetry and magnetometry. The modelling is completed in the same way as

laid out in Section 4 for each fracture and then summed to find the total halo system anomaly. The detection probability is calculated as laid out in Section 4.5.

Romanov *et al.*, (2002) modelled an idealised limestone aquifer with dissecting blocks of $7.5 \times 7.5 \times 1 \text{ m}^3$. As all of the following examples are within 6 m of the surface, fractures between blocks are not considered and the geology is assumed to be a solid limestone mass. Other fracture parameters are discussed and tested in the next Chapter.

6.6 Chapter summary

This chapter has sought to describe the halo effect through literature review. The parameters that are associated with a cavity halo region are identified, described and examples from the literature are presented. Both natural and excavation cavities are considered. These will inform the modelling parameters in the example in the next Chapter. The conditions within the cavity halo are seen to be complex and so by considering the key parameters, the modelling of the environment can be simplified while still considering the important aspects of the halo.

Although there is much qualitative discussion on the effect of the halo on geophysical results, little work has been completed on quantifying the effect. There exist a few rules of thumb which will be explored in the next Chapter. There appears to be no work in the literature related to the modelling of the halo effect. In this respect, this work is pioneering and will hopefully spur interest in further use of halo modelling when cavity detection is considered.

Finally, the general modelling approach is outlined, including the proposed method of halo generation and the application of the modelling method outlined in the previous Chapters.

Chapter 7

7 Halo Results

To assess the effect of a cavity halo on the geophysical results, the cavity and fracture system shown in Figure 6.8 was modelled and compared with the cavity without the halo (Figure 7.1). In all cases, the addition of a halo system increases the geophysical anomaly. The magnitude of the magnetic anomaly increased by 186% (from 0.0697 nT to 0.1996 nT) and the gravity anomaly increased by 183% (from 0.0012 mG to 0.0034 mG). Magnetic detection probability increased by 34 percentage points and gravity detection probability increased by 6.4 percentage points.

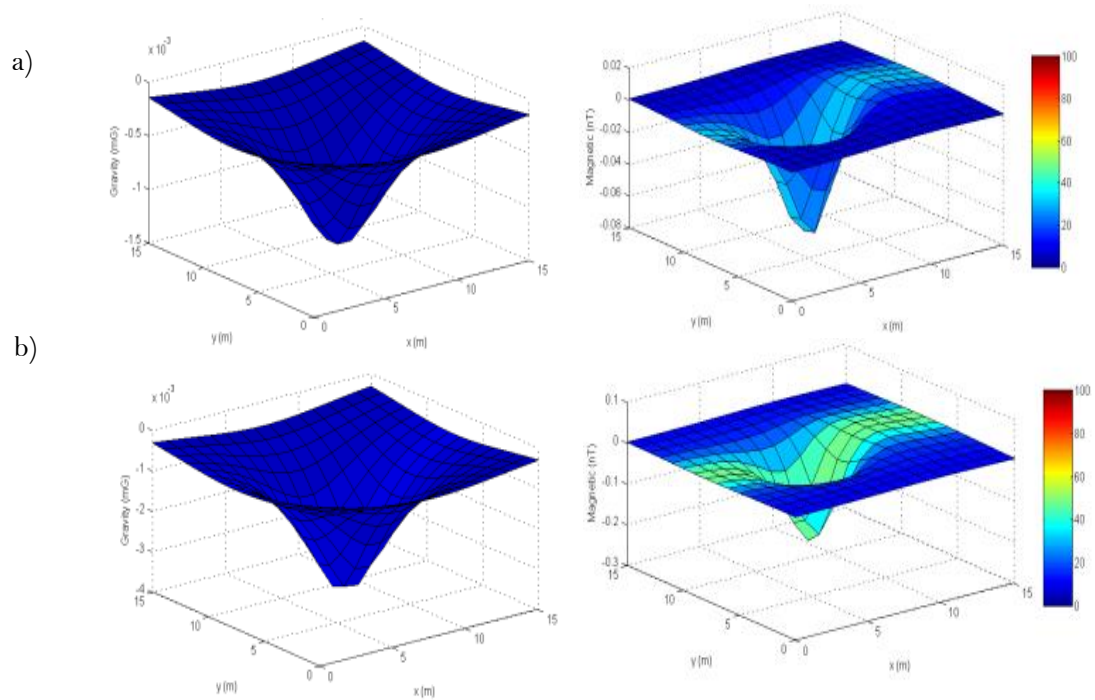


Figure 7.1. Modelling results with: a) no halo, b) halo as in Figure 6.8. Magnetic detection probability: 46.2% (A), 62.3% (B). Gravity detection probability: 92.9% (A), 98.8% (B). Fracture configuration

7.1.1 Fracture configuration

As the program creates the fractures from the cavity in a random manner (within the user input limitations), fracture configuration can vary between tests. A range of configurations were modelled to test the effect on the geophysical methods. Figure 7.2 shows three varied fracture configurations that all fill 0.5% of the 1 m halo area volume with 0.1 m fractures (around a 1-m cube air cavity at 2 m depth in limestone). Although the required 0.5% fracture volume is filled in different manners (A – a few large fractures, B – a lot of small fractures, C – a mixture) the effect on the geophysical results is small Table 7.1. Over 20 different fracture configurations, peak to peak amplitude varies by 0.05 nT and 0.0005 mG and detection probability by 0.008% for magnetic and 0.03% for the gravity method.

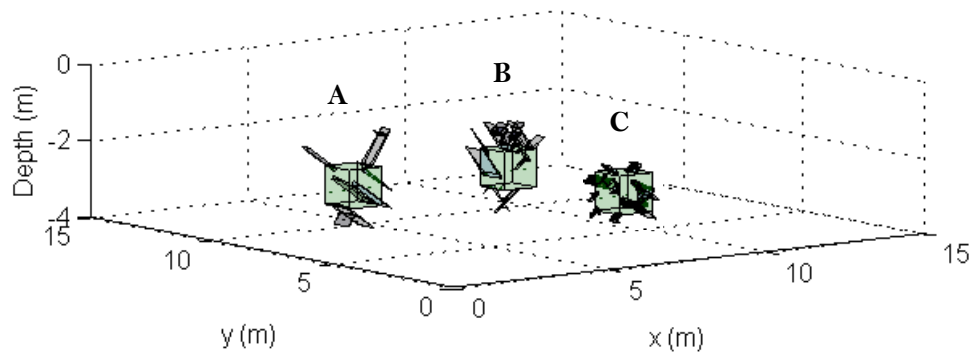


Figure 7.2. Three example fracture configurations with 0.5% of the halo area filled with fractures. Halo spread is 1 m and aperture is 0.1 m. System A: large fractures, B - a mixture of small and large fractures, C - many small fractures. Modelling results are shown in Table 7.1.

Table 7.1. Modelling results of fracture systems. Fracture systems A-C are those depicted in Figure 7.2 (0.5% fracture percentage) and D is the average results for 25% of halo area filled with fractures.

		Fracture system			
		A	B	C	D
Detection probability (%)	Magnetic	97.8	97.6	97.6	100
	Gravity	53.9	53	53.2	88.15
Anomaly size	Magnetic (nT)	0.258	0.266	0.247	2.095
	Gravity (mG)	0.00293	0.00292	0.00278	0.0235

As fractures fill more of the halo area, the variation in fracture configurations increases and consequently the variation in geophysical results increases. At 25% fracture volume peak to peak amplitude varies by 1.054 nT and 0.0118 mG over 19 different fracture configurations and detection probability by $8.25 \times 10^{-06}\%$ for magnetic and 0.0441% for gravity. The small variation in magnetic probability is due to the probability reaching 100% for most iterations. This increase in result range with fracture percentage can be seen in the wider error bars in Figure 7.4.

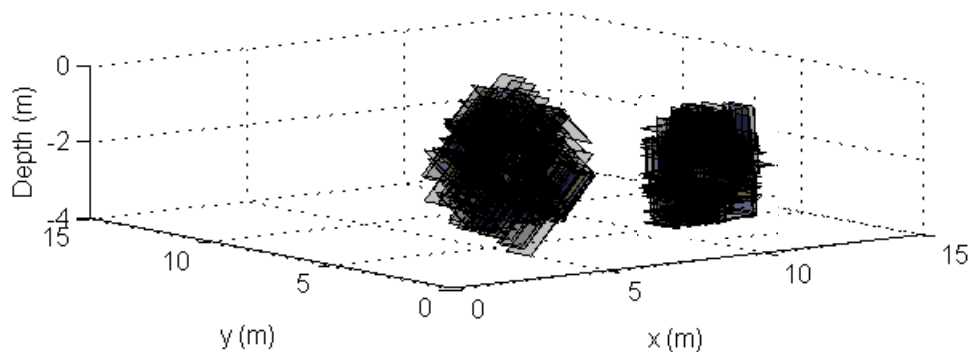


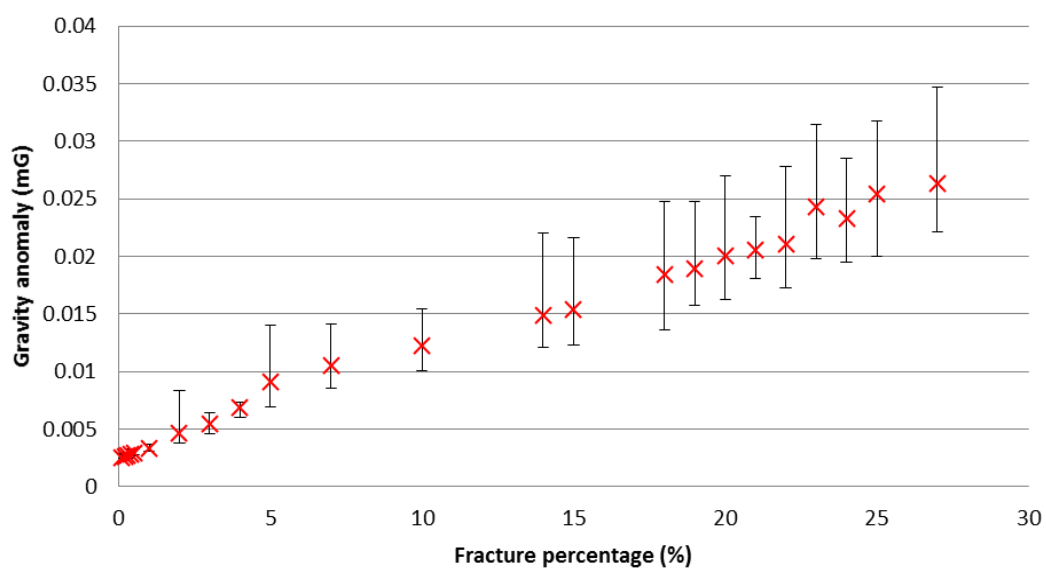
Figure 7.3. Two example fracture configurations for 25% of the halo area filled with fractures. From left (more angled fractures) to right (close to horizontal and vertical fractures): magnetic detection probability 100%, 100%; magnetic anomaly 2.44 nT, 1.75 nT; Gravity detection probability 89.2%, 87.1%; gravity anomaly 0.0269 mG, 0.0200 mG.

7.1.2 Fracture percentage

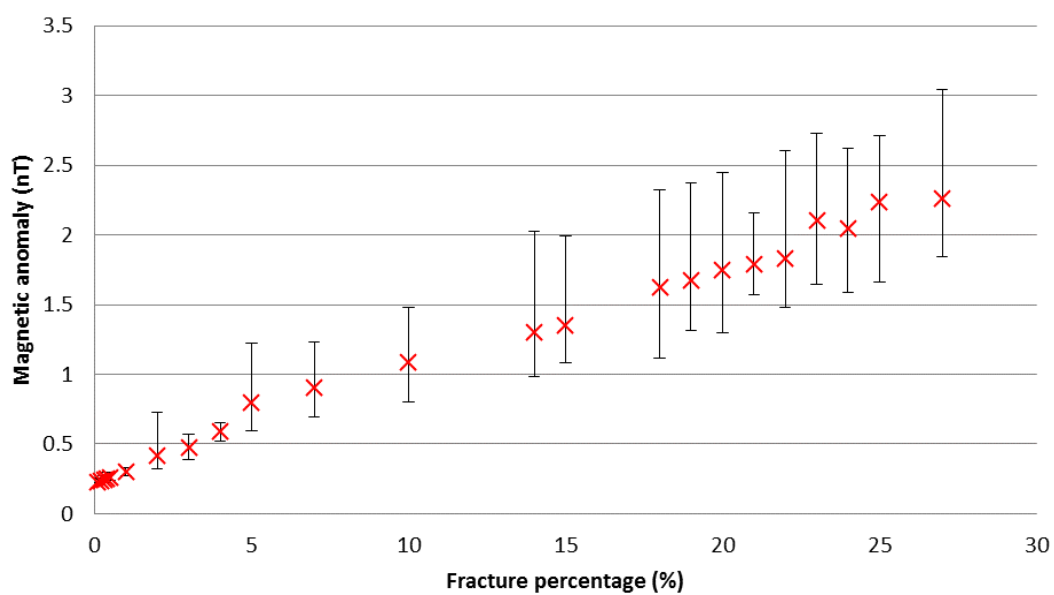
A clear limitation of using rules of thumb in halo assessment is the lack of consideration to the level of fracturing in the fracture system. Here, this is assessed by increasing the level of fracturing around a modelled cavity. Fractures are randomly generated around the cavity until the chosen fracture percentage (volume of fractures compared to the total volume within the halo spread) is reached. The geophysical response is then modelled and results recorded. This process is repeated 20 times at each fracture percentage level and the average result calculated (to account for fracture configurations variation).

Figure 7.4a-c show the effect of increased fracture percentage over a 1 m cube air cavity at 2 m depth in limestone, with up to 0.1 m fracture aperture. As expected, the anomaly size and the detection probability increase as fracture percentage increases. The rate of increase, though, is variable with technique (Figure 7.4c) and will depend on the parameters of the specific halo system. The results highlight that the rules of thumb often quoted are too simplistic; the increase in anomaly size is clearly related to the amount of fracture in the halo, not simply the presence of a halo.

a)



b)



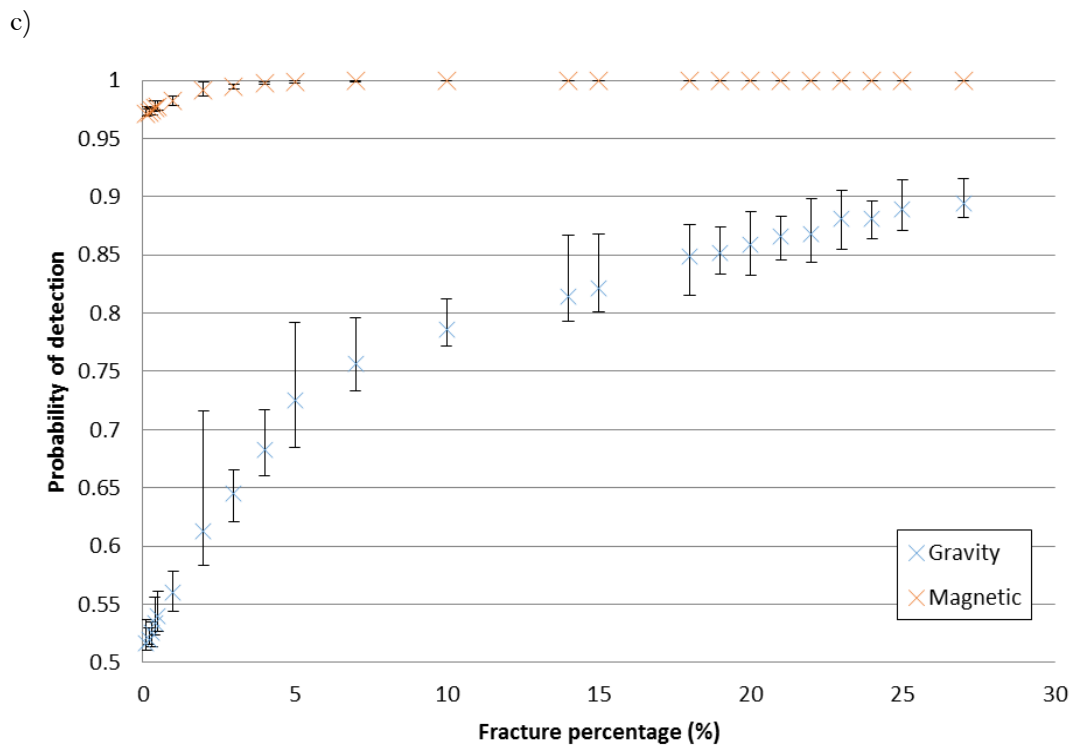
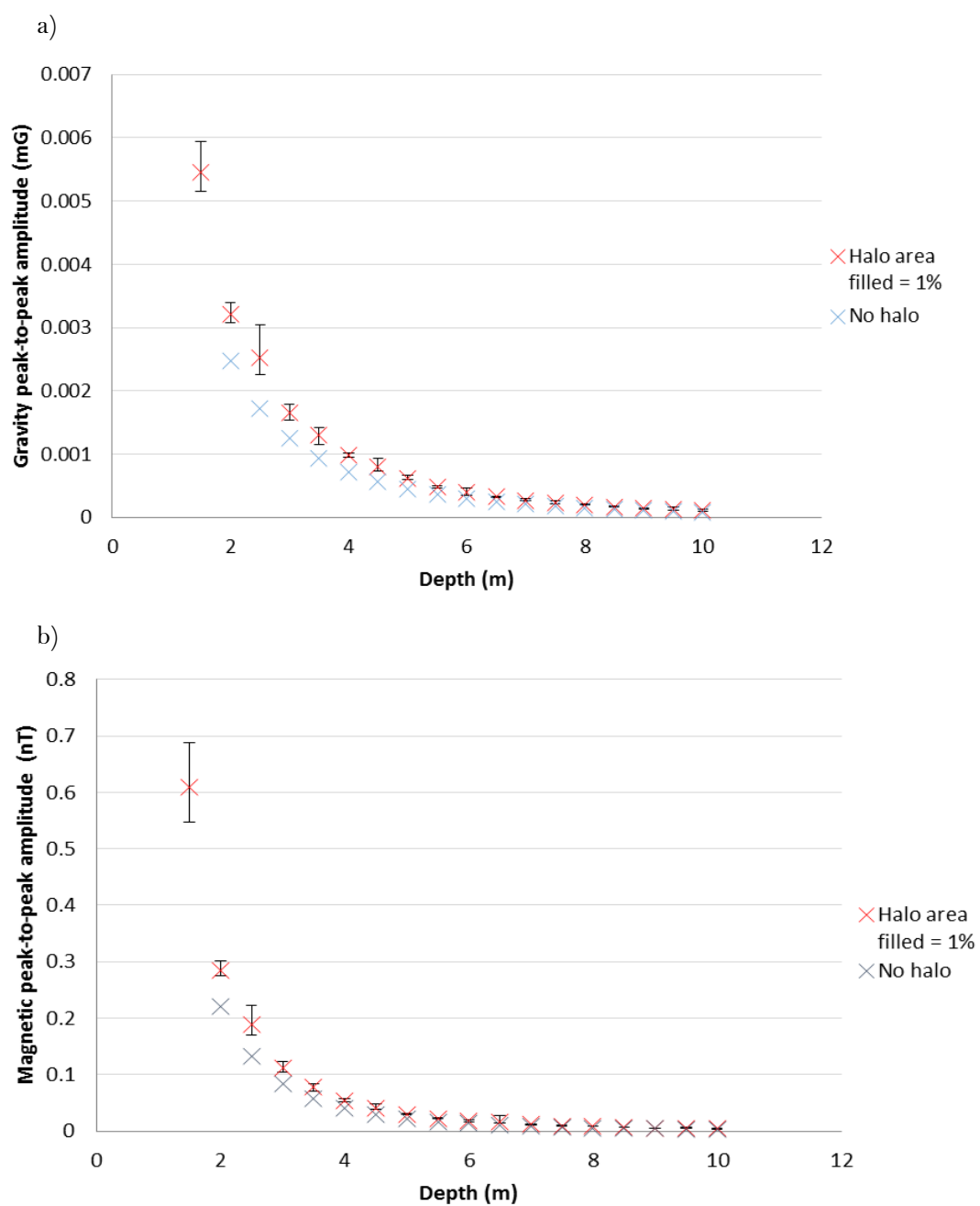


Figure 7.4. Modelled results over a 1 m cube air cavity at 2 m depth in limestone with up to 0.1 m aperture fractures. a, b) (previous page) Average size of anomaly as fracture percentage is increased. c) Increase in detection probability with fracture percentage. Crosses display the average peak-to-peak anomaly over 20 fracture systems generations and error bars show the maximum and minimum anomalies recorded.

7.1.3 Cavity depth

To critique the literature estimations of the effect of halos on the detectable depth of cavities, halo systems at various depths are modelled. Fracture systems around a 1-m air cube cavity were generated between 2 m and 10 m depth (Figure 7.5). The fracture percentage was 1% of the halo area, and the spread of fractures was 1 m (5 fracture iterations were run for each depth and the average results taken). The results show that in the shallow subsurface (up to 3 m) the halo system increases the both gravity and magnetic anomalies by a large amount. Beyond this shallow zone, the halo has less effect on the anomaly size.



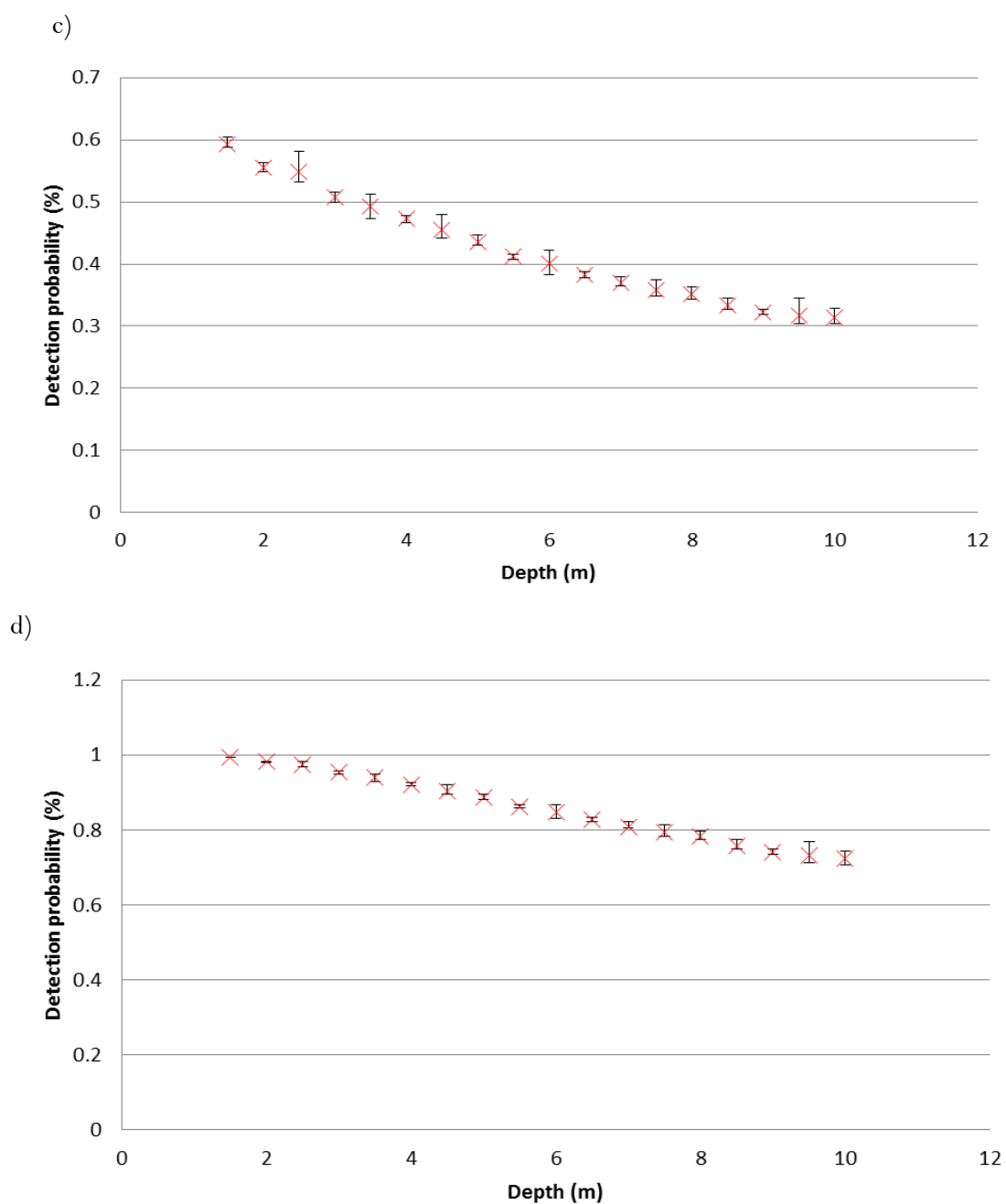


Figure 7.5. Modelled results of fracture systems around a 1-m air cube cavity between 2 m and 10 m depth. The fracture percentage was 1% of the halo area, and the spread of fractures was 1 m. Crosses show the average of 5 iterations (with varying fracture configurations) and the bars indicate the minimum and maximum results for the iterations. Blue crosses indicate the results for the same cavity without the halo system. a) (previous page) anomaly size for gravity modelling, b) (previous page) anomaly size for gravity modelling, c) detection probability for gravity technique, d) detection probability for magnetic technique.

The fracture volume percentage was also varied at each depth (Figure 7.6). In the shallow zone up to 3 m depth, the fracture percentage around the halo greatly affects the anomaly size, increasing 1.3 nT and 0.015 mG (both over 600% increase) between 0% and 16% fracture volume. With deeper cavities, the effect of the halo becomes less important. Anomalies deeper than 5 m see little increase magnitude at all fracture percentages up to 16%. At 10 m depth the effect becomes negligible.

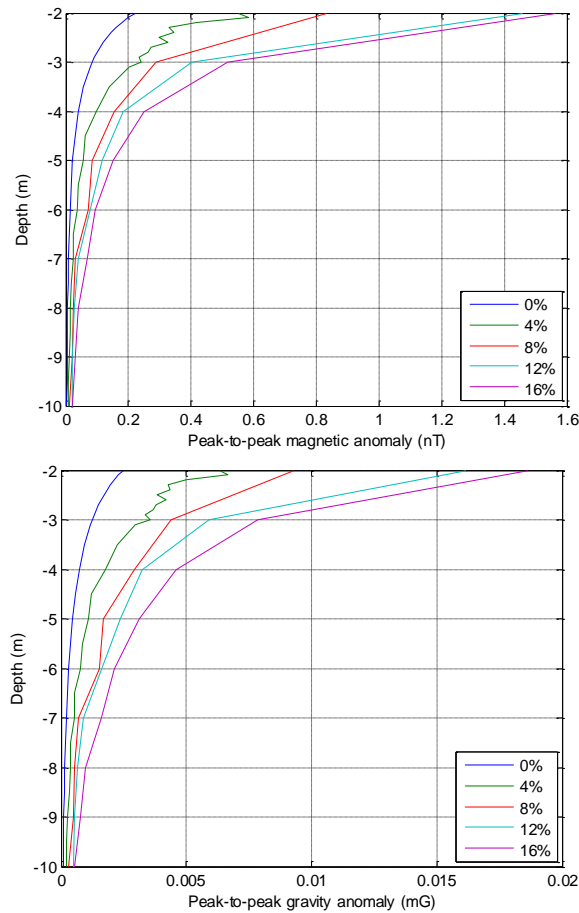


Figure 7.6. Modelled results of fracture systems around a 1-m air cube cavity between 2 m and 10 m depth. The fracture percentage was varied from 0-16% (legend) of the halo area, and the spread of fractures was 2 m. Left – magnetic results, right, gravity results. The modelled anomaly decreases in size with depth of cavity as does the impact of variation in fracture percentage.

7.1.4 Halo spread

The distance the halo extends beyond the cavity depends on a number of factors as discussed in Section 6.2.2. The effect of this variation on anomaly size and detection probability is assessed in this section. Halo spread (Figure 7.7) is varied between 0.5 m and 2 m and the effect on the magnetic and gravity techniques modelled (Figure 7.8).

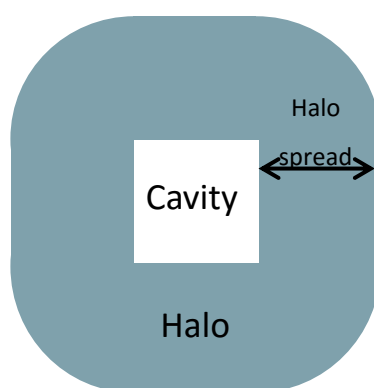
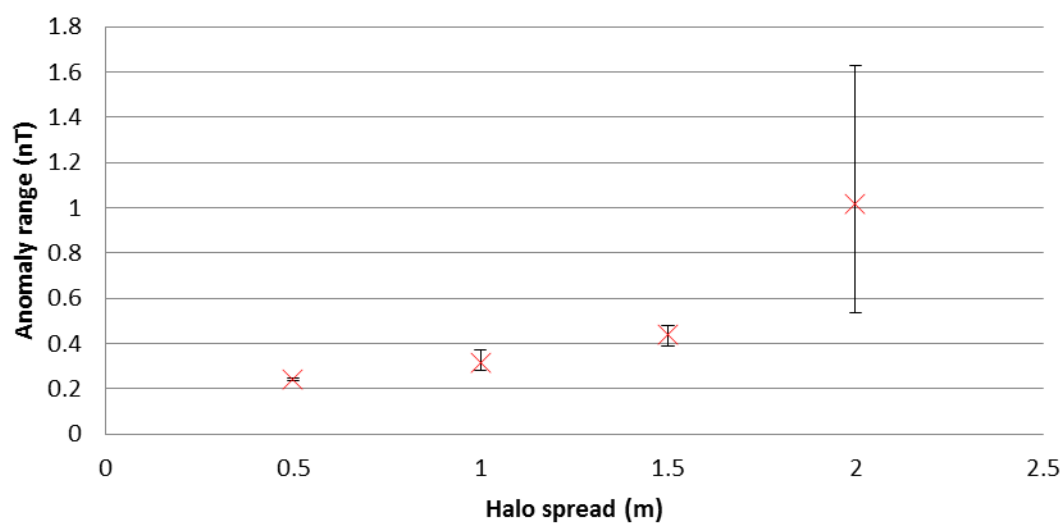


Figure 7.7. Schematic showing the halo zone and the halo spread distance. Cavities are randomly generated around the cavity until the chosen fracture percentage is reached (examples below use 1% fracture percentage).

a)



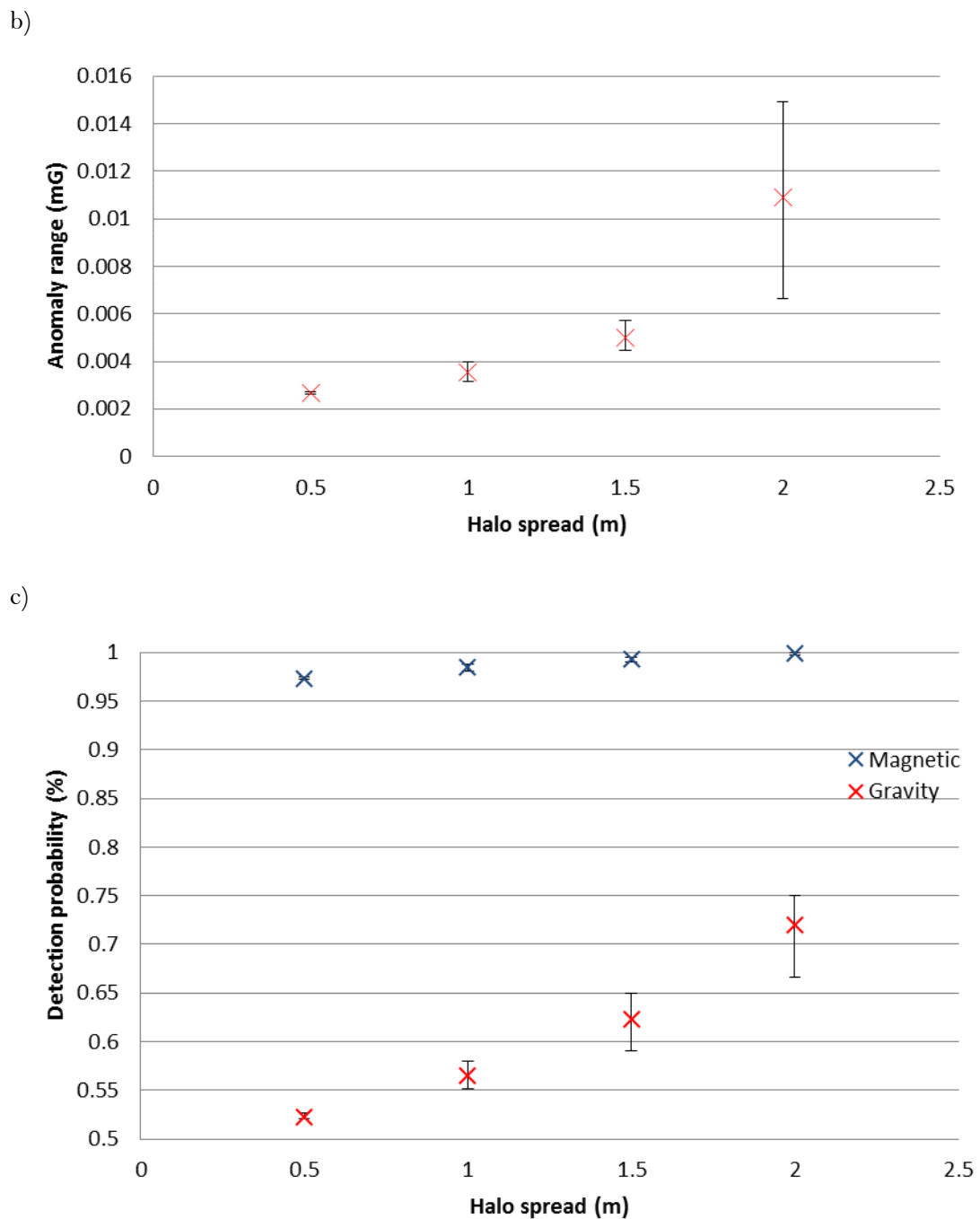


Figure 7.8. Change in a) (previous page) magnetic anomaly, b) gravity anomaly, c) detection probability with halo spread. Fracture systems are around a 1-m air cube cavity with fracture percentage always 1%. Crosses display the average peak-to-peak anomaly over 5 fracture systems generations and error bars show the maximum and minimum results.

For both the magnetic and gravity techniques anomaly amplitude and detection probability increase with halo spread (Figure 7.8). As fracture percentage is kept at a

constant 1%, this increase is clearly related to the increase in halo spread (and not simply the presence of a halo as simplified in previous literature).

To statistically test this, a single-factor analysis of variance (ANOVA) test was applied. The null hypothesis was that the mean anomalies at each halo spread are equal and the alternative hypothesis was that at least one of the means is different. For the magnetic method the p value is 8.4×10^{-5} and for gravity the p value is 1.7×10^{-6} . Since these are both under the chosen 0.05 level of significance the null hypothesis cannot be rejected and therefore halo spread has relevance to the anomaly size to a 5% level of significance. Similar results were found when testing the effect of halo spread on detection probability (both techniques had a significant effect: magnetic p value = 3.5×10^{-12} , gravity p value = 2.5×10^{-9}). In conclusion, the ANOVA test results show that halo spread has a significant effect on the size of the anomaly and the detection probability.

There is a large increase in the range of results across the 5 fracture configurations when halo spread is set at 2 m (Figure 7.8). At this large halo spread there is a wide range of potential fracture configurations (see Figure 7.2 for an example of a smaller halo spread). Configurations made of a few long fractures will show result in a larger anomaly and detection probability than a configuration with a lot of small fractures. At larger halo spreads this effect is amplified, as seen in the increased range of results as spread increases.

7.1.5 Fracture aperture

Fracture aperture was increased from 0.001 m to 0.2 m whilst fracture percentage was maintained at 0.5% and the effect on anomaly size was noted (Figure 7.9). Although there appears to be a small variation in the mean anomaly size (peaking at 0.02 m, 0.1 m and 0.16 m fracture aperture for both methods), the results of a single-factor analysis of variance (ANOVA) test on the data showed that fracture aperture has an insignificant effect on the size of the anomaly. The null hypothesis was that the mean anomalies at each fracture aperture are equal and the alternative hypothesis was that at least one of the means is different. For the magnetic method the p value is 0.078 and for gravity the p value is 0.051. Since these are both over the chosen 0.05 level of significance the null hypothesis cannot be rejected and therefore the fracture aperture has no relevance to the anomaly size to a 5% level of significance.

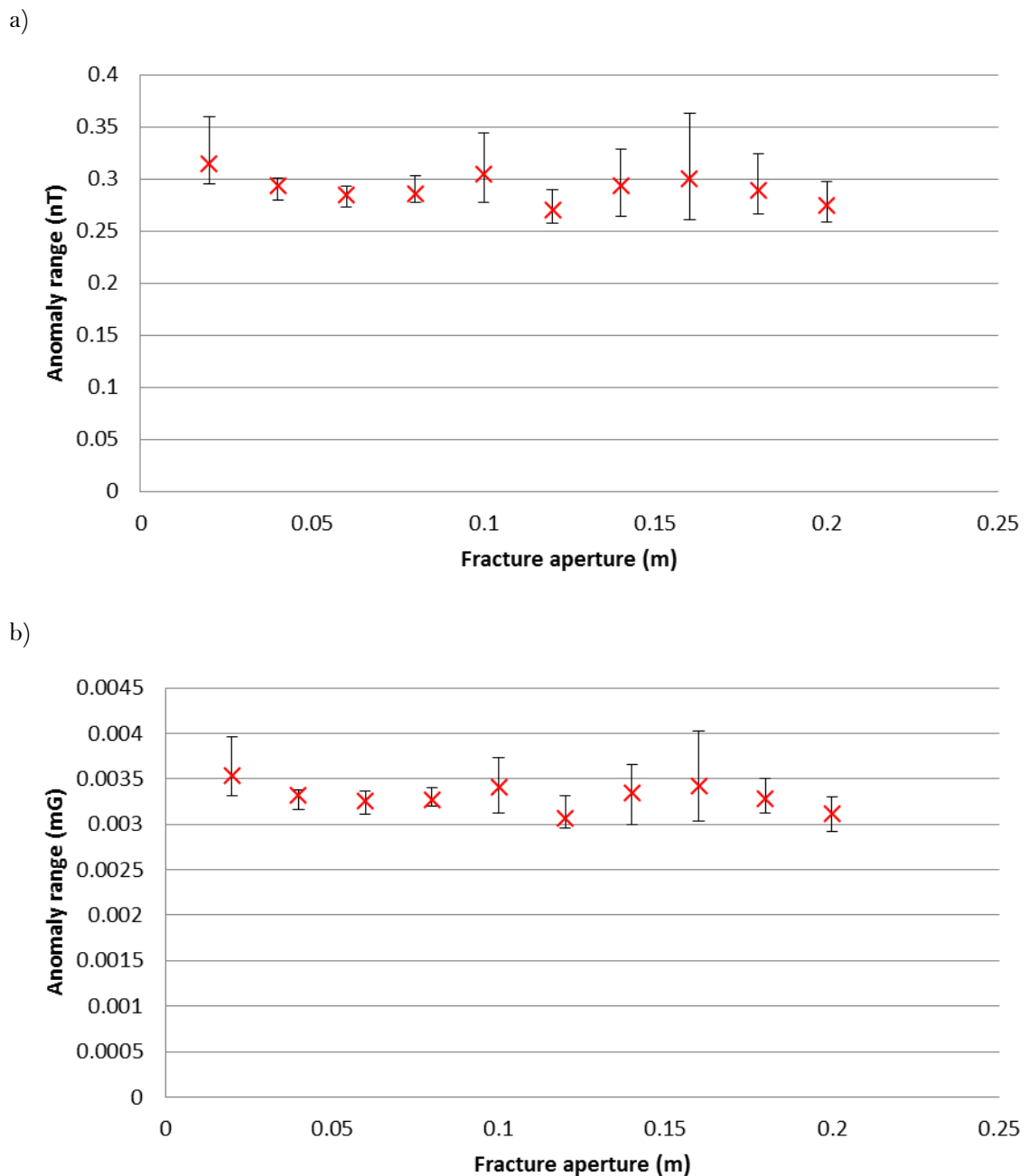


Figure 7.9. Effect of changing fracture aperture on a) gravity anomaly, b) magnetic anomaly. Fracture systems are around a 1-m air cube cavity in limestone with fracture percentage 1% and halo spread 1 m.

A paired T-test was used to test if fracture aperture altered the detection probability across a range of fracture percentages (0-5%) (Figure 7.10). The null hypothesis was that the detection probability did not change between pairs of fracture aperture results across all the fracture percentages tested. The alternative hypothesis was that there is some change. Analysis of all fracture apertures found that all p values were greater than the level of

significance (ranging from 0.12-0.87) and so we cannot reject the null hypothesis. In conclusion, there is not enough evidence to suggest fracture aperture makes a difference to the detection probability across all fracture percentages (for both magnetic and gravity techniques).

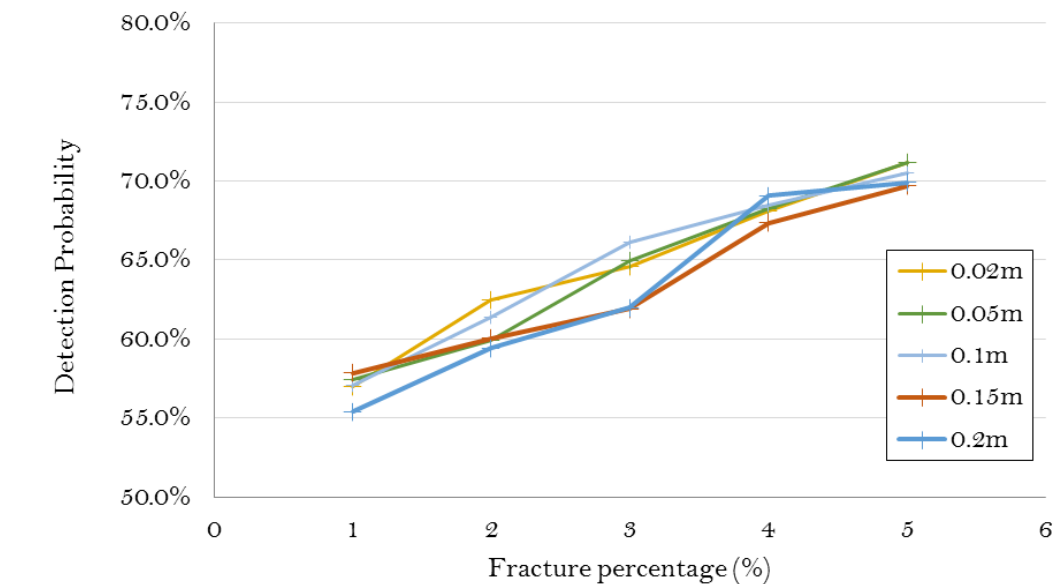
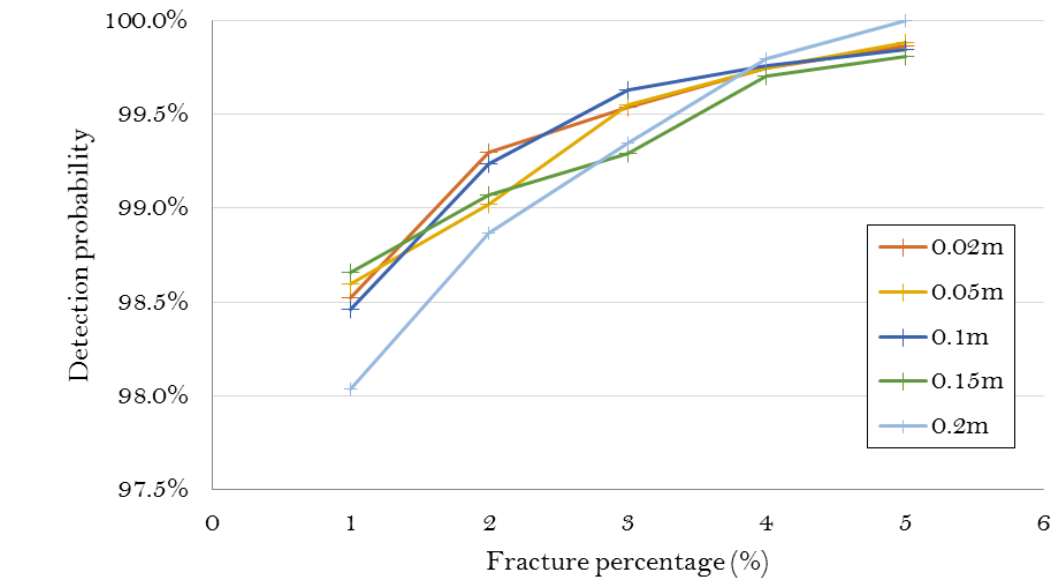
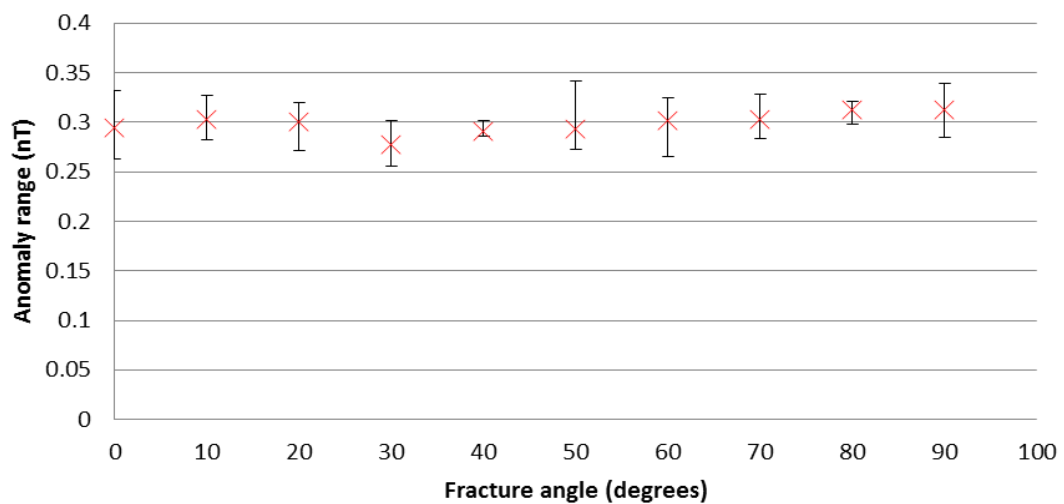


Figure 7.10. Increase in detection probability with increase in fracture percentage across a range of fracture apertures (see legend) for the a) magnetic technique and b) gravity technique. The change in fracture aperture has little influence on detection probability. Fracture systems are around a 1-m air cube cavity in limestone with fracture percentage 1% and halo spread 1 m in typical noise conditions. Note non-zero axis start.

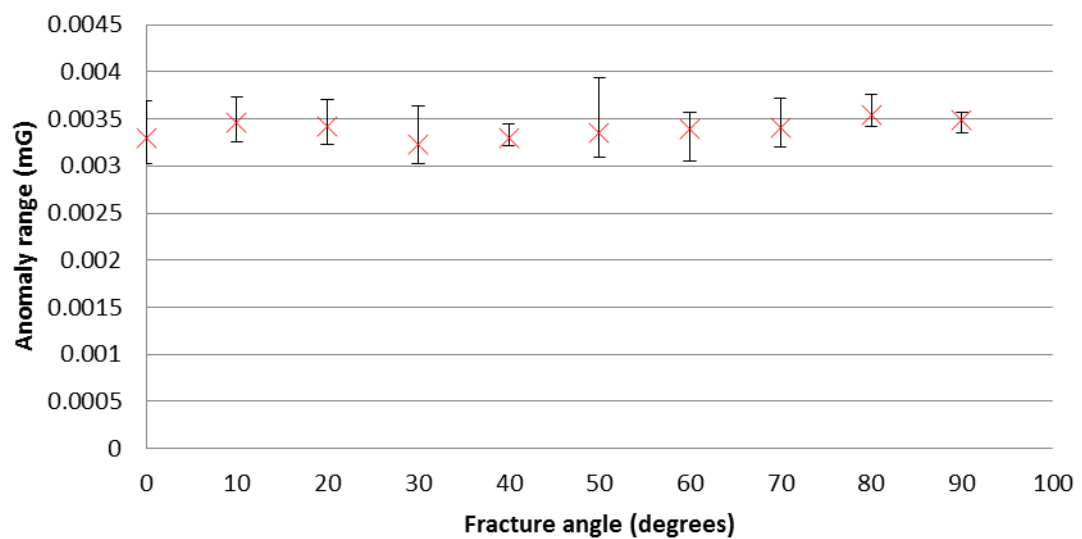
7.1.6 Fracture angle

The fracture angle is varied from 0-90° and the effect on the geophysical signal assessed (Figure 7.11). Fracture angle also has a minimal effect on the size of the anomaly. Although there appears to be a small variation in the mean anomaly size (peaking at around 20° and 40° for both methods) a single-factor ANOVA test finds no variation. The null hypothesis is that the mean anomalies at each angle are equal and an alternative hypothesis that at least one of the means is different. For the magnetic method the p value is 0.345 and for gravity 0.53. We cannot reject the null hypothesis and conclude that fracture angle has no effect on geophysical anomalies over cavity halos to 5% significance.

a)



b)



c)

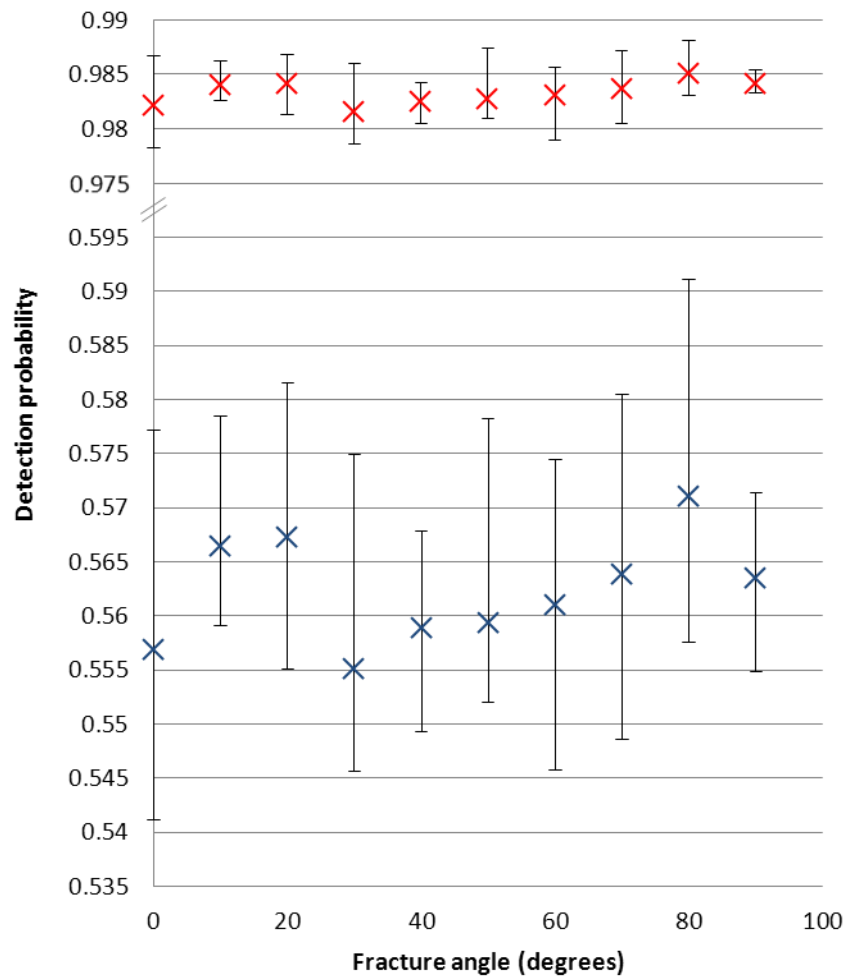


Figure 7.11. Varying fracture angle around a 1-m air cube cavity in limestone with fracture percentage 1% and halo spread 1 m in typical noise conditions. a) magnetic anomaly, b) gravity anomaly (previous page), c) detection probability (red crosses are the magnetic detection probability, blue gravity). Note non-zero axis start. Crosses mark the average for 5 fracture configurations; bars mark the maximum and minimum results.

The detection probability for the magnetic and gravity techniques was modelled with the same range of fracture angles and for fracture percentages from 1-5% (Figure 7.12). As above, there is little variance in detection probability across fracture angles for all fracture percentages.

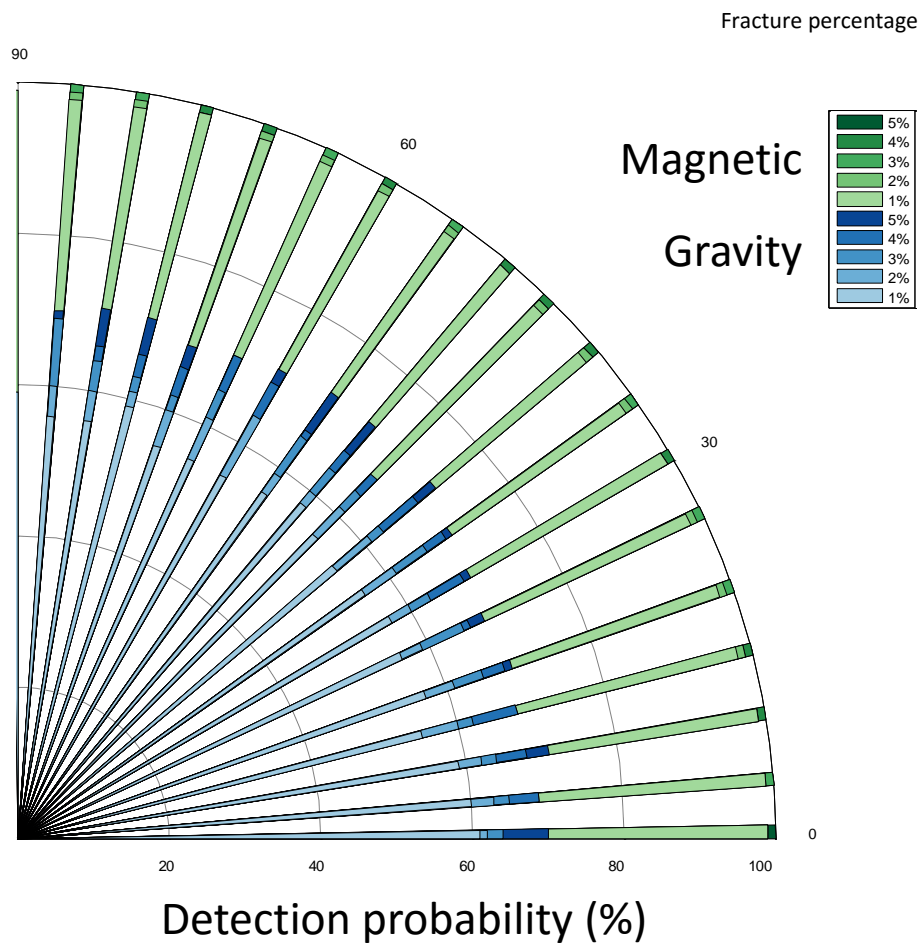


Figure 7.12. Varying fracture angle and fracture percentage around a 1-m air cube cavity in limestone with halo spread 1 m in typical noise conditions. Angle of bars represents the fracture angle; axis shows detection probability and legend show fracture percentage.

7.1.7 Fracture patterns

As noted in Section 6.2.9 stress distribution around cavities (especially tunnels and galleries) mean fractures can be concentrated around the side of cavities (Figure 7.13). In order to model these stress related fracture patterns, fractures generation was limited to the zone around the sides of the cavity, particularly by the corner of the cavity (Figure 7.14). In this way, the fracture pattern more closely resemble those suggested by Golshani *et al.* (2007) and Wang *et al.* (2012).

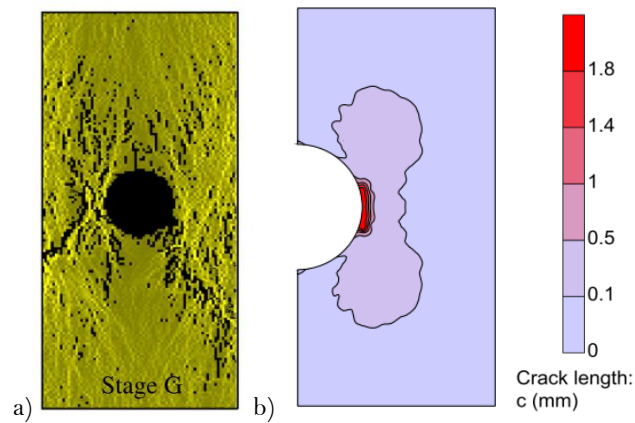


Figure 7.13. A later stage of a numerical simulation of crack evolution around a circular void. Small cracks are seen to develop and coalesce into larger cracks (Wang *et al.*, 2012). b) Microcrack configuration just before failure showing more cracks in the side walls as vertical stress is larger than horizontal stress (Golshani *et al.*, 2007). It should be noted that these patterns depend upon the rock strength and confining pressures.

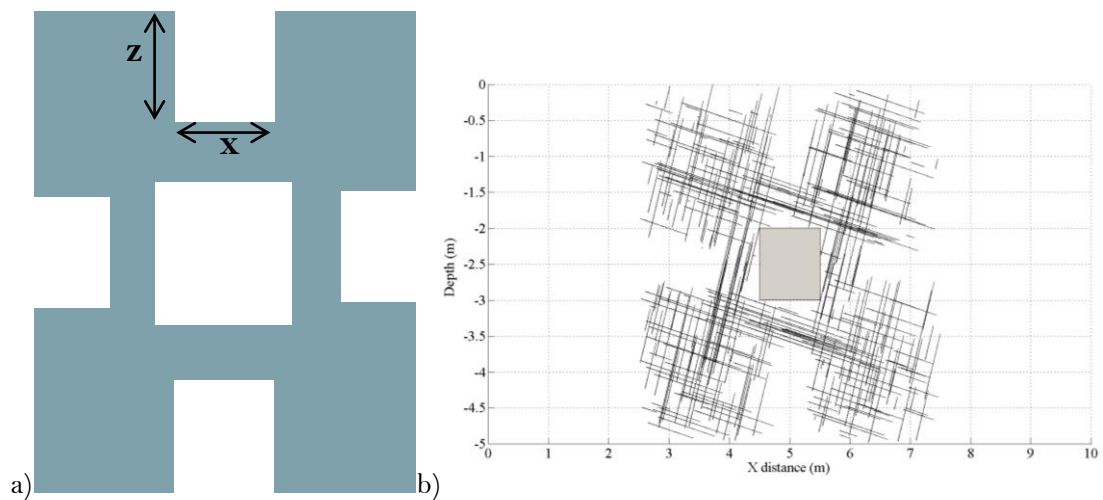


Figure 7.14. a) Schematic showing the creation of stress related fracture patterns. Indents are calculated as follows: $z = \text{halo spread} \times \text{indent}$, $x = \text{cavity size} \times \text{indent}$, where indent is user chosen. b) Example modelled fractures around a cavity (grey). Unlike previous models, these fractures don't necessarily have to be joined to the main cavity; the fractures just must within the stress distribution zone.

The impact of varying the indent size was tested by modelling a tunnel (Figure 7.15). Fracture percentage was kept at 1%, angle at 0° and halo spread at 1 m, while the indent size increased as a percentage of the halo spread (as shown in Figure 7.14).

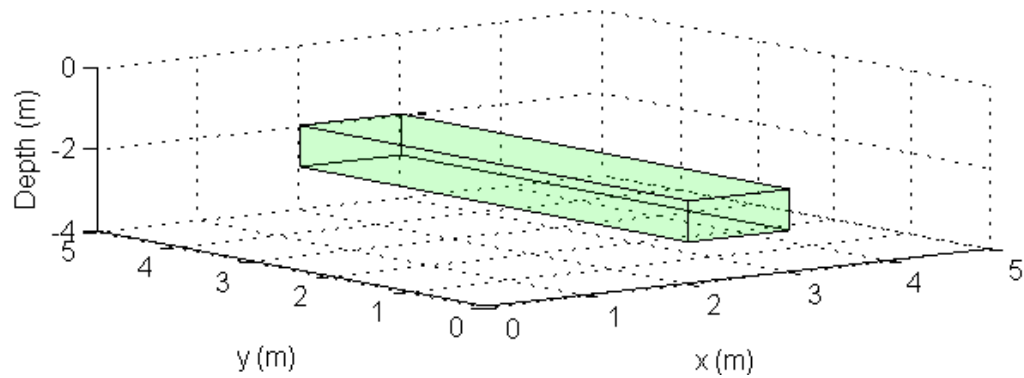
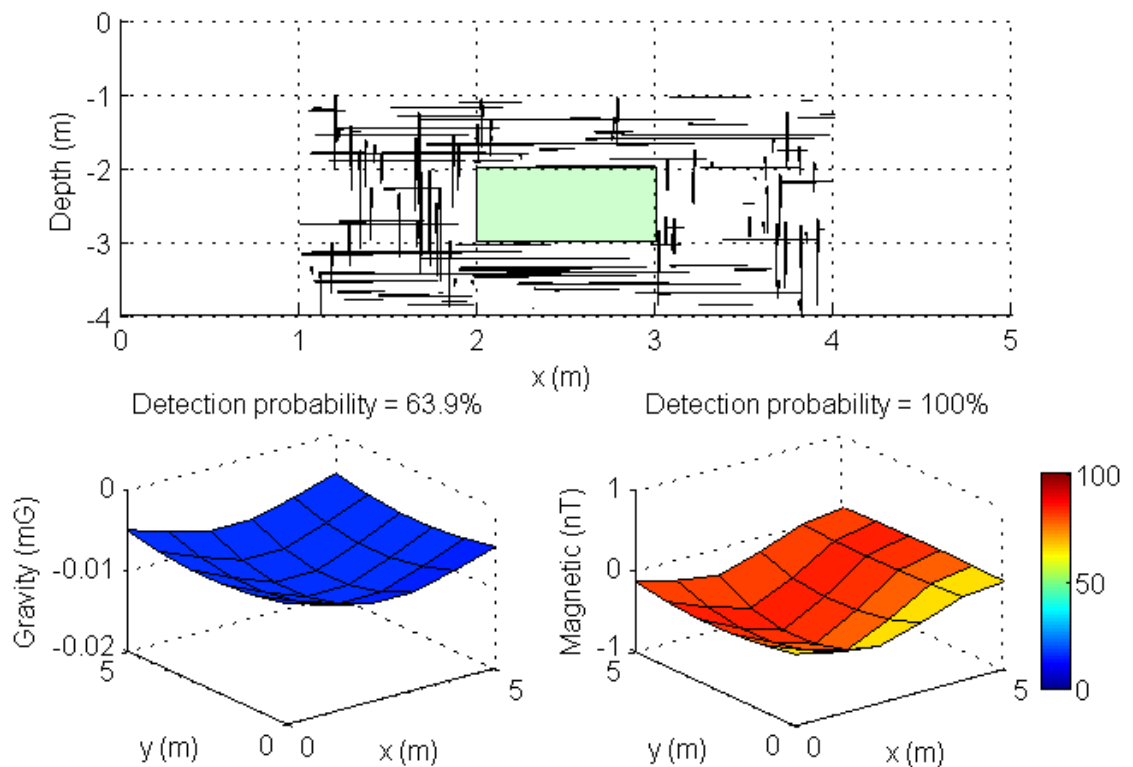


Figure 7.15. Modelled air tunnel: 1-m square, 5 m long, limestone surrounding material.

Figure 7.16 shows example fracture configurations for the 0.3 m and 0.7 m indentation of the halo area. Figure 7.17 shows the decrease in gravity anomaly with increased indentation of the halo area. Although fracture percentage is kept constant the concentration of fractures in the corners of the cavity lowers the overall anomaly size and consequently the detection probability (the same is true for the magnetic technique). This is an important consideration for modelling of halos. Should stress distribution patterns be expected around a cavity, the probability of detection will be lower than if fractures spread in all directions from the cavity.

a)



b)

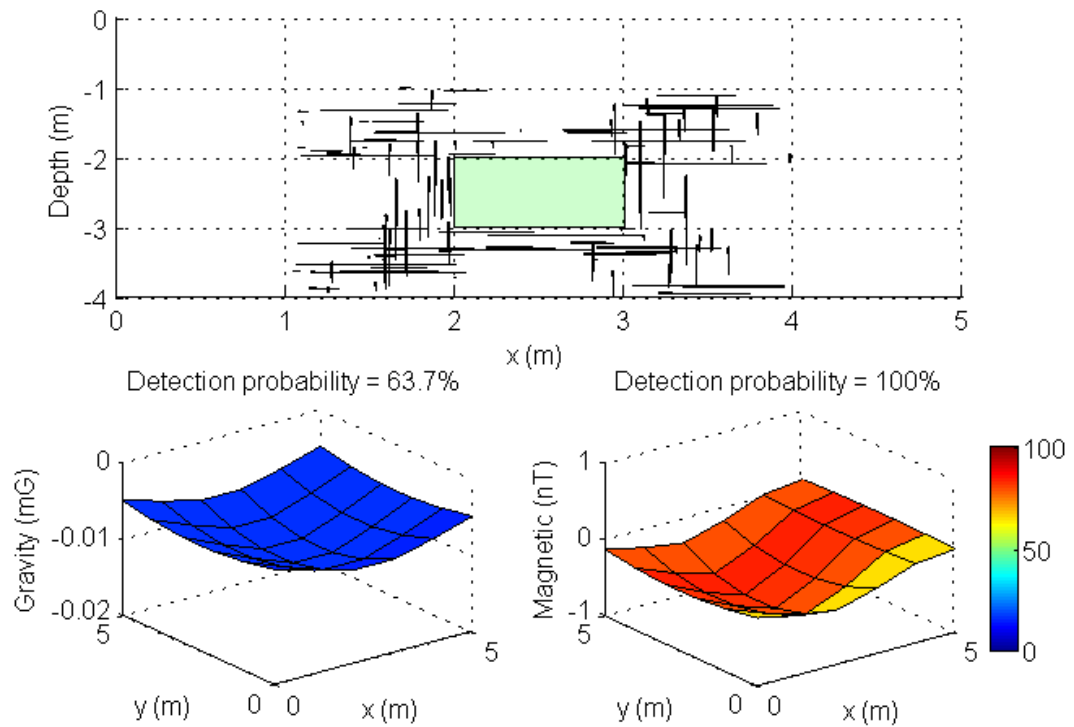


Figure 7.16. Example modelling outputs showing the air tunnel with a) (previous page) 30% of halo spread indentation (0.3 m) and b) 70% halo indentation (0.7 m). Other indentation percentage figures are in Appendix F. Green square represents the cavity, black lines are the fractures. Colour bar shows the detection probability.

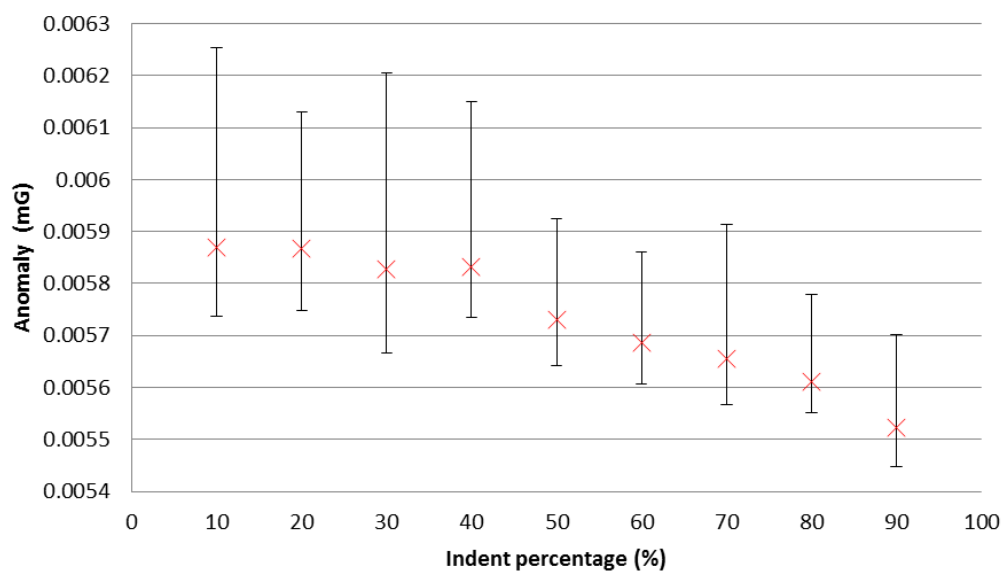


Figure 7.17. The effect of halo indentation on the gravity anomaly size. Results shown are modelled above the air tunnel in Figure 7.15. Crosses are the average of all 20 fracture configurations modelled at each indent percentage; bars are the minimum and maximum anomalies for all configurations.

7.1.8 Micro-fractures

In order to further develop the crack evolution system posited by Golshani *et al.* (2007) and Wang *et al.* (2012) halos made up of micro-fractures were modelled (code in Appendix Axviii). Figure 7.18 shows an example of a modelled halo system consisting of micro-fractures of random length, width and height up to 1 cm (based on the aperture for aged cavity fractures in limestone in Waltham *et al.* (2004)). Micro fractures are created in the halo zone (excluding the indented zone) until the chosen fracture volume percentage is reached (Figure 7.18).

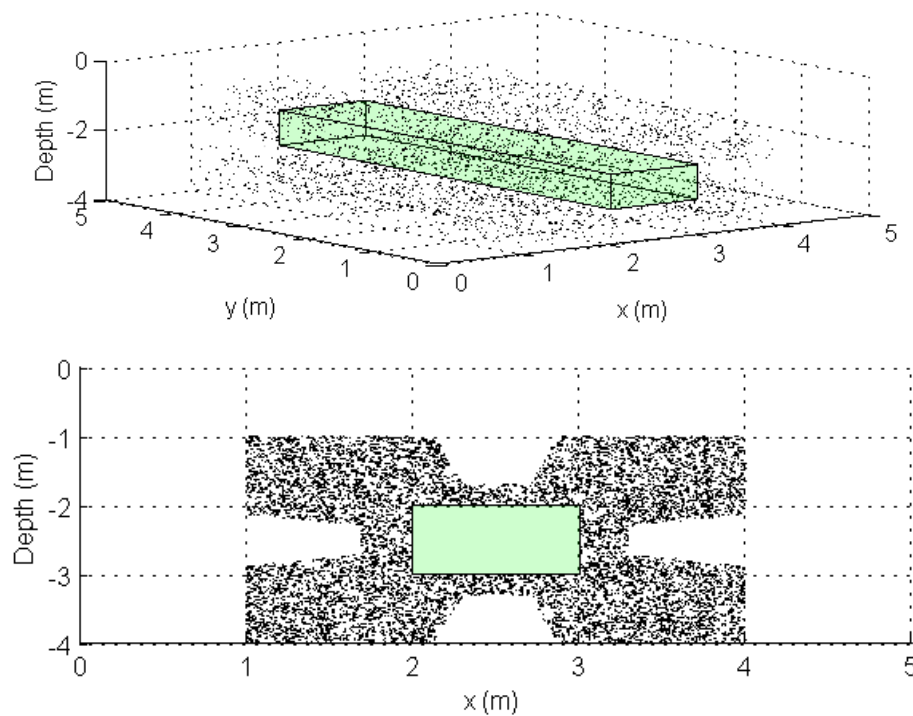


Figure 7.18. Micro-fracture halo system around a 1-m square, 5 m long air tunnel in limestone at typical noise level. Fractures are random dimensions up to 1 cm and the fracture percentage is 1%. Halo indentation is 0.7 m.

Modelled geophysical detection probabilities of this micro-fracture system are 63.6% for the magnetic method, and 99.9% for the gravity method. Even fractures this small (no bigger than 1 cm in any dimension) have the same effect on geophysical results as the larger fractures (Figure 7.16). As previously stated, the fracture width appears to have no effect on the overall detection probability. The main influence is the percentage of the halo filled with fractures and the halo spread.

Golshani *et al.* (2007) note that fracture size decreases with distance from the cavity. To test whether halo systems following this rule will have a larger effect on geophysical results, the same fracture system was modelled with fracture size decreasing with distance from the

cavity (Figure 7.19). Next to the halo, fractures can extend up to the halo spread distance (here 1 m), at the edge of the halo fractures are 1 cm. There is a linear decrease in fracture size with distance.

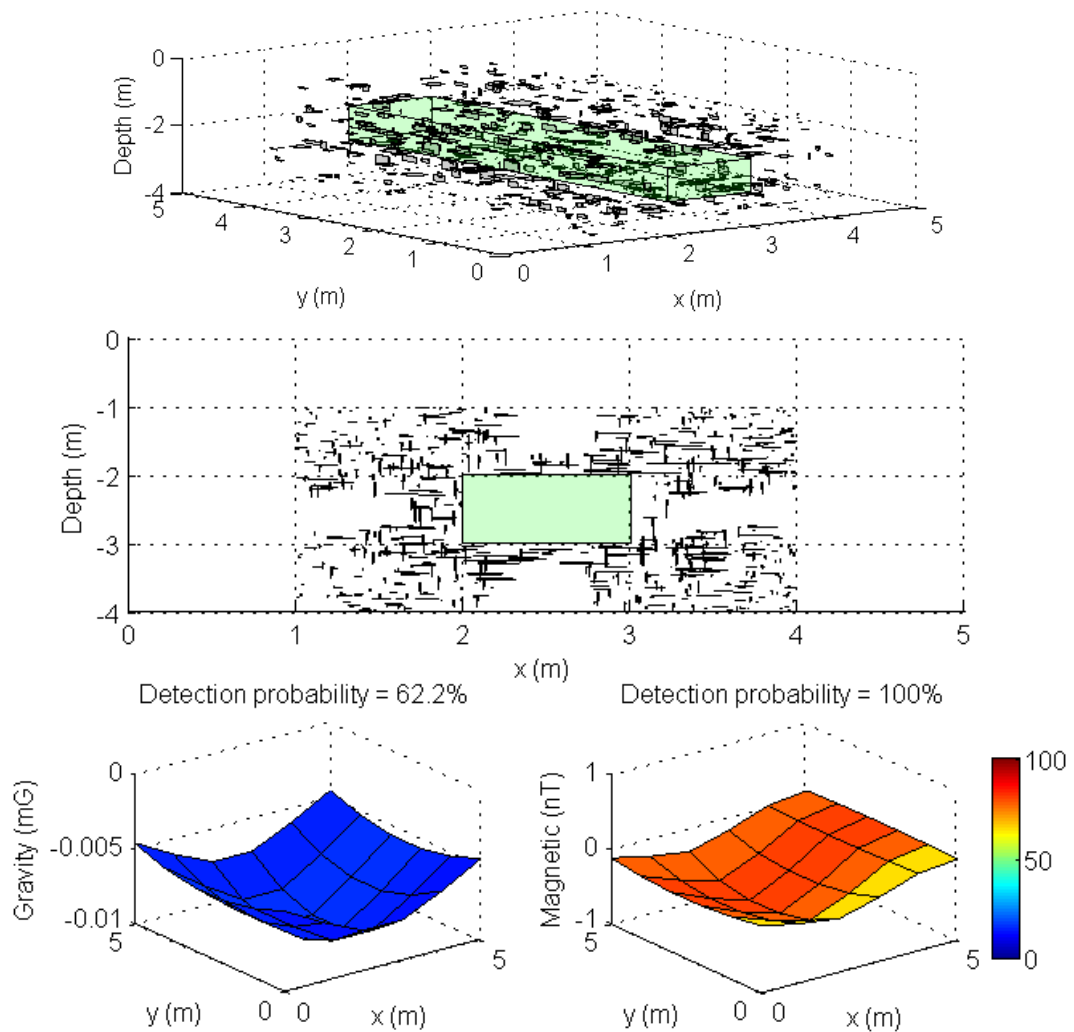


Figure 7.19. Micro-fracture halo system around a 1-m square, 5 m long air tunnel in limestone at typical noise level. Fractures range from 1 m to 1 cm, decreasing with distance from the cavity. The fracture percentage is 0.1%, fracture width 1 cm and halo indentation is 0.7 m. This low fracture percentage is shown here to highlight the change in fracture length with distance from the cavity. Bottom images show the modelled results for the gravity (left) and magnetic (right) techniques. Colour bar represents detection probability.

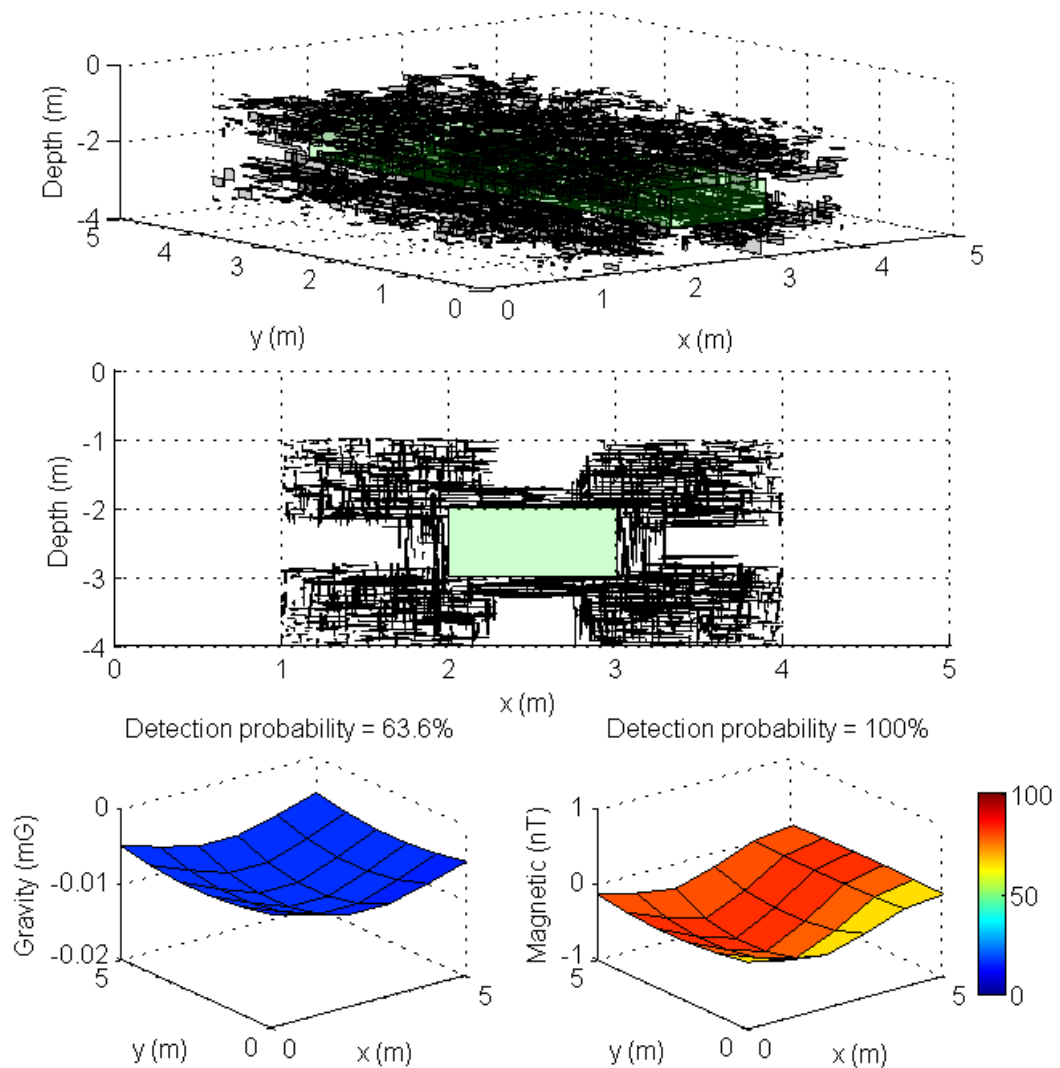


Figure 7.20. The same cavity and fracture conditions as Figure 7.19 but with 1% fracture percentage so comparisons can be made with previous results.

Using this methodology the halo system does increase the geophysical anomalies and the detection probability, when compared to a tunnel with no halo (Figure 7.2). Fracture percentage is only set at 1% and the detection probability results are not statistically different from the 70% indent results from the original method (see Figure 7.16).

Computing power is a limitation on modelling higher fracture percentages. Modelling so many small fractures takes a large amount of time. Improved speed is a future research aim of this project.

7.2 Comparison with rules of thumb

In estimating the effect of a cavity halo, previous literature only refers to rules of thumb. These rules will be compared to the results of this geophysical modelling. Butler (2008) suggests that a halo increases the size of a geophysical anomaly often larger than a factor of two. Chamon & Dobereiner (1988) found gravity anomalies specifically to be a factor of two larger than for the cavity alone. Figure 7.21 compares this rule with the modelled anomaly size for an air cavity in limestone across a range of fracture percentages (the percentage volume of the halo that the fractures occupy). As already established, the anomaly size is affected by more than just the presence of a halo. Because of this the rule of thumb is shown to be too simplistic. For the magnetic technique, at 3% fracture percentage the rule of thumb is approximately true; at all other percentages the rule is inadequate. Less than 3% fracture percentage and the rule overestimates the anomaly size, above 3% the rule underestimates. For the gravity technique the rule of thumb is only approximately correct at 2% fracture percentage. It should also be noted that this is just one modelled halo environment, the rules of thumb would not always be correct at these fracture percentages. The halo system would have to be modelled to determine this.

Benson & Yuhr (1993) suggest that the cavity halo allows detection 1.5-2 times deeper than the theoretical cavity alone. To test this rule, the anomaly size of a halo system at a range of depths (and across a range of fracture percentages) is compared with the anomaly with no halo (Figure 7.22). The cavity with no halo has a certain anomaly size (indicated by the blue dotted line). If it is assumed that the cavity is detectable at this anomaly size, the rule of thumb suggests that a halo system at 1.5-2 times the depth will need to have an anomaly at least as big as this (the arrowed line indicates this section on the figure).

For the magnetic technique, the halo anomaly is as large as the non-halo anomaly between 1.5-2 times the depth, but only for fracture percentages between 2% and 12%. This means, for these fracture percentages the rule of thumb is applicable. However, for a halo system with fracture percentage below 2% the cavity system will not be detectable. For a halo system with fracture percentage above 12%, the cavity will be detectable to even greater depths than the rule suggests.

For the gravity technique the rule is not as applicable. If the fracture percentage is 2% the rule applies, outside of this percentage the rule is inapplicable to the technique. This highlights that the rule do not apply across all techniques and, as with the previous rule, not for all fracture percentages.

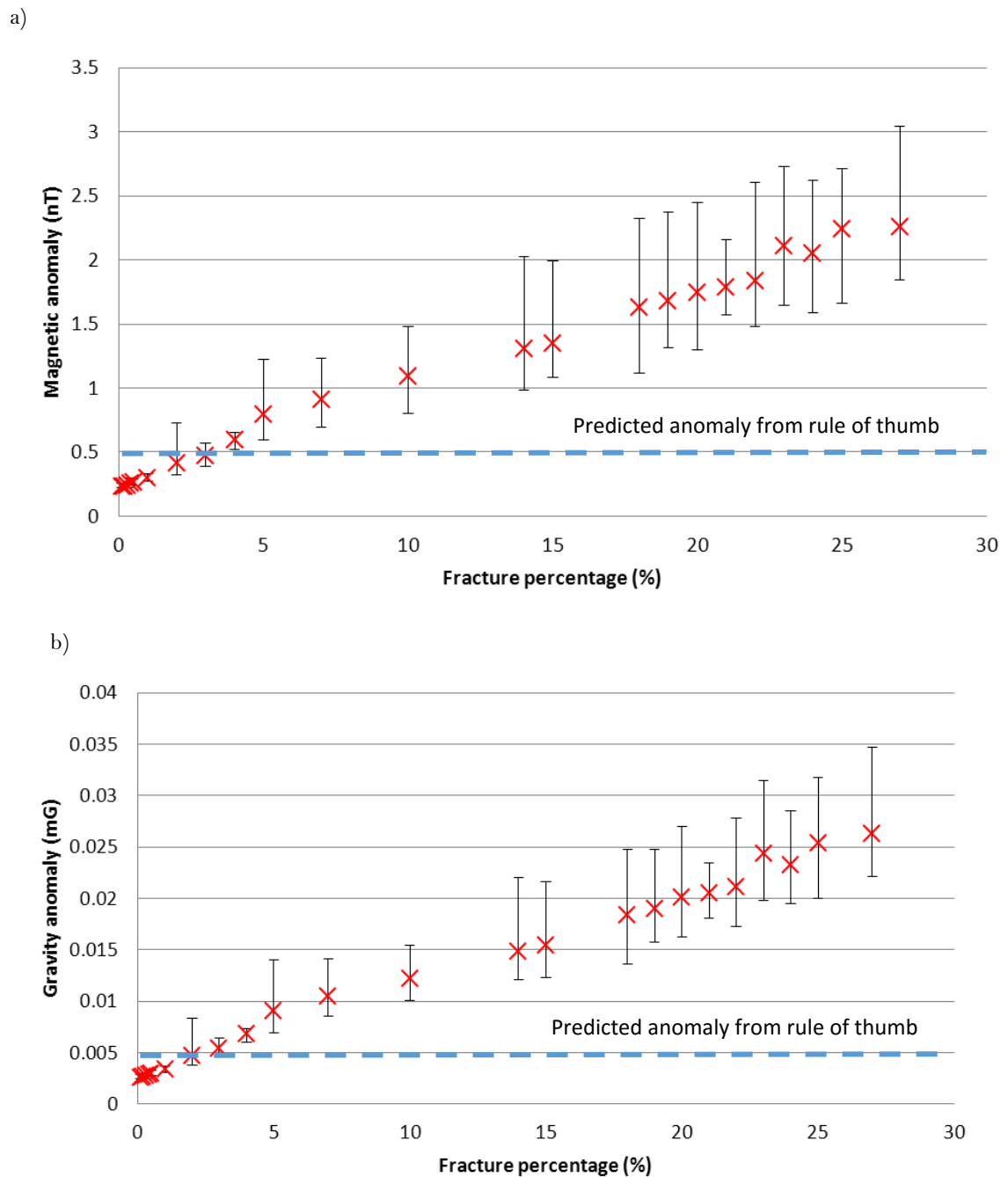


Figure 7.21. Modelled results compared with rule of thumb estimates. Modelled system is a 1-m cube air cavity at 2 m depth in limestone with up to 0.1 m aperture fractures. a) magnetic and b) gravity average size of anomaly as fracture percentage is increased. Crosses display the average peak-to-peak anomaly over 20 fracture systems generations and error bars show the maximum and minimum anomalies recorded. The blue dotted line indicates the anomaly size according to the rule of thumb (increase to the size of a geophysical anomaly by a factor of two over the cavity with no halo).

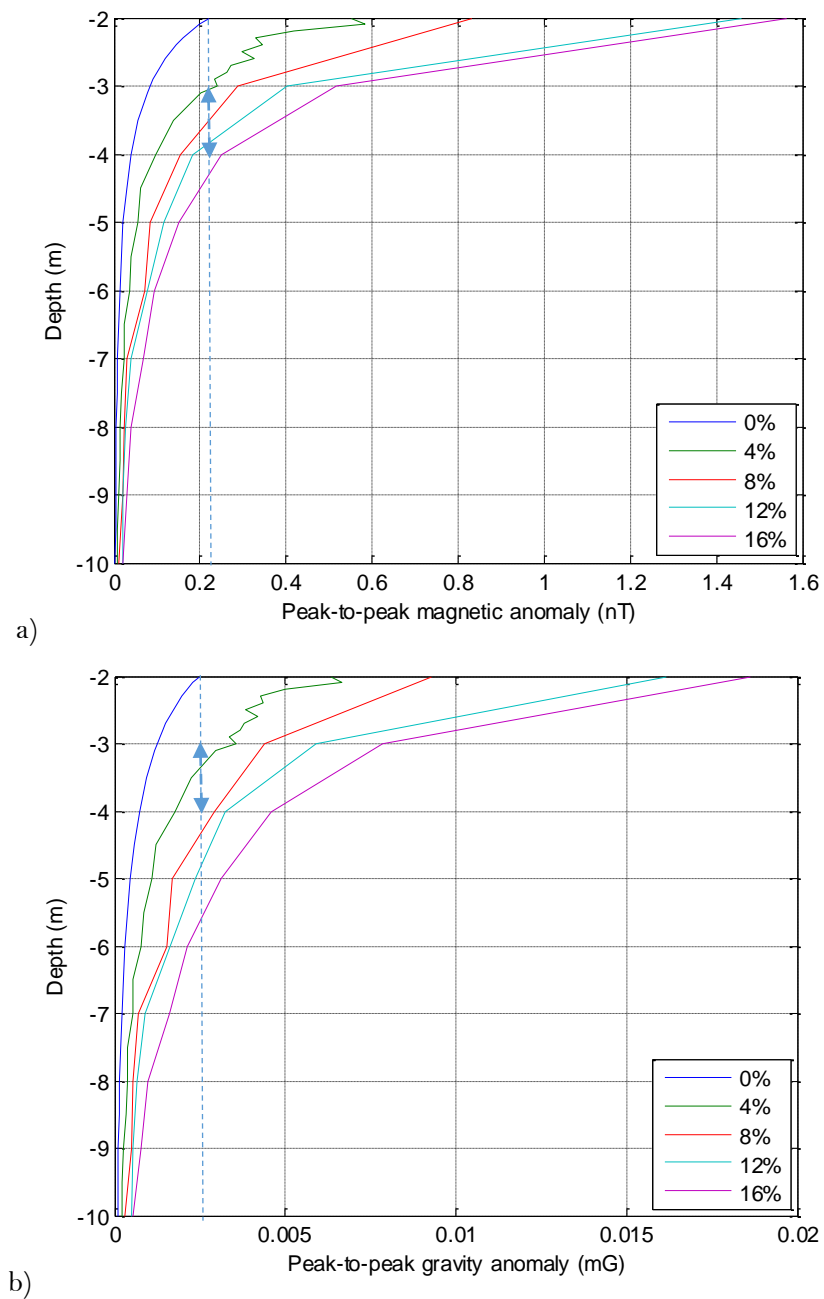


Figure 7.22. Comparison of anomaly size at depth with rules of thumb. Modelled results of fracture systems around a 1-m air cube cavity between 2 m and 10 m depth. The fracture percentage was varied from 0-16% (legend) of the halo area, and the spread of fractures was 2 m. a) magnetic results, b) gravity results. The blue dotted line highlights the anomaly size of the cavity with no halo at 2 m depth. The section indicated by the arrowed line is the depth the rule of thumb suggests the cavity with a halo will be detectable (1.5-2 times deeper than the cavity alone).

7.3 Comparison with previous work

Modelling is often used after the field work has been completed to interpret results. When doing so in the case of cavities, this author can find no examples of the modelled inclusion of the halo effect. It has been shown here that the halo does have an impact on signal size and detection probability, and should therefore always be considered.

The effect of the ignoring the halo in the interpretive modelling stage is to overestimate the size of the cavity. The modelled cavity will have to be bigger than in reality to make up the signal produced by the halo. Here, we compare an example of some interpretive modelling from the literature with the results using this halo modelling approach.

Pánisová & Pašteka (2009) successfully used the micro-gravity technique to detect a subsurface crypt in a Church in Pukanec, Slovakia. No modelling was completed before the survey but gravity modelling was used to interpret the measurements recorded (Figure 7.23).

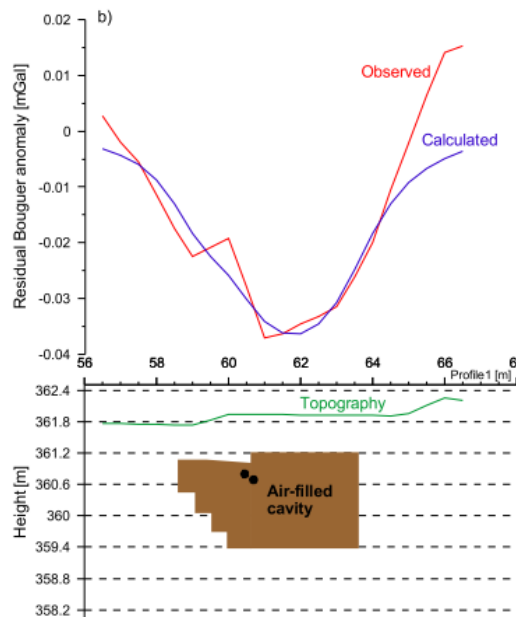


Figure 7.23. Interpretive modelling of an air filled cavity in comparison with the observed results (Pánisová & Pašteka, 2009).

A cavity of the same dimensions is modelled using the presented software with no halo for comparison with the Pánisová & Pašteka (2009) work (Figure 7.24). There is a good match between the two modelled results in anomaly size and shape. Now, it is hypothesised that the cavity could in fact be smaller than Pánisová & Pašteka (2009) interpreted but with halo surround. Figure 7.25 shows the cavity with a 5% reduction in all cavity dimensions but with the addition of a halo with fracture percentage of 2%. As can be seen, even though

the cavity is smaller, and a smaller anomaly would be expected, the halo increases the anomaly size up to the anomaly recorded for the original size cavity. That is to say, even though the cavity modelled by Pánisová & Pašteka (2009) matched the observations, the true subsurface could just as easily be a smaller cavity with a halo system.

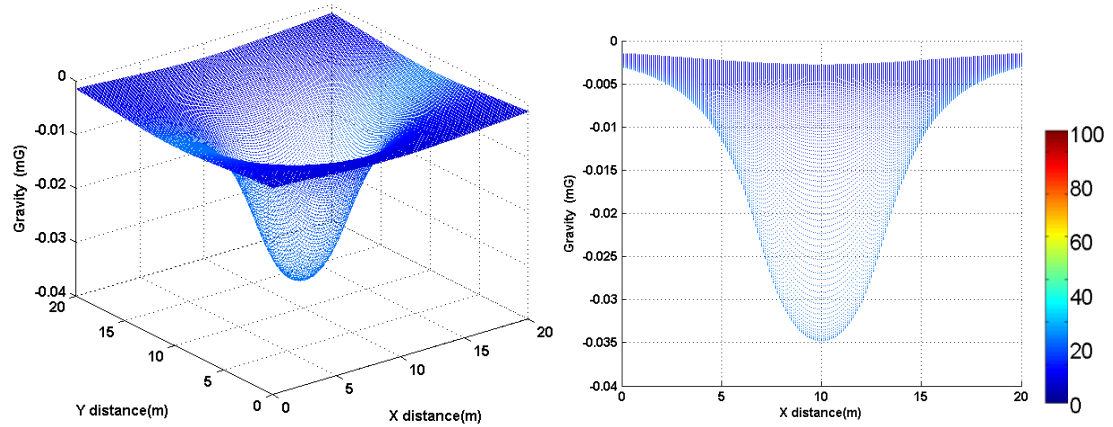


Figure 7.24. Modelled results of the cavity in Pánisová & Pašteka (2009). Dimensions used are from the paper (1.3 m depth, 5.5 m by 3 m across, 1.8 m tall in soil). The right image shows a profile view for comparison with Figure 7.23.

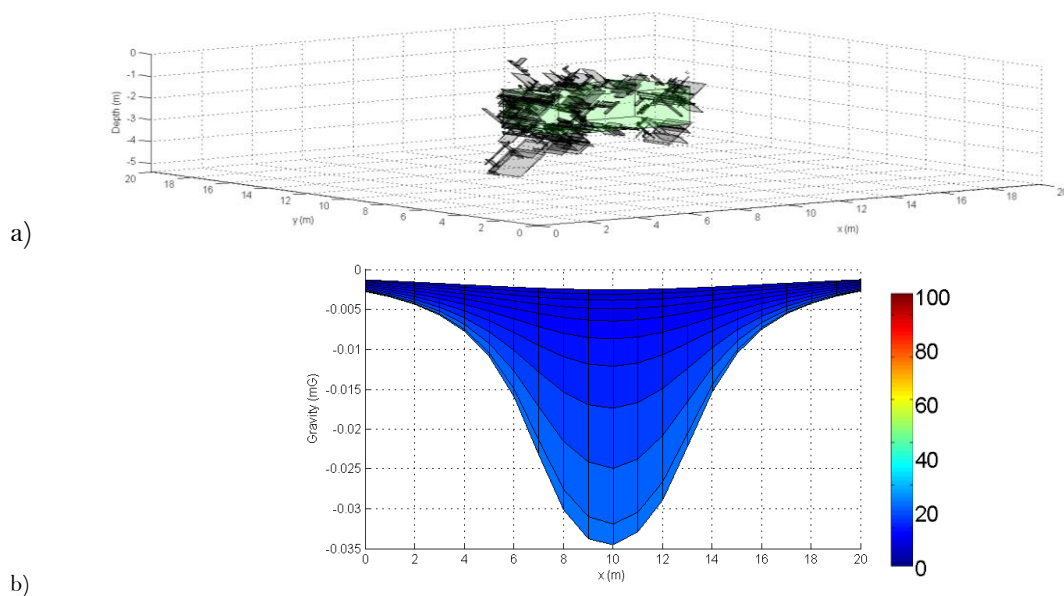


Figure 7.25. a) The original cavity dimensions reduced by 5%. A halo with 2% of the halo spread (1 m) filled with fractures. The percentage of fractures required was found by modelling the halo while increasing the fracture percentage until the gravity anomaly reached that of the original sized cavity. b) The modelled gravity result for the cavity and halo configuration. The amplitude and shape closely match that of the original cavity anomaly (Figure 7.24).

It should be noted, that these results are unlikely to be the actual configuration of the subsurface. It could just as likely be a smaller still cavity with a higher fracture percentage. However, the experiment does highlight the importance of consideration of the halo when using geophysical modelling around cavities.

This is just one example from the literature, and there are many more which don't consider the halo effect when completing interpretive modelling. This work highlights the importance of this step. Geophysical modelling, especially of potential fields, is known to be non-unique, and this finding adds a further complication to the problem.

7.4 Discussion

Although this work is an important iteration beyond rules of thumb in understanding the effect of the halo on geophysical methods, the subsurface is still much more complicated. Cavities can also be part of a larger cave system with other cavities and adjoining fractures and so the reality is much more complicated modelled here. As Golshani *et al.* (2007) suggest pre-existing cracks must be incorporated into calculations. The halo modelling must be further incorporated into the cavity modelling package, including rock specific fracture percentage and apertures based on previous field examples.

Work must be done on improving processing speed for micro-fractures. This may include comparisons of these results with halos composed of a solid volume of different geophysical parameters (for example, lower density material) surrounding the cavity. If results are in line with those presented here, this will be a much more computationally efficient method.

Although attempts have been made to accurately represent the halo system through realistic fracture parameters and by concentrating fractures on the side of the cavity, more can be done. Subsidence systems could be represented by higher density of fractures above the cavity. In the case of natural cavities, there is likely to be a system of cavities with adjoining fractures and halos. This will be difficult to predict on a specific site and complex to model, but is certainly worth considering.

7.5 Chapter summary

Of primary interest throughout this analysis is the effect that a cavity halo has on the gravity and magnetic methods. By modelling the halo around cavities caused by fracturing we have found that cavity halos have a significant effect on geophysical anomalies. Importantly, it is noted that this effect is not in line with current predictions in the

literature. In the near surface, the halo effect is much greater than known rules of thumb predicted. As cavity depth increases the halo has less effect on the anomaly size.

Through further analysis using the software it is shown that the fracture percentage in the halo area, the halo spread and halo indent all have a significant effect on the geophysical anomaly size above the cavity. Fracture width and fracture angle are shown to have insignificant effect on the geophysical anomalies. Of course, the nature of the software means that it can be used to calculate the geophysical anomaly and detection probability of any number of given cavity and halo scenarios.

Numerous fracture patterns configurations were modelled (chosen on the basis of the literature) including micro-fracture and fractures concentrated in the corners of the cavity. Beyond the influence of the shape of the cavity, micro-fracture halos did not make any significant difference to the geophysical results in comparison with larger fractures.

The comparison with the literature interpretive modelling highlights the importance of consideration of the halo in interpretive modelling. Any conclusions drawn from interpretive modelling should always be proven by intrusive techniques and this work adds further complication the issue. It is suggested that the halo effect should be considered in future cavity modelling and also possibly in reconsideration of past modelling.

As covered in the Discussion, there is further complexity that could be added to the halo modelling. Despite this, the analysis has shown the significance of the halo, and hopefully highlighted the need for consideration of the halo effect when considering any geophysical modelling of cavities (predictive and interpretive).

Chapter 8

8 Cavity Case Studies and Modelling Comparison

In order to verify the modelling techniques used in the program, four case studies have been chosen for testing. It is important to test a wide range of cavity types to properly test the program and the assumptions made within the modelling.

8.1 Equipment list

Geophysical equipment as used in the field on the case studies used to verify the modelling technique is as follows:

- Ground Penetrating Radar (GPR): Sensors and Software pulse EKKO PE-100A GPR (1000V) (100 MHz and 200 MHz antennae)
- Magnetometers: Geometrics 856 Proton Precision Magnetometer, Geometrics 858 Caesium Vapour Magnetometer.

8.2 Middlesex Hospital, London

A new mixed used development has been proposed on the now vacant site of Middlesex hospital (Figure 8.1). The old hospital has been razed leaving a construction site mostly covered with “made ground”. During site excavation, empty under-pavement vaults were encountered around some of the site perimeter; other potential vaults required delineation.

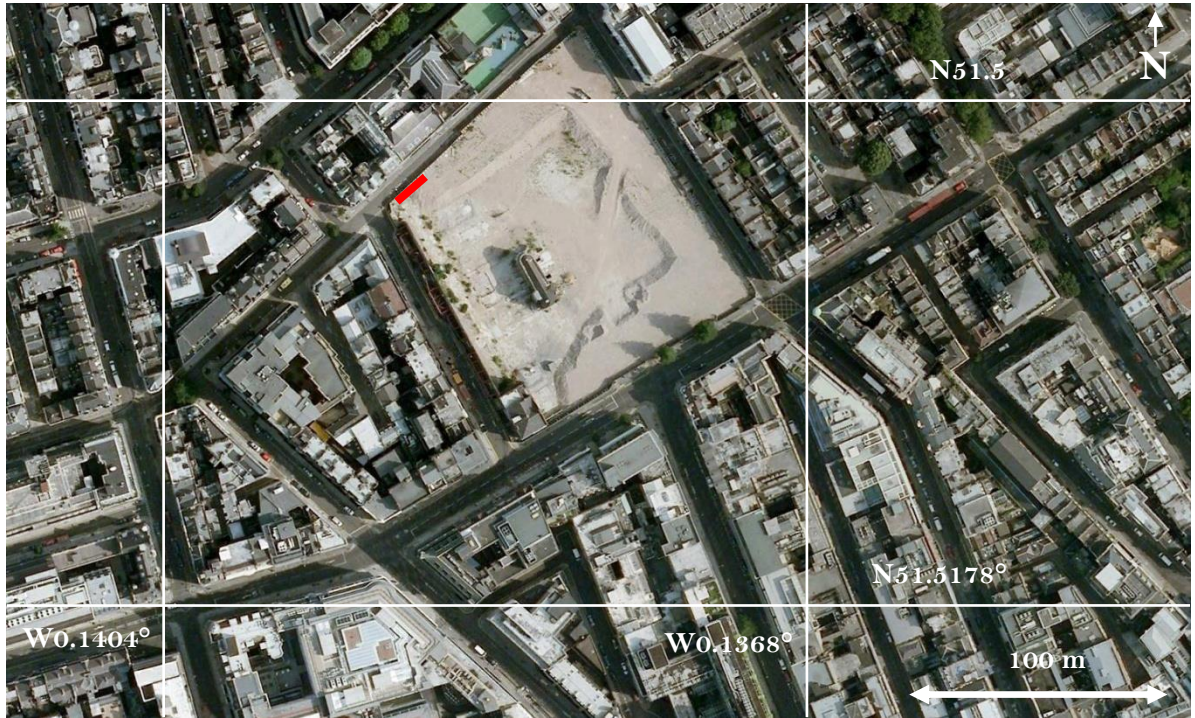


Figure 8.1. Satellite image of the Middlesex hospital site. Red line indicates location of survey (Google 2011).

8.2.1 Pavement vault modelling

The vaults were modelled to find the most suitable geophysical technique for detection on the site. The dimensions used were based on an exposed pavement vault on the site: 0.8 m deep, 1.5 m tall, and 2.8 m across. Typical brownfield levels of noise were chosen as the survey line is next to a road and the made ground contains an array of material. As a magnetic noise survey had already been undertaken in the area (section 4.3.2.4) the magnetic noise was constrained well at 16.3 nT. All techniques were modelled over the simulated vault across a 15 m square grid in concrete and the results are visualised in Figure 8.2a-d. The overall detection probabilities calculated were 84% (magnetic), 57% (gravity), and over 99% for gravity gradient and GPR. However, the confines of the site position (approximately 70 cm across) allowed just one survey line. The probabilities calculated for a single survey line directly over the cavity were 24% (magnetic), 7.5% (gravity), 98% (gravity

gradient), and over 99% (GPR). Hence, both the gravity gradient and GPR techniques were applicable for cavity detection on this site. The choice then becomes logistical and so GPR was chosen because the technique is much faster in the field.

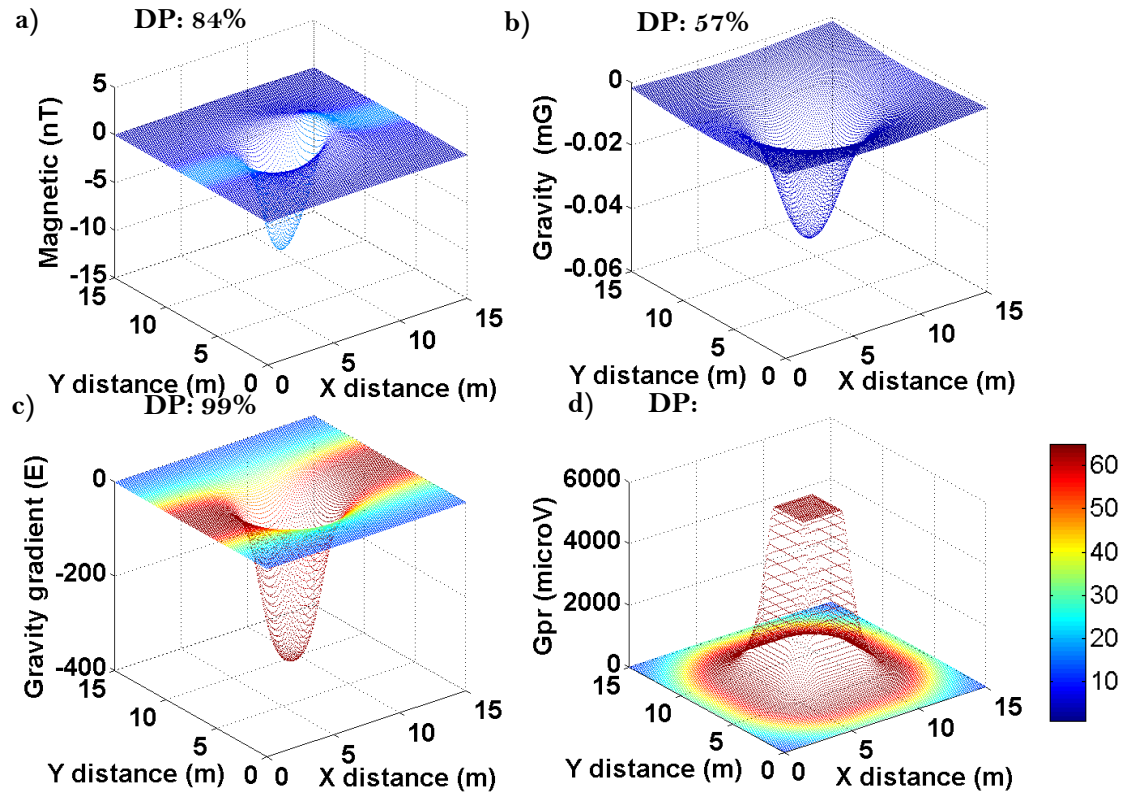


Figure 8.2. Geophysical signal modelled over pavement vaults with the same dimensions as an exposed vault at Middlesex Hospital site. DP= overall detection probability. a) magnetic, b) gravity, c) gravity gradient and d) GPR. Colour bar represents the detection probability on each survey line.

8.2.2 Field measurements

A pulseEKKO PE-100A GPR (1000 V) system with 200 MHz antenna was used to collect the data; this frequency was chosen as the target was known to be shallow. A 15 m survey in the NW corner of the Middlesex Hospital site was recorded (location shown in Figure 8.1). Standard survey parameters for this frequency were used: antenna separation 0.5 m, 32 stacks, 0.1 m step size (Sensors Software Inc. 2003). Data quality was good so processing was limited to: noisy trace deletion, dewow filter, SEC gain, and nth power attribute function to highlight strong amplitude reflections typical of cavities. The raw data is shown in Appendix G and processed data is shown in Figure 8.3. The GPR results show the technique choice was applicable as the strong amplitude reflections of the vaults were clearly detected (Figure 8.3).

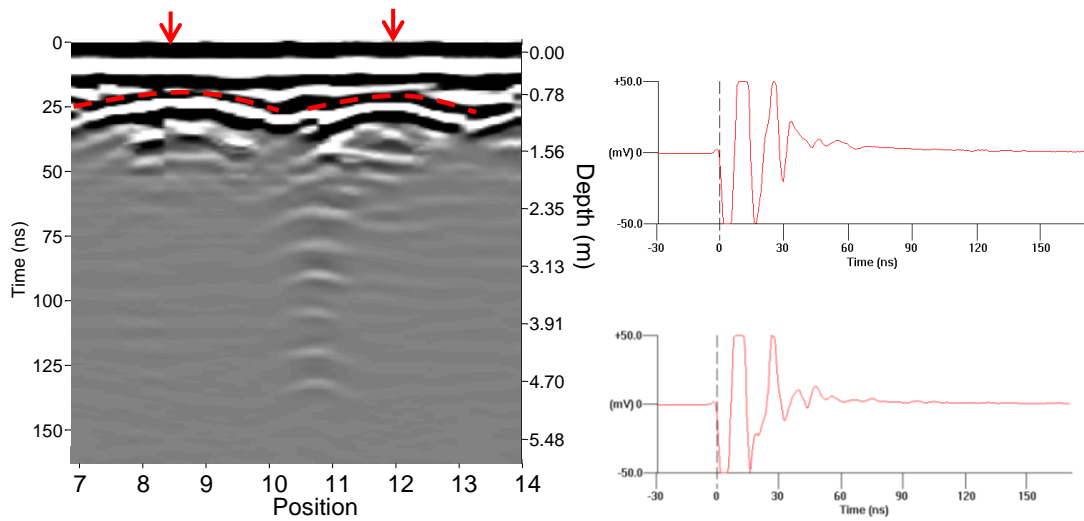


Figure 8.3. Left: processed section above two pavement vaults (survey location shown in Figure 8.1) showing the strong reflection from the vaults (red dotted line). Right: GPR traces directly above the vaults. Positions of traces are indicated by the arrows on the section (top trace is left arrow and bottom is right).

The vaults are shown to be at the same depth as the exposed vaults (0.8 m) and approximately the same width (the eastern vault is slightly wider - 3.5 m). The heights of the vaults are unknown as there is no reflection from the base of the vault and the single survey line means that the lateral extent is unknown.

Although the widths of the modelled anomalies match the measured anomalies, the amplitude is generally too small. Comparison of the amplitude recorded on individual traces directly over the pavement vaults and the modelled signal amplitude shows more energy was reflected from the vaults than was modelled (Figure 8.3). The modelled peak voltage directly above the cavity is 5.48 mV and the measured amplitude at the site ranged from 2-35 mV over both vaults. Estimation of the geophysical parameters of the concrete could be a source of error in the modelling. Experimenting with a range of dielectric constants found that Portland Cement (dielectric constant of 11 (Carino (2010))) creates an anomaly closest to that measured in the field (Figure 8.4). This highlights the importance of choosing the correct parameters for modelling.

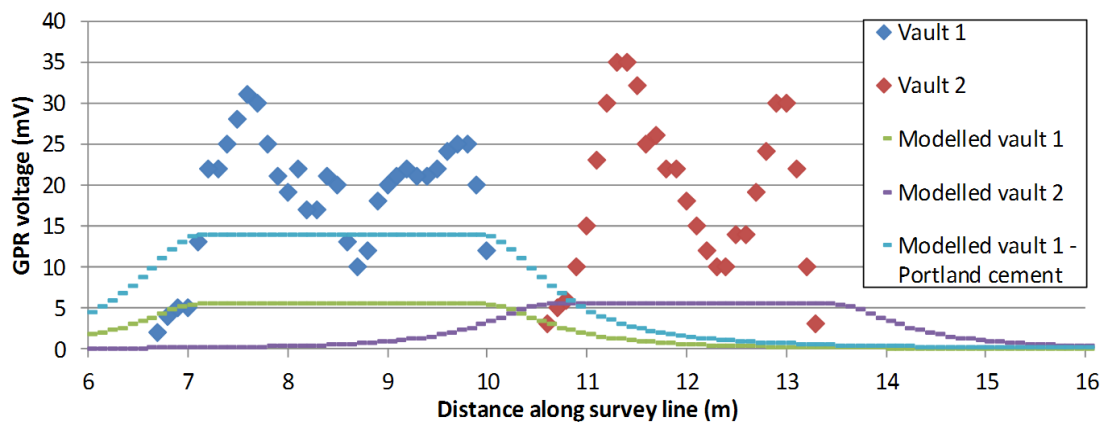


Figure 8.4. Magnitude of signal above both pavement vaults compared with the modelled results and with the modelled results when using the geophysical parameters of Portland cement. A much closer match is made when using the Portland cement parameters.

8.3 Oslo sewerage tunnel

A new sewerage tunnel was being installed in the vicinity of Oslo, Norway (unfortunately, specific locations cannot be shared). Above the new tunnel route, old sewerage maps indicated the presence of another smaller tunnel. This tunnel posed a hazard to the construction of the new tunnel, through collapse or through weakening the integrity of the tunnel surround. To make sure the smaller tunnel was far enough away from the construction of the new tunnel, geophysics was to be used to detect and delineate the old tunnel.

8.3.1 Tunnel modelling

A borehole in the tunnel roof identified the geology to be granite. Previous sewerage maps and plans estimated the location and size of the target tunnel (Figure 8.5). The dimensions of the tunnel were estimated to be: 5 m height, 4 m wide, extending towards the North and South direction (estimated to 3° north). The boreholes could be used for surveys if required.

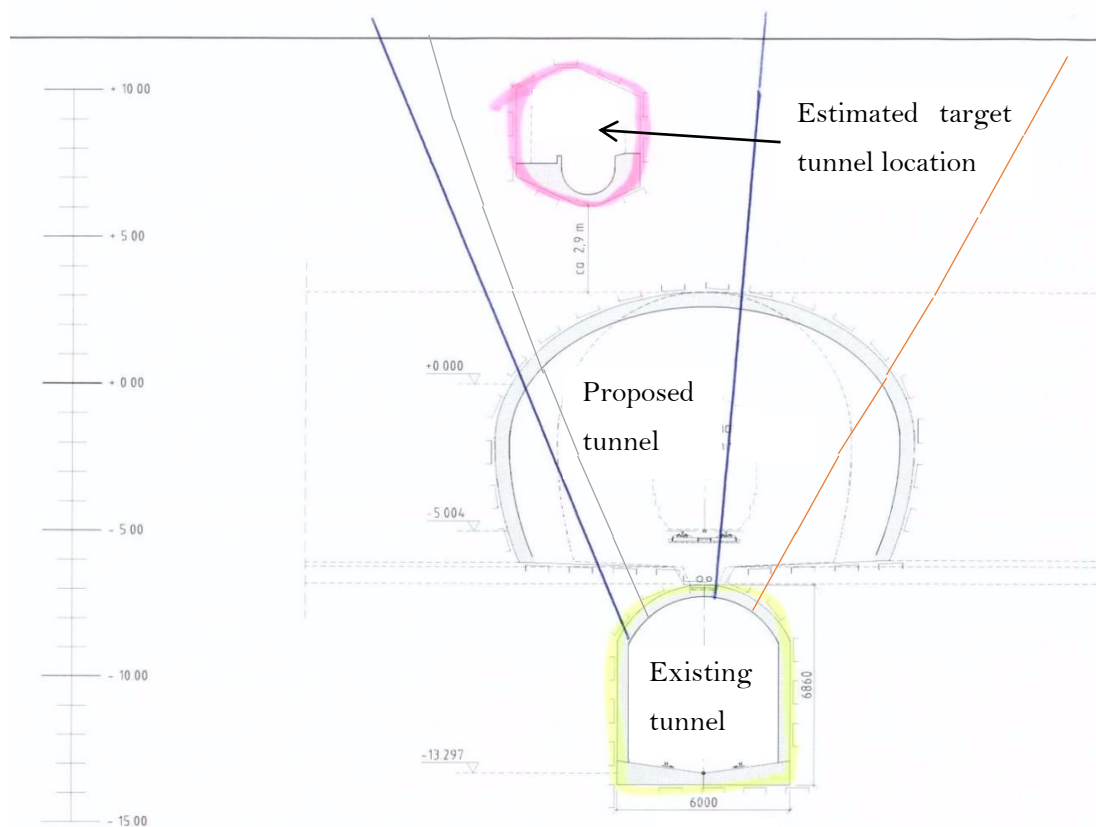


Figure 8.5. Estimated target tunnel location above the existing tunnel, and close to the proposed tunnel. The green line is the left borehole and the red line is the right borehole in the roof of the existing tunnel. North is into the page. Scale on the left is in meters.

The granite geophysical parameters used for the modelling were as in Table 4.1. The estimated positioning of the target cavity is used as the distance from the existing tunnel – 13 m. Magnetic was ruled out before the project began due to the metal rebars in the roof of the tunnel, leaving gravity and GPR techniques. The modelled results of both are shown in Figure 8.6. At brownfield noise levels (expected in the tunnel because of the passing construction vehicles and the metal material in the tunnels and walls), GPR has a much higher likelihood of detection of the tunnel, 99%, compared with 68%. It is also possible to use the boreholes to perform borehole radar analysis, putting the target much closer and consequently improve the detection probability even further. It was therefore decided, to use borehole radar to detect the target tunnel.

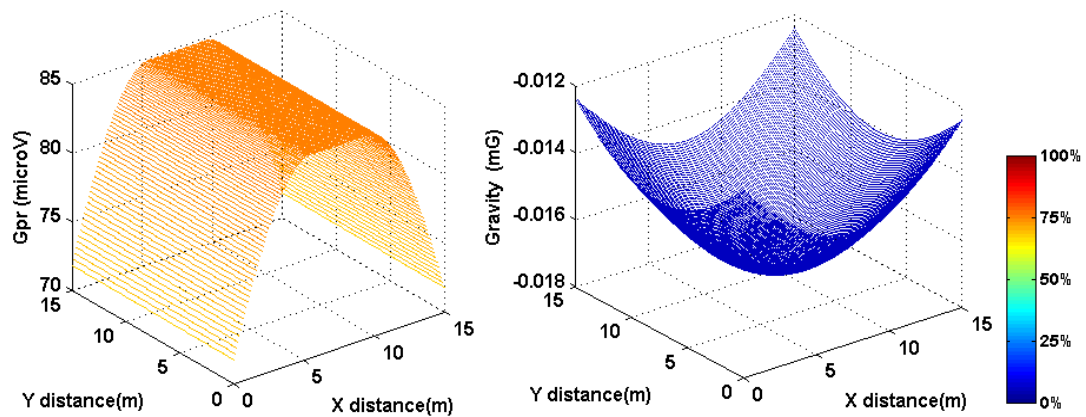


Figure 8.6. Modelled results of the estimated target tunnel location and dimensions (13 m from the existing tunnel, 4 m wide, 5 m high air tunnel in granite in brownfield noise). Left: GPR results, right: gravity results. GPR has an overall detection probability of 99% while gravity has 68%.

8.3.2 Field measurements

Borehole GPR is used to counteract the EM absorption loss commonly associated with using surface GPR to target deep objects (Liu & Yu, 2013). Using the technique in this context allows surveying much closer to the expected tunnel location than from the existing tunnel roof. Care must be taken in interpretation because borehole GPR, much like unshielded GPR, detects records reflections from all directions.

A 100 MHz frequency Mala borehole antenna system was used, with 2.75 m signal to receiver spacing, in reflection mode. Measurements were taken in both boreholes in the existing tunnel (Figure 8.5) to image the target tunnel from both sides. 21 m of measurements were taken in the left borehole and 16 m of measurements recorded in the right borehole.

Data was of a good quality so processing was minimal. Velocity was set at 0.135 m/ns after assessing hyperbolas present on the datasets (this fits well with the granite velocity of 0.13 m/ns (Milsom & Eriksen, 2011). Dynamic correction to correct for antenna offset was calculated using the signal to receiver spacing and the chosen velocity. As previously, a high frequency dewow filter was used and well as a median filter to remove artefacts from the dynamic correction. The data was smoothed and arrivals were picked by hand. The processed results are shown in Figure 8.7.

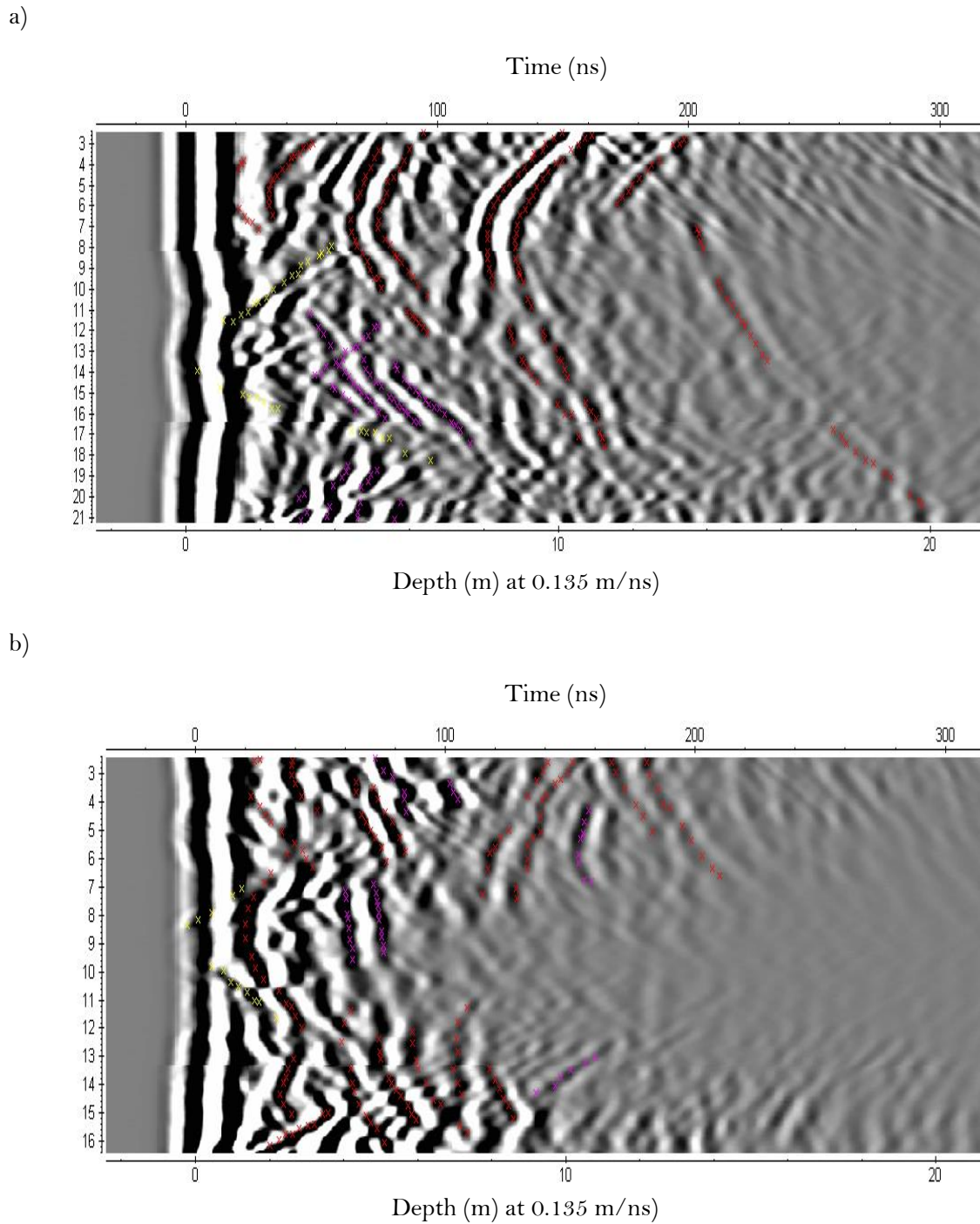


Figure 8.7. Processed radar sections from a) left borehole and b) right borehole. Y-axis shows distance along the profile. Red crosses indicate suspected reflections from point sources, yellow from fractures crossing the borehole, purple fractures within the rock.

A number of features stand out in the processed sections. In the left borehole (Figure 8.7a) there are two very strong point reflectors at 5 m and 9 m depth (highlighted by the red crosses). The hyperbola shape “limbs” have the angle that would be expected of a point

reflector in material with this EM velocity. On both sections there are two linear features which cut across beds and meet at the borehole (yellow crosses). As borehole radar receives information from all directions these features can be explained as a fracture cutting through the borehole; each feature representing the fracture on one side of the borehole.

The larger amplitude reflectors are plotted on the scale drawing of the existing and target tunnels (Figure 8.8). The separation between two largest reflectors from the left borehole is equal to the expected tunnel width. Therefore, these are expected to be reflection from the near and far side of the tunnel. From the right borehole there are two strong reflectors at 11 m depth. As these are still visible on the trace at such depth it is expected that they are the result of a large change in subsurface properties and interpreted to be the tunnel. Using these two sets of reflectors from the boreholes the tunnel can be positioned (shown in Figure 8.8). The location is slightly higher and to the east of the anticipated location.

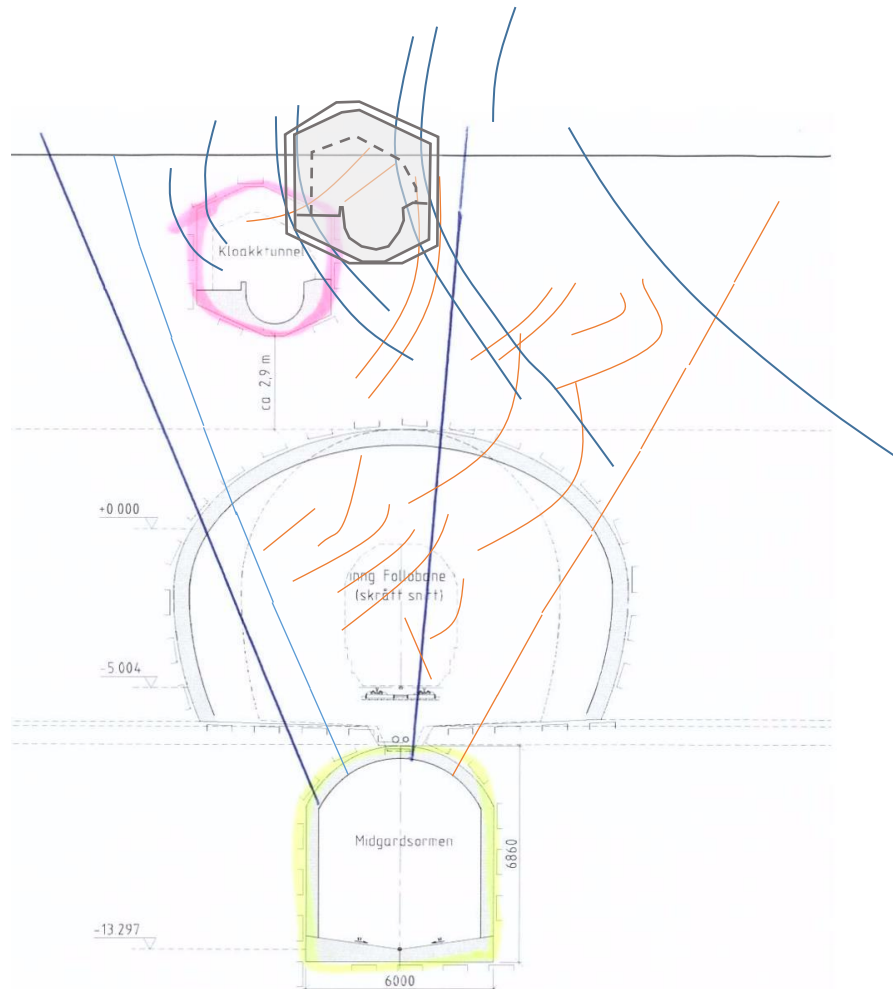


Figure 8.8. Strong amplitudes reflectors from the borehole radars overlaid on the tunnels profile. Blue reflectors are from the left borehole and red reflectors are from the right borehole. The anticipated tunnel location is drawn in brown.

8.3.3 Interpretation

To verify the interpretation of the signal, MATGPR R2 (Tzanis, 2006) was used to model the target tunnel using a ray-based approach (Figure 8.9). Geology velocity was set as per the hyperbola results at 0.135 m/ns and the air tunnel velocity was set at 0.3 m/ns. Frequency was set at the bore-hole radar frequency of 100 MHz. Split step 2D modelling was used.

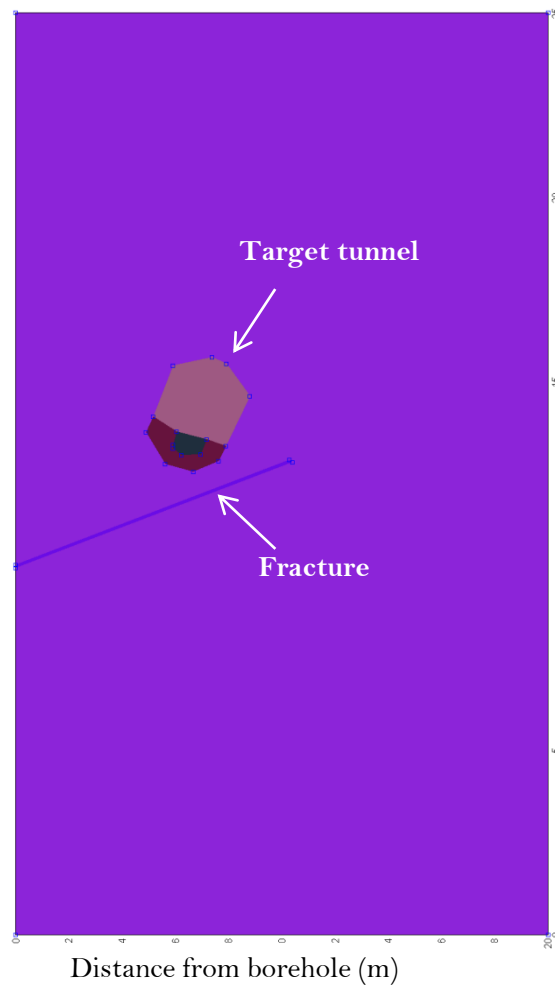


Figure 8.9. Modelled roof of tunnel with air fracture and air filled target tunnel in granite. The borehole is along the left axis. Y-axis shows distance along the borehole.

The modelling results are shown next to the recorded borehole results in Figure 8.10. The same features are seen on both sections; the linear signal of the fracture crossing the borehole and the reflection from the closest point of the tunnel. The features are noted at the same distance from the borehole, further verifying the interpretation of the tunnel on the GPR section. The reflection from the far side of the tunnel is however not as clearly apparent on the modelled results as on the recorded results. Although there are hyperbola

reflections at a similar depth, they are not as strong. This could be due to the loss of energy through reverberation within the tunnel that is shown on the modelled results.

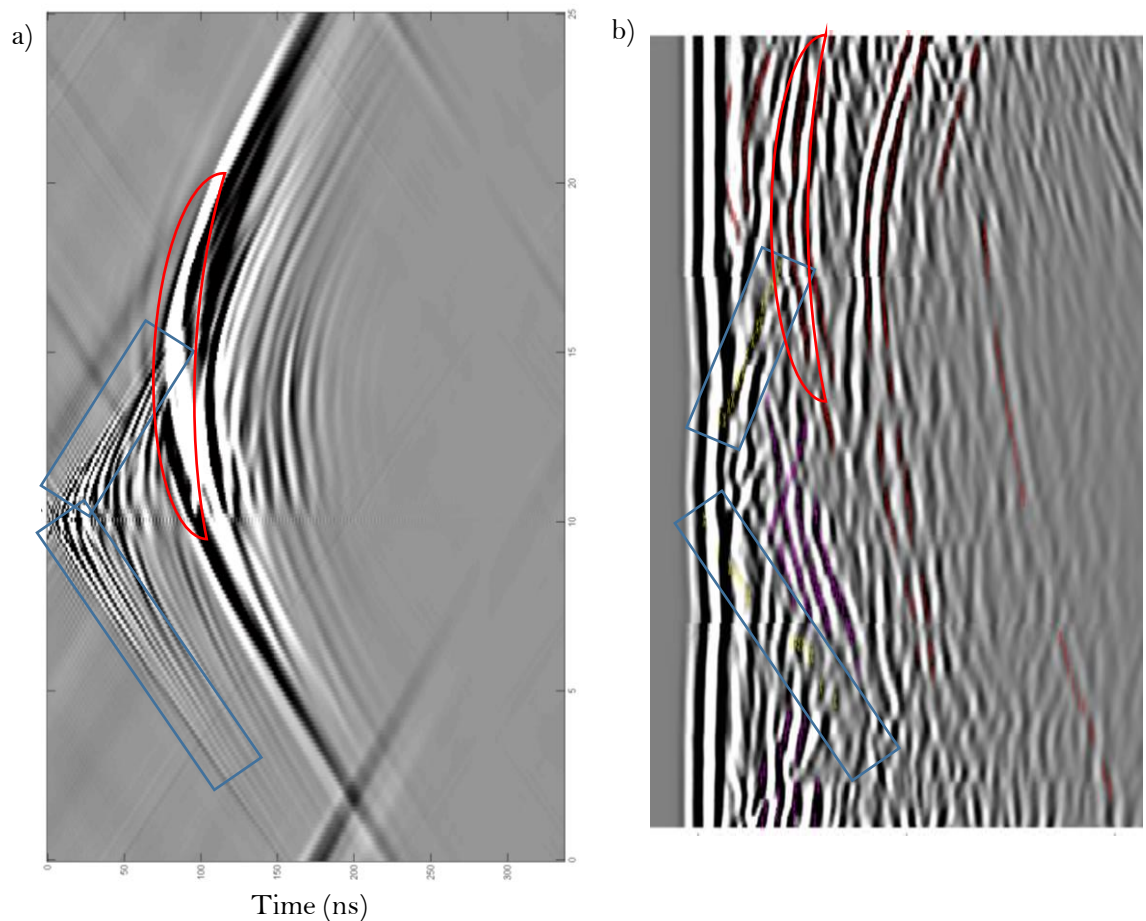


Figure 8.10. a) Modelling results from MATGPR R2 (Tzanis, 2006) for the tunnel and fracture shown in Figure 8.9. b) Recorded GPR results for the left borehole re-scaled to match the modelled results. Blue boxes highlight the signal from the fracture; red curves highlight the results from the tunnel. Y-axis shows distance along the borehole.

The similarities between the modelled and results sections help to verify the chosen location of the tunnel. It also confirms that it is the tunnel that was detected and consequently verifies the use of GPR on this environment (after the modelling choice).

8.4 West Wycombe Caves

Caves in West Wycombe were chosen for deeper testing of geophysical techniques. The caves are thought to be man-made mines of ancient origin. The caves were extended in the 1740s as chalk was excavated for use in the local area. It is thought that flint was mined from the caves to restore the Church and build a Mausoleum above the caves between 1748 and 1752. Famously, the caves were used by Sir Francis Dashwood's Brotherhood of St.

Francis of Wycombe (later known as The Hellfire Club) as a pagan meeting place during the 1740s and 1750s. After the disbandment of the Club in 1766 the caves were left unused until the 1940s when the caves were planned to be used as a large air raid shelter during World War 2, and were used as a tourist attraction. It remains an attraction today which posed access issues for the field work, overcome by accommodating staff. All historical information from the Hellfire Caves website and staff ("History Of The Caves," 2014).

8.4.1 Cave design

The design of the caves is elaborate (Figure 8.11) and thought to be inspired by either visits to the Ottoman Empire or based upon human anatomy. The tunnels are 1.5-2 m in height and extend for approximately $\frac{1}{4}$ mile with various sized caverns throughout. The Banqueting Hall is 12 m in diameter and height and is said to be one of the largest manmade chalk caverns in the world. The positioning of the cave with respect to the above structures is said to be of great importance with a long standing belief that certain parts of the caves lie beneath certain surface features. The Inner Temple is said to be directly below St. Leonard's Church and the Banqueting Hall beneath the Mausoleum (Figure 8.12) though no detailed mapping had been completed. Official West Wycombe literature (Hell Fire Caves, 2012) suggests the caves are 91 m below the surface, though no study has been completed on the site. Here, the positioning of the tunnels and caverns is investigated using surveying and geophysical techniques.

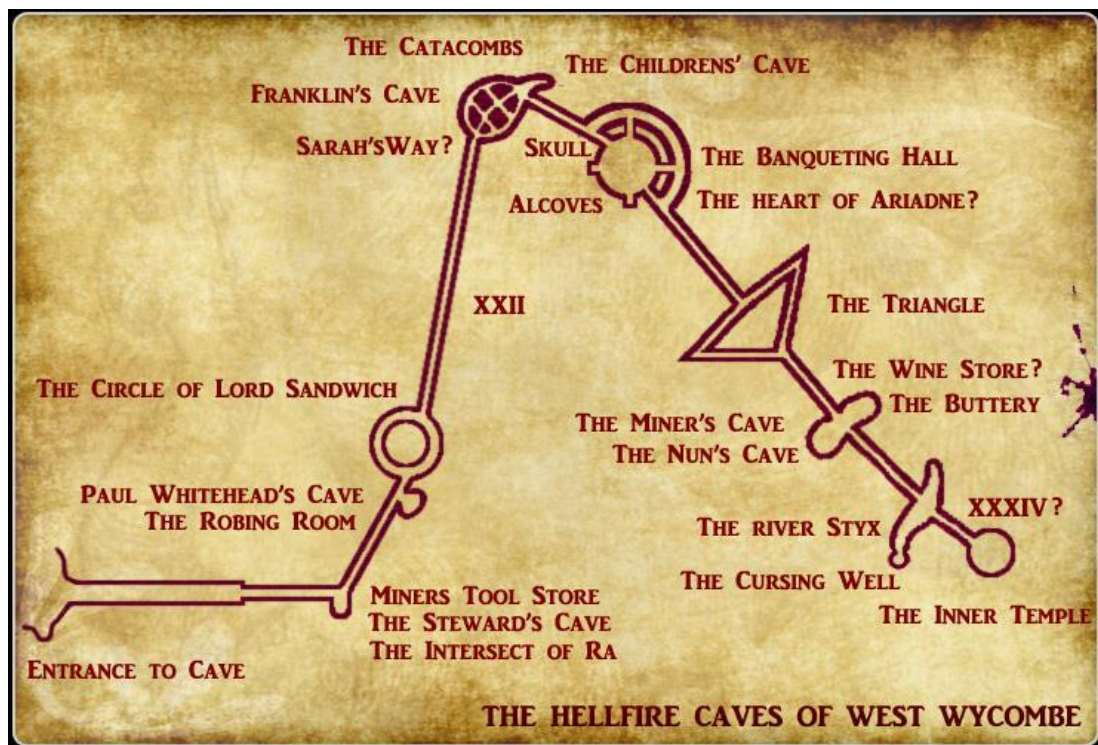


Figure 8.11. Currently accepted West Wycombe cave layout (not to scale). (Hell Fire Caves, 2012).



Figure 8.12. Satellite image of the West Wycombe Caves site (Google, 2011). Left inset is inside the tunnels, right inset shows the tunnel entrance.

In order to use the site as a test cavity it is important to ascertain the location of the caves with respect to the above landmarks and to clarify the cave depth. It is an interesting side-aim to challenge previously thought locations, especially as such relevance is held in the alignment of the subsurface and surface.

8.4.2 Land surveying

To assess the depth and position of the caves a land survey was completed using a Leica TC805 total station. The angle and distance between fifteen points within the cave were accurately measured. These measurements were converted into coordinates (Appendix G) and super-imposed on a satellite image of the area to show the surface expression of the cave (Figure 8.13). The general shape of the caves matches well with the existing map (Figure 8.11) but the established extent of the cave and the previously thought correspondence of above and below ground features are inaccurate. The inner temple is not underneath St. Leonard's church at the top of the hill, nor is the Banqueting Hall beneath the Mausoleum, contrary to the official literature.



Figure 8.13. Location of the caves beneath the surface (Google, 2011). White line indicates the cave route and the red dots are the Total Station survey locations.

The depth to the cave from the surface is calculated using the vertical angle and distance between the survey points. To calculate the depth from the surface the topography of the surface must be known. Three satellite digital elevation models (DEM) of the area were analysed and the average topography found (Appendix G). The first position of the Total Station survey was outside of the cave and could be calibrated with the DEM elevation. The depth from the first survey points were adjusted accordingly (Figure 8.14). The results show the cave descends 22.6 m from the entrance point. The deepest point is below the “The Triangle” area where the cave is 42.8 m below ground level. These results run contrary to official literature on the caves which suggest the caves are up to 91 m deep.

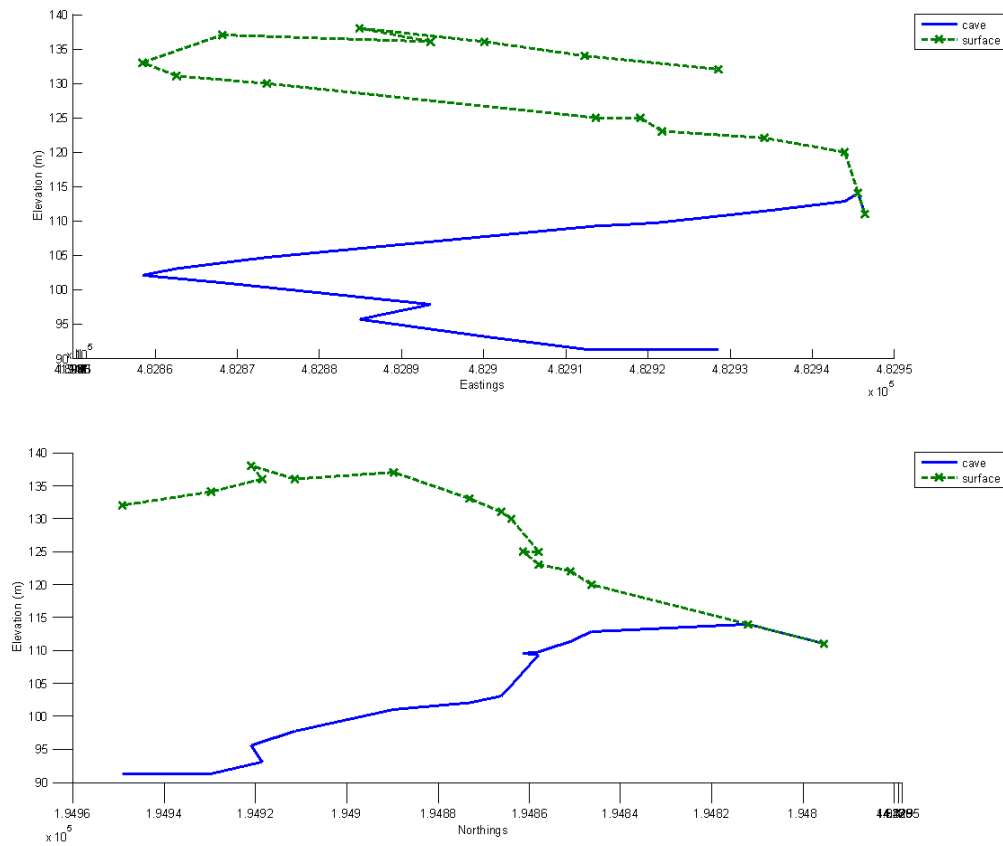


Figure 8.14. Elevation of the cave and the surface above the cave. Top: looking north, bottom: looking east.

This survey provided information to choose the best location for geophysical modelling and information for the geophysical modelling of the cave system. After a site reconnaissance, it was found that the shallowest point directly above the cave clear enough to be surveyed by geophysical techniques was between the “Stewards Cave” and “The Circle” (Figure 8.11). This straight part of the cave drops from 13.0 m to 21.5 m over this 25 m stretch. However, this depth is to the cave floor, and so the depth to the cave top is 2 m less this depth (the cave is almost uniform height throughout after the first section). The geological maps (Appendix G) show chalk outcropping across the hill with made ground on the Church site and so the cave was modelled in a chalk environment.

8.4.3 Cave geophysical modelling

The magnetic noise level was well constrained as on-site noise measurements had previously been measured on the site (0.007 nT) (see Section 4.4.2). The noise levels for other techniques were estimated from previous similar examples in the literature where available, else typical noise values were used (Table 5.1).

The modelled results show the effect of the descending cave with signal amplitude much larger above the shallow end of the cavity than the deeper end (Figure 8.15a-d). The higher detection probability on survey lines above the shallow end of the cave also reflects this.

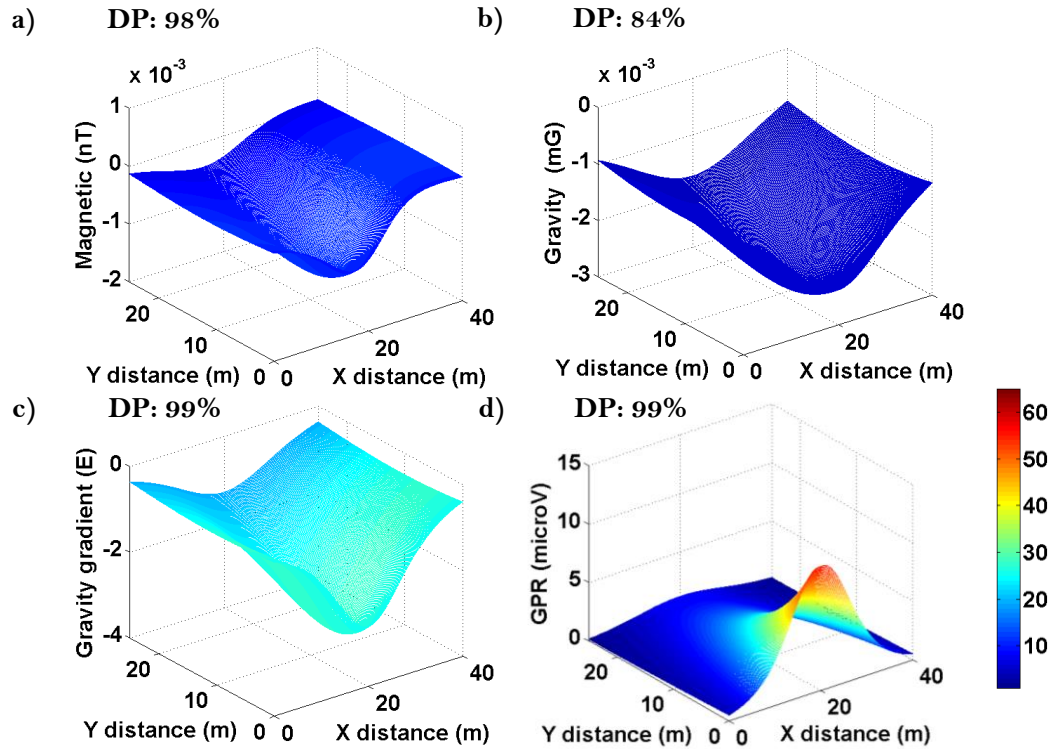


Figure 8.15. Modelled results above the descending cave (2-m height, 1-m width air gallery, descending 13.0 m to 21.5 m over this 25 m stretch in chalk) for four geophysical techniques: a) magnetic, b) gravity, c) gravity gradient, d) GPR. Colour scale indicates survey line detection probability (%). DP= overall detection probability.

The modelled results show that all the techniques have a high chance of detection at these noise levels across the 40 m by 25 m grid accessible on the site. At 1 m spacing magnetic, gravity gradient and GPR all have over 98% detection probability while gravity only has 84%. Rounding the top of the cavity to better represent the cave-shape (as in Figure 5.6) has only a small effect on the overall probability: 2% decrease for gravity and less than 1% for the other techniques.

The modelling parameters were adjusted as a sensitivity experiment to find the limitations of each technique. Parameters were adjusted until detection probability reduced to a threshold of 95%. Increasing the spacing to 2 m reduces the magnetic method detection probability below this threshold to 88%. Only increasing the noise level reduced the gravity method detection probability to below 95% threshold (71% at urban noise levels).

8.4.4 Field measurements

As the magnetic, gravity gradient and GPR methods were all applicable to the site, the technique choice becomes logistical. The magnetic method is chosen because it is faster and more portable than the other two techniques.

Magnetic data was collected every 0.1 s using a Geometrics 858 Caesium Vapour Magnetometer. As increasing the line spacing to 2 m reduces the magnetic detection probability below the 95% threshold, 1 m spacing was chosen. Parallel field lines were set up across the survey area with this 1 m spacing with waypoints every 5 m. The survey lines extended beyond the cavity by over two times the cavity depth to record the entire anomaly (at least 40 m where possible). A base station recorded diurnal changes every 20 minutes. By subtracting these values from the roaming magnetometer we can see the anomalous changes caused by the near subsurface.

Data was processed using MagMap2000 (Geometrics, 2010). The data was automatically despiked by the MagMap2000 programme and any residual spikes were manually removed. The data was then “destriped” in MagMap2000 to remove the herringbone effect of bidirectional data collection. The processed data is shown in location in Figure 8.16.

Diurnal data was smoothed with spline filters and removed from the measured results. A linear increase in total magnetic field up the hill was noted (Figure 8.16). This trend, assumed to be geological, was removed from all survey lines in order to highlight the smaller scale anomalies associated with the cavity. This resultant magnetic signal is shown in Figure 8.17.

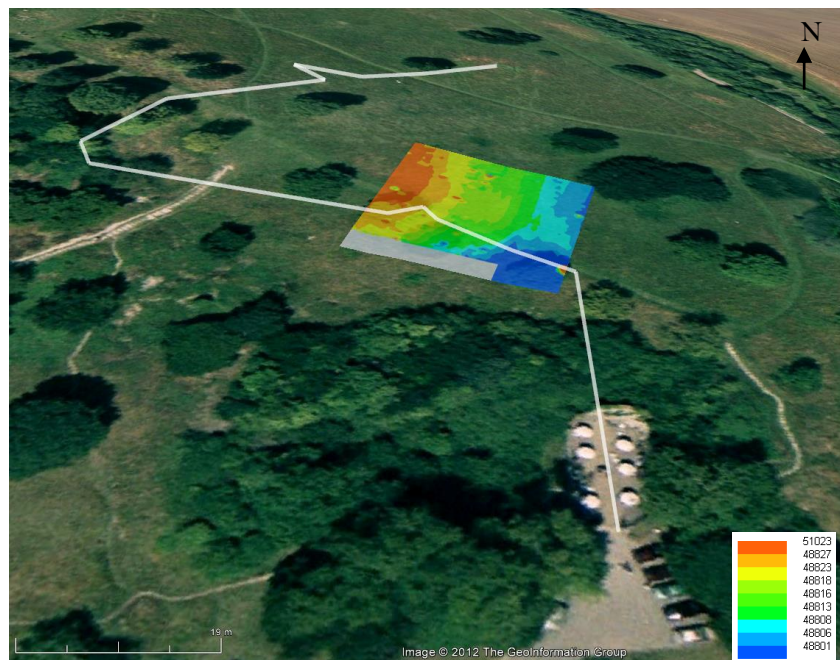


Figure 8.16. Total magnetic field measured over the cave. The inset shows the colour scale in nT. The measurements are positioned on a satellite and topographic image of the area with the white line representing the surface projection of the cave (Google, 2011).

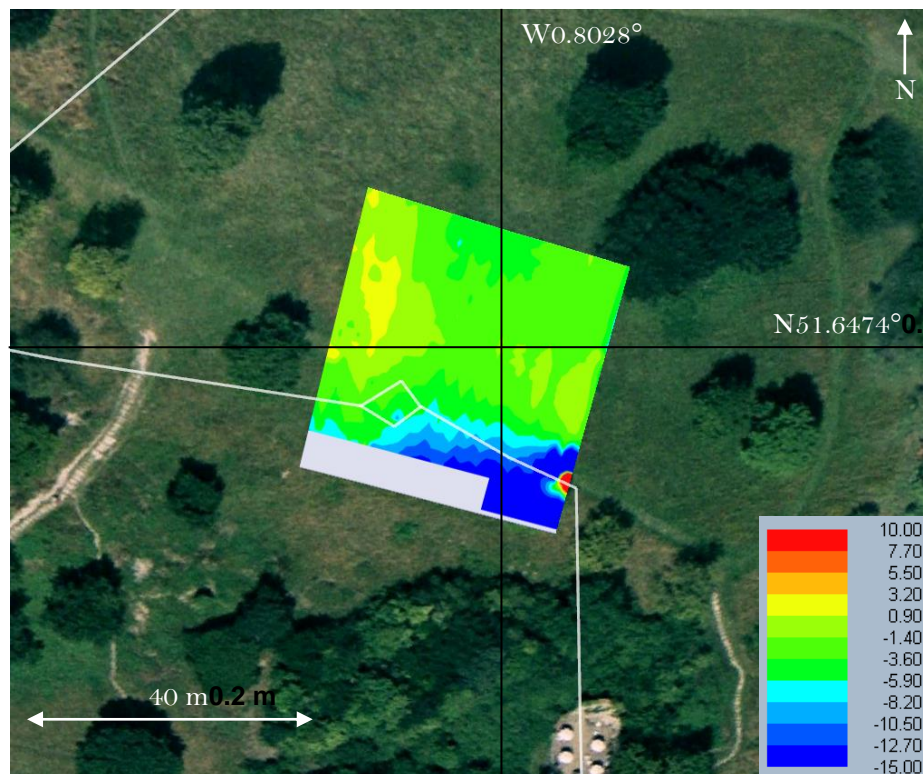


Figure 8.17. Magnetic field with diurnal change and linear uphill trend removed. The large magnetic high above the “Stewards gate” is still visible the red section to the east of the survey. The inset shows the colour scale in nT. The measurements are positioned on a satellite image of the area with the white line representing the surface projection of the cave (Google 2011).

With the linear trend removed, a clear and abrupt decrease in the magnetic field is noted running east-west across the survey area along the line of the cave. This decrease is most prominent over the cave in the eastern section of the survey. This is the shallower section of the cave. Over the deeper part of the cave in the west, the decrease exists but is more subtle. As expected, and shown in previous modelling results, a deeper cavity produces a smaller anomaly than a shallow cavity.

However, this noticeable decrease in the magnetic field over the cave is much larger than modelled (over 10 nT compared to 0.001 nT modelled). This disparity could be due to a number of factors. The depth of the cave was based upon three digital elevation models that showed large disparity in this region. Therefore, the cave could be shallower than modelled and explain the larger anomaly measured. The anomaly could have been exaggerated by the “halo effect”—the increase of subsurface cavity anomalies by the detection of the cracked and weakened area around the cavity. However, as shown in the previous chapter, the halo effect is unlikely to increase the cavity anomaly by so many orders of magnitude. There could be a number of fractures in the chalk around this area unrelated to the cave itself (and so not the cave’s halo). It was previously thought that this area was chosen for mining because of these fractures. These could explain an increase the anomaly measured in the area.

Also, the anomaly does not match the dipolar shape expected. It is most likely that the large decrease could be due to a change in geology and not the cavity itself. The orders of magnitude difference between the measured and modelled anomalies is too great for any true comparison. This highlights the importance of consideration of geological changes along the survey line and the consequent obscuration of the subtle cavity signal (see Discussion). For this reason it is often important to conduct more than one type of geophysical survey over a site.

Another interesting feature of the survey is the increase recorded above the cave at the very east of the survey (Figure 8.17). This is most likely caused by the large iron gating in “The Stewards Cave” (Figure 8.11). The anomaly has classic dipolar shape associated with a high susceptibility object beneath the surface (Figure 8.18). The amplitude of this anomaly is 4000 nT. Simple modelling of an iron object (with magnetic susceptibility of 720 SI) of the size of the gate would produce an anomaly of this size at 9 m depth. The estimated depth at this point is 11 m but this area had the biggest discrepancy in DEM height (Appendix G) and so the cave in fact be could be shallower at this position. There are also a number of other metal objects in “The Stewards Cave” which could have increased the signal.

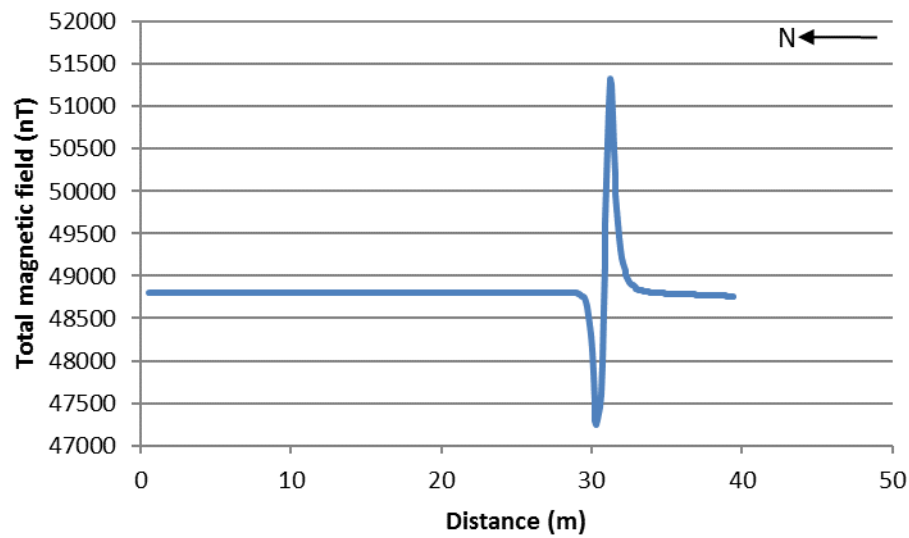


Figure 8.18. Most easterly magnetic survey line measurements. The large anomaly at 30 m is proposed to be metal inside the cave. The decrease in magnetic field over the cave is obscured by the scale used to show the larger anomaly.

8.5 Coatbridge, Scotland

A large playing field near Coatbridge, Scotland was due to be redeveloped as a school. Historical Ordnance Survey maps show the area has been mined in the past (Appendix G) and hence subsurface mine works are a hazard to be considered before construction begins. This hazard was shown when after a site investigation borehole was drilled the surrounding area subsided (Figure 8.19).



Figure 8.19. Collapsed borehole at site following an investigation borehole (photo courtesy of Ramboll, 2010).

8.5.1 Geology

The proposed site is on the Scottish Middle Coal Measures formation. This rock unit comprises of sandstone, siltstone and mudstone in repeated cycles, usually coarsening upwards. Coal seams in this formation are frequent and can exceed 0.3 m thickness (British Geological Survey, 2010c). The N.E.R.C. (2010) geological maps show the superficial deposit across most of the site is peat, with till to the North and East of the site, and glacial deposits in the South East (Figure 8.20). However, a more accurate picture of the near surface can be constructed from boreholes drilled on the site. The near surface geology is generally as follows: made ground of 0-6 m depth, then up to 6 m of peat, then 0-3 m of clay, and depth to bedrock ranging 10-16 m. (Figure 11.9, Figure 11.10 and Figure 11.11 show the depths of these strata across the school site (extrapolated from boreholes) and Table 11.7 and Table 11.8 show the borehole, trial-pit and hand-pit logs). Inferred coal seams and faults are mapped across the site (Figure 8.20) with further estimates of their positions by URS (Figure 11.12). The coal seams dip North to South and outcrop at the bedrock, where the mining is work is assumed. The faults are also of interest as they affect integrity and drainage on the site.

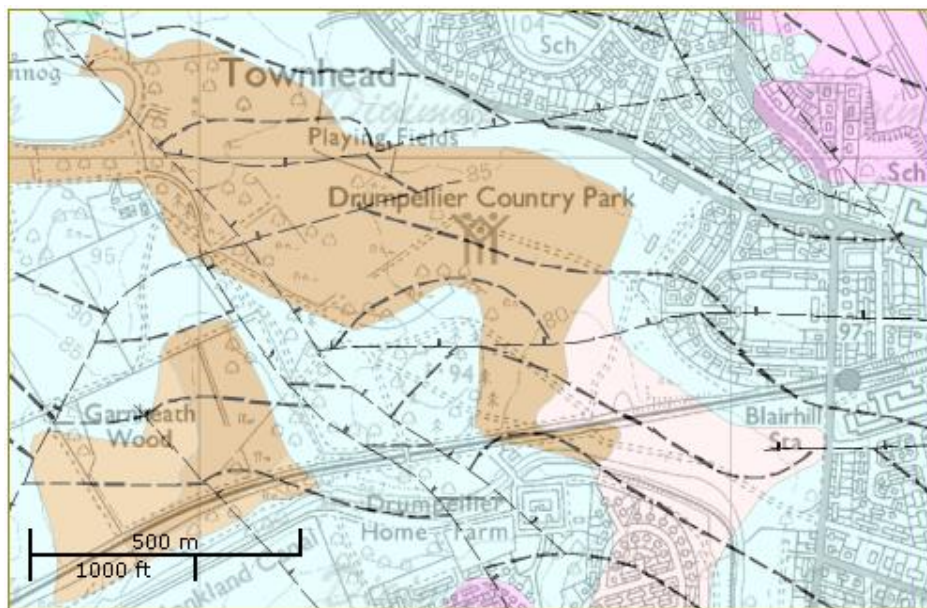


Figure 8.20. Geological map of survey area. The brown unit is a superficial deposit of peat of quaternary age. The blue unit is a superficial deposit of till (Devensian) of quaternary age. The light pink unit is a superficial deposit of Glaciolacustrine Deposits (Undifferentiated) (clay, silt and sand) of quaternary age. Dotted black lines are inferred coal seams, and dashed, dotted lines are inferred normal faults (N.E.R.C., 2010). A broader geological map can be seen in Figure 11.8.

8.5.2 Shaft modelling

The modelling software is used to decide upon the geophysical technique to utilise. The closest boreholes available show peat beyond the expected depth of shaft of 3 m and so geophysical parameters for a peat subsurface were set appropriately (**Table 4.1**). As the aim was to find mine shafts on the site, an air filled shaft was modelled as well as a capped and lined shaft as can be expected in this area.

Typical shaft dimensions were used, 2 m across, 3 m depth (expecting the shaft to have been covered) and 10 m tall in order to test the detectability of bell pits shaft on the site. Brownfield noise levels are used as the site is by a road and is cluttered with metallic and other materials. The magnetic, gravity and GPR results are shown in Figure 8.21.

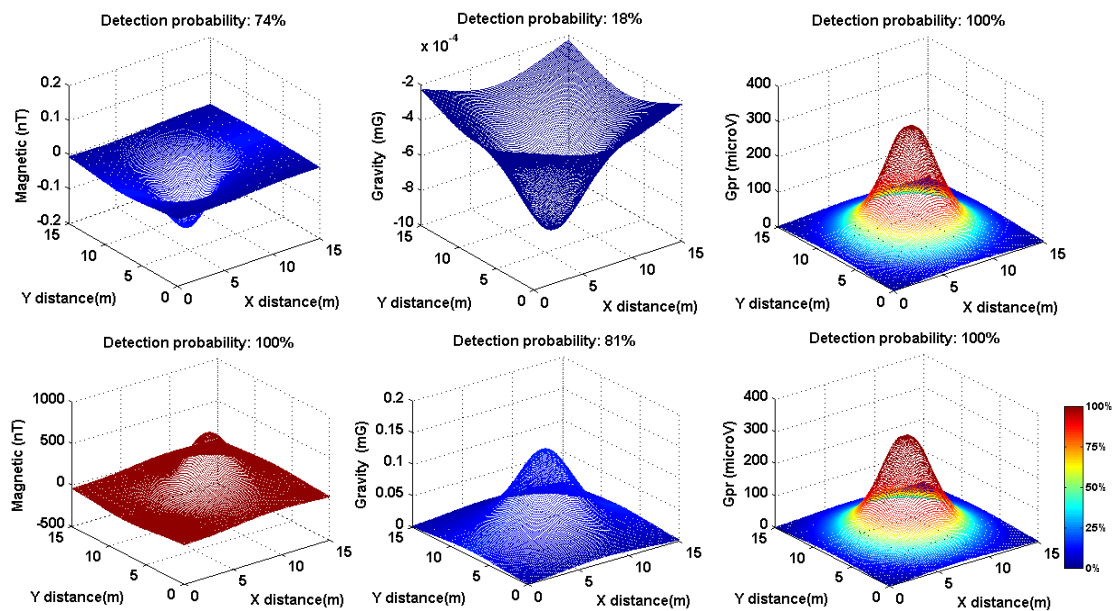


Figure 8.21. Modelled results over a 2-m square and 10-m tall air shaft at 3 m depth in peat. Left to right: magnetic, gravity and GPR techniques. Top row shows uncapped and lined, bottom shows a steel lined and capped shaft. Colour bar signals the detection probability on survey lines.

Magnetic and GPR both seem to be good choices to detect the air shaft on the site. The gravity method is inappropriate to detection on this site. Decreasing the profile spacing to 2 m reduces the magnetic detection probability to 49% and 3 m spacing reduces the detection probability to 38% and so profile spacing should be kept at 1 m where possible. GPR detection probability is above 99% for all of these spacings.

For the steel capped and lined shaft, the magnetic and GPR techniques have the highest detection probabilities, although gravity also has a high detection probability.

Based on these modelling results the magnetic and GPR techniques are best suited to the detection of either an air shaft or a lined shaft. It should be noted that should the near surface be clay, as is expected in some parts of the site, the GPR signal will suffer. Modelling

the same environment as above with clay instead of peat results in very low detection probability for the GPR method. If clay is noted on the site, the GPR method should not be used.

8.5.3 Geophysical survey

Following the modelling, a combined magnetic and GPR survey was used to find the mine shafts and potentially any faults across the site. Any information gained about the subsurface will also be analysed to demonstrate further integration into the current site investigation. Results will be used to corroborate and improve the planned site investigation.

8.5.4 Survey locations

The magnetic survey was used to cover the large site quickly, searching for anomalous regions and evidence of voiding. These anomalous areas were then explored in greater detail with GPR.

The location of the site and extent of the surveys over the site are shown in Figure 8.22. Survey positions were chosen based on a number of factors. A magnetic survey over area 1 was placed to cover most of the school site and was used as an exploration tool for areas of anomalous subsurface structure, which were then analysed in more detail with GPR (GPR survey area 2 was placed over one such anomalous region). The magnetic survey over area 1 was also chosen to cover the region of suspected faulting to the SE (Figure 8.20). GPR was run over area 3 because a borehole had encountered a void in this location (BH404 - **Table 11.7**).

By following the progression of historic O.S. Maps (Section 1.1), we can map mining activity through time to the current location. Magnetic surveys over areas 5 and 6 were located to find mine shafts inferred by these maps and by URS (Figure 11.12). While on site, a number of local people confirmed the previous existence of mining in these areas. When anomalous evidence of cavities was detected by magnetometry in sites 5 and 6, GPR surveys were conducted to verify, or disprove cavity existence and add detail to the subsurface picture.



Figure 8.22. Map showing site location (inset) and satellite image (Google Maps, 2010) showing the location of survey areas. Blue – magnetic survey, red – GPR, yellow – seismic (used in another project).

8.5.5 Field techniques

Data was collected by the author and a field assistant over 5 days in April, 2010. The data collected was used alongside the geological and historical maps, and information found through interviews with local people.

8.5.5.1 Ground penetrating radar survey

As mentioned, there is the potential for clay on the site which will cause attenuation of the radar signal. As the GPR is unshielded (a pulseEKKO PE-100A GPR (1000V) system was used) energy may reflect off surface objects and obscure subtle signals.

A rule of thumb (Milsom, 2003) states that for a resolution of 25% of the target depth, the product of depth and frequency should be 500; here, detecting to a depth of around 5 m (within the expected depth of the shaft) would require ~100 MHz antenna. A 100 MHz frequency antenna was used. As evidence of mining and cavities (shafts, collapses and fill)

will be shallower still, a 200 MHz was also used on some sites. It is the case that the antenna frequency is only the central frequency of the EM energy transmitted, and so 100 MHz antennas transmit frequencies from 50-150 MHz, increasing the chance of deeper penetration. 100 MHz antennas have detected cavities to depths of 13 m (Beres *et al.* (2001) and 14 m (Sellers & Chamberlain, 1998). With this antenna, in clay (the worst scenario), using (8.1), we can expect spatial resolution of 0.34-0.67 m (based on $\epsilon = 5-20$ for clay and shale (Milsom, 2003)) easily small enough for the expected mines and shafts which are expected to be greater than 2 m (Culshaw & Waltham, 1987).

$$f = 150/d\sqrt{\epsilon} \quad (8.1)$$

where f = frequency, d = spatial resolution, ϵ = dielectric constant (Milsom, 2003).

Step size was 0.25 m and antenna separation 1 m (recommended for 100 MHz as a minimum by the WIN_EKKO Pro PC Software) with 1, 2 or 3 m spacing between sample lines depending on the survey area (the modelling highlighted that the shaft should be detectable with all of these profile spacings). This will give a detailed picture of the subsurface and any voids and cover the sites in the given time constraints. GPR was used in the anomalous areas detected by the magnetic survey and areas of potential voids indicated by the boreholes and the desk study (Figure 8.22).

The topography of site was flat enough to consider variation negligible. Any surface objects were removed if possible, and permanent features were noted. The continuous reflection mode was used in successive 2D profiles. 32 stacks were recorded to maximise the signal to noise ratio. The time window was set at each site dependant on the depth of penetration required and to include all useful signal. After each profile, data was checked for excessive noise or interesting features, and repeat profiles were completed if necessary. Antennas were placed perpendicular to the strike of any cavity features for the highest resolution possible (Conyers, 2004). Gain was adjusted in the field to counter attenuation and enhance deeper reflections. All other variables were as suggested by the WIN_EKKO software.

Processing was completed using EKKO_View Deluxe (Sensors Software Inc., 2010). Bad traces were removed, and a low pass filter removed noise spikes. A high pass filter (DEWOW filter) removed noise from the induction of the ground and the limitations of instrument frequency response (due to the proximity of transmitter and receiver) (Sensors Software Inc., 2003). Various other filters (time and spatial) and gains (Average Gain Control and Exponential Compensation Gain) were tested on individual profiles to enhance features from depth lost through attenuation (based on suggestions by various authors: Mochales *et al.*, 2007a; El-Qady *et al.*, 2005; Gizzi *et al.*, 2010; Roberts *et al.*, 2009). The gain processes can result in excessive noise so a balance must be struck. Depth profiles were

constructed with velocities ascertained using the hyperbola calibration tool in EKKO_View. Velocities ranged from 0.04 - 0.104 m/ns dependant on site; typical of clay, silt, shale and wet sands (Milsom, 2003). This area, based on the site investigation and desk study, it is most likely clay, and so these results are typical.

8.5.5.2 Magnetic survey

The magnitude of the total magnetic field was measured by a magnetometer. Differences in susceptibility and remnant magnetism of the subsurface will result in anomalous results at the surface. The area of study is large (~500 m by 500 m), so a broad magnetic survey to find anomalous areas was to be carried out.

Finding the presence of brick or metal lined shafts is easier than wooden lined shafts that were popular in Scotland (Maxwell, 1976). However, an old mine may contain magnetic material (scrap iron, masonry). To achieve dense coverage needed to identify cavity anomalies 1 m spacing between survey lines was used on the areas with suspected shafts (as suggested by the modelling), and 2 m or 3 m spacing across the rest of the site. The presence of buildings and other surface objects may affect the signal and were noted.

Magnetic data was collected continuously using a Geometrics 858 Caesium Vapour Magnetometer. Parallel field lines were set up across the survey areas with waypoints at regular intervals. The survey lines extended beyond points of interest by at least two times the depth of the target in order to record the entire dipolar anomaly (in this case at least 20 m if possible, though roads and woods limited this). The survey lines were placed perpendicular to the strike of any suspected linear features so their entire cross sectional anomaly was recorded for use in depth estimations.

Any surface items seen on the survey that could contain magnetic materials were removed (permanent features were noted). Any sources of magnetic noise were removed from the operator and the sensor was held away from the operator by a non-magnetic pole.

A base station was set up to record diurnal changes (Geomatrics 856 Proton Precision Magnetometer). Recordings were taken every 3 minutes whilst the survey was being conducted. By subtracting these values from the roaming magnetometer we can see the anomalous changes in the reading caused by the near subsurface.

Data was processed using MagMap2000 (Geomatrics, 2010). Diurnal data was smoothed with spline filters. The data was automatically despiked by the programme and any residual spikes were manually removed.

Disruptions in the data came from the presence of cultural noise, buildings, goal posts, fences and cars, but all were noted in the field. The fact that the site is brownfield meant that there was numerous unseen ferrous objects in the near subsurface.

8.5.6 Results and interpretation

8.5.6.1 Area 1

Magnetic noise was problematic in area 1. The surface path is clearly defined on the results (Figure 8.23) but disguises any possible anomalies beneath. The path follows an old railway line (**Figure 11.16**) explaining the positive magnetic anomaly. North of the path is magnetically noisy. This is the area of an old landfill (local knowledge and O.S. Maps) so there is high chance of near surface ferromagnetic material, disguising any relevant features. The field is dotted with goal posts (Figure 8.23), causing huge magnetic anomalies for meters around them – preventing the detection of any subtler features in the vicinity.

When searching for air cavities in the Northern hemisphere we tend to see a dipole anomaly with the low in the south (Section 2.8.3.2). Examples such as this detected in area 1 are highlighted in Figure 8.23. These examples were further investigated with a GPR survey, unfortunately, the GPR surveys taken in this area (GPR 2 and 3 (Figure 8.22), profiles in Appendix G) had very limited penetration because of clay presence – only to around 3 m with no evidence of cavities. Time restricted further surveys over the area.

Linearity in anomalies across survey lines was noted to the east of the area (Figure 8.23). This is indicative of the strike of a magnetic material. These are likely to be the magnetic signature of faults and coal outcrops. Their positions match well with the faults and outcrops noted in the site investigation (Figure 11.12) and on geological maps (Figure 8.20). Of the three linear anomalies, the northern and southern anomalies have predominately negative peaks, and the centre anomaly a positive peak. A negative linear anomaly can be associated with the downthrown side of the fault (Reynolds, 1997); this would indicate the southern anomaly is downthrown to the north and the other two to the south. As coal has a low magnetic susceptibility, an outcrop is more likely associated with the northern and southern anomalies. The location of the southern anomaly is in the correct position to match the extension of the Pyotshaw and Main outcrop (Figure 11.12). It looks likely that the two most northerly anomalies are indicative of faults and the southern anomaly represents the Pyotshaw and Main coal outcrop. This information has been of great use to the site engineers, allowing them to more accurately map these features.

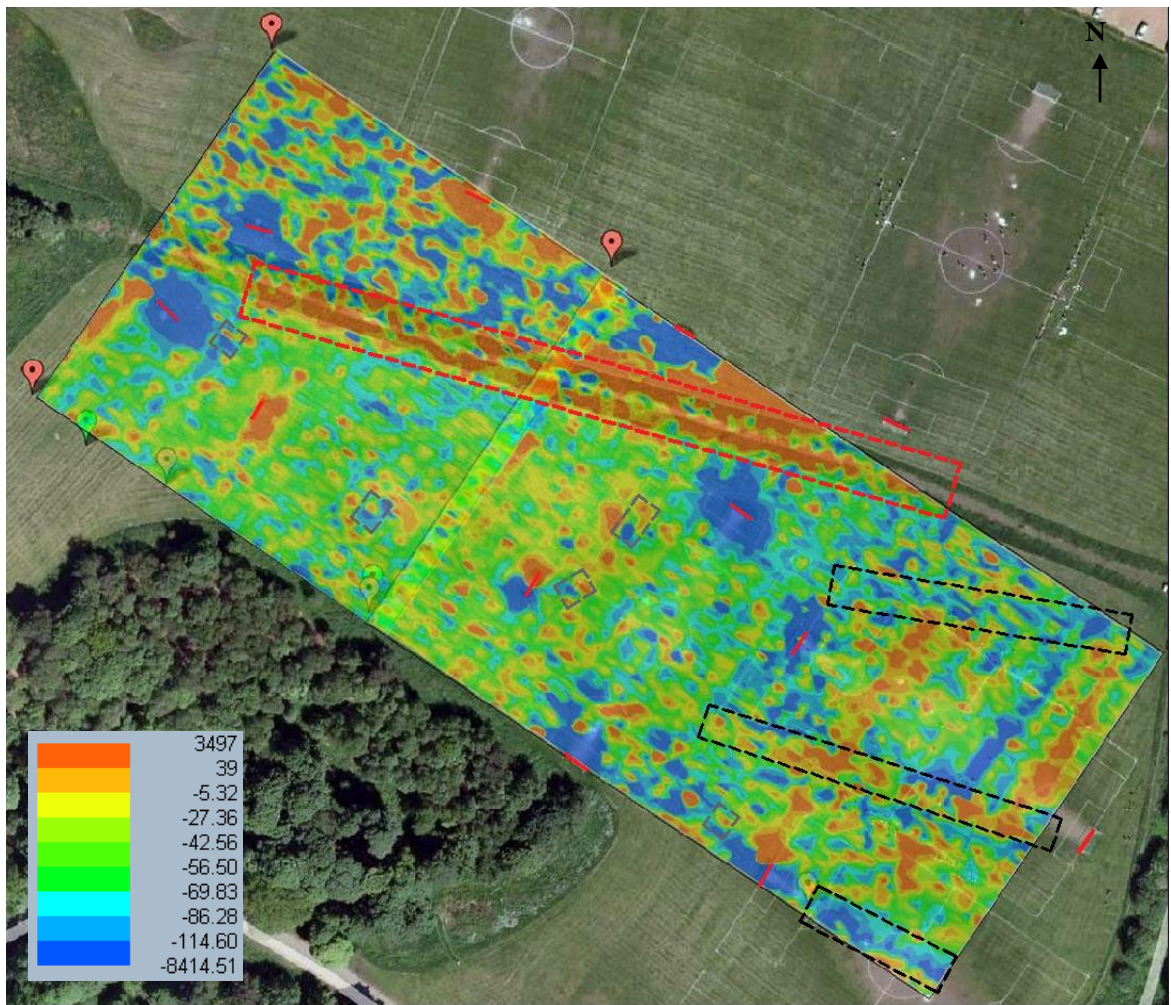


Figure 8.23. Satellite image (Google Maps, 2010) with magnetic results (diurnally corrected, in nT). Red line – goalposts, red dotted rectangle – path, black dotted rectangles – linear anomalies, grey dotted rectangles – dipole anomalies indicative of voids.

8.5.6.2 Area 6

A magnetic survey was conducted here to find evidence of the old mine shaft noted on the historic maps (Figure 11.16). The survey revealed a strong negative anomaly running 20 m from, and parallel to, the road (Figure 8.24). The negative anomaly has amplitude of 130 nT, much larger than any of the negative anomalies found for air cavities in the literature (see Section 2.8.3.2). It is therefore likely that this is the negative nadir of a dipolar pairing with a stronger positive peak to the south.

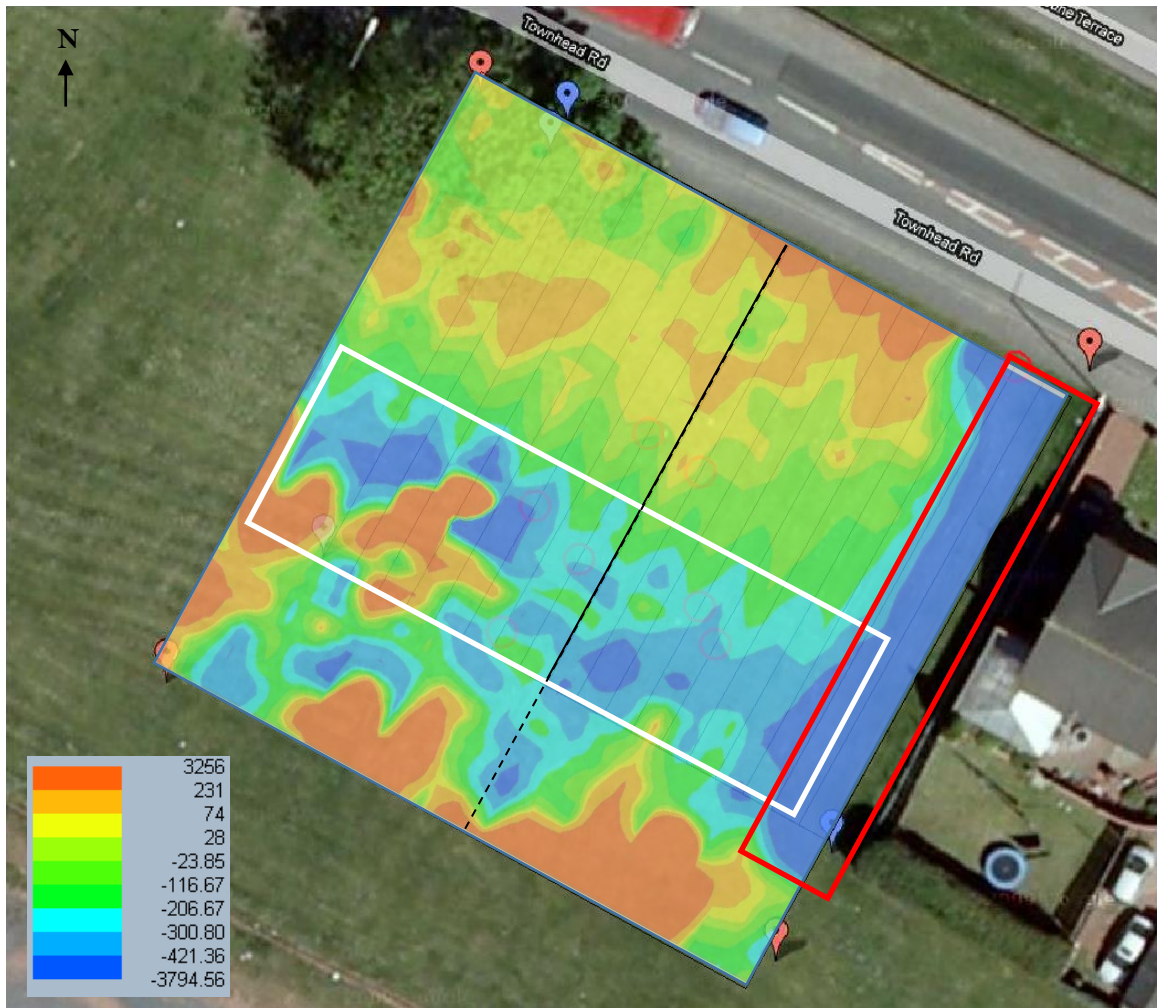


Figure 8.24. Satellite image (Google Maps, 2010) with magnetic results (diurnally corrected in nT). Red rectangle – anomaly from metal fence, white rectangle – linear negative anomaly, black lines – GPR survey lines (strong black line - survey shown in Figure 8.25, red circles – GPR evidence of voids. Note the herringboning on the anomaly caused by the offset of bi-directional field procedure.

To investigate further, a GPR survey was conducted over the area (example profiles in Appendix G). Reverberation patterns, indicative of cavities (Section 2.8.1.3.3), are represented by a series of high amplitude arrivals on numerous profiles, starting at around 2 m depth (an example profile is shown in Figure 8.25). To estimate the size of the void from the profiles we can take two approaches. Firstly, we can measure the lateral distance the void creates a disturbance on the profile as an estimate for the width of the void. In the example profile (Figure 8.25) this width would be approximately 3 m for the larger reverberation pattern. The second technique is to take a more theoretical approach. If the wave is reverberating within the void, the void must be bigger than the wavelength of an EM wave in air. Using $v=f\lambda$, for a 100 MHz antenna, we can calculate that wavelength as 3 m. Therefore, the void must be at least this in diameter. It should again be noted here that

the antenna will produce other frequencies (between 50-150 MHz) that would affect the calculation. Because the reverberation patterns obscure any reflections from the base of the cavity, direct height estimations are not possible. However, for reverberation to occur, Kofman *et al.* (2006) suggest the height of the void must not be significantly smaller than the cavity horizontal dimension, so here, little under 3 m.

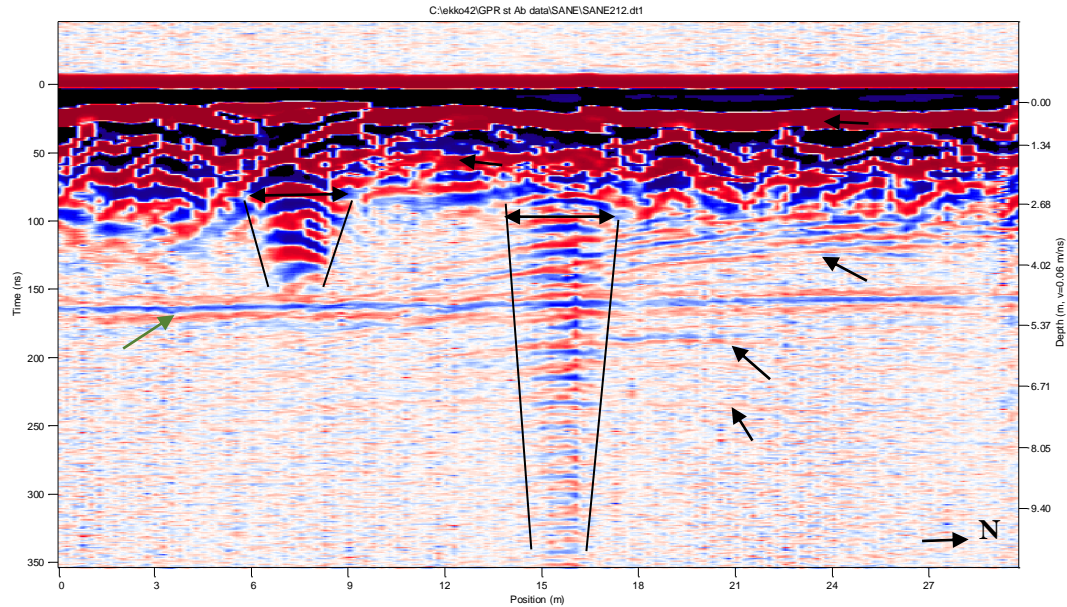


Figure 8.25. GPR section of line shown in Figure 8.24. Black lines indicate the reverberation. Black arrows point out significant strata. The double ended black arrow indicates the estimate of void width. The brown arrow indicates the reflection from the house. The first, strong arrival is the direct air wave.

The red circles on Figure 8.24 indicate the lateral positions of the reverberation patterns seen on the GPR sections. Many of these corroborate the position of possible voiding indicated by the linear magnetic anomaly. This supportive evidence strengthens a theory of voiding, probably associated with the mining activity in the area. If time had permitted, a useful profile would have been along the suspected line of voiding to map the change in depth of the structure.

The GPR also shows evidence of the soil layer and geological strata beneath. A strong horizontal reflection is seen on most of the profiles (at 5 m depth in Figure 8.25), appearing to be a geological layer. However, further analysis of the arrival time reveals that the arrival is most likely an airwave reflection from the house to the east of the survey. With knowledge of GPR speed in air (0.3 m/ns), and the time of arrival, the surface distance can be deduced, which then corresponded to distance to the house. A lack of boreholes in the area means the upper strata cannot be interpreted. The majority of the interpretable signal

is lost at 5 m depth due to probably clay– again a borehole would make this clear. We can use this information to map the depth of the clay (the depth at which the signal is lost) but this is not of interest to this study.

8.5.6.3 Area 5

A magnetic survey was taken over an area of suspected mining activity. As with area 6, a fence caused a large anomaly, here, to the south of the survey (

Figure 8.26). There is also an area with a strong positive magnetic signal. As discussed, we would expect a dipolar profile for a void. This positive anomaly could be due to strongly magnetic material in the subsurface. This could be a number of things, but as it covers a large area is of interest for investigation. In terms of mining, this anomaly could be due to any remnants of foundations (though typically wood lined shafts were used in Scotland), old mining equipment, or the fill of a shaft with relatively magnetic material. The anomaly was quite large, over 800 nT, but anomalies of this size have been noted in the literature (850 nT - Pueyo-Anchuela *et al.*, 2010; 650 nT - Mochales, *et al.*, 2007b).

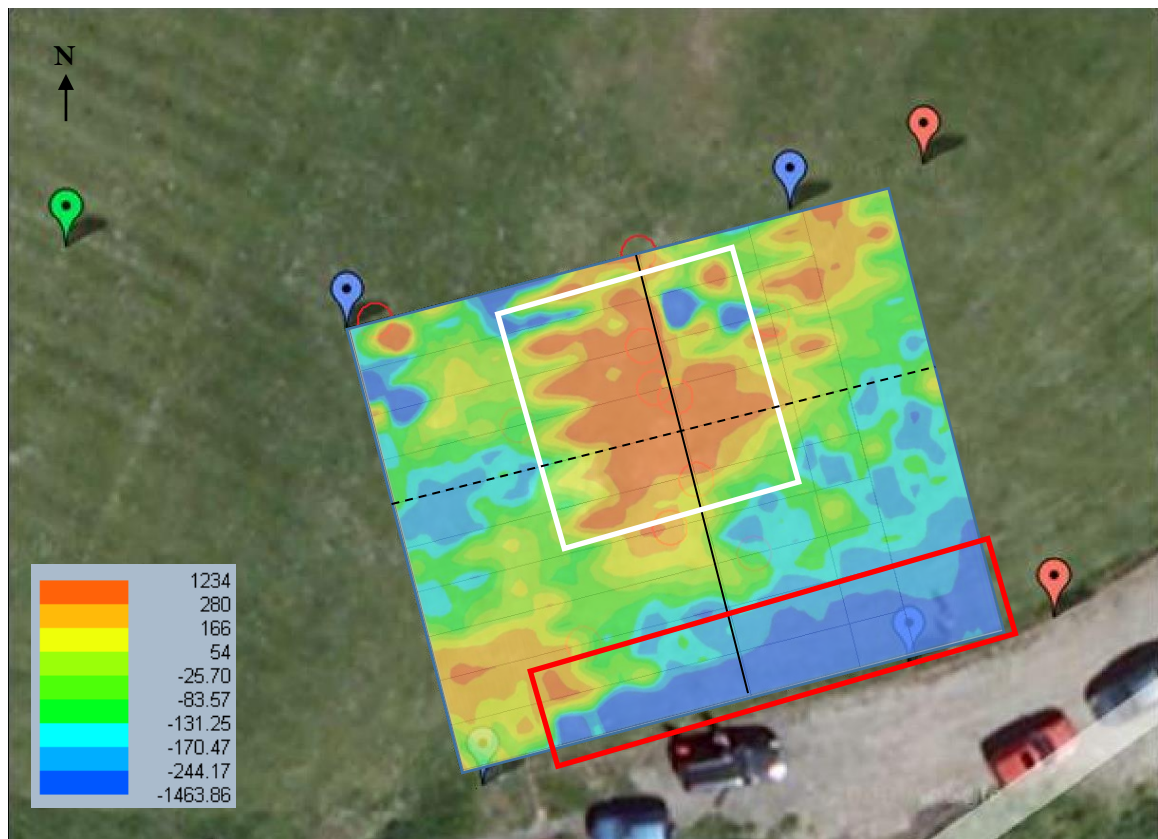


Figure 8.26. Satellite image (Google Maps, 2010) with magnetic results (diurnally corrected in nT). Strong black line - survey shown in Figure 8.27. See Figure 8.24 for further labels.

The anomaly was of enough interest to conduct a GPR survey across the area (profiles in Appendix G). The survey again showed evidence of reverberations (Figure 8.27),

indicative of voids. The depth of the reverberations are around 2 m. Estimating the width of the void by measuring the lateral disturbance of strata seen on the profiles gives a width of 2 m. The incidents of reverberation were again mapped over the magnetic survey contours and correlated well with the magnetic anomaly (Figure 8.26). This corroboration strengthens an interpretation of an anomalous subsurface region here; either mining activity or filled cavities. The GPR also showed numerous geological strata of the area. A strong reflector, probably a dipping bed, can be seen of most sections (dipping from the NE corner to the SW) at depth of around 5 m. Again a borehole in the area will verify the bed, and the possible presence of voids.

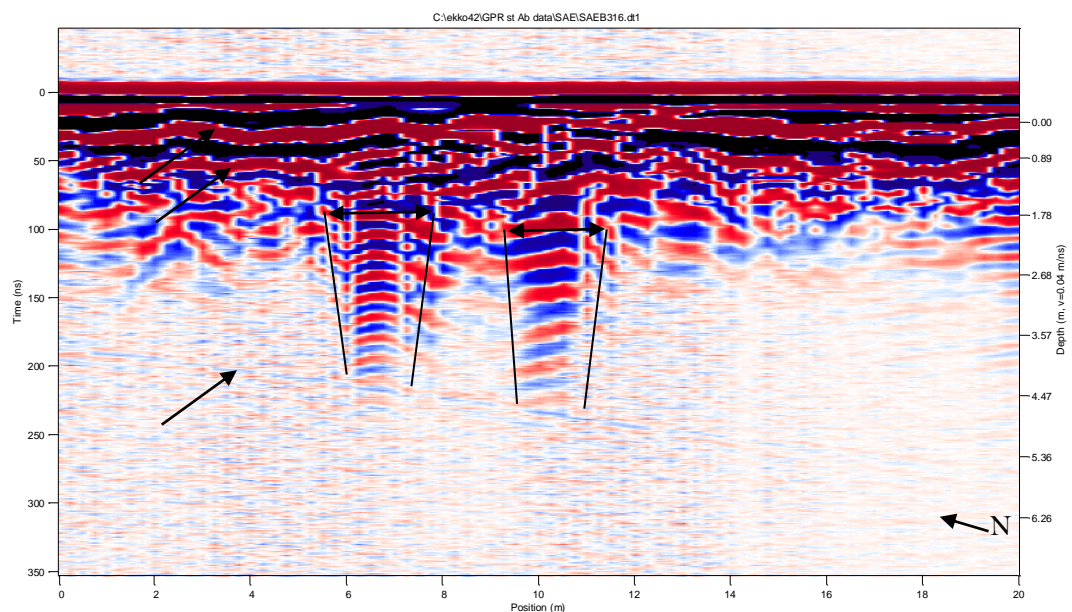


Figure 8.27. GPR section of profile shown in Figure 8.26. Black lines indicate the reverberation. Black arrows point out significant strata. The double ended black arrow indicates the estimate of void width. The first, strong arrival is the direct air wave.

8.5.7 Discussion

Though the surveys were limited by a magnetically noisy environment and attenuation of signal some interesting features were recorded and interpreted. The linear magnetic features in the SE area of the site closely match estimated fault and outcrop locations. This detail, though not the primary target, shows the potential benefits of a site-wide geophysical survey. With this information, features can be more accurately mapped, and used in engineering assessment.

The modelling implied that the suspected voids found with the surveys were not pure cavities (air or water filled cavities), but that the strong anomalies were indicative of mining activity, an old mine yard or a filled shaft. Another possibility is that the magnetic anomalies

are associated with iron within or above the air filled cavities. It is possible that more cavities are present across the site which are too deep to be detected by the GPR. Also, cavities of less than 0.6 m are not easily detected by 100 MHz antenna (Kofman *et al.*, 2006). It is however clear that both areas 3 and 6 show features incongruent with the surrounding subsurface and are therefore worthy of investigation.

That clear evidence of air or water filled cavities was not found, does not mean the process was unsuccessful. Firstly, there is no evidence that there are any voids in the areas investigated, so a lack of detection could be the correct interpretation. All previous studies in the literature knew the precise location of cavities, or created them, prior to any surveys. In this respect, the challenge of cavity detection in this study is vastly more difficult. Secondly, as a study of a procedure to cover a large site with complementary techniques, it was successful. Magnetometry indicated areas of potential voiding and the larger scale geological features. GPR confirmed the areas of potential voiding, allowed depth estimates and imaging the near surface geology. Much can be learned from the process. Magnetometry over the landfill was unusable and should be avoided as a technique in these areas. Potentially, high frequency filters could reduce some of the noise from near surface ferromagnetic materials and reveal large scale trends, but the noise will still obscure the subtle evidence of cavities. The magnetometry located numerous areas of potential voiding that went uninvestigated because of time restrictions. The survey was also not of use near fences, buildings, goalposts and old railway tracks; a walkover the site, if possible, before choosing technique is highly recommended. The GPR corroborated the magnetic results and added new information. However, attenuation was a major problem, only allowing the very near surface to be imaged in some areas.

8.6 Chapter summary

This Chapter aims to apply the modelling software outlined in this Thesis to geophysical technique choice on four real-world sites with potential cavities. The main interest is the evaluation of the benefits and limitations of the modelling and the techniques that were subsequently chosen.

The primary uses of the modelling software are detection feasibility analysis and choice of technique. In these aims the software was successful on at least three of the four sites. The modelling showed that cavity detection was possible in the estimated noise level on all sites, and indeed cavities were detected on three of the four sites. On the West Wycombe cave site the geological signal obscured any signal from the cavity although features within the cavity (the Stewards Gate) were detected. In choice technique, the modelling suggested radar on three occasions and magnetic on two. As the cavities were detected, these were concluded to

be the correct technique choices. That is not to say that other techniques would not have detected the subsurface cavities, but only that the software chose an appropriate technique in the majority of cases.

Naturally, the simplistic nature of the modelling compared to the complexity of the subsurface meant that there were some limitations to the modelling technique. Although the modelling improved technique choice, and in most cases survey parameter options (such as profile spacing and antenna frequency), the results of the field measurements did not always align with the modelled results. However, on sites where cavity depth and dimensions were fairly accurately known (Middlesex Hospital, and to a lesser extent the Oslo tunnel) the modelling did produce signal amplitudes roughly similar to the measured signal. A major source of error leading to this disparity was unknown subsurface geophysical parameters. On the sites where the cavity conditions were less well known (Coatbridge) it could not be expected that the predictive model would match the measured signal.

If treated as intended, a tool to test the feasibility of using geophysics and an aid in technique and technique parameter choice, these field examples proved the approach successful. Further testing is important on a wider variety of sites to test the approach further. It is also important to test more techniques on these sites to verify that the best technique has been chosen by the modelling.

It would have been useful to use all the techniques at all the sites in order to test whether the best technique was chosen. However, most of the sites were working geotechnical sites and so time was at a premium. Future work should attempt to find test sites to fully test all techniques with the modelling software.

Chapter 9

9 Summary and Conclusions

This Thesis has aimed to highlight the importance of modelling before undertaking a geophysical cavity detection survey and to introduce cavity detection feasibility analysis modelling software. There is very little evidence in the literature of a concerted effort prior to survey of assessing the feasibility of the techniques used for cavity detection and no quantified approach to technique comparison. The main geophysical techniques are all applicable to cavity detection in the right circumstance, and so should all be considered as an option. The presented work, allows quantifiable comparison between techniques through the calculation of detection probability. Survey parameters are often considered, but usually through rules of thumb or past experience. However, every site is different and so these approaches will not always be appropriate and are inhibiting for new practitioners. The approach outlined here, modelling the detection probability based on survey parameters, will aid practitioners to find optimum site-dependent survey parameters. It is therefore suggested that the techniques presented here represent a great improvement on the current approach of technique choice and survey design.

Alongside the creation of the software, a number of interesting results have been found, often against conventional thought in the literature. The incorporation of the cavity halo into the modelling of cavities is a fresh approach that will force practitioners to reassess their technique choice and also their current approaches to interpretive modelling.

In this Chapter, the main findings will be summarised and shown to meet the objectives set out in the Introduction. A critique of the methodology will be presented alongside an analysis of the limitations of the final software. Finally, possibilities for extension of this work into new research will be presented.

9.1 Review of objectives and findings

9.1.1 Objective 1

“Understand cavity processes and the likely subsurface conditions related to cavities. Review current approaches to cavity detection, including geophysical approaches, assessing their benefits and limitations”

Chapter 1 achieved this objective through a Literature Review outlining the current understanding of cavities and cavity detection. Through this review, the importance of cavity detection was highlighted and in doing so presented the reasoning for the need for the cavity modelling presented. The need for cavity detection will only become a more pressing concern as time goes by because space restrictions will force the construction sector to build upon land previously unconsidered. Brownfield sites and karstic environments will be built on, and the delineation of cavities will be of paramount importance. The Literature Review was vital to the modelling in ensuring that typical cavity conditions were used.

The second key area of review was the debate around current cavity detection techniques and their limitations. The current borehole approach is seen to be useful in certain uncommon situations where the subsurface conditions are well known but for most sites, where little is known about the cavity structure, the technique is slow expensive and produces an incomplete picture of the subsurface. It is therefore concluded that geophysics should be incorporated into the site investigation, working before or in tandem with intrusive methods.

Through discussion with engineers and field geophysicists, it is understood that geophysics has an uncertain reputation in the geotechnical engineering industry. This is due to assertions that a certain technique will detect cavities followed by failure in the field. It is hoped that the modelling approach here will not only improve technique choice (and so the success rate of cavity detection surveys), but the software will improve engineers understanding of the key drivers in survey success.

An important element of achieving objective 1 was understanding the current geophysical approaches to cavity detection. There is much work in cavity detection in the literature, but mostly of single case studies. This is very useful in understanding the popular techniques and this helped inform which techniques should be used in the modelling. However, there is little work, especially quantitative work, on technique choice or survey design. These were seen as limitations in the research base and hence this project aimed to produce software that allowed users to quantify the likelihood of survey success and optimise survey design. No such technique comparison software is available and it is thought that this would be a useful tool in both the geophysical and engineering industry.

In fulfilling objective 1 a better understanding of the current problem was gained and the insufficiencies in the current approach highlighted. The details of cavity review and the current geophysical modelling also informed the modelling choices made in the future Chapters.

9.1.2 Objective 2

“Develop modelling software that can simulate geophysical signal over cavities”

Chapter 3 outlines the methodological framework by which this objective is met. The detailed work lies within Chapters 4 and 5. Current modelling techniques are outlined and the chosen techniques discussed including the reasoning behind the choice (usually for practical purposes such the ability to model the typical cavity shapes identified in the Literature Review). The signal response of the gravity, gravity gradient, magnetic, magnetic gradient and GPR methods can be modelled over a range of typical cavity shapes. The modelled signal is from the surface above a 3D subsurface model of the cavity. It is possible to alter the subsurface geology, cavity shape, makeup, lining, depth, and size to meet specific site requirements.

Thereafter, the incorporation of the modelling technique into MATLAB is presented. This is an important element of the work as one of the aims of the software was to be as user friendly as possible so the geophysical and engineering community will be able to utilise the tool. A graphical user interface to the software was designed to fit this purpose and the notes in this Chapter act as a guide for any potential users highlighting the key parameters.

It is noted that despite little discourse in the literature, noise level on a site is of paramount importance to the likelihood of a successful geophysical survey and to survey planning. Here, it is at the centre of the modelling approach. Field noise measurements at typical sites are shown and the results embedded into the software. The modelling software will be a useful tool for the field geophysicist as well as the geotechnical engineer looking to use geophysics on a cavity detection project.

9.1.3 Objective 3

“Build in functions to allow the calculation of cavity detection probability for comparison between techniques, and to inform survey design”

The analysis and process of calculating the probability of detection of a signal in noise is laid out in Chapter 4 and the results of some modelling examples are presented in Chapter 5. This process is central to the general aim of the project: 1) assess the feasibility of using geophysics to detect cavities in the near surface, and 2) inform any subsequent geophysical survey design. This process is discussed in Chapter 4 and the functionality is added to the software. Ultimately, this enables the user to assess numerous geophysical techniques and the likelihood of survey success in any given cavity scenario.

The software can then calculate the minimum cavity detectable at any given depth giving precise information about the limitations of any geophysical survey proposed. This is presented in a simple but effective image of the smallest cavity detectable at a range of depths for each technique. The program can calculate the optimum profile spacing and survey point density at any given noise level through comparison of detection probability. This analytical and accurate technique of survey design will increase openness about the limits of particular geophysical techniques in given site conditions and optimise the geophysical survey to any specific site. The program improves survey design, allows open communication between engineers and geophysicists and, consequently, increases the likelihood of survey success.

Chapter 5 presented numerous tests on the range of techniques highlighting that technique use was conditional to site characteristics. It is therefore concluded that there is no “silver bullet” technique for cavity detection and that in order to choose the best technique for a site, modelling such as presented here should be completed.

Detection probability is shown to be dependent on site specific site parameters such as the geophysical parameters of the cavity and the host material, survey spacing and site noise level. Wide ranging probabilities of detection were modelled dependant on these parameters, and results are presented so the reader can see the impact of each individual parameter. Variation of each subsurface parameter affects the signal intuitively but the complexity of the combination of parameters, especially in 3D, and the requirement to accurately predict the magnitude of the effect, emphasised the need for mathematical modelling of geophysical methods rather than relying on rules of thumb or speculation based on previous field work.

Site noise level and survey profile spacing are shown to have the most influence on the minimum detectable cavity size and detection probability, while the host material and data deletion have a less significant effect. Cavity shape and makeup were shown to have a large effect on detection probability, and so the modelling of typical cavity shapes in this study,

which is new to the field in this work, is an important step towards accurate prediction of the feasibility of geophysics on a given site. In the tests conducted, bell pits are shown to have a higher detection probability for the gravity and magnetic methods than other typical cavity shapes. The magnetic technique detection probability is shown to be greatly influenced by the shaft lining material. Contrary to popular thought, modelling results showed that a north-south magnetic survey direction may not always be optimal and is dependent on the subsurface environment. The optimal survey direction is dependent upon anomaly size and the noise level on a site.

9.1.4 Objective 4

“Expand the investigation of cavities to include the area surrounding the cavities, the halo, and assess the impact on geophysical signal and detection probability”

Modelling the impact of the halo effect is novel work within this project. Chapter 6 describes the present knowledge of the halo effect through Literature Review and so fulfils the first half of this objective. This section is focused on describing the physical makeup of halo that then informs the modelling process. This process is especially important as the halo is seen to be a complex system and so identifying the key parameters the modelling process can be simplified while still representing a typical cavity system.

The Literature Review also highlighted the lack of research available on the quantification of the halo effect and no work completed related to the modelling of the halo effect. This is a major limitation of the research base. Natural cavities, and to a lesser extent tunnelled cavities, will always have a halo and so it is vital to consider it when modelling. This is especially important when using interpretive modelling based on field results. Without considering the halo, the interpretation cannot be sound. In this respect, this work is very inventive and one hope of this Thesis is to spur debate and future research around this topic.

The halo modelling approach is outlined as an addition to the work achieved in previous Chapters. The modelling generates fractures around the cavity based upon user input parameters outlining the fracture width, halo spread, fracture angle, fracture percentage and fracture fill. Chapter 7 then presents numerous scenarios that detail the effect of the halo on the geophysical anomaly and the detection probability and so fulfils the second part of objective 4. It is concluded that cavity halos have a significant effect on the geophysical anomalies and therefore the detection probability. As importantly, it is shown that current predictions in the literature do not accurately estimate the effect. Further detail was found by adjusting halo parameters and recording the effect on the geophysical results. The fracture percentage in the halo area, the halo spread and halo shape all have a significant

effect on the geophysical anomaly. Fracture width, fracture angle and fracture patterns are shown to have insignificant effect on the geophysical anomalies.

Through an assessment of a previous case study of cavity detection, it is shown that interpretive modelling which does not consider the halo effect does not consider the whole picture and may be interpreting cavities of the wrong size. It is suggested that halo analysis should be considered in all cavity modelling, predictive or interpretive.

9.1.5 Objective 5

“Evaluate the modelling technique by using the approach on real world cavity detection scenarios.”

Four case studies were used to test the modelling approach in order to complete objective 5. As the software was created for use within industry, it is important to test against real-world scenarios. The primary use of the software is feasibility analysis of geophysical and the correct choice of technique. In these objectives, the software was successful. The program picked out appropriate techniques on at least three of the four sites. The modelling results showed that, at the estimated or measured noise levels on site, cavities of the size estimated would be detectable on all of the case study sites. In agreement with this, cavities were detected on all sites. As such, it was concluded that the software chose a correct technique. Survey parameters used were also chosen by the software and so, in the cases of cavity detection, were proven to be correct. However, on one site, West Wycombe caves, the geological signal obscured the pure air cavity results and the cavity was only detected through the presence of metal with the tunnel.

The field measurements did not always align with the modelled results. This is not unexpected as in most cases the precise depth and geology was not precisely known before entering the field. On the Middlesex Hospital site where cavity depth and dimensions were fairly accurately known the GPR signal amplitude matched the modelled results fairly accurately.

If assessed as the software was intended, as a tool to test the feasibility of using geophysics and an aid in technique and technique parameter choice, the case studies chosen indicate the approach is sound. However, further testing must be completed on a wider variety of sites.

9.2 Discussion

9.2.1 Practical merits of approach

The proposed approach of using the modelling software before entering the field should benefit potential users in a number of ways.

- 1) *Improvement in survey design.* The software can aid survey spacing choice. If the potential size of the cavity is known, or if there is a known minimum cavity size before considered hazardous, the software can be used to find the spacing required to detect such a cavity to a chosen reliability. This may mean less survey lines, saving time in the field and hence money. If a cavity is small or the noise level is high, the software may suggest more survey lines than anticipated. By completing the modelling stage and increasing the number of profiles spacing, the likelihood of detection will be improved in such a situation.
- 2) *Improvement in technique choice.* The software compares a range of geophysical techniques in any given scenario. It does so by comparing detection probability, but also visually in the GUI to allow easier comparison for non-expert users. By directly comparing the techniques in the same environment a like-for-like comparison can be made, enabling the best choice possible.
- 3) *Cost saving.* A few of the cost savings as a result of the software are mentioned above. However, the key cost saving is made by the software highlighting inappropriate techniques. There will be situations where none of the techniques will be viable. The software will indicate this by low detection probabilities in all techniques. In these situations, the software will have saved money by stopping the user attempting to detect cavities with inappropriate equipment. This will make the user consider other techniques that might be applicable. In the long run, this more discerned approach to technique choice and whether or not to use geophysics will improve the reputation of geophysics within the engineering industry. Users of the software will be more likely to only choose projects they have confidence in completing successfully.
- 4) *Time saving.* Alongside the time savings as a result of better survey design and technique choice, a generalised protocol approach to detecting cavities that this thesis has presented (Section 2.11) will also save time. Using the quicker techniques to cover large areas, then honing in on key parts of the site as a result will make most efficient use of, often limited, field time.

9.2.2 Critique of methodology

Although the work presented in this Thesis has been shown to be novel and produced a unique piece of software which will aid survey analysis into the future, there may be criticism on some features of the approach. Some of these weaknesses have been mentioned throughout the Thesis, but here we explore some general limitations of this modelling.

9.2.2.1 Other noise sources

The detection probability calculations used here assume that signal measured in the field is a result of the cavity presence and randomly generated Gaussian noise. Noise may not be

random, and coherent noise is harder to predict and model, and noise may not be zero mean. It is also clear that other signal will be received by all techniques from elsewhere in the geological environment. Signal from undulating bedrock and from surface features may obscure a cavity or may be mistaken for a cavity in real data. The comparison of features amplitude will be assessed in future iterations of the software (section 9.3.6).

The noise level chosen for each site was done so either through measurements in the field or from similar examples in the literature. However, this process could be much more stringent. We can model or estimate particular noise sources that we know to be on the site: power cables, buildings, and underground communication and infrastructure routes. This could also extend to natural sources such as meteorological conditions and magnetic storms. This will give a much more accurate idea of the noise level.

The program allows some limitations of the field to be included in the analysis, such as the size of the survey site and the analysis into uneven ground. However, there are other site limitations that will have a large effect on the detection probability: rebars, concrete surfaces, trees. These should be considered in the probability calculations.

9.2.2.2 Data deletion estimations

One of the functions of the software is to assess the impact of data deletion (the deletion of noisy data points which occurs in most geophysical processing). In the analysis, data points are simply selected at random. However, in reality there will be an element of reconstruction to the data at the deleted point through smoothing or through kriging. This would improve the likelihood of detection of the signal. Such processing tools could be considered for future iterations of the work.

9.2.2.3 Detection probability calculation

There are numerous other approaches beside Kotelnikov's criterion for assessing the likelihood of detection of signal in noise. This could be as simple as calculating the ratio of signal to noise or the process chosen could be much more complicated such as using a Matched Filter to search for the signal within the noise. For this work, the approach taken was assessed to be the best for the balance of efficiency of programming and detail.

9.2.2.4 Parameter estimation

As shown in Section 5.2.7, variation in geophysical parameters causes a large difference in detection probability. The modelling can easily adjust the parameters but it is only as accurate as the input parameters. There are however some parameter variations that could be incorporated into the modelling. Dielectric properties are frequency dependant and so these could be altered with the modelled frequency is changed. Many properties also change

with depth mainly due to moisture (Loulizi, 2001) and this could also be incorporated (most likely along with the geological changes suggested in Section 9.2.4.2).

9.2.2.5 Use of the radar range equation

Daniels *et al.* (1988) state that the radar range equation is not suitable for GPR modelling with depths less than 2 m. However, fairly good results were found when comparing the modelled values with the Middlesex Hospital field measurements. This suggests that the technique could be viable. More research is recommended in comparing existing GPR modelling techniques at a range of depths.

9.2.3 Comparison with other modelling techniques

The modelling software presented has been designed to be as accessible as possible to a wide audience. It is hoped that the user base will extend beyond geophysics field practitioners. It is therefore much easier to use than other geophysical software available, although this comes with its own limitations (discussed in the next section). The inputs are purposefully kept simple, and the GUI and the results page show the bare minimum required to make a decision on the techniques presented. The software will not run as fast as a simple spherical magnetic or gravity field simulation software, but given the range of outputs, the model runs efficiently. The simplicity of the modelling approaches have been chosen to make sure it runs quickly so users can utilise the software without frustration.

However, this ease of use means that the modelling approach is limited in other respects. The simplicity of the shapes the model can produce do of course not come close to the complexity of the subsurface. More complex shapes with varying geophysical characteristics will be better modelled using techniques such as finite element modelling. This would be an interesting avenue to take the research, as this is a burgeoning field in geophysics. However, there is a risk that the usability may be lost by using more complex approaches. As long as the front end of the software is kept simple and useable, the back end can be more complicated.

A more complicated approach however may inhibit extension of the software by other developers. Currently, the software is set up in a modular way so that it is simple to add other techniques or extensions to the functionality. The code for each technique is straightforward, following established algorithms, and well commented and so adaption is possible. In more complicated software, this becomes harder, and in many cases, the code is not accessible to alteration at all.

The software was created in MATLAB as this is a well-used language across academia and the engineering sector. This means the user base is as wide as possible. Most other modelling software require a separate licence which may be a step too far for more casual users. The software could however be more useable if it was written in an open source language, such as Python or even VBA. This would mean users would not need to have MATLAB to be able to run and so would increase the potential user base. MATLAB does offer an option to create executable programs that can be run without a MATLAB licence. This has been used to create a small version of the software running only the GPR technique, but could be utilised to run the whole software package.

9.2.4 Modelling approach weaknesses

Due to the purposefully simple modelling methodology, there are some weaknesses associated with the approach. Of most importance, is the simplicity of the subsurface modelled. Currently, the software only models typical cavity shapes in a single geological background. Of course, the reality is much more complicated.

9.2.4.1 Cavity shape and makeup

When dealing with manmade cavities, the typical cavity shapes modelled represent the reality fairly well. However, natural cavities are much more complicated than represented by the software. Although the formation mechanisms of natural cavities are well known, the resultant shapes are very varied, and the perimeter of the cavity is certainly not as defined as the software shapes. There is a lot of interaction with rock fracture and with subsurface water features that make the edges of the cavity complicated. In reality, the cavity will also not be filled with a single material as modelled here. There may be loose rock material at the bottom of the cavity or water filling only a part of the cavity. In future versions of the modelling, these complexities can be included by simply including more polyhedrons, but with the price of processing speed.

9.2.4.2 Geological background

The modelling at present only allows one geological background. It is clear that the subsurface is much more complex than the modelling represents. This is the nature of modelling; to take something complex and simplify. However, in many cases, in the near surface, this assumption may not be too inaccurate. We may find cavities in the shallow zone within a single band of geology. Nevertheless, layered geology or the changing of geophysical parameters with depth would improve the modelling accuracy.

The area immediately surrounding of the cavity will have different geophysical properties to the host material. This is modelled in a simple way as a Halo in Chapter 6, but again, the reality is more complicated than modelled. There will be multiple interlocking fracture sets of varied apertures and geology of varying geophysical parameters.

Beyond the halo, the geological background is far more heterogeneous than is modelled. It is likely that the geology changes with depth and across the site. Even within each geological layer, there will be variation in the geophysical properties. In future versions these changes in geological background can be captured through the modelling of polyhedrons for each geological layer, or by polyhedrons within each geological layer of different geophysical parameters. However, it will be difficult to correctly represent smooth variation in parameters with this method.

The modelling of numerous polyhedrons of a range of geophysical parameters could also be used to represent the noise on the site. If we have an idea of the heterogeneity of the site geology, we could attempt to replicate this by randomly placing pockets of contrasting geophysical pockets across the subsurface. This approach would offer an alternative to estimating the site noise to the typical noise levels used currently in the modelling.

The shape of the geological layers is also of importance. As previously noted, undulation of a geological layer could obscure a cavity signal or lead to the false identification of the undulation as a cavity. To be able to accurately model all these variations would require much better information about the geological makeup of the site, which would again make the use of the software more limited to casual users. As with modelling the complex realities of cavities, accurately modelling the site geology in the software would take much longer to process due to the additional polyhedrons.

9.2.4.3 Techniques

Although many of the major cavity detection techniques are modelled in the software, a few are still missing that would be useful to include in future versions. 2D resistivity has been modelled but is not used in the final version of the software because the results are not directly comparable with the other techniques. As resistivity is a commonly used technique, especially karstic cavity detection, it not being provided is a weakness of the software. There will be situations when resistivity is the best technique, or the only technique, for cavity detection and the software does not currently communicate this. Other less commonly used techniques that could be included in future

versions are Multi-channel analysis of surface waves, borehole seismics, and electromagnetic induction.

9.2.5 Lessons learnt from the case studies

By applying the modelling approach to real world case studies, a number of strengths and weaknesses to the approach were identified.

9.2.5.1 Assessing all techniques

The modelling helped choose a technique in all cases but it would have been useful to have tested the other techniques as well on the site. This would have shown whether or not the modelled outputs were accurate. Unfortunately, the amount of time on each site was limited. St Ambrose, Middlesex Hospital and Oslo were all in the early stages of large engineering projects and West Wycombe caves is a working tourist attraction. If it was possible to return to the sites and test the other techniques we could have verified that the software correctly picked the best technique for the occasion. West Wycombe caves offered a particularly excellent site for this kind of testing as the cavity depth varied across the site allowing a range of depth tests.

9.2.5.2 Site choice

The sites chosen were a result of the relationship with the project's industrial partner, Ramboll. They offered the use of three of their sites whilst in the site evaluation phase. As part of the EngD is the collaboration between the university and the industrial partner, it was important to work on sites of interest to the partner. Although this gave access to applicable sites, the sites were not ideal for this type of testing.

Preferable to these sites are purpose built geophysical testing sites, such as the one at the University of Keele. Using such a site would allow direct comparison with the software used with well constrained parameters and the results of the real world site surveys. At such sites, not only is the depth, size and makeup of the test cavities well defined, but there have been numerous previous geophysical experiments on the site that have resulted in the measurement of a number of the background geophysical parameters. These parameters could have been used to better inform the modelling and get more accurate results of anomaly size and detection probability.

On such a site all techniques could easily have been tested over the exact same target for direct comparison with each other and with the modelled results. Tests could have been completed on the impact of changing various technique parameters (GPR frequency, line spacing) and again compared to the modelled results. All of these tests

could have informed the modelling, adjusting various parameters to better match the reality.

In this initial phase, this would have been very useful, not only to improve the accuracy of the modelling but to prove the concept. However, it is important to also conduct tests on the type of sites presented here. The modelling software has been created to use on the more complicated real world engineering sites and all of the complexities on those sites encountered in the case studies will inform future versions of the modelling.

9.2.5.3 Specific site lessons

In West Wycombe a large portion of the magnetic results were obscured by a large magnetic target in the cave (a gate). Combined with knowledge of the cavity contents, this was used to positively identify the cavity on the geophysical record. This approach may be useful in scenarios where the contents of a cavity will help detection. The best example of this is mining cavities, where the shaft may be filled with mining detritus. Currently the modelling allows the modelling of a shaft cap or shaft lining but not variability in the contents of the cavity. It would be worthwhile including the ability to model such materials in future versions.

However, in the case of natural cavities it is unlikely that the cavity will contain objects with such large geophysical contrasts. Objects of this type are more likely to be in the very near surface and will obscure the cavity rather than aid its detection. It could be useful in future versions to include an option in the software which can randomly assign such objects in the near surface. Options might include, the size of the object, the frequency of the object in the subsurface and the geophysical parameters of the object. This would allow the software to show whether the geophysical signal from the obscuring inclusions will reduce the detection probability.

At West Wycombe a total station was used to survey the depth and shape of the cave. This helped make sure the geophysical surveys were taken in the right place. The survey was also used in combination with digital elevation models to calculate the depth of the cavity from the surface. A better approach to this would be to use the same total station to survey the surface as well as the cave. This would have provided a more accurate depth calculation for use within the modelling and hence more accurate detection probability calculations.

As mentioned previously in this section, the limitations of a single geological background is a limitation to the modelling approach. In West Wycombe this was

highlighted in the magnetic results which showed an increase in the magnetic field to the west. This is most likely caused by a change in the geology up the hill. As this trend was linear, it was fairly easy to remove in post processing. However, a more complicated variation in geology would not be so simple to remove and may obscure the small signal from any subsurface cavities. To counteract this weakness in the modelling more complicated subsurfaces will have to be modelled using more polyhedrons (see Section 9.2.4.2).

9.3 Continuation and Future Work

The work presented here, though complete in and of itself, could be seen as a starting point for numerous other future pieces of work. The modelling software was designed modularly in order to make extension and adjustment simple. The use of an m-file for each function means that functions can easily be added or removed from the software. While the Section 9.2 covered weaknesses in the modelling approach and ways to rectify them, this section covers some suggestions for extensions and improvements to the presented work.

9.3.1 Alternative approach to halo modelling

The current halo modelling technique involves creating numerous fractures within the halo, individually as polyhedrons. Although this represents the reality well, it is computationally slow. There are other approaches that will approximate the halo effect that can be employed in the software. One approach is to model the halo at a less granular scale. Instead of modelling each of the fractures individually, the whole of the halo area could be modelled as one polyhedron using geophysical parameters based on the average for the whole of the halo area (both fractures and geological material). This would mean a heavily fractured halo would have a slightly different overall average than a less fractured halo. Although this approach would not represent the reality of the halo system, the results would be similar and much quicker to run and so is attractive.

Certainly for the potential field methods the approach could be utilised, but for the GPR method it might not be as applicable. Reflections from individual fractures of certain geophysical parameters will be different to the reflections from a large block of average geophysical parameter. If there is a large contrast in geophysical parameters between the fracture and the host material, the strength of the reflection will be big, but if we use the lowered average value, the reflection size may be underrepresented. The applicability of this approach to GPR needs to be considered carefully before altering the current technique.

9.3.2 Site specific parameter measurement

To limit the amount of error in inaccurate parameter estimation, site specific parameter measurements should be taken to constrain the parameters. These can then be incorporated into the modelling software.

As this work is envisioned to work in tandem with engineering site investigation, parameters can be measured directly from early site core samples or trial pits. There is equipment which can measure geophysical parameters directly from cores. The Geotek Multi-Sensor Core Logger can measure density, magnetic susceptibility, P-wave velocity and resistivity. Modelling before the main site investigation begins will provide geophysicists with results to present to engineers indicating that certain techniques will be applicable on a site.

Another option is to run a small geophysical survey on the site to record the relevant parameters before modelling and returning again with the most appropriate technique.

9.3.3 Further techniques

Future study on this work should incorporate further techniques including 3D resistivity and seismic techniques. These techniques will allow the modelling of detection of deeper cavities and a broader comparison.

Currently only 2D resistivity is available in the modelling, this can be extended to 3D modelling. Resistivity is a commonly used technique in cavity detection and so it is vital for full comparison of feasible techniques. Various 3D resistivity modelling theories do exist for forward modelling (Dahlin & Loke, 1997) and inversion (Jackson, Earl, & Reece, 2001), and RES3DMOD (Loke, 2011) is the most widely used computer program. However, conversion and incorporation into MATLAB code is currently unavailable.

Seismic techniques are not commonly used in near surface cavity detection but more commonly in situations where deeper penetration is required. However, recently Multi Channel Analysis of Surface Waves (MASW) (Park *et al.*, 1999) has been successfully adapted to the detection of cavities (Almalki & Munir 2012; Billington *et al.* 2006). As with resistivity, modelling of this technique does exist (Nasseri-Moghaddam *et al.* 2011 ;Donohue *et al.* 2008) but not in the MATLAB environment. The process will involve the creation of synthetic data for a given cavity environment and then processing using the MASW technique.

The electromagnetic induction technique is currently only suitable for a sphere and is only of the first order (Wait, 1951). A new technique is sought that can model typical cavity shapes in a more accurate manner.

9.3.4 Multiple techniques and joint inversion

The non-uniqueness of results means that it is often appropriate to use more than one technique. This gives a much better idea of the subsurface and will increase the likelihood of cavity detection. The program could in future calculate the detection probability for multiple techniques. A further, and much more complicated, continuation of this is the incorporation of joint inversion into the modelling.

9.3.5 Alternative modelling approaches

As discussed in Section 2.12, there are multiple approaches to modelling each technique. This project purposefully uses simple techniques where possible to encourage use amongst non-geophysical groups and to allow adaptation of the code and the software if required. However, to more accurately represent the complexity of the subsurface, more involved methods may be required. This may arise if a cavity is known to be in an area of complex heterogeneity. Currently the model only allows a single geological background. More detail may also be needed if the cavity has varying geophysical parameters, for example with loose rock around the perimeter or fill in the bottom.

In these cases, modelling using the current technique would be challenging as a large number of polyhedrons would have to be created of different geophysical parameters to represent the different areas.

If such complexity is required, finite element modelling might offer a good alternative. In more complex subsurfaces it is more efficient, and multiple geophysical parameters can be incorporated into the model to allow different techniques. The method is also used frequently in resistivity modelling and so it would be easier to extend the software to include this very important technique.

9.3.6 Comparison with other targets

It is important to realise that when in the field we may detect other subsurface and surface targets which we may confuse as cavities or may obscure the cavity signal. To analyse this effect on detection probability other targets will be modelled within the software. The comparison of the signal from these other targets with the cavity signal will allow a better idea of whether a cavity can be distinguished. For example, if we know that the signal from a cavity will be of similar size and shape to the known bedrock undulations (from site investigation) then we can suggest that the detection probability will be decreased as we may not interpret the correct signal. Other than bedrock and other geological layer undulations, targets that will be modelled for comparison include surface features and intrusions.

9.3.7 Application to other near surface targets

Currently the software is aimed at cavity detection, but with little alteration it can be used to model other subsurface objects. This could be useful elsewhere in engineering geophysics when trying to detect objects such as foundations.

Although the typical cavity shapes are modelled here, more complicated cavity shapes should be modelled, including the infill found beneath a migrating cavity and multiple cavity karstic systems.

9.3.8 Processing analysis

In a typical processing workflow noisy data may be eliminated by filtering. Usually this is achieved by a band, low or high pass frequency filter depending on the type of noise to be eliminated. Incorporating these filters into the modelling will give a more realistic estimation of real processing techniques and will therefore give a more accurate prediction of detection probability. Such filters are available in the MATLAB Signal Processing Toolbox and therefore the incorporation of this function should be possible.

9.3.9 On site noise measurements

Continuation of the noise measurements recorded for the magnetic technique (section 4.3.2.4) will follow. Further techniques noise levels will be recorded (GPR, gravity, EM, seismic) on a range of site types as with the magnetic noise measurements.

9.3.10 Field work and literature comparison

Further field work is vital in testing the modelling techniques and refining the functions. A wider range of sites and cavities should be tested with all the techniques. There are numerous references in the literature of cavity detection using geophysical techniques. These can be used as case studies for testing the modelling software. The parameters available in a paper will be used to model the cavity in the given environments and the modelled results can be compared with the measured signal in the paper. This will provide a wide range of case studies of cavities across the range of techniques for comparison with the modelling.

9.4 Final Conclusion

This Thesis has succeeded in its objective to create modelling software that improves geophysical technique choice and improves survey design. In creating user friendly software it is hoped that the work will be used in the geophysical and engineering industries to improve cavity detection techniques. The software produced a number of interesting results and presented innovative halo modelling that should be incorporated in future cavity

modelling analysis. The software was utilised in the successful detection of three field cavities. As noted, there are areas where progress can still be made in improving the modelling and approach. However, the software and surrounding results present an important contribution to the literature and the field in general.

10 References

- Alfares, W., Bakalowicz, M., Guerin, R., & Dukhan, M. (2002). Analysis of the karst aquifer structure of the Lamalou area (Hérault, France) with ground penetrating radar. *Journal of Applied Geophysics*, 51(2-4), 97–106. doi:10.1016/S0926-9851(02)00215-X
- Ali, S. H. (2008). Mining in China: A primary ecological and human health concern. Woodrow Wilson Center: China Environment Series, 10. Retrieved from <http://www.healtheffects.org/International/CES10.pdf>
- Almalki, H., & Munir, K. (2012). Efficiency of seismic attributes in detecting near-surface cavities. *Arabian Journal of Geosciences*, 1–8. doi:10.1007/s12517-012-0562-1
- Anderson, N., & Ismail, A. (2003). A generalized protocol for selecting appropriate geophysical techniques. In *Geophysical Technologies for Detecting Underground Coal Mine Voids: An Interactive Forum*.
- Anderson, N. L., Apel, D. B., & Ismail, A. (2002). Differentiating Rooms and Pillars on Reflection Seismic Profiles: A Seismic Investigation of Two Abandoned Coal Mines, 1, 58–70.
- Arrighini, G. P. (1968). Magnetic Properties of Polyatomic Molecules. I. Magnetic Susceptibility of H₂O, NH₃, CH₄, H₂O₂. *The Journal of Chemical Physics*, 49(2), 882. doi:10.1063/1.1670155
- Atkinson, T. C., Ward, R. S., & O'Hannelly, E. (2000). A radial-flow tracer test in Chalk: comparison of models and fitted parameters. In *Tracers and Modelling in Hydrogeology The International Association of Hydrological Sciences (IAHS) in the Series of Proceedings and Reports (Red Books)*, 7–15.
- Automation Creations. (2014). Online Materials Information Resource - MatWeb. Automation Creations. Retrieved August 23, 2014, from <http://www.matweb.com>.
- B.B.C. (2009a). Collapsed pipe causes huge hole. B.B.C. News. Retrieved August 16, 2010, from <http://news.bbc.co.uk/1/hi/england/manchester/8027205.stm>
- B.B.C. (2009b). Women die in Ghana mine collapse. B.B.C. News. Retrieved August 04, 2010, from <http://news.bbc.co.uk/1/hi/world/africa/8356343.stm>
- Balk, R., & Cloos, H. (1948). Structural behavior of igneous rocks. Published by the Geological Society of America.

- Ballard, R. F., Cuenod, Y., & Jenni, J. P. (1982). Detection of karst cavities by geophysical methods. *Bulletin of Engineering Geology and the Environment*, 26(1), 153–157.
- Barclay, C. (2010). *Greenfield, Brownfield Sites and Planning*. Science and Environment Section - House of Commons Library.
- Barnett, C. T. (1976). Theoretical modeling of the magnetic and gravitational fields of an arbitrarily shaped three-dimensional body. *Geophysics*, 41(6), 1353 – 1364. doi:10.1190/1.1440685
- Batayneh, A. T., Abuelad, A. A., & Moumani, K. A. (2002). Use of ground-penetrating radar for assessment of potential sinkhole conditions: an example from Ghor al Haditha area, Jordan. *Environmental Geology*, 41(8), 977–983. doi:10.1007/s00254-001-0477-8
- Bates, R., & Duff, M. (2006). Geophysical Surveys at an Industrial Archaeological site in Fife. In *British Archaeological Reports: British Series 416*, 1–19.
- Becerra, O. D. M. (2004). Creación de un programa para realizar modelado directo 2D de datos. Simon Bolivar University Thesis submission.
- Bell, F. G. (2004). *Engineering geology and construction*, Taylor & Francis Group, London, 797.
- Benson, R. C., & La Fountain, L. J. (1984). Evaluation of subsidence or collapse potential due to subsurface cavities. In *Proceedings 1st Interdisciplinary Symposium on Sinkholes*. Orlando, FL, 201–215.
- Benson, R. C., & Yuhr, L. (1992). A summary of methods for locating and mapping fractures and cavities with emphasis on geophysical methods. In *5th EEGS Symposium on the Application of Geophysics to Engineering and Environmental Problems*.
- Benson, R. C., & Yuhr, L. (1993). Spatial sampling considerations and their applications to characterizing fractured rock and karst systems. *Environmental Geology*, 22(4), 296–307. doi:10.1007/BF00767501
- Beres, M., Luetscher, M., & Olivier, R. (2001). Integration of ground-penetrating radar and microgravimetric methods to map shallow caves. *Journal of Applied Geophysics*, 46(4), 249–262. doi:10.1016/S0926-9851(01)00042-8
- Bieniawski, Z. T. (1976). Rock mass classification in rock engineering. In *Proceedings of Symposium Exploration for Rock Engineering*, Cape Town: Balkema, 97–106.
- Billington, E. D. (2006). 2D MASW abandoned mine detection. In *Highway Geophysics - NDE Conference*, 108–115.
- Bloushi, K. Al. (2011). Microgravity Investigation of the Subsurface Conditions at Al-Ain Wildlife Park and Resort area, Al-Ain, UAE. In *First International Conference on Engineering Geophysics*, EAGE.

- Branigan, T. (2010). Flood warnings “ignored” before Chinese mine disaster. *The Guardian*. Retrieved August 29, 2010, from <http://www.guardian.co.uk/world/2010/mar/31/china-coal-mine-disaster>.
- Branston, M. W., & Styles, P. (2003). The application of Time-Lapse Microgravity for the Investigation and Monitoring of Subsidence at Northwich, Cheshire. *Quarterly Journal of Engineering Geology and Hydrogeology*, 36(3), 231–244. doi:10.1144/1470-9236/03-243
- Breiner, S. (1999). Applications manual for portable magnetometers. Geometrics, San Jose, California.
- British Geological Society. (2010). Non-coal mining hazards. Retrieved March 02, 2012, from <http://www.bgs.ac.uk/research/informationProducts/newsSummer10.html>.
- British Geological Society. (2011). Soluble rocks (dissolution). Geosure: National Ground Stability Data. Retrieved May 10, 2011, from <http://www.bgs.ac.uk/products/geosure/soluble.html>.
- British Geological Survey. (2010a). Caves, subsidence and soluble rocks. Retrieved August 16, 2010, from http://www.bgs.ac.uk/science/landUseAndDevelopment/shallow_geohazards/dissolvableRocks.html.
- British Geological Survey. (2010b). Directory of Mines and Quarries. Minerals UK. Retrieved August 23, 2010, from <http://www.bgs.ac.uk/mineralsuk/mines/dmq.html>.
- British Geological Survey. (2010c). Scottish Middle Coal Measures Formation. BGS Lexicon of Named Rock Units. Retrieved August 17, 2010, from <http://www.bgs.ac.uk/lexicon/lexicon.cfm?pub=MCMS>.
- Buck, S. C. (2003). Searching for graves using geophysical technology: field tests with ground penetrating radar, magnetometry, and electrical resistivity. *Journal of Forensic Sciences*, 48(1), 5–11.
- Butler, D. (2008). Detection and characterization of subsurface cavities, tunnels and abandoned mines. *Near-Surface Geophysics & Human Activity, Science*, 578–584.
- Butler, D. K. (1984). Microgravimetric and gravity gradient techniques for detection of subsurface cavities. *Geophysics*, 49(7), 1084–1096. doi:10.1190/1.1441723
- Cai, J., & McMechan, G. A. (1995). Ray-based synthesis of bistatic ground-penetrating radar profiles. *Geophysics*, 60, 87–96.
- Cai, Y. & Wang, C.Y. (2005). Fast finite-element calculation of gravity anomaly in complex geological regions. *Geophysical Journal International*, 162(3), 696–708.
- Cardarelli, E., Cercato, M., Cerreto, A., & Di Filippo, G. (2009). Electrical resistivity and seismic refraction tomography to detect buried cavities. *Geophysical Prospecting*, 58(4), 685–695. doi:10.1111/j.1365-2478.2009.00854.x

- Carino, N. J. (2010). Nondestructive test methods. In *Concrete Construction Engineering Handbook*, CRC Press.
- Carter, B., Lajtai, E., & Petukhov, A. (1991). Primary and remote fracture around underground cavities. *International Journal for Numerical and Analytical Methods in Geomechanics*, 15, 21–40.
- Casas, A., Lazaro, R., Vilas, M., & Busquet, E. (1996). Detecting karstic cavities with ground penetrating radar at different geological environments in Spain. In *Proceeding of the 6th International Conference of GPR*, Sendai, Japan, 455–460.
- Chalikakis, K., Plagnes, V., Guerin, R., Valois, R., & Bosch, F. P. (2011). Contribution of geophysical methods to karst-system exploration: an overview. *Hydrogeology Journal*. doi:10.1007/s10040-011-0746-x
- Chambers, J. E., Wilkinson, P. B., Weller, A. L., Meldrum, P. I., Ogilvy, R. D., & Caunt, S. (2007). Mineshaft imaging using surface and crosshole 3D electrical resistivity tomography: A case history from the East Pennine Coalfield, UK. *Journal of Applied Geophysics*, 62(4), 324–337. doi:10.1016/j.jappgeo.2007.03.004
- Chamon, N., & Dobereiner, L. (1988). An example of the use of geophysical methods for the investigation of a cavern in sandstones. *Bulletin of Engineering Geology and the Environment*, 38(1), 37–43.
- Chavez Segura, R. E., Tejero-Andrade, A., Delgado-Solorzano, C., Cifuentes-Nava, G., Hernández-Quintero, E. (2011). L- and Corner-arrays for 3D electric resistivity tomography: An alternative for geophysical surveys in urban zones. In *American Geophysical Union, Fall Meeting*.
- Chung, C.-C., Lin, C.-P., & Yang, S.-H. (2013). Unsaturated Soil Water Content and Electrical Conductivity Characterization using Time Domain Reflectometry. In *Near Surface Geophysics, Asia Pacific Conference*.
- Clarke, B. G., Welford, M., & Hughes, D. B. (2006). The threat of abandoned mines on the stability of urban areas. In *IAEG 2006: Engineering geology for tomorrow's cities*, 379.
- Conyers, L. B. (2004). *Ground-penetrating radar for archaeology*, AltaMira, Lanham, Maryland, 203.
- Cooper, G. R. J. (2010). Geomodel - simultaneous magnetics and gravity modelling and inversion. School of Geosciences, University of the Witwatersrand.
- Culshaw, M. G., & Waltham, A. C. (1987). Natural and artificial cavities as ground engineering hazards. *Quarterly Journal of Engineering Geology and Hydrogeology*, 20(2), 139–150. doi:10.1144/GSL.QJEG.1987.020.02.04

- Dahlin, T., & Loke, M. H. (1997). Quasi-3D resistivity imaging-mapping of three dimensional structures using two dimensional DC resistivity techniques. Proceedings of the 3rd Meeting of Environmental and Engineering Geophysics.
- Daniels, D. J. (Ed.). (2004). Ground penetrating radar, Volume 1 (2nd edition), IET, 726.
- Daniels, D. J., Gunton, D. J., & Scott, H. F. (1988). Introduction to subsurface radar. IEE Proceedings, Part F, Communications, Radar and Signal Processing, 135(4), 278–320. doi:10.1049/ip-f-1.1988.0038
- Daniels, J. (1988). Locating caves, tunnels and mines. The Leading Edge (March), 32–38.
- David, A. (2008). Geophysical survey in archaeological field evaluation. English Heritage Research and Professional Services Guideline.
- Dearman, W. R., Baynes, F. J., & Pearson, R. (1977). Geophysical detection of disused mineshafts in the Newcastle upon Tyne area, North-East England. Quarterly Journal of Engineering Geology and Hydrogeology, 10(3), 257–269. doi:10.1144/GSL.QJEG.1977.010.03.07
- Dey, A., & Morrison, H. F. (1979). Resistivity modelling for arbitrarily shaped two-dimensional structures. Geophysical Prospecting, 27, 106–136.
- Doll, W. E., Nyquist, J. E., Carpenter, P. J., Kaufmann, R. D., & Carr, B. J. (1998). Geophysical Survey of a Known Karst Feature, Oak Ridge Y-12 Plant, Oak Ridge Tennessee. In Geo-engineering for underground facilities: American Society of Civil Engineering Special Publication 90.
- Donohue, S., Long, M., (2008). Assessment of an MASW approach incorporating discrete particle modeling. Journal of Environmental and Engineering Geophysics.
- Doolittle, J., & Collins, M. E. (1998). A comparison of EM induction and GPR methods in areas of karst. Geoderma, 85(1), 83–102. doi:10.1016/S0016-7061(98)00012-3
- EAGE Conference & Exhibition workshop discussion. (2012). Integrated Geosciences for Subsurface Instabilities, Offshore and Onshore. Copenhagen, 3rd June.
- Edmonds, C. N. (2008). Karst and mining geohazards with particular reference to the Chalk outcrop, England. Quarterly Journal of Engineering Geology and Hydrogeology, 41(3), 261–278. doi:10.1144/1470-9236/07-206
- Edwards, W., Okita, M., & Goodman, D. (2000). Investigation of a subterranean tomb in Miyazaki, Japan. Archaeological Prospection, 7(4), 215–224.
- Elawadi, E., El-Qady, G., & Salem, A. (2001). Detection of Cavities Using Pole-Dipole Resistivity Technique. Memoirs of the Faculty of Engineering, Kyushu University, 61(4).

- El-Qady, G., Hafez, M., Abdalla, M. A., & Ushijima, K. (2005). Imaging subsurface cavities using geoelectric tomography and ground-penetrating radar. *Journal of Cave and Karst Studies*, 67(3), 174–181.
- Engelder, T. (2012). Lecture 19: Joint Patterns. Penn State: Structural Geology Class.
- Erkan, K., & Jekeli, C. (2011). A comparative analysis of geophysical fields for multi-sensor applications. *Journal of Applied Geophysics*, 74(2-3), 142–150. doi:10.1016/j.jappgeo.2011.03.006
- Everett, M., & Meju, M. (2005). Near-surface controlled-source electromagnetic induction. *Hydrogeophysics*.
- Ewy, R., & Cook, N. (1990a). Deformation and fracture around cylindrical openings in rock—I: Observations and analysis of deformations. *International Journal of Rock Mechanics and Mining Sciences*, 27.
- Ewy, R., & Cook, N. (1990b). Deformation and fracture around cylindrical openings in rock—II: Initiation, growth and interaction of fractures. *International Journal of Rock Mechanics and Mining Sciences*, 27, 409–427.
- Fajkiewicz, Z., Glinski, A., & Sliz, J. (1982). Some applications vertical gradient of the underground tower gravity. *Geophysics*, 47(12), 1688–1692.
- Fehdi, C., Baali, F., Boubaya, D., & Rouabhia, A. (2010). Detection of sinkholes using 2D electrical resistivity imaging in the Cheria Basin (north-east of Algeria). *Arabian Journal of Geosciences*, 4(1-2), 181–187. doi:10.1007/s12517-009-0117-2
- Fenning, P. J., & Donnelly, L. J. (2004). Geophysical techniques for forensic investigation. *Geological Society, London, Special Publications*, 232(1), 11–20. doi:10.1144/GSL.SP.2004.232.01.03
- Filahi, M., Andrieux, P., Tabbagh, A., Rejiba, F., Najine, A., Jaffal, M., Casas, A., Angelova, D. (2008). Detection and mapping of the underground cavities by geophysical methods: ground penetrating radar, seismic waves and electrical imagery - case of Béni-Mellal city (Morocco). *Geophysical Research Abstracts*, 10, 8657–8657.
- Finck, F. (2003). Introduction of a ground penetrating radar system for investigations on concrete structures. *Otto-Graf-Journal*, 14, 35–44.
- Ford, D. C., & Williams, P. (2007). *Karst Hydrogeology and Geomorphology*, Wiley, 576.
- Franceschini, M. De, Marras, A. M., & Heritage, C. (2010). Advances in Geosciences New discoveries with geophysics in the Accademia of Hadrian ' s Villa near Tivoli (Rome). *Advances in Geosciences*, 3–13.

- Frumkin, A., Ezersky, M., Al-Zoubi, A., Akkawi, E., & Abueladas, A. (2011). The Dead Sea sinkholes hazard: Geophysical assessment of salt dissolution and collapse. *Geomorphology*. doi:10.1016/j.geomorph.2011.04.023
- Gardner, G. H., & Wu, K. K. (2005). Use Of Available And Emerging Methods For Location Of Air And Water Filled Cavities In Mines – Status Report On MSHA Demonstration Projects. SME Annual Meeting, Salt Lake City, Utah.
- Geomatrix. (2010a). How deep can ground penetrating radar (GPR) see? Sensors & Software Technical Paper.
- Geomatrix. (2010b). Land Magnetometer Training Course. In N.S.G.G Geophysical Field Exhibition.
- Geometrics. (2006). G-858 MagMapper datasheet. Retrieved from <https://www.geomatrix.co.uk/data-sheet/?q=/software/magnetic/magmap2000>.
- Geometrics. (2010). MagMap2000. Available from <http://www.geometrics.com/geometrics-products/geometrics-magnetometers/download-magnetometer-software>.
- Geophysical Software Solution & TGT Consulting. (2009). Pblock Version 1.06.0. Retrieved from www.geoss.com.au.
- Geoscan Research. (2012). FM256 Data Quality - Processing and Analysis with Geoplot. Retrieved January 04, 2013, from <http://www.geoscan-research.co.uk/page30.html>.
- Ghatge, S. (1993). Microgravity method for detection of abandoned mines. in New Jersey. Bulletin of the Association of Engineering Geologists.
- Gizzi, F., Loperte, A., Satriani, A., Lapenna, V., Masini, N., & Proto, M. (2010). Georadar investigations to detect cavities in a historical town damaged by an earthquake of the past. *Advanced in Geosciences*, 24, 15–21.
- Global Times. (2010). 38 Total number of dead in North China coalmine. Global Times. Retrieved August 29, 2010, from <http://china.globaltimes.cn/society/2010-04/526013.html>.
- Gochioco, L. M. (2003). Geophysical technologies for detecting underground coal mine voids – An interactive forum. *The Leading Edge*, 22(9), 848.
- Golshani, a., Oda, M., Okui, Y., Takemura, T., & Munkhtogoo, E. (2007). Numerical simulation of the excavation damaged zone around an opening in brittle rock. *International Journal of Rock Mechanics and Mining Sciences*, 44(6), 835–845. doi:10.1016/j.ijrmms.2006.12.005
- Google. (2011). Google Earth (6.1.0.5001). Retrieved from earth.google.co.uk.

Google Maps. (2010). Coatbridge (satellite). Retrieved August 16, 2010, from http://maps.google.co.uk/maps?hl=en&q=coatbridge&um=1&ie=UTF-8&hq=&hnear=Coatbridge,+Lanarkshire&gl=uk&ei=FlJpTIWaMqnZ4waovZWZBA&sa=X&oi=geocode_result&ct=image&resnum=1&ved=0CB0Q8gEwAA.

Grandjean, G., Gourry, J., & Bitri, A. (2000). Evaluation of GPR techniques for civil-engineering applications: study on a test site. *Journal of Applied Geophysics*, 45(3), 141–156. doi:10.1016/S0926-9851(00)00021-5

Grandjean, G., & Leparoux, D. (2004). The potential of seismic methods for detecting cavities and buried objects: experimentation at a test site. *Journal of Applied Geophysics*, 56(2), 93–106. doi:10.1016/j.jappgeo.2004.04.004.

Gritto, R. (2003). Subsurface void detection using seismic tomographic imaging. *Geophysical Technologies for Detecting Underground Coal Mine Voids: An Interactive Forum*. Retrieved from <http://www.escholarship.org/uc/item/10b3g07v>.

Guptasarma, D., & Singh, B. (1999). New scheme for computing the magnetic field resulting from a uniformly magnetized arbitrary polyhedron. *Geophysics*, 64(1), 70–74. doi:10.1190/1.1444531.

Hambling, D. (2010). Pentagon scientists target Iran's nuclear mole men. *Wired*. Retrieved August 05, 2010, from <http://www.wired.com/dangerroom/2010/01/irans-nuclear-molemen>.

Hammack, R. W. (2004). 2-D and 3-D resistivity for locating voids beneath highways; three case studies. In *Annual Meeting of the Interstate Technical Group on Abandoned Underground Mines*, Tucson, AZ.

Hartmann, S., Odling, N. E., & West, L. J. (2007). A multi-directional tracer test in the fractured Chalk aquifer of E. Yorkshire, UK. *Journal of Contaminant Hydrology*, 94(3-4), 315–31. doi:10.1016/j.jconhyd.2007.07.009.

Healy, P. R., & Head, J. M. (1984). Construction over abandoned mine workings. *International Journal of Rock Mechanics and Mining Sciences*, 21(4), 146–146. doi:10.1016/0148-9062(84)91032-5.

Hell Fire Caves. (2012). Explore the Caves. Promotional material. Retrieved April 02, 2012, from <http://www.hellfirecaves.co.uk/index.php?id=30>.

History Of The Caves. (2014). The Hellfire Caves. Retrieved September 07, 2014, from <http://www.hellfirecaves.co.uk/history/history-caves>.

Homes and Community Agency. (2010). Previously developed land that may be available for development. NLUD-PDL Database.

Hopey, D. (2008). Mine subsidence insurance rates to decrease. *Pittsburgh Post Gazette*. Retrieved August 04, 2010, from <http://www.post-gazette.com/pg/08265/913855-454.stm>.

- Huang, Q., & Angelier, J. (1989). Fracture spacing and its relation to bed thickness. *Geological Magazine* (126), 335–362.
- Hus, J., Ech-Chakrouni, S., & Jordanova, D. (2002). Origin of magnetic fabric in bricks: its implications in archaeomagnetism. *Physics and Chemistry of the Earth*, 27(25–31), 1319–1331. doi:10.1016/S1474-7065(02)00126-2.
- Hutchinson, P. J., & Barta, L. S. (2004). Deep-mine void detection through electrical imaging. In *Interstate Technical Group on Abandoned Underground Mines*, Tucson, Arizona.
- Inazaki, T., Kawamura, S., Tazawa, O., Yamanaka, Y., & Kano, N. (2005). Near-Surface Cavity Detection by High-Resolution Seismic Reflection Methods Using Short-Spacing Type Land Streamer. *Symposium on the Application of Geophysics to Engineering and Environmental Problems*, 959–970. doi:10.4133/1.2923554.
- Jackson, P. D., Earl, S. J., & Reece, G. J. (2001). 3D resistivity inversion using 2D measurements of the electric field. *Geophysical Prospecting*, 49(1), 26–39. doi:10.1046/j.1365-2478.2001.00241.x.
- Ji, S., & Saruwatari, K. (1998). A revised model for the relationship between joint spacing and layer thickness. *Journal of Structural Geology*, 20(11), 1495–1508. doi:10.1016/S0191-8141(98)00042-x.
- Johnson, B. (2008). A Portable Toolbox for the Visualization and Processing of Multimodal Geophysical Measurements. *Computer Engineering*, 351–355.
- Johnson, W. J. (2003). Applications of the electrical resistivity method for detection of underground mine workings. In *Geophysical Technologies for Detecting Underground Coal Mine Voids*, Lexington, Kentucky.
- Johnston, D. (2004). A metal mines strategy for Wales. *Mine Water 2004: Process, Policy, Progress* (Environment Agency Wales).
- Jol, H., & Smith, D. (1995). Ground penetrating radar surveys of peatlands for oilfield pipelines in Canada. *Journal of Applied Geophysics*, 34(2), 109–123. doi:10.1016/0926-9851(95)00018-6.
- Juerges, A., Pringle, J. K., Jervis, J. R., & Masters, P. (2010). Comparisons of magnetic and electrical resistivity surveys over simulated clandestine graves in contrasting burial environments, *Near Surface Geophysics* 8, 529–539. doi:10.3997/1873-0604.2010042.
- Kathage, A. (2010). GPR in the field. In *NSGG Geophysical Field Exhibition* (Leicester), 13th July.
- Keller, A. (1998). High resolution, non-destructive measurement and characterization of fracture apertures. *International Journal of Rock Mechanics and Mining Sciences*, 35(8), 1037–1050. doi:10.1016/S0148-9062(98)00164-8.

- Kendorski, F. S. (2004). Problems in “void” detection in coal mine water hazards. 23rd International Conference on Ground Control in Mining.
- Khesin, B. E., Alexeyev, V. V., & Eppelbaum, L. V. (1996). Interpretation of geophysical fields in complicated environments, Springer, 352.
- King, D., Hayden, J., Jackson, R., Holmans, A., & Anderson, D. (2000). Population of households in England to 2021. *Population Trends*, (99), 13–9.
- Kinlaw, A. E., Conyers, L. B., & Zajac, W. (2007). Use of Ground Penetrating Radar to Image Burrows of the Gopher Tortoise (*Gopherus polyphemus*). *Herpetological Review*, 38(1), 50.
- Kofman, L., Ronen, A., & Frydman, S. (2006). Detection of model voids by identifying reverberation phenomena in GPR records. *Journal of Applied Geophysics*, 59(4), 284–299. doi:10.1016/j.jappgeo.2005.09.005.
- Kosmatka, S. H. (2010). Properties and Performance of Normal-Strength and High-Strength Concrete. In *Concrete Construction Engineering Handbook*, 5–16.
- Kruse, S., Grasmueck, M., Weiss, M., & Viggiano, D. (2006). Sinkhole structure imaging in covered Karst terrain. *Geophysical Research Letters*, 33(16). doi:10.1029/2006GL026975.
- Laake, A., & Strobbia, C. (2012). Multi-measurement integration for near-surface geological characterization. *Near Surface Geophysics*, 591–600. doi:10.3997/1873-0604.2012008.
- Laswell, S., Engel, R., Cassidy, J., Courtier, N., & Henton, J. (2008). Recent observations of increased seismic background noise using gPhone gravity meters. In *Micro-G LaCoste* (<http://www.microglacoste.com/gPhoneNoise/gPhoneSeismicNoise.pdf>).
- Laubach, S., Marrett, R., Olson, J., & Scott, A. (1998). Characteristics and origins of coal cleat: A review. *International Journal of Coal Geology*, 35(1-4), 175–207. doi:10.1016/S0166-5162(97)00012-8.
- Lazzari, M., Loperte, A., & Perrone, A. (2010). Advances in Geosciences Near surface geophysics techniques and geomorphological approach to reconstruct the hazard cave map in historical and urban areas. *Advances in Geosciences*, 24, 35–44.
- Leckebusch, J. (2007). Short Report Pull-up/Pull-down Corrections for Ground-penetrating Radar Data. *Archaeological Prospection*, 145(February), 142–145. doi:10.1002/arp.
- Leucci, G. (2006). Contribution of Ground Penetrating Radar and Electrical Resistivity Tomography to identify the cavity and fractures under the main Church in Botrugno (Lecce, Italy). *Journal of Archaeological Science*, 33(9), 1194–1204. doi:10.1016/j.jas.2005.12.009.
- Lillie, R. J. (1998). *Whole Earth Geophysics: An Introductory Textbook for Geologists and Geophysicists*, Prentice Hall, 361.

- Linford, N. T. (1998). Geophysical Survey at Boden Vean, Cornwall, Including an Assessment of the Microgravity Technique for the Location of Suspected Archaeological Void Features. *Archaeometry*, 40(1), 187–216. doi:10.1111/j.1475-4754.1998.tb00833.x.
- Littlejohn, G. S. (1979). Surface stability in areas underlain by old coal workings. *Ground Engineering*, 12, 222–30.
- Liu, S., & Yu, J. (2013). Analysis of Fractures detectability by borehole radar: a numerical study. In *Near Surface Geophysics, Asia Pacific Conference*.
- Liu, X., Li, X., Li, F., Zhao, G., & Qin, Y. (2008). 3D cavity detection technique and its application based on cavity auto scanning laser system. *Journal of Central South University of Technology*, 15, 285–288. doi:10.1007/s11771.
- Loke, M. H. (2011). RES3DMOD: 3D resistivity and IP forward modeling. Available from <http://appliedgeophysics.berkeley.edu/dc/r3dmod/index.html>.
- Louis, F. I., Clark, R. A., Louis, I. F., & Makropoulos, C. C. (2005). Nondestructive imaging of small size voids at Akrotiri archaeological site, Thera Island, Greece, by seismic inversion techniques. *Journal of Applied Geophysics*, 57(4), 306–326. doi:10.1016/j.jappgeo.2005.04.001.
- Loulizi, A., Barker, R. M., Brown, G. S., Flintsch, G. W., & Riad, S. M. (2001). Development of Ground Penetrating Radar Signal Modeling and Implementation for Transportation Infrastructure Assessment. Virginia Polytechnic Institute and State University.
- Luke, B., & Chase, D. (1997). Detecting caves using seismic surface waves: a feasibility study. *The Engineering Geology and Hydrogeology of Karst Terranes*, Balkema, Rotterdam, 419–424.
- Ma, G., Li, L., & Huang, D. (2013). Alternative analytic signal methods for the interpretation of 2D magnetic anomaly data. In *Near Surface Geophysics, Asia Pacific Conference*.
- Mallick, K. & Sharma, K.K. (1999). A finite element method for computation of the regional gravity anomaly. *Geophysics*, 64(2), 461–469.
- Manzanilla, L., Barba, L., Chávez, R., Tejero, A., Cifuentes, G., & Peralta, N. (1994). Caves and Geophysics: an Approximation to the Underworld of Teotihuacan, Mexico. *Archaeometry*, 36(1), 141–157. doi:10.1111/j.1475-4754.1994.tb01070.x.
- Marinos, P. (2010). New proposed GSI classification charts for weak or complex rock masses. In *Proceedings of the 12th Bulletin of the Geological Society of Greece International Congress Patras*, 1248–1258.
- Marinos, P., & Hoek, E. (2000). GSI: a geologically friendly tool for rock mass strength estimation. In *Proceedings of GeoEng2000 Conference*, Melbourne.

- Marinos, V., Marinos, P., & Hoek, E. (2005). The geological strength index: applications and limitations. *Bulletin of Engineering Geology and the Environment*, 64(1), 55–65. doi:10.1007/s10064-004-0270-5.
- Martinez, A., Beaty, D. S., Feldman, H. R., & Kruger, J. M. (1996). Fluvial Sandstone Reservoir, Northeast Kansas, High-Resolution Ground-Penetrating Radar. Kansas Geological Survey, Open-file Report 95-58.
- Matthews, M. C., & Clayton, C. R. I. (2000). Locating dissolution features in the Chalk. *Journal of Engineering Geology*, 125–140.
- Maxwell, G. M. (1975). Some observations on the limitations of geophysical surveying in locating anomalies from buried cavities associated with mining in Scotland. *Mining Engineer*, 134, 277–285.
- Maxwell, G. M. (1976). Old mine shafts and their location by geophysical surveying. *Quarterly Journal of Engineering Geology and Hydrogeology*, 9(4), 283–290. doi:10.1144/GSL.QJEG.1976.009.04.01.
- McCann, D. M., Jackson, P. D., & Culshaw, M. G. (1987). The use of geophysical surveying methods in the detection of natural cavities and mineshafts. *Quarterly Journal of Engineering Geology and Hydrogeology*, 20(1), 59–73. doi:10.1144/GSL.QJEG.1987.020.01.06.
- McDowell, P. W. (1975). Detection of clay filled sink-holes in the chalk by geophysical methods. *Quarterly Journal of Engineering Geology and Hydrogeology*, 8(4), 303–310. doi:10.1144/GSL.QJEG.1975.008.04.05.
- McEnroe, S. A. (1998). Magnetic susceptibility measurements on concrete samples. Geological Survey of Norway Report, 98-122.
- McMechan, G., Loucks, R., Zeng, X., & Mescher, P. (1998). Ground penetrating radar imaging of a collapsed paleocave system in the Ellenburger dolomite, central Texas. *Journal of Applied Geophysics*, 39(1), 1–10. doi:10.1016/S0926-9851(98)00004-4.
- Meglich, T. (2013). Application of geophysical surveys to geotechnical investigations. In *Near Surface Geophysics, Asia Pacific Conference*.
- Mellet, J. (1995). Ground penetrating radar applications in engineering, environmental management, and geology. *Journal of Applied Geophysics*, 33(1-3), 157–166. doi:10.1016/0926-9851(94)00035-M.
- Miller, R. (2013). Near-surface Seismic: More than a Problem of Scale. In *Near Surface Geophysics, Asia Pacific Conference*.
- Miller, R., & Steeples, D. (1991). Detecting voids in a 0.6 m coal seam, 7 m deep, using seismic reflection. *Geoexploration*, 28(2), 109–119. doi:10.1016/0016-7142(91)90043-C.

- Milsom, J. (2003). *Field Geophysics*, 3rd Edition (Geological Field Guide). John Wiley and Sons Ltd.
- Milsom, J. J., & Eriksen, A. (2011). *Field Geophysics* (Geological Field Guide). Wiley-Blackwell.
- Mochales, T., Casas, A. M., Pueyo, E. L., Pueyo, O., Román, M. T., Pocoví, A., Ansón, D. (2007). Detection of underground cavities by combining gravity, magnetic and ground penetrating radar surveys: a case study from the Zaragoza area, NE Spain. *Environmental Geology*, 53(5), 1067–1077. doi:10.1007/s00254-007-0733-7.
- Mochales, T., Pueyo, E. L., Casas, A. M., & Soriano, M. A. (2007). Magnetic prospection as an efficient tool for doline detection: a case study in the central Ebro Basin (northern Spain). *Geological Society, London, Special Publications*, 279(1), 73–84. doi:10.1144/SP279.7.
- Monaghan, W., Trevits, M., Mucho, T., & Wood, J. (2003). Recent national institute for occupational safety and health research using ground penetrating radar for detection of mine voids. *Geophysical Technologies for Detecting Underground Coal Mine Voids: An Interactive Forum*, (2).
- Mine Safety and Health Administration (2001). MSHA Public Safety Campaign Stresses that Mines and Minors Don't Mix. MSHA Press Release. U.S. Department Of Labor.
- Munsch, M., Boulanger, D., Ulrich, P., & Bouiflane, M. (2007). Magnetic mapping for the detection and characterization of UXO: Use of multi-sensor fluxgate 3-axis magnetometers and methods of interpretation. *Journal of Applied Geophysics*, 61(3-4), 168–183. doi:10.1016/j.jappgeo.2006.06.004.
- N.E.R.C. (2010). Coatbridge Geological Map Data 1:10000. Ordnance Survey/EDINA/Crown Copyright.
- Narr, W., & Suppe, J. (1991). Joint spacing in sedimentary rocks. *Journal of Structural Geology* 13, 1037-1048.
- Nasseri-Moghaddam, A., Cascante, G., Phillips, C., & Hutchinson, D. (2007). Effects of underground cavities on Rayleigh waves—Field and numerical experiments. *Soil Dynamics and Earthquake Engineering*, 27(4), 300–313. doi:10.1016/j.soildyn.2006.09.002.
- Nasseri-Moghaddam, A., Park, C., & Cascante, G. (2011). Multi Geometry Approach for MASW Survey-Field and Synthetic Data Results. In *Symposium on the Application of Geophysics to Engineering and Environmental Problems* 24. doi:10.4133/1.3614276.
- Near Surface Geophysics Group. (2011). EIGG Test Site 1 Details. Geophysical Test Sites. Retrieved April 04, 2012, from <http://www.nsgg.org.uk/resources/Test-Sites/Site-1-Description.pdf>.

- Nikitin, A. A., & Tarchov, A. G. (1973). Estimation of the likelihood of the detection of geophysical anomalies. *Rarwied. Gieofiz.*, 59, 56–62.
- Norton, P. J. (1996). Mine closure and associated hydrological effects on the environment: some case studies. In *Minerals Metals and the Environment*, 2, 263–270.
- NSGG. (2011). Geophysics Test Sites. Retrieved June 13, 2011, from <http://www.nsgg.org.uk/test-sites/>
- Olhoeft, G. R. (1996). Application of ground penetrating radar. In *Proceedings of the Sixth International Conference on Ground Penetrating Radar*, 4.
- Ove Arup and Partners. (1976). *Reclamation of Derelict Land: Procedure for Locating Abandoned Mine Shafts*. Planning, Regional and Minerals Directorate, Department of the Environment, London.
- Palacky, G. J., & West, G. F. (1991). Airborne electromagnetic methods. In *Electromagnetic Methods in Applied Geophysics*, 2B, Society of Exploration Geophysics, 811–879.
- Pánisová, J., & Pašteka, R. (2009). The use of microgravity technique in archaeology: A case study from the St. Nicolas Church in Pukanec, Slovakia. *Contributions to Geophysics and Geodesy*, 39(3), 237–254.
- Parasnis, D. S. (1996). *Principles of Applied Geophysics*. Springer.
- Park, C. B., Miller, R. D., & Xia, J. (1999). Multichannel analysis of surface waves (MASW): *Geophysics*, 64, 800–808.
- Park Seismic. (2010a). Data Acquisition Parameters. Multichannel analysis of surface waves. Retrieved August 27, 2010, from <http://www.masw.com/ACQParaTables.html>.
- Park Seismic. (2010b). Dispersion. Multichannel analysis of surface waves. Retrieved August 26, 2010, from <http://www.masw.com/DispersionAnalysis.html>.
- Pasion, L. R. (2007). *Inversion of Time Domain Electromagnetic Data for the Detection of Unexploded Ordnance*. PhD Thesis, University of British Columbia.
- Pastoules, M., & Cripps, J. (1990). Survey of macro-and micro-fracturing in Yorkshire Chalk. In *Proceedings of the International Chalk Symposium*.
- Patterson, D. A., Davey, J. C., Cooper, A. H., & Ferris, J. K. (1995). The investigation of dissolution subsidence incorporating microgravity geophysics at Ripon, Yorkshire. *Quarterly Journal of Engineering Geology and Hydrogeology*, 28(1), 83–94. doi:10.1144/GSL.QJEGH.1995.028.P1.08.
- Pennsylvania Department of Environmental Protection. (2010). What is mine subsidence? Retrieved August 16, 2010, from <http://www.dep.state.pa.us/MSIHomeowners>.
- Petrovský, E., & Ivers, D. (2011). *The Earth's Magnetic Interior*, Springer.

- Pidlisecky, A., & Knight, R. (2008). FW2_5D: A MATLAB 2.5-D electrical resistivity modeling code. *Computers & Geosciences*, 34(12), 1645–1654. doi:10.1016/j.cageo.2008.04.001.
- Piggott, R. J., & Eynon, P. (1978). Ground movements arising from the presence of shallow abandoned mine workings. In *Proceedings of First International Conference on Large Ground Movements and Structures*, Cardiff, Pentech Press, London, 749–780.
- Pluijm, B. Van der, & Marshak, S. (2004). *Earth structure: an introduction to structural geology and tectonics*. W. W. Norton & Company (2nd International student edition).
- Pringle, J. K., Stimpson, I. G., Toon, S. M., Caunt, S., Lane, V. S., Husband, C. R., Jones, G. M., Cassidy, N. J., & Styles, P. (2008). Geophysical characterization of derelict coalmine workings and mineshaft detection: a case study from Shrewsbury, United Kingdom. *Near Surface Geophysics*, 6, 185–194, doi:10.3997/1873-0604.2008014.
- Pueyo-Anchuela, Ó., Casas-Sainz, A. M., Soriano, M. a., & Pocoví-Juan, A. (2010). A geophysical survey routine for the detection of doline areas in the surroundings of Zaragoza (NE Spain). *Engineering Geology*, 113(3-4), 382–396. doi:10.1016/j.enggeo.2010.05.015.
- Rákoš, M., Murín, J., Kafka, D., Varga, Z., & Olčák, D. (1984). NMR and magnetic susceptibility study of woods and cellulose. *Czechoslovak Journal of Physics*, 34(4), 332–340. doi:10.1007/BF01959497.
- Raybould, D. R., & Price, D. G. (1966). The use of the proton magnetometer in engineering geological investigations. In *the Proceedings of First Congress International Society of Rock Mechanics*. Lisbon, 11-14.
- Reches, Z. (1998). Tensile Fracturing of Stiff Rock Layers under Triaxial Compressive Stress State. *International Journal of Rock Mechanics and Mining Sciences*, 35(4-5), 456–457.
- Reynolds International. (2009). Micro-gravity: Technical Summary Sheet 8. Retrieved from <http://www.reynolds-international.co.uk/uploads/files/08tssmicrogravity.pdf>.
- Reynolds, J. M. (1997). *An Introduction to Applied and Environmental*. Wiley-Blackwell.
- Rives, T., Razack, M., Petit, J.-P., & Rawnsley, K. (1992). Joint spacing: analogue and numerical simulations. *Journal of Structural Geology*, 14(8), 925–937.
- Roberts, G. P., Raithatha, B., Sileo, G., Pizzi, A., Walker, J. F., Wilkinson, M., Pucci, S., McCaffrey, K., Phillips, R. J., Michetti, A. M., Guerrieri, L., Blumetti, A. M., Vittori, E., Cowie, P., Sammonds, P., Galli, P., Boncio, P., Bristow, C. & Walters, R. (2009). Paganica GPR Paper. In Preparation, (April).
- Roberts, R. L. (1997). Modeling near-field GPR in three dimensions using the FDTD method. *Geophysics*, 62(4), 1114–1126. doi:10.1190/1.1444212.

- Rodriguez Castillo, R., & Reyes Gutierrez, R. (1992). Resistivity identification of shallow mining cavities in Real del Monte, Mexico. *Engineering Geology*, 33(2), 141–149. doi:10.1016/0013-7952(92)90005-J.
- Roe, M. (2008). The Bell Pit. Lead Mining In the Yorkshire Dales. Retrieved March 08, 2012, from <http://www.martinroe.pwp.blueyonder.co.uk/bellpit.htm>.
- Romanov, D., Dreybrodt, W., & Gabrovsek, F. (2002). Interaction of Fracture and Conduit Flow in the Evolution of Karst Aquifers. *Hydrogeology and Biology of Post-paleozoic Carbonate Aquifers*, Karst Waters Inst. Spec. Publ. (7), 38–43.
- Roth, M., Mackeya, J. R., Mackeya, C., & Nyquist, J. E. (2002). A case study of the reliability of multielectrode earth resistivity testing for geotechnical investigations in karst terrains. *Engineering Geology*, 65(2-3), 225–232. doi:10.1016/S0013-7952(01)00132-6.
- Rybakov, M., Goldshmidt, V., Fleischer, L., & Rotstein, Y. (2001). Cave detection and 4-D monitoring: A microgravity case history near the Dead Sea. *The Leading Edge*, 20(8), 896–900. doi:10.1190/1.1487303.
- Rybakov, M., Rotstein, Y., Shirman, B., & Al-Zoubi, A. (2005). Cave detection near the Dead Sea - a micromagnetic feasibility study. *The Leading Edge*, 24(6), 585–590. doi:10.1190/1.1946210.
- Salem, A., Lei, K., Green, C., Fairhead, J. D., & Stanley, G. (2010). Removal of cultural noise from high-resolution aeromagnetic data using a two stage equivalent source approach. *Exploration Geophysics*, 41(2), 163–169. doi:10.1071/EG09047.
- Sargent, C., & Goulty, N. R. (2009). Seismic reflection survey for investigation of gypsum dissolution and subsidence at Hell Kettles, Darlington, UK. *Quarterly Journal of Engineering Geology and Hydrogeology*, 42(1), 31–38. doi:10.1144/1470-9236/07-071.
- Saribudak, M. (2001). Urban Geophysics: A Mapping of Mount Bonnell Fault And Its Karstic Features In Austin, Tx. 2010 SAGEEP Proceedings International Convention, Keystone, CO.
- Sasaki, Y. (1994). 3-D resistivity inversion using the finite-element method. *Geophysics*, 59(12), 1839–1848.
- School of Environment University of Auckland. (2010). World Map of Carbonate Rock Outcrops v3.0. Retrieved March 08, 2012, from http://web.env.auckland.ac.nz/our_research/karst.
- Scintrex. (2011). Scintrex CG-5 Brochure. Retrieved June 08, 2011, from [http://scintrexltd.com/dat/content/file/CG-5 New Brochure.pdf](http://scintrexltd.com/dat/content/file/CG-5%20New%20Brochure.pdf).
- Scollar, I., Tabbagh, A., Hesse, A., & Herzog, I. (2009). *Archaeological Prospecting and Remote Sensing*. Cambridge University Press.

- Scott, J., & Hunter, J. R. (2004). Environmental influences on resistivity mapping for the location of clandestine graves. *Geological Society, London, Special Publications*, 232(1), 33–38. doi:10.1144/GSL.SP.2004.232.01.05.
- Seigel, H. (1995). A guide to high precision land gravimeter surveys. Scintrex Ltd., Concord, Ontario.
- Sellers, B., & Chamberlain, A. (1998). Cave Detection Using Ground Penetrating Radar. *The Archaeologist*, 31, 20–21.
- Sensors Software Inc. (2003). EKKO_View Enhanced & EKKO_View Deluxe User's Guide. Mississauga, Ontario.
- Sensors Software Inc. (2010). EKKO_View Deluxe. Mississauga, Ontario.
- Sharma, P. V. (1997). *Environmental and Engineering Geophysics*. Cambridge University Press.
- Silc, T., & Stanek, W. (1977). Bulk density estimation of several peats in northern Ontario using the von Post humification scale. *Canadian Journal of Soil Science* (57).
- Singh, B., & Guptasarma, D. (2001). New method for fast computation of gravity and magnetic anomalies from arbitrary polyhedra. *Geophysics*, 66(2).
- Slater, L., & Glaser, M. (2001). Improving Understanding of Peatland Hydrogeology Using Electrical Geophysics Proceedings of the Symposium on the Application of Geophysics to Environmental & Engineering Problems (SAGEEP), March 4-7, 2001. Denver, Colorado.
- Sloan, S. D., & Harris, J. B. (2010). Shallow seismic investigation of surface deformation associated with the Kilmichael dome, Montgomery County, Mississippi, USA: Near Surface Geophysics, 8, 451–457. doi:10.3997/1873-0604.2010046.
- Snow, D. (1970). The frequency and apertures of fractures in rock. *International Journal of Rock Mechanics and Mining Sciences & Geomechanics Abstracts*, 7(1), 23–40. doi:10.1016/0148-9062(70)90025-2.
- Sternberg, B. (2004). Electromagnetic Geophysics Techniques for Location of Abandoned Underground Mines. In *Interstate Technical Group on Abandoned Underground Mines: 5th Biennial Workshop*, Tucson, AZ, 1–12.
- Stocco, S., Godio, A. & Sambuelli, L. (2009). Modelling and compact inversion of magnetic data: A MATLAB code. *Computers & Geosciences*, 35(10), 2111–2118.
- Stolarczyk, L. G., & Peng, S. S. (2003). Advanced Electromagnetic Wave Technologies for the Detection of Abandoned Mine Entries and Delineation of Barrier Pillars. In *Proceedings of the Interactive Forum on Geophysical Technologies for Detecting Underground Coal Mine Voids*, July 2003, Lexington, KY.

- Styles, P. (2003). Feature Environmental geophysics: a site characterization tool for urban regeneration in the post-mining era. *Geology Today*, 19(5), 173–178. doi:10.1046/j.1365-2451.2003.00407.x.
- Styles, P., McGrath, R., Thomas, E., & Cassidy, N. J. (2005). The use of microgravity for cavity characterization in karstic terrains. *Quarterly Journal of Engineering Geology and Hydrogeology*, 38(2), 155–169. doi:10.1144/1470-9236/04-035.
- Styles, P., Toon, S., Branston, M., Thomas, E., & McGrath, R. (2005). High resolution microgravity investigations for the detection and characterisation of subsidence associated with abandoned, coal, chalk and salt mines. *Postmining*, Nancy, France.
- Styles, P., Toon, S., Thomas, E., & Skittrall, M. (2006). Microgravity as a tool for the detection, characterization and prediction of geohazard posed by abandoned mining cavities. *First Break*, 24, 51–60.
- Talwani, M. (1965). Computation with the help of a digital computer of magnetic anomalies caused by bodies of arbitrary shape. *Geophysics*, 30, 797–817.
- Talwani, M., & Ewing, M. (1960). Rapid computation of gravitational attraction of 3D bodies of arbitrary shape. *Geophysics*, 25, 203–225.
- Talwani, M., Worzel, J. I., & Landisman, M. (1959). Rapid gravity computations for two-dimensional bodies with application to the Mendocino submarine fracture. *Journal of Geophysical Research*, 64, 49–59.
- Taner, M. T., Koehler, F., & Sheriff, R. E. (1979). Complex seismic trace analysis. *Geophysics*, 44(11), 1896. doi:10.1190/1.1440946.
- Taylor, J. (2000). Effects of abandoned shallow bord-and-pillar workings on surface development. *Transactions of the Institution of Mining and Metallurgy, Section A - Mining Technology*, 109, A140-A145.
- Telford, W.M., Geldart, L.P. & Sheriff, R.E. (1990). *Applied geophysics* (Vol. 1). Cambridge University Press.
- TerraDat UK Ltd. (2005). A Background to Shallow Geophysical Methods with Applied Engineering & Environmental Case Studies. Available from <http://www.terradat.co.uk/Company%20brochure.pdf>.
- Terzaghi, K. (1946). Rock Defects and Loads on Tunnel Supports. In *Rock Tunneling with Steel Supports* 1, 17–99. Youngstown, OH: Commercial Shearing and Stamping Company.
- Theimer, B., Nobes, D., & Warner, B. (1994). A study of the geoelectrical properties of peatlands and their influence on ground-penetrating radar surveying. *Geophysical Prospecting*, 42, 179–202.

- Trainum, M. (2006). A review and evaluation of the geological and geophysical surveys and general cost comparison: for the investigation of sinkholes on US 18 in Cerro Gordo County, Iowa. In *Highway Geophysics - NDE Conference*, 422–436.
- Tuckwell, G., Grossey, T., Owen, S., & Stearns, P. (2008). The use of microgravity to detect small distributed voids and low-density ground. *Quarterly Journal of Engineering Geology and Hydrogeology*, 41(3), 371–380. doi:10.1144/1470-9236/07-224.
- Twiss, R. J., & Moores, E. M. (2006). *Structural Geology*. W. H. Freeman.
- Tzanis, A. (2006). MATGPR: A freeware MATLAB package for the analysis of common-offset GPR data. *Geophysical Research Abstracts*, 8.
- U.S. Army Corps of Engineers. (1995). *Geophysical exploration for engineering and environmental investigations*. U.S. Army Engineering Manual.
- Uduwawala, D., & Norgren, M. (2005). A complete FDTD simulation of a real GPR antenna system operating above lossy and dispersive grounds. *Progress In Electromagnetics Research*, 50, 209–229.
- Ulriksen, C. (1982). *Application of Impulse Radar to Civil Engineering*. Doctoral Thesis, Department of Engineering Geology, University of Technology, Lund, Sweden.
- Ulugergerli, E. U., & Akca, I. (2006). Detection of cavities in gypsum. *The Journal of the Balkan Geophysical Society*, 9(1), 8–19.
- United States Geological Survey. (2006). Contaminated water at the Argo (mine) Tunnel, Idaho Springs. Retrieved March 02, 2012, from [http://libraryphoto.cr.usgs.gov/cgi-bin/show_picture.cgi?ID=ID.U.S. Geological Survey 91ct&SIZE=large](http://libraryphoto.cr.usgs.gov/cgi-bin/show_picture.cgi?ID=ID.U.S.GeologicalSurvey91ct&SIZE=large).
- Wadhwa, R. S., Ghosh, N., Chaudhari, M. S., Chandrashekhar, V., & Sinharay, R. K. (2008). Delineation of cavities in a canal bed by Geophysical Survey in Navargaon Project Area, Maharashtra. *The Journal of Indian Geophysical Union*, 12(1), 55–62.
- Wait, J. R. (1951). A conducting sphere in a time varying magnetic field. *Geophysics*, 16(4), 666. doi:10.1190/1.1437716.
- Walker, P. (2010). Tropical Storm Agatha blows a hole in Guatemala City. *The Guardian*. Retrieved August 29, 2010, from <http://www.guardian.co.uk/world/2010/jun/01/storm-agatha-hole-guatemala>.
- Walters, S. L., Miller, R. D., Steeples, D. W., Xia, J., & Zeng, C. (2009). Detecting tunnels and underground facilities using diffracted p-waves. In *Symposium on the Application of Geophysics to Engineering and Environmental Problems*, 937–942.
- Waltham, A. C., & Fookes, P. G. (2003). Engineering classification of karst ground conditions. *Quarterly Journal of Engineering Geology and Hydrogeology*, 36, 101–118.

- Waltham, T., Bell, F. G., & Culshaw, M. G. (2004). *Sinkholes and Subsidence: Karst and Cavernous Rocks in Engineering and Construction*. Springer.
- Wang, S. Y., Sloan, S. W., Sheng, D. C., & Tang, C. A. (2012). Numerical analysis of the failure process around a circular opening in rock. *Computers and Geotechnics*, 39, 8–16. doi:10.1016/j.compgeo.2011.08.004.
- Westerhoff, R., Hoegaerden, V. van, Brouwer, J., & Rijkers, R. (2004). ConsoliTest - Using Surface Waves for Estimating Shear-Wave Velocities in the Dutch Subsurface. In *Engineering Geology for Infrastructure Planning in Europe*, 104, 368–376. doi:10.1007/b93922.
- White, W. B. (1988). *Geomorphology and Hydrology of Karst Terrains* (p. 474). Oxford University Press.
- Wickham, G., & Tiedemann, H. (1974). Ground Support Prediction Model (RSR Concept). *Proceedings of the Rapid Excavation and Tunnelling Conference, AIME, New York*. 1974. 691–707.
- Wickham, G., Tiedemann, H., & Skinner, E. (1972). Support determinations based on geologic predictions. *Rapid Excavation and Tunneling Conference Proceedings*, Chapter 7.
- Wilkinson, P. B., Chambers, J. E., Meldrum, P. I., Ogilvy, R. D., & Caunt, S. (2006). Optimization of Array Configurations and Panel Combinations for the Detection and Imaging of Abandoned Mineshafts using 3D Cross-Hole Electrical Resistivity Tomography. *Journal of Environmental & Engineering Geophysics*, 11(3), 213–221. doi:10.2113/JEEG11.3.213.
- Wilkinson, P. B., Chambers, J. E., Meldrum, P. I., Ogilvy, R. D., Mellor, C. J., & Caunt, S. (2005). A Comparison of Self-Potential Tomography with Electrical Resistivity Tomography for the Detection of Abandoned Mineshafts. *Journal of Environmental and Engineering Geophysics* 10 (4), 381–389.
- Witten, A. (2004). A MATLAB-based three-dimensional viewer. *Computers & Geosciences*, 30(7), 693–703. doi:10.1016/j.cageo.2004.04.001.
- Won, I. J., & Bevis, M. (1987). Computing the gravitational and magnetic anomalies due to a polygon; algorithms and FORTRAN subroutines. *Geophysics*, 52(No. 2), 232–238.
- Wong, R. H., Lin, P., Tang, C., & Chau, K. (2002). Creeping damage around an opening in rock-like material containing non-persistent joints. *Engineering Fracture Mechanics*, 69(17), 2015–2027. doi:10.1016/S0013-7944(02)00074-7.
- Woods, R. D. (1968). Screening of surface waves in soils. *American Society of Civil Engineers, Journal of the Soil Mechanics*, 94, 951–979.
- Wu, H., & Pollard, D. D. (1995). An experimental study of the relationship between joint spacing and layer thickness. *Journal of Structural Geology*, 17(6), 887–905.

- Xia, J., Miller, R., Park, C., Hunter, J., & Harris, J. (2000). Comparing shear-wave velocity profiles from MASW with borehole measurements in unconsolidated sediments, Fraser River Delta, BC, Canada. *Journal of Environmental and Engineering Geophysics*, 5(3), 1–13.
- Xia, J., Nyquist, J., Xu, Y., Roth, M., & Miller, R. (2007). Feasibility of detecting near-surface feature with Rayleigh-wave diffraction. *Journal of Applied Geophysics*, 62(3), 244–253. doi:10.1016/j.jappgeo.2006.12.002.
- Xu, X., Zeng, Q., Li, D., Wu, J., Wu, X., & Shen, J. (2009). GPR detection of several common subsurface voids inside dikes and dams. *Engineering Geology*, 1–12. doi:10.1016/j.enggeo.2009.12.001.
- Xu, Y. (2013). Near-surface Geophysics in China. In *Near Surface Geophysics, Asia Pacific Conference*.
- Yang, X., Henderson, G., Mao, L., & Evans, A. (2009). Application of ground penetrating radar in detecting the hazards and risks of termites and ants in soil levees. *Environmental Entomology*, 38(4), 1241–9.
- Yang, Y. (2007). Coal Mining and Environmental Health in China. China Environmental Health Project Research Brief.
- Yanrong, W. (2009). Design of intrinsically safe intelligent water-level monitor used in coal mine. *IEEE International Conference on Automation and Logistics*, 1158–1162. doi:10.1109/ICAL.2009.5262596.
- Zerwer, A., Polak, M.A. & Santamarina, J.C. (2003). Rayleigh wave propagation for the detection of near surface discontinuities: Finite element modeling. *Journal of nondestructive evaluation*, 22(2), 39–52.
- Zhang, D. F., Ouyang, Z. Y., & Wang, S. J. (2001). Population resources environment and sustainable development in the karst region of southwest China. *China Population, Resources and Environment*, 11(1), 77–81.

11 Appendices

Appendix A Database of examples of cavity detection (GPR example)

Reference	Target depth (top) (m)	Target size (height x width x length) (m)	Target shape	Frequency (MHz)	Detected?	Test/real	Geology	Void makeup
Grandjean, G. <i>et al</i> 2000	2.5	~1x1x1	semi-sphere	300	Yes (hyperbola)	test	Limestone sand	air
Grandjean, G. <i>et al</i> 2000	2.5	~1x1x1	semi-sphere	500	Yes (hyperbola)	test	Limestone sand	air
Grandjean, G. <i>et al</i> 2000	2.5	~1x1x1	semi-sphere	900	No (limited by penetration)	test	Limestone sand	air
Xu, X. <i>et al.</i> , 2009	3.45	0.3 diameter, 1.5 length	cylinder	300	Yes (hyperbola)	Simulated test	Ferralsol	air
Xu, X. <i>et al.</i> , 2009	2.45	0.3 diameter, 1.5 length	cylinder	500	Yes (hyperbola)	Simulated test	Ferralsol	air
Xu, X. <i>et al.</i> , 2009	1.2	0.075 Diameter, 1.5 length	cylinder	300	Yes (hyperbola)	Simulated test	Ferralsol	air
Xu, X. <i>et al.</i> , 2009	1.2	0.075 Diameter, 1.5 length	cylinder	500	Yes (hyperbola)	Simulated test	Ferralsol	air
Xu, X. <i>et al.</i> , 2009	3.12	N/A	N/A	500	Yes (hyperbola)	Real	Ferralsol	Termite nest
Xu, X. <i>et al.</i> , 2009	15	N/A	N/A	50	Yes (hyperbola)	Real	Ferralsol dam	Termite nest

Mochales, T. <i>et al.</i> , 2007	0	2m across	doline	50	Yes (<i>high conductivity elements (multiple reflection anomalies in the GPR-profiles)</i>)	Real	Alluvial terrace, with urban debris filled doline	filled karstic collapse Filled with urnam debris-Doline
Mochales, T. <i>et al.</i> , 2007	5-9	N/A	elliptical	50	Maybe (<i>clustering of hyperbolae anomalies</i>)	Real	Alluvial terrace, with urban debris filled doline	<i>Paleo-collapse, a cavity with irregular roof shape</i>
Mochales, T. <i>et al.</i> , 2007	N/A	24 diameters	circular	50	Maybe(<i>onlap reflection geometries</i>)	Real	Alluvial terrace, with urban debris filled doline	filling of natural materials
El-Qady, G. <i>et al.</i> , 2005	2	4m width	spherical	200	Yes (hyperbola)	Real	Limestone	Air - Cave
Edwards, W., Okita, M. & Goodman, D., 2000	2.8	2.1-3.1 by 1.8-2.8	Rectangular	N/A	Yes (hyperbola)	Real	Volcanic soils	Air - Tomb
Sternberg, B., 2004	16	N/A	N/A	16	Yes (hyperbola - highest reflection strength)	Real	Limestone	air - mine
(Lazzari, Loperte, & Perrone, 2010)	1-3	7 deep	various - house (cuboid)	200	Yes (hyperbola)	Real	Well cemented sands	air - Cave houses
Gizzi, F. <i>et al.</i> , 2010	0.8	5 wide	dug out cave	400	Yes (hyperbola)	Real	pyroclastic deposits	air - cave/grotto, some maybe water
Gizzi, F. <i>et al.</i> , 2010	1	4 wide	dug out cave	400	Yes (hyperbola)	Real	pyroclastic deposits	air - cave/grotto, some maybe water
Gizzi, F. <i>et al.</i> , 2010	1.2	N/A	dug out cave	400	Yes (hyperbola)	Real	pyroclastic deposits	air - cave/grotto, some maybe water
Gizzi, F. <i>et al.</i> , 2010	0.7	N/A	dug out cave	400	Yes (hyperbola)	Real	pyroclastic deposits	air - cave/grotto, some maybe water
Gizzi, F. <i>et al.</i> , 2010	0.4	N/A	dug out cave	400	Yes (hyperbola)	Real	pyroclastic deposits	air - cave/grotto, some maybe water
Leucci, 2006	1.5	N/A	N/A	400	Yes (strong reflection)	Real	carbonate rock formation	air
Yang, X. <i>et al.</i> , 2009	0.61	0.4-1.5 diameter	spherical	400	Yes (hyperbola)	Real	soil levee	Termite nest

Kofman, L., Ronen, a. & Frydman, S., 2006	1	1.5 diameter	cylinder	500	Yes (<i>reverberation phenomenon</i>)	Test	Homogenous, dry sand	fibreglass
Kofman, L., Ronen, a. & Frydman, S., 2006	1	1.5	cylinder	300	Yes (<i>reverberation phenomenon</i>)	Test	Homogenous, dry sand	fibreglass
Kofman, L., Ronen, a. & Frydman, S., 2006	1	0.6 diameter	cylinder	100	Not really - too small	Test	Homogenous, dry sand	fibreglass
Kofman, L., Ronen, a. & Frydman, S., 2006	N/A	4 diameter	N/A	100	Yes (reverberation patterns)	Real	N/A	Empty cavity
Kofman, L., Ronen, a. & Frydman, S., 2006	N/A	4 diameter	N/A	300	Yes (reverberation patterns)	Real	N/A	Empty cavity
Beres, M., Luetscher, M. & Olivier, R., 2001	13	10	cylinder and linking cave systems	100	Yes (hyperbola)	Real	karstic Limestone with less than 0.5m of topsoil	shallow karstic features - air filled cave
Batayneh, A.T., <i>et al</i> 2002	12.5	47 wide	semi-sphere	100	Yes (diffractions and refractions in sinkhole)	Real	karstic limestone	depression/filled sinkhole
Sellers, B. & Chamberlain, A., 1998	14 and 6	N/A	N/A	100	yes (strong reflections hyperbola)	Real	Devonian limestone	air
Mellet, J., 1995	1	N/A	N/A	500	yes (multiple echoes)	Real	canal (concrete)	air
Doolittle, J., 1998	N/A	N/A	N/A	120	yes (Multiple dark reflections)	Real	<i>electrically resistive sands overlying loamy marine sediments and limestone bedrock.</i>	Solution or collapsed features
Doolittle, J., 1998	N/A	N/A	N/A	120	No (lack of penetration)	Real	<i>clayey residuum and limestone bedrock</i>	

Pueyo-Anchuela, Ó. <i>et al.</i> , 2010	N/A	N/A	N/A	50	Yes (<i>adaptation features, plane-concave geometry, apparent lower reflectivity</i>)	Real	various filling	Collapse and doline
Pueyo-Anchuela, Ó. <i>et al.</i> , 2010	N/A	N/A	N/A	100	Yes (<i>adaptation features, plane-concave geometry, apparent lower reflectivity</i>)	Real	various filling	Collapse and doline
Pueyo-Anchuela, Ó. <i>et al.</i> , 2010	N/A	N/A	N/A	250	Yes (<i>adaptation features, plane-concave geometry, apparent lower reflectivity</i>)	Real	various filling	Collapse and doline
Wadhwa, R. <i>et al.</i> , 2008	1	9.27 across	N/A	250	Yes (<i>trough like pattern of radar diffractions</i>)	Real _canal	Limestone	clay filled void
Wadhwa, R. <i>et al.</i> , 2008	1	N/A	N/A	250	Yes (<i>hyperbola</i>)	Real _canal	Limestone	air void
Wadhwa, R. <i>et al.</i> , 2008	varying depths	N/A	N/A	250	Yes (<i>hyperbola and trough</i>)	Real _canal	Limestone	air and clay void
Kinlaw, A., Conyers, L. & Zajac, W., 2007	3.6	0.25-0.35 width, 0.11-0.18 height	cylinder	900	Yes (<i>hyperbola</i>)	Real	dry Aeolian sand	air void (turtle tunnel)
Butler, D., 2008	2	1.2 diameter	cylinder	N/A	Yes (<i>hyperbola</i>)	Real	N/A	gas pipe
Butler, D., 2008	11-20	1.5 diameter	cylinder	50	No (<i>Electromagnetically lossy soil conditions</i>)	Real	N/A	tunnel (drug smuggling)
(Alfares, Bakalowicz, Guerin, & Dukhan, 2002)	20	height 1-3 , width 3-8	cave	50	Yes (<i>strong reflections numerous hyperbolas</i>)		Limestone	cave (air)
Ulugergerli, E. & Akça, I., 2006	6	N/A	N/A	25	Yes (<i>intrabed reflections of subsidence - indicative of cavity</i>)	Real	gypsum	air cavity

Appendix B Parameters of geologies recorded with GPR

		Silt	Limestone sand	Gneiss 14/20	Gneiss 0/20	Ferrososil	Alluvial terrace	Limestone	pyroclastic deposits	carbonate rock formation	air	soil levee	air dry dune sand	Limestone	karstic limestone	overl marine sediments	clayey residuum	dry aeolian sand	limestone
wave param	v (m/ns)	0.09 0.07	0.12 0.1	0.17 0.15	0.12 0.1	0.076	0.075	0.121	0.05	0.075	0.3	0.0801		0.10–0.13 0.10–0.13	0.08 to 0.10	0.09	0.06	0.08	0.1
	α (dB/m) attenuation	9.5 15-45	4.3 "6-20"	2.6 1.5-4.5	6.9 9-27					12.8			0.1 0.108 0.105						
	wavelength										0.6 1 3		0.35 0.57 1.73						
dielectric property	K (relative)	13	6	3	5.5														
	Q (Quality factor)	7	20	30	7														
	ϵ (dielectric)					17.3										11	25		
	ϵ_r (real part of dielectric permittivity)												3.1 2.9 2.9						
	ϵ_s = electrical conductivity σ													0.6 2					
Performance param	P (m) penetration	1.5-1	4.5-2 18	4.5–4.5	2.5–1.5			10	–3			0.61			15			3.68	20-30
	r (m) wave	0.15–0.03	0.14–0.03	0.23–0.06	0.16–0.04														
Reference		Grandjean et al	Grandjean et al	Grandjean et al	Grandjean et al	Xu et al 2009	Mochales et al	El Qady et al 2005	Gizzi et al 2010	Leucci 2006	Kofman et al 2006	Yang et al 2009	Kofman et al 2006	Beres et al 2001	Batayneh et al 2002	Doolittle, 1997	Doolittle, 1998	Kinlaw et al 2007	Alfares et al 2002

Appendix C Choice of geophysical technique

Example Objectives	Seismic Refraction	Seismic Reflection	Ground Penetrating Radar	Electrical Resistivity	Electromagnetic Induction	Induced Polarization	Microgravity	Airborne Sensing	Magnetic Methods
Geologic mapping	①	①	①	①	②	②	②	②	②
Hydrogeology characteristics	①	②	①	①	③	②	③	na	na
Water table depth	①	②	②	①	③	na	②	②	na
Top of bedrock	①	②	③	①	③	②	③	③	na
Cavity detection	②	②	①	①	③	①	③	③	③
Disposal trench mapping	③	②	①	①	na	②	②	②	②
Nature of trench fill	③	na	①	①	?	①	na	①	①
Inorganic contaminant plume	na	na	①	①	?	na	②	na	na
Organic contaminant plume	na	na	②	?	?	na	②	na	na
Disposal container (metal drum)	na	na	①	②	③	③	na	①	①
Underground storage tanks	③	③	①	②	③	②	na	①	①
UXO detection	na	na	①	①	na	na	③	③	③
Coal "Void" Detection	2	1	2	2	3	1	3	3	3

KEY: ① = primary applicability; ② = secondary supporting applicability; ③ = limited applicability; na = no general applicability or not widely used; and ? = area of active research and rapidly evolving technology or questionable application.

→ (NRC 2002)

Table 11.1– Applicability of methods (adapted from National Research Council 2000 and 2002) (Butler, 2008).

Feature type	Mag area survey	Earth res survey	GPR	EM (cond)	Mag susc
other cavities	n	Y	Y	?	N

Table 11.2– Matching survey type to feature in the UK. ? = technique may work well in some conditions (David, 2008).

Application	Seismic Refraction	Seismic Reflect.	Seismic Tomo.	GPR	EM	Resist.	IP	SP	Mag.	Grav.
Mapping air-filled cavities, tunnels, (<10m depth)	x	x	x	M	x	M			x	
Mapping air-filled cavities, tunnels, (>10m depth)	x	M	M		x	x			x	
Mapping water-filled cavities, tunnels	X (P-wave)	M (P-wave)	M	x						
Mapping clay-filled cavities, tunnels	x	M	M		x	x				
Mapping abandoned underground mines		M	x			x				
Detecting abandoned Mine shafts		x	x	M	M	x		x		

Table 11.3– Application of geophysical techniques. M = major, x = minor application (Anderson & Ismail, 2003).

Appli cation	G ravity	Ma gnetic	Seis mic refraction	Sei smic reflection	Resi stivity	Sponta neous potential	Induc ed polarisation	M	M - VLF	PR	Ma gneto-telluric
Dete ction of subsurface cavities	s	m	s	m	P	m	m				!

Table 11.4– Application of geophysical techniques. P = primary, s = secondary, m = may not be best method or hasn't been developed, ! = not applicable (Reynolds, 1997).

Applica tion	G ravity	Ma gnetic	Sei smic refraction	Sei smic reflection	Resistivity and Induced polarisation	Self -potential	Radioa ctivity	M	E PR	G
Locatio n of cavities/voids	+	+	O	O	+	-	-			+

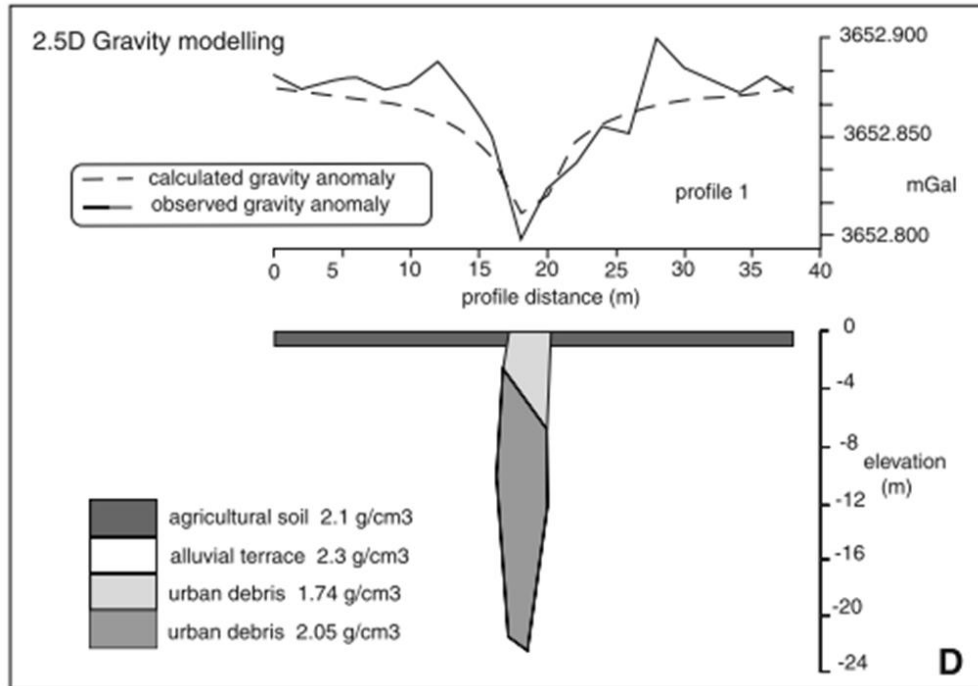
Table 11.5 - Application of geophysical techniques. + = applicable, O = limited applicability, - = not applicable (Sharma, 1997).

Applic ation	M icro Gravit y	Ma gnetic	Seis mic refraction	Seis mic reflection	Ea rth resistivit y	Self-potential, Vertical electrical sounding, induced polarisation	Rad ioactivity	M	E PR	G
Locati on of cavities/voi ds	P				P					

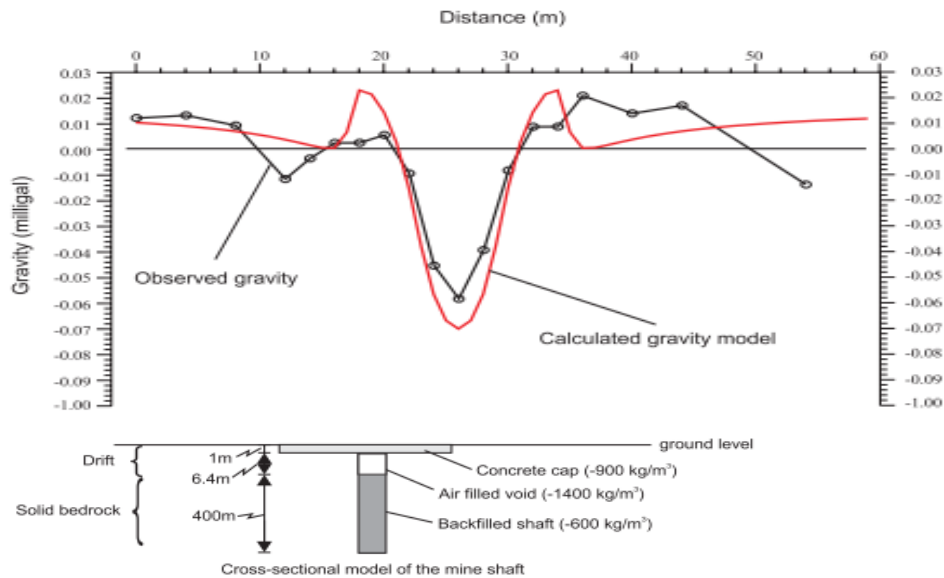
Table 11.6 - Application of geophysical techniques. P = primary method (Parasnis, 1996).

Appendix D Detection examples

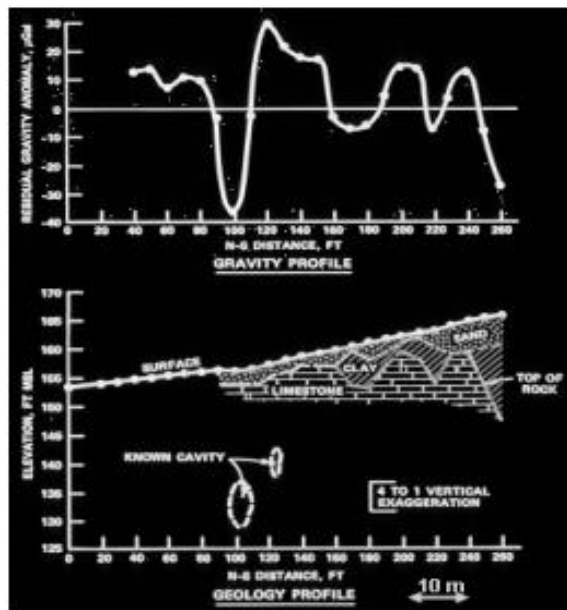
Gravity



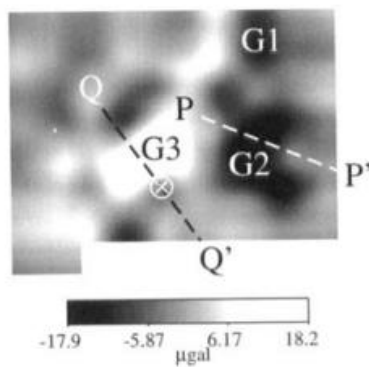
Observed and 2.5D modelled of a filled doline in north east Spain (Mochales *et al.*, 2007)



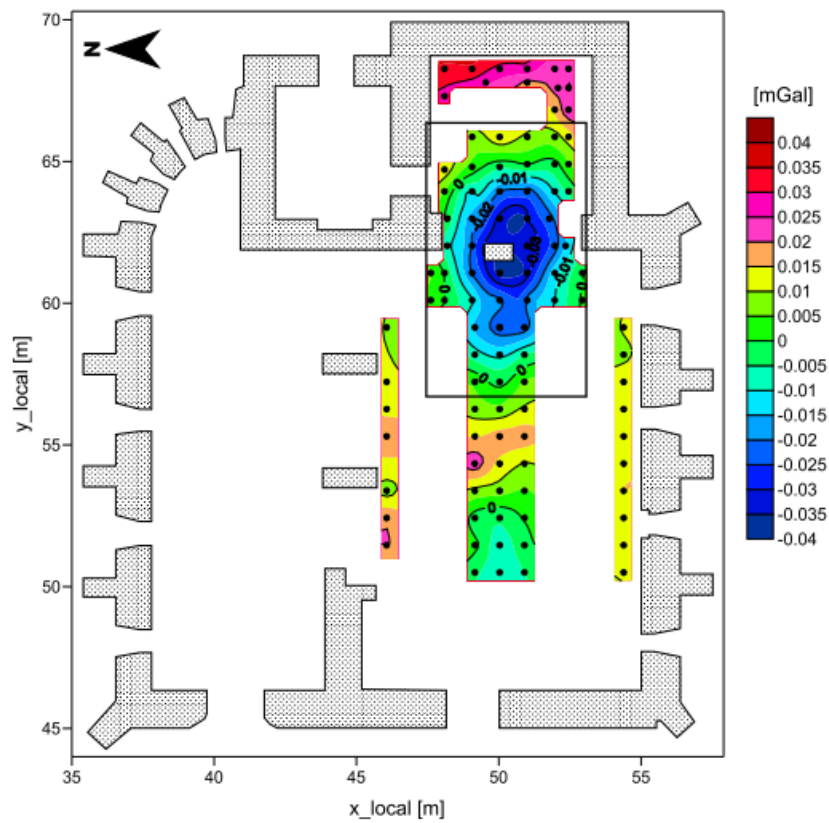
Observed and modelled gravity anomaly above a capped and filled mine-shaft used to find the backfill depth (TerraDat UK Ltd., 2005).



Matching of known geology with a gravity profile, showing anomaly related to cavities but also the deepening of bedrock ((Butler, 2008).



Cross section results of a gravity survey in Cornwall, UK. The results show negative gravity anomalies thought to represent air-filled voids.(Linford, 1998).

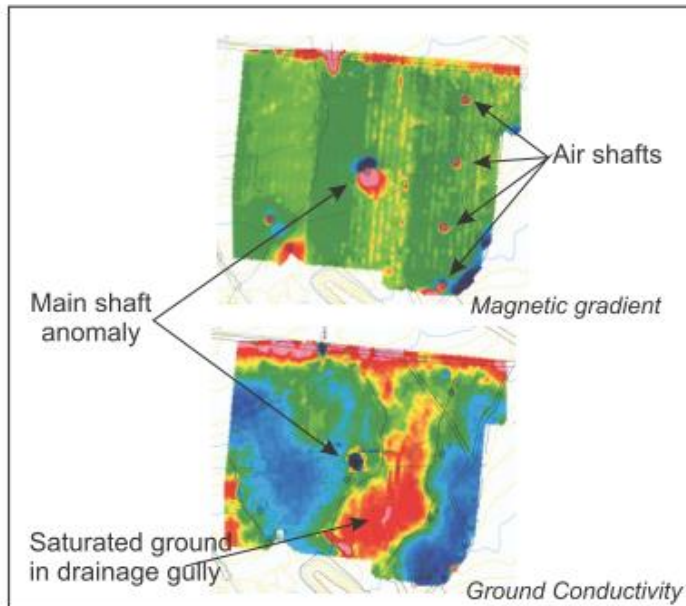


Resultant negative anomaly thought to be caused by an underground crypt in a church in Pukanec, Slovakia (Pánisová & Pašteka, 2009).



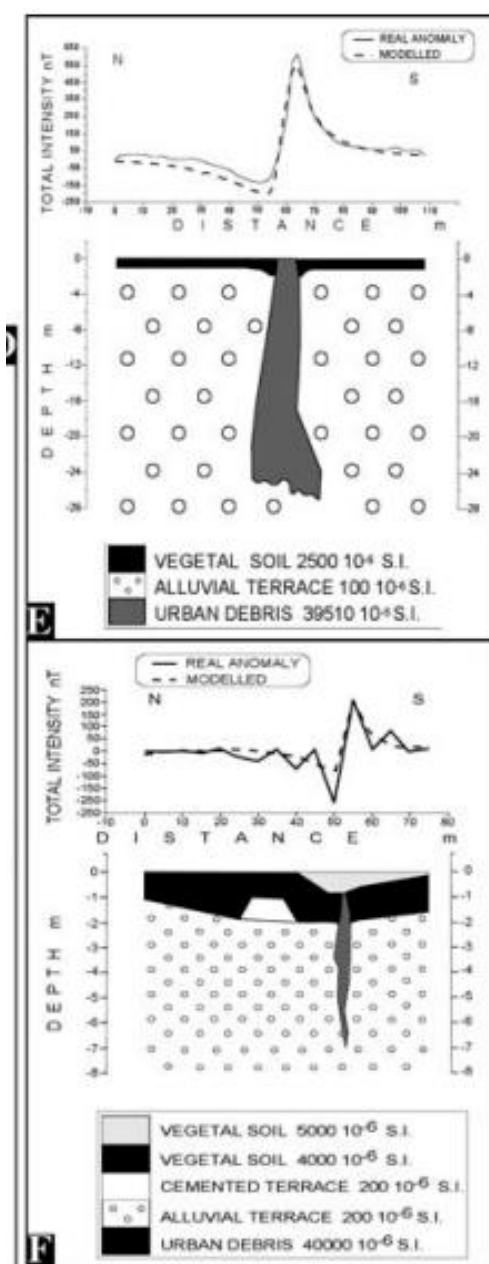
Resultant gravity anomaly over subsidence detected in an area with salt mining in Northwich, UK (Branston & Styles, 2003).

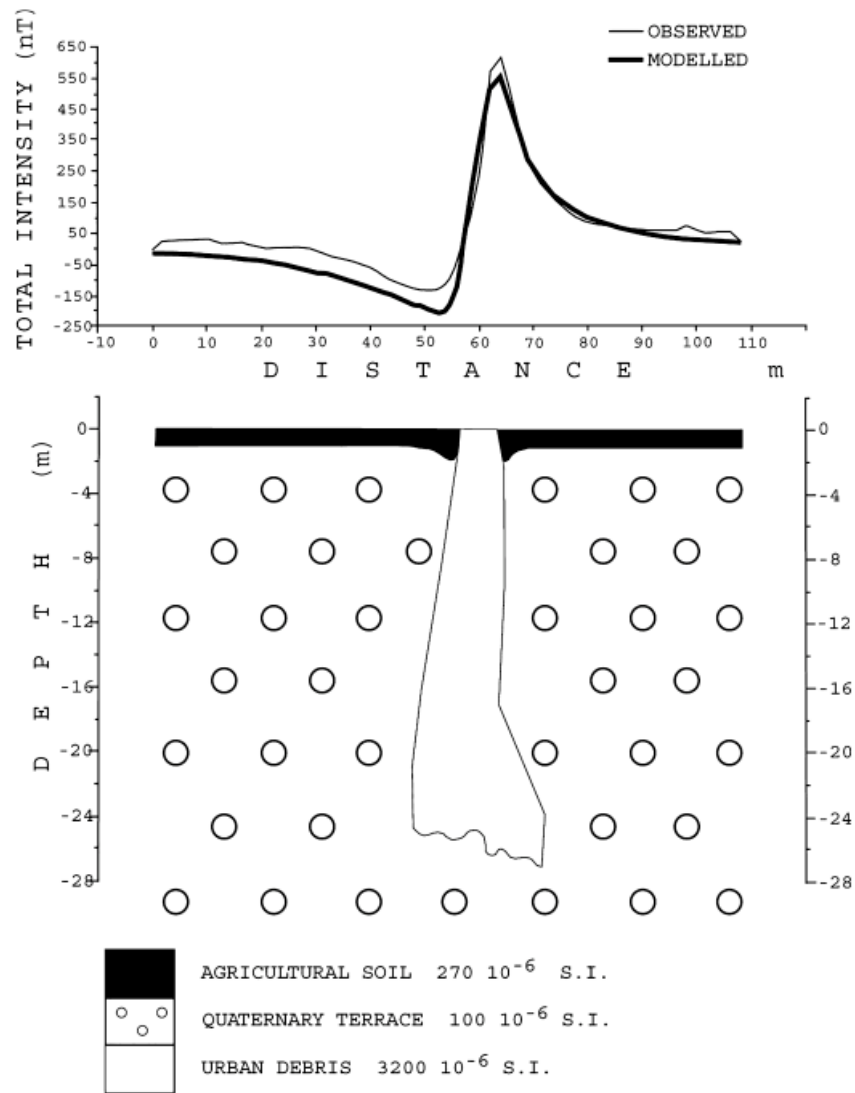
Magnetic



(ABOVE) A combined magnetic and conductivity survey was carried out over an abandoned colliery site in South Wales. A large shaft containing scrap metal is clearly evident in the centre of the site. In addition, four air shafts above an adit have been located using magnetic gradient mapping.

Magnetic gradient (and conductivity) results of a survey completed above and abandoned colliery in South Wales. The central shaft is easily identifiable as it contains scrap metal (TerraDat UK Ltd., 2005).





Magnetic results and subsequent modelling over a filled doline in (top) north-east Spain (Mochales, Casas, *et al.*, 2007) and (bottom) northern Spain (Mochales, Pueyo, *et al.*, 2007).

Appendix A Modelling code

Key programs are shown here. For all .m files or for these files in a more convenient way, please email the author.

i 2D polygon magnetic code

```
function [anom_z,anom_x,anom_t] = m_poly(xs,zs,x,z,N,CMT,INC,STR,SUS)
dtr=pi/180;
SUS=SUS/(4*pi);
c1=sin(INC*dtr);
c2=sin(STR*dtr)*cos(INC*dtr);
c3=2*SUS*CMT;
```

```

nstn = length(xs);
for is=1:nstn
xst=xs(is);
zst=zs(is);
hz=0;
hx=0;

for ic=1:N
x1=x(ic)-xst;
z1=z(ic)-zst;

if ic==N
x2=x(1)-xst;
z2=z(1)-zst;
else
x2=x(ic+1)-xst;
z2=z(ic+1)-zst;
end

if x1 == 0 & z1 == 0
    continue
else
    th1=atan2(z1,x1);

end

if x2 == 0 & z2 == 0
    continue
else th2=atan2(z2,x2);
end

if sign(z1) ~= sign(z2)
    test=x1*z2-x2*z1;
    if test > 0.0
        if z1 >= 0
th2=th2+2*pi;
        else
            continue
        end
    elseif test < 0.0
        if z2 >= 0
th1=th1+2*pi;

```

```

else
continue
end
else
continue
end
end

t12=th1-th2;
z21=z2-z1;
x21=x2-x1;
x21s=x21*x21;
z21s=z21*z21;
xz12=x1*z2-x2*z1;
r1s=x1*x1+z1*z1;
r2s=x2*x2+z2*z2;
r21s=x21*x21+z21*z21;
r1n=0.5*log(r2s/r1s);
p=(xz12/r21s)*((x1*x21-z1*z21)/r1s - (x2*x21-z2*z21)/r2s);
q=(xz12/r21s)*((x1*z21+z1*x21)/r1s - (x2*z21+z2*x21)/r2s);

if x21 == 0
dzz=-p;
dzx=q-z21s*r1n/r21s;
dxz=q;
dxx=p+z21s*t12/r21s;
else
z21dx21=z21/x21;
x21z21=x21*z21;
fz=(t12+z21dx21*r1n)/r21s;
fx=(t12*z21dx21-r1n)/r21s;
dzz=-p+x21s*fz;
dzx=q-x21z21*fz;
dxz=q-x21s*fx;
dxx=p+x21z21*fx;
end

hz=c3*(c1*dzz+c2*dzx) + hz;
hx=c3*(c1*dxz+c2*dxx) + hx;

end

anom_z(is)=hz;

```

```

anom_x(is)=hx;
anom_t(is)=c1*hz+c2*hx;

```

```

end
return

```

ii Polyhedron field calculation

(adapted via Singh & Guptasarma 2001)

```

%Program file: grvmag3d.m
%Comments: Program for simultaneous computation of gravity
%& magnetic fields from a 3-D polyhedron. With all distances
%in meters, model density in g/cm3, ambient magnetic induction
%and remnant magnetization in gamma, and the magnetic susceptibility
%in SI, it gives gravity fields in milligals and magnetic
%fields in gamma.

%preparedem3
%down_slope
trapezod
%slope
%prepdemeinat
%threebricks

%for i=1:2,close(figure(i)),end %clear old figures if present

Nedges=sum(Face(1:Nf,1)); Edge=zeros(Nedges,8);%create Edge for use later,
Nedges - number of edges of polyhedra
% Get edgelengths
for f=1:Nf %for each face
    indx=[Face(f,2:Face(f,1)+1) Face(f,2)];%vector of all the corners in each
    face, plus 1st corner again (to finish face)
    for t=1:Face(f,1)%for each edge on a face (ie 4 on a cube)
        edgeno=sum(Face(1:f-1,1))+t;% give the current edge number a number
        ends=indx(t:t+1);%find both ends (corners) of current edge
        p1=Corner(ends(1),:);%x y z coords of first corner
        p2=Corner(ends(2),:);%x y z coords of second corner
        V=p2-p1; L=norm(V);Edge(edgeno,1:3)=V;%find diff, normalise length, put x y
        z into Edge matrix
        Edge(edgeno,4) =L;%put length into Edge matrix
        Edge(edgeno,7:8)=ends;%put corner numbers into Edge matrix
    end
end
%create vectors perp to face

```

```

for t=1:Nf
    ss=zeros(1,3);
    for t1=2:Face(t,1) - 1;%from 2 to number of corners-1
        v1=Corner(Face(t,t1+2),:) - Corner(Face(t,2),:);%diff in coords of corners
        v2=Corner(Face(t,t1+1),:) - Corner(Face(t,2),:);
        ss=ss+cross(v2,v1); %vector perpendicular to face
    end
    Un(t,:)=ss./norm(ss); %normalised vectors perp to faces
end
clear v1 v2 ss

%create x and y grid
%[X,Y]=meshgrid(s_end:stn_spcng:n_end,w_end:prof_spcng:e_end);original
%[npro nstn]=size(X);

%set grav field to zero
if calgrv,Gx=zeros(size(X)); Gy=Gx; Gz=Gx;end

if calmag
    Hin=Hincl*pi/180; % change to radians
    Dec=Decl*pi/180;
    cx=cos(Hin)*cos(Dec); %x direction of decl and hin
    cy=cos(Hin)*sin(Dec);%x direction of decl and hin
    cz = sin(Hin);%x direction of decl and hin
    Uh=[cx cy cz];%vector direction of field
    H=Hintn .* Uh; % vector magnetic field strength
    Ind_magn=Susc.*H/(4*pi); % Induced magnetization (4pi for conversion of
susceptibility
http://en.wikipedia.org/wiki/Magnetic\_susceptibility#Conversion\_between\_SI\_and\_CGS\_units)

    Min=Mincl*pi/180; Mdec=Mdecl*pi/180;% in radians
    mcx=cos(Min) *cos(Mdec);% directions
    mcy=cos(Min)*sin(Mdec); mcz=sin(Min);
    Um=[mcx mcy mcz];
    Rem_magn=Mstrength .* Um; % Remnant magnetization
    Net_magn=Rem_magn+Ind_magn; % Net magnetization
    Pd=(Un * Net_magn')'; % perpendicular vector pole densities
    Hx=zeros(size(X)); Hy=Hx; Hz=Hx; %create matrix for total mag field
    clear cx cy cz Uh Hin Dec mcx mcy mcz Um Min Mdec Rem_magn Ind_mag Net_magn
end

%Comments: Now, for each observation point do the following:
%For each face find solid angle; for each side find p,q,r, and

```

```

%add p,q,r of sides to get P,Q,R for the face; if calmagD1, find
%hx,hy,hz; if calgrvD1, find gx,gy,gz. Add the components from
%all the faces to get Hx,Hy,Hz and Gx,Gy,Gz at the station.
for pr=1:ny %for all profiles
    curr_pr = pr;
    for st=1:nx %for all stations
        opt=[X(pr,st) Y(pr,st) 0];%x and y values at current observation point (0
for surface)
        fsign=zeros(1,Nf); Omega=zeros(1,Nf);
        for t=1:Ncor
            cor(t,:) = Corner(t,:) -opt; %diff in coords from corner to obbserveration
point
            end % shift origin

            for f=1:Nf%for all faces
                nsides=Face(f,1);% number of sides of face
                cors=Face(f,2:nsides+1);%corners for each face
                Edge(:,5:6)=zeros(Nedges,2); % Clear record of integration
                indx=[1:nsides 1 2];
                for t=1:nsides
                    crs(t,:)=cor(cors(t,:),:);%matrix of coords of corners of current side
                end
                %Find if the face is seen from inside
                fsign(f)=sign(dot(Un(f,:),crs(1,:)));
                % Find solid angle W subtended by face f at opt
                dp1=dot(crs(indx(1,:),:),Un(f,:)); %distance to face%cos of angle between
face and observation point to polyhedra
                dp=abs(dp1);
                if dp==0%at right angles
                    Omega(f)=0;
                end
                if dp~=0, W=0; %some other angle
                    for t=1:nsides%for each side of current face
                        p1=crs(indx(t,:),:); p2=crs(indx(t+1,:),:); p3=crs(indx(t+2,:),:);%coords for
current side and two after
                        W=W + angle(p1,p2,p3,Un(f,:)); %finds angle of polar coordinate coords
                    end
                    W=W-(nsides-2).*pi; %nsides - 2 because last loop added two more phase
angles
                    Omega(f)=-fsign(f)*W; %change back to solid angle (in degrees) for each
face
                end
                indx=[1:nsides 1 2]; %already defined
            end
        end
    end
end

```

```

for t=1:nsides
crs(t,:)=cor(cors(t),:);%already defined
end
% Integrate over each side, if not done, and save result
PQR=[0 0 0];
for t=1:nsides
p1=crs(indx(t),:); %coords of corner
p2=crs(indx(t+1),:);%coords of next corner
Eno=sum(Face(1:f-1,1))+t; % current Edge number ie total edge number of all
edges
if Edge(Eno,6)==1 %if the edge in the opp direction has already been
calculated
I2=Edge(Eno,5);
V=Edge(Eno,1:3);%vector direction of edge
pqr=I2 .* V; PQR=PQR+pqr;
end
if Edge(Eno,6) ~=1 %
chsgn=1; %change sign
if dot(p1,p2)/(norm(p1)*norm(p2))==1 % if origin,p1 & p2 are on a st line
if norm(p1)>norm(p2) % and p1 farther than p2
chsgn=-1; psave=p1; p1=p2; p2=psave;%interchange p1,p2
end
end
V=Edge(Eno,1:3); %vector direction of edge
L=Edge(Eno,4); L2=L*L;%edge length squared
b=2*(dot(V,p1));%2* angle b/t edge and corner to obs point
r1=norm(p1); r12=r1*r1; b2=b/L/2;
if r1+b2 == 0%because we can't divide by zero
V=-Edge(Eno,1:3);b=2*(dot(V,p1));b2=b/L/2;
end
if r1+b2 ~= 0
I2 = (1/L).* log ((sqrt(L2 + b + r12) + L + b2)./(r1 + b2));%from paper
end
s=find(Edge(:,7)== Edge(Eno,8) & Edge(:,8) ...
== Edge(Eno,7));%edge in opposite direction
I2=I2*chsgn; % change sign of I if p1,p2 were interchanged
Edge(Eno,5)=I2;Edge(s,5)=I2;Edge(Eno,6)=1;Edge(s,6)=1;%set edge in opp
direction the same I and Edge 6 as 1 so iteration ends
pqr=I2 .* V; %components of field for each edge
PQR=PQR+pqr;%total contribution from side
end
end
%From Omega,l,m,n,PQR, get components of field due to face f

```

```

l=Un(f,1);m=Un(f,2);n=Un(f,3);%x y z normalised direction of face
p=PQR(1,1);q=PQR(1,2);r=PQR(1,3);%x y z field contribution to each face
if calmag== 1
hx=Pd(f)*(l*Omega(f)+n*q-m*r); % x direction mag field for each side
Hx(pr,st)=Hx(pr,st)+hx;%total x direction mag field
hy=Pd(f)*(m*Omega(f)+l*r-n*p); Hy(pr,st)=Hy(pr,st)+hy;
hz=Pd(f)*(n*Omega(f)+m*p-l*q); Hz(pr,st)=Hz(pr,st)+hz;
end
if calgrv== 1
if dp~=0 %if distance to face is non-zero
gx=-dens*Gc*dp1*(l*Omega(f)+n*q-m*r);
Gx(pr,st)=Gx(pr,st)+ gx;
gy=-dens*Gc*dp1*(m*Omega(f)+l*r-n*p);
Gy(pr,st)=Gy(pr,st)+ gy;
gz=-dens*Gc*dp1*(n*Omega(f)+m*p-l*q);
Gz(pr,st)=Gz(pr,st)+ gz;
end
end
end,
end
end % end of faces, stns, profiles

```

```

if Gz<0
Gtotal=-sqrt((Gx).^2 + (Gy).^2 + (Gz).^2);
else Gtotal=sqrt((Gx).^2 + (Gy).^2 + (Gz).^2);
end
Htot=sqrt((Hx+H(1,1)).^2 + (Hy+H(1,2)).^2 + (Hz+H(1,3)).^2);
Dtotal=Htot-Hintn;

clear Susc calgrv calmag Nedges Ncor Nf Gx Gy Gz Hx Hy Hz Htot Pd V I2 pr st
dp dp1 gx gy gz hx hy hz lm n p q r Un PQR Edge Eno s chsgn r1 r12 b b2 L L2
psave p1 p2 t f indx W Omega crs cors fsign cor opt Corner Face edgeno ends

```

iii Simple sphere modelling code

```

for i=1:nx
x(i)=delx*(i-1);%position along the survey
end
for j=1:ny
y(j)=dely*(j-1);
end
z=abs(z0);

```

```

for i=1:nx
xi=(x(i)-x0);%distance from target
    for j=1:ny
        yj=(y(j)-y0); %depth of target
        g(j,i)=grav_sphere(xi,yj,z,a,rho1,rho0);% send values to function
    end
end

```

```

function f = grav_sphere(xi,yj,z,a,rho1,rho0)

```

```

g=0.00673;% gravitational constant
delrho=rho0-rho1;% change in density

```

```

%for sphere
    r2=xx*xx+yy*yy+zz*zz;
    r=sqrt(r2);
    rr3=mx*mx*mx;%radius cubed
    f=g*delrho*4*pi*rr3*zz/(3*r2*r);
end

```

iv Ground penetrating radar range code

Using theory in Daniels 2004

```

% model gpr signal

```

```

%tand

```

```

tandel=sigmal/(2*pi*frequency*E0*e1);

```

```

% propagation constants

```

```

attconst=2*pi*frequency*((E0*e1*mu0*mu1)/2)*(((1+tandel^2)^0.5)-1)^0.5;

```

```

b=2*pi*frequency*((E0*e1*mu0*mu1)/2)*(((1+tandel^2)^0.5)+1)^0.5;

```

```

k=attconst+imaginary*b;

```

```

%%%%%%%%%%%%%%%%%%%%%%%%%%%%%%%%%%%%%%%%%%%%%%%%%%%%%%%%%%%%%%%%%%%%%%%%

```

```

%impedance

```

```

ng=(mu0*mu1/(E0*e1*(1-tandel)))^0.5;% electrical impedance of ground (Ohms)

```

```

pg=(ng-n0)/(ng+n0);%ground refelective coefficient

```

```

tg=(2*ng)/(ng+n0);%ground transmission coefficient

```

```

%%%%%%%%%%%%%%%%%%%%%%%%%%%%%%%%%%%%%%%%%%%%%%%%%%%%%%%%%%%%%%%%%%%%%%%%

```

```

% target parameters

```

```

nt=(mu0*mu1/(E0*e0))^0.5;% electrical impedance of target (Ohms)

```

```

pt=(nt-ng)/(nt+ng);%target refelective coefficient

```

```

ta=Xcav*Ycav;% area of target

%%%%%%%%%%%%%%%%%%%%%%%%%%%%%%%%%%%%%%%%%%%%%%%%%%%%%%%%%%%%%%%%%%%%%%%%
%distance to target
j=1;
for ydist=0:dely:yl
    i=1;
    for xdist=0:delx:xl
        if xdist>=(xl/2)-(Xcav/2) && xdist<=(xl/2)+(Xcav/2) && ydist>=(yl/2)-(Ycav/2) && ydist<=(yl/2)+(Ycav/2) %above cavity
            R(i,j)=z0*1000;
        end
        if xdist>=(xl/2)-(Xcav/2) && xdist<=(xl/2)+(Xcav/2) && ydist<=(yl/2)-(Ycav/2)
            R(i,j)=(z0^2+(yl/2-Ycav/2-ydist)^2)^0.5)*1000;
        end
        if xdist>=(xl/2)-(Xcav/2) && xdist<=(xl/2)+(Xcav/2) && ydist>=(yl/2)+(Ycav/2)
            R(i,j)=(z0^2+(ydist-yl/2-Ycav/2)^2)^0.5)*1000;
        end
        if ydist>=(yl/2)-(Ycav/2) && ydist<=(yl/2)+(Ycav/2) && xdist<=(xl/2)-(Xcav/2)
            R(i,j)=(z0^2+(xl/2-Xcav/2-xdist)^2)^0.5)*1000;
        end
        if ydist>=(yl/2)-(Ycav/2) && ydist<=(yl/2)+(Ycav/2) && xdist>=(xl/2)+(Xcav/2)
            R(i,j)=(z0^2+(xdist-xl/2-Xcav/2)^2)^0.5)*1000;
        end

        if xdist<(xl/2-Xcav/2) && ydist<(yl/2-Ycav/2)
            R(i,j)=(z0^2+(((xl/2-Xcav/2)-xdist)^2+((yl/2-Ycav/2)-ydist)^2)^0.5)^2)^0.5)*1000;
        end
        if xdist<(xl/2-Xcav/2) && ydist>(yl/2+Ycav/2)
            R(i,j)=(z0^2+(((xl/2-Xcav/2)-xdist)^2+(ydist-(yl/2+Ycav/2))^2)^0.5)^2)^0.5)*1000;
        end
        if xdist>(xl/2+Xcav/2) && ydist>(yl/2+Ycav/2)
            R(i,j)=(z0^2+((xdist-(xl/2+Xcav/2))^2+(ydist-(yl/2+Ycav/2))^2)^0.5)^2)^0.5)*1000;
        end
        if xdist>(xl/2+Xcav/2) && ydist<(yl/2-Ycav/2)

```

```

R(i,j)=((z0^2+(((xdist-(x1/2+Xcav/2))^2+((y1/2-Ycav/2)-
ydist)^2)^0.5)^2)^0.5)*1000;
end
i=i+1;
end
j=j+1;
end

%%%%%%%%%%%%%%%%%%%%%%%%%%%%%%%%%%%%%%%%%%%%%%%%%%%%%%%%%%%%%%%%%%%%%%%%
% front surface reflection
vs=(V0/pw)*(1/C)*(aa/((pi*(radar_height/100)^2)*tand((theta/2))^2))*num_avg*
pg*10^-3;
efp=(pi*(((radar_height/1000)*tand(theta/2))*(1/(tand(asind((sind(theta/2)
/e1))))))+R/1000)*(tand(asind(sind(theta/2)/e1))))).^2);

for m=1:nx% for changing target size
for i=1:ny
x_gpr=(aa*ta*num_avg);
xefp=(x_gpr/efp(m,i));
V1=(1/C)*(V0/pw)*(xefp)*tg*pt*(10^-3);
V2=exp(-(2*k*(R(m,i)/1000)));
V3(m,i)=V1*V2';
end
end

```

v Set_parameters.m

```

%define all parameters from gui and standard parameters

x1 = findobj('Tag','survey_length');
x1 = get(x1,'string');
x1=sscanf(x1,'%f');
y1 = findobj('Tag','survey_width');
y1 = get(y1,'string');
y1=sscanf(y1,'%f');
zf = findobj('Tag','layer1_depth1');
zf = get(zf,'string');
zf=sscanf(zf,'%f');
% set depth at last point as z1
z1 = findobj('Tag','layer1_depth2');
z1 = get(z1,'string');
z1=sscanf(z1,'%f');
z2f = findobj('Tag','layer2_depth1');
z2f = get(z2f,'string');
z2f=sscanf(z2f,'%f');
% set depth at last point as z1
z2l = findobj('Tag','layer2_depth2');
z2l = get(z2l,'string');
z2l=sscanf(z2l,'%f');

```

```

z0 = findobj('Tag','cavity_depth');
z0 = get(z0,'string');
z0=sscanf(z0,'%f');
shaft_depth = findobj('Tag','shaft_depth');
shaft_depth = get(shaft_depth,'string');
shaft_depth=sscanf(shaft_depth,'%f');
Xcav = findobj('Tag','X_dimension');
Xcav = get(Xcav,'string');
Xcav=sscanf(Xcav,'%f');
Ycav = findobj('Tag','Y_dimension');
Ycav = get(Ycav,'string');
Ycav=sscanf(Ycav,'%f');
Zcav = findobj('Tag','Z_dimension');
Zcav = get(Zcav,'string');
Zcav=sscanf(Zcav,'%f');
X_shaft = findobj('Tag','shaft_X_dimension');
X_shaft = get(X_shaft,'string');
X_shaft=sscanf(X_shaft,'%f');
Y_shaft = findobj('Tag','shaft_Y_dimension');
Y_shaft = get(Y_shaft,'string');
Y_shaft=sscanf(Y_shaft,'%f');
Z_shaft = findobj('Tag','shaft_Z_dimension');
Z_shaft = get(Z_shaft,'string');
Z_shaft=sscanf(Z_shaft,'%f');
horiz_dip = findobj('Tag','horiz_cavity_dip');
horiz_dip = get(horiz_dip,'string');
horiz_dip=sscanf(horiz_dip,'%f');
time = findobj('Tag','survey_time');
time = get(time,'string');
time=sscanf(time,'%f');
cost = findobj('Tag','survey_cost');
cost = get(cost,'string');
cost=sscanf(cost,'%f');
delete_percentage = findobj('Tag','delete_perc');
delete_percentage = get(delete_percentage,'string');
delete_percentage=sscanf(delete_percentage,'%f');
delete_percentage=delete_percentage/100;
spacing = findobj('Tag','spacing_step');
spacing = get(spacing,'string');
spacing=sscanf(spacing,'%f');

%%%%%%%%%%%%%%%%%%%%%%%%%%%%%%%%%%%%%%%%%%%%%%%%%%%%%%%%%%%%%%%%%%%%%%%%%%%%%%
% Survey parameters
delx=0.1;
dely=0.1;
nx=x1/delx+1;%no. of stations
ny=y1/dely+1;%no. of profiles
[X,Y]=meshgrid(0:delx:x1,0:dely:y1);
x0=x1/2;
y0=y1/2;
% cavity parameters
cap_thickness=0.2;
line_thick=0.2;

load('C:\Documents and Settings\uces051\My Documents\MATLAB\cavity
model\data_files\Used\geology.mat')%rows: conductivity(S/m),dielectric
constant,em velocity(m/ns),density(Mg/m3),mag susc SI, mu, bulking
factor (decimal percentage)

```

```

% columns: typical, min, max
%geology{?}; 1 sandstone, 2 clay, 3 limestone, 4 concrete, 5 soil, 6
air, 7
%water 8 mining
%bulking factors from http://www.engineeringtoolbox.com/soil-rock-
bulking-factor-d_1557.html
%bulking factor for concrete 60%
http://www.wrap.org.uk/downloads/Site_Layout_Plan.e95ddfdf.1761.pdf

sigma1=geology{layer1_geology}(1,1);
e1=geology{layer1_geology}(2,1);
c1=geology{layer1_geology}(3,1);
rho1=geology{layer1_geology}(4,1);
susc_rock1=geology{layer1_geology}(5,1);

%cavity parameters
sigma=geology{cavity_makeup+5}(1,1);
e0=geology{cavity_makeup+5}(2,1);
c0=geology{cavity_makeup+5}(3,1);
rho0=geology{cavity_makeup+5}(4,1);
susc_cav=geology{cavity_makeup+5}(5,1);
mu=geology{cavity_makeup+5}(6,1);%set as 200 in geophysica

%GPR parameters
frequency=1*10^8;%100Mhz
%ground propagation parameters
E0=8.85419*10^-12;% permittivity of free space (F/m)
mu0=4*pi*10^-7;% mag constant (N/A^2)free space mag permeability
mul=1;%relative magnetic permeability - assumed to be unity in gpr
(Milsom)
imaginary=(-1)^0.5;%imaginary number
C=3*10^8;%speed of light in air m/s
n0=377;% electrical impedance of air (Ohms)

% antenna parameters
theta=20;
ar=0.15;% antenna radius
aa=pi*ar^2;% antenna area
% radar system params
V0=1000;%Ekko view value. peak radiated voltage (volts) Daniels pg
697=10V
pw=0.3*10^-9;% pulse width (ns)
num_avg=5; %number of averages
radar_height=0;% radar initial height

%%%%%%%%%%%%%%%%%%%%%%%%%%%%%%%%%%%%%%%%%%%%%%%%%%%%%%%%%%%%%%%%%%%%%%%%
% EM parameters
wxy=9.8; %9.8kHz is EM31 frequency. spatial plot frequency. also em34:
10m at 6.4 kHz

% switch layer1_geology
% case 1%sandstone
% sigma1=0.01;% Erkan and Jekeli (2011). also min conductivity
of dry sand S/m(min in Milsom 2011)
% e1=5;%dielectric constant/relative permittivity Erkan and
Jekeli (2011)but max of dry sand in Milsom 2011

```

```

%      c1=.15;% Martinez et al 1996. Or velocity of radar m/ns in
DRY Sand Milsom 2011
%      rho1=2.35;%density avg, min and max (siegel 1995). 2.5 in
Mg/m3 Erkan and Jekeli (2011)
%      susc_rock1=0.00002;%magnetic susceptibility SI Milsom (2011)
but Erkan and Jekeli (2011) diff
%      case 2%clay
%      sigma1=0.04350;%from eiggg test site
%      e1=5;%min of shales and clays in Milsom 2011
%      c1=.08;%for shales and clays Milsom 2011
%      rho1=2.21;%1.63-2.6 (SEigel 199%) or 1.5-2.2 Milsom 2011
%      susc_rock1=0.00001; % min in Milsom (2011)
%      case 3%limestone
%      sigma1=0.0001;%min in Milsom 2011
%      e1=8;%Erkan and Jekeli (2011) though 4-8 in (Milsom)
%      c1=.12;%Milsom 2011
%      rho1=2.55;%range 1.93-2.9 siegel 1995. or 2.65% avg in
Milsom 2011 (range 2.6-2.7 ),2.700 in Erkan and Jekeli (2011
%      susc_rock1=0.0001; % Erkan and Jekeli (2011). BUT Milsom
20110.5-2
%
%      case 4%concrete
%      sigma1=0.001;%min in reynolds
%      e1=7;%average from range 3-11 Portland 6-11, Asphalt 3-5
Carino (2010) OR
http://www.foundationperformance.org/pastpresentations/gehrig\_paper\_mar
ch2004.pdf
%      c1=0.1;%reynolds
%      rho1=2.3;%2.240-2.4 KOsmatka 2010 OR conventional concrete
http://hypertextbook.com/facts/1999/KatrinaJones.shtml
%      susc_rock1=0.00165; % average from concrete block McEnroe
1998
%      case 5%soil
%      sigma1=0;%0.01(5% water content ), 0.03(10%, 0.06(15%,
0.1(20%) (Tiejun et al 2000). typical water content is 15-45% Sands
2001
%      e1=4.5;%4-5 ludwig et al 2011
%      c1=0;%
%      rho1=1.92% 1.2-2.4 (Seiegel 1995). or 1.5;%Erkan and Jekeli
(2011)
%      susc_rock1=0.001; % Erkan and Jekeli (2011) ORRR Topsoil
magnetic susceptibility falls within a range of 5 - 30 x10-5 (SI)
http://www.eng-h.gov.uk/reports/tower\_hill/
%
%      chalk: sigma1
%      e1=2.1; http://www.ohmartvega.com/downloads/Forms-
Certificates/Dielectric\_Constants\_List.pdf
%      c1=0;%
%      rho1=2;% 1.9-2.1 from (J. J. Milsom & Eriksen, 2011)
%      susc_rock1=0.00003;% from (Olesen, 1996)
% end

sigma2=geology{layer2_geology}(1,1);
e2=geology{layer2_geology}(2,1);
c2=geology{layer2_geology}(3,1);
rho2=geology{layer2_geology}(4,1);
susc_rock2=geology{layer2_geology}(5,1);

```

```

sigma3=geology(layer3_geology)(1,1);
e3=geology(layer3_geology)(2,1);
c3=geology(layer3_geology)(3,1);
rho3=geology(layer3_geology)(4,1);
susc_rock3=geology(layer3_geology)(5,1);
%%%%%%%%%%%%%%%%%%%%%%%%%%%%%%%%%%%%%%%%%%%%%%%%%%%%%%%%%%%%%%%%%%%%%%%%
%cavity makeup

% switch cavity_makeup
%     case 1 %air
%         c0=.3;%Milsom 2011
%         e0=1;%Milsom 2011
%         sigma=0;%Milsom 2011
%         mu=1;%a vacuum is zero%air and water are non-ferrous so mag
permeability close to vacuum and hence relative permeability of 1%mag
permeability
%         rho0=0.0012252; %Mg/m^3 density air (at sea level and 15
degrees)- wiki
%         susc_cav=0;%Milsom, 2011,
%     case 2 %water (fresh)
%         c0=.033;%Milsom 2011
%         e0=80;%Milsom 2011
%         sigma=0.00005;%Milsom 2011
%         mu=1;%mu=-0.0000090;%
ref:http://info.ee.surrey.ac.uk/Workshop/advice/coils/mu/#sus
%         rho0=1;%Milsom 2011
%         susc_cav=-0.000009035;%water at 20 degrees
%     case 3 %soil
%         c0=.08;% Milsom
%         e0=4;%Erkan and Jekeli (2011)
%         sigma = 0.01;% min topsoil in Milsom 2011
%         mu = 200;% geophysica-
%         rho0=1.5;%value for topsoil (infill) Erkan and Jekeli (2011)
%         susc_cav=0.0000001;%min of topsoil in Milsom 2011, but 0.001
value for topsoil (infill) Erkan and Jekeli (2011)
% end

switch lining_makeup
    case 2 %wood
        ksusc_cap=0-susc_rock1;%
http://www.springerlink.com/content/q6m435w83036uu14/
        rho_cap=0.7-rho1;%http://www.simetric.co.uk/si_wood.htm
    case 3 %steel
        ksusc_cap=0.73-susc_rock1;%http://hyperphysics.phy-
astr.gsu.edu/hbase/tables/magprop.html
        rho_cap=7.085-rho1;%http://www.simetric.co.uk/si_metals.htm
    case 4 % concrete
        rho_cap=2.3-rho1;%2.240-2.4 KOsmatka 2010 OR conventional
concrete http://hypertextbook.com/facts/1999/KatrinaJones.shtml
        ksusc_cap=0.00165-susc_rock1; % average from concrete block McEnroe
1998
    case 5 % brick
        rho_cap=2.25-rho1;%mean from wolfram alpha
        ksusc_cap=0.001297-susc_rock1;% avg for baked loam brick (Hus
et al 2002). 0.06 to 0.5*10^-3SI mud bricks
end

ksusc=susc_cav-susc_rock1;

```

```

rho=rho0-rho1;
Hintn=47500;%uk 47500
Hincl=70;Decl=-5;%uk 70 ,-5
%spacing=1;%magnetic and gravity spacing
resist_type=3;%type of resistivity survey
I=1;%current of resistivity survey
Gc = 6.6732e-3; % Universal Gravitational constant

%%%%%%%%%%%%%%%%%%%%%%%%%%%%%%%%%%%%%%%%%%%%%%%%%%%%%%%%%%%%%%%%%%%%%%%%
%%%
% add noise
load('noise.mat')%rows are noise type, columns are method
load('west_wycombe_noise')% {1}by mauseleum, {2}by computer, {3}by
trees, {4}open
%grav noise from GEOPHYSICAL EXPLORATION FOR ENGINEERING AND
ENVIRONMENTAL
%INVESTIGATIONS 1995: instrumental 0.01  $\mu\text{m/s}^2$ , typical 0.05  $\mu\text{m/s}^2$ , but
new
%electronic 0.02-0.03  $\mu\text{m/s}^2$ , pessimist 0.08 to 0.1  $\mu\text{m/s}^2$ . hilly eastern
coal field on a rainy day, 0.22  $\mu\text{m/s}^2$ 
%of error is optimistic
% mccann, jackson, culshaw. size of anomaly detected. gravity:0.01mGal,
more realistic 0.03mGal
%also mag anom, lgamma, more realistically 5 gamma
% switch real_noise_choice
%     case 1%zero
%         mag_noise_scale=0;
%         mag_noise_grad_scale=0;
%         grav_noise_scale=0;
%         grav_grad_noise_scale=0;
%         gpr_noise=0;
%         em_phase_noise=0;
%         em_quad_noise=0;
%     case 2%instrumental
%         mag_noise_scale=0.01;
%         mag_noise_grad_scale=0.01;
%         grav_noise_scale=0.005;%0.01mGals, sensitivity of most manual
instruments Milsom. Automatic and microgravity meters manufacturers
claim 3 micro gals (Milsom)
%         grav_grad_noise_scale=1;
%         gpr_noise=1;
%         em_phase_noise=1;
%         em_quad_noise=1;
%     case 3%typical
%         mag_noise_scale=0.1;%Erkan
%         mag_noise_grad_scale=0.2;%Erkan
%         grav_noise_scale=0.1;%Laswell, S. et al. Recent observations
of increased seismic background noise using gPhone gravity meters.
(2008)
%         grav_grad_noise_scale=3;%Erkan
%         gpr_noise=10;%Erkan in micro volts
%         em_phase_noise=2;
%         em_quad_noise=2;
%     case 4% brownfield
%         mag_noise_scale=1.4;%Munschy, M. et al. Magnetic mapping for
the detection and characterization of UXO: Use of multi-sensor fluxgate
3-axis magnetometers and methods of interpretation. Journal of Applied
Geophysics 61, 168-183(2007).

```

```

%         mag_noise_grad_scale=3;
%         grav_noise_scale=1;
%         grav_grad_noise_scale=10;
%         gpr_noise=100;
%         em_phase_noise=3;
%         em_quad_noise=3;
%         case 5%rural
%             mag_noise_scale=0;%Munsch, M. et al. Magnetic mapping for
the detection and characterization of UXO: Use of multi-sensor fluxgate
3-axis magnetometers and methods of interpretation. Journal of Applied
Geophysics 61, 168-183(2007).
%             mag_noise_grad_scale=0;
%             grav_noise_scale=0;
%             grav_grad_noise_scale=0;
%             gpr_noise=0;
%             em_phase_noise=0;
%             em_quad_noise=0;
% end

```

vi Cavity.m

```

layer1_geology=1;
layer2_geology=1;
layer3_geology=1;
cavity_makeup=1;
cavity_type=1;
lining_makeup=1;
noise_scale=0;
noise_type=0;
real_noise_choice=1;
bulk_geometry=1;
limit_technique=1;
limit_parameters=1;
limit_running=0;
dip_diff=0;

addpath(genpath(' ../cavity model'))

parameters;

```

vii Parameters.m

```

% Opens a gui to input parameters

% open window
figure('Position',[10 500 1150 430],'Name','Set
Parameters','NumberTitle','off');

%draw cavity parameters box and title
uicontrol('Position',[10 200 205 220], ...
    'Style','frame');
uicontrol('Position',[50 400 120 15], ...
    'String','Cavity parameters', ...
    'Style','text', 'FontWeight' , 'Bold' );

% depth
uicontrol('Position',[20 360 100 15], ...

```

```

        'String','Depth to top (m)', ...
        'Style','text');
uicontrol('Position',[125 380 40 15], ...
        'String','Cavity', ...
        'Style','text');
uicontrol('Position',[125 360 40 15], ...
        'String','3', ...
        'Style','edit', ...
        'Tag','cavity_depth');
uicontrol('Position',[170 380 40 15], ...
        'String','Shaft', ...
        'Style','text');
uicontrol('Position',[170 360 40 15], ...
        'String','3', ...
        'Style','edit', ...
        'Tag','shaft_depth');

% dimensions
uicontrol('Position',[20 340 100 15], ...
        'String','X dimension (m)', ...
        'Style','text');
uicontrol('Position',[125 340 40 15], ...
        'String','0.5', ...
        'Style','edit', ...
        'Tag','X_dimension');
uicontrol('Position',[170 340 40 15], ...
        'String','0.5', ...
        'Style','edit', ...
        'Tag','shaft_X_dimension');
uicontrol('Position',[20 320 100 15], ...
        'String','Y dimension (m)', ...
        'Style','text');
uicontrol('Position',[125 320 40 15], ...
        'String','0.5', ...
        'Style','edit', ...
        'Tag','Y_dimension');
uicontrol('Position',[170 320 40 15], ...
        'String','0.5', ...
        'Style','edit', ...
        'Tag','shaft_Y_dimension');
uicontrol('Position',[20 300 100 15], ...
        'String','Z dimension (m)', ...
        'Style','text');
uicontrol('Position',[125 300 40 15], ...
        'String','0.5', ...
        'Style','edit', ...
        'Tag','Z_dimension');
uicontrol('Position',[170 300 40 15], ...
        'String','0.5', ...
        'Style','edit', ...
        'Tag','shaft_Z_dimension');

% makeup
uicontrol('Position',[20 280 100 15], ...
        'String','Makeup', ...
        'Style','text');
uicontrol('Callback','cavitymakeup', ...
        'Position',[125 280 80 15], ...

```

```

        'String','Air|Water|Mining|rubble', ...
        'Style','popup', ...
        'Tag','cavity_makeup');

% cavity shapetype
uicontrol('Position',[20 250 30 15], ...
        'String','Type', ...
        'Style','text');
uicontrol('Callback','cavitytype', ...
        'Position',[55 250 60 15], ...
        'String','Cube|Bellpit|Shaft|Capped shaft|Capped and lined
shaft|Horizontal tube', ...
        'Style','popup', ...
        'Tag','cavity_type');

% horizontal cavity dip
uicontrol('Position',[120 250 30 15], ...
        'String','Dip', ...
        'Style','text');
uicontrol('Callback','cavitytype', ...
        'Position',[170 250 40 15], ...
        'String','0', ...
        'Style','edit', ...
        'Tag','horiz_cavity_dip');

% lining type
uicontrol('Position',[20 220 100 15], ...
        'String','Cap and lining', ...
        'Style','text');
uicontrol('Callback','liningmakeup', ...
        'Position',[125 220 80 15], ...
        'String','None|Wood|Steel|Concrete|Brick', ...
        'Style','popup', ...
        'Tag','lining_makeup');

%%%%%%%%%%%%%%%%%%%%%%%%%%%%%%%%%%%%%%%%%%%%%%%%%%%%%%%%%%%%%%%%%%%%%%%%
% area text box
uicontrol('Position',[10 70 205 125], ...
        'Style','frame');
uicontrol('Position',[40 170 140 15], ...
        'String','Survey parameters', ...
        'Style','text', 'FontWeight', 'Bold' );

% survey width
uicontrol('Position',[20 140 100 15], ...
        'String','Width (m)', ...
        'Style','text');
uicontrol('Position',[125 140 40 15], ...
        'String','15', ...
        'Style','edit', ...
        'Tag','survey_width');

% survey length
uicontrol('Position',[20 120 100 15], ...
        'String','Length (m)', ...
        'Style','text');

```

```

uicontrol('Position',[125 120 40 15], ...
    'String','15', ...
    'Style','edit', ...
    'Tag','survey_length');

% survey time span
uicontrol('Position',[20 100 100 20], ...
    'String','Days', ...
    'Style','text');
uicontrol('Position',[125 100 40 15], ...
    'String','2', ...
    'Style','edit', ...
    'Tag','survey_time');

% survey cost
uicontrol('Position',[20 80 100 20], ...
    'String','Survey cost (£)', ...
    'Style','text');
uicontrol('Position',[125 80 40 15], ...
    'String','1500', ...
    'Style','edit', ...
    'Tag','survey_cost');

%%%%%%%%%%%%%%%%%%%%%%%%%%%%%%%%%%%%%%%%%%%%%%%%%%%%%%%%%%%%%%%%%%%%%%%%
%file name
uicontrol('Position',[430 30 100 40], ...
    'Style','frame');
uicontrol('Position',[440 50 80 15], ...
    'String','Save parameters as...', ...
    'Style','text');
uicontrol('Position',[450 35 60 15], ...
    'String','cavity1', ...
    'Style','edit', ...
    'Tag','gprfile');

%%%%%%%%%%%%%%%%%%%%%%%%%%%%%%%%%%%%%%%%%%%%%%%%%%%%%%%%%%%%%%%%%%%%%%%%
% geology parameters
uicontrol('Position',[220 200 300 220], ...
    'Style','frame');
uicontrol('Position',[240 400 240 15], ...
    'String','Subsurface parameters', ...
    'Style','text', 'FontWeight' , 'Bold' );

%table headings
uicontrol('Position',[230 360 60 20], ...
    'String','Depth (m)', ...
    'Style','text');
uicontrol('Position',[290 360 50 20], ...
    'String','Start', ...
    'Style','text');
uicontrol('Position',[350 360 50 20], ...
    'String','End', ...
    'Style','text');
uicontrol('Position',[410 360 50 20], ...
    'String','Geology', ...
    'Style','text');

```

```

% layer 1
uicontrol('Position',[230 340 60 15], ...
    'String','Layer 1', ...
    'Style','text');
uicontrol('Position',[300 340 40 15], ...
    'String','4', ...
    'Style','edit', ...
    'Tag','layer1_depth1');
uicontrol('Position',[360 340 40 15], ...
    'String','4', ...
    'Style','edit', ...
    'Tag','layer1_depth2');
uicontrol('Callback','layer1geology', ...
    'Position',[410 340 90 15], ...
    'String','Sandstone|Clay|Limestone|Concrete|Soil', ...
    'Style','popup', ...
    'Tag','layer1_geology');

% layer 2
uicontrol('Position',[230 310 60 15], ...
    'String','Layer 2', ...
    'Style','text');
uicontrol('Position',[300 310 40 15], ...
    'String','0.5', ...
    'Style','edit', ...
    'Tag','layer2_depth1');
uicontrol('Position',[360 310 40 15], ...
    'String','0.5', ...
    'Style','edit', ...
    'Tag','layer2_depth2');
uicontrol('Callback','layer2geology', ...
    'Position',[410 310 90 15], ...
    'String','Sandstone|Clay|Limestone|Soil', ...
    'Style','popup', ...
    'Tag','layer2_geology');

% layer 3
uicontrol('Position',[230 280 60 15], ...
    'String','Layer 3', ...
    'Style','text');
uicontrol('Callback','layer3geology', ...
    'Position',[410 280 90 15], ...
    'String','Sandstone|Clay|Limestone|Soil', ...
    'Style','popup', ...
    'Tag','layer3_geology');

%%%%%%%%%%%%%%%%%%%%%%%%%%%%%%%%%%%%%%%%%%%%%%%%%%%%%%%%%%%%%%%%%%%%%%%%
% add noise
uicontrol('Position',[220 30 195 165], ...
    'Style','frame');
uicontrol('Position',[250 170 140 15], ...
    'String','Noise', ...
    'Style','text', 'FontWeight' , 'Bold' );
% noise real
uicontrol('Callback','real_noise', ...
    'Position',[230 140 90 20], ...
    'String','Real', ...
    'Style','radiobutton', ...

```

```

        'Tag','real_noise',...
        'Value', 1);
uicontrol('Callback','realnoise', ...
    'Position',[310 140 90 15], ...
    'String','zero|instrumental|typical|brownfield|rural', ...
    'Style','popup', ...
    'Value', 2, ...
    'Tag','real_noise_choice');

% artificial noise
uicontrol('Callback','artificial_noise', ...
    'Position',[230 100 90 20], ...
    'String','Artificial', ...
    'Style','radiobutton', ...
    'Tag','artificial_noise');
uicontrol('Callback','noise', ...
    'Position',[310 100 90 20], ...
    'Style','slider', ...
    'Tag','noise_scale', ...
    'Value',0);
uicontrol('Position',[300 80 40 15], ...
    'String','Rural', ...
    'Style','text');
uicontrol('Position',[370 80 40 15], ...
    'String','Urban', ...
    'Style','text');

%deletion percentage
uicontrol('Position',[230 60 100 15], ...
    'String','Data deletion %', ...
    'Style','text');
uicontrol('Position',[360 60 40 15], ...
    'String','0', ...
    'Style','edit', ...
    'Tag','delete_perc');

uicontrol('Position',[230 40 100 15], ...
    'String','Spacing', ...
    'Style','text');
uicontrol('Position',[360 40 40 15], ...
    'String','1', ...
    'Tag','spacing_step',...
    'Style','edit');
%%%%%%%%%%%%%%%%%%%%%%%%%%%%%%%%%%%%%%%%%%%%%%%%%%%%%%%%%%%%%%%%%%%%%%%%

% push button "run" that invokes check_filename.m
uicontrol('Style','pushbutton','String','Run',...
    'Position', [430 160 50 30],...
    'Callback','check_filename');
% draw "show" button - invoking draw_subsurface.m
uicontrol('Style','pushbutton','String','Show',...
    'Position', [430 120 50 30],...
    'Callback','draw_subsurface;');
% draw "exit" button - invoking clear
uicontrol('Style','pushbutton','String','Exit',...
    'Position', [430 80 50 30],...
    'Callback','clear; close');

```

```

    % push button "limits" that invokes probdepthsize.m
    uicontrol('Style','pushbutton','String','Limits',...
        'Position',[1070 20 50 30],...
        'Callback','limit');
    %%%%%%%%%%%%%%%%%%%%%%%%%%%%%%%%%%%%%%%%%%%%%%%%%%%%%%%%%%%%%%%%%%%%%%%%%
    % draw graph
    axes('Position',[0.5 0.1 0.45 0.8]);

    %migration calc
    uicontrol('Position',[540 400 100 15], ...
        'String','Migration type', ...
        'Style','text');
    uicontrol('Callback','bulkgeometry', ...
        'Tag','bulk_geometry', ...
        'Position',[660 400 120 15], ...
        'String','Rectangular|Wedge|Conical', ...
        'Style','popup');
    draw_subsurface

```

viii Draw_subsurface.m

```

% draws an image of the subsurface and calculates the migration height
set_parameters
% clear speed x y z;
cla% clear current axis

max_depth(1)=(Zcav+dip_diff+z0)*1.2;%maximum depth of axis
max_depth(2)=zf+z2f;
max_depth(3)=zl+z2l;
max_depth(4)=(shaft_depth+Z_shaft)*1.2;
max_depth=max(max_depth);

view(3); axis([0 xl 0 yl -max_depth 0]); grid on;
alpha(.3)
hold on
patch([0,xl,xl,0], [yl,yl,0,0], [-zf,-zl,-zl,-zf], 'g'); alpha(.3)
patch([0,xl,xl,0], [yl,yl,0,0], [-zf-z2f,-zl-z2l,-zl-z2l,-zf-z2f],
'b'); alpha(.3)

% calculate migration height in loops based on piggott and Eynon 1978
in Bell 2004
% rectangular collapse
% H(migration height) (m)=h(height of void) (m)/bt(bulking
factor)(percentage as a decimal)

%cube
if cavity_type==1 || cavity_type==2
zt=-z0;%top of void
zb=-(z0+Zcav);%bottom of void
xw=x0-(Xcav/2);%west end of void
xe=x0+(Xcav/2);%east end of void
ys=y0-(Ycav/2);%south end of void
yn=y0+(Ycav/2);%north end of void
xcube=[xw xe xe xw xw xw;xw xe xe xw xw xw;xw xw xe xe xe xe;xw xw xe
xe xe xe];

```

```

ycube=[ys ys yn yn ys ys;ys ys yn yn yn yn;yn ys ys yn yn yn;yn ys ys
yn ys ys];
zcube=[zb zb zb zb zb zt;zt zt zt zt zb zt;zt zt zt zt zb zt;zb zb zb
zb zb zt];
for i=1:6
    patch(xcube(:,i),ycube(:,i),zcube(:,i),'k');
    alpha(.3)
end
H=bulk_geometry*Zcav/geology{layer1_geology}(7,1);
end

if cavity_type==2 || cavity_type==3 || cavity_type==4 || cavity_type==5
%shaft
zt=-shaft_depth; %height of bell pit section
zb=-(shaft_depth+Z_shaft);%shaft bottom
xe=x0+(X_shaft/2);
xw=x0-(X_shaft/2);
yn=y0+(Y_shaft/2);
ys=y0-(Y_shaft/2);
xcube=[xw xe xe xw xw xw;xw xe xe xw xw xw;xw xw xe xe xe xe;xw xw xe
xe xe xe];
ycube=[ys ys yn yn ys ys;ys ys yn yn yn yn;yn ys ys yn yn yn;yn ys ys
yn ys ys];
zcube=[zb zb zb zb zb zt;zt zt zt zt zb zt;zt zt zt zt zb zt;zb zb zb
zb zb zt];
for i=1:6
    patch(xcube(:,i),ycube(:,i),zcube(:,i),'k');
    alpha(.3)
end
H=bulk_geometry*Z_shaft/geology{layer1_geology}(7,1);
if cavity_type==2 %bellpit
    H=bulk_geometry*(Z_shaft+Zcav)/geology{layer1_geology}(7,1);
end
end

if cavity_type==4 || cavity_type==5
%cap
zt=-shaft_depth+cap_thickness; %height cap
zb=-(shaft_depth);%cap bottom
xe=x0+(X_shaft/2);
xw=x0-(X_shaft/2);
yn=y0+(Y_shaft/2);
ys=y0-(Y_shaft/2);
xcube=[xw xe xe xw xw xw;xw xe xe xw xw xw;xw xw xe xe xe xe;xw xw xe
xe xe xe];
ycube=[ys ys yn yn ys ys;ys ys yn yn yn yn;yn ys ys yn yn yn;yn ys ys
yn ys ys];
zcube=[zb zb zb zb zb zt;zt zt zt zt zb zt;zt zt zt zt zb zt;zb zb zb
zb zb zt];
for i=1:6
    patch(xcube(:,i),ycube(:,i),zcube(:,i),'r');
    alpha(.3)
end
end
if cavity_type==5
%cap
zt=-shaft_depth; %height cap
zb=-(shaft_depth+Z_shaft);%shaft bottom

```

```

xe=x0+line_thick+(X_shaft/2);
xw=x0-line_thick-(X_shaft/2);
yn=y0+line_thick+(Y_shaft/2);
ys=y0-line_thick-(Y_shaft/2);
xcube=[xw xe xe xw xw xw;xw xe xe xw xw xw;xw xw xe xe xe xe;xw xw xe
xe xe xe];
ycube=[ys ys yn yn ys ys;ys ys yn yn yn yn;yn ys ys yn yn yn;yn ys ys
yn ys ys];
zcube=[zb zb zb zb zb zt;zt zt zt zt zb zt;zt zt zt zt zb zt;zb zb zb
zb zb zt];
for i=1:6
    patch(xcube(:,i),ycube(:,i),zcube(:,i),'r');
    alpha(.3)
end
end

%horizontal tube
if cavity_type==6
    zt=-z0;%top of void
    zb=-(z0+Zcav);%bottom of void
    xw=x0-(Xcav/2);%west end of void
    xe=x0+(Xcav/2);%east end of void
    ys=y0-(Ycav/2);%south end of void
    yn=y0+(Ycav/2);%north end of void
    xw_slant=xw+Xcav/3;%west end of slant
    xe_slant=xw_slant+Xcav/3;%west end of slant
    z_slant=zt-Zcav/3;%bottom of slant
    dip_diff=tand(horiz_dip)*yl/2;%change in depth from centre
    xcube=[xw xe xe xw xw xw_slant;xw xe xe xw xw xw_slant;xw xe_slant xe
xw_slant xe xe_slant;xw xw_slant xe xe_slant xe xe_slant;0 xw 0 xe 0
0;0 xw 0 xe 0 0];
    ycube=[ys ys yn yn ys ys;ys ys yn yn yn yn;yn ys ys yn yn yn;yn ys ys
yn ys ys;0 ys 0 yn 0 0;0 ys 0 yn 0 0];
    zcube=[zb+dip_diff zb+dip_diff zb-dip_diff zb-dip_diff zb+dip_diff
zt+dip_diff;z_slant+dip_diff z_slant+dip_diff z_slant-dip_diff z_slant-
dip_diff zb-dip_diff zt-dip_diff;z_slant-dip_diff zt+dip_diff
z_slant+dip_diff zt-dip_diff zb-dip_diff zt-dip_diff;zb-dip_diff
zt+dip_diff zb+dip_diff zt-dip_diff zb+dip_diff zt+dip_diff;0
z_slant+dip_diff 0 z_slant-dip_diff 0 0;0 zb+dip_diff 0 zb-dip_diff 0
0];
    for i=[1,3,5,6]
        patch(xcube(1:4,i),ycube(1:4,i),zcube(1:4,i),'k');
    end
    for i=[2,4]
        patch(xcube(:,i),ycube(:,i),zcube(:,i),'k');
    end
    alpha(.3)
    H=bulk_geometry*Zcav/geology{layer1_geology}(7,1);
end

%draw possible migration
uicontrol('Position',[930 400 220 15], ...
    'String','Black=cavity, green=crowning limit', ...
    'Style','text');

migrate_depth=(-zt)-H;
zb=zt;%bottom of void
zt=-migrate_depth;%top of migration

```

```

if zt>=0 %ie migration crowns
    uicontrol('Position',[950 380 180 15], ...
        'String','Possible crowning of cavity', ...
        'Style','text');
    %    zt=0;
else
    uicontrol('Position',[950 380 180 15], ...
        'String','No crowning of cavity', ...
        'Style','text');
end

bulk_change_x=0;
bulk_change_y=0;
if bulk_geometry==2
    bulk_change_x=abs(xe-xw)/2;
    bulk_change_y=0;
end
if bulk_geometry==3
    bulk_change_x=abs(xe-xw)/2;
    bulk_change_y=abs(yn-ys)/2;
end

xcube=[xw xe xe xw xw xw+bulk_change_x;xw+bulk_change_x xe-
bulk_change_x xe-bulk_change_x xw+bulk_change_x xw
xw+bulk_change_x;xw+bulk_change_x xw+bulk_change_x xe-bulk_change_x xe-
bulk_change_x xe xe-bulk_change_x;xw xw xe xe xe xe-bulk_change_x];
ycube=[ys ys yn yn ys ys+bulk_change_y;ys+bulk_change_y
ys+bulk_change_y yn-bulk_change_y yn-bulk_change_y yn yn-
bulk_change_y;yn-bulk_change_y ys+bulk_change_y ys+bulk_change_y yn-
bulk_change_y yn yn-bulk_change_y;yn ys ys yn ys ys+bulk_change_y];
zcube=[zb zb zb zb zb zt;zt zt zt zt zb zt;zt zt zt zt zb zt;zb zb zb
zb zb zt];
for i=1:6
    patch(xcube(:,i),ycube(:,i),zcube(:,i),'k','FaceColor','g');
    alpha(.3)
end

rotate3d on
ylabel('Width (m)')
zlabel('Depth (m)')
xlabel('Length (m)')

clear max_depth zt zb xw xe ys yn xcube ycube zcube H migrate_depth
bulk_change_x bulk_change_y

```

ix Check_filename.m

```

% redraws subsurface, checks if file exists, either closes or
overwrites
% and starts modelling
draw_subsurface;
gprfile = findobj(gcf,'Tag','gprfile');
filenm = get(gprfile,'string');
fid=fopen(filenm);
clear gprfile filenm

```

```

if fid == -1
    clear fid
    start;
else
    clear fid
figure('Position',[500 500 180 100],'Menubar','none');
uicontrol('Position',[10 65 150 15], ...
    'String','File exists. Overwrite?', ...
    'Style','text');
uicontrol('Callback','start', ...
    'Position',[30 20 40 40], ...
    'String','Yes');
uicontrol('Callback','close', ...
    'Position',[90 20 40 40], ...
    'String','No');
end

```

x Start.m

```

%start modelling
close

mag_sim
gpr_volt
em_sim
resist_sim

data={Dt, Dt_grad, Gtot, grav_grad,hr,hi,abs(V3)};
probability_calc
plot_data

```

xi Probability_calc.m

```

%calculate the detection probability
nsamples=100;%number of iterations of monte carlo simulation
for i=1:7 %for each technique
    for k=1:nsamples%start monte carlo loop
        if i==3 || i==4%spacing for gravity measurements

sample=data{i}(randi(spacing*10,1,1):spacing*10:end,randi(spacing*10,1,
1):spacing*10:end);
            else%spacing for other techniques
                sample=data{i}(randi(spacing*10,1,1):spacing*10:end,:);
            end

sample(randperm(numel(sample),round(numel(sample)*(delete_percentage)))
)=NaN;%delete percentage
        if i<=6
            for j=1:length(sample(:,1))
                rms=sqrt(nanmean(sample(j,:).^2));%root mean square

erf_data{i}(j)=erf(0.5*sqrt(rms/noise(real_noise_choice,i)));%error
function
            end
            erf_data{i}(isnan(erf_data{i}))=0;%change those lines where
no value was taken to zero probability

```

```

        prob{i}(k)=1-(prod(1-erf_data{i}));%total probability of
detection for this run of simulation
    else%gpr
        for m=1:length(sample(:,1))
            for n=1:ny

SNR(m,n)=abs(sample(m,n)/noise(real_noise_choice,7));%signal to noise
ratio for each GPR survey point
                erf_data{7}(m,n)=abs(erf(SNR(m,n)));
            end
        end
        erf_data{i}(isnan(erf_data{i}))=0;%change those lines where
no value was taken to zero probability
        prob{i}(k)=1-(prod(prod(1-erf_data{7})));%total probability
of detection for this run of simulation
    end

end
% %draws histogram of probability for all runs of simulations
%     figure;
%     hist(prob{i},50)
data_prob(i,:)=prob{i};
    prob_total(i)=mean(prob{i});%total prob
    sample_test(i)=sample;
    clear rms SNR sample erf_data
end
clear nsamples

```

xii Plot_data.m

```

%plot images
% open window
scrsz = get(0,'ScreenSize');
figure('OuterPosition',[1 scrsz(4)/4 scrsz(3)/2
3*scrsz(4)/4],'Name','Results');
zlabel1= cellstr(['Magnetic (nT)'; 'Mag grad (nT)'; 'Gravity (mG)';
'Grav grad (E)'; 'Em phase (nT)'; 'Em quad (nT)'; 'Gpr (microV) ']);
for i=1:6%calc erf for all techniques across area
    for j=1:ny
        rms=sqrt(mean(data{i}(j,:).^2));%root mean square

erf_data_1{i}(j,1)=erf(0.5*sqrt(rms/noise(real_noise_choice,i)));%error
function
    end
    for j=1:nx
        erf_data_1{i}(:,j)=erf_data_1{i}(:,1);
    end
end
for m=1:nx%calc gpr erf across survey
    for n=1:ny
        SNR(m,n)=abs(data{7}(m,n)/noise(real_noise_choice,7));%signal
to noise ratio for each GPR survey point
        erf_data_1{7}(m,n)=abs(erf(SNR(m,n)));
    end
end
end

```

```

for i=1:7%plot
    subplot(3,3,i);
    if i==7
        plot3k({X' Y' data{i}},erf_data_1{i}*100,[0 100],{'o',1},5);
    else
        plot3k({X Y data{i}},erf_data_1{i}*100,[0 100],{'o',1},5);
    end
    xlabel('X distance(m)')
    ylabel('Y distance(m)')
    zlabel(zlabell(i))
    title(['Detection probability: ', num2str(prob_total(i)*100)],'')
end

%plot apparent resistivity
subplot(3,3,[8 9]);
xlin=linspace(min(app(:,1)),max(app(:,1)),100);
ylin=linspace(min(app(:,2)),max(app(:,2)),100);
[Xres,Yres]=meshgrid(xlin,ylin);
Zres=griddata(app(:,1),app(:,2),app(:,3),Xres,Yres,'cubic');
mesh(Xres,Yres,Zres);
contourf(Xres,-Yres,Zres)
colorbar

rotate3d on

clear erf_data_1 erf_data_1 zlabell rms %clear ready for replotting

% back button closes window and clears data
uicontrol('Callback','close;', ...
    'Position',[230 15 50 30], ...
    'String','Back');
% compare button keeps window open and clears data
uicontrol('Callback','movegui("southeast")', ...
    'Position',[290 15 50 30], ...
    'String','Compare');
% field button keeps window open and clears data
uicontrol('Callback','field;', ...
    'Position',[350 15 50 30], ...
    'String','Field');
% field button keeps window open and clears data
uicontrol('Callback','replot_options;', ...
    'Position',[410 15 50 30], ...
    'String','Replot');

```

xiii Field.m

```

%calculate the time and cost required in field

%disatnce or no. of stations for each technique
measurements([1 2 5 6 7])=xl*(yl/spacing);%in meters
measurements(3)=(xl*yl)/spacing^2;%in stations
measurements(4)=2*(xl*yl)/spacing^2;%in stations

time(1)=measurements(1)/40000;%in days
time(2)=measurements(2)/40000;%in days

```

```

time(3)=measurements(3)/100;%in days
time(4)=measurements(4)/100;%in days might be faster
time(5)=measurements(5)/40000;%in days
time(6)=measurements(6)/40000;%in days
time(7)=measurements(7)/1512;%in days
for i=1:7
    if time(i)<=1
        time(i)=time(i)*24;
        time_unit{i}={'hours'};
    else
        time_unit{i}={'days'};
    end
end

cost(1)=376.83/7*time(1);
cost(2)=376.83/7*time(2);
cost(3)=669.92/7*time(3);
cost(4)=669.92/7*time(4);
cost(5)=669.92/7*time(5);
cost(6)=669.92/7*time(6);
cost(7)=376.83/7*time(7);

scrsz = get(0,'ScreenSize');
figure('OuterPosition',[scrsz(3)/2 scrsz(4)/2 scrsz(3)/4
scrsz(4)/2],'Name','Field','NumberTitle','off');

for i=0:spacing:xl
    subplot(2,1,1);plot(i,0:dely:yl,'--','color','k')
    subplot(2,1,1);plot(i,0:spacing:yl,'.','MarkerSize',10,'color',
'r')
    hold on
end
xlabel('East (m)');
ylabel('North (m)');
title('Field measurements');

zlabel1= cellstr(['Magnetic'; 'Mag grad'; 'Gravity '; 'Grv grad'; 'Em
phase'; 'Em quad '; 'Gpr      ']);

for i=1:7
    uicontrol('Position',[10 i*15 410 15], ...
        'String',['Time for ' zlabel1{i} ' = ' num2str(time(i), '%.2f')
time_unit2{i} '. Rental cost = £' num2str(cost(i), '%.2f')], ...
        'Style','text', 'FontWeight' , 'Bold' );
end

```

xiv Limit.m

```

%open option window for limit of depth and size study
scrsz = get(0,'ScreenSize');
figure('Position',[scrsz(4)/2 scrsz(4)/2 scrsz(3)/4
scrsz(4)/4],'Name','Limit parameters','NumberTitle','off');
uicontrol('Position',[40 200 150 15], ...
    'String','Parameter to alter', ...
    'Style','text');
uicontrol('Callback','limitparameter', ...

```

```

        'Tag','limit_parameter', ...
        'Position',[200 200 120 15], ...
        'String','Noise|Geology|Spacing|Delete %', ...
        'Style','popup');
uicontrol('Position',[40 170 150 15], ...
        'String','Technique', ...
        'Style','text');
uicontrol('Callback','limittechnique', ...
        'Tag','limit_technique', ...
        'Position',[200 170 120 15], ...
        'String','magnetic|Gravity|GPR', ...
        'Style','popup');
uicontrol('Position',[40 135 150 15], ...
        'String','Limit percentage', ...
        'Style','text');
h1=uicontrol('Position',[200 135 40 15], ...
        'String','0.95', ...
        'Style','edit');
% push button "limit" that invokes probdepthsize.m
uicontrol('Style','pushbutton','String','Run limit',...
        'Position',[100 100 100 30],...
        'Callback','probdepthsize');
uicontrol('Position',[40 80 150 15], ...
        'String','This will take some time', ...
        'Style','text');

```

xv Probdepthsize.m

```

% Runs a loop to calculate the minimum size cavity required to reach a
% certain probability limit
clear prob_depth_size

limit_percentage=get(h1,'String');
limit_percentage= str2num(limit_percentage);
close; %close option window

limit_running=1;%for a test to see if a limit is running
[Dt, Dt_grad, Gtot, grav_grad,hr,hi,V3]=deal(zeros(nx)+1);%+1 to
prevent errors from not postive numbers
if limit_parameters==1, start_parameter=4;%
else start_parameter=1;
end
add=0.1;%start cavity size (0.6 for mag)
depth_increase=1;
cavity_increase=0.2;
maximum_depth=15;
start_depth=1;
maximum_cavity_size=30;

for changing_parameter=start_parameter:4%
switch limit_parameters
case 1, real_noise_choice=changing_parameter;
case 2, layer1_geology=changing_parameter;
case 3, spacing=changing_parameter;
case 4, delete_percentage=changing_parameter/10;
end
signal=geology{layer1_geology}(1,1);

```

```

e1=geology(layer1_geology)(2,1);
c1=geology(layer1_geology)(3,1);
rho1=geology(layer1_geology)(4,1);
susc_rock1=geology(layer1_geology)(5,1);
ksusc=susc_cav-susc_rock1;
rho=rho0-rho1;

for z0=start_depth:depth_increase:maximum_depth%increase depth
    prob_total=[0,0,0,0,0,0,0];count=1;%count2=1;
    for j=add:cavity_increase:maximum_cavity_size% size of cavity
        tic% start timer
        Xcav=j;Ycav=Xcav;Zcav=Xcav;%set cavity dimensions (only cube)
        z0
        Xcav

% Model signal if prob still less than 95%
        if min(prob_total(7))<=limit_percentage
            if limit_technique<=2, mag_sim
                else gpr_volt
                    z0
                end
            end
        end

%
% Calculate probability of detection
        data={Dt, Dt_grad, Gtot, grav_grad,hr,hi,abs(V3)};
        probability_calc
%if prob greater than 95% change start position for next time
        if limit_parameters==2, addition=0.1; %if geology parameter always
            start a cavity size 0.1
        else
            if prob_total(7)>=limit_percentage
                addition(count)=Xcav;
                count=count+1;
            end
        end
    end

    prob_depth_size(changing_parameter)(round(z0*(1/depth_increase)),round(
    Xcav*(1/cavity_increase)))=prob_total(7);
    %
        toc

        if prob_total(7)>limit_percentage
            break
        end

    end
    add=addition(1);

end

end
clear add addition changing_parameter maximum_depth start_depth
maximum_cavity_size count
drawdepthsize;

```

xvi Executable GPR

```
%set parameters

load('geology')
load('noise')

% layer1_geology=1;
% cavity_makeup=1;
Xcav=size;
Ycav=size;
z0=depth;

real_noise_choice=4;
yl=15;
xl=15;
spacing=1;
delete_percentage=0;
dely=0.1;
delx=0.1;
nx=(xl/delx)+1;
ny=(yl/dely)+1;
[X,Y]=meshgrid(0:delx:xl,0:dely:yl);
sigma1=geology{layer1_geology}(1,1);
e1=geology{layer1_geology}(2,1);
c1=geology{layer1_geology}(3,1);

%cavity parameters
sigma=geology{cavity_makeup+5}(1,1);
e0=geology{cavity_makeup+5}(2,1);
c0=geology{cavity_makeup+5}(3,1);
mu=geology{cavity_makeup+5}(6,1);%set as 200 in geophysica

%GPR parameters
frequency=1*10^8;%100Mhz
%ground propagation parameters
%d=2000;tandel=tan((d+0.01)/1000);% tand for soil=0.1, for second layer of
soil=0.5 page 17 daniels,more on pg 42
% tandel=sigma1/(2*pi*frequency*e1)
E0=8.85419*10^-12;% permittivity of free space (F/m)
mu0=4*pi*10^-7;% mag constant (N/A^2)free space mag permeability
mu1=1;%relative magnetic permeability - assumed to be unity in gpr (Milsom)
imaginary=(-1)^0.5;%imaginary number
```

```

C=3*10^8;%speed of light in air m/s
n0=377;% electrical impedance of air (Ohms)

% antenna parameters
theta=20;
ar=0.15;% antenna radius
aa=pi*ar^2;% antenna area
% radar system params
V0=1000;%Ekko view value. peak radiated voltage (volts) Daniels pg 697=10V
pw=0.3*10^-9;% pulse width (ns)
num_avg=5; %number of averages
radar_height=0;% radar initial height
% model gpr signal

%tand
tandel=sigma1/(2*pi*frequency*E0*e1);

% propagation constants
attconst=2*pi*frequency*((E0*e1*mu0*mu1)/2)*(((1+tandel^2)^0.5)-1))^0.5;
b=2*pi*frequency*((E0*e1*mu0*mu1)/2)*(((1+tandel^2)^0.5)+1))^0.5;
k=attconst+imaginary*b;

%%%%%%%%%%%%%%%%%%%%%%%%%%%%%%%%%%%%%%%%%%%%%%%%%%%%%%%%%%%%%%%%%%%%%%%%
%impedance

ng=(mu0*mu1/(E0*e1*(1-tandel)))^0.5;% electrical impedance of ground (Ohms)
pg=(ng-n0)/(ng+n0);%ground refelective coefficient
tg=(2*ng)/(ng+n0);%ground transmission coefficient

%%%%%%%%%%%%%%%%%%%%%%%%%%%%%%%%%%%%%%%%%%%%%%%%%%%%%%%%%%%%%%%%%%%%%%%%
% target parameters
nt=(mu0*mu1/(E0*e0))^0.5;% electrical impedance of target (Ohms)
pt=(nt-ng)/(nt+ng);%target refelective coefficient
% t=1:10; %range t from 1 to 10
% tr=t/40; %radius
% ta=pi*tr.^2;% arean of target
% t=1;
ta=Xcav*Ycav;% area of target

%%%%%%%%%%%%%%%%%%%%%%%%%%%%%%%%%%%%%%%%%%%%%%%%%%%%%%%%%%%%%%%%%%%%%%%%
% radar target geometries

%distance to target

```

```

j=1;
for ydist=0:dely:yl
    i=1;
    for xdist=0:delx:xl
        if xdist>=(xl/2)-(Xcav/2) && xdist<=(xl/2)+(Xcav/2) && ydist>=(yl/2)-(Ycav/2) && ydist<=(yl/2)+(Ycav/2) %above cavity
            R(i,j)=z0*1000;
        end
        if xdist>=(xl/2)-(Xcav/2) && xdist<=(xl/2)+(Xcav/2) && ydist<=(yl/2)-(Ycav/2)
            R(i,j)=(z0^2+(yl/2-Ycav/2-ydist)^2)^0.5)*1000;
        end
        if xdist>=(xl/2)-(Xcav/2) && xdist<=(xl/2)+(Xcav/2) && ydist>=(yl/2)+(Ycav/2)
            R(i,j)=(z0^2+(ydist-yl/2-Ycav/2)^2)^0.5)*1000;
        end
        if ydist>=(yl/2)-(Ycav/2) && ydist<=(yl/2)+(Ycav/2) && xdist<=(xl/2)-(Xcav/2)
            R(i,j)=(z0^2+(xl/2-Xcav/2-xdist)^2)^0.5)*1000;
        end
        if ydist>=(yl/2)-(Ycav/2) && ydist<=(yl/2)+(Ycav/2) && xdist>=(xl/2)+(Xcav/2)
            R(i,j)=(z0^2+(xdist-xl/2-Xcav/2)^2)^0.5)*1000;
        end

        if xdist<(xl/2-Xcav/2) && ydist<(yl/2-Ycav/2)
            R(i,j)=(z0^2+(((xl/2-Xcav/2)-xdist)^2+((yl/2-Ycav/2)-ydist)^2)^0.5)^2)^0.5)*1000;
        end
        if xdist<(xl/2-Xcav/2) && ydist>(yl/2+Ycav/2)
            R(i,j)=(z0^2+(((xl/2-Xcav/2)-xdist)^2+(ydist-(yl/2+Ycav/2))^2)^0.5)^2)^0.5)*1000;
        end
        if xdist>(xl/2+Xcav/2) && ydist>(yl/2+Ycav/2)
            R(i,j)=(z0^2+((xdist-(xl/2+Xcav/2))^2+(ydist-(yl/2+Ycav/2))^2)^0.5)^2)^0.5)*1000;
        end
        if xdist>(xl/2+Xcav/2) && ydist<(yl/2-Ycav/2)
            R(i,j)=(z0^2+((xdist-(xl/2+Xcav/2))^2+((yl/2-Ycav/2)-ydist)^2)^0.5)^2)^0.5)*1000;
        end
    end
    i=i+1;
end

```

```

j=j+1;
end

%%%%%%%%%%%%%%%%%%%%%%%%%%%%%%%%%%%%%%%%%%%%%%%%%%%%%%%%%%%%%%%%%%%%%%%%
% front surface reflection
vs=(V0/pw)*(1/C)*(aa/((pi*(radar_height/100)^2)*tand((theta/2))^2))*num_avg*
pg*10^-3;
efp=(pi*(((radar_height/1000)*tand(theta/2))*(1/(tand(asind(sind(theta/2)
/e1)))))+R/1000)*(tand(asind(sind(theta/2)/e1))))).^2);

for m=1:nx% for changing target size
    for i=1:ny
        x_gpr=(aa*ta*num_avg);
        xefp=(x_gpr/efp(m,i));
        V1=(1/C)*(V0/pw)*(xefp)*tg*pt*(10^-3);
        V2=exp(-(2*k*(R(m,i)/1000)));
        % test(1)=(V0/pw)*(1/C)*((aa*ta(m)*num_avg)/efp(i))*tg*pt*(10^-3)*(exp(-
(k*2*(R(i)/1000))));
        V3(m,i)=V1*V2';
    end
end
V3=abs(V3);

%prob calc
%calculate the detection probability
nsamples=100;%number of iterations of monte carlo simulation

for k=1:nsamples%start monte carlo loop

    sample=V3(randi(spacing*10,1,1):spacing*10:end,:);

    sample(randperm(numel(sample),round(numel(sample)*(delete_percentage))))=NaN
;%delete percentage

    for m=1:length(sample(:,1))
        for n=1:ny
            SNR(m,n)=abs(sample(m,n)/noise(real_noise_choice,7));%signal to noise ratio
        for each GPR survey point
            erf_data(m,n)=abs(erf(SNR(m,n)));%
        end
    end
end

```

```

    erf_data(isnan(erf_data))=0;%change those lines where no value was taken to
zero probability
    prob(k)=1-(prod(prod(1-erf_data)));\%total probability of detection for this
run of simulation

end

prob_total=mean(prob);\%total prob
sample_test=sample;

%plot
scrsz = get(0,'ScreenSize');
figure('OuterPosition',[1                scrsz(4)/4                scrsz(3)/2
3*scrsz(4)/4],'Name','Results');
for m=1:nx%calc gpr erf across survey
    for n=1:ny
        SNR(m,n)=abs(V3(m,n)/noise(real_noise_choice,7));%signal to noise ratio for
each GPR survey point
        erf_data_1(m,n)=abs(erf(SNR(m,n)));
    end
end
plot3k({Y' X' V3'},erf_data_1,[0 1],{'o',1},5);
colorbar('off');
xlabel('X (m)')
ylabel('Y (m)')
zlabel('GPR microV')
title(['Detection probability: ', num2str(prob_total)],'')

```

xvii Halo calculation

```

function [mag_field_total,grav_field_total,
detect_prob,h,recreate_count] =
halo(x,y,spacing,cavity_size,cavity_depth,geology,fill,fracture_percent
age,halo_spread,fracture_width,noise_level,loop,recreate_count,fracture
_method)
%
% USAGE:[gravity_field, detect_prob] =
halo(x,y,spacing,cavity_size,cavity_depth, geology, fill,
fracture_percentage, halo_spread, fracture_width,noise_level, loop);
% eg: [mag_field_total,grav_field_total, detect_prob,h,recreate_count]
= halo(10,10,1,1,2,3,1,0.03,2,0.01,3,1,1,3)
% Inputs:
%         x=x survey length
%         y=y survey width
%         spacing= station and profile spacing
%         cavity_size=dimension of square air cavity
%         cavity_depth=depth of cavity from top

```

```

%          geology=surrounding material (1 sandstone, 2 clay, 3
limestone,4 concrete, 5 soil)
%          fill = cavity fill type (1=air, 2=water, 3=mining)
%          fracture_percentage=percentage of halo area that is
fractured
%          halo_spread=distance from cavity that fracture spreads
%          fracture_width=fracture width, tapers to zero
%          noise_level=1) zero 2)instrumental 3)typical 4)brownfield
5)rural
%          loop=loop number for saving of image
%          fracture_method=type of fracture system generated
%
% Output:
%          mag_field_total=value of magnetic field at each survey
point
%          grav_field_total=value of gravity field at each survey
point
%          detect_prob=overall detection probability of survey
%
% Operation: calculates the gravity and mag field and probability of
using
% gravity and magnetic
% method over a cavity with given halo size and fracture percentage

disp('Creating fracture network')
tic
switch fracture_method
    case 1
        % create sheets and cavity (fills whole halo area)
        %
        [xcube,ycube,zcube,fracture_coord_x,fracture_coord_y,fracture_coord_z,d
        elete_fracture_coord_x_calc,delete_fracture_coord_y_calc,delete_fractur
        e_coord_z_calc,recreate_count] =
        vert_horiz_sheet_fracture(x,y,cavity_size,cavity_depth,fracture_percent
        age,halo_spread,fracture_width,recreate_count);

        [xcube,ycube,zcube,fracture_coord_x,fracture_coord_y,fracture_coord_z,d
        elete_fracture_coord_x_calc,delete_fracture_coord_y_calc,delete_fractur
        e_coord_z_calc,recreate_count] =
        vert_horiz_sheet_fracture_user_input(x,y,cavity_size,cavity_depth,fract
        ure_percentage,halo_spread,fracture_width,recreate_count);

    case 2
        % create sheets and cavity with fractures concentrated at sides

        [xcube,ycube,zcube,fracture_coord_x,fracture_coord_y,fracture_coord_z,d
        elete_fracture_coord_x_calc,delete_fracture_coord_y_calc,delete_fractur
        e_coord_z_calc,recreate_count] =
        sheet_fractures_concentrated_at_sides(x,y,cavity_size,cavity_depth,frac
        ture_percentage,halo_spread,fracture_width,recreate_count);

    case 3
        % create sheets and cavity with radomly distributed fractures
        concentrated
        % at sides (not necesarily connected to the cavity)

        [xcube,ycube,zcube,fracture_coord_x,fracture_coord_y,fracture_coord_z,d
        elete_fracture_coord_x_calc,delete_fracture_coord_y_calc,delete_fractur
        e_coord_z_calc,recreate_count] =

```

```

dispersed_fractures(x,y,cavity_size,cavity_depth,fracture_percentage,ha
lo_spread,fracture_width,recreate_count);
    case 4
        % create sheets and cavity with radomly distributed fractures
        concentrated
        % at sides (not necesarily connected to the cavity).Limited to
        % micro fractures based on Golshani 2007.

        [xcube,ycube,zcube,fracture_coord_x,fracture_coord_y,fracture_coord_z,d
        elete_fracture_coord_x_calc,delete_fracture_coord_y_calc,delete_fractur
        e_coord_z_calc,recreate_count] =
        micro_fractures(x,y,cavity_size,cavity_depth,fracture_percentage,halo_s
        pread,fracture_width,recreate_count);
    case 5
        % create fractures and cavity - point fractures only

        [xcube,ycube,zcube,fracture_coord_x,fracture_coord_y,fracture_coord_z]
        =
        shape_coords(x,y,cavity_size,cavity_depth,fracture_percentage,halo_spre
        ad,fracture_width);
    end
    toc

    % calculate fields

    %cavity coords and field
    %xcube,ycube,zcube
    disp('Calculating cavity field')
    tic
    [Corner, Face] = polygons(6,xcube,ycube,zcube);
    [Gtotal(:, :, 1), Dtotal(:, :, 1)] = grvmag3d_halo(6, 8, Face, Corner, 70, -
    5, 47500, 0, 0, 0, geology, fill, spacing, x, y);
    toc
    % %fractures coords and field
    % for i=1:length(fracture_coord_x(:,1))
    % [Corner, Face] =
    polygons(5,fracture_coord_x(i,:),fracture_coord_y(i,:),fracture_coord_z
    (i,:));
    % [Gtotal(:, :, i+1), Dtotal(:, :, i+1)] =
    grvmag3d_halo(5, 5, Face, Corner, 70, -
    5, 47500, 0, 0, 0, geology, fill, spacing, x, y);
    % end

    %fractures sheets

    for i=1:length(fracture_coord_x(:,1))
        tic
        [Corner, Face] =
        polygons(7,fracture_coord_x(i,:),fracture_coord_y(i,:),fracture_coord_z
        (i,:));
        [Gtotal(:, :, i+1), Dtotal(:, :, i+1)] =
        grvmag3d_halo(5, 6, Face, Corner, 70, -
        5, 47500, 0, 0, 0, geology, fill, spacing, x, y);
        if max(max(Gtotal(:, :, i+1))) < 0 %account for change in orientatioo
        oof shape
            Face(1,1:5)=[4 1 4 3 2];

```

```

        Face(2,1:4)=[3 2 5 1];
        Face(3,1:5)=[4 3 6 5 2];
        Face(4,1:4)=[3 4 6 3];
        Face(5,1:5)=[4 1 5 6 4 ];
        [Gtotal(:,:,i+1),Dtotal(:,:,i+1)] =
grvmag3d_halo(5,6,Face,Corner,70,-
5,47500,0,0,0,geology,fill,spacing,x,y);
    end
    str=['Calculated fracture field ', num2str(i), ' in ',
num2str(toc), ' secs'];
    disp(str);
end

if delete_fracture_coord_x_calc~=0
    %minus overlaps
    disp('Deleting overlaps')
    tic
    for i=1:length(delete_fracture_coord_x_calc(1,1,:))

        [Corner, Face] =
polygons(6,delete_fracture_coord_x_calc(:,:,i)',delete_fracture_coord_y
_calc(:,:,i)',delete_fracture_coord_z_calc(:,:,i)');

        delete_fracture_coord_x_calc(:,:,i);
        delete_fracture_coord_y_calc(:,:,i);
        delete_fracture_coord_z_calc(:,:,i);
        x_order=sort(delete_fracture_coord_x_calc(:,:,i),'descend');

        z_choice_1=find(delete_fracture_coord_x_calc
(:,:,i)==x_order(3));
        z_choice_2=find(delete_fracture_coord_x_calc
(:,:,i)==x_order(4));

        z_now=delete_fracture_coord_z_calc ((:,:,i);
if z_now(z_choice_1(1))>z_now(z_choice_2(1))
            one=[x_order(3),z_now(z_choice_1(1))];
            two=[x_order(4),z_now(z_choice_2(1))];
        else
            one=[x_order(4),z_now(z_choice_2(1))];
            two=[x_order(3),z_now(z_choice_1(1))];
        end

        z_choice_3=find(delete_fracture_coord_x_calc
(:,:,i)==x_order(2));
        z_choice_4=find(delete_fracture_coord_x_calc
(:,:,i)==x_order(1));
        if z_now(z_choice_4)>z_now(z_choice_3(1))
            five=[x_order(1),z_now(z_choice_4(1))];
            six=[x_order(2),z_now(z_choice_3(1))];
        else
            five=[x_order(2),z_now(z_choice_3(1))];
            six=[x_order(1),z_now(z_choice_4(1))];
        end

        Corner=[one(1,1),min(min(delete_fracture_coord_y_calc(:,:,i))),-
one(1,2)];
    end
end

```

```

        two(1,1),min(min(delete_fracture_coord_y_calc(:, :, i))), -
two(1,2);
        two(1,1),max(max(delete_fracture_coord_y_calc(:, :, i))), -
two(1,2);
        one(1,1),max(max(delete_fracture_coord_y_calc(:, :, i))), -
one(1,2);
        six(1,1),max(max(delete_fracture_coord_y_calc(:, :, i))), -
six(1,2);
        five(1,1),max(max(delete_fracture_coord_y_calc(:, :, i))), -
five(1,2);
        five(1,1),min(min(delete_fracture_coord_y_calc(:, :, i))), -
five(1,2);
        six(1,1),min(min(delete_fracture_coord_y_calc(:, :, i))), -
six(1,2)];
        Face(1,1:5)=[4 2 3 5 8];
        Face(2,1:5)=[4 8 7 1 2];
        Face(3,1:5)=[4 1 4 3 2];
        Face(4,1:5)=[4 6 5 3 4];
        Face(5,1:5)=[4 5 6 7 8];
        Face(6,1:5)=[4 4 1 7 6];
        [Gminus(:, :, i), Dminus(:, :, i)] =
grvmag3d_halo(6,8,Face,Corner,70,-
5,47500,0,0,0,geology,fill,spacing,x,y);
        test_corner(:, :, i)=Corner;

    end
    toc
    save('test_corner','test_corner')
else Gminus=0;Dminus=0;
end

grav_field_total=-(sum(real(Gtotal),3)-sum(real(Gminus),3));
mag_field_total=-(sum(real(Dtotal),3)-sum(real(Dminus),3));%
save('test','Dtotal','Dminus','Gtotal',
'Gminus','delete_fracture_coord_x_calc','delete_fracture_coord_y_calc',
'delete_fracture_coord_z_calc','fracture_coord_x','fracture_coord_y','f
racture_coord_z','xcube','ycube','zcube')
% calculate detection percentage
disp('Calculating detection probability')
tic
[detect_prob,erf_grav,erf_mag] =
detection_probability(grav_field_total,mag_field_total,noise_level);
toc
h=1;
%draw cavity
disp('Visualising results')
tic
[h]=draw_cavity(x,y,cavity_size, cavity_depth,
halo_spread,loop,xcube,ycube,zcube,fracture_coord_x,fracture_coord_y,fr
acture_coord_z,detect_prob,erf_grav,erf_mag,spacing,grav_field_total,ma
g_field_total,
delete_fracture_coord_x_calc,delete_fracture_coord_y_calc,delete_fractu
re_coord_z_calc);
toc

```

xviii Microfractures

```
function
[xcube,ycube,zcube,fracture_coords_x,fracture_coords_y,fracture_coords_
z,
delete_fracture_coord_x_calc,delete_fracture_coord_y_calc,delete_fractu
re_coord_z_calc, recreate_count] = micro_fractures(x,y,cavity_size,
cavity_depth,fracture_percentage, halo_spread,
fracture_width,recreate_count)

%This function creates a fracture system that has more fractures
situated
%around the side of the void without the limitation of eing joined to
the cavity. The literature suggest that this is more
%realistic.It also creates a tunnel fracture.

%%%%%%%%%%%%%%%%%%%%%%%%%%%%%%%%%%%%%%%%%%%%%%%%%%%%%%%%%%%%%%%%%%%%%%%%
%%%
%cavity coords
zb=-(cavity_depth+cavity_size);%bottom of void
xw=x/2-(cavity_size/2);%west end of void
xe=x/2+(cavity_size/2);%east end of void
ys=0;%south end of void
yn=y;%north end of void
xcube=[xw xe xe xw xw xw;xw xe xe xw xw xw;xw xw xe xe xe xe;xw xw xe
xe xe xe];
ycube=[ys ys yn yn ys ys;ys ys yn yn yn yn;yn ys ys yn yn yn;yn ys ys
yn ys ys];
zcube=[zb zb zb zb zb -cavity_depth;-cavity_depth -cavity_depth -
cavity_depth -cavity_depth zb -cavity_depth;-cavity_depth -cavity_depth
-cavity_depth -cavity_depth zb -cavity_depth;zb zb zb zb zb -
cavity_depth];

%how many fractures?
indent=.3;
total_halo_area=y*((2*halo_spread+cavity_size)^2-cavity_size^2-
4*(halo_spread*(1-indent)*cavity_size*(1-2*indent)));%volume of halo
area

%possible fracture positions
x_coords=x/2-cavity_size/2-
halo_spread:0.01:x/2+cavity_size/2+halo_spread;%the increment increase
can be altered to reflect a uniform fracture spacing
z_coords=-(cavity_depth-
halo_spread:0.01:halo_spread+cavity_size+cavity_depth);
y_coords=0:0.1:y;

%fracture system angle
frac_angle=deg2rad(45);%randi(90));

fracture_volume_total=0;%initiate volume matrix
delete_fracture_coord_x_calc=[];delete_fracture_coord_y_calc=[];delete_
fracture_coord_z_calc=[];% initiate depete matrices
count=1;%start count to increase with evrey fracture
while fracture_volume_total<=total_halo_area*(fracture_percentage/100)
    if round(count/100)==count/100
```

```

        fracture_volume_total-total_halo_area*(fracture_percentage/100)
    end
    %randomly choose fracture position
    x_coord=x_coords(randi(size(x_coords)));
    z_coord=z_coords(randi(size(z_coords)));
    y_coord=y_coords(randi(size(y_coords)));

    %Use this section for microfractures
    width=fracture_width;
    length=2*rand(1);

    % choose whether vertical or horizontal
    v_or_h=randi(2);

    %create fracture
    if v_or_h==1%vertical
        fracture_coord_x=[x_coord x_coord-fracture_width x_coord-
fracture_width x_coord x_coord-fracture_width/2+(width*sin(frac_angle))
x_coord-fracture_width/2+(width*sin(frac_angle))];
        fracture_coord_z=[z_coord z_coord z_coord z_coord z_coord-
width*cos(frac_angle) z_coord-width*cos(frac_angle)];
        fracture_coord_y=[y_coord+length y_coord+length y_coord y_coord
y_coord+length y_coord];
    else%horizontal
        fracture_coord_x=[x_coord x_coord x_coord x_coord
x_coord+width*cos(frac_angle) x_coord+width*cos(frac_angle)];
        fracture_coord_z=[z_coord z_coord-fracture_width z_coord-
fracture_width z_coord (z_coord-
fracture_width/2)+(width*sin(frac_angle)) (z_coord-
fracture_width/2)+(width*sin(frac_angle))];
        fracture_coord_y=[y_coord+length y_coord+length y_coord y_coord
y_coord+length y_coord];
    end

    %remove any fractures entering the cavity or leaving the halo

    % check if fracture enters cavity
    xlimit = x/2+[-cavity_size cavity_size]/2;
    zlimit = -[cavity_depth cavity_depth+cavity_size];
    xbox = xlimit([1 1 2 2 1]);
    zbox = zlimit([1 2 2 1 1]);
    x_line=[fracture_coord_x(1) fracture_coord_x(5)];
    z_line=[fracture_coord_z(1) fracture_coord_z(5)];
    [cross_polygon, yi] = polyxpoly(x_line, z_line, xbox, zbox);
    cross_polygon=isempty(cross_polygon);
    if cross_polygon==1

        % Then check if fracture goes outside halo (new shape to match
        % literature)

        xlimit = x/2+[-cavity_size/2-halo_spread -cavity_size/2-
halo_spread*indent -cavity_size/2+cavity_size*indent cavity_size/2-
cavity_size*indent cavity_size/2+halo_spread*indent
cavity_size/2+halo_spread];
        zlimit = -cavity_depth+[halo_spread halo_spread*indent -
cavity_size*indent -cavity_size+cavity_size*indent -cavity_size-
halo_spread*indent -cavity_size-halo_spread];

```

```

xbox = xlimit([1 1 2 2 1 1 3 3 4 4 6 6 5 5 6 6 4 4 3 3 1]);
zbox = zlimit([1 3 3 4 4 6 6 5 5 6 6 4 4 3 3 1 1 2 2 1 1]);

x_line=[fracture_coord_x(1) fracture_coord_x(5)];
z_line=[fracture_coord_z(1) fracture_coord_z(5)];
[cross_polygon, yi] = polyxpoly(x_line, z_line, xbox, zbox);

cross_polygon=isempty(cross_polygon);
if cross_polygon==1

    %check if starts outside halo [this actually curves off the
    %halo square corners so is more representative
    x_line=[fracture_coord_x(1) x/2];%creat line from start to
cavity centre and see if it crosses the halo line
    z_line=[fracture_coord_z(1) -cavity_depth-(cavity_size/2)];
    [cross_polygon, yi] = polyxpoly(x_line, z_line, xbox,
zbox);

    cross_polygon=isempty(cross_polygon);
    if cross_polygon==1

        %then remove all fractures that end in the cavity
        if fracture_coord_x(5)>=(x-cavity_size)/2 &&
fracture_coord_x(5)<=(x+cavity_size)/2 && fracture_coord_z(5)<=-
cavity_depth && fracture_coord_z(5)>=-cavity_depth-cavity_size
            else
                fracture_coords_x(count,:)=fracture_coord_x;
                fracture_coords_y(count,:)=fracture_coord_y;
                fracture_coords_z(count,:)=fracture_coord_z;

                %Calculate volume

fracture_volume(count)=polyarea(fracture_coord_x([1,2,5]),fracture_coord_z([1,2,5]))*range(fracture_coord_y(:));

                %calculate volume of overlaps
                [delete_fracture_coord_x_calc_2,
delete_fracture_coord_y_calc_2,delete_fracture_coord_z_calc_2,overlap_v
olume(count)]=overlaps(fracture_coords_x,fracture_coords_y,fracture_coor
ds_z);

                % combine matrices
                if
isempty(delete_fracture_coord_x_calc_2)==0

delete_fracture_coord_x_calc=cat(3,delete_fracture_coord_x_calc,
delete_fracture_coord_x_calc_2);

delete_fracture_coord_y_calc=cat(3,delete_fracture_coord_y_calc,
delete_fracture_coord_y_calc_2);

delete_fracture_coord_z_calc=cat(3,delete_fracture_coord_z_calc,
delete_fracture_coord_z_calc_2);
                    end
                    fracture_volume_total=sum(abs(fracture_volume));%
                    count=count+1;
                end
            end
        end
    end
end

```

```

end

end
disp('Fracture volume percentage reached')

```

Appendix B Program variables

Variable	Details
layer1_geology	choice of geology for layer 1
layer2_geology	choice of geology for layer 2
layer3_geology	choice of geology for layer 3
cavity_makeup	choice of cavity material
cavity_type	choice of cavity shape
lining_makeup	choice of lining material
noise_scale	choise of noise level by slider
noise_type	real or artificial
real_noise_choice	level of noise by type (zero to brownfield)
bulk_geometry	type of migration
limit_technique	parameter changed in depth size limit study
limit_parameters	technique used in depth size limit study
limit_running	check to see if limit is running
x1	survey length
y1	survey width
zf	depth of layer 1 at length 0m
zl	depth of layer 1 at length [end]
z2f	depth of layer 2 at length 0m
z2l	depth of layer 2 at length [end]
z0	cavity depth
shaft_depth	shaft depth
Xcav	x dimension of cavity
Ycav	y dimension of cavity
Zcav	z dimension of cavity
X_shaft	x dimension of shaft
Y_shaft	y dimension of shaft
Z_shaft	z dimension of shaft
time	survey time
cost	survey cost
delete_percentage	percentage of data deleted
spacing	spacing of survey lines and survey positions
delx	spacing of survey lines and survey positions in x direction for modelling - set at 0.1
dely	spacing of survey lines and survey positions in y direction for modelling - set at 0.2
nx	number of survey points in x direction

ny	number of survey points in y direction
X	matrix with y coordinates
Y	matrix with x coordinates
x0	centre of cavity. Set as half survey length
y0	centre of cavity. Set as half survey width
geology	cell containing various parameters (max and min and average) of geologies
sigma1	conductivity S/m (layer 1)
e1	dielectric constant/relative permittivity (layer 1)
c1	velocity of radar m/ns (layer 1)
rho1	density Mg/m ³ (layer 1)
susc_rock1	magnetic susceptibility SI (layer 1)
sigma	conductivity S/m (cavity)
e0	dielectric constant/relative permittivity (cavity)
c0	velocity of radar m/ns (cavity)
rho0	density Mg/m ³ (cavity)
susc_cav	magnetic susceptibility SI (cavity)
mu	mag permeability
sigma2	conductivity S/m (layer 2)
e2	dielectric constant/relative permittivity (layer 2)
c2	velocity of radar m/ns (layer 2)
rho2	density Mg/m ³ (layer 2)
susc_rock2	magnetic susceptibility SI (layer 2)
sigma3	conductivity S/m (layer 3)
e3	dielectric constant/relative permittivity (layer 3)
c3	velocity of radar m/ns (layer 3)
rho3	density Mg/m ³ (layer 3)
susc_rock3	magnetic susceptibility SI (layer 3)
ksusc_cap	magnetic susceptibility SI (lining wood or steel)
rho_cap	density Mg/m ³ (lining and cap - wood or steel)
ksusc	difference in susceptibility between cavity and surrounding
rho	difference in density between cavity and surrounding (g/cm ³)
Hintn	magnetic field in the uk
Hincl	inclination
Decl	declination
resist_type	type of resistivity survey
I	current of resistivity survey
Gc	Universal Gravitational constant (6.6732e-3)
noise	cell containing a range of noise levels
limit_percentage	the minimum percetage for detetion probability
data	cell containing all the probability values of the techniques
prob_depth_size	store the probaility od detection for each technique in the depth size study
prob_total	

start_parameter	the number of the option that loop should start on (in depth size analysis)
depth_increase	iterative increase value for cavity size
cavity_increase	iterative increase value for depth
grad_distance	distance between gradient sensors
Dt	matrix of magnetic response
Gtot	matrix of gravity response
Dt_grad	matrix of magnetic gradient response
grav_grad	matrix of magnetic gradient response
Ncor	number of corners of the model
Nf	number of faces
Mstrength	remnant magnetic induction
Mincl	remnant magnetic declination
Mdecl	remnant magnetic inclination
cap_thickness	cap thickness (set at 0.5m)
Corner	matrix of corner coords
Face	the first number is the number of corners forming a face; the following are row numbers of the Corner array with coordinates of the corners which form that face
Nedges	number of edges
Edge	vector direction of edge(1,2,3), and length of edge(4), I2 (5), and if integration required (6) and corner (end) numbers (7,8)
indx	vector of all the corners in each face, plus 1st corner again (to finish face)
Uh	vector direction of field
H	vector magnetic field strength
Rem_magn	Remnant magnetization
Ind_magn	Induced magnetization
Net_magn	Net magnetization
Omega	solid angle for each side at each observation point (angle the edges of the shape make from the obs point)
V	vector direction of edge
I2	Contribution of field from edge
nsamples	number of iterations of monte carlo simulation
start_position	'nsample' random starting points from 0-spacing distance
sample	sample of data after spacing deletion percentage taken
rms	root mean square
erf_data	error function for each monte carlo simulation (cell containing each technique)
prob	probability for each monte carlo simulation
SNR	signal to noise ratio for each GPR survey point
prob_total	total average probability of survey
xlin	
ylin	
Xres	

Yres	
Zres	
measurements	distance covered or no. of stations for each technique
time	time for each survey
cost	cost of each survey
frequency	frequency of radar (Hz)
E0	8.85419×10^{-12} ; % permittivity of free space (F/m)
mu0	$4\pi \times 10^{-7}$; % mag constant (N/A ²)
mu1	1; %relative magnetic permeability - assumed to be unity in gpr (Milsom)
imaginary	$(-1)^{0.5}$; %imaginary number
C	3×10^8 ; %speed of light in air m/s
n0	377; % electrical impedance of air (Ohms)
theta	20; % antenna parameters
ar	0.15; % antenna radius
aa	$\pi \times ar^2$; % antenna area
% radar system params	
V0=10; %peak radiated voltage (volts) Daniels pg 697	
pw= 0.3×10^{-9} ; % pulse width (ns)	
n=5; %number of averages	
H=0; % radar initial height	
EM	
w	angular frequency ($2\pi \times wxy \times 1000$) = ($2\pi \times f$). f=spatial plot frequency*1000 to change to Hz
wxy	spatial plot frequency. set at 9.8kHz is EM31 frequency
k	$\sqrt{\text{imaginary} \times \mu \times \sigma \times w}$; from theory in Wait <i>et al</i> 1951
mu2	change from relative to original mag permeability. ($\mu_0 \times \mu$)
ka	$\text{real}(k \times X_{\text{cav}})$ - in theory (Wait <i>et al</i> 1951)
cap_thickness	thickness of cap
line_thick	thickness of lining

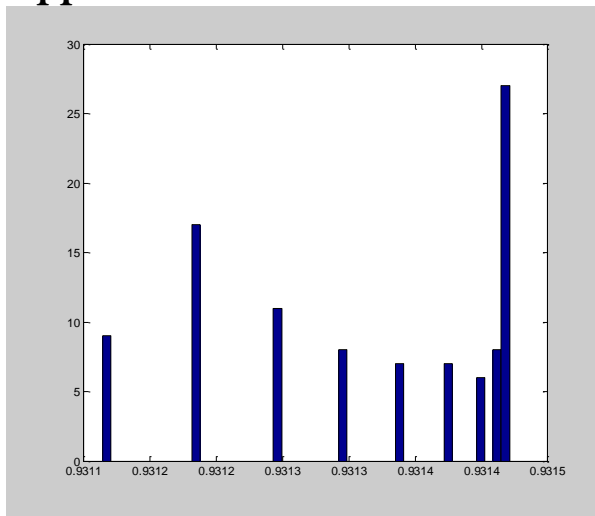
Appendix A Cavity depth results

Anomaly size over a 1-m cube air cavity in limestone at typical noise levels

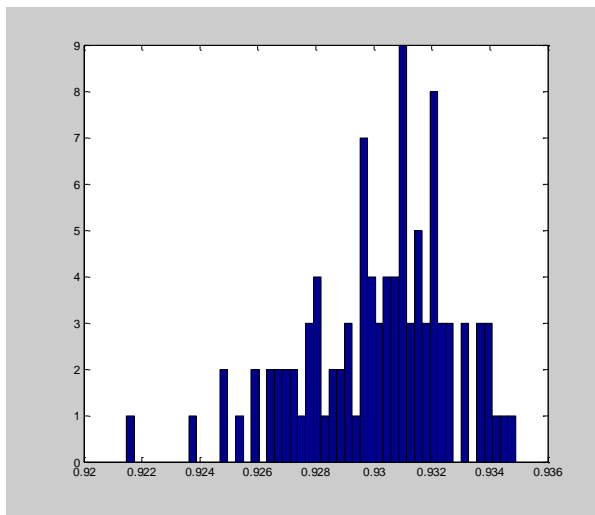
Cavity depth (m)	Magnetic (nT)	Magnetic (nT)	gradient	Gravity (mG)	Gravity gradient
1	1.09378	2.204585		0.007598	100.7111
2	0.242561	0.30376		0.002674	22.44004
3	0.088777	0.079742		0.001301	8.153917
4	0.041821	0.029232		7.40E-04	3.787129
5	0.022912	0.013113		4.60E-04	2.028889
6	0.013881	0.006726		3.04E-04	1.191154

8	0.006125	0.002301	1.49E-04	0.487581
10	0.003193	0.000986	8.10E-05	0.230564
12	0.001827	0.000485	4.74E-05	0.119817
14	0.001111	2.65E-04	2.93E-05	0.066749
16	0.000709	1.54E-04	1.90E-05	0.039293
18	0.00047	9.46E-05	1.28E-05	0.024208
20	0.000322	6.04E-05	8.88E-06	0.015501

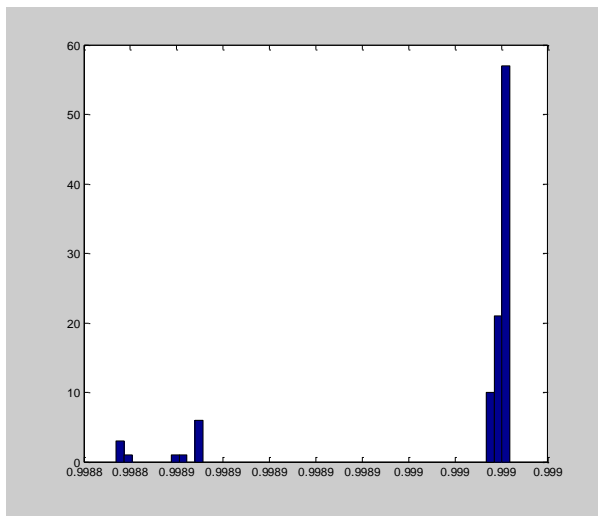
Appendix B Data deletion



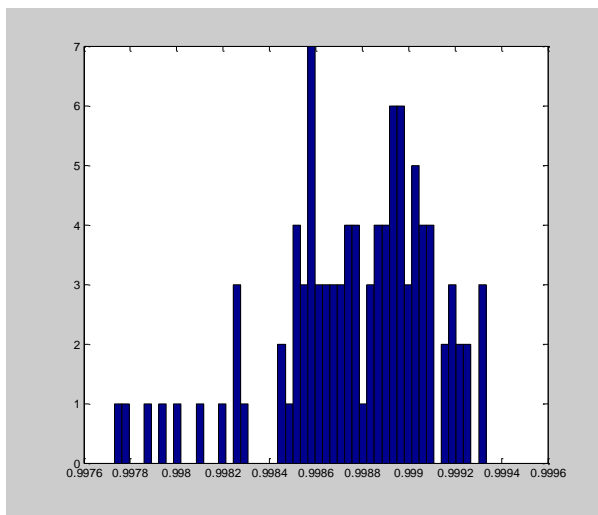
mag 1m spacing 0% data deletion



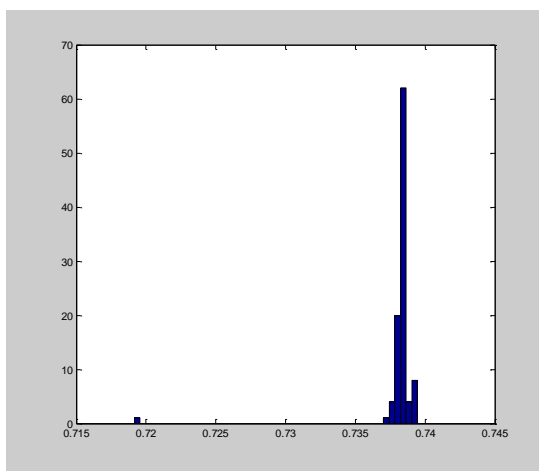
mag 1m spacing 50% data deletion



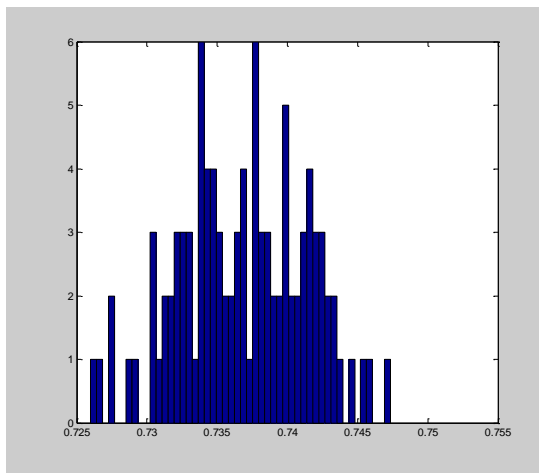
grav grad 1m spacing 0% data deletion



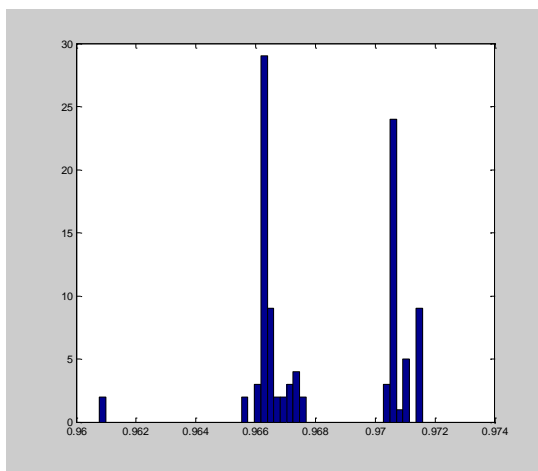
grav grad 1m spacing 50% data deletion



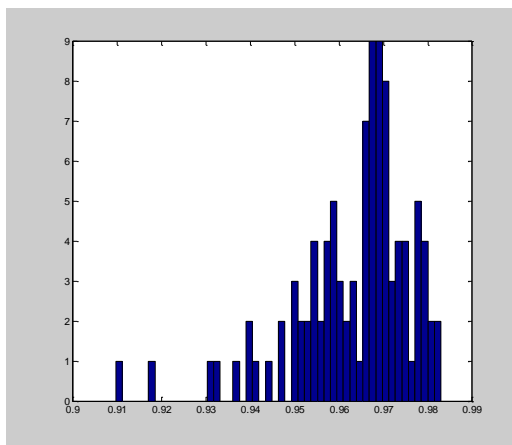
mag 2m spacing 0% data deletion



mag 2m spacing 50% data deletion



grav grad spacing 2m 0% data deletion



grav grad spacing 2m 50% data deletion

Appendix C Noise measurement data



Figure 11.1. Regents Park noise measurements.

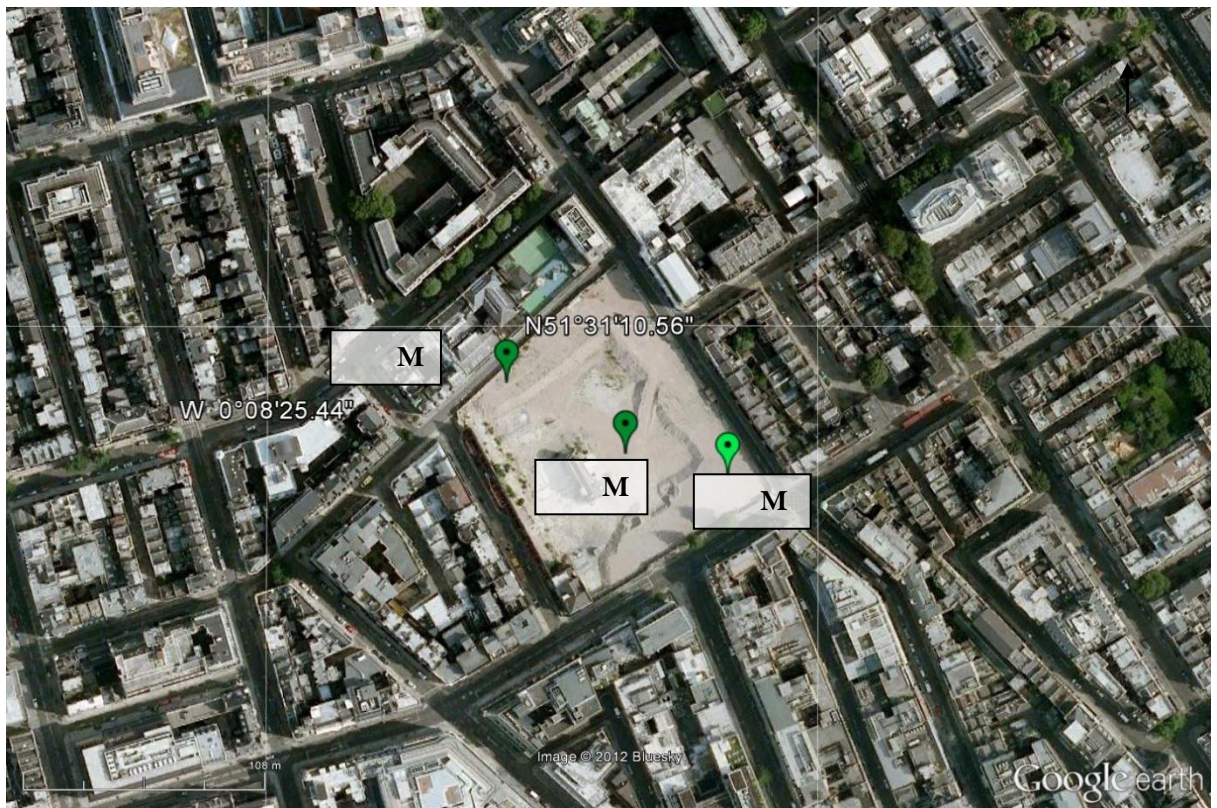


Figure 11.2. Middlesex noise measurements.

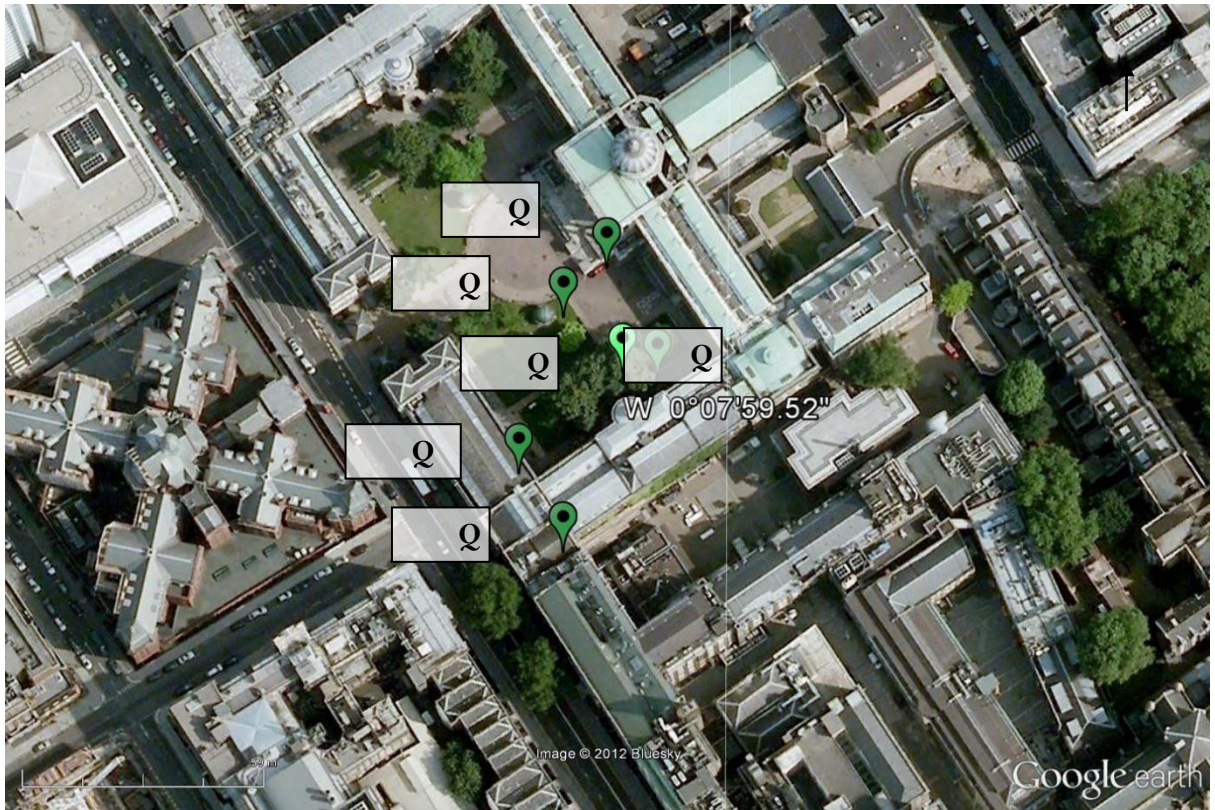
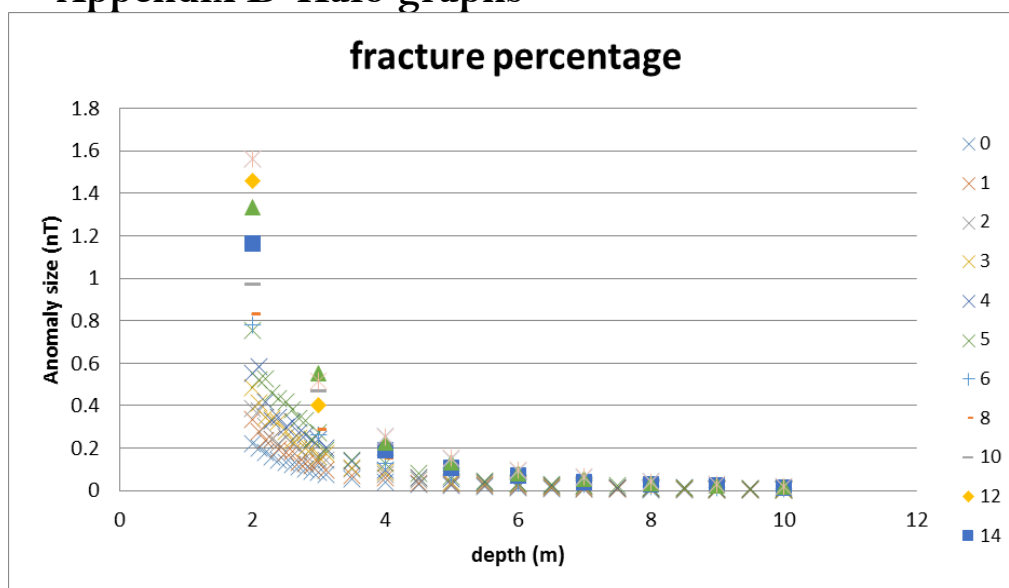


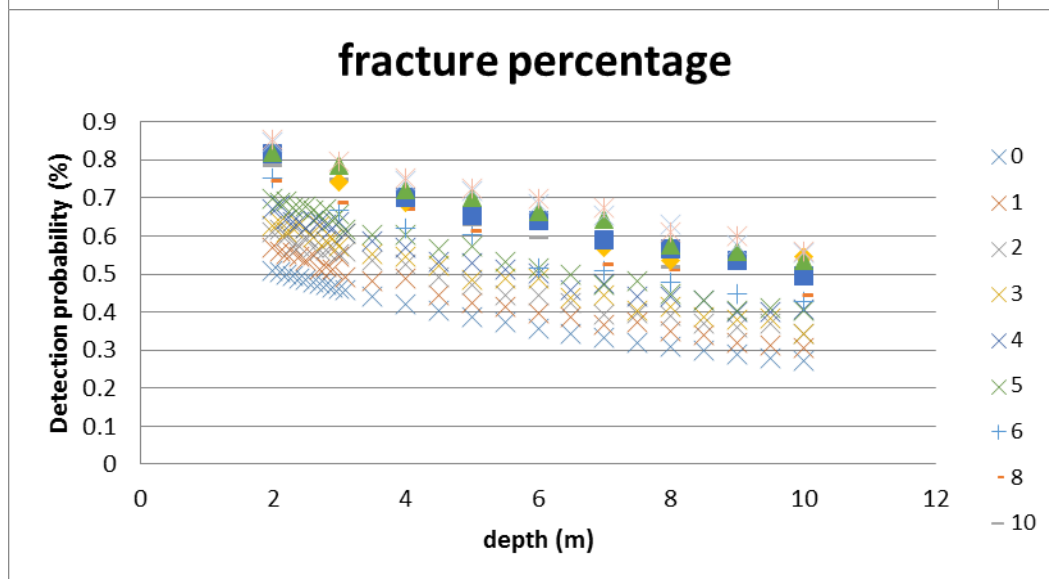
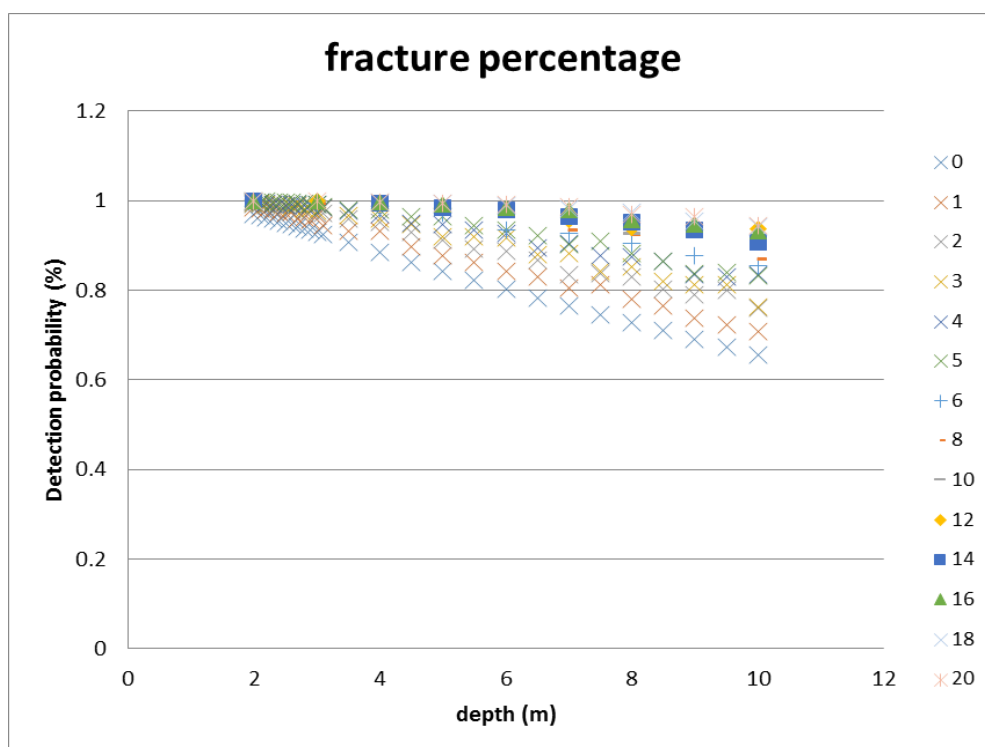
Figure 11.3. UCL Quad noise measurements.



Figure 11.5. West Wycombe noise measurements.

Appendix D Halo graphs





Appendix E Statistical test results

0.02-0.05

t-Test: Paired Two Sample for Means

	0.9	0.985
	852	93
	0.9	0.995
Mean	96121	504
	6.2	1.42E-
Variance	1E-06	05
Observations	4	4
	0.9	
Pearson Correlation	79012	
Hypothesized	Mean	
Difference	0	
df	3	
	0.8	
t Stat	6393	
	0.2	
P(T<=t) one-tail	25586	
	2.3	
t Critical one-tail	53363	
	0.4	
P(T<=t) two-tail	51172	
	3.1	
t Critical two-tail	82446	

0.02-0.1

t-Test: Paired Two Sample for Means

	0.9	0.9
	852	8463
	0.9	0.9
Mean	96121	96175
	6.2	7.2
Variance	1E-06	2E-06
Observations	4	4
	0.9	
Pearson Correlation	73027	
Hypothesized	Mean	
Difference	0	
df	3	
	-	
t Stat	0.17161	
	0.4	
P(T<=t) one-tail	37333	
	2.3	
t Critical one-tail	53363	
	0.8	
P(T<=t) two-tail	74665	
	3.1	
t Critical two-tail	82446	

0.2-0.15

t-Test: Paired Two Sample for Means

	0.9	0.9
	852	8659
	0.9	0.9
Mean	96121	94673
	6.2	1.2
Variance	1E-06	E-05
Observations	4	4
	0.9	
Pearson Correlation	87162	
Hypothesized	Mean	
Difference	0	
df	3	
	2.6	
t Stat	92572	
	0.0	
P(T<=t) one-tail	37126	
	2.3	
t Critical one-tail	53363	
	0.0	
P(T<=t) two-tail	74252	
	3.1	
t Critical two-tail	82446	

0.5-0.1

t-Test: Paired Two Sample for Means

	0.9	0.984
	8593	63
	0.9	0.996
Mean	95504	175
	1.4	7.22E-
Variance	2E-05	06
Observations	4	4
	0.9	
Pearson Correlation	9962	
Hypothesized	Mean	
Difference	0	
df	3	
	-	
t Stat	1.22894	
	0.1	
P(T<=t) one-tail	5335	
	2.3	
t Critical one-tail	53363	
	0.3	
P(T<=t) two-tail	06699	
	3.1	
t Critical two-tail	82446	

0.1-0.15

0.5-0.15

t-Test: Paired Two Sample for Means

	0.9	0.9
	8593	8659
	0.9	0.9
Mean	95504	94673
	1.4	1.2
Variance	2E-05	E-05
Observations	4	4
	0.9	
Pearson Correlation	39311	
Hypothesized	Mean	
Difference	0	
df	3	
	1.2	
t Stat	80804	
	0.1	
P(T<=t) one-tail	45151	
	2.3	
t Critical one-tail	53363	
	0.2	
P(T<=t) two-tail	90303	
	3.1	
t Critical two-tail	82446	

0.1-0.2

0.5-0.2

t-Test: Paired Two Sample for Means

	0.9	0.9
	8593	8037
	0.9	0.9
Mean	95504	9503
	1.4	2.5
Variance	2E-05	4E-05
Observations	4	4
	0.9	
Pearson Correlation	77856	
Hypothesized	Mean	
Difference	0	
df	3	
	0.6	
t Stat	07572	
	0.2	
P(T<=t) one-tail	93188	
	2.3	
t Critical one-tail	53363	
	0.5	
P(T<=t) two-tail	86376	
	3.1	
t Critical two-tail	82446	

0.15-0.2

t-Test: Paired Two Sample for Means

	0.9	0.986
	8463	59
Mean	96175	673
Variance	7.2	1.2E-05
Observations	4	4
Pearson Correlation	0.9	29788
Hypothesized Mean Difference	0	
df	3	
t Stat	2.1	77086
P(T<=t) one-tail	0.0	58835
t Critical one-tail	2.3	53363
P(T<=t) two-tail	0.1	1767
t Critical two-tail	3.1	82446

0.01-0.2

t-Test: Paired Two Sample for Means

t-Test: Paired Two Sample for Means

Means

t-Test: Paired Two Sample for Means

	0.9	0.9
	8463	8037
Mean	96175	9503
Variance	7.2	2.5
Observations	4	4
Pearson Correlation	0.9	71753
Hypothesized Mean Difference	0	
df	3	
t Stat	0.9	13147
P(T<=t) one-tail	0.2	14248
t Critical one-tail	2.3	53363
P(T<=t) two-tail	0.4	28496
t Critical two-tail	3.1	82446

0.02-0.2

t-Test: Paired Two Sample for Means

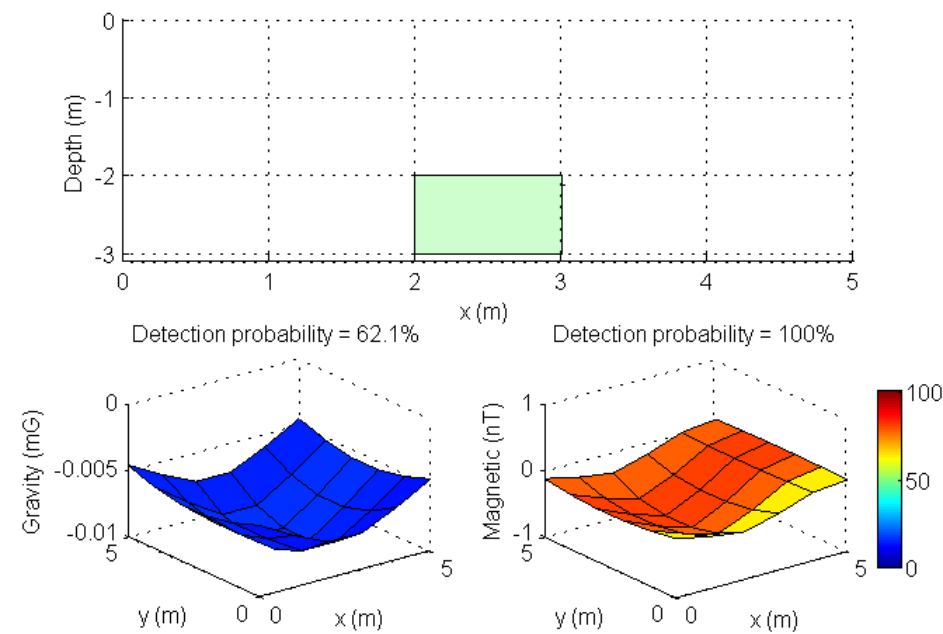
	0.9	0.9
	8659	8037
Mean	94673	9503
Variance	1.2	2.5
Observations	4	4
Pearson Correlation	0.9	89614
Hypothesized Mean Difference	0	
df	3	
t Stat	-	0.42347
P(T<=t) one-tail	0.3	5024
t Critical one-tail	2.3	53363
P(T<=t) two-tail	0.7	0048
t Critical two-tail	3.1	82446

	0.9	0.980
	8335	37
	0.9	0.995
Mean	90128	03
	2.4	2.54E-
Variance	9E-05	05
Observations	4	4
	-	
Pearson Correlation	0.2248	
Hypothesized	Mean	
Difference	0	
df	3	
	-	
t Stat	1.24964	
	0.1	
P(T<=t) one-tail	50022	
	2.3	
t Critical one-tail	53363	
	0.3	
P(T<=t) two-tail	00043	
	3.1	
t Critical two-tail	82446	

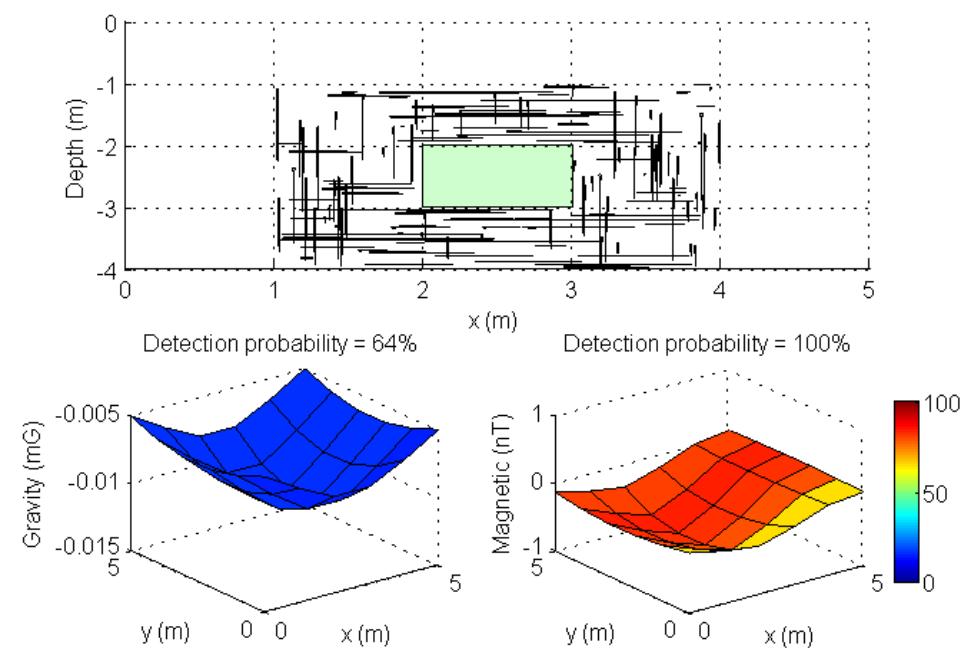
	0.9	0.9
	852	8037
	0.9	0.9
Mean	96121	9503
	6.2	2.5
Variance	1E-06	4E-05
Observations	4	4
	0.9	
Pearson Correlation	99672	
Hypothesized	Mean	
Difference	0	
df	3	
	0.8	
t Stat	57043	
	0.2	
P(T<=t) one-tail	27214	
	2.3	
t Critical one-tail	53363	
	0.4	
P(T<=t) two-tail	54428	
	3.1	
t Critical two-tail	82446	

Appendix F Stress distribution halo examples

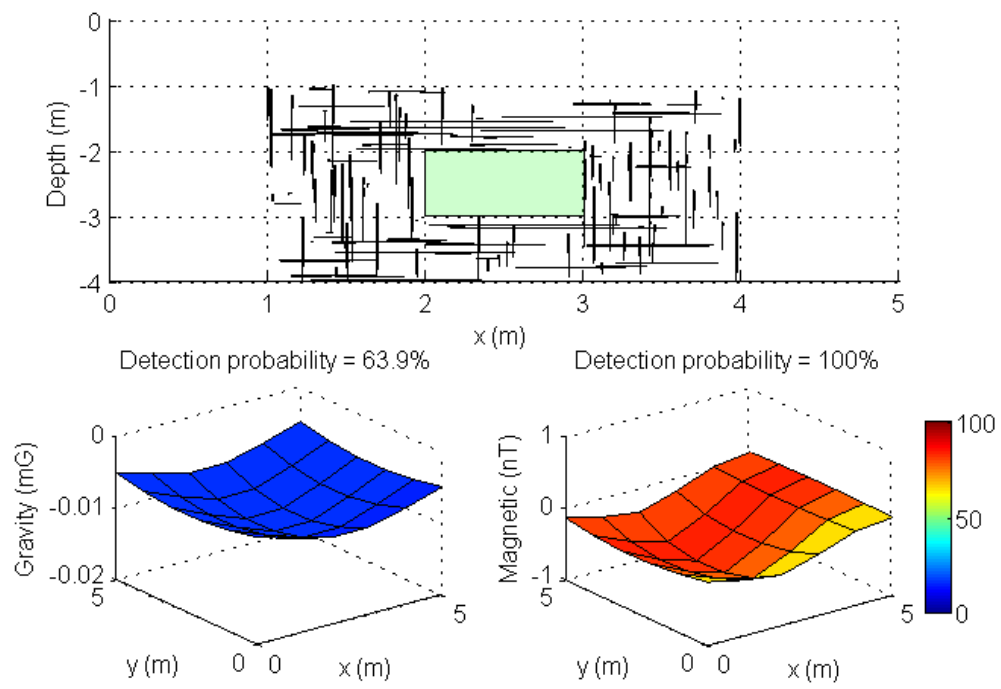
No halo



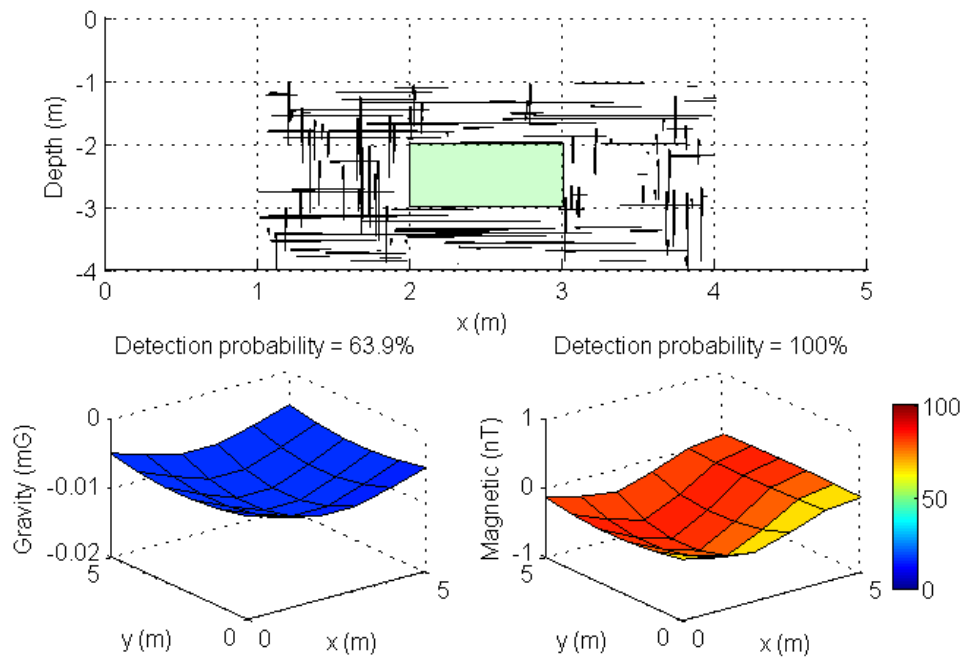
10% indent



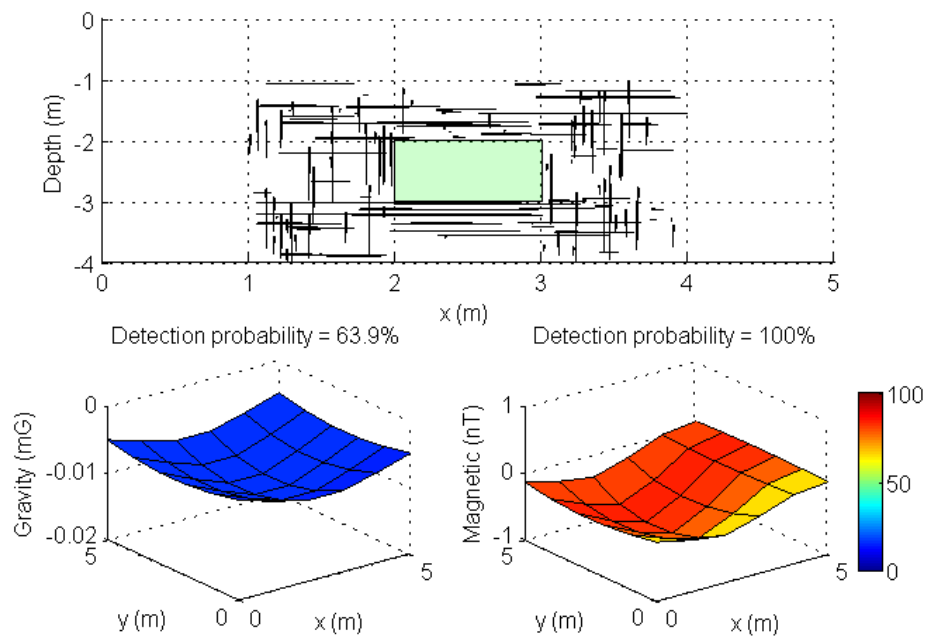
20% indent



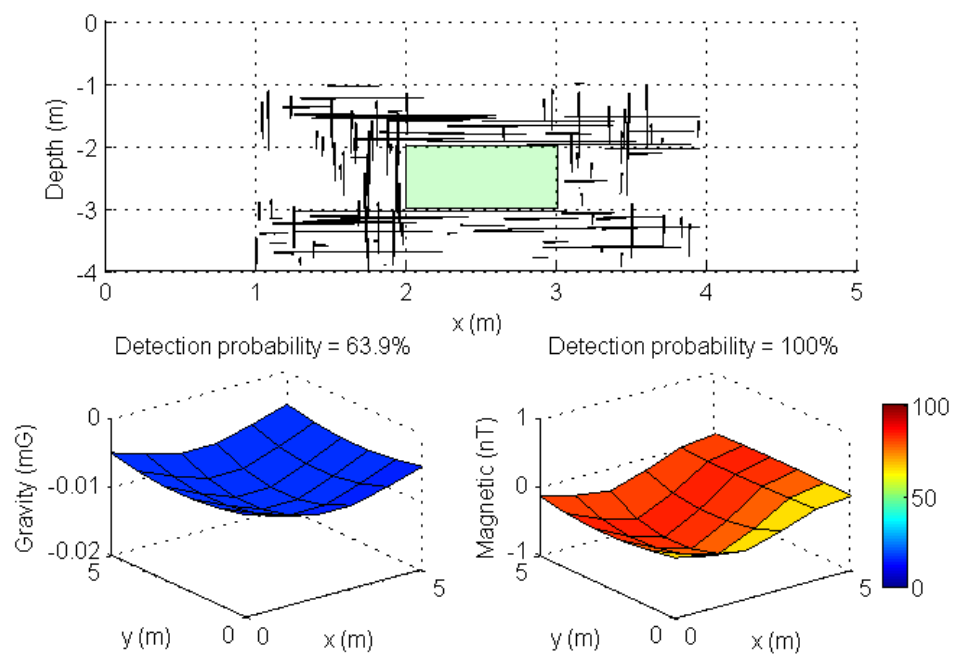
30% indent



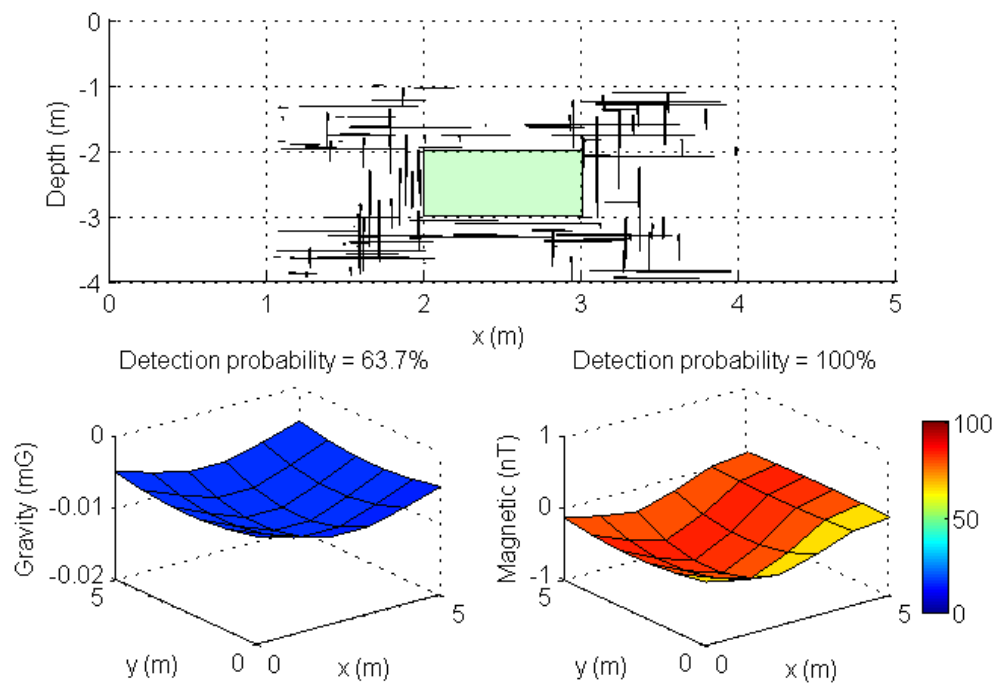
40% indent



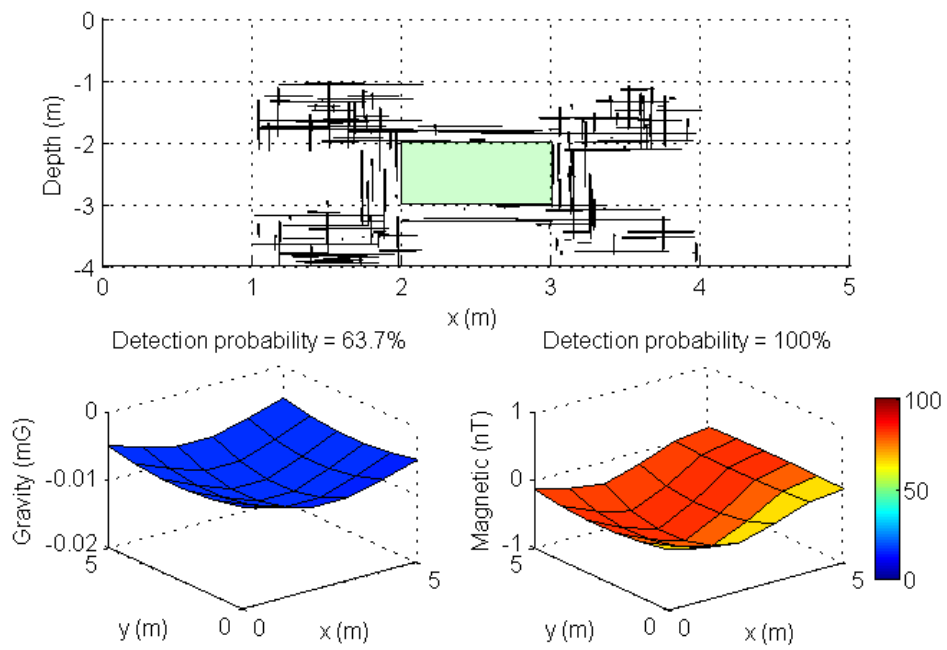
50% indent



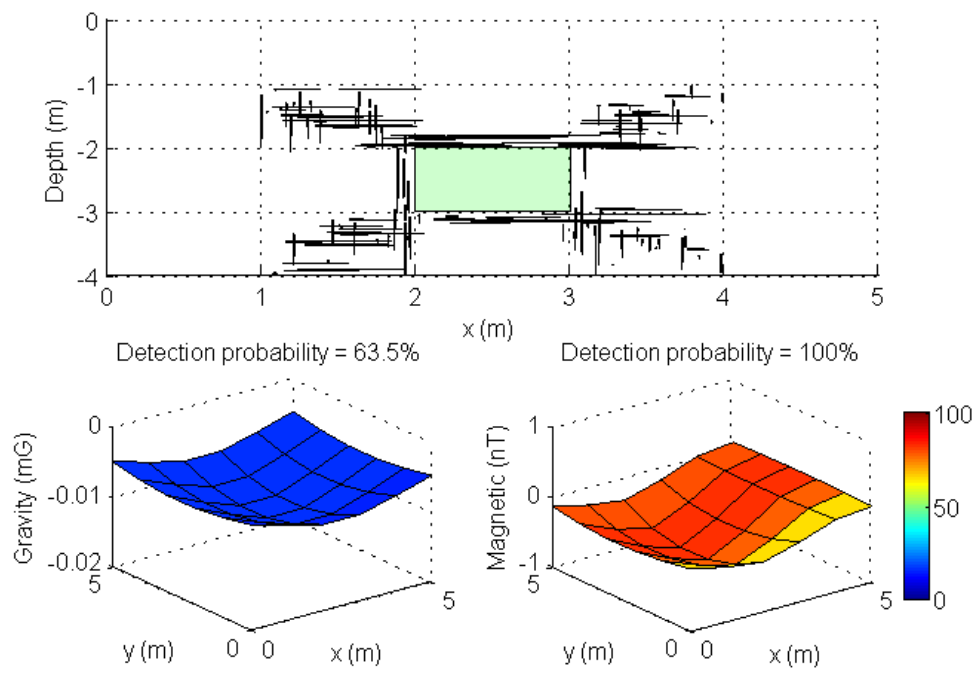
60% indent



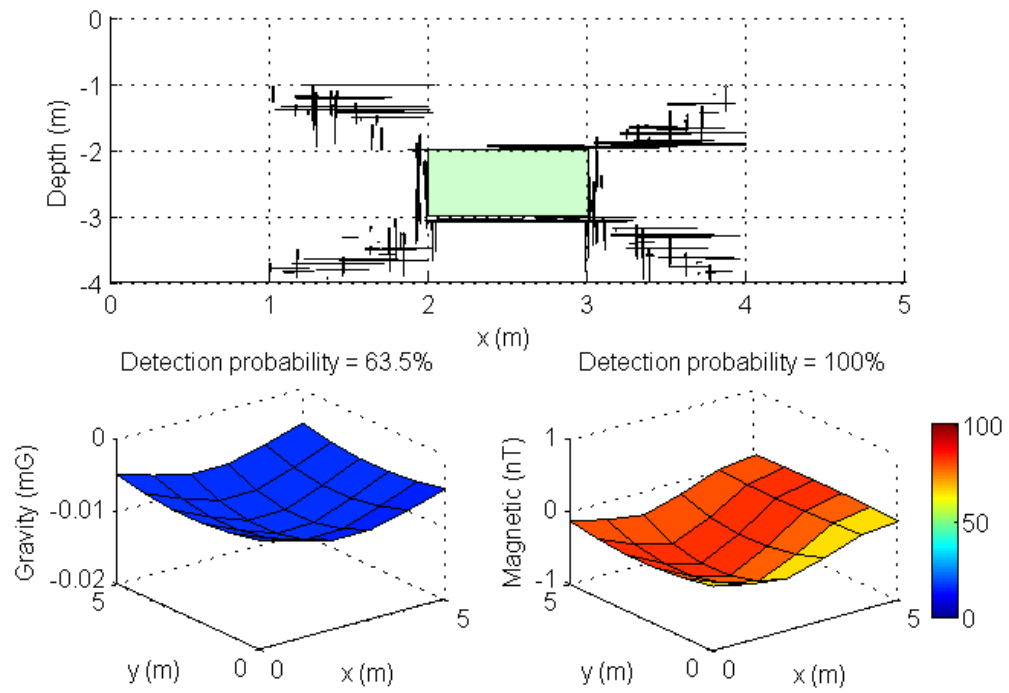
70% indent



80% indent



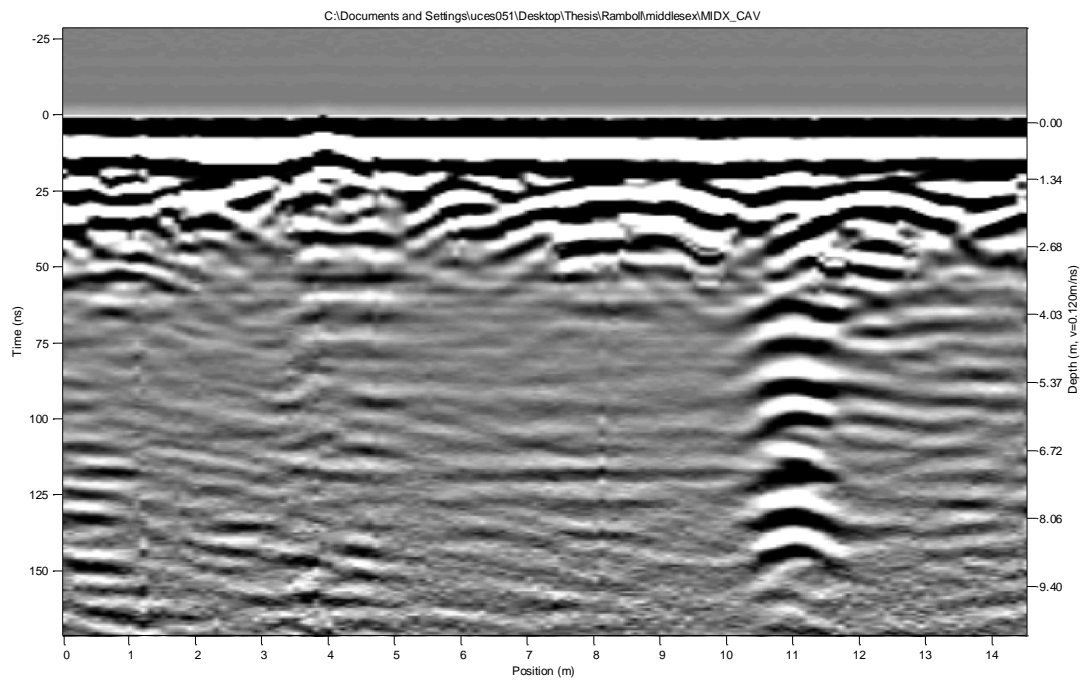
90% indent



Appendix G Case study data

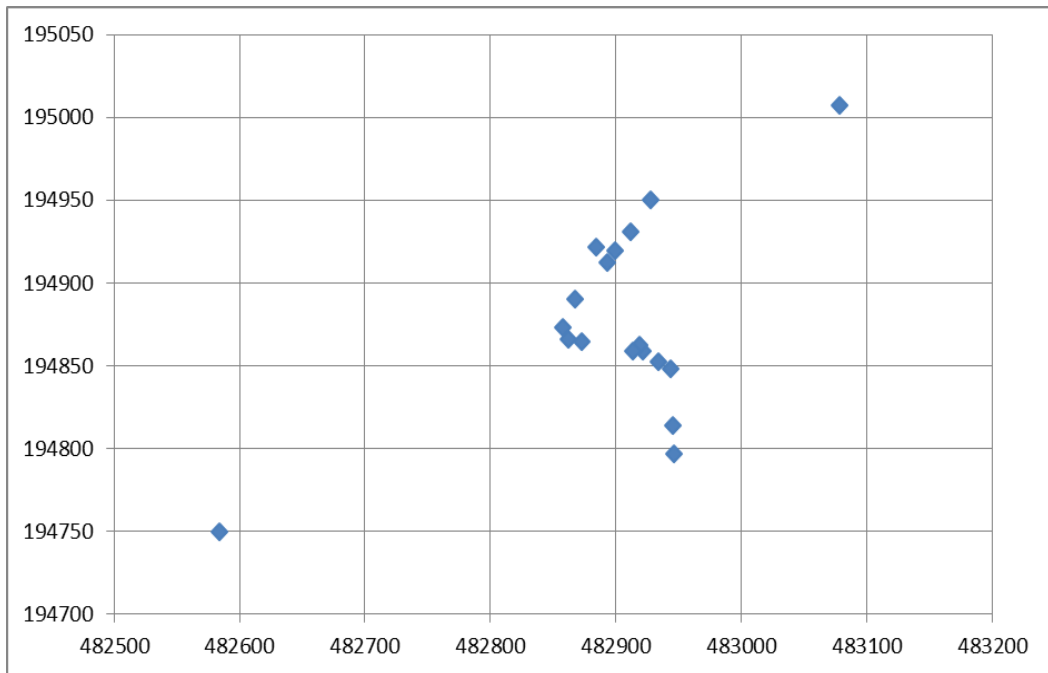
Middlesex

GPR data



West Wycombe caves

Coordinate location



Variation in DEM depths

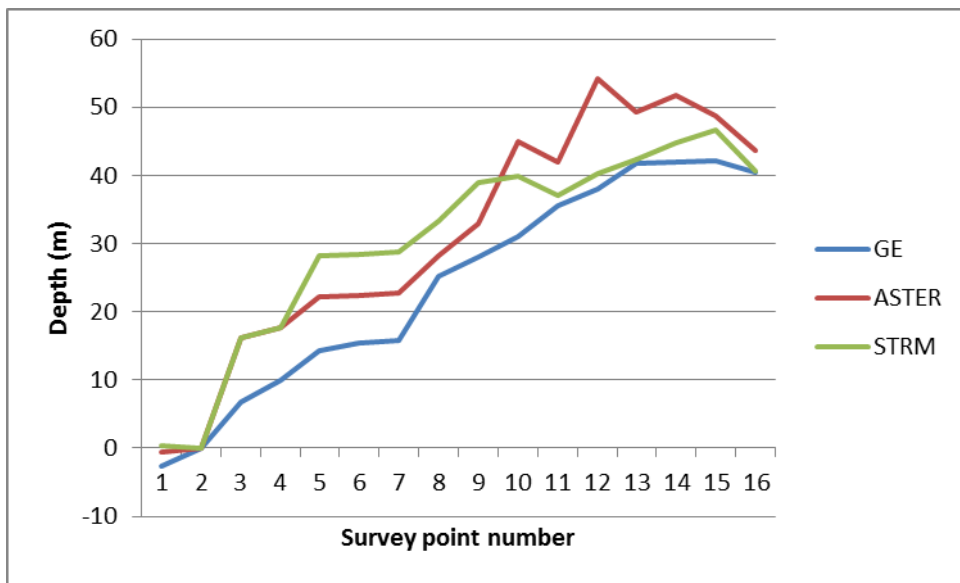


Figure 11.6. Depth to cave from surface at survey points. Digital Elevation models: GE – Google Earth, ASTER - Advanced Spaceborne Thermal Emission and Reflection Radiometer, STRM - Shuttle Radar Topography Mission.

West Wycombe geological maps

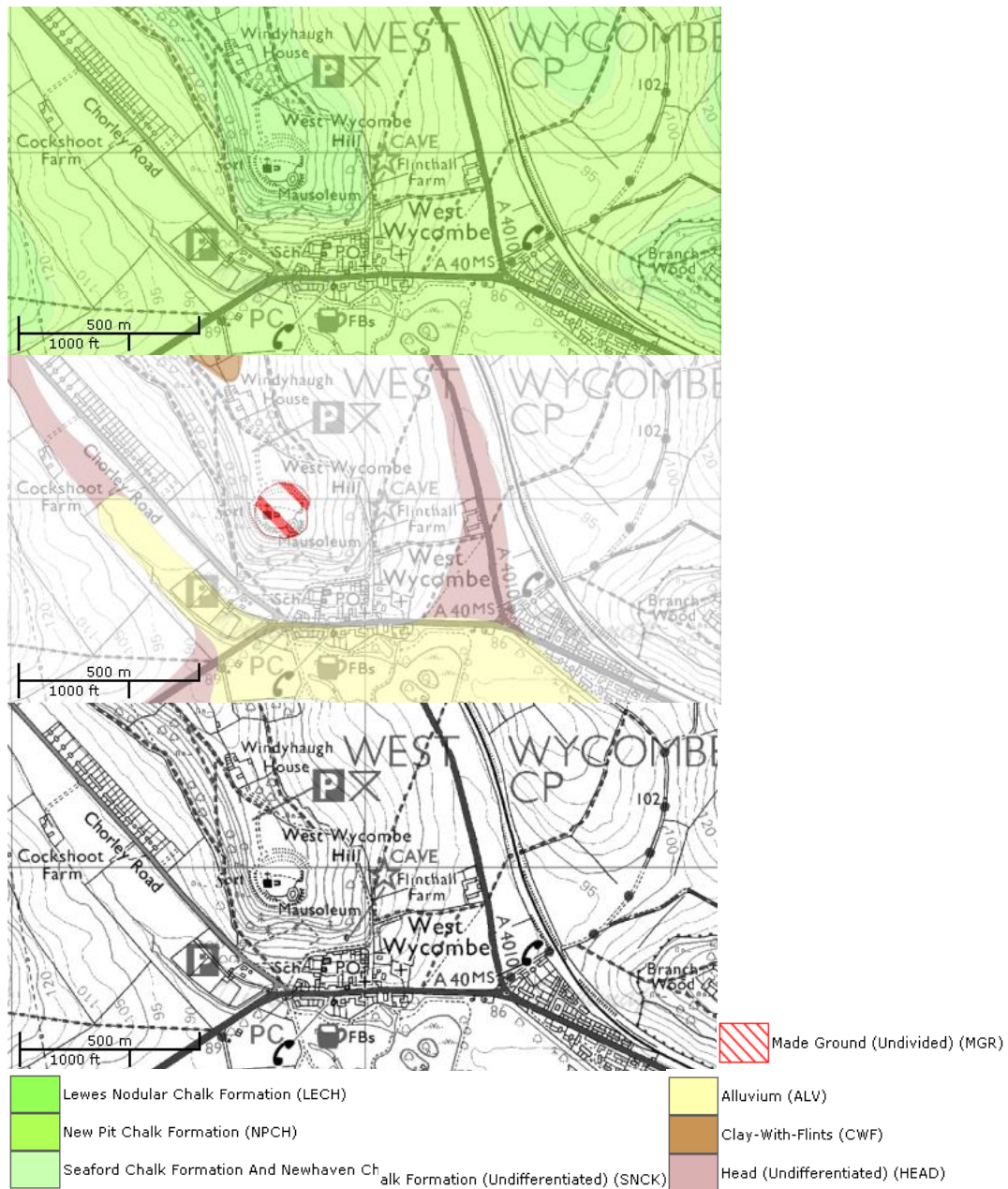
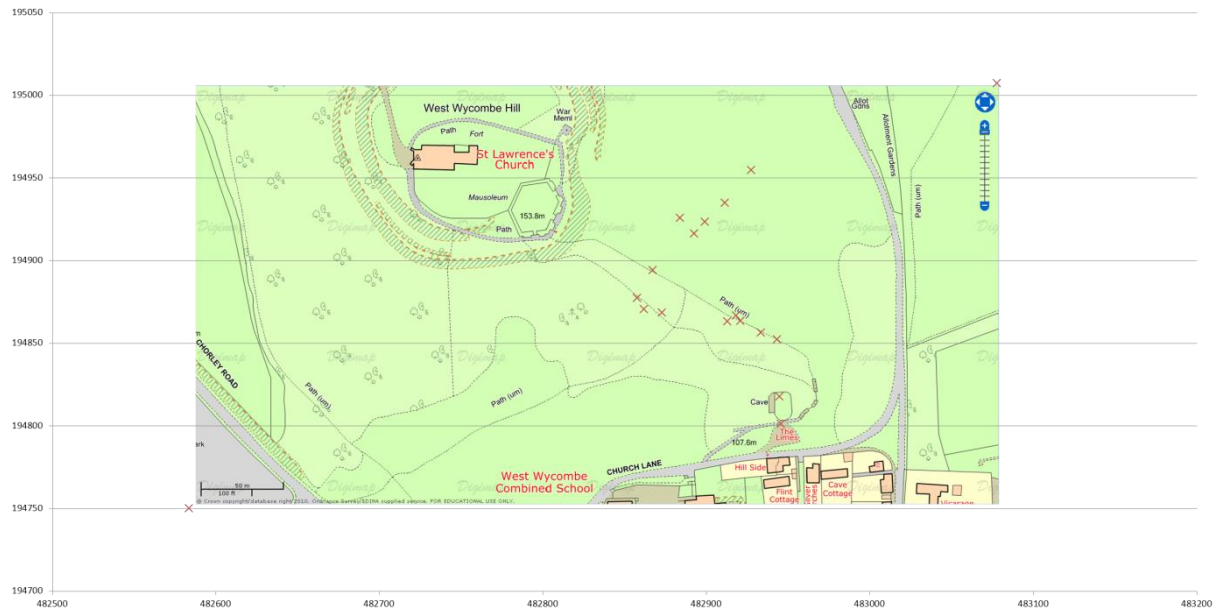


Figure 11.7 Geological and OS maps. Top: basement geology. Middle: Superficial geology. Bottom: OS map.



Location of tunnel

St. Ambrose

Site geology

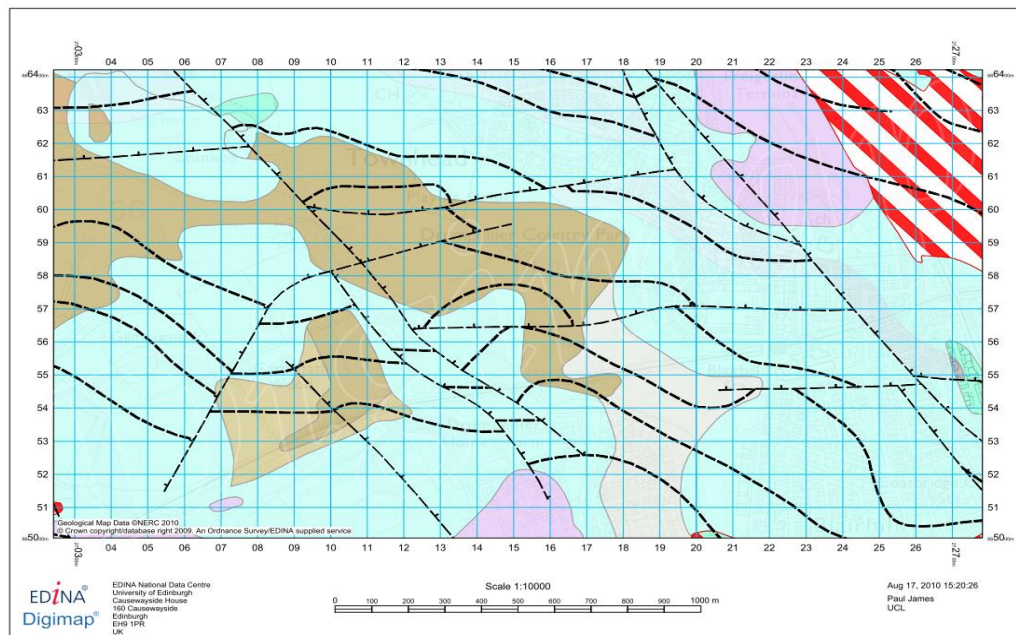


Figure 11.8 - Geological map of survey area. The brown unit is a superficial deposit of peat of quaternary age. The blue unit is a superficial deposit of till (Devensian) of quaternary age. The pink unit is a superficial deposit of Glaciolacustrine Deposits (Undifferentiated) (clay, silt and sand) of quaternary age. Dotted black lines are inferred coal seams, and dashed, dotted lines are inferred normal faults (N.E.R.C., 2010).

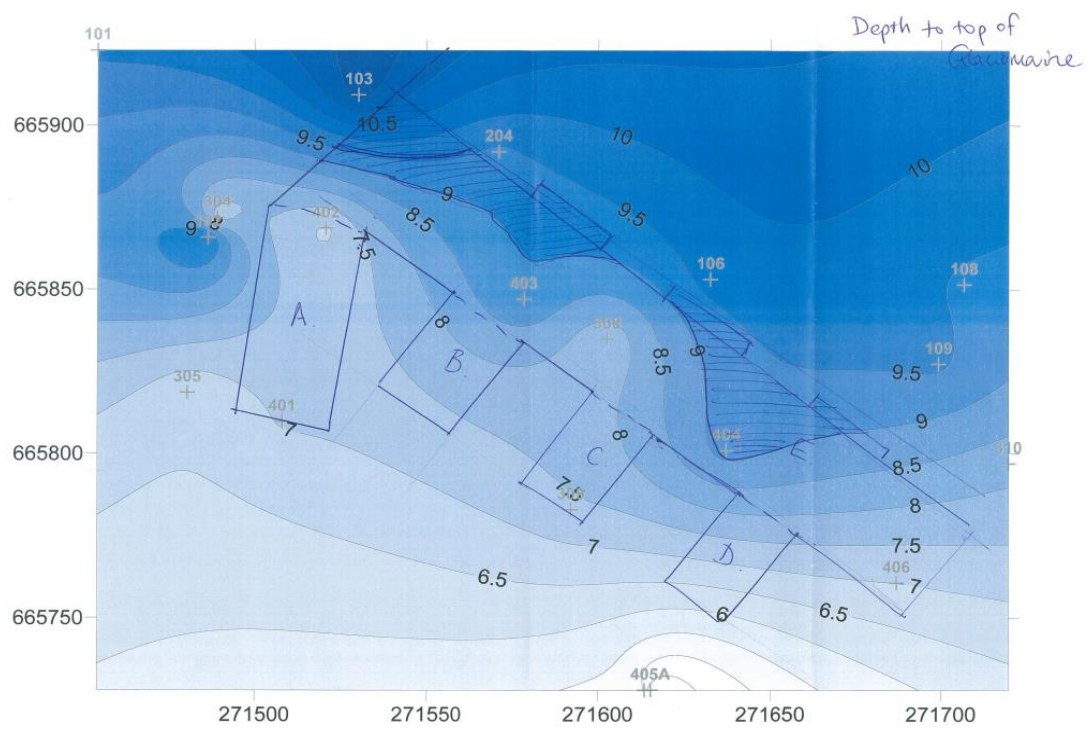


Figure 11.11 - Depth to Glaciomarine (m)

BH401		BH402		BH403		BH404		BH405		BH405A		BH406	
Depth (m)		Depth (m)		Depth (m)		Depth (m)		Depth (m)		Depth (m)		Depth (m)	
0	made ground (mg)	0	mg	0	mg	0	mg	0	mg	0	ash fill	0	mg
2.3	peat	1.6	peat	1.8	peat	3.4	peat	0.5	mg - gravelly sandy clay	1.5	peat	3.5	peat
7.05	silt	6.9	silt	8	clayey peat	5.8	peat	1.4	peat	4	boulder clay	7	clay
9	clay	7.8	clay	9	clay	9.2	clay	5.2	sand	9.9	void	8.4	weathered bedrock
10	sand	15.3	weathered rockhead	9.5	gravelly sandy silty clay	10.8	gravelly sandy clay	9.6	weathered bedrock	10.4	broken ground - sandstone coal shale	9.63	sandstone and silts
13	clay	15.55	sandstone	13.4	weathered rockhead	13	weathered bedrock	9.92	sandstone - fragments of coal	18		10.5	broken ground - sandstone ss, mudstone
13.8	sand	18.35	mudstone	14.24	mudstone	13.77	sandstone	10.54	siltstone			12.2	sandstone and ss
14.1	rockhead	20.5	siltstone	14.34	dark green crystalline to coarse grained igneous	16	mudstone	10.6	void			14.97	weak thin layered
14.3	sandstone and siltstone	25.5		14.46	mudstone	16.55	sandstone and siltstone	11.5	broken ground			15.02	mudstone
17.25	mudstone			15.2	broken ground	18.1	mudstone	13				15.2	sandstone and silts
17.5	sandstone and siltstone			16	sandstone and siltstone	18.25	sandstone and siltstone					19.6	
18.4	coal			19.44	coal	19.5	void						
18.56	sandstone and siltstone			20.1	mudstone	20.1	broken ground						
22.97	mudstone			20.31	sandstone and siltstone	20.5	sandstone and siltstone						
23.5	ss and ss			24.1		24.25							
24.5													

Table 11.7 - Borehole logs. For borehole locations see Figure 11.12.

TP01		TP02		TP03		TP04		TP05		TP101	
Depth (m)		Depth (m)		Depth (m)		Depth (m)		Depth (m)		Depth (m)	
0	grass over topsoil	0	grass over topsoil	0	grass over topsoil	0	grass over topsoil	0	grass over topsoil	0	grass over topsoil
0.07	made ground	0.1	made ground	0.1	made ground	0.07	made ground	0.1	made ground	0.15	made ground
1.8	peat	2	peat	2.3	clay	1.5	sand gravelly clay	2.9	sandy clay	2.9	clay
3.2		2.8		3		3		3.3		3.5	
TP102		TP103		TP104		TP105		TP106		Handpits (general)	
Depth (m)		Depth (m)		Depth (m)		Depth (m)		Depth (m)		Depth (m)	
0	grass over topsoil	0	grass over topsoil	0	grass over topsoil	0	grass over topsoil	0	grass over topsoil	0.03-0.15	grass over topsoil
0.2	made ground	0.2	made ground	0.1	made ground	0.17	made ground	0.18	made ground	0.85-1.2	made ground
3.8		3.4		3.4	clay	4.1		3.3			
				3.6							

Table 11.8 - Trial pit and hand pit logs. For trial pit and hand pit locations see Figure 11.12.

Historical O.S. Maps

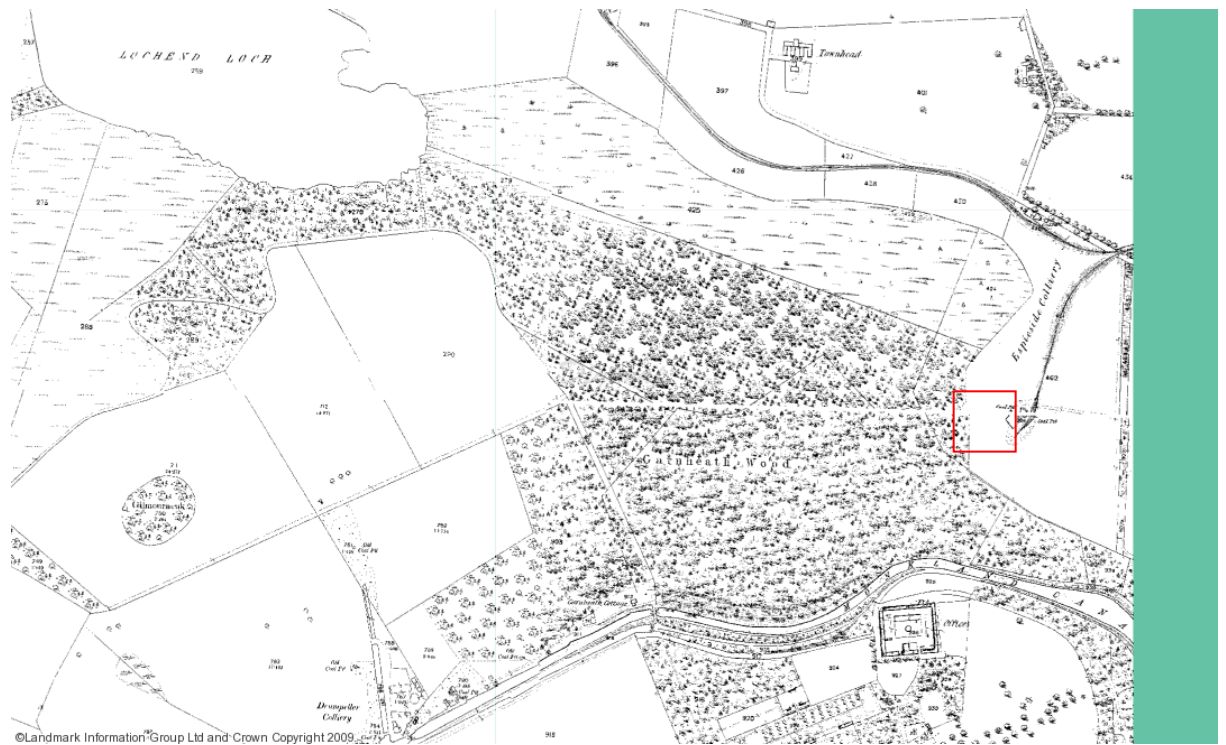


Figure 11.13 – 1859 O.S. Map. Red box indicates location of coal pit.

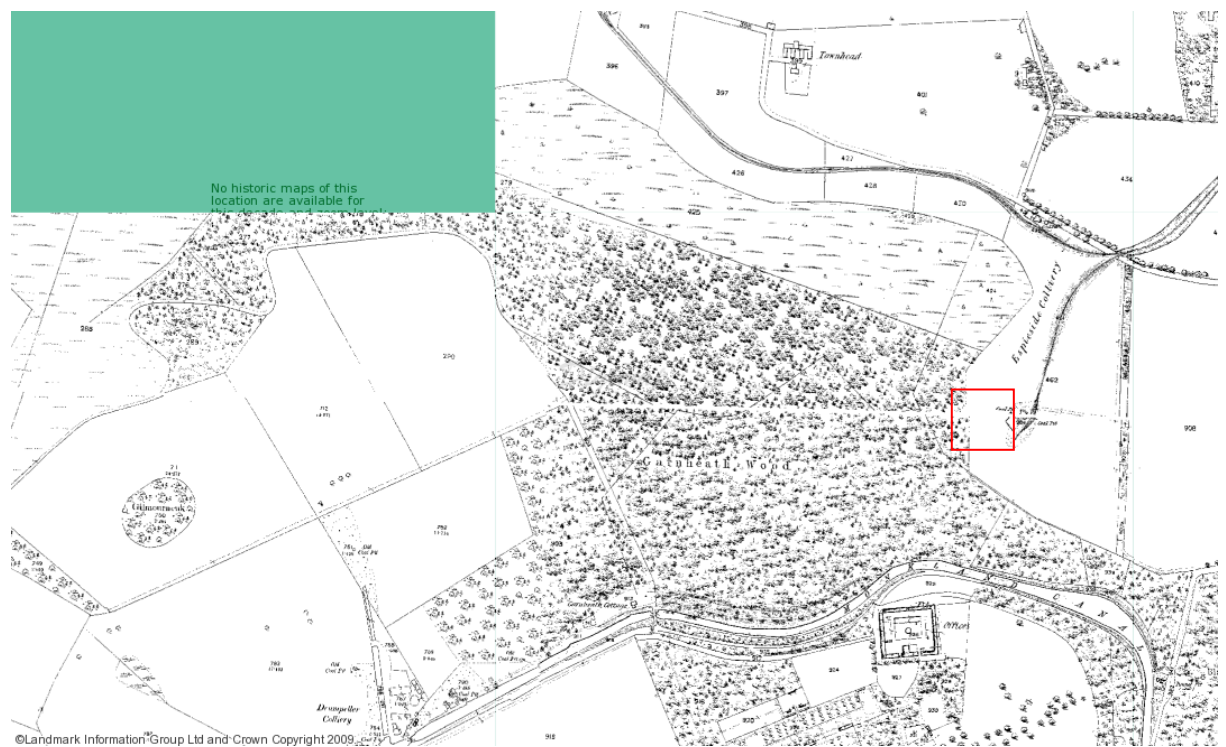


Figure 11.14 – 1860 O.S. Map. Red box indicates location of coal pit.

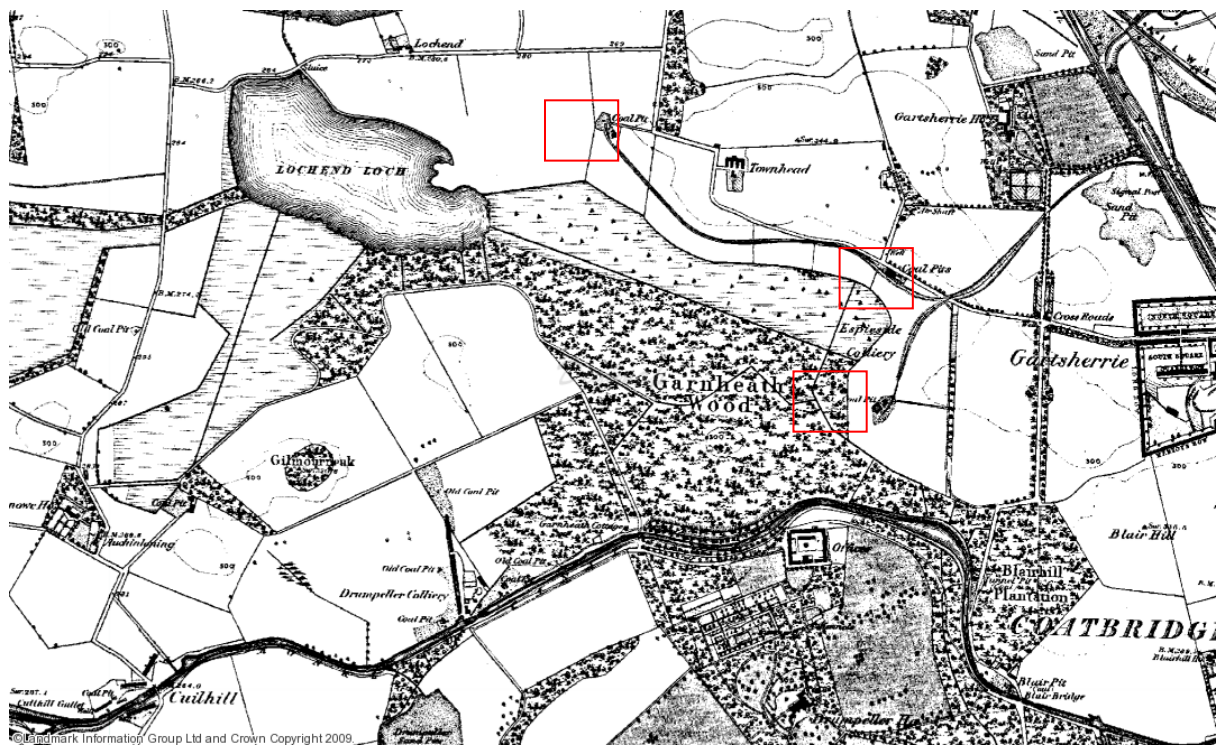


Figure 11.15 – 1864 O.S. Map. Red box indicates location of coal pit.

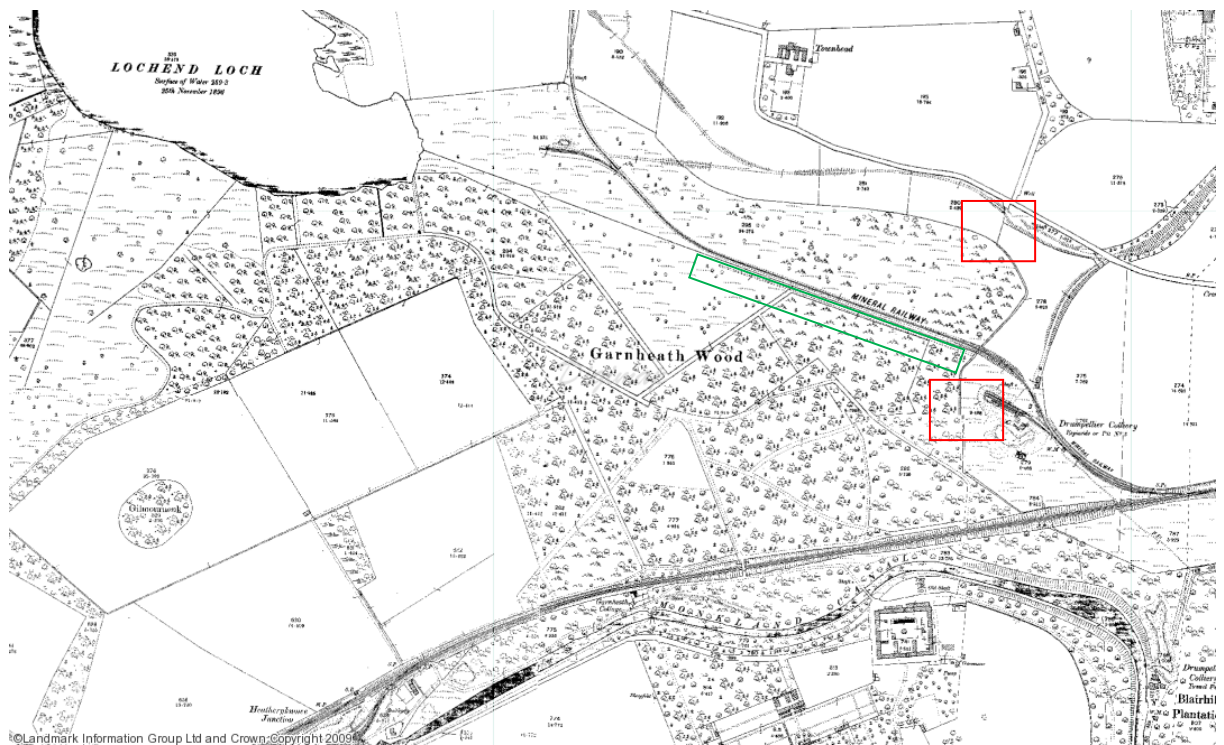


Figure 11.16 – 1898 O.S. Map. Red boxes indicate shafts. Green box indicates old railway – now a path.

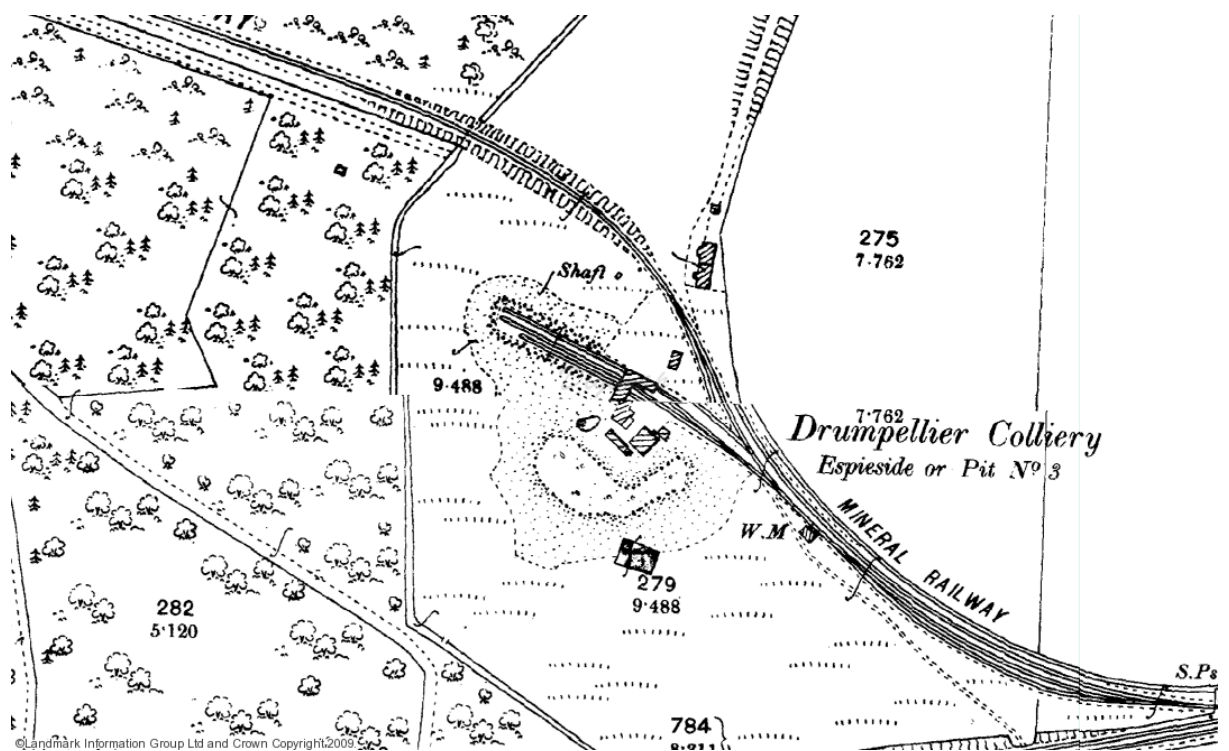


Figure 11.17 - 1898 O.S. Map. Zoom of shaft area.

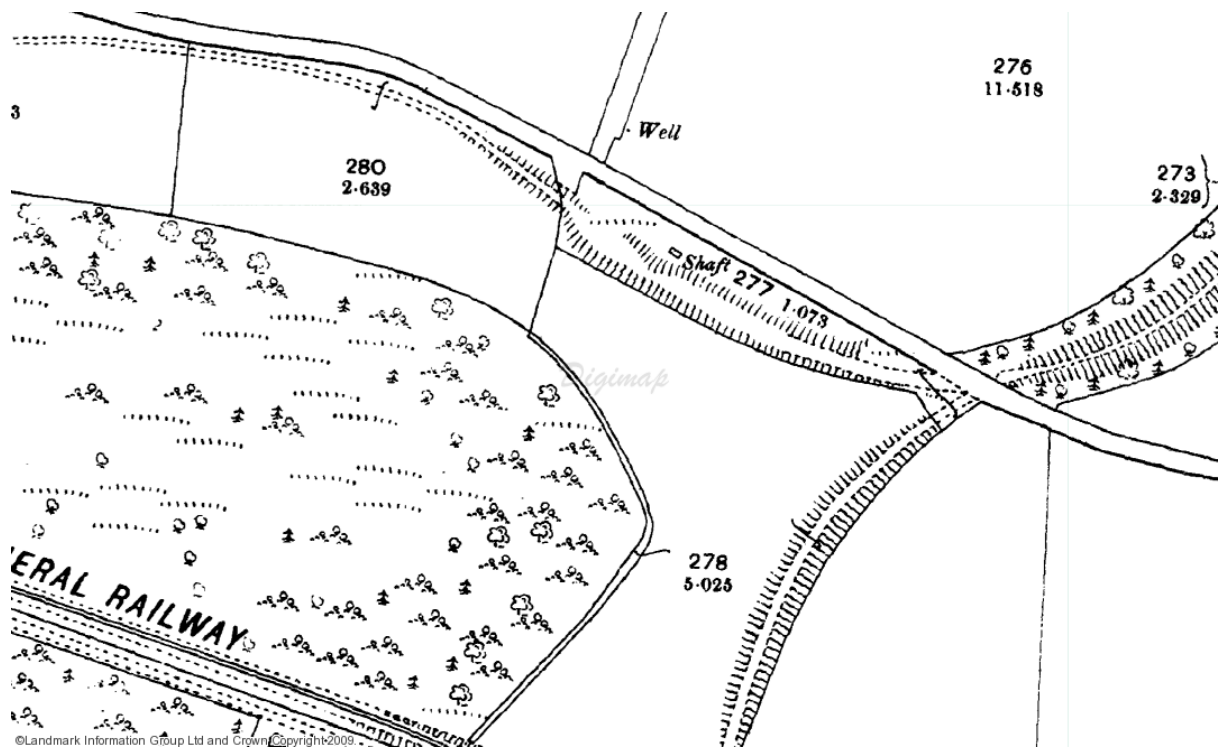


Figure 11.18 - 1898 O.S. Map. Zoom of northern shaft area.

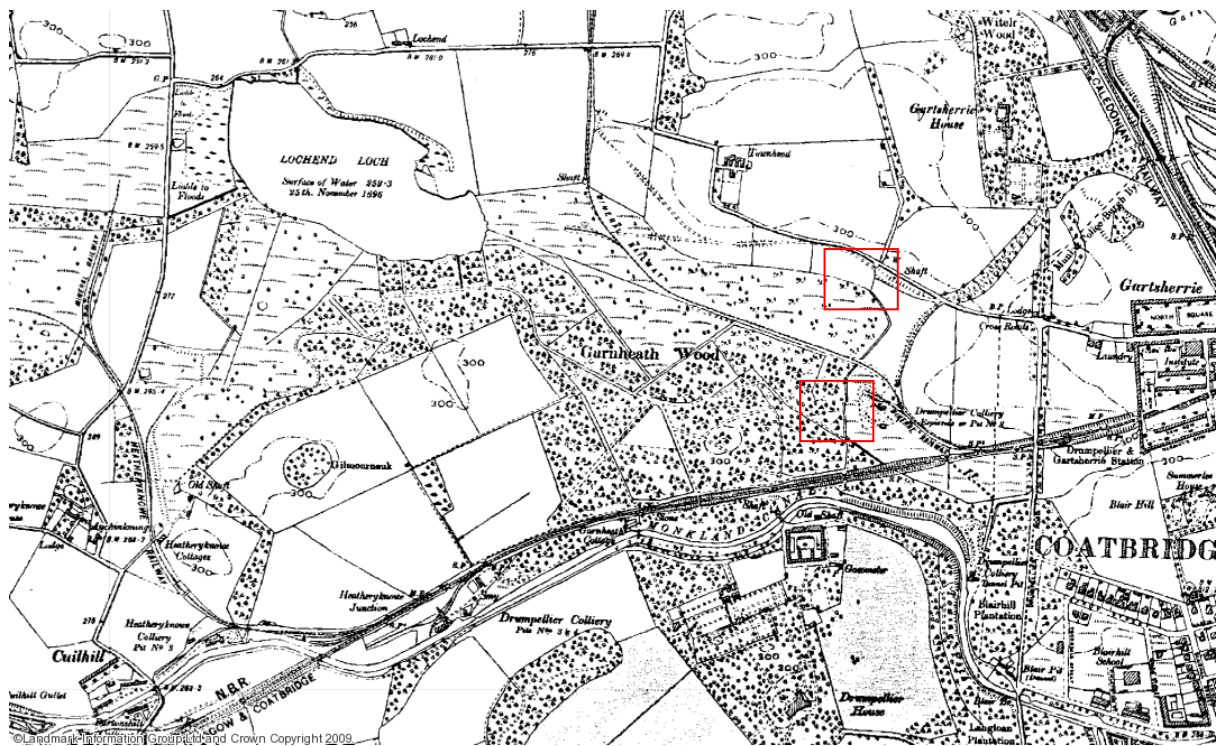


Figure 11.19 – 1899 O.S. Map. Red box indicate shaft and mine (here not labelled as such).

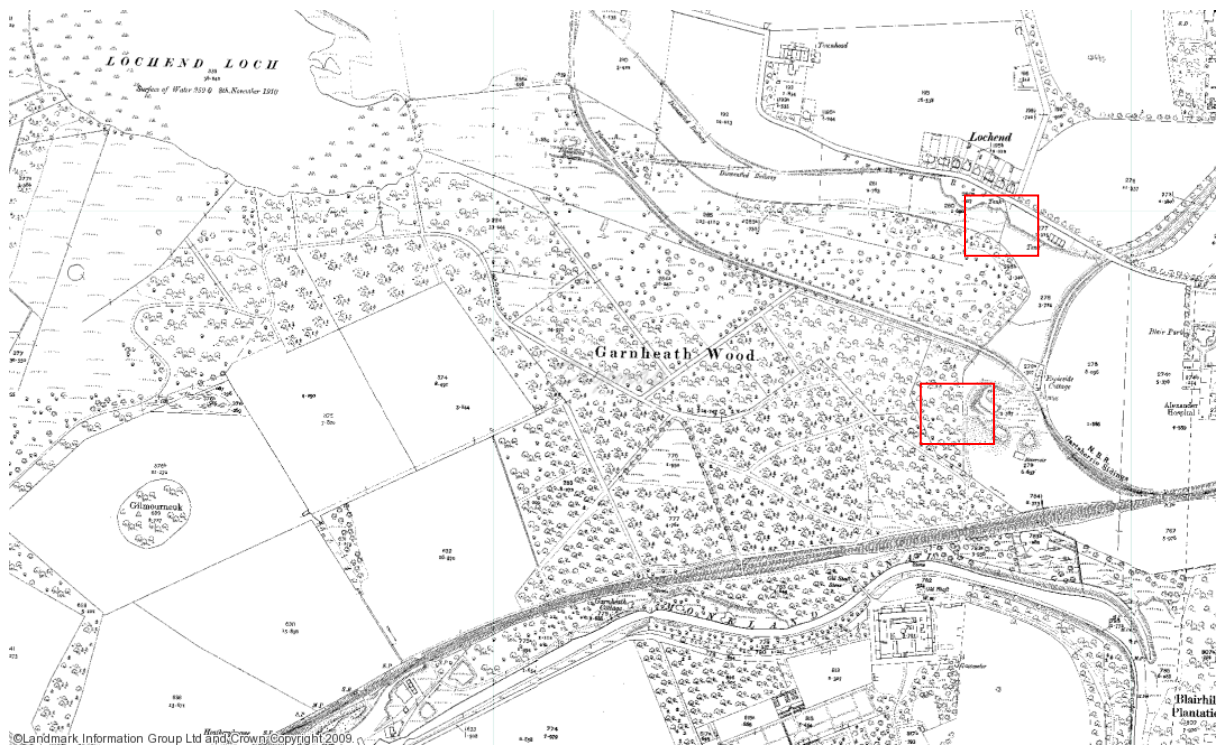


Figure 11.20 – 1912 O.S. Map. Red boxes indicate areas of shafts – no longer marked on these maps indicating inactivity. Railway now noted as dismantled.

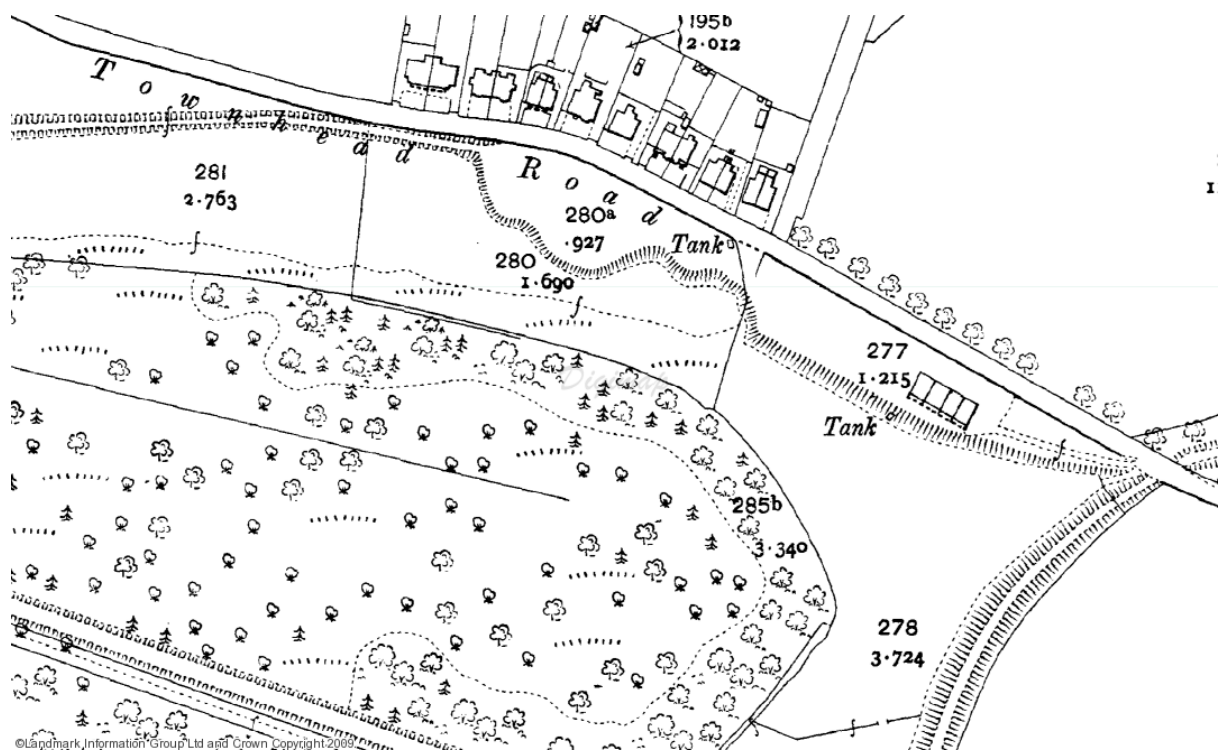


Figure 11.21 - 1912 O.S. Map. Zoom of tank.

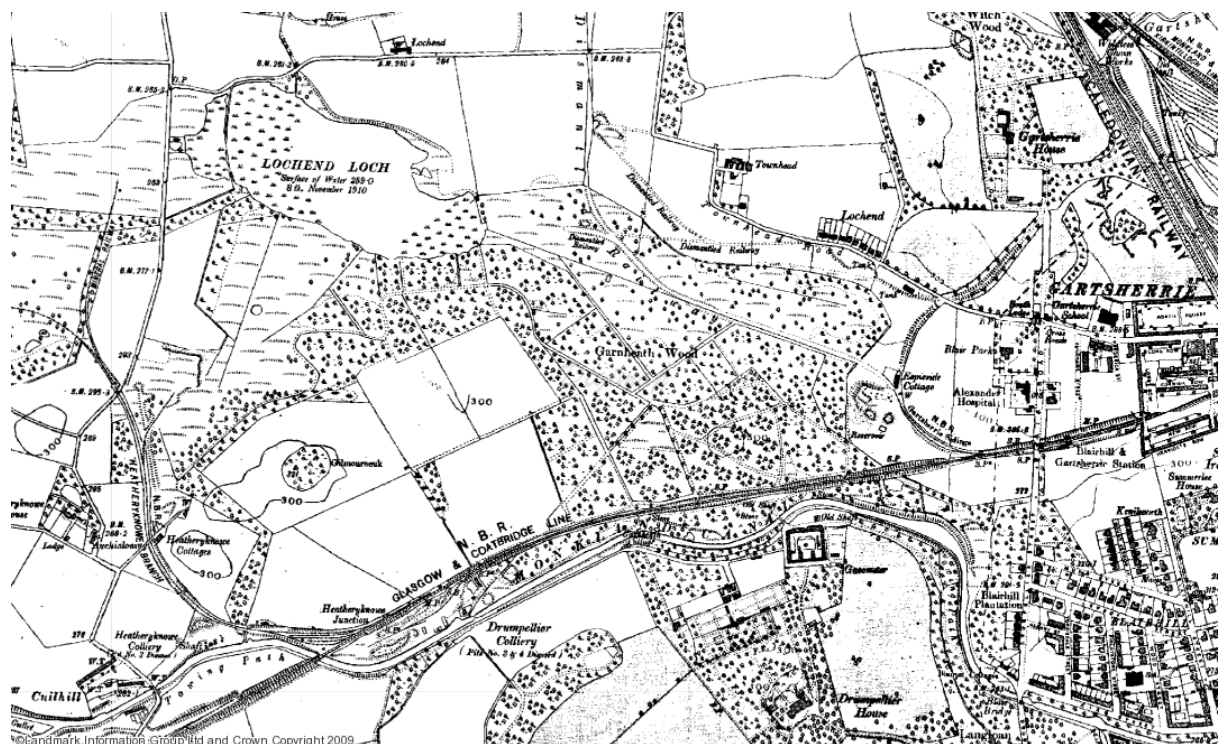


Figure 11.22 - 1914 O.S. Map. Mining activity no longer noted.

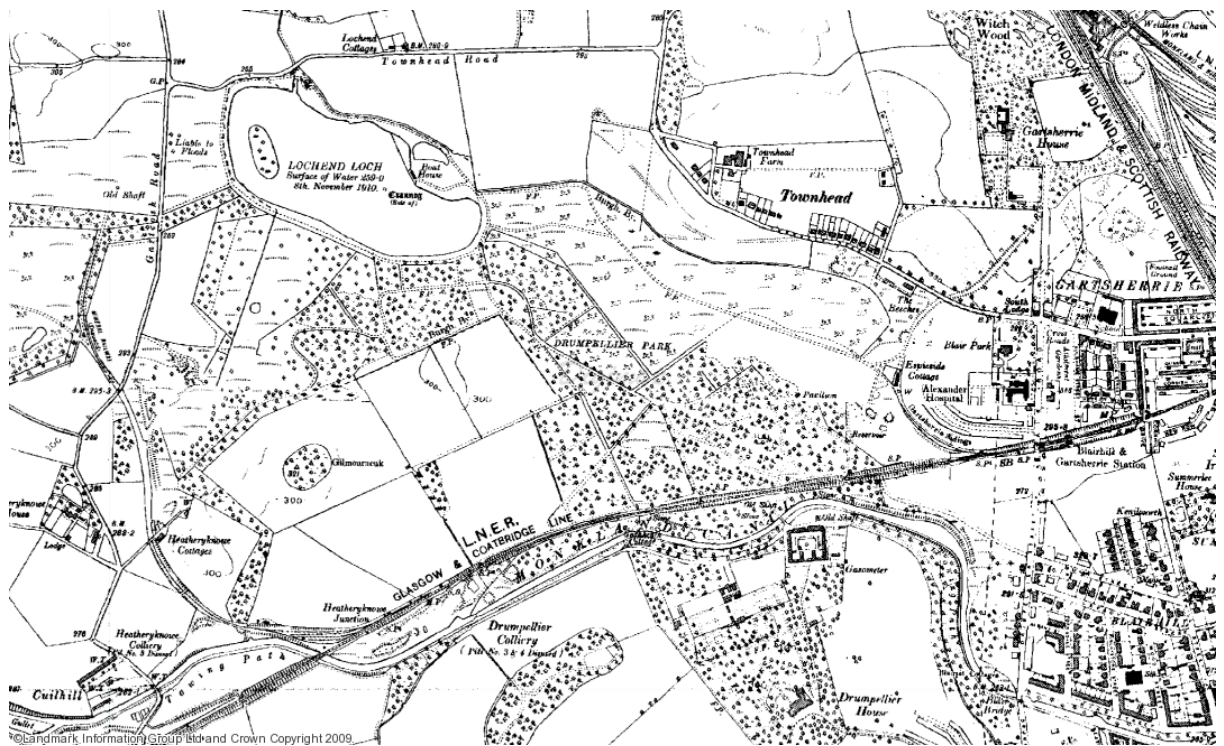


Figure 11.23 – 1935 O.S. Map. No mention of mining activity. Railway line now path.



Figure 11.24 – 1936 O.S. Map. No mention of mining activity.

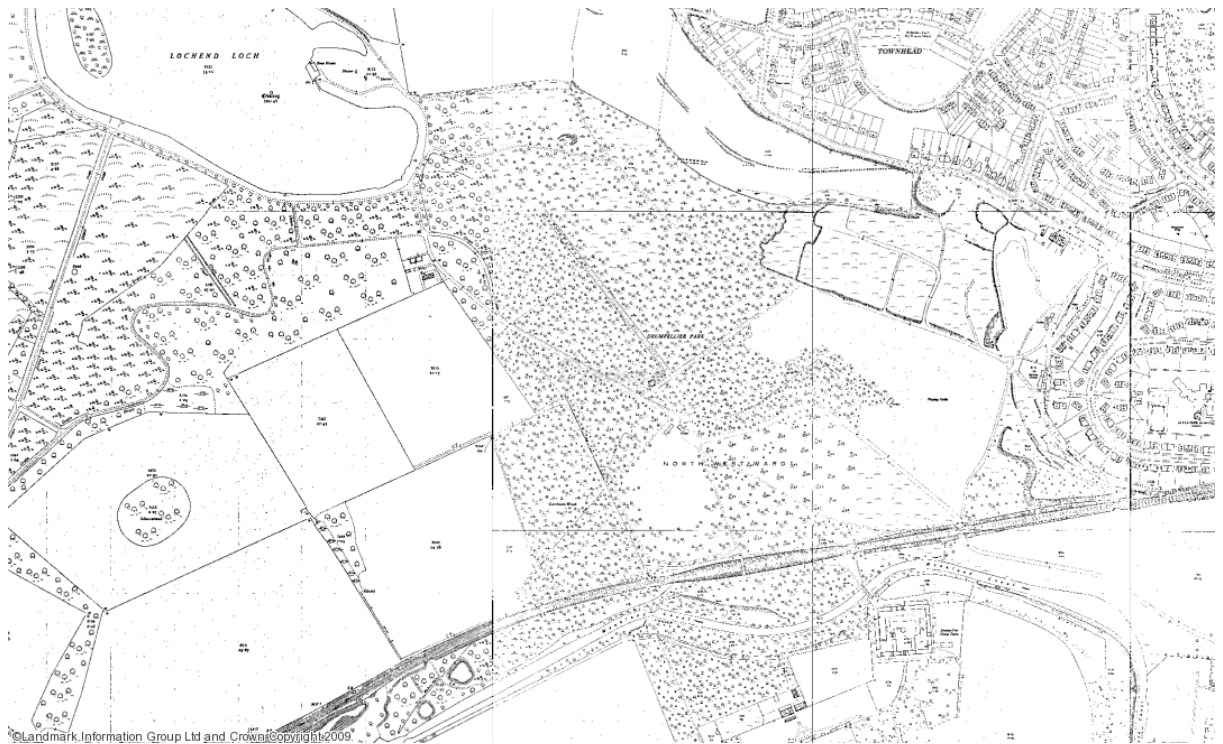


Figure 11.25 – 1955 O.S. Map. New cutting activity..

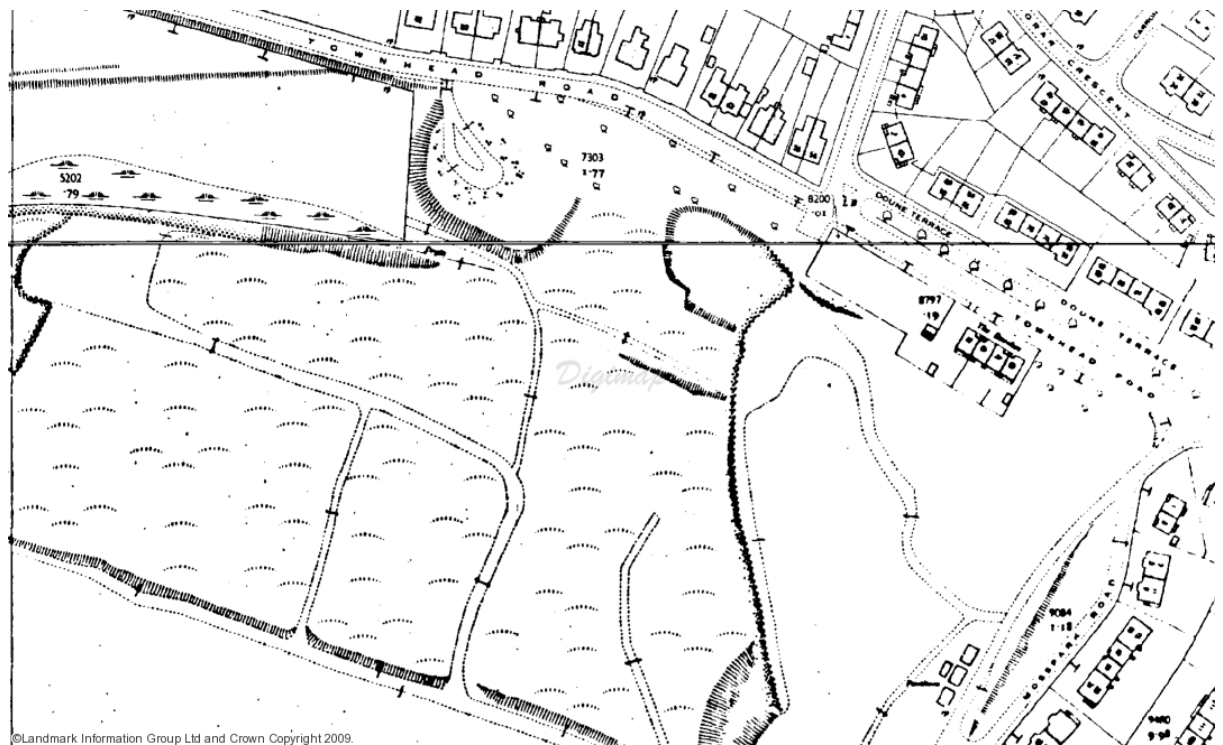


Figure 11.26 - 1955 O.S. Map. Zoom of cutting.

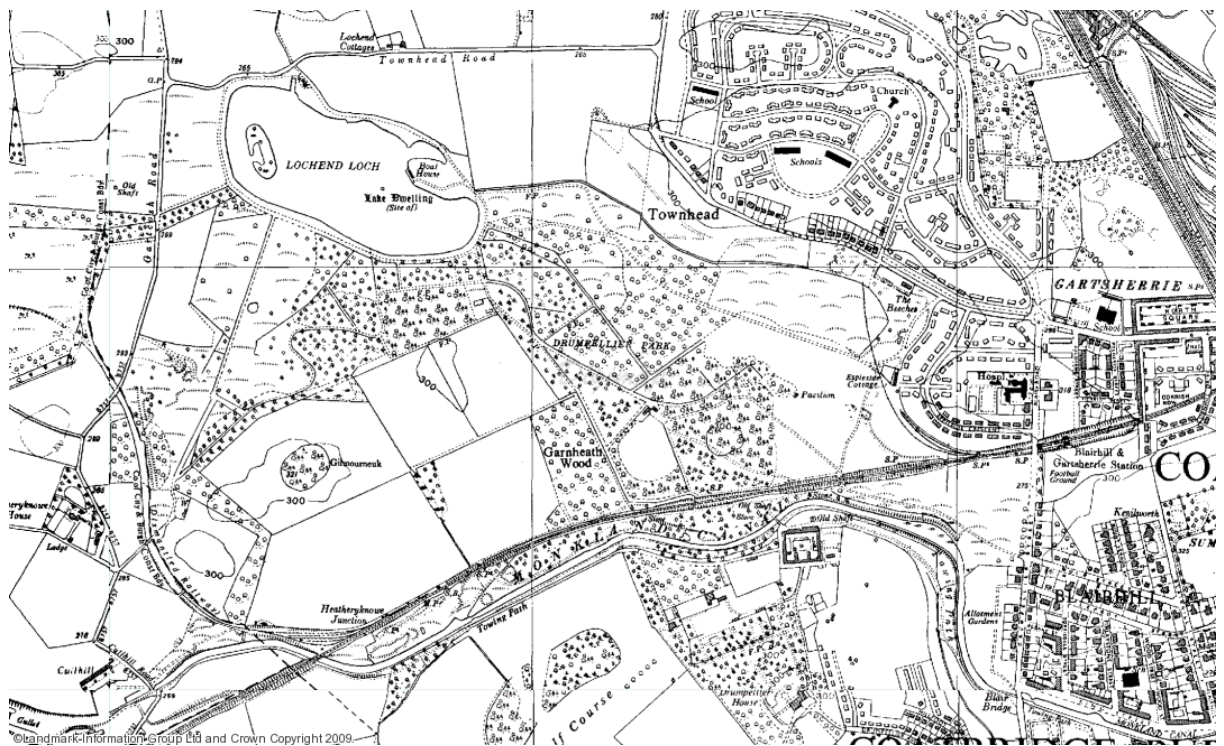


Figure 11.27 – 1958 O.S. Map.

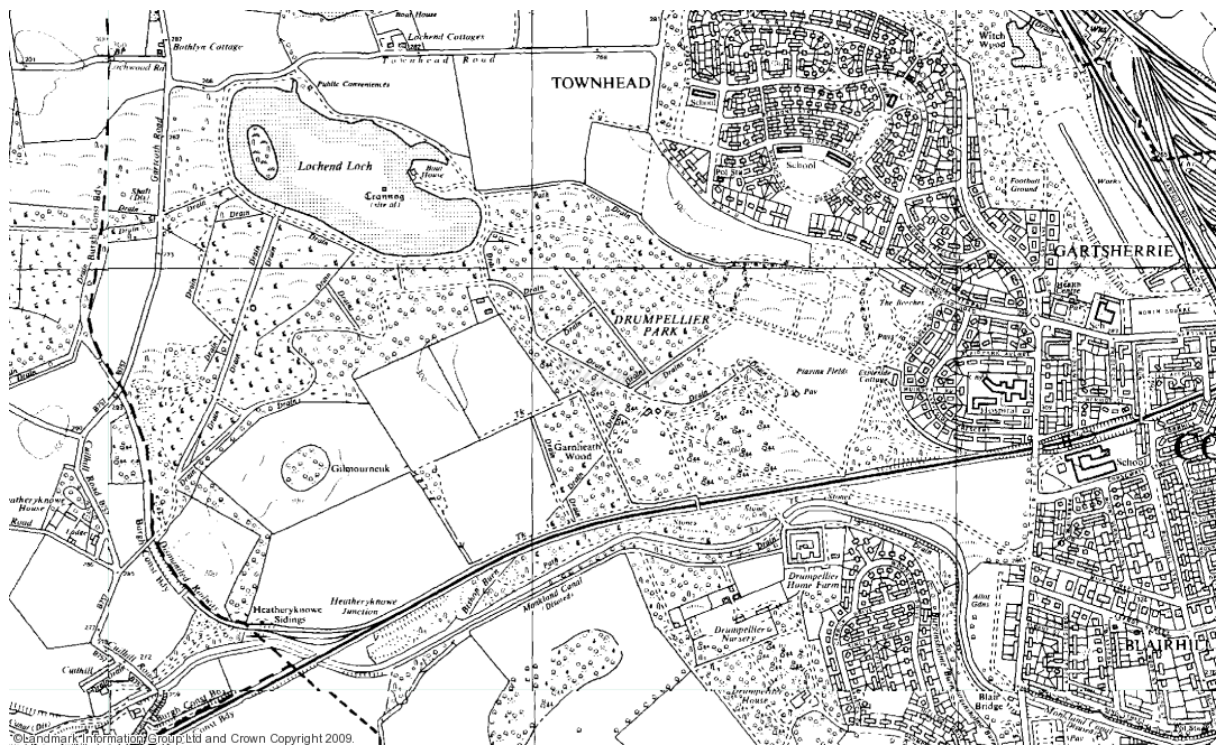


Figure 11.28 – 1967 O.S. Map.

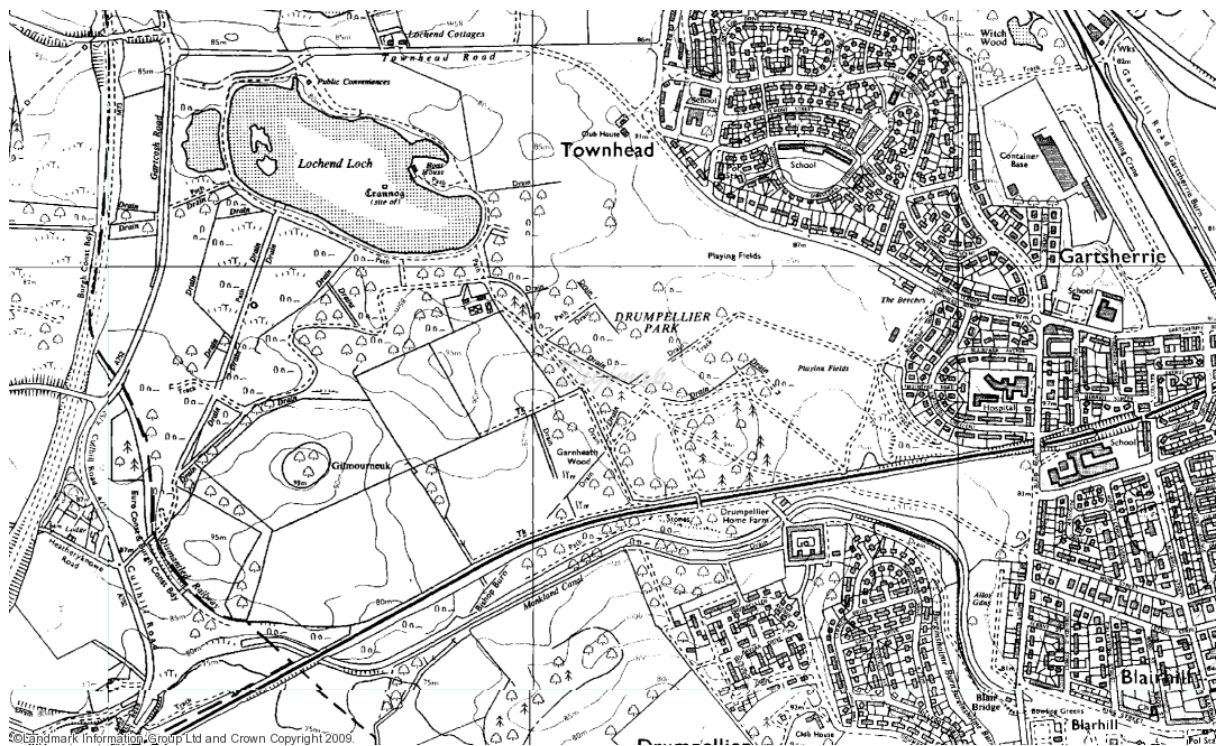


Figure 11.29- 1982 O.S. Map. Landfill area now playing fields.

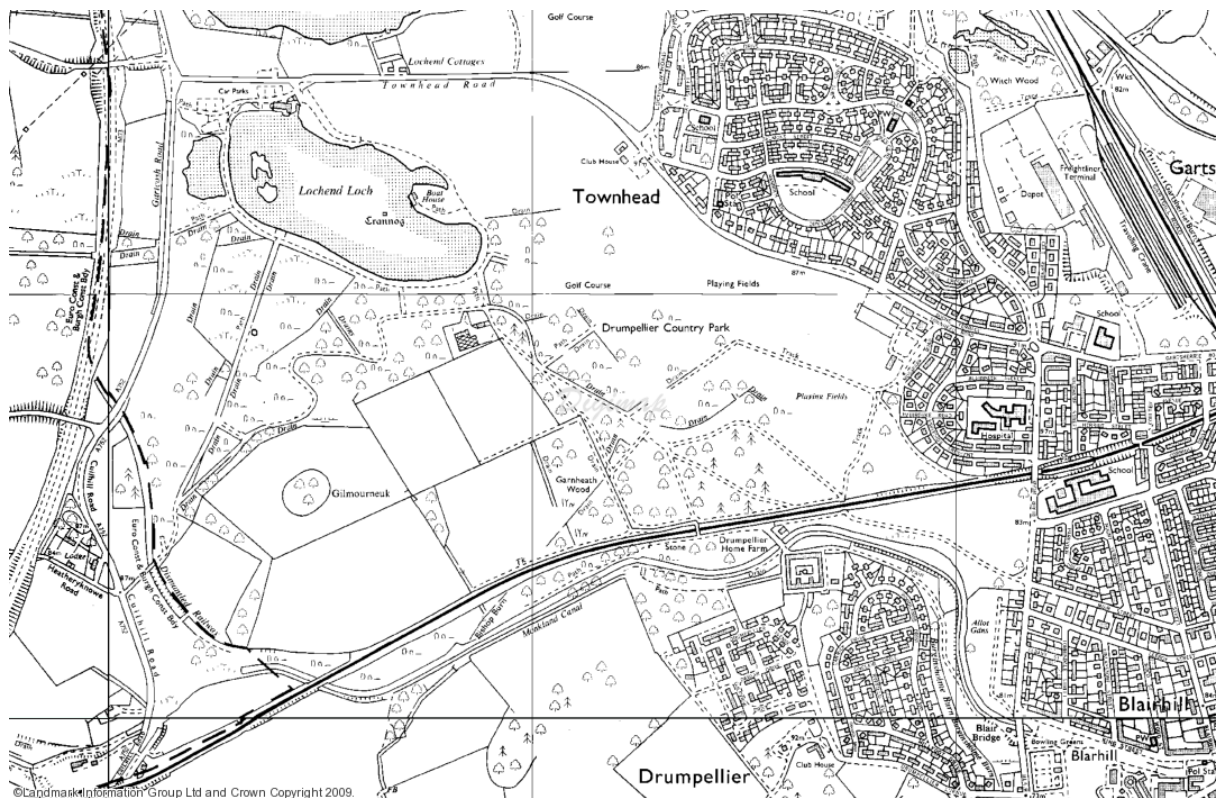
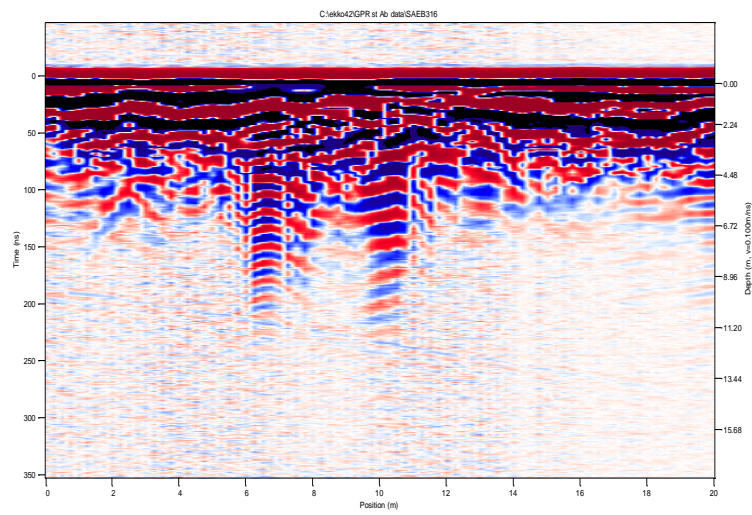
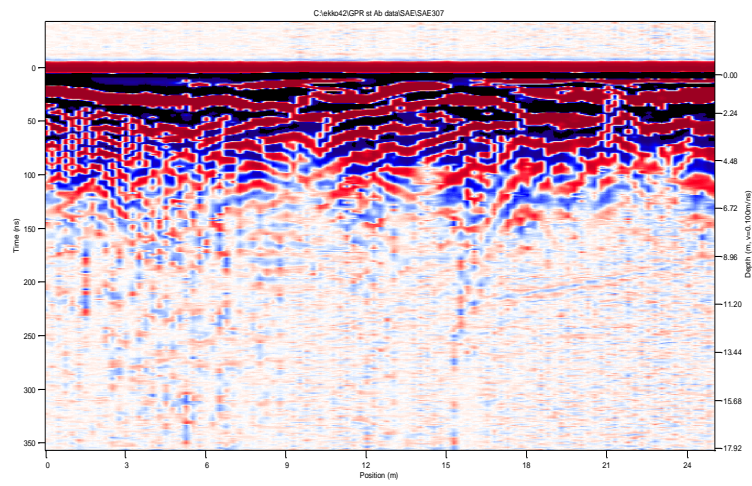


Figure 11.30 - 1993 O.S. Map.

GPR sections

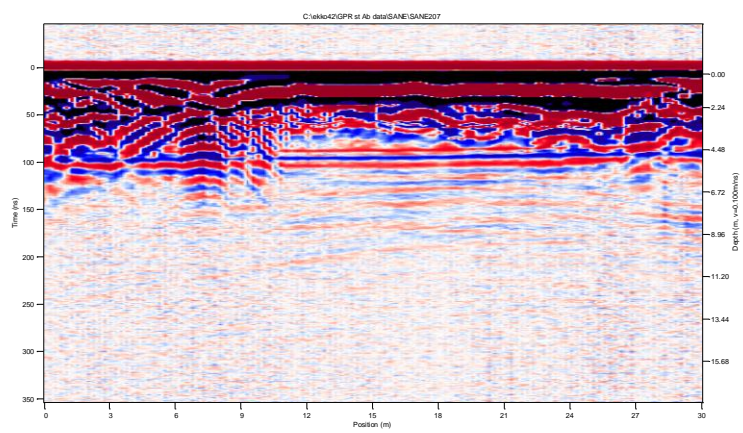
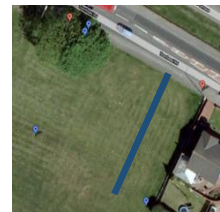
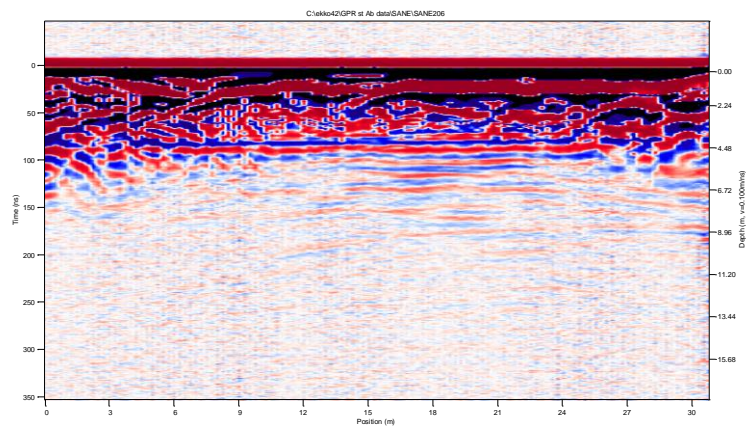
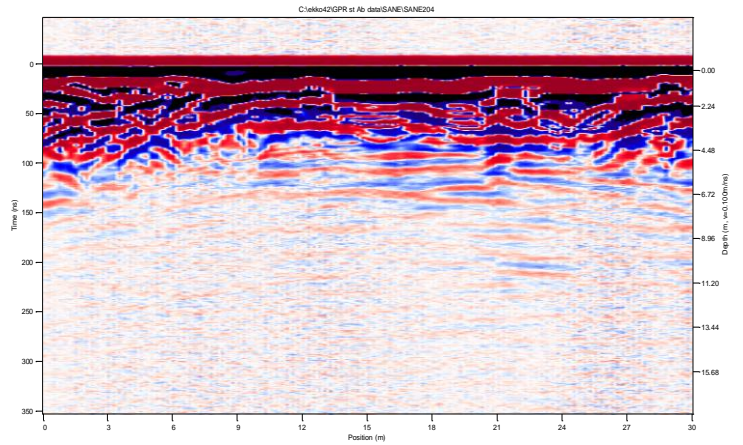
Area 5

Example GPR lines



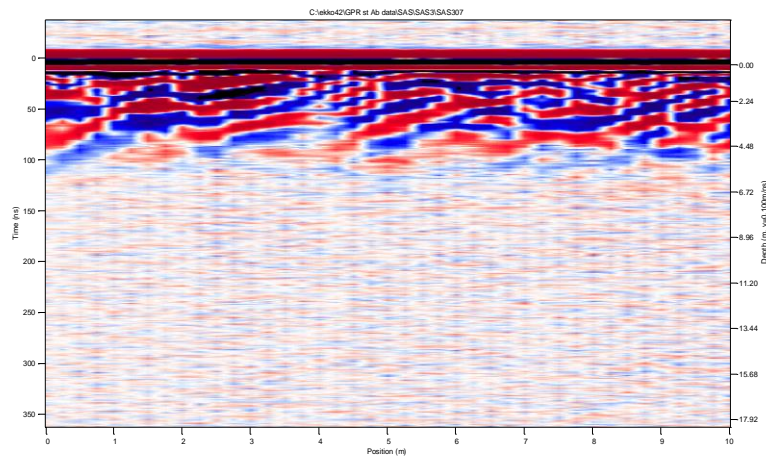
Area 6

Example GPR lines



Area 3

Example GPR line



Area 2

Example GPR line

